UNIVERSITY OF SOUTHERN QUEENSLAND

Faculty of Engineering and Surveying

Managing the Effect of Infiltration Variability on the Performance of Surface Irrigation

A dissertation submitted by

Malcolm Horace Gillies

For the Award of

Doctor of Philosophy

2008

ABSTRACT

Infiltration variability is a major issue during the design phase and management for all types of irrigation systems. Infiltration is of particular significance for furrow irrigation and other forms of surface irrigation as the soil intake rate at any given position not only determines the depth applied but also governs the distribution of water to other locations in the field. Despite this, existing measurement and evaluation procedures generally assume homogeneous soil infiltration rates across the field to simplify data collection and computational requirements. This study was conducted to (a) determine whether spatial and temporal variations in soil infiltration characteristics have a significant impact on the performance of surface irrigation and (b) identify more appropriate management strategies that account for this variability and substantially improve irrigation performance.

The soil infiltration rate is typically expressed as an empirical function of opportunity time. The infiltration function parameters cannot be directly measured but are commonly estimated from field hydraulic measurements using an appropriate simulation model. The volume balance model as used in the inverse solution for infiltration (e.g. Two Point Method) was modified to enable runoff data collected during the inflow period to be used in the estimation of the infiltration parameters. The resulting model, IPARM also accommodates the full (variable) inflow hydrograph rather than relying on a constant inflow assumption. Inclusion of runoff data in the inverse solution improved the accuracy of the infiltration curve during the runoff phase and hence offered the greatest benefit where the irrigation time exceeded the completion of advance. Analysis of field data collected from multiple furrows at a single site indicated that accounting for the variable inflow in IPARM both reduced the variability (e.g. reduction in the coefficient of variance (CV) of cumulative infiltrated depths of 18.6% and 11.5% at opportunity times of 100 and 500 minutes, respectively) and standardised the shape of the estimated infiltration curves. Hence, a significant proportion of the apparent variability in soil infiltration rates was shown to be a consequence of the constant inflow assumption. Sensitivity analysis indicated that IPARM is highly sensitive to the runoff measurements but is not influenced by the relative numbers of advance and runoff data points. Validation of IPARM

estimated infiltration parameters using the full hydrodynamic model SIRMOD showed that the inclusion of runoff data in the inverse procedure did not compromise the ability to predict the measured advance trajectory but significantly improved the fit to the measured runoff volumes (average decrease in absolute error of simulated runoff volumes of 84%). Whereas the use of runoff data enabled SIRMOD to estimate runoff volumes, accounting for variable inflow improved the fit of the predicted runoff rates to the shape of the measured outflow hydrograph.

Field data collected from several sites across the Darling Downs, Queensland has shown that the infiltration rates vary significantly (e.g. by up to 65% at 500 minutes), both spatially between furrows and temporally over the season. For the sites studied, the spatial variance in infiltration was surpassed by the seasonal variance (e.g. average CV of infiltration of 33.1% compared to 12.5%) but no consistent trends were identified. It was found that the lognormal distribution provided the best fit for the variance in the infiltration curves which was in turn strongly related to the statistical distribution of the infiltration term of the volume balance. From this research, a procedure was developed to predict the infiltration parameters using a single advance point and any number of “known” infiltration curves from the same field.

The IrriProb model was developed to extend the process of simulation from a single furrow scale to the whole field scale. IrriProb performs the full hydrodynamic simulation for multiple independent furrows which are combined to form a spatial representation of the water application. Each furrow can have a unique infiltration rate, inflow rate (Q), time to cut off (TCO) and soil moisture deficit. Validation of IrriProb using multiple sets of field data demonstrated that the single furrow simulations failed to predict the true whole field irrigation performance (e.g. furrow distribution uniformity (DU) between 72.2% and 86.2% compared to the whole field DU of 64.8%).

An optimisation routine was developed within IrriProb to maximise irrigation performance through identification of optimal values of Q and TCO. The optimisation objective function is comprised of a Boolean combination of customisable

performance criteria. The user selects the appropriate performance terms and the optimal management is determined through a graphical overlay of the complying ranges of Q and TCO. Hence, the objective function of IrriProb retains the importance of each individual performance term, an advantage over those based on numerical combinations of weighted terms. Simulation of the whole field application under practical ranges of Q and TCO demonstrated the complex interactions between the performance indices (e.g. the trade off between requirement efficiency (RE) and application efficiency (AE)). In cases of low infiltration variability it was possible to optimise the whole field performance using a single value of Q and TCO. However, under increased infiltration variability it was more appropriate to manage the field using two or more different management strategies. Irrigation optimisation based on measurements from a single furrow or the average infiltration curve, cannot identify the optimal combination of Q and TCO for the whole field. Simulation of field management based on the optimisation strategy obtained from single furrow measurements results in lower whole field performance than estimated from simulation of the single furrow data (e.g. field RE, AE and distribution uniformity of the root zone up to 26%, 18% and 66% lower than predicted). Field trials were used to demonstrate the ability to estimate whole field infiltration variability, evaluate whole field irrigation performance and optimise whole field irrigation management while taking into account the influence of spatial variability.

CERTIFICATION OF DISSERTATION

I certify that the ideas, designs, experimental work, software code, results, analyses and conclusions presented in this dissertation are entirely my own effort, except where otherwise indicated and acknowledged.

I further certify that the work is original and has not been previously submitted for assessment in any other course or institution, except where specifically stated.

_____ _____

Malcolm Horace Gillies, Candidate **Date**

Endorsement:

_____ _____

Prof. Rod Smith, Principal supervisor **Date**

_____ _____

Prof. Steven Raine, Associate supervisor **Date**

ACKNOWLEDGEMENTS

The completion of this research is a testimonial to the assistance I have received from a great many people. I would like to take the time here to express my gratitude to some of those who have helped and inspired me during the past three and a half years.

I would like to express my thanks to my supervisors Prof. Rod Smith and Prof. Steven Raine for their guidance during the last few years. I sincerely thank them for their enthusiasm, technical assistance and patience during my PhD studies. Finally I would like to thank Steve and Rod for the proof reading of this dissertation, I know that my English expression can be a little crude at the best of times.

To the staff at the NCEA for their support during my research and help in the collection of irrigation data. In particular to Dr J. McHugh and Dr J. Eberhard for assistance in collection of data for the Lagoona field trial. I would also like to thank John Hornbuckle (CSIRO) for use of his field data. A major part of this research would have not been possible without the simulation model and guidance provided by David McClymont.

I acknowledge the scholarship funding provided by the University of Southern Queensland and the Australian Federal Government. Also to the CRC for Irrigation Futures for providing additional funding for operational costs. I am grateful to the members of the CRC IF for their support and constructive criticism during my study.

To my brother and sisters and especially Mum and Dad who have encouraged me throughout my life. I am forever indebted to you for all your support and inspiration that has led me to this point.

Finally, to my wife Dennielle, words cannot express the appreciation I have for your love and understanding over the past few years. To you Dennielle, I dedicate this work.

LIST OF PUBLICATIONS FROM THIS RESEARCH

Gillies, M.H. and Smith, R.J. (2005), Infiltration parameters from surface irrigation advance and run-off data, *Irrigation Science*, Vol. 24, No.1, pp 25-35.

Gillies, M.H. and Smith, R.J. and Raine, S.R. (2006) Is it possible to extract infiltration rates for variable inflow furrow irrigation? National Conference, Irrigation Association of Australia. 9-11 May, Brisbane. pp 63-64.

Gillies, M.H. and Smith, R.J. and Raine, S.R. (2007), Accounting for temporal inflow variation in the inverse solution for infiltration in surface irrigation, *Irrigation Science*, Vol. 25, No.2, pp 87-97.

TABLE OF CONTENTS

TABLE OF FIGURES

LIST OF TABLES

LIST OF ABBREVIATIONS

ADU	absolute distribution uniformity
AE	application efficiency
AELQ	application efficiency of the low quarter
AER	application efficiency accounting for tail water recycling
AT	average advance time (time of the final advance point for a set of furrows)
CV	coefficient of variation
CU	Christiansen's uniformity coefficient
DD	deep drainage/deep percolation below the root zone
D_{DD}	average depth of deep drainage
DU	low quarter distribution uniformity
DURZ	distribution uniformity of the root zone
EC	electrical conductivity
EM	electromagnetic survey
ESP	exchangeable sodium percentage
ET_c	crop evapo-transpiration calculated from the reference evaporation
FIDO	Furrow Irrigation Design Optimiser
Fur	furrow
GPS	global positioning system
IPARM	infiltration parameters from advance and runoff model
Irr	irrigation
MIC	model infiltration curve
NCEA	National Centre for Engineering in Agriculture
NSW	New South Wales
Opt	optimisation (objective function to optimise performance)
PAM	Polyacrylamide
PRD	partial root-zone drying
Q	inflow rate
Qld	Queensland
RE	requirement efficiency
RMSE	root mean square error
SAR	sodium adsorption ratio
SCS	US Soil Conservation Service
SSE	standard square error
SSS	surface storage smoothing (technique to estimate the surface storage term)
TCO	time of cut-off (termination of inflow relative to irrigation start time)

LIST OF SYMBOLS

α	significance level
β	curvature constant for surface water storage
γ	semivariance
ζ	empirical exponent of Q for variation of infiltration with inflow
η	dynamic viscosity (Pa s)
θ	decrease in infiltration over time from Horton equation
λ	ratio of current time to end of advance
μ	population mean
σ	population standard deviation
σ_s	sample standard deviation
σ_y	surface storage coefficient for advance phase
σ_{ys}	surface storage coefficient for storage phase
σ_{z1}	subsurface storage coefficient of the transient infiltration term
σ_{z2}	subsurface storage coefficient of the steady infiltration term
τ	infiltration opportunity time (min)
τ_{f_0}	time constant of the Branched Kostiakov equation
φ	empirical parameter for variation of infiltration with wetted perimeter
χ^2	chi squared statistic
ω_{CV}	coefficient to calculate $CV_{Infiltration}$ from CV_{VB}
ω_{ZVal}	coefficient to calculate $ZVal_{Infiltration}$ from $ZVal_{VB}$
a	empirical Kostiakov/Modified Kostiakov infiltration parameter
A	cross-sectional area of flow (m^2)
A_0	upstream area of flow (m^2)
ACF	autocorrelation coefficient
AT	average time value of the last measured advance point (min)
c	coefficient of the power relationship of furrow width to depth
C	crack infiltration term ($m^3 m^{-1}$)
$CV_{Infiltration}$	time averaged CV for the logarithm of the Modified Kostiakov infiltration
CV_{VB}	CV for the logarithm of the infiltration term of the volume balance
D	volume of infiltration per unit area of soil (m)
$\overline{D_{LQ}}$	average of D over the quarter of the field with the lowest infiltration (m)
$\overline{D_{RZ_{LQ}}}$	average of D_{RZ} over the quarter of the field with the lowest infiltration (m)
D_{DD}	volume of deep drainage per unit area of soil (m)
D_{min}	minimum value of D across the field (m)
D_{req}	required volume of infiltration per unit area or soil moisture deficit (m)
D_{RZ}	volume infiltrated and stored in the root zone per unit area of soil (m)
$E[]$	the expected value
E_R	efficiency of the tail-water recycling system
f_0	semi-empirical steady state infiltration parameter of the Modified Kostiakov ($m^3 m^{-1} min^{-1}$)
F	rapid surface storage term from the Horton equation
F_S	scaling factor of infiltration function for the MIC approach
g	acceleration due to gravity (9.81 m s^{-2})
G	group iteration factor (default = 0.01)
h	lag distance (between samples)
H	pressure head (m)
I	infiltration rate ($m^3 m^{-1} min^{-1}$)
ICF	irrigation condition factor
Ja	direction and number of increments for Kostiakov a in the individual parameter search

Ja_{temp}	record of Ja for the last round of individual parameter searches
JC	equivalent to Ja but for C
JC_{temp}	equivalent to Ja_{temp} but for JC
Jf_0	equivalent to Ja but for f_0
Jf_{0temp}	equivalent to Ja_{temp} but for Jf_0
Jk	equivalent to Ja but for k
Jk_{temp}	equivalent to Ja_{temp} but for Jk
k	empirical Kostiakov/Modified Kostiakov infiltration parameter ($m^3 m^{-1} min^{-a}$)
K	hydraulic conductivity ($m^3 m^{-2} min^{-1}$)
K_s	saturated hydraulic conductivity ($m^3 m^{-2} min^{-1}$)
K_{wet}	hydraulic conductivity at field capacity ($m^3 m^{-2} min^{-1}$)
L	field length (m)
m	exponent of the power relationship of furrow width to depth.
n	Manning roughness coefficient
N	number of data points
N_a	number of advance points
N_r	number of runoff points
OBJ	objective function for optimisation of irrigation management
p	parameter of the power advance function
P	wetted perimeter (m)
P_0	upstream wetted perimeter (m)
q_r	steady runoff rate ($m^3 min^{-1}$)
Q	discharge ($m^3 s^{-1}$)
Q_0	inflow rate at upstream end of furrow ($m^3 min^{-1}$)
Q_r	outflow discharge ($m^3 s^{-1}$)
Q_x	flow rate at point x in a furrow ($m^3 s^{-1}$)
r	exponent of power advance function
R	Pearson correlation coefficient
s	distance measured from the upstream end of the field (m)
s_Z^2	variance of Z
S	sorptivity as present in the Phillip equation
S_0	field slope
S_f	friction slope
t	time (min or sec)
t_{Stat}	t statistic from the t-distribution
t_x	time taken to reach point x (min)
t_w	time taken for a change in upstream area to have effect over the wetted furrow length (min)
$T_{advance}$	length of the advance phase at the current time (min)
$T_{depletion}$	length of the depletion phase (min)
v	flow velocity ($m s^{-1}$)
v_x	flow velocity at point x ($m s^{-1}$)
V_f	volume surface storage at end of storage phase (m^3)
V_I	volume of infiltration (m^3)
V_R	volume of runoff (m^3)
V_{R_i}	measured runoff volume at data point, i (m^3)
V_S	volume of surface storage (m^3)
V_w	velocity of a wave or small disturbance ($m s^{-1}$)
V_{Zx}	volume of infiltration at the time t_x (m^3)
Vol_{DD}	volume of infiltration that drains below the rootzone as deep percolation (m^3)
$Vol_{Infiltration}$	volume of infiltration (m^3)
Vol_{RZ}	volume of infiltration stored in the root zone (m^3)
Vol_{req}	volume of infiltration required to refill the rootzone (m^3)
Vol_{Runoff}	volume of runoff (m^3)
Vol_{Inflow}	volume of inflow (m^3)
w	weighting factor for advance and runoff errors in IPARM (%)
W	top width of flow within the furrow (m)
W_B	bottom width of the furrow (m)
W_M	furrow width at half the total height (m)
Ws	furrow spacing (m)
W_T	furrow width at the total height (m)
x	advance distance (m)
x_i	measured advance distance at data point, i (m)

x_t	predicted advance distance if the advance continued beyond the end of the field (m)
X	a continuous variable
X_i	a continuous variable measured at point *i*
y	depth of flow (m)
y_0	upstream depth of flow (m)
Y_T	total height of furrow (m)
$\bar{y}$	centroid of the area of flow (m)
y_w	depth of the wetting front (m)
Z	infiltrated depth per unit length of furrow ($m^3 m^{-1}$)
Z_S	scaled infiltration depth per unit length of furrow ($m^3 m^{-1}$)
Z_x	infiltrated depth at distance x ($m^3 m^{-1}$)
$ZVal$	standard normal variate
$ZVal_{Infiltration}$	time averaged *ZVal* for the logarithm of the Modified Kostiakov infiltration
$ZVal_{VB}$	*ZVal* for the logarithm of the infiltration term of the volume balance

CHAPTER 1

Introduction

This thesis deals with the issue of infiltration variability and its influence over the performance and management of surface irrigation. As such, this introductory chapter establishes the purpose and importance of irrigation whilst covering the characteristics of different application systems. The concise discussion herein provides the necessary background to define the objectives of this research.

1.1 Background

1.1.1 Irrigation

Irrigation is defined by the Oxford English dictionary (Simpson and Weiner 1989) as "The action of supplying land with water by means of channels and streams; the distribution of water over the surface of the ground in order to promote the growth and productiveness of plants". Water is required by almost every aspect of life on Earth. It makes up a large proportion of all plant and animal tissue, serves as the essential for the fundamental processes of photosynthesis and respiration.

Through history, humans have learnt to use irrigation to enhance the production and reliability of crops and facilitate the growing of many plants outside their natural environment. Full irrigation describes the situation where little or no effective rainfall occurs during the growing season and all moisture must be supplied artificially. Supplementary irrigation differs in that water is applied in order to complement the natural precipitation and is often preferred over the full irrigation strategy.

Irrigation has been an essential component of agriculture for thousands of years for numerous civilisations across the globe. It is thought that the agricultural society began 10,000 years ago in the Middle East where the rainfall was plentiful and local plants were suited to domestication. Sometime later (approximately 4,000 BC) a group of people migrated from the northern Mesopotamian highlands to the fertile

plains between the Tigris and Euphrates Rivers in modern day Iraq. The crops germinated but the lack of follow up rain caused them to wither and die. The farmers fixed this problem by digging a network of channels and ditches to supply water to the fields (Postel 1999). These early irrigation systems resembled what we now call flood and furrow irrigation. The Egyptians and Indians pioneered a system of "inundation canals" that are dug parallel to the river and rely on regular seasonal flooding (Cantor 1970). In Egypt, these canals were used to supply water to the field in a basin type irrigation where the water was ponded on the soil surface and later drained. Basin irrigation can still be seen relatively unchanged in the region to this day. Irrigation must have been an integral part of the Egyptian civilisation as a historic relief dated from 3,100 BC shows the Scorpion King using a hoe to cut a ditch in a network grid (Postel 1999). Evidence for similar primitive irrigation systems has also been found in other regions such as China and Mexico. The advent of irrigation was a turning point for society as it assisted farmers to produce excess food and therefore freed up labour. These non-farm workers could then pursue other occupations in areas diverse as from metalworking to mathematics. Considering this, irrigated agriculture led to the creation of the urban society that is so prevalent in the modern age.

Crops have been grown with the aid of irrigation for thousands of years but technological advances over the past few centuries have provided farmers with new techniques to apply water to the field. The wide range of irrigation techniques can be grouped into three main categories, namely surface, sprinkler and drip irrigation. This dissertation deals with surface irrigation systems.

1.1.2 Irrigation Performance

The term irrigation performance has different significance and meaning depending on its context. This thesis deals with measuring, evaluating and managing the technique of surface irrigation with little or no consideration of the plant response. Hence, the term performance is used to describe the hydraulic performance or the ability to apply water efficiently and uniformly to the field. Irrigation efficiency is defined in terms of the requirement efficiency, ability to completely refill the soil moisture deficit and the

application efficiency, volume added to the root zone divided by the total applied. Uniformity refers to the spatial distribution of infiltrated depths and is typically expressed in terms of the distribution uniformity, average low quarter divided by the average infiltrated depth or the coefficient of uniformity, average deviation from the mean of applied depths.

1.1.3 Surface Irrigation

Surface irrigation is defined as the group of application techniques where water is applied and distributed over the soil surface by gravity. It is the oldest technique and is also the simplest to implement. Surface irrigation is often referred to as flood irrigation, implying that the water distribution is uncontrolled and therefore, inherently inefficient. In reality, the various irrigation practices grouped under this name often involve some degree of management. In some cases (e.g. surge irrigation), the implementation of surface irrigation actually demands a high level of control and expertise. Surface irrigation is further divided into the three types; level basin, border strip and furrow irrigation, which is the primary focus of this dissertation.

1.1.3.1 Level Basin

Level basin irrigation has historically been used in small areas having level surfaces that are surrounded by earth banks. Basin irrigation is favoured in soils with relatively low infiltration rates (Walker and Skogerboe 1987). Paddocks are traditionally set up to follow the natural contours of the land but the introduction of laser levelling and land grading has permitted the construction of large rectangular basins that are more appropriate for broadacre cropping (e.g. Figure 1-1). The water is applied quickly to the entire basin and ponded until the required infiltration has occurred. Individual basins may be linked sequentially so that drainage from one basin is diverted into the next once the desired soil water deficit is satisfied. Alternatively, closed basin systems are characterised as those in which all of the water applied to the individual basin is expected to infiltrate (Khanna and Malano 2006).

1.1.3.2 Furrow

Furrow irrigation is the most common form of irrigation throughout the world (Burt 1995). The furrow itself is a small trench, typically between 200 to 800 millimetres wide, 100 to 300 millimetres deep and orientated in the direction of predominant slope. They are traditionally closely spaced with the plants located on the crest of the ridge between adjacent furrows. Alternatively, the field may be formed into beds, which are flat elevated regions between the furrows rather than a single narrow ridge. The actual distance between furrows is governed by a combination of the plant spacing, machinery track-width, irrigation management and the soils capacity for horizontal redistribution of water. Shorter furrows are commonly associated with higher uniformity of application and increased potential for runoff losses. However, farmers in Australia tend towards longer furrows (e.g. 950m in Figure 1-2) to reduce the labour requirements and to minimise the area of land occupied by irrigation infrastructure.

Water is applied to the top end of each furrow and moves along the furrow under the influence of gravity. The “advance” phase refers to that time where the water front is travelling towards the downstream end. Inflow usually continues for some time after the completion of advance, aptly termed the “storage” phase. As inflow ceases there is a short period where the entire length of the field remains submerged, termed the “depletion”. Finally, the “recession” describes the retreat of water towards the downstream end of the furrow. Furrow inflow may be applied to individual furrows or small groups of furrows through siphons or gated pipe. Siphon application requires a head ditch running across the upstream end of the field in which the water level is higher than the base of the furrow. Gated pipe systems, commonly used by the Australian sugar industry comprise a low pressure, large diameter rigid or flexible walled pipe running across the upstream end of the furrows. Gates or cups are located in the wall of the pipeline according to the furrow spacing. The discharge from each outlet is governed by the outlet dimensions, pipeline pressure and flow velocity at that point (Smith 1990). Recently, in an effort to reduce labour requirements, farmers have looked towards a number of alternative application techniques. One such technique, termed “bankless channel”, removes the requirement for manual siphons or gated pipe

by extending the furrow upstream into the head ditch. Water automatically flows into each furrow when the depth in the head-ditch is higher than the bottom of the furrow cross-section.

Figure 1-1 Large scale level basin irrigation of rice/wheat field in Griffith region, southern NSW

Figure 1-2 Furrow irrigation of cotton near Moree, northern NSW showing siphon application

Furrow irrigation is particularly suited to broad-acre row crops such as cotton, maize and sugar cane. It is also practiced in various horticultural industries such as citrus, stone-fruit and tomatoes. It does not involve wetting the canopy which can be a benefit in some crops by reducing the risks of disease transmission and infestation. Furrow irrigation offers better performance and greater flexibility than other types of surface irrigation largely since only part of the soil surface needs to be wetted. This offers the possibility of smaller application volumes and more rapid advance times than other types of surface irrigation.

1.1.3.3 Border Strip

Border strip or bay irrigation could be considered as a hybrid of level basin and furrow irrigation. The borders of the irrigated strip are longer and the strips are narrower than for basin irrigation and are orientated to align lengthwise with the slope of the field. The water is applied to the top end of the bay, which is usually constructed to facilitate free-flowing conditions at the downstream end.

1.1.4 Irrigation in Australia

Australia is often given the title of the driest continent on earth, and in reality it is only surpassed by Antarctica. Situated approximately 30° from the equator positions Australia on the latitudes that contain a large portion of the desert regions of the world, including the Sahara and Arabian deserts. These zones are characterised by lower rainfall due to the persistent high pressures caused by dry colder air sinking from high altitudes as part of the Hadley Cell system (Hidore and Oliver 1993). The majority of Australia receives low rainfall and experiences high rainfall variability from season to season. It is therefore necessary for many farmers to look to irrigation in order to minimise the risk associated with agricultural production.

Irrigation emerged in many locations in Australia during the 19th century but was generally limited to individuals or small groups of individuals. The first major development occurred in 1882 with the formation of the Loddon Irrigation Works (Hallows and Thompson 1995). Other schemes soon followed in nearby catchments as the area surrounding Mildura and Goulburn was suitable for agricultural production while the development was partly funded by income from the Victorian Goldfields. This development later spread downstream to South Australia and upstream into the Murray, Murrumbidgee and various tributaries of the Darling River. Still to this day, the Murray-Darling irrigation system remains the largest of its type in Australia

Australia’s economy has traditionally been reliant on the agricultural sector. Statements such as “riding on the sheep’s back” have become an integral part of Australia’s cultural identity. Over the past few decades the rise of the mining and

manufacturing sectors has somewhat diminished the role of agriculture. However, it still remains an important contributor to exports and employment.

In the year 2004-2005 Australia's total water consumption was 18767 GL, with irrigation being the single largest user by far at 12,191GL or 65% (ABS 2006a). In the same year, the gross value of irrigated agricultural production was $9,076 million representing 23% of the total value of agriculture. This large portion of income is generated from 2.4 million hectares or a mere 0.5% of the total land area used for agriculture (ABS 2006a). The largest user of irrigation is the pasture industry which accounts for the largest percentage of irrigation establishments covering 42.7% of the total irrigated land area using 35.6% of the total volume of irrigation water (ABS 2006b). In the 2004-2005 year surface irrigation was the most common form of irrigation considering both the number of properties (27%) and the area irrigated (60.2%) (ABS 2006b). Almost three quarters and 69.5% of the irrigated area of New South Wales and Victoria respectively is surface irrigated (Table 1-1). This is significant considering that combined these states account for the majority of the irrigation that takes place in Australia.

Table 1-1 Irrigation area, volume and type by state (Created from data included in ABS 2006b)

	State	NSW[1]	VIC	QLD	SA	WA	Tas	NT	Aus
	Volume of water (GL)	3717	2364	2613	878	267	232	14	10085
	Area Irrigated (1000 Ha)	910	636	542	184	45	86	4	2405
Percentage by Area	Surface	74.5	69.5	50.6	17.9	31.1			60.2
	Surface Drip	4.7	7.2	5.4	30.4	31.1	4.7	25.0	8.1
	Subsurface Drip	1.2	0.9	2.0	0.5	2.2	0.0	0.0	1.3
	Microspray	1.1	2.8	3.7	9.2	8.9	1.2	50.0	3.0
	Portable irrigators	3.5	2.5	4.6	2.2		14.0		3.7
	Hose Irrigators	3.4	3.6	22.5	2.7	6.7	39.5	0.0	9.1
	Large Mobile Machines	6.9	5.7	8.9	24.5		31.4		9.1
	Solid Set	1.3	4.1	2.6	7.6	6.7	2.3	0.0	3.0
	Other	0.1	0.2	0.4	0.0	0.0			0.2
	TOTAL	100.0	100.0	100.0	100.0	100.0	100.0	100.0	100.0

[1] includes the Australian Capital Territory

Many of the crop growing regions of Australia are situated on heavy clay soils with low permeability, which makes them ideally suited to surface irrigation. Over recent decades there has been a definite trend towards other more efficient application techniques. However, the change has been slow due to the associated capital costs of conversion, increased level of expertise required, low water costs and low return for agricultural commodities. It is interesting that in the years between 2002 and 2005

both the total and fractional area under surface irrigation has increased marginally (ABS 2006b).

1.1.5 The Surface Irrigation Debate

Alternative irrigation techniques with potentially higher efficiencies and uniformities have been available for a number of decades but their uptake has generally been low or non-existent. There are a number of factors underpinning this trend. One the most important is the cost, as surface irrigation systems are generally inexpensive compared to pressurised systems. Most alternative techniques are pressurised and hence have additional pumping requirements and higher energy consumption. The current trend in oil prices and possible future limitations on the use of fossil fuels to reduce the greenhouse effect will serve to increase the operating costs further. It is reasonable to expect that future land developments will involve some form of pressurised systems while it is less likely for existing surface irrigated land to be converted. The changes to field layout will require large capital investment whereas the farmer may have not as yet recouped the installation costs of the current system.

Pressurised irrigation systems are usually associated with higher investment for installation, operation and maintenance. A cost-benefit analysis study conducted in Portugal found that centre pivot and hose reel irrigation systems provide 9.5% higher and 5.7% lower returns per unit area compared to optimised surface irrigation (floppy pipe irrigated furrows) but simultaneously involve 60.7% and 40.7% higher total costs (Sousa et al. 1999). The centre pivot system may offer higher gross returns but in reality produce a 27.7% lower net return than for furrow irrigation. The adoption of linear move and subsurface drip systems may reduce some of the crop production costs (e.g. land preparation and labour) but the benefits are often overcome by the associated increase in capital cost. Wichelns and Oster (1990) found that for cotton, the installation costs of a linear move could be offset by a reduction in infiltration variability (estimated by standard deviation of soil electrical conductivity) of 50%.
Although effective management of surface irrigation may require a high level of understanding, it is possible to conduct the technique with minimal knowledge of the soil-crop environment. Sprinkler and drip irrigation require a different mindset,

particularly regarding the process of irrigation scheduling. Associated with the ability to apply smaller volumes more frequently is the importance of correctly identifying the crop demand. Many farmers are resistant to change, they are willing to remain using proven scheduling and application techniques while being hesitant to take a risk with new technology.

Drip irrigation, particularly subsurface drip may be perceived as the best alternative for broadacre crops due to the potential for high application uniformity and reduced evaporation losses compared with sprinkler irrigation. This translates to higher crop yields and water productivity compared to surface and sprinkler systems (O'neill et al. 2006). However, the direct comparison between application techniques is usually invalid due to different scheduling procedures and sub-optimal irrigation management. Field trials have shown that subsurface drip may have lower uniformity in the surface soil layers compared to furrow (Amali et al. 1997), and therefore may require a secondary irrigation system to “wet up” the soil prior to the establishment of the root profile.

Some agricultural industries are better suited to surface irrigation due to plant agronomy (e.g. rice in cool climates must be grown in ponded conditions to avoid cold damage). For many plants, the long duration between irrigation events practiced in surface irrigation may encourage deeper root systems. Many soils such as the cracking clays of Australia appear to be suited to furrow irrigation due to their rapid infiltration in dry conditions and particularly low intake at field capacity. Surface irrigation on these soils will often have high distribution uniformities while high application efficiencies are possible providing irrigation times are managed to minimise runoff. Conversely, sandy soils are not suited to furrow irrigation due to the high potential for water loss to deep percolation.

The debate between furrow and pressurised systems is not as simple as one outside the industry may perceive. It is obvious that much of the land currently under furrow and other forms of surface irrigation will ultimately be converted to some form of pressurised system. However, a significant proportion of farmers will continue to use

surface irrigation systems where the soil crop and economic conditions are appropriate. These people will require the improved tools and management practices in order to remain economically, environmentally and socially sustainable.

1.1.6 The Issue of Infiltration Variability

The design and management of any irrigation system should be conducted to maximise irrigation performance. The design of the irrigation system should ensure adequate and uniform water application over the entire field area with minimal loss via runoff or deep drainage. For most pressurised irrigation techniques, the uniformity of application is almost entirely dependent on the characteristics of an engineered mechanical system. Pipes and nozzles can be added, altered or exchanged throughout the design phase and to a limited extend during regular maintenance in order to alter application rates or improve uniformities. Surface irrigation differs in that the water infiltrated at any point and hence the distribution of water throughout the field is affected by a multitude of soil properties (section 2.3) over which the designer and operator have little or no control. Soil is complex and its many variable characteristics combine to regulate the hydraulic behaviour of the surface irrigation system.

Many soil characteristics vary considerably both spatially and temporally. The majority of these soil properties cannot be readily measured at the field or furrow scale and furthermore it is difficult to relate them directly to soil infiltration rates. The temporal and spatial variability in soil infiltration rates is a major impediment to the accurate simulation of furrow irrigation and prohibit the consistent level of high efficiencies possible with other forms of irrigation (Elliott and Walker 1982).

This thesis while dealing with the issue of infiltration variability relies on the assumption that the infiltration characteristic of a furrow can be expressed as a spatial average over the field length. In this way the analysis is restricted to the inter-furrow variation in the soil infiltration characteristic.

1.2 Hypothesis

This study will firstly propose and provide evidence for the following:

1) *Spatial and temporal variations in soil infiltration characteristics have a significant impact on the performance of surface irrigation at the field scale.*

2) *It is possible to determine more appropriate management strategies that account for that variability and substantially improve irrigation performance.*

1.3 Objectives

The main objectives of this work are to:

1) Develop an improved inverse procedure to estimate the parameters of the Modified Kostiakov infiltration equation from runoff data that can also accommodate variable inflow conditions.
2) Evaluate the nature of infiltration variability at the field scale and develop a technique to estimate the spatial and temporal variability using minimal field measurements.
3) Develop a model to evaluate and optimise the irrigation performance at the whole field scale under heterogeneous infiltration conditions.
4) Investigate management options and develop techniques to optimise the irrigation performance while accounting for the effects of both spatial and temporal variability of soil characteristics.

1.4 Structure of this Dissertation

This chapter has provided a brief background to the subject area and introduced the objectives of the remaining eight chapters of this dissertation. Chapter 2 serves as a comprehensive review of the theory of infiltration, summarising previous findings. The literature review covers many of the soil factors responsible for infiltration variability and the problems this presents for field measurement. Chapter 2 also

discusses the nature of infiltration variability, its impact on irrigation performance and a number of alternative application techniques that can reduce the impact of this variability. Chapter 3 deals with hydraulic simulation modelling by presenting the different options and their potential applications in the evaluation and management of surface irrigation. It discusses the limitations of these models focussing on the assumptions that may lead to apparent infiltration variability in both the inverse solution techniques and performance evaluation processes.

Chapter 4 describes the development of an improved technique to estimate the infiltration characteristic from field data (objective 1). The validation of this model includes comparison with existing procedures and sensitivity analysis of selected input parameters. Chapter 5 describes the statistical nature of infiltration variability by using three selected case studies (objective 2). This study provides the groundwork for a procedure to predict infiltration curves from limited field measurements. Chapter 6 describes the development of the whole field simulation model (objective 3). It discusses the methodology and demonstrates the need for surface irrigation models to consider the whole field rather than single furrow performance. Chapter 7 uses the IrriProb simulation model to observe the process of surface irrigation optimisation. This work serves as the justification for the development of the whole field optimisation technique (objective 4). The proposed optimisation routine is compared against alternative procedures such as single furrow and recipe optimisation. Chapter 8 presents an additional case study which is used to demonstrate how the techniques developed in the four objectives of this study can be combined to measure, evaluate and optimise irrigation performance at the field scale. Finally, chapter 9 discusses the key findings of this work and presents a number of recommendations for further research in this area.

CHAPTER 2

Review of Infiltration and Infiltration Variability

2.1 Introduction

Before proceeding with any analysis, it is necessary to recognise the body of research on the theory and field behaviour of infiltration variability and its affect on furrow irrigation. This chapter provides an introduction to the process of infiltration and describes the factors that can influence the process. It discusses techniques used to estimate the soil infiltration and their suitability for use at the field scale. The chapter concludes with some of the previous attempts deal with this variability and improve irrigation performance through alternative surface irrigation techniques.

2.2 Infiltration

Infiltration is defined as the process by which a fluid passes through or into another substance travelling through pores and interstices (Simpson and Weiner 1989). For surface irrigation that fluid, water, is ponded on the soil surface and the infiltration rate, intake rate or infiltrability describes the flux into the soil profile. For many types of irrigation systems and natural rainfall events the application rate does not exceed the potential for infiltration. In these circumstances, the water flux is governed by, and limited to, the water application rate. As long as this application rate remains appreciably below the infiltration potential and the soil characteristic is non-limiting, the uniformity of water applied should be distinctly defined by the irrigation system design. Where this is not the case, such as for surface irrigation, the soil hydraulic properties will govern the infiltration rate and surface ponding. The water volume that does not infiltrate immediately remains on the soil surface and can then move under gravity to other parts of the field. In this way, the distribution of water will be partly determined by the infiltration at other locations in the field.

Water movement within the soil is governed by Darcy's law, which states that the flux is equal to the hydraulic conductivity multiplied by the hydraulic gradient. The hydraulic gradient is comprised of the gravity, pressure, osmotic and matric (movement of water from wet or full pores to dry soil) potentials (Singer and Munns 1999). Starting with a dry soil the suction gradient (matric potential) is high causing a high infiltration rate. As the pores fill with water the suction gradient decreases and time permitting approaches zero (Lal and Shukla 2004). The infiltration rate experiences a similar reduction until at saturation is almost entirely reduced to that caused by the forces of gravity and pressure.

2.2.1 Infiltration Equations

There are two main approaches to describe the time dependent function of infiltration. Some are physically based, derived from the interaction between soil physical characteristics while others are empirically based, composed from the results of experiments and statistical analysis. Physically based relationships include the Green-Ampt and Philip equations. Many empirical models have been developed, of which three major examples are the Horton, Kostiakov and Modified Kostiakov equations. The infiltration rate I (m^3 min^{-1} m^{-2}) and infiltration volume Z (m^3 m^{-2}) are commonly expressed in units of infiltrated volume per unit area. However, for furrow irrigation these terms are usually described in terms of infiltration per unit length of furrow (i.e. I (m^3 min^{-1} m^{-1}) and Z (m^3 m^{-1})).

2.2.1.1 Green-Ampt Equation

The Green-Ampt equation applies the Darcy equation to the soil through the use of a distinct wetting front approach. The soil immediately below the wetting front is dry and that behind the front is at saturation, hence often referred to as piston flow. The infiltration rate I (m^3 min^{-1} m^{-2}) in the vertical direction (Lal and Shukla 2004) is given by:

$$I = K_s\left(1+\frac{\Delta H}{y_w}\right) \quad \text{..... Eq 2-1}$$

where K_s (m^3 min^{-1} m^{-2}) is the hydraulic conductivity in saturated conditions, ΔH (m) is the hydraulic head difference between the wetting front and the soil surface while

y_w (m) is the depth of the wetted region. Since the wetted layer of soil is rarely at saturation, the K_s term is commonly replaced with the hydraulic conductivity at field-saturated conditions (Enciso-Medina et al. 1998; Warrick et al. 2005). This value, denoted by K_{wet} is close to but slightly less than the value of K_s.

2.2.1.2 Philip Equation

The Philip equation is based on the sorptivity parameter S (m^3 $min^{-½}$ m^{-1}), which is a function of the initial and boundary water contents:

$$I = \frac{1}{2} S \tau^{-\frac{1}{2}} + f_0 \qquad Z = S\tau^{\frac{1}{2}} + f_0\tau \quad \text{..... Eq 2-2}$$

where τ (min) is opportunity time (water ponding time), Z is the cumulative infiltrated depth per unit length of furrow (m^3 m^{-1}) and f_0 is the steady infiltration rate (m^3 min^{-1} m^{-1}) and is closely related to the saturated hydraulic conductivity and slightly influenced by the water content (Or and Silva 1996). The parameters of this equation have physical meaning when applied to the simple case of a one-dimensional homogenous media. It is sometimes preferred in the study of infiltration variability over strict empirical formulae such as the Kostiakov equation due to the ability to separate variation into components (Tarboton and Wallender 1989). However, in the practical example of furrow irrigation, soil cracks, roots and macro-pores from earthworm activity undermine the theoretical significance of this equation (Gish and Starr 1983). Austin and Prendergast (1997) found that the Philip equation yielded a poor representation of the infiltration under bay irrigation and hence concluded that it was unsuitable for use on cracking clay soils. Philip (cited in Hopmans 1989) himself concedes that his equation is less accurate for large values of opportunity time, providing further evidence for its unsuitability for use in surface irrigation modelling.

2.2.1.3 Horton Equation

The Horton infiltration equation is empirical and has the feature of a defined initial infiltration rate as apposed to other equations (e.g. Kostiakov) which have an infinite intake rate at $\tau = 0$.

$$I = F\theta e^{-\theta\tau} + f_0 \qquad Z = F\left(1 - e^{-\theta\tau}\right) + f_0\tau \quad \text{..... Eq 2-3}$$

F is the initial infiltration rate (rapid surface storage) and θ represents the decrease of the infiltration over the transient time period (Renault and Wallender 1994).

2.2.1.4 Kostiakov Equation

The well known Kostiakov equation (Walker and Skogerboe 1987) is given by

$$I = ak\tau^{a-1} \qquad Z = k\tau^{a} \quad \text{..... Eq 2-4}$$

where a and k (m^3 min^a m^{-1}) are empirical constants that must be calibrated. The Kostiakov equation assumes that the infiltration rate approaches zero at long times. This may be satisfactory for basin and border irrigation with short ponding times as the expression adequately estimates intake rates where the opportunity time does not exceed 3 to 4 hours (Walker et al. 2006). In most soils, the infiltration rate does not decline to zero but approaches a steady state at larger opportunity times. For longer irrigations this steady intake rate may dominate the shape of the infiltration function (Walker and Willardson 1983).

Kostiakov himself realised that equation 2-4 would not suffice for greater times and proposed the Branched Kostiakov equation (Clemmens 1983) composed of two components, one before and the other after steady state conditions have been reached (Bali and Wallender 1987):

$$I = ak\tau^{a-1} \qquad Z = k\tau^{a} \qquad \textbf{for} \qquad \tau \le \tau_{f_0} \quad \text{..... Eq 2-5}$$

$$I = f_0 \qquad Z = k(1-a)\tau_{f_0}{}^{a} + f_0\tau \qquad \textbf{for} \qquad \tau \ge \tau_{f_0}$$

where τ_{f_0} is the time defined by making I for the two branches equal.

2.2.1.5 Modified Kostiakov Equation

In some cases the soil may approach the final infiltration rate soon after wetting (Elliott et al. 1983). The Kostiakov-Lewis variant, also known as the Modified Kostiakov equation corrects for this by adding a steady state intake term (Walker and Skogerboe 1987).

$$I = ak\tau^{a-1} + f_0 \qquad Z = k\tau^{a} + f_0\tau \quad \text{..... Eq 2-6}$$

In this case the f_0 term is an empirical parameter that shows close relationship to the final infiltration rate of the soil. Comparisons between the standard Kostiakov and the

Modified Kostiakov for surface irrigation evaluations have found that both provide adequate predictions of the water front advance but that the later provides better estimates of the cumulative infiltration depth and hence also irrigation performance (Hanson et al. 1993). In some instances, this equation fails to adequately describe the cracking nature of the soil. The shape of the two parameter infiltration curve cannot adapt to the rapid infiltration that occurs on many clay soils. To correct for this, some have proposed the inclusion of a fourth term, C (m^3 m^{-1}) to the Modified Kostiakov equation to account for cracking and depression storage:

$$I = ak\tau^{a-1} + f_0 \qquad Z = k\tau^a + f_0\tau + C \quad \text{..... Eq 2-7}$$

2.2.1.6 Linear Equation

Of the candidate equations presented thus far, all use curves to describe the gradual decline in the intake rate over time. An alternative is to assume that the time dependent cumulative infiltration can be described by an instantaneous depth (the crack volume C) followed by a constant rate (the steady intake term f_0.).

$$Z = C + f_0\tau \quad \text{..... Eq 2-8}$$

The resulting equation has the advantage that both terms have physical significance and can be evaluated independently (Austin and Prendergast 1997). In addition, the linear nature of this expression simplifies any hydraulic model and permits the use of standard statistical techniques. Mailhol and Gonzalez (1993) used the linear equation within a real-time control system, where f_0 is adjusted based on the wetted perimeter and C is fitted using the end advance time. While the linear equation performs well, it tends to over predict infiltrated depth at early times (Austin and Prendergast 1997). Similarly, experience has shown that the parameter a often tends to zero during numerical calibration of the Modified Kostiakov function for cracking clay soils indicating the suitability of the simple linear equation.

2.2.1.7 Soil Intake Families

The concept of infiltration families assumes that soils can be grouped into a number of different classes according to their hydraulic properties. This assumption reduces the analysis requirement since it reduces the number of infiltration curves within a

field down to a small number of units. Although the technique is not widely used, it can be of enormous benefit in the initial irrigation design phase where soil properties must otherwise be inferred from similar fields in the region.

The US Soil Conservation Service (SCS) devised a system of intake families based on a large number of field trials. They used the following expression to represent infiltration:

$$Z = \left(k\tau^{a} + 0.007\right)\frac{P}{W_s} \quad \text{..... Eq 2-9}$$

where k and a are unique to each family and are dependent on each other (Valiantzas et al. 2001), 0.007 is the constant assumed value for initial infiltration, P is the wetted perimeter (m) and W_s is the furrow spacing (m). The resulting function has the advantage of only containing one unknown parameter. Soils are grouped into families according to their final infiltration rate (Maheshwari and Kelly 1997).

2.2.1.8 Choosing an Infiltration Function

A number of equations have been formulated to describe the process of infiltration. None of these could be considered as universally applicable as there may be circumstances or soil types that favour the use of each alternative. Physically based equations are convenient due to their ability to relate the infiltration to measurable soil characteristics. However, the simple empirical equations often provide better approximations to the infiltration curve. Clemmens (1983) evaluated the performance of several alternative expressions for the infiltration function using both infiltrometer and border irrigation measurements. He found that the empirical equations consistently out-performed the physically based Philip and Green-Ampt equations and concluded that the Modified Kostiakov and Branched Kostiakov provided the best compromise of simplicity and accuracy for both cumulative infiltrated depths and intake rates.

2.3 Factors Influencing Infiltration

The infiltration rate is determined by the interaction of a number of physical and chemical soil characteristics. These soil properties vary from one location to another

and change over time due to cultural practices (e.g. tillage and compaction), water management and biological processes (e.g. macro and micro-organisms). This section provides a summary of the various factors that influence the soil infiltration rate within a surface irrigated field.

2.3.1 Soil Texture

The hydraulic conductivity of the soil is strongly influenced by the soil texture, i.e. the relative proportions of sand, silt and clay. Clay particles are particularly important as their small size makes them able to fill the voids between larger particles while their charge orientation gives them a crucial role in binding the soil matrix into larger structures. For a media with a single particle size the hydraulic conductivity is approximately proportional to the square of the particle diameter (Iwata et al. 1995). However, in a natural soil the particle sizes range from the microscopic clay colloids (< 0.0002 mm) to the much larger sand grains (0.05 – 2 mm) up to large boulders (Singer and Munns 1999). The textural composition and soil properties vary considerably between soil types therefore attempts are commonly made to position field and property boundaries based on the soil characteristics. However, the field layout, particularly in the case of furrow irrigation, is usually based on regular sized rectangular shaped fields. Hence, it is likely that a single field may contain a number of distinct soil types.

Hydraulic properties which are strongly influenced by texture and structure vary considerably even within a single soil class. For example, a general trend was observed (Vervoort et al. 2003) amongst the Vertosols found throughout the cotton growing areas of south-eastern Australia running in the north-south direction with the soils in the northern regions, close to the New South Wales/Queensland border having a more developed, crumb-like structure due to higher clay contents. It was also found that the hydraulic conductivity declined significantly with depth between the surface and 400 mm depth for these soils.

One might expect coarser sandy soils to have higher infiltration due to larger pore sizes. Regions of lighter textured, or sandy soil within a field often have higher intake

rates (Childs et al. 1993). However, van Es et al. (1991) found a positive correlation between the clay content and the initial infiltration rate while the silt content was negatively correlated. Also, stones within the soil matrix can serve to reduce the pore areas available for water storage and transport (Mehuys et al. 1975). Attempts have been made to correlate the hydraulic conductivity with soil texture with the promise of predicting infiltration using measurable physical properties. For example, Bresler et al. (1984) found that between 24-45% of the variability in K_s could be related to the sand content and 10-25% was explained by the interaction between electrical conductivity and sand content.

Variations in soil horizon thickness and texture may have significant effects on the spatial variation in soil infiltration rates, particularly as the wetting front reaches that layer. Considering a vertical soil column, the long term infiltration rate is determined by the most restrictive layer. The existence of a coarse sand layer within a finer textured loam or clay soil has been found to reduce rates of infiltration and upwards movement from a water table (Brady and Weil 2002). The larger pores within the sand cannot generate the same level of matric potential therefore no water passes through that layer until the moisture content of the finer soil rises sufficiently to generate the same level of matric suction.

The natural topography of the land is inherently random in nature and is determined by geological features and history of erosion. Hence, fields are often graded using laser guided or manual scrapers and buckets to aid in drainage and irrigation management. Consequently, soil is excavated and relocated to other areas. In parts of the field, this may uncover underlying soil horizons with differing chemical and hydraulic properties. Brye et al. (2006; 2003) found that field levelling altered soil texture and increased the average bulk density by 3% for a clay loam and 12% for a silt loam. However, the variance decreased due to the compaction and exposure of the denser subsoil. Brye et al. (2006) also observed changes in the spatial variability as the bulk density became spatially auto-correlated while the silt content became more spatially independent after levelling.

2.3.2 Soil Erosion

Soil erosion is the process by which material is dislodged, transported and deposited elsewhere in the landscape via the effects of wind or water. Disregarding wind, the severity of erosion is determined by the soil particle size, field slope and water flow velocity. In furrow irrigation, maximum flow velocity is realised close to the inlet and gradually declines over the furrow length. Hence, the sediment load generally increases throughout the first quarter of the field length and steadily declines over the second half of the field (Trout 1996). Soil erosion from the upstream end can be up to six times (Fernandez-Gomez et al. 2004), or 20 times greater (Trout 1996) than the furrow average. Some of the eroded material may be removed in the tail water but a majority of the suspended load is deposited before the water reaches the end of the field. Despite this, erosion is usually only considered a problem where soil material is removed from the field even though any degree of erosion along the furrow length will result in non-uniform re-distribution of soil particles.

The suspended load for a given particle size is deposited once the flow declines below a threshold velocity. Therefore, the gradual reduction in velocity observed in furrow irrigation will introduce systematic heterogeneous conditions as the soil particles are deposited spatially according to size and density. Surface seals may form in areas where fine sediment is deposited and consolidated, creating areas of low infiltration at the downstream end of the field. Infiltration rates have been observed to be 50-100% higher (for a silt loam) at the upstream compared to the downstream end of the furrow (Brown et al. 1988). The effect of this decline becomes even more significant considering the tendency for shorter opportunity times at the downstream end of the field. Brown et al. (1988) found that the addition of fine sediment to the supply water could replace the sediment removed from the upstream end of the field and hence increase the uniformity of applied depths. In some cases, soil colour can be used as a remote indicator of soil erosion. van Es et al. (1991) found that the colour development equivalent (a combination of redness and chroma) was the best predicative variable for initial infiltration rates as it was related to the clay and silt contents.

In the field, erosion is often observed as alterations in furrow cross section (Horst et al. 2005). Furrows are typically formed into a V shaped cross-section at the start of the season. A combination of soil erosion and slumping causes the channels to widen and become shallower with a flat bottom (Izadi and Wallender 1985; Kemper et al. 1988; Segeren and Trout 1991). This decreases the dependency of the wetted perimeter on the flow depth and discharge, in some instances overcoming the otherwise strong relationship between inflow rate and infiltration that occurs at non-erosive discharges (Antonio and Alvarez 2003). In contrast, furrows in fields with steeper slopes tend to become deeper and narrower (Trout and Kemper 1983). The alteration in cross section is also affected by the flow regime as surge inflow was found to remove greater amounts of material from the side walls (which is deposited on the furrow bed) compared to continuous inflow (Horst et al. 2007).

2.3.3 Soil Structure and Compaction

The majority of factors influencing the infiltration rate have a direct effect on the soil structure namely the soil porosity. Porosity refers to the ratio between the volumes of solid and fluid components of a soil sample. However, for infiltration the average pore size, distribution of pore sizes and connectivity of pores are of greater importance. The soil pores must be large enough and offer sufficient continuity in order for infiltration to occur. Soil pores are classified by size into macropores (> 0.075 mm), mesopores and micropores (< 0.03 mm) (Singer and Munns 1999). Soil pores may be created or altered through biological activity, shrinkage from temperature or moisture effects, formation of ice lenses, cultivation and collapse or plugging of larger pores (Lal and Shukla 2004). Intuitively, the infiltration should be associated with the pore size distribution. However, Baker (1979) failed to find any direct relationship due to the complex interactions between other soil properties. The bulk density is calculated by dividing the mass of solid material by the volume that it occupies. Hence, it is inversely proportional to the porosity for a fixed particle density. Several attempts have been made to link the bulk density to the saturated hydraulic conductivity or infiltration rates with mixed results. House et al. (2001) found that 58% of the variability in Ln(K_s) was due to differences in bulk density. Jaynes and Hunsaker (1989) found that only 25% of the variation in infiltrated

volumes could be explained by the variance in surface bulk density but they expected that the correlation would increase when considering a greater depth of soil.

Compaction and tillage are the two major cultural practices that affect soil hydraulic properties. Compaction will generally result in increased bulk density while tillage should have the opposite effect providing that it does not destroy the soil structure. Compacted layers may occur naturally but in agricultural soils usually form due to farming practices. Soil compaction may be caused by livestock (Shafique and Skogerboe 1983) or repeated cultivation at the same depth resulting in the formation of plough plans. However, for cultivated fields, the primary source of compaction is machinery wheel traffic. The greatest compaction was found to occur during the first machinery pass of the season or following tillage (Allen and Musick 1992) and subsequent passes did not result in a significant further decrease in infiltration rates. The severity of compaction also increases with increasing soil moisture content (up to the optimum water content) during machinery operations (Allen and Musick 1997).

Some have attempted to link changes in the infiltration rate to the incidence of compaction. For example, Trout and Mackey (1988a) measured a 20% higher infiltration rate in uncompacted furrows in Idaho and more than a 50% reduction in alternate wheeled furrows for two Colorado fields. Focussing on individual infiltration curve parameters, Hunsaker et al. (1999) found that the Kostiakov k parameter (Eq. 2-4) and cumulative infiltration at four hours were 25% lower for wheeled furrows while a also tended to be lower. However, the greatest effect is observed in the value of the steady infiltration rate f_0 (Elliott and Walker 1982), with reported declines in the order of 50% (Trout and Kemper 1983), 70% (Fattah and Upadhyaya 1996) and 75-80% (Li et al. 2001). The large difference suggests that modelling may require one set of input parameters for freshly tilled soil and a second set for compacted soil (House et al. 2001). Wheel-slip associated with machinery traffic acts to further reduce infiltration rates. On a self-mulching Vertisol in the Lockyer Valley, Queensland, increasing the wheel-slip from 3% to 10% had a notable effect (Li et al. 2001), with no further significant reduction in infiltration rates with further increases in wheel-slip. The wheel-slip influence increases as the soil moisture

content approaches the plastic limit, which is significant since cultivation and sowing often occur soon after rainfall.

The recent introduction of controlled traffic farming restricts compaction to the same locations with each pass, thereby resulting in a small number of furrows with high compaction and the remainder with little or no compaction. For surface irrigated fields, the decrease in intake associated with soil compaction causes an increase in water advance rates, ultimately improving the uniformity of applied depths in those furrows but increasing the variance between wheeled and non-wheeled furrows. This complicates irrigation management since the advance rates can differ by as much as 45% (Allen and Musick 1992) between adjacent furrows in the same irrigation.

Furrow smoothing and/or compaction by dragging a torpedo shaped object behind a tractor (Hunsaker et al. 1999) or by using weighted v-shaped wheels (Fornstrom et al. 1985) can be used to decrease infiltration rates, increase advance velocities and improve uniformities. Furrow smoothing can reduce Manning's *n* (surface roughness coefficient) by up to a factor of five but increasing the flow rate tends to overcome any advantage (Hunsaker et al. 1999). Allen and Musick (1992) found that machinery traffic can reduce the intake rates by 17% for the first irrigation after tillage and reduce the cumulative applied depth by an average of 13% with no adverse effects on yield.

Soil tillage will usually result in higher infiltration rates due to the increase in porosity and decrease in bulk density. Often the first irrigation of the season experiences greater infiltration rates and excessive deep drainage due to the loosened soil conditions through tillage and winter frost action (Allen and Musick 1992). The tillage effect is greater for medium and fine textured soils and is influenced by the initial moisture content (van Es et al. 1999). Although soil cultivation acts to reverse the effects of soil compaction, machinery traffic during planting, cultivation or even from previous seasons can influence the variability of intake rates (Trout and Kemper 1983). Ripping of compacted furrows can reduce the bulk density to a value lower than that of the uncompacted soil (Allen and Musick 1992). The practice of minimum

tillage in sugarcane has been found to result in decreased infiltration rates (Raine and Bakker 1996). However, in sugar cane the presence of crop residues on the soil surface may impede surface irrigation advance thereby increasing infiltration.

2.3.4 Soil Moisture Content and Cracking

In an unsaturated soil, the initial infiltration rate is dominated by the matric potential, which is an inverse function of the moisture content. Hence, the soil hydraulic properties are strongly linked to the water content and its distribution within the soil profile. In addition, the moisture content will change both spatially and temporally due to rainfall (Raine et al. 1998), uniformity of previous irrigations, evaporation and plant extraction. However, surface irrigation events tend to reduce the spatial variability of soil moisture contents (e.g. a reduction in the coefficient of variance (CV) of 2 to 3% (Jaynes and Hunsaker 1989)) because the dryer areas of the field tend to have increased intake rates and vice versa.

Soil water content also has a direct impact on the degree of soil cracking which in turn has a large impact on the infiltration function (Mailhol and Gonzalez 1993). Cracking occurs within many clay soils, (e.g. those found in the irrigation areas of Queensland and New South Wales) where the soil shrinks excessively on drying. During irrigation, these cracks serve as pathways through which water can quickly enter the soil. Furrow irrigation is particularly sensitive to cracked soils as the advancing water front may be effectively brought to a standstill while a large crack is filled. Generally, the variability of infiltration rates is greatest during the initial stages of ponding. Therefore, soil cracking appears to be a significant source of variation in applied depths (Bali and Wallender 1987; Bautista and Wallender 1985), particularly under conditions where the surface water is flowing (Izadi and Wallender 1985). However, Hodges et al. (1989) found that increased levels of soil cracking need not affect the level of infiltration variability. Compared to the lighter textured soils, the cracking nature of heavy clay soils and the resultant shape of the infiltration curve may make them more suitable to furrow irrigation (Mitchell and van Genuchten 1993). It is possible to achieve uniform water application with minimal deep percolation since the

majority of infiltration occurs in the initial moments of water ponding and the cracks serve as paths for lateral subsurface re-distribution between furrows.

Despite the obvious influence of moisture content, it is not explicitly represented in empirical infiltration functions such as the Modified Kostiakov equation (Bautista and Wallender 1985). Bakker et al. (2006) replaced the infiltration equation with a single crack-fill term determined by the moisture deficit prior to irrigation. They found this approach worked best for broad furrows but failed with deep V-shaped furrows. Others have accounted for the crack fill by using a linear infiltration function (Eq. 2-8) (Mailhol et al. 1999) or adding the *C* term to the Modified Kostiakov (Walker 2003) (Eq. 2-7).

Since the crack fill volume is strongly related to moisture content, its value can be estimated by multiplying the soil moisture deficit, measured using soil probes or estimated from ET_c values by a constant factor (e.g. 0.75 (Robertson et al. 2004) or 0.67 (Mitchell and van Genuchten 1993)). Enciso-Medina et al. (1998) devised a system of equations to relate crack formation to moisture content and the coefficient of linear expansion. They accounted for the infiltration that occurs through the sidewalls of large cracks by assuming standard crack geometry.

Considering the linear infiltration equation (Eq. 2-8) the magnitude of the cracking term can be inferred from the water advance velocity. A 30% variance in f_0 only results in a 2% difference in the advance time whereas the advance is much more sensitive to variations in the crack term (Mailhol et al. 1999). In addition, the variance of the *C* term is positively correlated with its mean (Mailhol et al. 1999). Hence, a dryer soil will have greater crack volume variability. Where infiltration parameters are calibrated from advance measurements, ignoring soil cracking will cause the estimated infiltration curve to over predict infiltration volume at large times (Bali and Wallender 1987). Where the cracking term is omitted from the infiltration function the influence of the crack volume and hence the initial soil moisture content is reflected in the terms of the infiltration function responsible for initial intake rates (i.e. *a* and *k* from the Kostiakov and Modified Kostiakov and *S* from the Philip equation).

Most soils, regardless of the existence of cracks, tend to exhibit a strong inverse relationship between initial infiltration and moisture content. Experimentation by Robertson et al. (2004) has shown that this dependency follows a strong linear relationship. However, Gish and Starr (1983) could not find any correlation between the initial moisture content and the cumulative infiltration at 15 minutes. Numerical studies using HYDRUS 1D (Furman et al. 2006) found that the Modified Kostiakov k had similar values at saturation over a range of soils and followed an inverse relationship with moisture content that differed between soil types. Unexpectedly, the sensitivity of k to the moisture content was greatest for a sandy loam soil (i.e. non-cracking). Similar work failed to find any significant relationship between f_0 or a and the initial moisture content (Furman et al. 2006; Robertson et al. 2004).

2.3.5 Water Quality and Soil Structural Stability

Water quality has significant impacts on the crop yield (Wallender et al. 1990), however it also has a profound influence over the infiltration rate. The composition of irrigation water, through its effect on soil surface conditions, may be more important than the chemical properties of the soil itself (Oster and Schroer 1979). Some farmers may have the ability to choose between different water sources but the majority rely on a single supply. In addition, the tail-water collected from the end of the field may have significantly altered chemistry, increased temperature and elevated levels of suspended material compared with the initial water supply.

Wastewater is becoming increasingly popular as a source for irrigation due to the tightening competition for limited water supplies. This water may contain suspended solids and dissolved chemicals that can influence crop growth and alter the hydraulic properties of the soil. With wastewater application both loam and clay soils experience a decrease in the infiltration rate that appears to be restricted to clogging of the soil pores in the top layers the profile (Viviani and Iovino 2004). This decline in intake rates increased with sediment loading whilst a clay soil exhibited the greatest sensitivity. However, the infiltration rates were restored by microbial breakdown of the organic material combined with soil expansion and shrinkage, and was accelerated through cultivation (Viviani and Iovino 2004).

Sediment loading also affects infiltration. Trials have shown that clay suspension levels of 5 g L^{-1} caused a 50% reduction in the saturated hydraulic conductivity (Ragusa et al. 1994). However, turbidity levels in irrigation supply water rarely reach this high loading. Sediment-laden water can form a thin surface seal on the wetted perimeter that reduces infiltration (Brown et al. 1988) and creates a tension gradient of 0.5 to 1.0 kPa. This seal is self-enhancing since the resultant tension increases the ability of the surface to hold onto the fine particles. Brown et al (1988) suggested that for the silt loam studied, significant amounts of fine sediment applied to the supply water can reduce the risk of erosion and increase the irrigation uniformity.

Surface seals and crusts are typically thin (1 to 6 mm), relatively impervious layers (Chiang et al. 1993) characterised by high bulk density and low porosity, formed at the soil surface due to soil aggregate breakdown. These layers may impede crop emergence and have significantly lower hydraulic conductivity than the underlying soil and therefore govern the infiltration rate. The severity of a surface seal is influenced by soil texture, chemistry, aggregate stability and organic matter content. Soil aggregate stability is positively related to the moisture content, particularly in the near-surface layer (Trout and Kemper 1983). Surface seals are not easily modelled. The most appropriate technique to include the effect of a surface seal is to divide the soil profile into a number of layers with each having a unique infiltration curve (e.g. the three level Green-Ampt model by Enciso-Medina et al. (1998)).

Aggregate breakdown takes place by slaking and/or dispersion (Young and Young 2002). Slaking is a physical process where water moves into the soil aggregate and displaces and compresses the air contained within. As the compressed air escapes, it exerts a force that may overcome the strength of the soil aggregate. Often the smaller particles will coalesce to form a hard-setting mass on drying. Soil slaking is prevalent under furrow irrigation since the surface soil is initially dry and is then suddenly immersed in water. Furrow pre-wetting with drip tape may reduce the severity of aggregate breakdown and resultant soil erosion (Bjorneberg et al. 2002).

The physical aggregate breakdown of non-slaking soils is caused by external energy inputs including raindrop impact (Glanville and Smith 1988), and surface water flow. Crust formation intensity has been found to be strongly correlated with the raindrop kinematic energy (Lal and Shukla 2004). Heavy rainfall events are common during the summer cropping season in southeast Queensland. Field trials within this region have indicated that significant aggregate breakdown occurs within the initial minutes of rainfall for both covered and bare soil (Glanville and Smith 1988). However, further breakdown was only detected in the unprotected soil. In addition, it was found that the soil slaking in the absence of raindrop impact did not influence infiltration (Glanville and Smith 1988). The reduction in hydraulic conductivity as the result of heavy rainfall occurs rapidly on sandy soils but for loam and clay soils the decline occurs slowly over durations that may exceed 60 minutes (Chiang et al. 1993). Flowing water exerts forces on soil aggregates causing them to break into smaller pieces that roll and bounce along the furrow bed. The resultant particles impact with the furrow perimeter causing further structural breakdown (Kemper et al. 1988).

Soil dispersion is a chemical process governed by the attraction of cations to clay and humus particles. Clay particles will quickly dissociate in water since their surfaces are covered in repelling negative charges. In the soil, positively charges ions are attracted to these particles to help bind them into larger aggregates. Cations like magnesium and calcium have the best ability to flocculate and bind soil colloids while the attractive power of sodium is easily overcome by water. As such, those soils with higher exchangeable sodium percentage (ESP) (as a percentage of total exchangeable cation capacity), termed sodic soils, tend to disperse upon wetting (Young and Young 2002). A similar term, the sodium adsorption ratio (SAR) is used to describe the ratio of the concentration of sodium ions ($[Na^+]$) to the concentrations of calcium ($[Ca^{2+}]$) and magnesium ($[Mg^{2+}]$) ions (mmol L^{-1}) in the soil solution (Brady and Weil 2002).

$$SAR = \frac{[Na^+]}{\left(0.5\left[Ca^{2+}\right] + 0.5[Mg^{2+}]\right)^{\frac{1}{2}}} \quad \text{..... Eq 2-10}$$

Sodic soils are generally described as those with an ESP > 15% (ESP > 6% in Australia (Northcote 1979)) whilst sodic water has a SAR > 13 (Brady and Weil

2002). Sodic soils are prone to structural decline as the clay and humus particles readily dissociate in water in conditions of low salinity (Singer and Munns 1999). The severity of dispersion and flocculation cannot be described by the sodium ratio (SAR) alone, the total salt load must also be considered. The salinity is often measured by and expressed in terms of the electrical conductivity (EC). Ragusa et al. (1994) provided two expressions to predict the critical thresholds for flocculation (Eq. 2-11) and dispersion (Eq. 2-12) in irrigation water:

Flocculation: $EC > 0.1(SAR) + 0.3$ ..... **Eq 2-11**

Dispersion: $EC < 0.056(SAR) + 0.06$ ..... **Eq 2-12**

When the EC is greater than the value given by Eq. 2-11 the hydraulic conductivity will increase by over 15% due to flocculation. Hence, the addition of saline water will result in increased seepage rates. Emdad et al. (2004) found that final infiltration rates declined for successive irrigations early in the season regardless of water quality but the decline only continued (15% lower than the control) in the later part of the season for those soils receiving high SAR and EC water. The quality of the irrigation water did not affect the thickness of the surface seal but it did influence the density of that layer. The additional application of low EC water (i.e. rainfall) to those fields with the poor water treatment is expected to cause further aggregate breakdown and reductions in infiltration (Emdad et al. 2004). Similarly, Oster and Schroer (1979) found that the intermittent application of high SAR water with distilled water resulted in the greatest reduction in infiltration. Hence, fields receiving poor quality water to supplement natural rainfall are at greatest risk of aggregate dispersion and crust formation. In soils with high sodicity, calcium application through addition of gypsum can greatly improve infiltration rates (Dowling et al. 1991). Similarly, the application of $CaCO_3$ as agricultural lime has been shown to increase infiltration rates (Ersahin 2003).

Segeren and Trout (1991) lined the perimeter of a flow furrow infiltrometer to observe the decrease in infiltration rates as the result of sealing under normal field conditions. The surface seal reduced the intake rate and cumulative infiltration at 300 minutes by 57% and 46%, respectively. Ben Hur et al. (1987) found that sealing arising from raindrop impact reduced the infiltration rate from 57.8 to 8.6 mm hr^{-1} on

the comparison of a sprinkler and ring infiltrometer. Surface seals may have no effect on the variability of infiltration rates (Segeren and Trout 1991) while Ben Hur et al. (1987) found that seals reduced the variability of the final intake rate and caused the frequency distribution of measurements to become more positively skewed. Soil cracking tends to reverse the decline in infiltration due to surface soil crusts. For layers less than 6 mm thick, cracking entirely overcomes the reduction in hydraulic conductivity (Fattah and Upadhyaya 1996). On a cracking soil, crusts with thicknesses between 8.7 and 13.5 mm reduced the transient infiltration rates. For thicker crusts (> 13.5 mm) the soil cracks swelled shut on wetting to reduce the intake from 45.3 mm hr^{-1} to 35 and 9.2 mm hr^{-1} for initially dry and wet soil, respectively (Fattah and Upadhyaya 1996).

The application of water will gradually alter the chemical composition of the soil solution. Depending on the irrigation management, the surface layer of soil will tend towards a similar electrical conductivity (EC) (Emdad et al. 2004) and SAR (Oster and Schroer 1979) to that of the water source. Soil changes at greater depths will depend on the leaching rate and plant uptake of both water and solutes. High water infiltration volumes, either from infiltration or rainfall will result in the leaching of mobile ions hence, potentially lowering the EC and SAR (Wichelns and Oster 1990). The opposite will occur in areas of low infiltration where the presence of any dissolved salts in the irrigation water may slowly build up in the soil profile if not leached.

2.3.6 Soil Organisms

The soil is a combination of mineral, liquid, gas and living components. Living soil organisms include micro-organisms (invisible to the naked eye), larger animals living in and on the soil surface and finally the roots of crops and weeds. Most of these organisms influence the soil hydraulic conductivity by influencing aggregate stability, pore sizes and pore connectivity.

The crop is not simply a passive inhabitant of the soil environment. Plants extract nutrients and moisture from the soil at different rates depending on the location in the

profile, spatial distance from the plant line, growth stage and plant species. As the crop matures the root zone extends and increases the soil volume available for extraction, hence altering the matric gradient component of infiltration. The crop can also influence the large-scale variability in hydraulic properties through spatial variations in crop growth from a combination of the non-uniformities in nutrient availability, disease, sowing density, soil type or previous irrigation applications. Plant cover and crop residues left on the soil surface also influence infiltration through protection of the soil from raindrop impact or the restriction of advance hence increasing ponding depths (e.g. for squash, Shafique and Skogerboe 1983). Li et al. (2001) observed a strong linear relationship between the straw residue and steady infiltration which increased by 0.66 mm hr^{-1} for each percent increase in residue cover.

When roots die, they leave behind relatively large interconnected macro-pores that serve as channels for accelerated rates of infiltration. Root channels may be responsible for a large fraction of the variability in late season infiltration rates (Gish and Starr 1983). Similarly, living organisms such as earthworms, ants and termites create pathways as they move through the soil profile. The resulting macro-pores have the greatest effect when the soil is close to saturation as they serve as paths for preferential flow. Laboratory measurements may employ techniques such as refrigeration, electrical currents or chemicals to suppress organic activity (McKenzie and Cresswell 2002). However, in agriculture these organisms are usually encouraged due to the benefits of improved soil structure and increased aeration.

Micro-organisms can cause significant reductions in the hydraulic conductivity through the destruction of soil structure and production of gases and other metabolic products which accumulate in soil pores (McKenzie and Cresswell 2002). Ragusa et al. (1994) discovered an inverse linear relationship between the polysaccharide (an example of a metabolic product) content in the top 5 mm of soil caused by algal and bacterial growth and the hydraulic conductivity of the soil in an irrigation channel. Interestingly the algal growth was not influenced by the addition of phosphorus or nitrate to the soil. Land levelling can decrease the magnitude of bacterial and fungal

biomass in the soil by over 50% (Brye et al. 2006; Brye et al. 2003) since the majority of microbial activity is situated within the top 100 mm of the profile. Microbial activity has been correlated with soil properties (e.g. bulk density and sand content) before and after levelling but the relationships are often difficult to generalise (Brye et al. 2006).

2.3.7 Other Irrigation Water Effects

Water viscosity, also known as the fluid friction, quantifies a liquid's internal resistance to flow and is inversely related to its temperature. Viscosity directly affects the furrow hydraulics by reducing the flow velocity of surface water but more importantly, it determines the flow rate of water through soil pores. Corrections for temperature variations are seldom considered during field measurements even though this effect may be a potential source of error (McKenzie and Cresswell 2002). The measured hydraulic conductivity can be converted to a reference temperature using:

$$K_{rt} = K_t\left(\frac{\eta_t}{\eta_{rt}}\right) \quad \text{..... Eq 2-13}$$

where K_t and K_{rt} are the hydraulic conductivities at the measured and reference temperatures, respectively while η_t and η_{rt} are the dynamic viscosity of water at the same temperatures. Note that the value of K at a water temperature of 35˚C is twice that of a temperature of 7˚C (Iwata et al. 1995).

The temperature of water supplied to the field may change both seasonally and diurnally by as much as 10˚C (Lentz and Bjorneberg 2001). More importantly, the soil, ambient air and sunlight will cause the temperature to vary significantly over the furrow length. For example, Duke (1992) measured temperature increases over the furrow length of 22˚C for unshaded and 2˚C for shaded conditions. A temperature increase of 22˚C reduces the viscosity sufficiently to increase the hydraulic conductivity by 70% (Duke 1992) and may result in an improvement in the distribution uniformity of applied depths. Lentz and Bjorneberg (2001) found that average infiltration increased by 2.3% $^{\circ}C^{-1}$ for furrow measurements but in some cases declined back to the original values after 0.5 to 1.5 hours. Where the infiltration

rate is governed by the properties of the surface layer it may be more sensitive to changes in temperature (Duke 1992).

The majority of infiltration equations (e.g. section 2.2.1) neglect the influence of the ponding depth even though it has a direct impact on the hydraulic gradient at the soil surface. However, on a dry soil the high matric potential caused by negative pore pressures far outweighs any influence as large variations in ponding depths only translate to infiltration changes of a few percent (Strelkoff and Souza 1984). In furrow irrigation, the significance of surface water depths is almost entirely dependent on the importance of the wetted perimeter available for infiltration. Furman et al. (2006) identified relationships between the parameters of the Modified Kostiakov and surface water depths but concluded that the dependencies were soil type dependent. A sandy loam displayed the greatest sensitivity to changes in ponding depth compared to silt or loam soils. Both k and a increased with increasing water level along with a slight decrease in f_0. The nature of the infiltration equation indicates that the ponding depth should principally influence the final infiltration term (f_0) as at higher ponding times the soil intake rate is exclusively determined by the gravity potential.

2.4 Measuring Soil Infiltration

2.4.1 Soil Moisture and Laboratory Measurements

Laboratory measurements of hydraulic conductivity are preferred in many disciplines because of the ability to control all aspects of the environment. Where a researcher is attempting to observe the effect of a single treatment they do not want any other environmental variable to be changing at the same time. However, laboratory measurements conducted on small soil cores are of limited value to field studies of infiltration and irrigation performance, because of their high spatial variability and inability to recreate field conditions. It is difficult to correlate laboratory measurements to field values due to the difference in the scale of measurement. For example Lentz and Bjorneberg (2001) measured steady infiltration rates amongst soil columns of between 0.8 and 20.8 mm hr^{-1} while furrow infiltrometer measurements conducted on the same site varied between 1.3 and 3.2 mm hr^{-1}.

Several techniques are available to estimate the cumulative infiltrated volume after the irrigation event is completed. The most simplistic of these methods is direct volumetric soil sampling where a sample is collected, weighed, oven dried and re-weighed to calculate the mass of water present. The difference in moisture content of pre and post irrigation samples is the cumulative infiltration volume.

Capacitance and neutron probes also provide indirect estimates of the moisture content by measuring its influence on the dielectric constant and quantity of thermalised neutrons, respectively (Allmaras and Kempthorne 2002). Although these tools are designed primarily for irrigation scheduling, provided they are calibrated correctly, they can provide reliable estimates of the changes in soil water content. The measurements can also describe the re-distribution of water that occurs below the soil surface both during and after irrigation. However, since they only provide information on the moisture content they can not measure that portion of the infiltration that percolates below the measurement zone (Shepard et al. 1993). This may be a problem for furrow irrigation where the soil profile may start draining before the end of the event. Childs et al. (1993) found that the mean and variance of infiltration estimated using a neutron probe compared favourably with infiltrometer measurements. However, Purkey and Wallender (1989) found that neutron probes overestimated the mean and standard deviation of intake rates by 30% and 50% respectively, compared to blocked furrow infiltrometer measurements.

2.4.2 Field Infiltrometers

The general term, “infiltrometer” is usually used to describe the single and double ring variants, although it may also refer to the sprinkler and furrow types. Ring infiltrometers (e.g. Figure 2-1) consist of cylinder(s), 250 to 600 mm in diameter, positioned vertically, partially inserted into the soil and filled with water. The soil intake rate is measured directly by observing the rate at which the water level declines with respect to time. Where no further water is added, they are termed “falling head” while “constant head” refers to the situation where the water is automatically or manually added to the ring to maintain the initial water depth. Lateral water re-distribution is a problem for these instruments due to their relatively small size. The

double-ring design (Figure 2-1.b) attempts to eliminate this error by enclosing a smaller measuring ring within a larger outside ring. This ensures that the water lost from the inner ring contributes solely to vertical flow. Despite best efforts to install rings with minimal soil disturbance, it is conceivable that there will be considerable disruption of the normal water flow paths around the circumference. Ring infiltrometers have limited application to furrow irrigation, but they are often used to measure the steady infiltration rate (f_0) for use in simple "infiltration from water advance" techniques (Eldeiry et al. 2005). Ring infiltrometers are often chosen due to simplicity, time and expense considerations. However, they do not provide reliable results for soils with vertic (soils with high clay contents that experience appreciable shrinking and swelling) properties (McKenzie and Cresswell 2002).

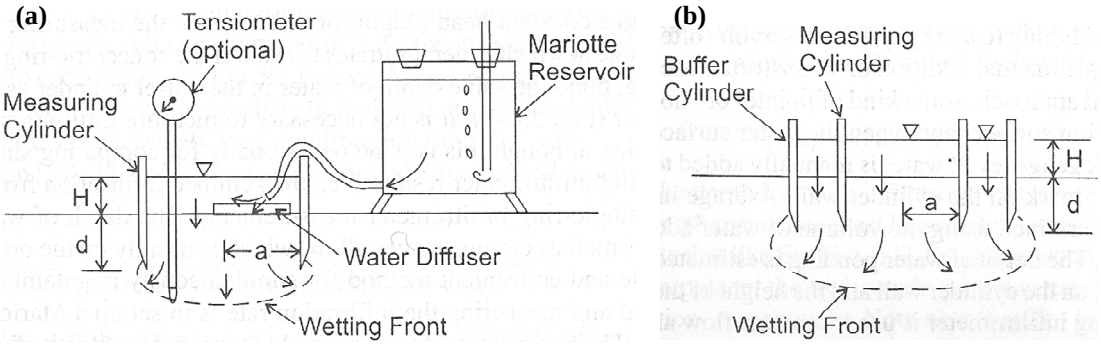

Figure 2-1 Cross section view of the (a) single ring and (b) double ring infiltrometer (Reynolds et al. 2002)

The small size of the ring infiltrometer implies that it is only capable of making point scale measurements. Soil infiltration rates can have considerable spatial variability, even over small distances. A point measurement at one location could yield a totally different estimate to another location spaced only metres away. Consequently, large numbers of measurements are necessary to reliably determine the average hydraulic properties but such measurements are time-consuming and costly. The representative elementary volume principle (McKenzie and Cresswell 2002) defines the minimum number of soil peds (20) that should be sampled within a single measurement to overcome small scale heterogeneity. This poses a problem on many Australian soils such as for Vertosols and Sodosols, where 20 soil peds corresponds to a soil volume of 2.5 m^3 (McKenzie and Cresswell 2002). The variation between infiltration measurements is inversely related to the size of the sample area, therefore ring

infiltrometer tests typically yield higher estimates of the infiltration variability (Bautista and Wallender 1985). Within a basin, infiltration obtained using values from ring infiltrometers were compared with soil moisture measurements and were found to produce lower infiltration rates and underestimate the cumulative infiltration by one third (Jaynes and Hunsaker 1989). In the same trials the infiltrometers yielded predictions of the coefficient of variation that were up to double that indicated by measured soil storage volumes, thereby underestimating the distribution uniformity. Jaynes and Hunsaker (1989) suggested that this effect may be caused by soil disturbance during installation or changes in flow geometry.

The intake family approach (section 2.2.1.7) classifies the intake function on the basis of the final infiltration rate. An alternative, the Time-Rated infiltration families, developed by Merriam and Clemmens (cited in Maheshwari and Kelly 1997), may be more relevant to surface irrigation since it considers the time required to infiltrate a specified depth. The infiltration curves are in the Kostiakov form and the family is selected by the time taken to infiltrate 100 mm. Maheshwari and Kelly (1997) modify the technique by basing the selection of the intake family on the time taken to infiltrate depths of 25, 50, 75 and 100 mm. Their approach performed well in trials across a range of fields with an average error in the required infiltration time of 20%, while 80% of tests had errors of less than 35%.

Usually it is not possible to undertake soil measurements with infiltrometers at the same time as the irrigation event within the same field let alone on the same soil. As soil properties change with time, field trials have observed discrepancies between infiltrometer measurements and those obtained from the irrigation advance phase data. Often the results from the infiltrometers are significantly lower in the initial moments of opportunity time (Oyonarte and Mateos 2002).

Sprinkler infiltrometers, often called rainfall simulators, are generally used to define maximum permissible application rates for sprinkler systems or to determine the runoff and erosion that would occur under a given rainfall intensity. They are not suited to studies of furrow infiltration since they do not consider the soil behaviour

under ponded conditions and can only be used to characterise the uppermost layers of the soil profile (McKenzie and Cresswell 2002). The expense and technical complexity of rainfall simulators has encouraged the use of flood infiltrometers to predict soil hydraulic behaviour under rainfall conditions. However, no significant statistical relationship has been found between these two techniques (Ben-Hur et al. 1987). As measurements obtained from flood infiltrometers cannot be used to predict the values under rainfall, the reverse hypothesis should also hold.

Furrow infiltrometers are more applicable to furrow irrigation since they measure the water intake through the sides and bottom of a typical furrow cross section. Several different variations have been proposed (Bautista and Wallender 1985). Basically they are constructed by portioning off a short length of furrow to which water is applied in either a flowing (flowing furrow infiltrometer) or stagnant (blocked furrow infiltrometer) manner. The former is often preferred since it more closely represents field conditions. Alterations to the standard design have mainly focussed on the technique used to sustain the flowing water. One example of a flowing infiltrometer is the prototype developed by Childs et al. (1993). This device can be inserted into the furrow during the irrigation event since water can pass through the instrument normally when measurements are not being collected. During measurement, both ends of the infiltrometer are blocked and water is gradually applied to maintain similar water depths within and around the instrument. Probably the most accurate technique is the recirculating furrow infiltrometer (Lentz and Bjorneberg 2001), which utilises a greater length of furrow where inflow is applied and runoff is collected and measured in such a way to replicate the normal furrow hydraulics. Infiltration measurement can be improved by measuring the water level in a small storage chamber rather than using flow meters at the inlet and outlet (Walker and Willardson 1983). This design was further improved to recreate the normal furrow sediment loads without breakdown of the soil particles by lifting the water from the downstream end of the measured section using a low speed Archimedes screw (Segeren and Trout 1991) and feeding that water back into the supply.

Holzapfel et al. (1988) found that those techniques considering two dimensional infiltration such as the blocked furrow method yielded values close to that of the flowing furrow infiltrometer. These techniques also consistently yielded infiltration rates that were larger than the single dimension measurements such as ring and basin infiltrometers. Field trials of seven different measurement apparatus (Holzapfel et al. 1988) including both stagnant and flowing techniques resulted in seven different infiltration functions and final intake rates. However, smaller variance existed between those methods under stagnant conditions where the infiltration could be considered one-dimensional. As discussed in section 2.3, soil infiltration is influenced by many factors, some of which are determined by, or require the action of, flowing water. Non-flowing ponded methods cannot take many of these important factors (e.g. the effect of flowing water on the soil and the wetted perimeter determining the area available for infiltration) into account (Walker and Willardson 1983). Tests using stagnant water commonly produce lower estimates of the infiltration rate than those that use flowing water (Holzapfel et al. 1988). They may result in lower (Izadi and Wallender 1985) or higher (Jaynes and Hunsaker 1989) estimates of the variability. The velocity dependence of infiltration rates appears to be influenced by soil cracking as the difference between flowing and stagnant blocked furrow measurements is greatest where significant soil cracking has occurred (Bautista and Wallender 1985). After cracks have been filled the difference in intake rates between flowing and stagnant tests is no longer significant (Izadi and Wallender 1985).

2.4.3 Inverse approach

An alternative to direct measurement is to estimate the infiltration rate from other measurements obtained during the irrigation event. Inverse methods solve for the parameters of one of the infiltration equations by attempting to fit the results from a hydraulic simulation model to measured field data. The volume balance model is the most common choice for the inverse approach due to its simplicity. Chapter 3 introduces some of these inverse techniques whilst chapter 4 describes a new inverse procedure built on existing volume balance techniques.

2.5 Infiltration Variability

For simplicity, field measurement and analysis often considers the soil to be homogeneous. However, the infiltration rate will vary, between all locations in the field and also over time. In addition, any errors in field measurements or violations within the inverse solution techniques will cause further uncertainty in infiltration estimates which contribute to the observed variation.

Traditional approaches to infiltration measurement assume the only source of variability in applied depths under surface irrigation is due to differences in the opportunity time. This suggests that the farmer can improve uniformities by simply increasing advance velocities. However, the random nature of soil cracks, sediment distribution and alteration of pore size often results in greater variance in infiltrated depths than that due to the effect of the opportunity time alone (Amali et al. 1997). In addition, as the volume applied increases the importance of the within furrow variation remains while the influence of opportunity time declines (Wallender 1986). Childs et al. (1993) measured infiltration rates across a cotton field and determined that soil variability caused more variability in infiltrated volumes than variations in intake opportunity time. This is further confirmed by Cavero et al. (2001) who found that simulations based on variable infiltration produced better estimates of the variance and average crop yield than those that considered opportunity time as the only source of variability. Where parameter *a* from the Modified Kostiakov infiltration equation (Eq 2-6) is low the soil will tend to also have a low final infiltration rate. In such situations, a variation in the opportunity time will have minimal impact on the total volume of water infiltrated.

The nature of the influencing factors (section 2.3) suggests that infiltration variability is greatest during the transient infiltration phase and declines as the intake approaches the steady state. Hence, the steady infiltration rate appears to be less spatially and temporally variable than the transient components (Walker and Willardson 1983). However, measurements taken by Hopmans (1989) at 50 locations within a field contradict this general conclusion as the variability in infiltration rates did not change noticeably over an opportunity time of 7 hours. In this case, infiltration rates were

influenced by both the surface soil properties and then later by those of the soil at depth. Others (e.g. Oyonarte et al. 2002) have found that up to 90% of the variation in infiltrated depths can be explained by the final infiltration rate (f_0).

Naturally, the severity of the variation is influenced by the interaction between soil properties and management. Properly designed fields with minimal variation in soil type combined with uniform cultivation history, crop growth and irrigation management would be expected to have reduced infiltration variability. However, under commercial field conditions it is likely that none of the contributing factors are homogeneous. Even a field having uniform cultivation history, machinery compaction, flow rates and initial moisture content demonstrated significant variances (CV ≈ 25%) in water intake (Trout and Kemper 1983).

2.5.1 Spatial Variability

Soil intake rates can vary spatially, obviously between separate paddocks or between different properties but also across a single field. However, significant variation can also be observed at smaller scales, with infiltration rates differing significantly between positions less than one metre apart. Field tests carried out on four soil types (clay loam, fine sand loam and two different silt loams) indicated that 66% of the variability in infiltration between the sites and 100% of the variation expected across the field could be observed within the area of 1 m^2 (van Es et al. 1999).

Spatial variability is an important consideration for many furrow irrigated fields due to their large size and management. Much of the field scale spatial variability is a result of the natural changes in soil type and topography across the field. The practice of land levelling can also significantly alter the spatial variability of infiltration rates (Brye et al. 2006) by exposing underlying soil layers. This may lead to large areas of the field with different soil properties related to the areas of cut and fill. During any given machinery operation, the tractor wheels will only come into contact with a proportion of the furrows. In controlled traffic farming, the same furrows are compacted each time. This produces regular spatial infiltration patterns perpendicular to the furrow orientation with spacing determined by the implement width.

The process of surface irrigation produces a general trend in the cumulative infiltrated volumes due to the natural reduction in opportunity time along the field length. Field measurements of infiltration variability should be careful to separate this predictable and systematic component from the analysis. The distribution of moisture contents immediately following the irrigation event will be directly correlated to the infiltration variability assuming only small differences in opportunity time. However, the processes of root uptake, evaporation and water re-distribution in the days after the irrigation may tend to dampen the initial soil moisture variation. In some instances the patterns in water content may persist between irrigations (Amali et al. 1997). Interestingly, Amali et al. (1997) found that the variability of soil moisture content caused by surface irrigation does not extend below a depth of 0.6 m. Spatial differences in the soil moisture content become more significant under limiting water conditions, especially where the lower part of the field is deficit irrigated (Enciso-Medina et al. 1998).

Where the variability in soil moisture content is caused by soil properties, the spatial patterns would be expected to persist throughout the season. Jaynes and Hunsaker (1989) collected measurements of soil water storage at 44 points within a surface irrigated border. The ranking of the soil moisture content at each location generally remained consistent over the season relative to the field mean. Similarly, the soil moisture storage was well correlated between the pre- and post-irrigation measurements. Although the magnitudes of water storage changed considerably over time, analysis of the variogram indicated that the spatial trends were conserved. Infiltration depths exhibited a similar degree of temporal stability, with 66 to 81% of the variability explained by the previous irrigation (Jaynes and Hunsaker 1989). Similarly, Mailhol and Gonzalez (1993) measured a significant cross correlation between the advance times of irrigations late in the season and concluded that this was caused by the similarity in spatial distribution of soil cracking between irrigations. Van Es et al. (1991) also identified a spatial dependence of infiltration rates present as a autocorrelation in the sorptivity parameter, which was greater for dry soil. Hence, in wet conditions the variability tends to be random while the localised differences in sorptivity become more apparent in a dry soil. Generally, the results suggested the

possibility of greatly reducing the measurements required to evaluate the field variability. The nature of the observed spatial variability is also influenced by the measurement technique as Izadi and Wallender (1985) found that the spatial correlation distance was greater under flowing conditions.

Trends in the spatial variability may also present a problem for infiltration estimation using the inverse techniques. Bautista and Wallender (1993c) simulated irrigation advance using furrows where the infiltration varied along the furrow following (a) low to high , (b) high to low or (c) had a random distribution in infiltration rates along their length. With the exception of the first 100 m of advance there was no effect on the simulated advance trajectories. However, the inverse technique failed to adequately identify the average infiltration under both the increasing with distance and decreasing with distance trends. Hence, spatial dependence in soil properties undermines the ability of the inverse models to predict the infiltration parameters of the Kostiakov and Modified Kostiakov equations (Bautista and Wallender 1993c). This problem is also reflected in the comparison between simulated and measured runoff hydrographs. For the randomly variable infiltration, the simulation based on the averaged optimal Kostiakov parameters provided an adequate prediction of the shape, peak value and arrival time of the runoff hydrograph. Where the measured inflow rates exhibited rising or declining trends the same simulations still predicted the final advance time but failed to predict the shape and volume of the runoff hydrograph compared to the variable infiltration simulations. Bautista and Wallender (1993c), postulated that these issues would become more significant in instances of higher variability.

2.5.2 Seasonal Variability

The infiltration characteristic will experience substantial variation over time through soil structure degradation, crop growth, climate or farming practices. In many instances, this temporal change in soil hydraulic properties may be more important than the spatial variability. Field trials within a commercial sugar cane crop have shown that temporal variation is greater than the underlying spatial variation due to soil properties (Raine et al. 1998). Measurements collected in commercial fields have

identified temporal variations in cumulative infiltration of 1.3 to 2.4 ML ha^{-1} at an opportunity time of 500 minutes on a high infiltration Dermosol (Raine et al. 1997) and 0.2 to 2 ML ha^{-1} at 2000 minutes for a low infiltration Sodosol (Raine et al. 1998). Similarly, van Es et al. (1999) found that the spatial variation between different sites was soil texture dependent but was generally overshadowed by within season temporal variations caused by management differences. Hence, as the infiltration rate has been known to vary by a factor of four over the season (Elliott et al. 1983) it is essential that the design and management process can account for temporal variation.

Often the performance of the first irrigation of the season is somewhat unpredictable due to high and widely variant infiltration rates (Childs et al. 1993; Izadi et al. 1991). Generally, the infiltration rate is significantly higher for the first irrigation and declines over the season. In most instances, the infiltration rate declines significantly between the first and second irrigations as a result of the soil changes arising from cultivation during field preparation and planting (Childs et al. 1993). As the soil surface conditions tend to stabilise after several irrigation events, the infiltration variations are generally smaller in the second half of the season and do not necessarily follow the same decline (Elliott et al. 1983). Infiltration rates have been found to change significantly between irrigation events. However, for annual crops the soil behavioural change between successive years is minimal due to similar cultivation practices with each season (Shafique and Skogerboe 1983). The situation is different for perennial crops such as fruit trees where changes in infiltration behaviour are observed between irrigations, but a general decline may also be apparent between seasons.

The decline in infiltration rates over the season due to factors such as compaction (Li et al. 2001) are commonly correlated to a decrease in the final infiltration rate parameter f_0. Observations of trends in the other parameters of the Modified Kostiakov equation are weak and conflicting. Horst et al. (2005) measured a slight increase in k and a decrease in a, while Hunsaker et al. (1999) found that k increased by 33% with no trend for a. Similarly, Shafique and Skogerboe (1983) did not find any significant trend in the value of a with the majority of the general decline in infiltration rates caused by a decrease in the parameter k.

Many of the factors influencing soil intake rates have a significant effect when first applied but a smaller effect with subsequent applications. For example, soil compaction from a first tractor pass will have a large effect on infiltration while additional passes will have a diminished effect since the soil is already compacted. The first irrigation following cultivation will often induce erosion rates greater than subsequent irrigations. Soil cultivation is responsible for a large amount of temporal variation in the infiltration rate but its effect appears to be dampened out over time (Gish and Starr 1983). Other causes of temporal variability such as the application of high SAR water (Emdad et al. 2004) and changes in initial moisture content with summer rainfall (Raine et al. 1998) can generate more complex trends in the infiltration rate.

As the crop matures, the increasing root zone depth and shading effect will cause temporal changes in the soil hydraulic properties. As a result, Gish and Starr (1983) set out to scale infiltration based on the process of plant growth. However, due to the low levels of correlation they conclude that these trends are small compared with the inherent spatial variability in soil properties.

Childs et al. (1993) found that the infiltration rates measured at a fixed location were well correlated between successive irrigations late in the season, the strength of which increased with time. However, the same analysis resulted in poor correlation values early in the season, particularly between the pre-plant and first in-season irrigation. This suggests that the temporal variability may be more important early in the season but that spatial trends become more prominent over time. More importantly, excluding the early season irrigations, this supports the practice of predicting future infiltration rates based on measurements of the previous irrigation event. Realising that the greatest change in infiltration occurs during the initial irrigation Walker et al. (2006) proposed an irrigation condition factor (*ICF*) to predict the parameters of the Modified Kostiakov equation from measurements of the initial (or following cultivation) irrigation of the season. All three fitted equation parameters are scaled by a value of $ICF = 0.8$ for continuous flow.

2.6 Effect of Infiltration Variability on Irrigation Performance

Infiltration variability is an issue for the identification of infiltration rates but more importantly, it has a significant detrimental impact on the performance of surface irrigation.

2.6.1 Consequence of Assuming Spatially Average Infiltration

Ignoring the effects of infiltration variability will generally provide false and usually optimistic perceptions of the irrigation performance. Comparisons between spatially averaged and variable simulation models have produced mixed messages of the impact on performance estimates. Fonteh and Podmore (1994a) found that a spatially averaged model under predicted application and requirement efficiency by greater than 10% while at the same time over predicted the distribution uniformity (DU). However, Fonteh and Podmore (1994b) conclude that spatial averaging of infiltration rates does not greatly compromise estimates of the application and requirement efficiencies but overestimates the uniformity and underestimates the volume of deep drainage. Bali and Wallender (1987) also found that the predicted uniformity was lower when considering variable conditions but that the difference decreased rapidly as the average infiltrated volume increased. Further comparisons have indicated that the effects of variable soil intake are most apparent in the upper reaches of the furrow, most likely emphasised by the increase in wetted perimeter (Schwankl et al. 2000). It is likely that variability at the downstream end is more sensitive to variations in opportunity time caused by variations in the inflow rate.

Where a significant proportion of the inflow volume is accounted for by the runoff, the spatial averaging of infiltration does not greatly affect the predictions of performance values such as the application efficiency (AE) and deep percolation ratio. However, the DU is overestimated. For three irrigations, the DU was estimated as being approximately 95-98% when simulating with constant infiltration but when infiltration variability was considered the uniformity was found to be 73% (Mateos

and Oyonarte 2005). Similarly, accounting for the within furrow variation of the final infiltration rate resulted in accurate estimates for the distribution of applied depths whereas the use of a spatially uniform infiltration model over predicted the uniformity by up to 40% (Oyonarte and Mateos 2002).

2.6.2 Using a Single Furrow to Estimate the Irrigation Performance

Regardless of the actual source of in-field variability, the use of a single furrow to estimate field performance is fraught with danger. The furrow selected for evaluation may not exhibit soil properties representative of the field, and therefore may provide inappropriate values when compared to the spatial average. An infiltration curve derived using a single furrow is wrongly termed the spatial average when in reality it only reflects the soil intake in that furrow. Ignoring the effects of lateral infiltration variability between furrows can result in underestimates of the water losses by as much as 80% for deep percolation and 90% for runoff (Popova and Kuncheva 1996). Depending on the furrow selected for consideration within a single irrigation event, the estimates of average infiltrated depth, coefficient of uniformity and DU have been found to vary by 31, 17 and 35%, respectively (Schwankl et al. 2000).

2.6.3 Variability and Performance

Spatial and/or temporal variability will affect the selection of inflow rates and cut-off times required to optimise irrigation performance. Greater volumes of water are generally required to achieve the same requirement efficiency (RE) for a heterogeneous than a homogeneous soil (Bautista and Wallender 1993b; Raghuwanshi and Wallender 1997). However, at higher levels of adequacy (the percentage of the field having its deficit fully satisfied) there is minimal difference between the optimised inflow rates and times (Raghuwanshi and Wallender 1997). Even considering only furrow to furrow infiltration variability and within furrow opportunity time variations, the farmer must over irrigate by 30% to refill the root zone across 80% of the field (Trout 1990). Wallender (1986) found that an average infiltrated depth of 0.15 m^3 m^{-1} was required to replenish the root zone using spatially

averaged characteristics along the furrow length whereas 0.17 m^3 m^{-1} must be applied when variable soil conditions were considered. The required increase in application volume ultimately results in increased volumes of runoff and deep percolation. In addition, for a given level of RE, the maximum achievable AE was reduced under heterogeneous conditions. This decline in performance is more noticeable when attempting to reach higher requirement efficiencies (Bautista and Wallender 1993b).

One of the major issues for furrow irrigation is the variation of opportunity times at the downstream end of the field. If within furrow variability is ignored, a furrow with lower infiltration will have increased advance rates therefore increasing the opportunity time at the downstream end and increasing the DU along the furrow length. The opposite situation occurs in furrows with high infiltration rates where the advance may be sufficiently slowed to prevent water from reaching the end of the field. On the completion of an irrigation event, the water is typically distributed in a decreasing fashion, from head ditch to tail drain. The inverse relationship between infiltration and moisture content introduces the reverse trend into the spatial distribution of infiltration rates (increasing over the furrow length). During the following irrigation the infiltrated depths at the downstream end will be increased due to a combination of increased infiltration rates and increased opportunity times caused by higher advance velocities at the upstream end. Hence, the interaction between infiltration rates and advance velocities will reduce the cumulative infiltration variation at the lower end of the field (Trout 1990). However, this will have no influence on the variability of infiltrated depths at the supply end.

Simulation models using homogeneous soil information suggest that it is possible to achieve almost perfectly uniform applied depths across the field. In reality, the spatial infiltration variability places an upper limit on the achievable coefficient of uniformity of approximately 85%, even under the maximum permissible inflow rates (Wallender and Rayej 1987). In addition, the uniformity becomes more sensitive to changes in inflow rate and irrigation time under variable infiltration conditions.

The existence of spatial trends acts to further decrease the reliability of predicted irrigation performance, although they may not have much effect on the total volume applied to the field. Where infiltration rates continuously increase over the length of the furrow the uniformity of applied depths will be greater than the randomly variable case, while the opposite is true where infiltration rates decrease over the field length (Bautista and Wallender 1993c).

2.6.4 Impact of Infiltration Variability on Crop Yields and Productivity

Throughout this dissertation, the term irrigation performance primarily refers to volumetric efficiency and uniformity of the water applied to the root zone. However, the ultimate purpose of irrigation is not to supply water to the soil but to supply water to a growing crop. Therefore, the irrigation performance should also consider the crop yield and profitability rather than simply considering the water distribution. Although crop yield is greatly influenced by the water availability, it is also linked to other factors that also tend to vary over space and time. Crop yield is determined by the interactions between the soil fertility, weather conditions, soil moisture, pest and disease pressures and time. An effective crop growth model that takes these factors into account is a useful tool for management but one that can take into account the effects of water availability on plant stress combined with the spatial irrigation application is particularly valuable (Cavero et al. 2001).

In many cases, the link between applied depths of irrigation water and crop yields will be obvious, particularly for deficit irrigation strategies on some crops (e.g. sugar cane). In other circumstances, where water is not limited or where the crop yield is maximised in stressed conditions (e.g. cotton), the link may not be apparent. Wichelns and Oster (1990) measured a significant correlation between pre-irrigation depths and crop yield but failed to find any link with the season total applied water depths. They found that crop yields were generally highest where soil moisture contents were maintained between field capacity and the refill point. Reductions in yield caused by plant stress may occur both in water limited and waterlogged conditions. This adds extra complexity to the relationships between water applied and yield that can be

overcome by combined crop growth and soil-water balance models. For example, Cavero et al. (2001) evaluated the B2D basin irrigation simulation model with variable infiltration combined with the EPICphase crop model. When considering the water application as the only source of variability they found that they could explain between 50 and 70% of the spatial variation in maize yield.

A surface irrigation volume balance model was used to study the effects of spatially homogeneous and heterogeneous soil conditions on the relationships between drainage costs, water costs and yield of a cotton crop (Wallender et al. 1990). As expected, predicted yields and profits were greater on uniform soils. Under variable conditions, the yield is more sensitive to the drainage cost than the water cost whereas for homogeneous conditions the yield is equally sensitive to drainage and water costs. Similarly, the influence of drainage costs on the profit increases relative to the water cost for the non-uniform soil. The optimised flow rate and time to cut off is also influenced by variable soil conditions. For non-uniform soil, the inflow rate must increase and irrigation time decrease to reduce risks of excessive deep drainage in those areas with increased infiltration rates. Similarly, simulations of the SOFIP model indicate that to maintain crop yields under highly variable conditions increased volumes of water need to be applied (Mailhol et al. 2005). A separate study by Wallender and Rayej (1987) found that for variable infiltration rates the maximum yield occurs at the highest non-erosive flow. In these situations, the yield is higher due to increased infiltration. However, as the opportunity time increases yield declines in those areas of the field affected by waterlogged conditions. Profit does not behave in the same manner, as higher flow rates result in increased runoff costs (i.e. costs associated with tailwater recycling) which may outweigh the benefits associated with high uniformities. The financial penalty caused by optimisation based on limited infiltration information has been found to be greatest under low inflow rates (Ito et al. 1999). The benefits associated with higher inflow rates were greater than the additional water related costs.

Raghuwanshi and Wallender (1996) constructed a seasonal irrigation model combining irrigation scheduling, furrow hydraulics and yield sub-models with

temporal and spatial variation in inputs. The optimised irrigation designs did not differ greatly between homogeneous and heterogeneous water balance, soil and root zone depth. However, assuming heterogeneous conditions did have a significant influence on the predicted crop yield and expected return for water (Raghuwanshi and Wallender 1997). Further tests with the four combinations of spatially and temporally constant and variable infiltration conditions indicated that variability did not have a significant influence on the crop yield since the average ET was relatively insensitive to the variability.

2.7 Estimating Infiltration Rates while Accounting for Infiltration Variability

2.7.1 Relating Infiltration to Other Parameters

Acknowledging that infiltration is determined by various soil parameters, a number of attempts have been made to predict intake rates from more readily available field data. Many of the factors influencing of soil infiltration rates (section 2.3) can be quantified and used to estimate the spatial pattern of infiltration rates. For example, Naney et al. (1983) described a technique to estimate the distribution of soil hydraulic properties over a large area using limited measurements of the hydraulic properties and other soil physical measurements taken elsewhere in the field. They successfully correlated the saturated hydraulic conductivity with measurements of macro-porosity, clay content and bulk density and demonstrated that similar information could be obtained with fewer measurements. In most cases however, it is excessively difficult and time consuming to measure sufficient soil characteristics to adequately define these relationships.

The infiltration rate and infiltrated volumes may be strongly linked to the volumetric moisture content of the soil after irrigation. The apparent electrical conductivity (EC), measured by electromagnetic conductivity meters such as the EM-38, has been traditionally used to quantify soil salinity but these instruments are also responsive to changes in the soil moisture. The EM-38 measurements increase linearly with water content but the slope of the regression line increases as the salinity increases (Hanson

and Kaita 1997). This is a problem for salinity measurement but highlights the ability to estimate soil moisture status. On a clay soil, Sudduth et al. (2001) found that the EC reading (apparent EC given by the EM-38) increased by 1.1 mS m^{-1} for every percent increase in soil moisture. However, the relationship is site specific. Hedley et al. (2004) attempted to use electromagnetic (EM) sensing combined with GPS technology to differentiate between different zones contained on a soil map and also to predict various soil physical and chemical properties. The EC was correlated with a number of different properties but importantly it was able to explain 72% of the variation in clay content, 42% of the variation in moisture content and possibly also predicted areas of compaction.

EM surveys have the major advantage of being able to quickly infer soil properties at depth without actually disturbing the profile. The electric conductivity of the soil is influenced by salinity, clay content, cation exchange capacity, clay mineralogy, pore size distribution, moisture content and temperature (Sudduth et al. 2001). Before using an EM survey to describe one or more of these characteristics, it is crucial that efforts are made to identify the magnitudes and distribution of the other parameters within the study area. Considerations must be given to the ambient air temperature, the field should be sampled quickly, and future measurements taken at the same site should be collected at a similar time of the day (Sudduth et al. 2001).

2.7.2 Estimating Infiltration Variability through Statistical Analysis

The variability in a population can only be accurately quantified when the whole population has been measured. Hence, it is impractical, if even possible, to measure the full extent of infiltration variability. However, there are statistical techniques that can be applied to reduce the quantity of field measurements needed to adequately assess the variability in soil properties. The same concept applies to the measurement of limited furrows within a surface irrigated field. However, it is conceivable that analysis based on measurements from a limited number of furrows may underestimate the total extent of field scale variability (Mailhol et al. 1999).

2.7.2.1 Spatial Dependence

Standard statistical methods generally require that the quantity of interest is independent in both a spatial and temporal sense. In reality, the infiltration rate is not entirely random over space (particularly over small distances) and time. The validity of the random assumption is also influenced by the spatial scale and sampling size of the measurement technique itself. Geostatistical analysis encompasses the tools and procedures used to identify and separate this spatial dependence from the pure random oscillation. The parameters are not necessarily fully dependent but are instead semi-related at different spatial scales. In regards to field sampling, geostatistical techniques may be used to determine the optimal spacing of samples in order to provide the best description of the population with a minimum of measurements.

Autocorrelation describes the linear relationship between values of the same random variable spaced a constant distance apart (Upton and Cook 2002). Autocorrelation is generally used to find repeated patterns within a time series but when applied to spatial data it becomes a tool to determine the minimum measurement spacing to gain the maximum information from a limited number of soil measurements (Bautista and Wallender 1985). The autocorrelation coefficient (*ACF*) is found by dividing the autocovariance (average cross product) of a continuous variable, X_i at a given lag *h*, by the variance (square of the standard deviation, σ^2):

$$ACF = \frac{E\left[\left(X_i - \mu\right)\left(X_{i+h} - \mu\right)\right]}{\sigma^2} \quad \text{..... Eq 2-14}$$

where μ is the mean of all X_i (Haining 2003). In the case of spatial variability, that lag term (*h*) would be distance. The correlogram is constructed by plotting the *ACF* against increasing values of the lag. A positive value of *ACF* indicates positive spatial correlation whilst a negative value corresponds to negative correlation between measurements spaced at a given distance (lag). Generally the *ACF* is positive between closely spaced points and declines asymptotically with distance (Gupta et al. 1994) as measurements move away from each other, they become more independent. Two measurements are considered dependent where the autocorrelation coefficient is larger in magnitude than the bounds calculated for a specified significance level.

Gupta et al. (1994) found that the hydraulic conductivity had a higher magnitude of variation (CV of 80%) and lower degree of correlation than the infiltration rate (CV of 39%). They then used a model with a deterministic and stochastic component to describe the spatial variability between measurements spaced 5 m apart but found that the deterministic component only accounted for 12 to 22% of the variation.

Another technique to study spatial dependence between neighbouring measurements is the semi-variogram (commonly shortened to variogram) (Vieira et al. 1981), which describes the similarity between measurements at locations separated by a given distance. It is constructed by plotting half the average square difference, the semi-variance function ($\gamma(h)$) :

$$\gamma(h) = \frac{1}{2N(h)} \sum_{i=1}^{N(h)} \left[X_{i+h} - X_i \right]^2 \quad \text{..... Eq 2-15}$$

against the lag (h), where $N(h)$ is the total number of pairs at lag h (Vieira et al. 1981). Similarly, a plot of the autocovariance against the lag is termed the covariogram (Upton and Cook 2002). Variograms should be used with care where nestled structures appear at different spatial scales, such as that observed by Sharma et al. (1983). The $\gamma(h)$ function can be standardised by dividing by the average (of X) to form the coefficient of semi-variation. This standardised term enables the direct comparison of different quantities. For example, Sakai et al. (1992) used the coefficient of semi-variation to simplify the spatial trend of infiltration to the spatial dependence of f_0 from the Horton equation.

2.7.2.2 Kriging

Kriging is a regression technique that provides information at a smaller scale than the measured data, providing that the sample grid is fine enough to establish the pattern of spatial variation. Hence, kriging has been used to describe spatial variance of infiltration along the length of a furrow from widely spaced field measurements (Fonteh and Podmore 1994b). The kriging process can only be performed if the variogram does not exhibit a nugget effect, i.e. it requires that the variogram approaches zero as the separation distance declines to zero (Vieira et al. 1981). Also, the technique should not be applied where complexities can be seen within the

variograms (Sharma et al. 1983). Where these requirements are not met, the sampling must be repeated on a finer grid. Vieira et al. (1981) found that kriging could predict 1280 field measurements of infiltration with an correlation coefficient of 0.8 using just 128 measured points. Kriging of the same field using 256 measured samples improved the correlation coefficient to 0.95.

Cokriging extends this process by combining the spatial autocorrelation with the spatial relationship of another auxiliary variable such as bulk density, texture or water content (Ersahin 2003). Ersahin (2003) found that cokriging of infiltration based on bulk density offered no advantage over kriging alone where sufficient data was available. However, cokriging outperformed kriging where reduced numbers of measured points were available.

2.7.2.3 Scaling

Scaling is the collective term used to describe a range of techniques that reduce the measurements necessary to describe the properties of a variable soil. In this case it refers to the technique of assessing soil hydraulic properties using detailed measurements obtained at one point in the field combined with limited data collected from other locations (Ahuja and Williams 1991). It offers the advantage of being able to describe the spatial variability of infiltration using a single term, the scaling factor. Scaling is best suited to those processes that are modelled using physically based parameters which can be obtained with field measurements (Mailhol et al. 1999). For example, Gish and Star (1983) attempted to scale the two parameters of the Philip equation but lack of agreement between the two factors led them towards the use of a single scaling coefficient for the cumulative furrow intake. Hopmans (1989) made the same conclusion when considering the Modified Kostiakov infiltration function. Rasoulzadeh and Sepaskhah (2003) formulated an expression to scale the infiltration function based on the characteristic furrow width and the difference between initial and saturated moisture contents. Their approach enables the intake functions for a wide range of soils to be scaled to a single infiltration curve. The result is a scaled form of the Modified Kostiakov equation where k and f_0 are functions of the furrow width.

Scaling can be also used to describe the adjustment of the infiltration function in the time dimension. One such example uses the results from short duration tests combined with other data from long-term tests to predict the infiltration rate at greater times (Childs et al. 1993).

2.7.3 Real-Time Estimation of Infiltration Parameters

Considering temporal variation, maximum irrigation performance is only likely to be achieved using real-time system control. To implement this approach for surface irrigation, the system must be able to measure or at the least estimate the soil properties in real-time. Real-time estimation is desirable since infiltration parameters change both with space and over time (Bautista and Wallender 1993c). However, the field measurement and data processing procedures usually prolong the feedback process. Many of the available numerical tools, particularly those based on the advance phase, can already cope with the real-time procedures as the parameter estimation is completed within a matter of seconds. The major impediment to real-time control is the capture and compilation of field measurements. It is likely that the necessary simplifications to enable real-time processing of field measurements will require new or adapted procedures to identify infiltration rates.

2.7.4 Cost of Sampling

Effective measurement of infiltration in heterogeneous conditions requires the development of new field sampling techniques and/or new types of equipment (e.g. to measure within furrow variation). However, the existing tools could be better utilised in order to characterise some aspects of field variation. One major issue is the large quantity of measurements required to adequately describe the variation of the soil properties. The collection of such quantities of data is often impractical and cost prohibitive. Also, since soil parameters change over time, the field data must be collected quickly to avoid the temporal effects. Consideration must also be given to the influence of sampling on the viability of the agricultural production system as the apparatus or testing procedures may hinder machinery access or the plant development. Any practical attempt to quantify variable soil hydraulic properties must be able to function using minimal field measurements. The push to achieve maximum

benefit from minimal field measurement has led to the development of a number of techniques such as the method used to calibrate the Phillip infiltration equation by Shepard et al. (1993) using a single advance point and a similar approach by Khatri and Smith (2006) for the Modified Kostiakov equation.

Ito et al. (2005) combined an economic model with the hydraulic simulation to determine the optimal measurement step size to maximise profit. Under the assumed unit costs they found that sampling costs are prohibitive for small fields (≤ 400 furrows or 9.1 ha). Optimal sample sizes ranged from three furrows for fields with less than 500 furrows up to ten furrows for fields with more than 700 furrows (15.9 ha) and 1800 furrows (41 ha) for the two cost functions considered (Ito et al. 2005). In the calculation of the sampling costs, it was assumed that one technician is required for every three sampled furrows at a cost of $100 per day with an additional $150 independent of the sample size. Clearly, these costs will be reduced considerably with the adoption of automated measurement and processing equipment.

2.7.5 Accuracy versus Sample Number

It is important to optimise the sampling size to achieve the required soil information while minimising costs. Increasing the number of sampled furrows will always increase the accuracy of variability estimates but the incremental improvement declines as the number of measurements increase. Statistical tests performed with field data have found that the average predicted infiltration variance decreases dramatically when the number of measured furrows increases from one to three (where each furrow contained ten blocked furrow infiltrometers spaced 30 m apart). However, further increases in sample size have a diminished effect on the accuracy (Tarboton and Wallender 1989). The sample number necessary is determined by the required accuracy of the infiltration information.

2.8 Irrigation Strategies to Reduce Infiltration Variability and/or Improve Performance

It is possible to improve the uniformity of applied depths through physical alteration of key soil properties (section 2.3). One notable example is the use of compaction to reduce infiltration and increase advance rates. This section introduces a number of other irrigation practices that can be used to decrease the influence of infiltration variability and improve irrigation performance.

2.8.1 Surge Irrigation

In traditional furrow irrigation the inflow rate remains constant throughout the entire event or at least throughout the duration of the advance phase. Surge irrigation is a technique where the inflow is pulsed on and off, usually in regular time increments that are significantly shorter than the advance time (Figure 2-2.a).

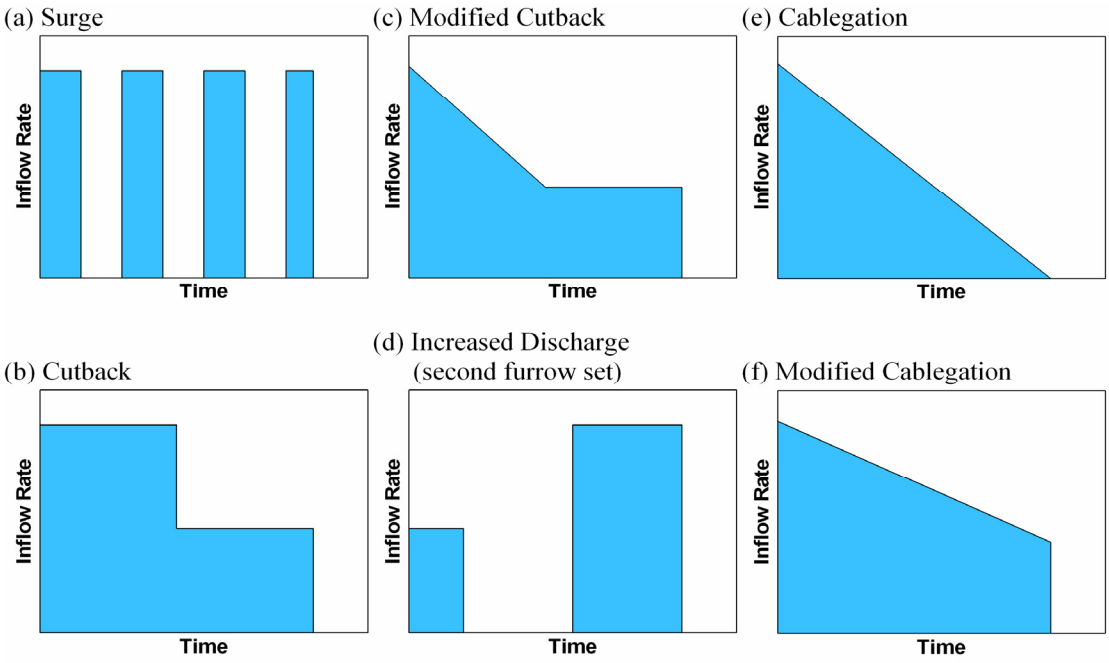

Figure 2-2 Sample inflow hydrographs for alternative inflow regimes
These figures have been created from information contained within Alazba (1999) and Vazquez-Fernandez et al. (2005)

Surge irrigation was originally devised as a method to cutback inflow volumes during later stages of the irrigation because of the difficulty of automatically reducing flow rates. Now the technique is more commonly used to accelerate the advance phase

while reducing the volume of applied water (Walker and Skogerboe 1987) and increasing the uniformities of applied depths (Purkey and Wallender 1989). The ability of surge irrigation to alter soil surface characteristics offers the possibility of increasing the uniformity of application rates. Surge irrigation does not necessarily reduce the variability of infiltration rates. The benefits of the technique are derived from the ability to reduce intake rates. The primary mechanisms responsible for this decline are consolidation of the soil surface, filling of cracks with water and/or sediment load, surface sealing during the recession of each inflow cycle and accelerated disintegration of soil aggregates as the result of rapid wetting (Kemper et al. 1988). Decreased infiltration rates translate to faster water advance rates so that the advance phase can be completed more quickly with far less water. Hence, the surging technique reduces the absolute difference in opportunity times between the two ends of the field. Surge irrigation acts to reduce the differences in the opportunity time which is one of the great limitations of surface irrigation.

Trials conducted on both a loam (fine-silty Aridisol) and a Willard loam (fine Entisol) comparing surge with conventional inflow under the same field conditions (El-Dine and Hosny 2000) found that surge irrigation improved the distribution uniformity (DU) of applied depths from 82% and 77%, to 90% and 91%, respectively. When flow rates remained constant, surge irrigation increased the application efficiency (AE) and saved almost 40% of total water use, time and energy costs. On a Yolo clay loam soil, the infiltration rate was found to decline by 42% between the first and second surges and by 17%, 10% and 8% between the subsequent surges (Purkey and Wallender 1989). Surging with constant inflow rates also caused a reduction in intake rates of 20 to 30% on a silt loam soil (Trout and Kemper 1983). Hence, the greatest change in soil behaviour occurs after the first surge but the reduction in intake rates appears to continue with the following surges.

Simulation of the surging phenomenon is difficult since the change in infiltration cannot be easily explained by mathematical equations. Prediction of infiltration parameters under surge conditions is more difficult than under conventional inflow due to the wetting and drying cycles (Fekersillassie and Eisenhauer 2000). Trout and

Kemper (1983) proposed a step infiltration function to represent soil behaviour under surge irrigation where intake rates are adjusted after each surge. Other furrow irrigation models require the user to calibrate different infiltration functions for the first and following surges (e.g. SIRMOD (Walker 2003)).

The effectiveness of surge irrigation is largely dependent on the soil texture and stability. Unstable clay soils experience rapid declines in intake rates under traditional inflow regimes and therefore surging has limited benefit (Walker and Skogerboe 1987). Measurement of the distribution of applied depths in a fine textured soil did not identify any benefits of surge irrigation as it was unable to overcome the variability of infiltration rates (Amali et al. 1997). Sandy loam soils are best suited to the technique because of the large reduction in infiltration rates during the recession after each surge. Such reduction would otherwise require long periods of time under continuous flow (Walker and Skogerboe 1987). The most noticeable change in infiltration occurs during the first irrigation in spring where the soil has low stability (Kemper et al. 1988). However, surge irrigation has a diminished effect where the soil has been compacted. Field trials have shown that surge irrigation can reduce the inflow required to complete the advance phase by 40% (Horst et al. 2007) for the first irrigation of the season but later in the season no advantages were evident since the furrow surface was already smooth. Horst et al. (2007) found that surge irrigation decreased the value of f_0 by half while the parameter a was double that of the continuous flow.

Many soils within the surface irrigated areas of Australia are cracking clays and therefore surge inflow techniques might be expected to offer little benefit. Field evaluations on two Australian soils having different clay contents (25% and 74 to 82%) could not identify the benefits of the surging techniques because any changes in the infiltration rate were smaller than the spatial variability in soil properties (Smith et al. 1992). On black clay soil, the surging technique appeared to cause an initial increase in the intake rate followed by the expected slight decrease later in the opportunity time. Even though surge irrigation did not cause significant changes in the infiltration function, the technique still improved the irrigation performance on the

soils studied. Similarly, field evaluations of border irrigated pasture located on cracking clay soil found that surging reduced the steady infiltration rate from 1.5 to 1 mm hr^{-1}. This reduction combined with a reduction in opportunity time resulted in a substantial decrease in the average infiltration (Turral et al. 1992).

2.8.2 Cutback Irrigation

Increasing inflow rates is a simple way to accelerate the advance phase and therefore improve the uniformity of opportunity times and applied depths. However, higher inflows may result in excessive runoff losses from the end of the field, particularly where the irrigation time far exceeds the advance time. One method to reduce these losses is to commence the irrigation with a high inflow rate that ensures rapid advance but then reduce the inflow when the water has reached the end of the field. In this case, inflow rates are typically "cutback", often by as much as half, at a time approximately equal to or immediately after completion of the advance phase. A 50% reduction in discharge is often selected due to ease of implementation. For example, in Spain the common practice uses a flexible pipe to supply water to each furrow through two holes, one of which is blocked at the completion of the advance time (Mateos and Oyonarte 2005). Care is required to ensure that the reduced inflow rate is sufficient to prevent tail-end recession.

Izadi et al. (1991) proposed a furrow set cutback regime that reduces the flow rate when the advance of the slowest advancing furrow reaches the end of the field. In this case, inflow is stopped when the requirement efficiency (RE) reaches 100% for all furrows. Both the cutback and a comparable surge system increased the AE with a reduction in water use by 5% and 7%, respectively. The cutback inflow regime was preferred over the other two techniques since it returned high performance over a wide range of inflow rates. However, the genuine benefits may be greater since the maximum inflow rate was limited by the recommended erosion limits and the simulation model used in the evaluation could not account for the reduction in wetted perimeter during the cutback phase. Although cutback and modified cutback regimes offer higher performance than a constant inflow they are more sensitive to field parameters (Alazba 1999).

An alternative approach to cutback involves the use of a high constant inflow during the advance phase followed by a continuous slow reduction in the inflow rates during the cutback phase. The time pattern of this reduction may be determined by the average soil intake in the furrow in each time step (Lal and Pandya 1970). For simplicity, the calculations may only consider infiltration rates at either end of the furrow and assume a linear trend. Modified cutback irrigation (Alazba 1999) is another variant where the inflow is slowly reduced during the initial phase.

2.8.3 Increased Discharge

The increased discharge flow method, otherwise known as inverse cutback (Vazquez-Fernandez et al. 2005) is another, less common alternative to the constant inflow regime. Water is applied to the furrows at a low flow rate until the advance reaches the end of the field. At this point, the flow is diverted to only half of the furrows and sustained until the desired volume is applied. The flow is then diverted to the remaining furrows, which are irrigated in the same manner (Figure 2-2.d). The primary advantage of this technique is the reduction in soil erosion from the upper reaches. As mentioned previously (section 2.3.1), erosion is reduced when water advances over wet rather than dry soil. To improve uniformity, Vazquez-Fernandez (2006) proposed that the inflow should be increased earlier, when the advance has reached ¼ of the field length. The increased discharge technique has performed favourably on blocked furrows resulting in values of DU of 90.5% compared to 83.2% (Vazquez-Fernandez et al. 2005) and 83% compared to 69% (Vazquez-Fernandez 2006) for a conventional constant inflow.

2.8.4 Alternate and Wide Spaced Furrow

In conventional furrow irrigation, the field is designed with furrows located between each plant row or bed and each furrow receives the same inflow rate. However, in an effort to conserve water, many farmers choose to supply water to every second furrow. Compared to every-furrow irrigation, it should be possible to complete the advance phase more rapidly with the same total field inflow rate, hence improving uniformity.

In cracking soils, the benefits of lower water use may be limited because of the high degree of lateral re-distribution that occurs in cracks. Alternate furrow also encourages the development of deep root systems with greater biomass and higher uniformity across the row width. Hence, the plants can utilise a greater proportion of the applied water reflected by the reduced deep percolation.

For every-furrow irrigation, the crop may extract water from either neighbouring furrow hence reducing the significance of between furrow variability. In fact, individual furrow variability overstates the actual plant water variability by between 25 and 50% (Trout and Mackey 1988a). In contrast, for alternate and wide spaced irrigation the inter-furrow variation in infiltration rates requires careful consideration. Many of the clay soils in Australia experience significant lateral infiltration and later re-distribution which reduces variations in moisture content across the wetted and unwetted furrows. This may not be the case for other soil types with excessive infiltration rates where water moves downward rather than horizontally or for soils with relatively low intake rates. Field root density measurements of a maize crop with watered furrows between every second plant row have been undertaken on a low infiltration brown Mediterranean soil (Oliveira et al. 1998). The root density within the plant row was 356 g m^{-3} and 55.6 g m^{-3} under and between plants, respectively. However, the root density was found to be 22.2 g m^{-3} next to the watered furrow and only 0.5 g m^{-3} between crop rows in the unwatered furrow (Oliveira et al. 1998). These findings indicate that the furrow spacing at this site could be reduced to improve nutrient and soil utilisation.

Intermittent furrow irrigation, a variant of alternate furrow is carried out by applying water to every second furrow in the first irrigation and then to the remaining dry alternate furrows during the following event. Field trials suggest that this technique has the ability to reduce water use while retaining comparable yields to the conventional practice (Kang et al. 2000). Consequently, the intermittent technique performed better than conventional or normal alternate furrow irrigation in water limited conditions. It is believed that for maize, this intermittent application of water to furrows on each side of the plant row (termed partial rootzone drying (PRD)) can

induce a stomatal response which reduces transpiration. However, in this case the authors failed to take the necessary measurements to verify the physiological plant response. It is likely that successful application of PRD is only possible under appropriately controlled drip irrigation systems.

2.8.5 Cablegation

Cablegation is an alternative, automated system to supply inflow to irrigation furrows offering both reduced labour requirements and water savings. The system is comprised of a rigid walled gated pipe positioned along the top end of the field on a constant cross-slope greater than 0.002 (Kemper et al. 1987). Water is supplied to the pipeline at such a rate to ensure the cross-section is flowing part full. A plug (piston) is slowly moved along the pipe length controlled by a length of wire cable or rope, travelling with the slope. As water flows down the pipe, it backs up against the plug and begins to flow through the nearby outlets. Considering a single furrow, the inflow will commence as the plug moves past and continuously decline over time as the plug moves further down the pipeline (e.g. Figure 2-2.e is one possible example but the decline is not necessarily linear). The high initial flow rate accelerates the advance phase of the irrigation promoting uniformity of opportunity time. The cablegation system could be classed as an automated cutback regime except the inflow rates decline over the entire inflow time. The application rate for each furrow is dictated by the system layout and speed of the plug movement. Cablegation has a number of benefits such as the reduction in inflow variability by removing the need to manually open and close gates, decreases in labour requirements and ability to match the flow regime to the infiltration function which potentially reduces runoff (Kemper et al. 1987). Cablegation was found to be the most appropriate option in water limiting conditions but was found to be sensitive to field parameters and had lower efficiencies compared to cutback irrigation (Alazba 1999). However, these findings are site specific and cablegation may perform better for different field configurations.

2.8.6 Deficit Irrigation

Deficit irrigation is used to describe the practice of irrigation scheduling where the soil profile is kept in a constant condition of deficit. The imposed plant stress reduces

transpiration and hence, the crop uses a smaller quantity of water. Ignoring surface runoff and considering the reduced potential for deep percolation, one of the major reasons for adoption of this technique is the potential to increase the AE (Sepaskhah and Ghahraman 2004). Conventional thinking suggests that it is impossible to add less water to the soil storage than the current deficit on cracking soils with furrow irrigation. However, field trials conducted on a self-mulching clay soil near Narrabri, in NSW, Australia indicated that the 150 mm rootzone capacity is seldom completely refilled by furrow irrigation (Chan and Hodgson 1981). In cracking soils the stability of cracks is undermined by rapid wetting, during furrow irrigation they quickly swell shut and seal to restrict further infiltration

Where AE is increased under deficit irrigation, the non-uniformity of applied depths will be more pronounced (Sepaskhah and Ghahraman 2004). The shorter irrigation times associated with deficit irrigation result in an increased proportional variance in the opportunity time between the two ends of the field. In addition, the infiltration variability is often greatest at shorter opportunity times. Both effects will add together to decrease the uniformity of applied depths. Sepaskhah and Ghahraman (2004) provided mathematical relationships between the water reduction compared to the full irrigation strategy and the relative benefit due to effects on yield and ability to grow larger areas of crop under deficit irrigation. They found that such relationships differed depending on the AE, irrigation uniformity and crop species.

2.8.7 Real-Time Control

The process of surface irrigation optimisation currently involves using measurements from a previous irrigation event to calibrate a simulation model and identifying appropriate adjustments for the next irrigation. The idea of real-time control requires that the measurement, optimisation and control are integrated into an automated system. This offers the possibility to almost completely remove the problem of temporal variability in infiltration rates that occurs between irrigation events. True real-time control systems are rare but many researchers have used simulation models to investigate the possible performance under such a system. The potential performance is estimated by combining the applications of several furrows where

each irrigation event or furrow is optimised individually with a unique inflow time or possibly also an individual inflow rate.

Application efficiencies for a sugar cane field in Queensland measured over a season ranged between 27 to 55% for individual furrows with an average of 41% while the RE was 98% (Raine et al. 1997). SIRMOD modelling assumed that irrigation performance for all furrows could be improved using a single flow rate of 3.7 L s^{-1} and time of 190 minutes. The resulting average AE was improved to 71%, however the RE declined to 83%. Where individual optimisations using the real-time control were performed on the irrigation events the AE was increased to 93% whilst the RE remained high at 90% (Raine et al. 1997). Similarly, Reddell and Latimer (1987) concluded that a real-time control system would be able to improve the AE to 90% with distribution uniformities of 85%.

Infield implementation of real-time control systems are rare. The high requirement for automated sensing and water control requires a great degree of technical skill and financial expense compared to traditional surface irrigation. One such system, outlined in the description of the Advanced Rate Furrow Irrigation System (ARFIS) (Reddell and Latimer 1987) comprises a water advance sensor, telemetry system, microcomputer and two-position solenoid valve. Constant inflow is supplied to the furrow for the duration of the advance phase. Thereafter the discharge required to supply the current infiltration rate is calculated by integrating the volume required over the field length for two times and then subtracting. The inflow is then switched on and off in a form of surge technique where the inflow rate is decreasing through the event. Real-time control systems must be able to collect advance measurements at different locations in the field and transfer this data to a central processing unit that will optimise and implement the control. The advance sensors may be hard-wired to the computer as in the prototype described by Turnell et al. (1997) as part of RIOS (Developed at the Federal University of Paraìba, Brazil) where 14 water detectors were connected to a maximum of 1000 m length of twin wire. In the future, it may be possible to download the sensor data using wireless technology over a radio network.

2.8.8 Application of Polyacrylamide

Polyacrylamide (PAM) has many variants and a equally diverse range of uses. A water soluble anionic form with a molecular weight between 12 and 15 Mg mol^{-1} and charge density of 8 to 35% has been found to be the most effective in erosion remediation (Lentz 2000, cited in Lentz and Bjorneberg 2003). When PAM is applied to irrigation water it attaches itself to soil surfaces, thereby increasing soil stability and also flocculating fine soil particles so they fall out of suspension rather than exiting the field as part of the tailwater (Lentz and Bjorneberg 2003). PAM offers the possibility of reducing erosion rates, reducing severity of surface seals and increasing flow rates without the associated runoff losses (Santos and Serralheiro 2000).

Many soils have problems with low permeability such as those found in southern Portugal. Santos and Serralheiro (2000) applied two different treatments of high molecular weight anionic PAM to irrigated furrows. It was found that the PAM increased the cumulative infiltration at 5 hours by 20% for a continuous application of 1 mg L^{-1} and 14% for a concentrated application of 10 mg L^{-1} during the advance phase. However, the soil treated with PAM experienced a higher level of infiltration variability compared to the control. Regardless of the treatment method, the application of PAM reduced the severity of the surface sealing. Saturated hydraulic conductivity was 168% higher for the surface seals in the treated furrows compared to the control with similar results for unsaturated measurements (Santos and Serralheiro 2000). Lentz and Bjorneberg (2002) also found that the continuous application resulted in the largest increase in infiltration but concentrated application during the advance phase provided the best protection against erosion.

2.9 Conclusion

The hydraulic properties of the soil are influenced by many physical and chemical factors, the majority of which are difficult to measure and almost impossible to control. Both spatial and temporal infiltration variability is present within fields. Some of this variation can be linked to observable soil factors while much of it remains unexplained. Infiltration variability poses a significant problem for the performance of surface irrigation systems. Not only does it reduce the existing and

potential irrigation performance, it also limits the ability to specify improved irrigation strategies.

The nature of soil properties does not facilitate direct measurement of the infiltration function. In addition, many of the soil physical measurement techniques do not re-create the same physical phenomena, and therefore cannot reflect the behaviour, of a furrow irrigated soil. Hence, there is a genuine need to estimate the parameters of the chosen infiltration function using measured field data. The high variance of soil properties means that these measurements must be collected during or close as possible to the irrigation event using a representative sample of the field area.

There are a number of alternative irrigation strategies that have been proposed to improve irrigation performance. Some of these strategies also offer the potential to reduce the variability of infiltration rates or minimise its influence over the distribution of applied depths. The initial testing and ongoing evaluation of these and the traditional irrigation strategies requires (a) the collection of accurate soil infiltration information and (b) the use of hydraulic simulation models which may need to be specifically designed for that irrigation technique. The complexity of the soil-water interactions prevents direct measurement of the field distribution of applied depths and hence also hinders in measurement of the irrigation performance. For this reason, simulation models are often utilised to study the hydraulic behaviour of surface irrigation. Chapter 3 follows to discuss the available modelling techniques in relation to calibration, performance evaluation and their ability to represent heterogeneous field conditions.

CHAPTER 3
Hydraulic Simulation of Furrow Irrigation

3.1 Purpose of the Simulation Model

In recent decades, a number of computer packages have been developed to simulate the process of surface irrigation. In general, they have three main uses where each package may perform one or more of the following, usually undertaken in the presented sequence:

1) Identification of the infiltration curve and hydraulic characteristics
2) Evaluation of the current irrigation performance, and
3) Optimisation of field design and management.

The selection of models is diverse, where each has been developed with a specific purpose in mind, ranging from the simple direct solution of the volume balance to the complex Saint Venant equations.

3.1.1 Identification of Field Characteristics

A number of the field characteristics required for irrigation simulation cannot be directly measured and therefore must be estimated from other field characteristics. The infiltration rates and surface roughness are commonly estimated using optimisation techniques that minimise the differences between measured and simulated field data (section 3.3).

3.1.2 Evaluation of the Current Irrigation Performance

Irrigation performance is the general term given to the suite of efficiencies and indicators used to describe the irrigation adequacy, distribution of applied water and proportion of applied water that is beneficially used or wasted. Irrigation evaluations can be used to compare the performance between different fields and application

techniques or serve as a benchmark for future changes to the irrigation management. Direct physical measurement of the data required for irrigation evaluations (e.g. the distribution of applied water and the volume of deep percolation) is expensive, labour intensive and difficult to perform. Apart from detailed research experiments it is not practical to measure the volume and distribution of moisture applied by surface irrigation to all parts of the field. Other quantities such as runoff rates from the end of the field may be easier to measure but instead are often also estimated through computer simulation. Before the irrigation can be evaluated, the model must be first calibrated to represent measured field conditions using the inverse solution approach (step 1 from above) or some other technique.

3.1.3 Optimisation of Field Design and Management

Simulation models offer an opportunity to test and evaluate potential alterations to irrigation design and management (section 3.5). Traditionally, optimisation of irrigation management entails extensive field trials, which require substantial time to conduct and analyse. Alternatively, computer models provide the capability for the user to propose a change, simulate the irrigation and evaluate the likely performance, all within a matter of minutes. However, prior to any optimisation it is paramount to evaluate the current performance to provide a benchmark for any improvements.

3.2 Hydraulic Model Theory

The flow of water within an irrigated furrow can be classified as unsteady open channel flow, where the depth varies both with distance and over time. The system is further complicated by the soil infiltration which is described by a time variant lateral outflow. The system is simplified by assuming that the water velocity at any position across the furrow or border cross section is constant and perpendicular to that cross section. The flow of water within the furrow must satisfy the principles of conservation of mass (continuity) and conservation of momentum, commonly expressed in the Saint-Venant form as follows.

First, consider a control volume of length Δx (Figure 3-1). The continuity principle states that the net volume out is equal to the negative change in storage over a time interval, Δt (Sturm 2001). In this case the net volume out is equal to the change in discharge, ∂Q plus the unit infiltration rate I at position x. Rearranging this equation gives the first of the two Saint Venant equations (Walker and Skogerboe 1987):

$$\frac{\partial Q}{\partial x} + \frac{\partial A}{\partial t} + I_x = 0 \quad \text{..... Eq 3-1}$$

where Q is the discharge (m^3), A is the cross-sectional area of flow (m^2) at a depth of y (m), x is the distance (m) and I is the infiltration rate ($m^3\ m^{-1}\ s^{-1}$).

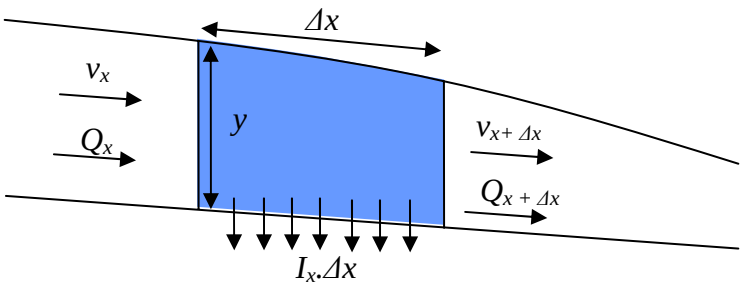

Figure 3-1 Control volume for Saint-Venant equations

Conservation of momentum following Newton's second law states that any unbalanced force (combination of pressure, gravity and shear forces) acting on the control volume must be compensated by a change in momentum. The expression for momentum, making up the second half of the Saint Venant equations can be presented in number of different forms. The equation commonly used in furrow irrigation is developed by expressing the unsteady momentum terms as a function of flow area and discharge (Walker and Skogerboe 1987):

$$\frac{v}{g}\frac{\partial v}{\partial x} + \frac{v}{gA}\frac{\partial Q}{\partial x} + \frac{v}{gA}\frac{\partial A}{\partial t} + \frac{1}{g}\frac{\partial v}{\partial t} + \frac{\partial y}{\partial x} = S_0 - S_f \quad \text{..... Eq 3-2}$$

where v is the velocity of flow ($m\ s^{-1}$), g is the acceleration due to gravity ($m\ s^{-2}$) and S_0 and S_f are the bed slope and friction slope respectively. This equation can be presented in a number of different ways. For example, the continuity equation (Eq. 3-1) can be substituted for $\partial A/\partial t$ or the velocity terms and velocity derivative expressions can be replaced with their equivalent discharge terms. In order to describe the hydraulics of more complex systems such as irregular basins the same expressions must be extended to describe flow in two dimensions.

3.2.1 Full Hydrodynamic Model

The full hydrodynamic approach includes the momentum and continuity equations in their entirety and is therefore the most accurate but also the most complex model. In the past, this model was considered as too computationally intense for practical use, being primarily suited to research purposes (Walker and Willardson 1983). However, the unprecedented improvements in microprocessor speed and software development over the past two decades have eventually made this the most favoured choice for irrigation evaluation and optimisation.

The full hydrodynamic model is commonly used to validate the performance of less complex hydraulic models. Ideally these models should be evaluated by assessing their ability to predict measured field characteristics. In reality the simulation approach is more practical and cost effective due to problems with field measurements (e.g. variations in surface roughness, infiltration and furrow shape) and the difficulty in measuring water recession times (Abbasi et al. 2003b).

3.2.2 Zero Inertia Model

The complexities of the Saint-Venant equations led to the development of a number of simplified hydraulic models. As the name suggests, the zero inertia model neglects the inertia and acceleration terms of the momentum equation. Doing this simplifies equation 3-2 to:

$$\frac{\partial y}{\partial x} = S_0 - S_f \quad \textbf{..... Eq 3-3}$$

This approach requires the assumption that the omitted terms are insignificant within a typical irrigated furrow (Walker and Skogerboe 1987). This assumption holds under free flowing conditions typically observed in the field (Schwankl and Wallender 1988). Zero inertia models are less accurate than the full hydrodynamic but are often preferred due to the reduction in computational requirements (Alazba 1999; Schmitz and Seus 1992).

3.2.3 Kinematic Wave Model

The kinematic wave model takes the simplification of the momentum equation one step further by assuming that the change in energy with distance for a constant discharge is equal to the slope of the furrow bed, hence simplifying equation 3-3 to:

$$S_0 = S_f \quad \text{..... Eq 3-4}$$

This approach is so named because it describes the movement of a kinematic shock wave along a water surface (Walker and Skogerboe 1987). In the absence of an expression to describe the flow depth the flow at any point is assumed to be steady, therefore one of the uniform flow equations must be used to solve the system (also known as the normal depth approximation). The most common uniform flow expression used by these models is the Manning equation:

$$Q = \frac{1}{n} S_0 \frac{A^{\frac{5}{3}}}{P^{\frac{2}{3}}} \quad \text{..... Eq 3-5}$$

where n is the Manning coefficient which describes the roughness of the furrow bed and P is the wetted perimeter (m). Since this model assumes that the flow is governed entirely by the field slope, it may only function correctly for fields with a considerable slope (e.g. > 0.1% (Gharbi et al. 1993)). The kinematic wave approximation improves the speed of convergence over the zero inertia and therefore opens up opportunities for real-time calibration and control (e.g. the IPE model (Camacho et al. 1997)). The simplicity of the kinematic wave model has also facilitated its use in schemes that consider the temporal (Raghuwanshi and Wallender 1996) and spatial variability (Fonteh and Podmore 1994a) of infiltration.

3.2.4 Volume Balance Model

The volume balance model is the most basic of the hydraulic models. It uses the same continuity equation (Eq. 3-1) but completely neglects all components of the momentum equation. Hence, the volume balance must rely on broad assumptions describing the water depth along the furrow length. The simplicity of the volume balance model lends itself to analytical expressions which can be solved directly without the need for computers. The numerical formulation of the volume balance model is covered in detail in chapter 4.

3.2.5 Simulating Longitudinal (Within Furrow) Variation

Studies of furrow irrigation commonly consider the variation of infiltration rates between furrows in the same field. However, they rarely attempt to account for the within furrow variations probably due to the complexity of interactions between infiltrated depths at points within the furrow. This may be justified since field measurements of 315 furrow irrigation events from California and France showed that only one quarter of the events exhibited a non-standard advance velocity trajectory (Renault and Wallender 1994). However, it is recommended that the assumption of a uniform furrow infiltration is at least initially verified using closely spaced advance measurements.

Most simulation models utilise a pre-determined, fixed time-step in the solution of the hydrodynamic equations. To facilitate study of the longitudinal variation in infiltration rates it is more appropriate to alter the solution grid by using fixed space steps to calculate unknown advance times (Rayej and Wallender 1988). This permits specification of different infiltration characteristics for each distance interval (Oyonarte and Mateos 2002) which may be fixed or variable in size. Rayej and Wallender (1988) developed a time based solution of the kinematic wave equations capable of varying infiltration and wetted perimeter along the furrow length and used the resulting model to compare results between spatially averaged and variable infiltration. Whereas the model with spatially averaged infiltration estimated the coefficient of uniformity (CU) at 93%, the spatially variable model estimated a CU of 79% and the measured data indicated that the CU should be closer to 68%. The average predicted infiltration depth also agreed more closely between the spatially variable model and field measurements. The spatially variable model provided accurate predictions of the advance during the majority of the irrigation but diverged from the measured values during the last 20% of the advance distance (Rayej and Wallender 1988).

An alternative approach is to split the length of the furrow into a number of fixed sections, where the infiltration rate remains constant within each segment but varies between different segments. One example, The ALIVE model was adapted to model

heterogeneous conditions by applying advance linear theory to segments within an irrigated furrow (Renault and Wallender 1994). The analysis merely involves dividing the furrow into two sub-lengths but clearly demonstrated the possibility of identifying separate infiltration characteristics from a single advance trajectory where the water moves from a permeable to a less permeable soil and vice versa. Others have used similar techniques by dividing the furrow length into greater numbers of intervals and using the volume balance (e.g. Wallender 1986), kinematic wave (e.g. Raghuwanshi and Wallender 1996) and zero inertia models (e.g. Schwankl et al. 2000; Schwankl and Wallender 1988). Although it may be possible to develop spatially variable hydraulic models and generate individual infiltration curves for each field unit, the approach might not always be practical or necessary (Jaynes and Clemmens 1986).

Fonteh and Podmore (1994b) created a computer program that estimated the average infiltration in a section of furrow based on the results of kriging. This information was combined with a kinematic wave simulation model that allowed intake rates to vary spatially. Field trials confirmed that the model provided more realistic predictions of the application and requirement efficiencies, tail water ratio and distribution uniformity than an equivalent spatially averaged model.

The combination of variance technique offers an alternative method to assess the impact of infiltration variability. It involves taking the mean and variance of a selection of variables that influence the irrigation and then combining them in such a way to estimate the uniformity of applied water (Clemmens 1988). For example, Jaynes and Clemmens (1986) develop a procedure that can estimate the variability of applied depths within an irrigated border using only the results from a single simulation combined with the statistical distributions of the infiltration parameters. Oyonarte et al. (2002) apply the combination of variance technique to furrow irrigation by assuming that the variability of infiltration depths is due to the variability of the f_0 and k parameters, P and τ (opportunity time). Mateos and Oyonarte (2005) adopt a similar combination of variance procedure within a simple spreadsheet model that calculates the infiltration parameters using the Two Point method and estimates the irrigation performance using an assumed level of field variability.

3.3 Estimating Infiltration through Inverse Simulation of Surface Irrigation

There have been numerous techniques devised to estimate the infiltration characteristic from field data. Basically, they operate by attempting to fit a hydraulic simulation model to certain irrigation measurements, most commonly advance distances and times. However, it is possible to carry out similar inverse procedures using other measurements such as advance velocities, runoff rates, water flow depths and recession times. The infiltration curve is calibrated by altering the parameters of the infiltration equation until the simulation model provides the best fit to the measured data. It is theoretically possible to use any surface irrigation model for the inverse procedure by manual optimisation of the parameters. However, it is more common to use software tools and techniques that are purpose designed for the task to arrive at the solution via an automated process. Some notable examples of inverse procedures include:

3.3.1 Full Hydrodynamic Model

Bautista and Wallender (1993a) devised a finite difference approach for the inverse solution of the hydrodynamic equations with a wetted perimeter dependent infiltration characteristic. The resulting model could estimate the infiltration parameters using advance distances but had faster convergence when minimising the differences between measured and simulated advance velocities. Their approach could not successfully optimise the three parameters of the Modified Kostiakov equation but performed well when considering only the *a* and *k* parameters.

Recently a “step-wise multilevel scheme” was developed to perform infiltration calibration using the hydrodynamic model capacity of the surface irrigation model SIRMOD (Walker 2005a). Rather than attempting to optimise the three parameters of the Modified Kostiakov and Manning’s *n* using all available data, the process is split into several stages. Sensitivity analysis (Walker 2005a) indicated that the parameters did not share equally in their influence over the different stages of the irrigation. Consequently the parameter *k* is optimised by reducing the errors between observed

and predicted advance measurements, f_0 from the runoff magnitude, a from the shape of the runoff hydrograph, and n from the recession trajectory, preferably in that order. This procedure performed favourably compared to the Two Point method (Walker 2005a). However, the major advantage is the added ability to estimate f_0 from irrigation measurements, particularly where short irrigation durations do not permit the system to reach steady state conditions.

3.3.2 Zero Inertia Model

Katopodes et al. (1990) derived a numerical zero inertia model for the advance phase of border irrigation to calibrate Kostiakov parameters a, k and Manning n. The process was successful but convergence for all three parameters simultaneously proved difficult owing to the inability to separate the effects of infiltration and roughness in the objective function. Later a direct solution to solve for either, parameter k or Manning n was derived from the same model (Clemmens 1991). Clemens (1991) found that it was difficult to produce reliable estimates of a from advance because its value is highly sensitive to the accuracy of field measurements.

Yinong et al. (2006) develop an inverse solution technique to estimate the parameters of the modified Kostiakov equation and Manning n from advance and/or recession data. The optimisation is performed by an iterative application of the SRFR (Clemmens and Strelkoff 1999) simulation model. They found that optimising the infiltration and roughness parameters based on advance data alone caused SRFR to provide poor predictions of the recession trajectory and vice versa. The best estimate for the field occurs when the inverse procedure solves for the infiltration parameters using advance and recession data simultaneously (Yinong et al. 2006).

3.3.3 Volume Balance Model

The volume balance model, being the most basic model available is the most common choice for the inverse procedure. Prior to the use of the personal computer, a number of volume balance approaches were developed based on the use of characteristic curve shapes or using graphical estimation from log-log plots. Norum and Gray (1970) identified the parameters of the Kostiakov or Philip equations from

dimensionless advance distances and dimensionless advance times plotted on logarithmic paper. DeTar (1989) describes a method where the average infiltrated depths from a simple volume balance calculation are plotted on log-log paper against the average opportunity time based on a fitted power function advance. The Kostiakov parameter *a* is determined graphically from the slope of the line and *k* is read off the same plot as the intercept. Similarly, Sepaskhah and Afshar-Chamanabad (2002) used regression analysis between $ln(V_{Zx})$ (volume infiltrated at t_x) and $ln(t_x)$ to determine the value of *a*. The parameter *k* is found by simple substitution into the volume balance for t = 1 minute. They also used a similar approach to calculate infiltration during the storage phase.

Two major developments in the inverse volume balance, namely the Two Point (Elliott and Walker 1982) method and INFILT (McClymont and Smith 1996) are discussed later (in sections 4.2.2.1 and 4.2.2.2, respectively) as these techniques are the precursors of the procedure developed in chapter 4. Foroud et al. (1996) extend the method to include recession data by fitting power functions to both the advance and recession trajectories for an irrigated border. Many others have developed similar numerical schemes to predict infiltration rates from advance measurements, each with a unique advantage or purpose (Valiantzas 2000).

The simplicity of the volume balance model has also encouraged its use in the calibration of infiltration functions other than the Kostiakov and Modified Kostiakov. It has for example, been used to calibrate the parameters of the Horton equation for both loamy and cracking clay soils (Mailhol 2003). This approach (i.e. inverse application of the RAIEOPT furrow simulation model) was later included as part of the whole field crop model SOFIP (Mailhol et al. 2005). Similarly, Shepard et al. (1993) employed the volume balance approach to estimate the two parameters of the Philip infiltration equation from a single advance point. This method has the advantage of being able to estimate the final infiltration rate from minimal data. In a similar manner, Valiantzas (2001) developed a procedure to calibrate the SCS intake function from a single advance point.

An alternative of the volume balance is the flow balance model, which considers infiltration rates and advance rates rather than advance distances and infiltration volumes. One example, the ALIVE model uses the Horton equation to represent soil intake (Renault and Wallender 1994). The authors believe that the advance velocity can capture more information compared to the advance time, adding the possibility of identifying infiltration rates in heterogeneous conditions.

3.3.4 Discussion of the Inverse Procedures

For volume balance methods, the accuracy of the fitted infiltration parameters has been found to be compromised (Bautista and Wallender 1993c) under higher inflow rates, corresponding to shorter advance times. This finding should be universal amongst all hydraulic models. Longer times increase the possibility of successfully identifying the steady state component of the infiltration function from the advance trajectory. Some methods account for this limitation by specifying that these steady components are evaluated separately (e.g. the Two Point method (Elliott and Walker 1982)).

Reliability of infiltration estimation increases while data requirements decrease when two rather than three parameters are estimated from advance measurements, for this reason optimisation of a and k should be the preferred strategy (Bautista and Wallender 1993c). Bautista and Wallender (1993c) also found that estimating infiltration parameters from advance velocities rather than distances results in poor predictions of the steady infiltration rate but improved estimates of the transient terms (a and k) of the Modified Kostiakov equation.

The typical inverse scheme does not consider within furrow variability. The estimated infiltration curve represents the soil intake rate averaged over the length of the field. In reality the infiltration curve is not a strict average due the differences in opportunity time along the field length. Field trials have shown that the infiltration variance is up to ten times greater (Tarboton and Wallender 1989) when the within furrow variability in intake rates is considered compared to the standard furrow averaged infiltration parameters.

3.4 Apparent Infiltration Variability in the Inverse Solution and Simulation Processes

Apparent infiltration variability is a particular problem of the techniques used to estimate the infiltration parameters from field measurements. The inverse solution requires many assumptions, most of which yield erroneous results whenever they are violated. In some cases, the errors in estimation are confused with authentic variations in soil intake rates. Consequently, the estimated variation in infiltration rates may be greater than the true variability in infiltration. Some of the limitations of the inverse methods, such as the assumption of constant within-furrow infiltration rates will always mask the true extent of the infiltration variability.

3.4.1 Inflow Rate

The discharge into the furrow is the most important item of information required in both the inverse solution for infiltration parameters and the simulation process. Regardless of the application technique, the discharge into the furrow is influenced by a number of factors which can be controlled to differing extents. For siphon systems, the variation of inflow is determined by field geometry, siphon attributes (length, roughness) and water level in the supply ditch. For gated pipe application, discharge rates are a function of the pipeline pressure and pipeline characteristics. Field trials indicate that as much as half of the observed variability in uniformity estimates between furrows is caused by inflow variability between furrows (Schwankl et al. 2000). High variations in inflow rates have been found to overwhelm expected seasonal trends in infiltration (Mailhol et al. 2005).

Schwankl et al. (2000) conducted a sensitivity analysis of the zero inertia model using randomised values of the input parameters within expected ranges and confirmed the importance of the inflow rate. It was found that the inflow variability between furrows had the greatest effect on the variation of average infiltrated depths, CU, distribution uniformity and advance times. The infiltration variability rated second most important followed by the furrow geometry and surface roughness. These findings were based

on a field that was considered to be spatially uniform therefore the infiltration will increase in significance for conditions of higher spatial soil variability.

Budget and labour constraints limit the number of measurements that can be practically carried out in the field. Hence, a single discharge reading is often recorded for the entire field and constant inflow is assumed between furrows. Higher resolution measurements may be possible for specialised research purposes but are not practical or indeed possible in commercial agriculture. Measurements of layflat gated pipe have exposed CV's (coefficient of variance) of 35% between furrows which under correct management can be reduced to 15% (Mailhol et al. 1999) or less than 5% (Mailhol and Gonzalez 1993). Although the uniformity of siphon inflow is determined by manual pipe placement, there is reduced interdependence of flow rates compared to gated pipe. Hence, high uniformity should be expected where siphons are started and positioned with care. For siphons, a 50% decrease in head will only cause a 25% reduction in the flow rate whilst a change in gate opening of 1 to 5 mm can cause the flow to differ by 25% (Trout and Mackey 1988a). The CV of inflow between 15 siphons was measured at 5% (Mailhol et al. 1999), while Trout and Mackey (1988a) measured CV's of 14% for siphon, 25% for gated pipe and 29% for feed ditch inflows. Complicating the matter, the farmer will often manually adjust the inflows between furrows in the same set to maintain a uniform advance.

Flow measurements suffer from both systematic and random errors. Where inflow measurements are used to estimate the infiltration function parameters (either within the inverse solution of advance or using simple inflow-outflow measurements), these errors will usually increase the variability in estimated infiltration curves above the actual level of variation. For the inflow-outflow technique, errors in the infiltration curve increase as the percentage of inflow that has infiltrated decreases (Trout and Mackey 1988b). Extra care should be taken when using short sections of furrow as the infiltrated volume becomes smaller relative to the inflow and runoff volumes. However, longer measurement lengths provide less information regarding spatial variability. Systematic errors introduced by the apparatus may be reduced by using the same device to collect both inflow and outflow measurements.

3.4.2 Wetted Perimeter

Most irrigation models assume that the furrow dimensions are uniform both between furrows and along the furrow length. In reality, furrow dimensions differ substantially along the furrow length and will change over time due to the process of slumping and erosion (section 2.3.2). Since infiltration occurs through the wetted perimeter of the furrow, any changes in the wetted perimeter will have some influence on the water intake. The importance of the wetted perimeter effect is determined by the soil type and field configuration (e.g. the size of the wetted perimeter has minimal effect in a dry heavy cracking clay).

Furrows with uniform cross-section will also experience changes in wetted perimeter due to the variation in water flow depth. Water depth within the furrow is determined by a non-linear function of the flow rate with increasing inflow resulting in a corresponding increase in the wetted perimeter. The wetted perimeter is far more sensitive to changes in the flow depth for a narrow furrow compared to a wide flat furrow profile (Holzapfel et al. 2004). Abbasi et al. (2003a) measured a positive correlation between infiltrated volumes and in-furrow water depths on a sand loam soil. However, the small sample size did not permit any general conclusions. Izadi and Wallender (1985) also found a correlation between the infiltration rate and wetted perimeter, but they discovered that the influence declined with increasing opportunity time. In the absence of cracks and holes, approximately one-third of the variation in soil intake can be attributed to the wetted perimeter effect (Izadi and Wallender 1985). Others have observed weaker relationships, Oyonarte et al. (2002) found that in two seasons, only 17% and 10% of the variance in infiltration could be directly explained by the wetted perimeter.

If infiltration parameters are determined while neglecting the wetted perimeter effect, those parameters are only valid for the inflow rate at which those parameters were determined (Bautista and Wallender 1993a). Hence, some adjustment may be necessary any time that infiltration curve is used to describe the intake under differing inflow rates.

Considering the two parameter Kostiakov infiltration equation, Antonio and Alvarez (2003) discovered that the parameter *a* remains constant for different inflow rates while the changes in *k* followed a power relationship with the wetted perimeter:

$$k_{new} = k_{old}\left(\frac{P_{new}}{P_{old}}\right)^{\varphi} \quad \text{..... Eq 3-6}$$

where P_{old} and P_{new} are the wetted perimeters for k_{old} and k_{new}, respectively and φ is a function of *a* and furrow geometry. However, at higher discharges the process of erosion appeared to reduce or even eliminate any effect on infiltration rates due to the consequential increases in wetted perimeter. The same relationship has been applied to (a) the saturated hydraulic conductivity (K_s) (Mailhol et al. 2005) where $\varphi = 0.6$, (b) the steady state term f_0 (Mailhol and Gonzalez 1993) ($\varphi = 1$) and (c) the cumulative infiltration depth *Z* (Oyonarte et al. 2002). Some research suggests that the value of φ is in fact greater than 1.0 indicating that the proportional change in infiltration is larger than the change in wetted perimeter. Field trials with blocked furrow infiltrometers have produced values of $\varphi = 0.64$ for the first irrigation and $\varphi = 0.29$ for subsequent irrigations (Oyonarte et al. 2002) suggesting a much weaker relationship after the first irrigation.

Walker et al. (2006) describe a similar approach to adjust the parameters of the infiltration intake families to different wetted perimeters *P* resulting from continuous and surge flow:

$$a = ICF \times a_{ref}\text{,}\quad k = ICF \times k_{ref} \times \left(\frac{P}{P_{ref}}\right)\text{,}\quad \textbf{and}\quad f_0 = ICF \times f_{0ref} \times \left(\frac{P}{P_{ref}}\right) \quad \text{..... Eq 3-7}$$

where *ICF* = 0.8 (defined in section 2.5.2) and *ref* denotes the reference infiltration parameters and wetted perimeter unique for that infiltration family.

Strelkoff and Souza (1984) compared a range of expressions to scale the infiltrated depth *Z* as given by the Kostiakov equation (Eq. 2-4) by functions of the wetted perimeter or top flow width at the measured, upstream, and normal depths. They found that field measurements of the advance were best predicted by the simulation using infiltration scaled according to wetted perimeter at the measured depth closely followed by the flow width at the measured depth. Scaling based on the upstream

flow depth also performed satisfactory but the infiltration predicted using the normal flow depth resulted in the poorest reproduction of the measured advance.

A different approach is to scale the whole infiltration equation based on a function of the inflow rate (Sepaskhah and Afshar-Chamanabad 2002):

$$Z = \left(kt^{a} + f_{0}t\right)Q^{\zeta} \quad \text{..... Eq 3-8}$$

where ζ is an empirical exponent fitted from field measurements. The results of Sepaskhah and Afshar-Chamanabad (2002) indicated that the cumulative infiltration *Z*, estimated from measurements during the advance phase is not dependent on the wetted perimeter for the first irrigation. For wide-spaced (every-other) irrigation however, the cumulative infiltration was strongly related to the wetted perimeter and inflow rate indicated by a high value for ζ. This effect is more pronounced under wide-spaced furrow irrigation since the potential for irrigation per unit width remains the same but the flux is restricted by halving the wetted area. Where the infiltration curve was estimated using data collected during both the advance and storage phases the dependency on wetted perimeter was reduced for conventional every furrow and every other furrow irrigation (Sepaskhah and Afshar-Chamanabad 2002).

Schwankl and Wallender (1988) developed a zero inertia model that alters soil intake by simply multiplying the infiltration rate by the wetted perimeter at that time. The model performed favourably compared to field measurements and was subsequently used to study the implications of ignoring wetted perimeter effects. The advance trajectory is initially slower for the constant wetted perimeter simulation since the flow depth and wetted perimeter is overestimated early in the irrigation. This continues until the actual wetted perimeter reaches the average value, after which the constant wetted perimeter model underestimates the infiltration depth compared to the variable model. It is important to note that the two advance curves do not converge at the end of the irrigation as might be expected, therefore the two models have different advance completion times. Hence, ignoring the wetted perimeter effect results in overestimation of advance times and application efficiencies. Camacho et al. (1997) take this approach further by developing a simulation model that changes the infiltration parameters at every location and time by adjusting for the wetted

perimeter. On comparison with the spatially averaged approach of SIRMOD they found that ignoring the wetted perimeter effect instead results in a overestimation of the infiltrated depths, conflicting with the findings of Schwankl and Wallender (1988).

A combination of field trials and experiments carried out by Trout (1992a) undermines many of these simple practices to include the wetted perimeter effect. He identified a weak positive relationship between the infiltration and wetted perimeter that was less than proportional (60 to 80% increase in Z for increase in wetted perimeter at average field values) and diminished as the wetted perimeter increased. The negative relationship between flow velocity and infiltration caused by erosion and subsequent formation of surface seals overcomes most of the expected increase in infiltration caused by the wetted perimeter. Therefore, on moderate slopes the infiltration is mostly independent of the inflow discharge while on steep slopes the relationship becomes negative. The influence of velocity will decrease on non-erosive soils.

3.4.3 Surface Storage

Apart from the wetted perimeter effect, uncertainty in the furrow dimensions and flow depths also poses a problem to the inverse procedures due to the changes in the surface storage. During the early stages of the irrigation (i.e. the advance stage), the surface storage will account for a significant part of the volume balance. One approach to account for the spatial uncertainty of measured furrow geometry, field slope or surface roughness is to include the surface storage parameter within the inverse solution of infiltration as an additional empirical parameter (McClymont and Smith 1996). However, this technique does require a greater number of measured and reliable advance points to ensure realistic estimates. Altering the surface storage term will have similar effects to that of the transient infiltration term (i.e. k), change in one will have an equal and opposite effect on the other.

3.5 Simulation Models to Evaluate and Optimise Performance

3.5.1 SIRMOD

SIRMOD (Walker 2003), developed by Utah State University applies the full hydrodynamic, Saint-Venant equations (Eq. 3-1 and 3-2) to describe the process of surface irrigation in one dimension. Alternatively, where the solution is unstable, the zero inertia or kinematic wave models (version III only) can be used.

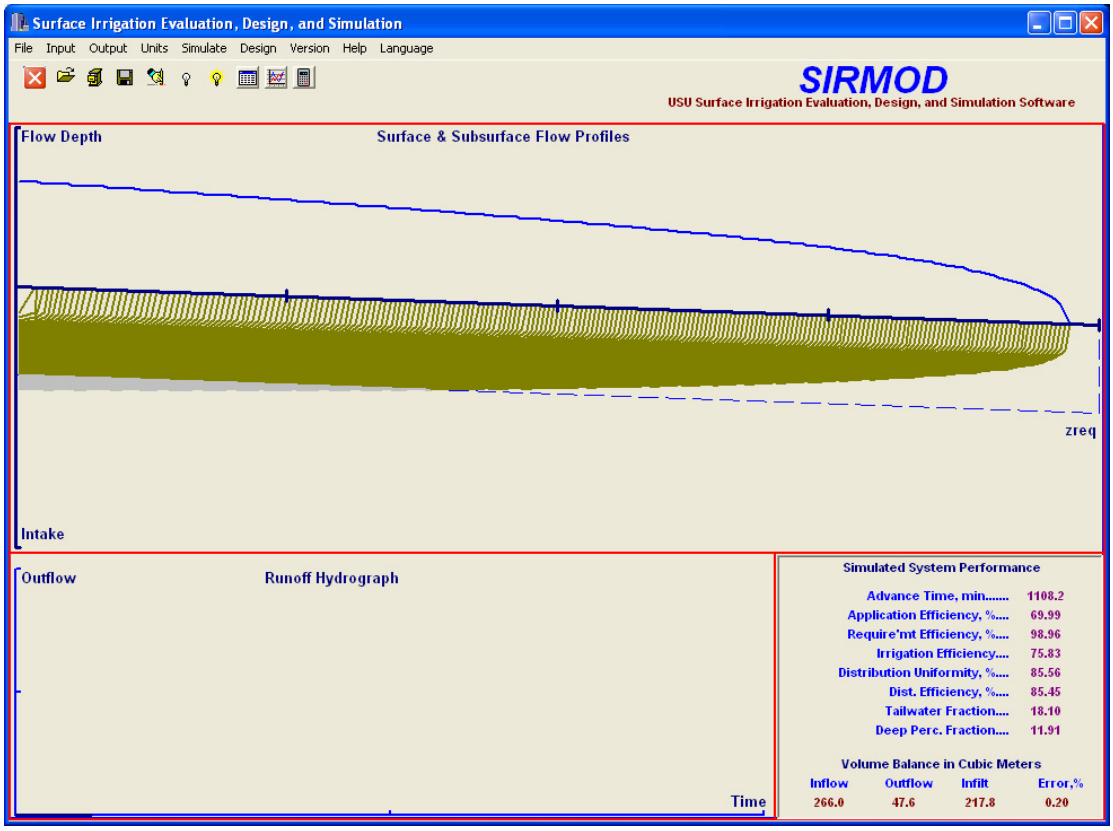

Figure 3-2 Screenshot of SIRMOD III: simulation of the Kooba field with variable inflow (infiltration estimated using advance and runoff with variable inflow)

During this research, two versions of SIRMOD were utilised, versions II and III. In Australia, SIRMOD II has been widely adopted as the standard for the evaluation and optimisation of furrow irrigation (e.g. within the Irrimate™ field evaluation system (section 5.4.1)). Considering the numerical model, Version III is almost identical to the preceding version with the capacity to model variable inflow and the ability to adjust intake rates based on the wetted perimeter at the upstream end of the field. It is

worth noting that both of these options do not function simultaneously, the infiltration rate is not adjusted to account for temporal changes in the inflow hydrograph. The infiltration rate is described by the Modified Kostiakov equation with an optional cracking term as in equation. 2-7. The required field characteristics such as furrow geometry are determined from simple field measurements. Following completion of the simulation, SIRMOD provides various descriptors of the irrigation performance, predicted advance and recession trajectories, outflow hydrograph and final distribution of applied depths.

3.5.2 SRFR

SRFR (Clemmens and Strelkoff 1999), developed at the United States Water Conservation Laboratory employs the zero inertia or kinematic wave models to simulate the process of irrigation. Unlike SIRMOD, it can cope with outflows from either or both ends of the field. Hence, SRFR can simulate furrow irrigation carried out on the reverse grade. In addition, it can accommodate variable inflow rates and has the capability to model variations in furrow dimensions, field slope and soil intake rates over both distance and time. The infiltration characteristic may be presented in the form of the Modified Kostiakov equation, time related intake curves, branch infiltration, known characteristic infiltration time or SCS intake curve. Although SRFR is not discussed extensively within this dissertation, its provision for variable inflow proved vital in the early development of IPARM (chapter 4).

3.5.3 FIDO

FIDO, Furrow Irrigation Design Optimiser is a tool for the design and management of furrow irrigation systems (McClymont et al. 1999). It can accurately simulate all phases of the irrigation event to calculate reliable estimates of irrigation efficiency and uniformity values. Fido contains many features such as parameter calibration, management optimisation and presentation of graphical outputs. The software package is founded on the implementation the full hydrodynamic equations (Eq. 3-1 and 3-2). The simulation engine of FIDO is used as the basis for the development of the whole field simulation model discussed in chapter 6.

Some of the main strengths of FIDO are derived from its database capabilities. A relational database (in XML format) is used to store a wide range of parameters (e.g. field location, farm owner, irrigation date, soil type) in addition to the standard soil infiltration and field design characteristics. This facilitates the study of seasonal trends and variations in field performance.

3.5.4 Other Models

The AIM irrigation model proposed by Austin and Prendergast (1997) combines kinematic wave theory with the linear infiltration function to produce a analytical solution for surface irrigation. Consequently, this approach can be hard-wired into electronic equipment since it does not require use of computers and is not subject to numerical instability. Field trials have shown that this approach performs favourably compared to the numerical models of Walker (SIRMOD) and Strelkoff (SRFR) and is particularly suited to heavy textured soils (Austin and Prendergast 1997).

ZIMOD proposed by Abbasi et al. (2003b) applies the zero inertia model to describe furrow irrigation. The authors conclude that the model provides excellent predictions of advance and runoff but suffers from slower convergence compared with the Priessman double sweep algorithm used by SIRMOD. ZIFA (Schmitz and Seus 1992), another model based on the zero inertia approach and can accommodate both level and sloping furrows and can take into account the variable nature of infiltration using any infiltration equation.

Mailhol (2005) developed the SOFIP model (Simulation of Furrow Irrigation Practices) that can simulate and predict the whole field behaviour by assuming that a number of irrigation characteristics are stochastic in nature. It includes the RAIEOPT hydraulic model to predict the advance process using a volume balance approach. The soil moisture content is predicted using a volumetric water balance within the crop model, PILOTE which predicts the temporal variation in infiltration rates. These components are combined with a Monte Carlo simulation to generate realistic parameter values. The completed model has been used to study the compounded effects of different sources of variability and to identify optimal management

strategies to maximise irrigation performance and crop yield at the same time (Mailhol et al. 2005).

3.6 Conclusions

The simulation of surface irrigation provides the opportunity to observe hydraulic, soil and crop behaviour while greatly reducing the need for time-consuming field trials and intensive irrigation measurements. Irrigation models encompass a wide range of different numerical approaches, each being suited to a particular task or series of tasks.

Simplification of the hydraulic process has lead to several schemes to estimate infiltration parameters from field data. However, as these inverse techniques are typically based on the most basic hydraulic models, they are restricted by a number of simplifying assumptions. These assumptions are valid under controlled homogeneous conditions. However, in non-ideal field conditions such assumptions can compromise the predictive capability of these models leading to unreliable estimates of soil infiltration and possibly false estimations of variability. It should be possible to improve the performance of these schemes taking into account many of these issues whilst still maintaining the simplicity required for the iterative processes.

Several software packages to evaluate irrigation performance have been identified. However, these models generally consider the furrow as the basic hydraulic unit. Hence, the prediction and subsequent optimisation of irrigation performance at the field scale is tedious. It is proposed that this use of limited field information not only reduces the accuracy of performance estimates but also prevents the identification of the true optimal combination of irrigation management practices.

CHAPTER 4

Development of IPARM

4.1 Introduction

Chapter 3 introduced a number of different numerical simulation models that have been applied to surface irrigation. From the discussion in section 3.3 it is clear that the volume balance model is the most appropriate option for use in the inverse solution for infiltration from field data due to its simplicity compared to alternative models. The accuracy of these inverse techniques is often compromised by the complete reliance on data collected during the advance phase. As a result the estimated infiltration curve is only representative for times less than the final advance time and must be extrapolated past this point to predict infiltration volumes for longer times. The traditional volume balance model assumes constant inflow, an assumption which is often violated in the field. As a result these techniques perform well where the steady inflow assumption is satisfied but frequently fail to provide satisfactory results for fields with non-steady inflow rates.

It is hypothesised that a proportion of the apparent infiltration variability between furrows and over time is the result of errors in the estimation of the infiltration parameters associated with the limitations of the volume balance model. This chapter discusses the development, operation and validation of a new inverse solution for the infiltration parameters. This procedure, IPARM is based on a modification of the volume balance model to include runoff data and account for temporally varying inflow rates. Before description of the IPARM procedure, it is necessary to review previous developments in the inverse volume balance approach.

4.2 Volume Balance Model for Inverse Solution of Infiltration

4.2.1 Volume Balance Model

The volume balance model (Figure 4-1) is constructed by applying the principle of mass continuity to the flow of water within an irrigated furrow, border or basin. It states that the volume of water applied to the field, calculated by multiplying the constant inflow rate Q_0 (m^3 min^{-1}) by elapsed irrigation time t (min) must equal the sum of the volume temporally stored on the soil surface V_S (m^3) and the volume infiltrated V_I. Over time, the leading edge of the water front x (m), described by the term "advance" moves down the furrow and eventually reaches the end of the field L (m), at which point the runoff term V_R (m^3) is added to the equation:

$$Q_0 t = V_I + V_S + V_R \quad \text{..... Eq 4-1}$$

The volume infiltrated V_I can be described by any of the infiltration equations mentioned in section 2.2.1. The Modified Kostiakov equation (Eq. 2-6) is commonly used to describe the cumulative infiltrated depth at a given opportunity time (τ):

$$Z = k\tau^a + f_0\tau \quad \text{..... Eq 4-2}$$

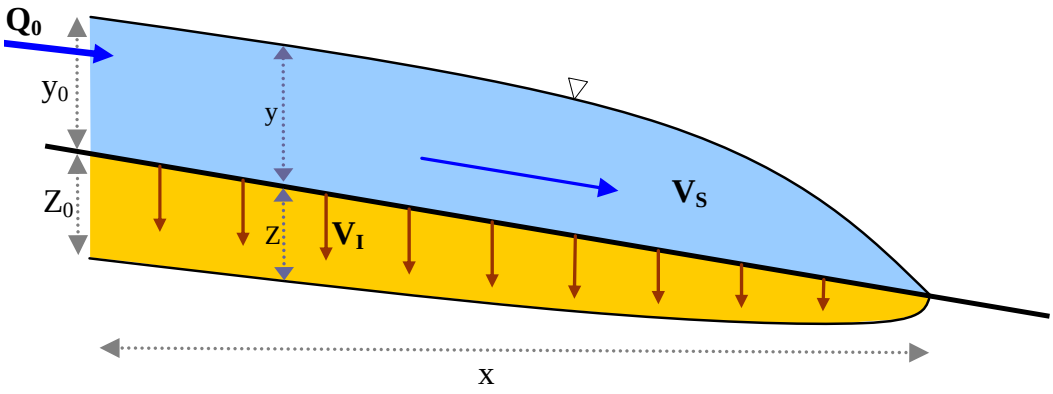

Figure 4-1 Volume balance model during the advance phase

4.2.2 Advance Phase

The expression selected to describe infiltration (Eq. 4-2) merely yields the cumulative infiltrated depth at a particular location for a given value of opportunity time τ. For the advance phase, the opportunity time at the upstream boundary is equal to the

irrigation time but at any other location the infiltrated depth Z_x is a function of the advance time t_x to that point.

$$Z_x = k(t - t_x)^a + f_0(t - t_x) \quad \text{..... Eq 4-3}$$

More complex models (e.g. zero inertia) divide the field length into a number of intervals where the opportunity time is based on the simulated advance time at that position. Instead it is proposed that the advance trajectory can be described using a power curve function:

$$x = pt^r \quad \text{..... Eq 4-4}$$

where p and r are selected so that the function best represents a series of measured advance data comprised of the time taken, t of the water front to reach various distances, x. Alternatively, the data requirement can be reduced by using a pre-determined curvature by specifying a constant value for r (e.g. r = 0.5 (Shepard et al. 1993)).

By substituting equation 4-4 into 4-3 and integrating over the field length the expression for the total volume infiltrated at any point in time during the advance phase is given by:

$$V_I = \sigma_{z1} k t^a x + \sigma_{z2} f_0 t x \quad \text{..... Eq 4-5}$$

Where σ_{z1} and σ_{z2} are the subsurface storage coefficients for the advance phase (Walker and Skogerboe 1987) given by:

$$\sigma_{z1} = \frac{a + r(1 - a) + 1)}{(1 + a)(1 + r)} \quad \text{..... Eq 4-6}$$

$$\sigma_{z2} = \frac{1}{1 + r} \quad \text{..... Eq 4-7}$$

Alternately, to simplify calculations the value of σ_{z1} may be fixed independent of irrigation measurements. For example, Levien and de Souza (1987) assumed a value of σ_{z1} = 0.8 and Reddell and Latimer (1987) assumed a value of σ_{z1} = 0.78.

Ideally, the volume stored on the soil surface (V_S) can be estimated based on water depth measurements taken at numerous locations down the furrow length. However, this approach is almost exclusively limited to research applications owing to the

difficulties and costs associated with obtaining this data. Consequently, V_S is commonly approximated as a function of the up-stream area of flow A_0 (m^2) during constant inflow multiplied by the advance distance:

$$V_S = \sigma_y A_0 x \quad \text{..... Eq 4-8}$$

The coefficient σ_y describes the ratio of average area of flow relative to the upstream area which is assumed to be constant and is referred to as the surface storage shape factor. Various values have been proposed for the shape factor (typically ranging between 0.7 and 0.8) including 0.74 (Scaloppi et al. 1995), 0.75 (Levien and de Souza 1987; Sepaskhah and Afshar-Chamanabad 2002), 0.77 (Elliott and Walker 1982; Valiantzas et al. 2001; Walker 2003), 0.79 (Renault and Wallender 1997) and 0.8 (Mailhol and Gonzalez 1993). DeTar (1989) discovered that most of the inconsistencies in the model can be corrected by making slight adjustments to the average area of surface storage.

Field trials conducted by Esfandiari and Maheshwari (1997) do not support the use of a constant value for σ_y. They found that the value of σ_y changes over the advance time, differs between individual furrows and also changes during the season (declining with time). Esfandiari and Maheshwari (1997) also found that the parameter was often much higher than conventionally adopted values and varied between 0.96 and 1.8. In this case, differences were most likely the result of non-uniformities in the bed slope and changes in surface roughness. Hence, these results should not be used to draw general conclusions on the correct value of the surface storage. However, they do raise some questions regarding the collection of furrow profile and water depth measurements. Furrow geometries may vary considerably between furrows and will change over time due to erosion. Consequently, the location(s) selected for geometry and water depth measurements must be representative of the field.

Valiantzas (1997) devised an expression for the surface storage coefficient as a function of non-dimensionalised time. In this approach, the value of σ_y begins at a value marginally less than 1 for very small times and gradually decreases approaching a final value dependent on the Kostiakov parameter *a* and furrow geometry. When

this time dependent surface storage calculation was included in the volume balance the results were found to be almost identical (Valiantzas 1997) to the more computationally intensive kinematic wave model.

Volume balance models using a constant value for σ_y tend to underestimate (by approximately 25%) the advance velocity over the upper section of the field (e.g. first 25 m of a 150 m long furrow) with respect to the zero inertia model (Guardo et al. 2000). The hydraulic gradient is greater at the start of the irrigation, and therefore the surface storage coefficient should be higher for that portion of the advance. Hence, Guardo et al. (2000) proposed an improved volume balance technique for level basins where the hydraulic gradient is re-calculated for each advance distance based on Manning's equation, hence providing better advance predictions over the entire length. Alternatively, the most simple approach is to neglect the surface storage completely (Or and Silva 1996; Reddell and Latimer 1987). However, this simplification may lead to significant errors in the simulated advance (Valiantzas 2000) or estimated infiltration curve.

Cahoon (1995) recommends that the cross section should be measured with a profilemeter with no less than 20 measurements across the width of the furrow, recorded at least three times along the field length. Ideally, the functions relating area and wetted perimeter to flow depth are represented by linear interpolation between points. The validity of such an approach is limited by the spatially and temporally variable nature of the cross-section. Also, the high data requirement for this method does not lend itself to practical use on a commercial enterprise.

Substitution of the infiltration (4-5) and surface storage (4-8) terms into the volume balance (Eq. 4-1) results in the completed equation:

$$Q_0 t = \sigma_y A_0 x + \sigma_{z1} k t^a x + \sigma_{z2} f_0 t x \quad \text{..... Eq 4-9}$$

Rearrangement of this equation produces an expression for the advance distance:

$$x = \frac{Q_0 t}{\sigma_y A_0 - \sigma_{z1} k t^a + \sigma_{z2} f_0 t} \quad \text{..... Eq 4-10}$$

4.2.2.1 Two Point method

The Two Point method (Elliott and Walker 1982) is one of the most well known examples of the inverse solution for the volume balance. The Two Point method is commonly used to predict infiltration rates due to its high stability and performance over wide ranging conditions (Mateos and Oyonarte 2005). Holzapfel (2004) tested a number of different inverse procedures, including one based on the kinematic wave model but found that the Two Point method performed much better than the other methods when applied to wide (0.6 m top width) furrows and only slightly worse when used in narrow (0.4 m top width) furrows.

As the procedure relies on two measured advance points, x_1,t_1 and x_2,t_2 the values of the power curve trajectory constants p and r of equation 4-4 can be evaluated directly.

$$r = \frac{\ln\left(\frac{x_1}{x_2}\right)}{\ln\left(\frac{t_1}{t_2}\right)} \quad \text{..... Eq 4-11}$$

$$p = \frac{x_2}{t_2^{\,r}} \quad \text{..... Eq 4-12}$$

Similarly as the Two Point method uses only two advance points the values of a and k can also be expressed analytically. Rearrangement of equation 4-10 leads to the following expressions (Walker 2003):

$$a = \frac{\ln\left(\frac{V_{L,2}}{V_{L,1}}\right)}{\ln\left(\frac{t_2}{t_1}\right)} \quad \text{..... Eq 4-13}$$

$$k = \frac{V_{L,2}}{\sigma_{z1} t_2^{\,a}} \quad \text{..... Eq 4-14}$$

where the volume at point i is calculated from:

$$V_{L,i} = \frac{Q_0 t_i - \sigma_y A_0 x_i - \sigma_{z2} f_0 t_i x_i}{x_i} \quad \text{..... Eq 4-15}$$

The Two Point method does not include the ability to calibrate the steady infiltration rate therefore it must be estimated separately. Although it is possible to measure the steady intake directly at a single point, the preferred approach remains the inflow-outflow method. At some time after the runoff has stabilised at the final value of q_r (m^3 min^{-1}), f_0 is calculated from the difference between the inflow and outflow rates:

$$f_0 = \left(\frac{Q_0 - q_r}{x} \right) \quad \text{..... Eq 4-16}$$

hence effectively using the whole furrow length as an infiltrometer. This technique assumes that the irrigation duration is sufficient to approach steady conditions over the majority of the field. Hence, problems arise where inflow rates fluctuate over time. Alternatively, where runoff data is not available or does not reach steady state within the irrigation time the value for f_0 may be assumed to be zero reducing the infiltration equation to the Kostiakov form.

4.2.2.2 INFILT

The inverse technique (INFILT) proposed by McClymont and Smith (1996) is based on a similar form of the volume balance equation (Eq. 4-10) but overcomes a number of the shortcomings of the Two Point method. INFILT estimates the parameters of the Modified Kostiakov infiltration equation from three or more advance measurements. The parameters can no longer be expressed analytically, hence the approach converges to the solution by minimising the differences between measured and predicted advance distances. Most importantly, INFILT does not require a separate calculation of the steady intake rate as f_0 is calibrated simultaneously with the other two parameters. The use of an increased number of advance points also reduces the sensitivity of the infiltration curve to individual measurement point errors. Finally, INFILT treats the surface storage as a fourth empirical parameter to account for variations in furrow geometry and surface roughness. However, experience has shown that optimisation of the $\sigma_y A_0$ term can produce unreliable results, particularly where the number of advance points is limited. Often the value for $\sigma_y A_0$ will approach unrealistically high or values below zero and is only prevented from doing so by pre-defined limits specified by the user. Comparisons with other inverse methods has shown that this technique is the most versatile and appropriate alternative for use in

Australian conditions (Khatri and Smith 2005). Over recent years, the INFILT calibration method has been tested and verified with a large number of irrigation events as part of the commercial Irrimate™ system. It has also been the basis for research applications within the sugar cane (Raine et al. 1998) and cotton (Smith et al. 2005) industries.

4.2.3 Runoff Phase

Where the parameters of the Modified Kostiakov equation are evaluated exclusively from advance data, the resulting function should be able to predict the infiltration at any time during the advance phase. However, to estimate the infiltration during the storage and recession phases, the same infiltration curve is simply extrapolated to greater times. This approach assumes that the advance data contains sufficient information to capture the true shape of the infiltration curve. Inverse procedures based entirely on the advance phase have great difficulty in identifying the correct value for f_0, particularly for short fields. This becomes more of an issue for clay soils since the contribution of f_0 to the volume of infiltration during the advance phase is insignificant relative to that of the transient term, or in the case of the linear infiltration function, the cracking term (Mailhol and Gonzalez 1993). Simulations (e.g. SIRMOD) using infiltration parameters estimated solely from advance measurements usually provide adequate reproductions of the measured advance data but often fail to predict measured runoff volumes and recession trajectories. The accurate simulation of advance is not essential as the purpose of irrigation evaluation is to calculate values of irrigation performance, water use and uniformity. Hence, it is more important to gain accurate knowledge of the infiltrated profile and runoff hydrograph rather than the advance trajectory.

The wetted perimeter dependent nature of infiltration presents a significant problem for furrow irrigation. The sensitivity of infiltration rates to wetted perimeter is greatest during the early stages of the advance phase but is much lower during the storage phase. For this reason those approaches that utilise measurements collected during both the advance and storage phases perform favourably compared to the simple inverse solution of advance (Sepaskhah and Afshar-Chamanabad 2002). This is

particularly important for every-other or widely spaced irrigation where the infiltration potential is greater.

The surface storage component makes up a significant proportion of the volume balance during the advance phase. This can be an issue considering that its value is based on a simplification of the physical model. The simplifying assumption found in equation 4-8 introduces an unknown error into the volume balance model. Such errors are significant where the volume stored on the soil surface accounts for a large proportion of the inflow volume. Over time, the volumes of inflow, infiltration and later, runoff (Eq. 4-1) continue to increase while the surface storage component firstly follows a semi-constant ratio of the advance distance and then remains essentially static during the storage phase. Therefore, any inaccuracy in the assumed value of σ_y looses importance where infiltration parameters are estimated from runoff measurements or other data collected during the storage phase.

The relationship of the surface storage volume to the upstream conditions changes after the completion of the advance phase. Generally, the value of the surface storage coefficient will increase as infiltration rates decline and the water level at the downstream end increases. Renault and Wallender (1997) determined that σ_y was equal to 0.91 for the storage phase. Sepaskhah and Afshar-Chamanabad (2002) adopted the constant ratio for σ_y during the advance stage but during the storage phase the volume was calculated from water depth measurements spaced at 10 m increments along the field length. Scaloppi et al. (1995) instead developed an expression that calculates the surface water depth at any point within the standard shape of the advance profile:

$$y = y_0\left(1-\frac{s}{x}\right)^{\beta} \quad \text{..... Eq 4-17}$$

where y is the flow depth (m) at some distance s (m) from the supply end, x (m) is the current length of the advance profile, and β is the curvature constant. The empirical parameter β usually ranges between 0.25 and 0.45 with Scaloppi et al. (1995) proposing a value of 0.35 for typical surface irrigated fields.

Previous studies have demonstrated the benefits of including data collected during the storage phase in the calibration of the infiltration function. Scaloppi et al. (1995) modified the volume balance equation to estimate the parameters of the infiltration function based on the advance phase, runoff phase or a combination of both and found that parameters based on both phases provide superior predictions of irrigation measurements when compared to those derived from the advance or runoff separately.

4.2.4 Variable Inflow

The constant inflow requirement is one of the most restrictive limitations if not the greatest limitation of the volume balance model. Procedures based on the inverse solution from field data assume perfectly managed water application where inflow rates remain steady for the duration of the irrigation. It is true that variations in slope and roughness both influence the shape and magnitude of the advance curve but the variation in inflow rates has an overriding effect (Renault and Wallender 1996). From the expression for the advance (Eq. 4-10), a temporary increase in the inflow will cause the upstream area of flow to change thereby changing the surface storage. The extra surface storage translates to increased advance rates for that period, hence also altering the subsurface water distribution. Similarly during the runoff phase, a change in inflow rates will immediately alter surface storage volumes and at some later time cause variations in the runoff rates.

Considering the inverse solution, variations in inflow rates have significant influence over the calibrated infiltration function. Experience using the INFILT technique suggests that a seemingly small change in the constant inflow rate can have considerable implications for the values of the individual parameters, the magnitude of infiltrated depths and to a lesser extent, the form of the infiltration curve. Therefore, it is postulated that temporal changes in intake discharges during the irrigation event will have a similar influence over the soil intake function. It would be expected that the effect would be more evident within the shape of the estimated infiltration curve than the total cumulative applied depth.

The majority of inverse techniques and irrigation models employ the step inflow approach (otherwise known as the constant inflow assumption) to simplify the solution procedure. This practice is not exclusive to the volume balance model as it is also commonplace amongst some of the more complex simulation techniques (e.g. SIRMOD II). Step inflow implies that the inflow commences at time zero, immediately reaches its final constant rate (Q_0), and remains at that level until the cut-off time where it instantly declines back to zero. The step inflow assumption is purely an idealised representation. In practice the inflow will always experience some form of variation, (particularly during the initial minutes of the irrigation) as even the best managed systems require a certain period for the discharge to stabilise. This initial variation in inflow rate may adversely affect the performance of the infiltration calibration process, especially where the technique is based on advance data alone (Renault and Wallender 1996).

Some alternative forms of surface irrigation include designated changes in inflow rates but for the most part system design and management strive for uniform discharges over time and space. Despite best efforts, the greatest majority of furrow irrigation systems suffer from time-variant discharges, particularly during the first moments of the irrigation. Often the variable nature of inflow rates is only identified during analysis of field data. Here the extension officer or consultant must decide either to ignore the issue at the expense of accuracy or discount the evaluation and wait for following irrigation events. Depending on the timing and magnitude of an inflow variation, it can have significant impacts on the application efficiency, requirement efficiency and distribution uniformity (Gharbi et al. 1993). Hence, it can be concluded that techniques that ignore these influences during the calibration of intake functions and the following simulation and evaluation process will be unable to correctly identify the field performance.

4.3 IPARM Model Development

For the inverse method developed herein, the original expression for infiltration (Eq. 4-2) is modified to include the cracking term C to account for that proportion of infiltration that occurs immediately on wetting.

$$Z = k\tau^a + f_0\tau + C \quad \text{..... Eq 4-18}$$

Similarly, the infiltration volume of equations 4-5 and 4-9 is modified by including the cracking volume Cx. Hence, equation 4-10 becomes:

$$x = \frac{Q_0 t}{\sigma_y A_0 - \sigma_{z1} k t^a + \sigma_{z2} f_0 t + C} \quad \text{..... Eq 4-19}$$

No shape factor is required for the cracking volume (Cx) because unlike the other terms of the infiltration equation, its magnitude is independent of the opportunity time.

4.3.1 Advance Phase

Where more than two advance points are available equations 4-11 and 4-12 can be applied to one of the middle points and the final advance point to produce suitable starting estimates for p and r. The values of p and r are refined using a non-linear regression scheme to minimise the difference between measured advance times and those predicted using the power advance function (Eq. 4-4).

The upstream area of flow (A_0) for the surface storage term (Eq. 4-8) can be either: (a) estimated directly, (b) calculated from field measurements of water depth or (c) estimated based on the flow rate by solution of Manning's equation:

$$Q_0 = \frac{1}{n} S_0^{\frac{1}{2}} \frac{A_0^{\frac{5}{3}}}{P_0^{\frac{2}{3}}} \quad \text{..... Eq 4-20}$$

where Manning n is an empirical parameter based on the surface roughness, S_0 is the field slope and P_0 is the upstream wetted perimeter corresponding to A_0.

Estimation of the surface storage through either the measured depth or flow rate requires an expression to calculate the cross-sectional area and wetted perimeter from

values of water depth. In IPARM, the furrow geometry is described as a power curve with provision for a flat bottom. Other models use similar equations (e.g. Scaloppi et al. 1995; Sepaskhah and Afshar-Chamanabad 2002) but have no allowance for the flat bottom. The expression proposed here, and used within IPARM to relate the dimension of upper flow width with respect to depth is:

$$W = W_B + cy^m \quad \text{..... Eq 4-21}$$

where W is the top width of flow, W_B is the bottom width of the furrow, y is the flow depth and c and m are fitted empirical parameters. In order to be compatible with the data requirements of SIRMOD, the values of c and m are determined from measurements of the total furrow height Y_T (m), the corresponding top width W_T (m), width at half the furrow height W_M (m) and bottom width W_B (m). Rearrangement of equation 4-21 and substitution of the measured dimensions results in two expressions to evaluate these parameters, which have a single value for each furrow cross section:

$$m = \frac{\log\left(\frac{W_T - W_B}{W_M - W_B}\right)}{\log(2)} \quad \text{..... Eq 4-22}$$

$$c = \frac{W_T - W_B}{Y_T^{\,m}} \quad \text{..... Eq 4-23}$$

Once the upstream depth of flow is known, the corresponding flow area (A_0) is calculated from the integral of equation 4-21 between $y = 0$ and y_0.

$$A_0 = W_B y_0 + \frac{c y_0^{\,m+1}}{m+1} \quad \text{..... Eq 4-24}$$

It is not possible to devise a similar simple formulation for the wetted perimeter. Hence, the wetted perimeter is expressed in terms of the sum of a large number of small elements. A furrow width is calculated for each increment of furrow depth and the perimeter is calculated by drawing straight lines between adjacent calculated points:

$$P_0 = W_B + 2\sum_{i=1}^{num}\sqrt{\left(\left(\sqrt{c}\right)\left(\left(\frac{i}{num}y_0\right)^m - \left(\frac{i-1}{num}y_0\right)^m\right)\right)^2 + \left(\frac{1}{num}y_0\right)^2} \quad \text{..... Eq 4-25}$$

Within IPARM, the water depth is divided into up to 500 increments (*num*).

The resultant value for A0 is substituted into the surface storage volume (Eq. 4-8). The completed model, IPARM contains three different options to calculate the surface storage coefficient σ_y. By default a value of σ_y = 0.77 is assumed. Alternatively, the user can calculate this coefficient by integrating the flow area (Eq. 4-24) over the wetted length of furrow where the flow depth is given by equation 4-17. The constant term, β of equation 4-17 can be specified by the user or calibrated from measured depths at the inlet and midpoint of the surface profile during the advance phase. Within IPARM, this term defaults to β = 0.25 as this value was found to result in a surface storage coefficient of $\sigma_y \approx 0.77$ during the advance phase for most furrow geometry shapes. The infiltration terms of the volume balance equation remain as defined for the Two Point and INFILT methods (i.e. Eq. 4-9).

4.3.2 Runoff Phase

During the storage phase, the expressions for the subsurface storage are no longer directly proportional to the infiltrated depth at the upstream boundary. The values of σ_{z1} (Eq. 4-6) and σ_{z2} (Eq. 4-7) become functions of time that slowly approach unity. The coefficient of the unsteady term (σ_{z1}) can be represented by an incomplete gamma function approximated by the following binomial expression (Scaloppi et al. 1995):

$$\sigma_{z1} = \left[\begin{array}{l} 1 - \frac{ar\lambda}{r+1} + \frac{a(a-1)r\lambda^2}{2!(r+2)} - \frac{a(a-1)(a-2)r\lambda^3}{3!(r+3)} + \\ \frac{a(a-1)(a-2)(a-3)r\lambda^3}{4!(r+4)} - \frac{a(a-1)(a-2)(a-3)(a-4)r\lambda 4}{5!(r+5)} + .. - .. \end{array} \right] \quad \text{..... Eq 4-26}$$

And for the steady term;

$$\sigma_{z2} = 1 - \frac{r\lambda}{r+1} \quad \text{..... Eq 4-27}$$

where λ is the ratio of complete advance time ($T_{advance}$) to the current advance time (t).

$$\lambda = \frac{T_{advance}}{t} \quad \text{..... Eq 4-28}$$

During the advance phase, t is equal to $T_{advance}$, therefore λ is equal to 1. In this case, the wetted perimeter terms from the original formulation (Scaloppi et al. 1995) of equation 4-26 have been omitted to simplify the data requirements.

During the development of IPARM, it was found that computing any more than the first ten terms of the binomial sequence in equation 4-26 did not appear to change the value of the σ_{z1} coefficient. However, increasing the number to 20 improved the stability of the numerical procedure through reducing the random error in the objective function between adjacent iterations. In the original formulation, Scaloppi et al. (1995) multiplied equation 4-26 by the factor λ^r to simplify the numerical techniques where both advance and storage phases were included. This assumes that the advance trajectory for the transient term follows the power curve, hence removing the need for the distance x in that term in the volume balance equation. This approach was not considered in the development of IPARM since it may increase the significance of the power curve in the model and decrease the sensitivity of advance distance to the values of a and k. In addition, the advance distances are already known, therefore there is no benefit in removing the x variable from the volume balance equation. The expressions for the subsurface storage (4-26 and 4-27) also apply to the advance phase if $\lambda = 1$. Hence, IPARM uses these same expressions for the advance phase instead of the original terms (4-6 and 4-7) found within the Two Point method. Any difference between the two alternative formulations is minor.

During the storage phase, the advance trajectory is assumed to continue at the same velocity past the end of the field. An assumption that is only valid under open-ended furrow conditions with no impediment to runoff. From equation 4-17 an expression was developed to relate the surface storage coefficient of the storage phase σ_{ys} to that of the advance phase σ_y by assuming that the advance continues unimpeded past the end of the field:

$$\sigma_{ys} = \sigma_y \frac{x_t}{L}\left(1-\left(1-\frac{L}{x_t}\right)^{\frac{1}{\sigma_y}}\right) \quad \text{..... Eq 4-29}$$

where x_t (m) is the imaginary distance reached by the water front if the advance trajectory continues past the end of the furrow, calculated by evaluating equation 4-19 at time t. Note that this distance x_t is predicted using the volume balance equation, not by extrapolating the power advance function past the end of the field. The volume stored in the furrow at some time greater than the end of the advance phase but prior

to cut-off is calculated by replacing the surface storage coefficient in the original equation 4-8.

$$V_S = \sigma_{ys} A_0 L \quad \text{..... Eq 4-30}$$

The new formulations for the surface (Eq. 4-30) and subsurface storage (Eq. 4-26 and 4-27) are substituted into the volume balance equation to create a similar expression for the storage phase as that of the advance phase (Eq. 4-9):

$$Q_0 t = \sigma_{ys} A_0 L + \sigma_{z1} k t^a L + \sigma_{z2} f_0 t L + CL + V_R \quad \text{..... Eq 4-31}$$

Re-arrangement of this equation yields the expression to predict the runoff volume at a given time during the storage phase:

$$V_R = Q_0 t - \sigma_{ys} A_0 L - \sigma_{z1} k t^a L - \sigma_{z2} f_0 t L - CL \quad \text{..... Eq 4-32}$$

4.3.3 Depletion and Recession Phases

The equations developed in the previous sections apply exclusively to the advance and storage phases as they are only valid during the inflow time. A different set of equations are required to describe the hydraulic behaviour in terms of the volume balance during the depletion and recession phases (e.g. those presented by Walker and Skogerboe (1987)).

The length of time taken for the depth at the upstream end to reach zero after termination of inflow (i.e. the end of the depletion phase) may be calculated from (Walker and Skogerboe 1987):

$$T_{depletion} = \frac{V_f \left(1 - \sigma_y\right)}{Q_0} \quad \text{..... Eq 4-33}$$

where V_f is the volume of surface storage at the completion of the storage phase. The following example (Table 4-1), based on realistic field measurements will be used to demonstrate the relative importance of the depletion phase.

Table 4-1 Calculating the length of the depletion phase

Field Parameters	**Infiltration**
L = 565 m	a = 0.1410
Q_0 = 3.2372 L s^{-1} (0.1942 m^3 min^{-1})	k = 0.0323
A_0 = 0.02933 m^2	f_0 = 0.000228
σ_y = 0.77	C = 0.0
r = 0.7541 (from power curve)	
T_{co} = 560 min	

At t = 560 minutes calculate V_f:

Subsurface storage components for the imaginary advance past end of furrow.

σ_{z1} = 0.8977 *(from Eq. 4-26)*

σ_{z2} = 0.5701 *(from Eq. 4-27)*

x_t = (0.1942*560)/(0.77*0.02933+0.8977*0.0323*$560^{0.141}$+0.5701*0.000228*560)
= 654.6 m *(from Eq. 4-10)*

σ_{ys} = 0.77*(654.6/565)*(1-(1-565/654.6)$^{1/0.77}$) *(from Eq.* 4-29*)*
= 0.8247

Volume stored

V_f = 0.8247*0.02933*565 *(from Eq. 4-30*)
= 13.67 m^3

Length of depletion phase

$T_{depletion}$ = 13.67*(1-0.77)/0.1942
= **16.2 min**

The length of the depletion phase at 16 minutes (Table 4-1) is insignificant relative to the duration of the advance and storage phases at 424 minutes and 136 minutes, respectively. In this case, a typical logging interval of 5 or 10 minutes (Irrimate™ logging equipment (section 5.4.1)) would translate to a maximum of three measured runoff data points during this period.

Although the recession phase may account for a significant portion of the irrigation time (120 minutes for the example in Table 4-1), it has not been considered as part of this inverse procedure. Field observations have indicated that the recession trajectory does not reflect that of the simulation models since it is extremely sensitive to longitudinal variations in field slope and field roughness. Experimentation with SIRMOD has shown that the recession phase is influenced by the value of Manning *n* but insensitive to the infiltration parameters *a* and *k* (Walker 2005a).

Although the full hydrodynamic model can successfully predict water movement during depletion and recession, it is often difficult to reproduce observed data for these phases. Drainage of water from the field during recession is greatly influenced by small imperfections in ground levelling and surface roughness. In addition, these models generally require either free-flowing or blocked end conditions. Although the majority of fields in Australia are designed as free draining, in reality drainage is usually restricted to some extent by tail-drain dimensions, culvert design and placement, and pumping capacities. Therefore it was considered inappropriate to use measurements taken during these later stages to calculate infiltration except for well designed research trials.

4.3.4 Variable Inflow

4.3.4.1 Adjusting Surface Storage Based on the Inflow Discharge

IPARM accommodates variable inflow rates by simply replacing the $Q_0 t$ term found in the prediction of advance points (Eq. 4-19) and runoff volumes (Eq. 4-32) with the integral of the inflow hydrograph ($\sum Q(t)dt$) for each measured advance and runoff time point. The inflow rate at any given time is estimated by performing a linear interpolation between the two adjacent measured inflow times. This approach is sufficient in most cases due to the close spacing of inflow measurements (e.g. 5 minute intervals with Irrimate™ siphon or flume loggers (section 5.4.1)) and gradual changing nature of the inflow hydrograph.

Prior to optimisation, the model searches through the inflow hydrograph to locate the position of each advance and runoff time. Once this point is found, the inflow volume is determined by integrating the inflow hydrograph between that time and the irrigation start time. The surface storage for each point is estimated by interpolating the instantaneous inflow rate at the required time and then using trial and error of the Manning equation (Eq. 4-20) to calculate the upstream flow area in normal conditions.

This modification includes the implicit assumption that the advance distance or runoff volume at any time is determined by all the inflow up to that time. However, some of

the other assumptions included within the volume balance model may limit the capabilities of IPARM under extreme changes in discharge. As with previous methods, the exponent of the power advance function is present within the expressions for subsurface storage (equations 4-26 and 4-27). Hence, problems may occur when inflow rates cause advance trajectories to depart significantly from the conventional power curve shape. The power curve function (Eq. 4-4) will only cope with minor changes in inflow and will particularly struggle where inflow rates increase significantly causing the advance trajectory to reverse its usual concavity partway through the irrigation. Most importantly it is assumed that the volume temporally stored on the soil surface can be described by the same simple function based on the upstream area of flow (Eq. 4-8). Thereby, the model requires that the rate of inflow change is slow and the surface storage has sufficient time to adjust to the new inflow rate. This approach will not function correctly where the inflow changes suddenly or cope with data collected after the time of cut-off.

4.3.4.2 Surface Storage Smoothing Technique

The simple approach used by IPARM to account for inflow variation causes the surface storage to change immediately on any change in inflow. This can be a problem where the inflow rates change significantly over a short space of time. In reality, the shockwave resulting from the inflow change will propagate downstream and take some time to reach the advance front or the end of the furrow in the case of the storage phase. The volume balance in pure form is unable to represent this phenomenon since it assumes that surface storage is proportional to the current upstream flow area. An alternative approach, Surface Storage Smoothing (SSS) was proposed to calculate the surface storage by averaging the cross sectional area over the time taken for the influence of the inflow change to reach the advancing water tip or end of the field. This averaging time could be based on application of a kinematic approach, wave propagation theory or simply an arbitrary pre-determined time period.

If the change in discharge is sudden, the movement of the disturbance downstream can be likened to the behaviour of a surge wave. The speed at which a positive surge wave moves downstream V_w (m s^{-1}) is given by (Featherstone and Nalluri 1995):

$$V_w = V_C + V_2 \quad \text{..... Eq 4-34}$$

where points 1 and 2 are positions immediately upstream and downstream of the wave respectively, V_2 is the velocity of normal flow (m s^{-1}) at point 2 and V_C (m s^{-1}) is the wave celerity given by:

$$V_C = \left[\frac{g\left(A_1\bar{y}_1 - A_2\bar{y}_2\right)}{A_1 - A_2} \frac{A_1}{A_2} \right]^{\frac{1}{2}} \quad \text{..... Eq 4-35}$$

where $\bar{y}$ is the depth (m) of the centre of flow area A (m^2). This expression can be further simplified where the furrow can be approximated by a rectangular shape. In this case, y is calculated by dividing the cross sectional area by the width of flow:

$$V_C = \left[\frac{gy_1}{2y_2}\left(y_1 + y_2\right) \right]^{\frac{1}{2}} \quad \text{..... Eq 4-36}$$

Where the disturbance is small, this can be further simplified by forcing y_1/y_2 to approach unity.

$$V_C = \sqrt{gy} \quad \text{..... Eq 4-37}$$

For the purposes of the volume balance model, the depth y is evaluated by converting the current upstream area of flow to an average area using the surface storage factor (σ_y) and then dividing that area by the width of flow at that cross-sectional area. The velocity of normal flow within the furrow (V_2) is calculated by applying the Manning equation at the estimated average cross-sectional area of flow. This yields an approximate velocity for the surface storage disturbance and hence, the time taken for that disturbance to travel along the wetted furrow length (t_w in Figure 4-2). The upstream area for the surface storage equations 4-8 and 4-30 is estimated by averaging the upstream area over the predicted wave travel time based on past inflow rates and the Manning equation (4-20). The schematic in Figure 4-2 provides an overview of the numerical process.

Initial testing of the above approach yielded wave propagation times far in excess of that expected in the field. The expression for the wave celerity (V_C) indicates that a perturbation in the inflow will reach the downstream end of a typical field length (e.g. 500 m) in less than 10 minutes. To rectify this situation, the V_C term in equation 4-34 is ignored which assumes that a step change in inflow will travel at a velocity

equivalent to normal flow. A similar approach is used to model the water flow within an irrigated bay in the AIM model (Austin and Prendergast 1997). The AIM model uses a kinematic shock of velocity to predict the time taken for the influence of the up-stream depletion to reach the down stream end.

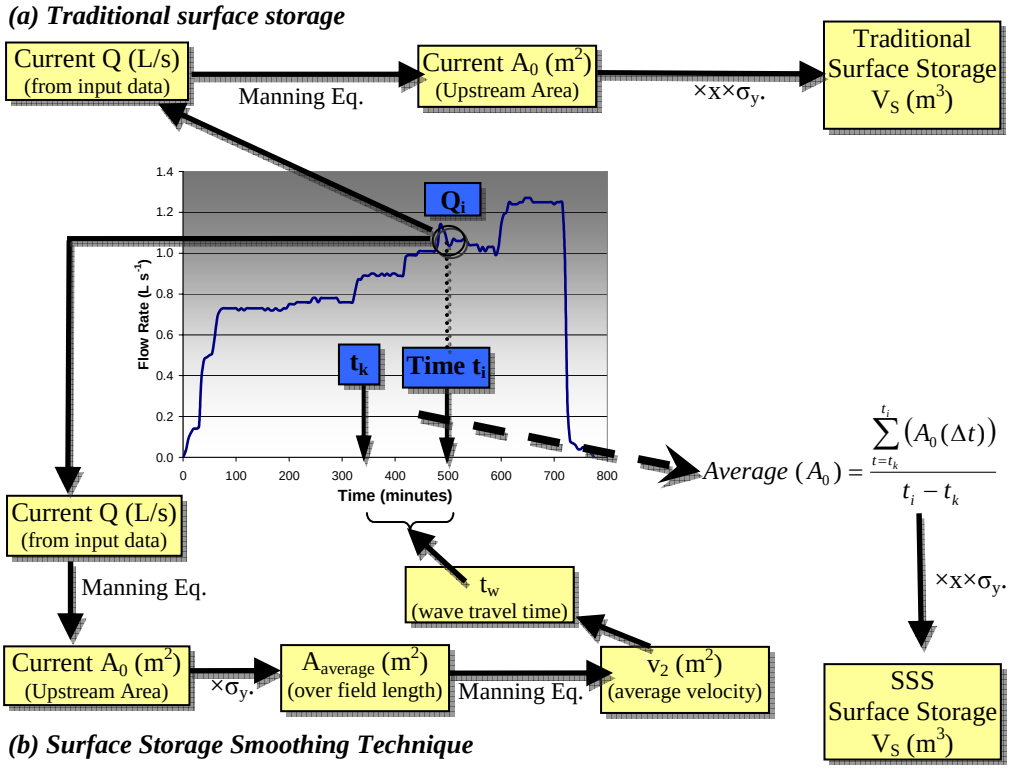

Figure 4-2 Explanation of the Surface Storage Smoothing calculation

In the original procedure, IPARM merely estimated a single value of the surface storage term $\sigma_y A_0$ for each inflow rate. The surface storage smoothing approach (SSS) differs in that the surface storage term is re-calculated depending on the velocity of the surface storage disturbance. This approach is merely a simple procedure to smooth out the effect of sudden changes in inflow rates. However, it should provide more appropriate predictions of surface storage compared to the original volume balance formulation. The averaging process should offer the greatest advantage where the advance and runoff measurements are widely spaced in time as the surface storage estimate is based on the upstream area over a period of time rather than an instantaneous value. Unless otherwise stated, all attempts to estimate the infiltration using IPARM contained within this dissertation use the original surface storage approximation (i.e. not using the surface storage smoothing approach).

4.3.5 Objective function

The numerical procedure attempts to minimise differences between measured irrigation data and results of computer simulation by altering the parameters of the soil intake function. The difference between predicted and measured data is expressed as a sum of square errors. For the advance phase this error is calculated using the expression originally used by INFILT (McClymont and Smith 1996) while including the cracking term C and correcting the inflow volume term in the numerator to accommodate variable inflow hydrographs:

$$SSE_{advance} = \sum_{i=1}^{N_a} \left[x_i - \frac{\sum_{t=0}^{t_i} Q(t)dt}{\sigma_y A_{0i} + \sigma_{z1} k t_i^{\,a} + \sigma_{z2} f_0 t_i + C} \right]^2 \quad \text{..... Eq 4-38}$$

This expression is evaluated at all of the non-zero advance measurements, i up to the last measurement N_a.

Similarly, the equation for prediction of runoff volume (Eq. 4-32) is re-arranged to produce an error term for the difference between measured and predicted runoff volumes where N_r is the number of runoff measurements taken during the storage phase:

$$SSE_{runoff} = \sum_{i=1}^{N_r} \left[V_{R_i} - \left(\sum_{t=0}^{t_i} Q(t)dt - \sigma_y A_{0i} L - \sigma_{z1} k t_i^{\,a} L - \sigma_{z2} f_0 t_i L - CL \right) \right]^2 \quad \text{. Eq 4-39}$$

Each error is non-dimensionalised by dividing by the sum of squares of the measured advance distances and runoff volumes, respectively to eliminate problems that arise due to both the difference in units and numbers of measured points. Generally, the advance distance will be greater in magnitude whilst the runoff predictions are expected to have larger relative errors. Taking this into account the two halves of the objective function are combined using a weighting factor, w.

$$Objective.function = \left(\frac{SSE_{advance}}{\sum_{i=1}^{N_a} x_i^{\,2}} \right) + w \left(\frac{SSE_{runoff}}{\sum_{i=1}^{N_r} V_{ri}^{\,2}} \right) \quad \text{..... Eq 4-40}$$

This factor is set by the user according to the relative importance and/or accuracy between the advance and runoff data sets. A value of w = 1 (100%) will give equal weighting between the two errors while increasing w will increase the sensitivity of the infiltration curve to the runoff data. Where no runoff data is available the objective function is calculated in the same way except the bracketed term following the weighting factor is removed.

At first glance, it may appear more appropriate to re-arrange the equations to express both halves of the objective function as errors in time measurements. It should be easy to combine the errors in the predicted advance and runoff data since they are presented in the same units. A pre-cursor of IPARM used this approach. However, solving for unknown advance and runoff time required excessive numbers of computations since many of the terms within the volume balance model (e.g. the subsurface shape factors in equations 4-26 and 4-27) are time dependent. Hence, this approach required large numbers of iterations merely to calculate a single advance or runoff time. By contrast solving for advance distances and runoff volumes within IPARM only requires a single iteration at each data point. As a result, the objective function converges rapidly to the solution with minimal stability problems. It should be noted that the infiltration parameters identified by the two different techniques are essentially equivalent.

4.3.6 Solution Scheme

Prior to the optimisation procedure, IPARM must process the supplied data to fit the furrow geometry relationship and evaluate the upstream flow areas. The power function (Eq. 4-4) is fitted to the advance measurements by a simple search style regression scheme in order to evaluate the value for r.

The optimisation scheme for the parameters of the Modified Kostiakov equation follows a similar procedure to that outlined by McClymont and Smith (1996) for the INFILT model. In that case, they attempted to solve for the parameters using the Steepest Descent and Newtons method but found that a simple “line-search”

technique provided the best results. The process outlined below has been developed from the INFILT approach, based on trial and evaluation.

(1) A starting estimate for each infiltration parameter is determined. Results differ slightly according to the values selected but experience has shown that the values in Table 4-2 facilitate rapid convergence to the optimal solution in the majority of cases. The initial step sizes are also pre-determined. The default values (Table 4-2) roughly follow the expected relative magnitudes of the parameters and have been refined during the design phase. Alternatively, the user may constrain one or more of the parameters to known values (e.g. setting f_0 to zero) and optimise the other parameters.

Table 4-2 Default starting estimates and initial step sizes for IPARM

Parameter	Starting Estimate	Initial Step Size	Lower Bound	Upper Bound
a	0.3	0.01	1.0×10^{-10}	0.9999
k	0.05	0.001	0	0.9999
f_0	0.0001	0.00001	0	0.9999
C	0	0.001	0	0.9999

(2) The parameter *a* is incremented in either direction until the objective function (Eq. 4-40) cannot be reduced any further. The number and direction of iterations are stored within the parameter Ja_{temp}.

$$a_{new} = a \pm Ja_{temp} Step_a \quad \text{..... Eq 4-41}$$

(3) This process is repeated for the remaining three parameters to arrive at improved estimates of *k*, f_0 and *C* and a record of the iterations is kept within Jk_{temp}, $Jf0_{temp}$, and JC_{temp}. Each *J* parameter contains both a magnitude and direction.

(4) The new J_{temp} values are added to the sum of the previous values of *J*, which in the case of the first iteration will be equal to zero.

$$\begin{aligned} Ja &= Ja + Ja_{temp} \\ Jk &= Jk + Jk_{temp} \\ Jf_0 &= Jf_0 + Jf_{0\,temp} \\ JC &= JC + JC_{temp} \end{aligned} \quad \text{..... Eq 4-42}$$

(5) The individual values from equation 4-42 for each parameter are combined to create a crude form of group step. All four infiltration parameters are incremented simultaneously using the following:

$$\begin{aligned} a &= a + G \times Ja \\ k &= k + G \times Jk \\ f_0 &= f_0 + G \times Jf_0 \\ C &= C + G \times JC \end{aligned} \quad \text{..... Eq 4-43}$$

Hence moving the values of the four parameters in the same direction as the individual steps. The value of *G* is included to reduce the size of each increment to some smaller proportion of the individual step sizes. In the absence of *G*, the group search tends to move too far past the minimum objective function in a single group step. The value for *G* is fixed at 0.01 within the code (i.e. it will take 100 group iterations to move the same distance as the sum of the individual iterations). The group iteration process continues until the objective function cannot be reduced any further.

(6) The values of *Ja*, *Jk*, Jf_0 and *JC* are stored and the optimisation continues back to step 2.

(7) When steps 2 through 6 fail to further reduce the error term the step sizes are divided in half, the values of *Ja*, *Jk*, Jf_0 and *JC* are set back to zero and the process commences at step 2.

This process is repeated 25 times in IPARM to arrive at the optimal set of infiltration parameters. Usually only minimal improvements are achieved with further iterations. Experience has shown that the parameters appear to change little and then converge suddenly within the space of one or two step size groups.

Note that the presence of the cracking term (*C*) within the model does not necessitate its use. The Modified Kostiakov equation should suffice in most conditions. Hence, *C* is ignored within the validation and is hidden from the user unless it is requested. Where IPARM is used to optimise all four infiltration parameters simultaneously, the

C value reduces that part of the infiltrated volume accounted by the transient term of the infiltration function (i.e. reduces the value of kt^a).

4.3.7 The IPARM Computer Software

The numerical optimisation technique was coded using Borland C++ Builder 6 to produce a stand-alone executable program that can be operated on any personal computer running under Microsoft Windows. IPARM is designed to be run under Windows XP or later versions. Some issues (with the user interface) may be encountered while attempting to use the program in the Windows 98/ME environments, mainly due to the limited multi-tasking capabilities of these operating systems. The graphical user interface (Figure 4-3 and Figure 4-4) has been designed to be simple and intuitive with online help available. IPARM does not have any specific system requirements but is best viewed on a screen with resolution greater than 800x600 pixels. After a number of minor versions, the first IPARM release version (1.1.2) (Figure 4-3) was completed in late 2005 and has been utilised for both research and commercial applications.

A second major release, IPARM V2 was developed (Figure 4-4) to incorporate some extra minor features and to address some of the operational problems with the initial release. Improvements in IPARM V2 include:

- choice of units for most inputs;
- automatic creation of SIRMOD input files from entered data and estimated infiltration parameters;
- option to use the alternative surface storage estimation (surface storage smoothing technique) for variable inflow (see section 4.3.4.2); and
- general improvements to the user interface.

Figure 4-3 Screen shot of main user interface for IPARM version 1.1.2

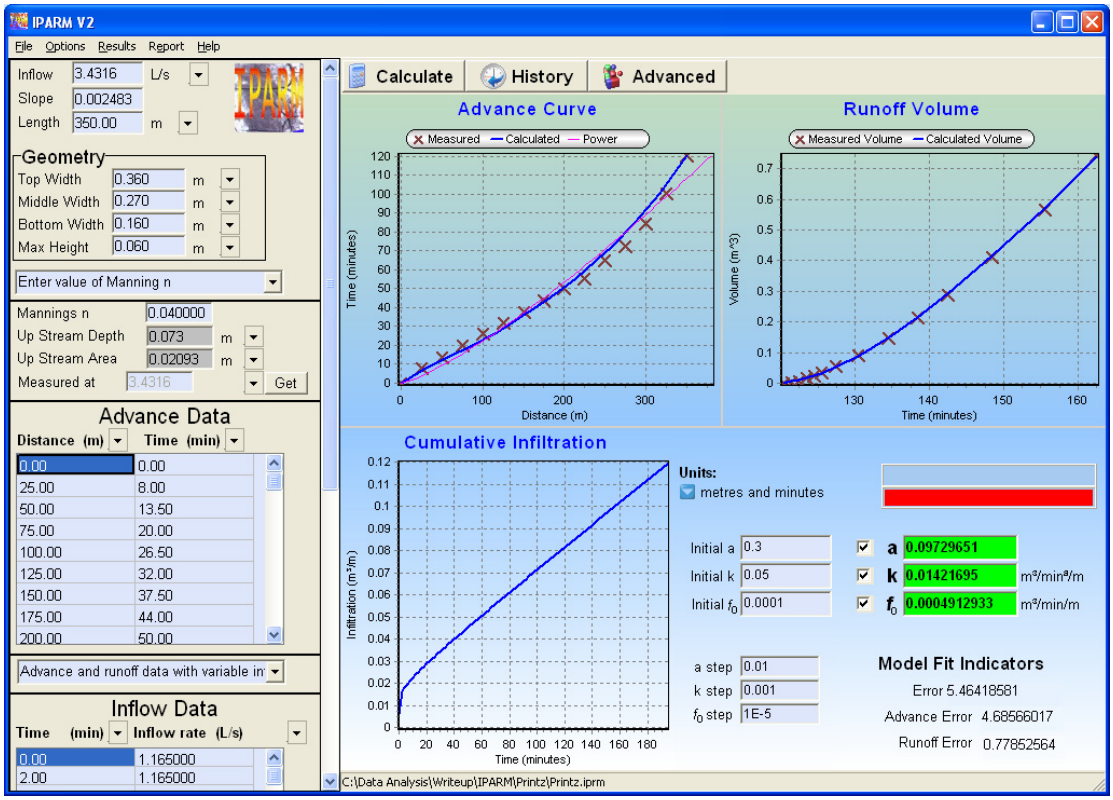

Figure 4-4 Screen shot of main user interface for IPARM version 2

4.4 Evaluation of IPARM

4.4.1 Input Data

A number of irrigation data sets were used to test and validate the IPARM technique. Data was selected to cover a range of soil types, field lengths, inflow patterns and irrigation durations. The inflow variation for each irrigation is presented in Figure 4-5, the dotted line indicates the relationship of the advance and storage phases to the hydrograph.

IPARM requires a value for Manning *n* to adjust the surface storage for changes in the inflow rate. The user may choose to calibrate *n* based on either a measured depth, estimated cross sectional flow area or in the absence of such information may configure the roughness directly. The furrow roughness cannot be measured directly and may vary considerably over the field. During the irrigation the flowing water will smooth the furrow thereby reducing the furrow roughness. Taking this effect into account, Trout (1992b) attempted to determine the relationship between roughness and flow velocity. They found that the inherent longitudinal velocity decline within a single furrow can cause a significant change in Manning's *n*. For example, the 30% reduction in flow rate as the water reaches the tail end of the field (Trout 1992b) caused a 50% higher roughness (i.e. 0.03 compared to the field average of 0.02). Other experimentation (Mailhol and Gonzalez 1993) has suggested the use of a *n* value of 0.05 for the first irrigation and 0.04 for subsequent irrigations. The value of *n* varies from 0.02 to above 0.36 for irrigated pasture (Robertson et al. 2004). Some typical values are 0.02 to 0.03 for very smooth furrows and 0.05 to 0.06 for very rough furrows (ASAE 2003). The US Soil Conservation Service (SCS) recommends a value of $n = 0.04$ for smooth bare soil (ASAE 2003; Clemmens 2003), hence this value is used throughout the dissertation in the absence of any description of the furrow surface condition.

4.4.1.1 Benson

The Benson irrigation was carried out in Colorado, USA on a clay loam soil (Walker 2005a). This event was selected as an example of an irrigation where the advance phase (199 minutes) only comprises a small portion of the inflow time relative to the

storage phase (506 minutes). In addition, the inflow rate experienced a significant decrease (1.11 to 0.79 L s^{-1}) during the advance but was relatively stable throughout the storage phase. No information was provided regarding the depth of flow, therefore Manning's *n* was estimated. Walker (2005a) has used a value of 0.015 which is indicative of smoother surfaces such as concrete or wood (Chow 1959), instead a value of $n = 0.02$ was used in this analysis.

4.4.1.2 Printz

The Printz data set was collected in Colorado, USA on a loamy sand soil (Walker 2005a). Both the Printz and Benson data sets were used to verify the multilevel calibration of infiltration parameters by SIRMOD (Walker 2005a) and comparisons with the results from the Walker (2005a) paper serve as further validation of IPARM. No information on flow depth or surface condition was available therefore the roughness was assumed to be equal to 0.04. The Printz inflow hydrograph displays minimal temporal variance (Figure 4-5.b) where the discharge requires approximately 17 minutes to reach steady-state conditions. For the purpose of the validation of IPARM this data was considered as having constant inflow.

4.4.1.3 Downs

The Downs data used here represents a single furrow (irrigation 2 furrow 3) from the Downs data set presented in chapter 5. This data was collected from a cracking clay soil typical of the Macalister district on the Darling Downs in southern Queensland (Dalton et al. 2001). This irrigation is typical of many in the Darling Downs area where the inflow is stopped a few hours after the water has reached the end of the field. The inflow hydrograph displays a characteristic instability during the first 30 minutes but afterwards is almost constant (Figure 4-5.c). Hence, this data is also considered as an example of constant inflow. No information was available regarding flow depths or surface conditions therefore the roughness was assumed to be 0.04.

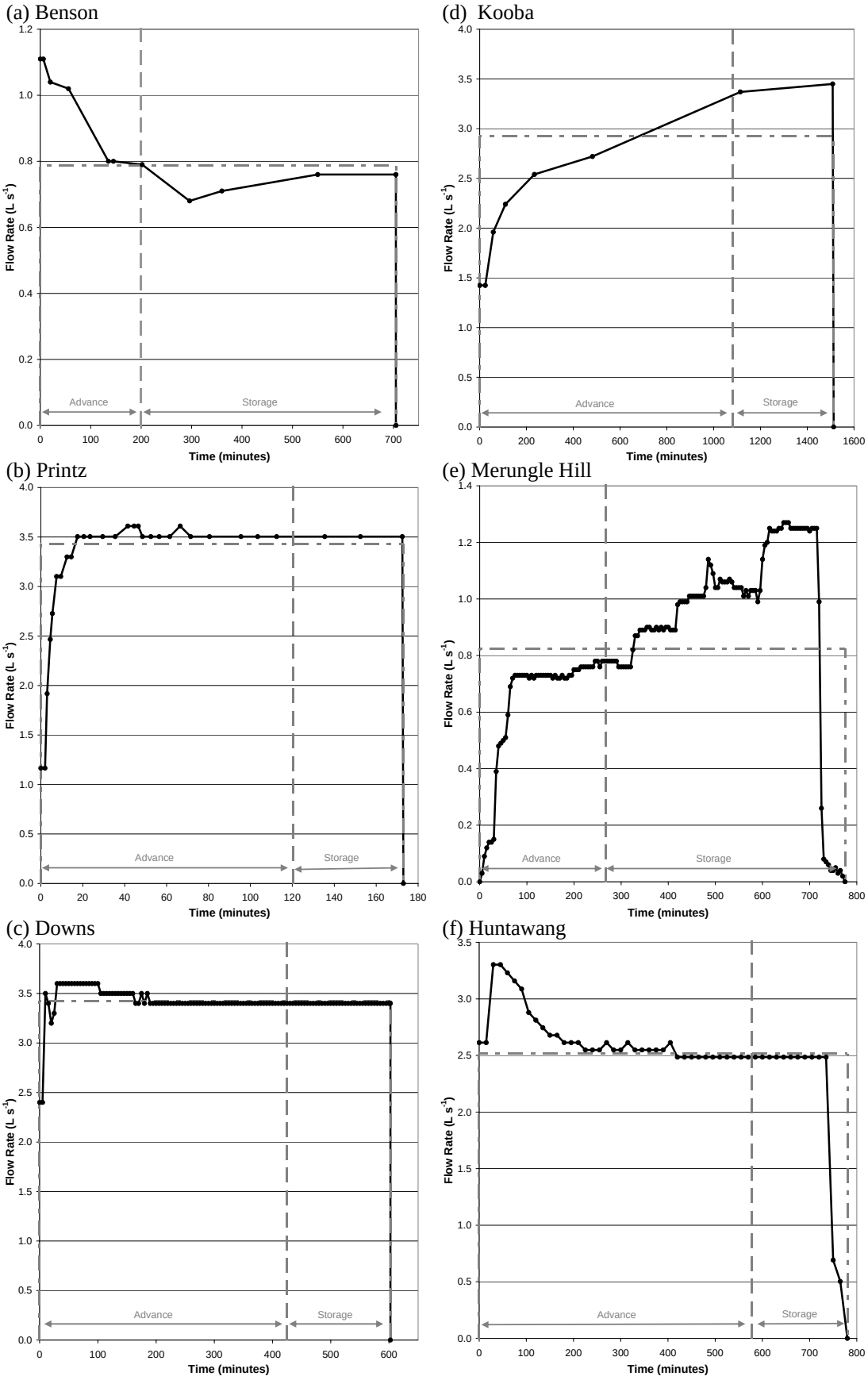

Figure 4-5 Measured inflow hydrographs for IPARM validation

4.4.1.4 Kooba

The Kooba irrigation data (Hornbuckle 1999) was collected on a cracking clay soil planted to maize in southern NSW. The data includes measurements from the same four irrigated furrows collected from three separate events during the 1998/1999 season. The data from irrigation 1 furrow 1 was selected for this evaluation. As previously, Manning *n* was assigned a value of $n = 0.04$ due to the absence of suitable flow depth measurements. In this example, the inflow increased 1.4 to 3.5 L s^{-1} over the entire irrigation duration. The majority of this inflow variation occurred within the advance phase (Figure 4-5.d). In this instance, only a limited number of runoff measurements were available to describe the outflow hydrograph therefore the weighting of runoff to advance data (*w* in Eq. 4-40) was set to 50%.

4.4.1.5 Merungle Hill

The Merungle Hill field data (Hornbuckle 1999) was obtained from a citrus orchard with wide furrow spacing and some weed and grass cover. Hence, Manning *n* was assumed equal to 0.2 to account for the anticipated increase in surface roughness arising from the surface conditions and low flow depths (resulting from the large furrow dimensions). As for Kooba, the inflow rate increased throughout the entire irrigation event. However, the majority of the increase took place during the runoff phase with the average inflow rate during the runoff phase being more than 50% larger than that of the advance phase (Figure 4-5.e). No information was available regarding the soil moisture deficit hence all calculations are based on a assumed value of 0.03 m (far in excess of the infiltrated depth).

4.4.1.6 Huntawang

The Huntawang data set (Hornbuckle J.W., 2005, personal communication) was collected in a cotton field near Griffith, NSW. In this case, the upstream flow depth was measured hence Manning *n* was estimated by assuming normal flow conditions. A flow depth of 117 mm at the average inflow rate of 2.516 L s^{-1} produced an *n* value of 0.0318 using the supplied furrow dimensions. The inflow rate decreased within the first 3 to 4 hours reaching its final value well before the onset of runoff (Figure 4-5.f).

4.4.2 Estimation of Infiltration Parameters

IPARM was used to estimate the parameters of the Modified Kostiakov equation for each data set using each of the following options:

1. Advance data only with constant inflow equal to the average inflow rate.
2. Advance data only with the measured inflow hydrograph.
3. Advance data and run-off hydrograph with a constant inflow equal to the average inflow rate.
4. Advance data and run-off hydrograph with the measured inflow hydrograph.

*Note that IPARM only accommodates runoff data collected during the storage phase.

Option 1 is comparable to traditional infiltration from advance schemes such as the INFILT optimisation. For options 3 and 4, the weighting of runoff to advance data (parameter *w* in equation 4-40) was maintained at 100% for all irrigations with the exception of the Kooba data set (explained in 4.4.1.4).

Calibration of the infiltration function was successful for all case studies with the results presented in Table 4-3. The advance and runoff errors were calculated using the relevant parts of the objective function (Eq. 4-40) and are provided as standard outputs of IPARM. The multiplication by 100 does not serve any other purpose than to simplify the user's understanding. The total error is the same value used to drive the optimisation process within IPARM.

$$Ad\_Error = 100 \times \left(\frac{SSE_{advance}}{\sum_{i=1}^{N_a} x_i^{\,2}} \right) \quad \text{..... Eq 4-44}$$

$$Run\_Error = 100 \times \left(\frac{SSE_{runoff}}{\sum_{i=1}^{N_r} V_{ri}^{\,2}} \right) \quad \text{..... Eq 4-45}$$

$$Total\_Error = Ad\_Error + w \times Run\_Error \quad \text{..... Eq 4-46}$$

The extra shaded line included for Benson and Printz (Table 4-3) contains the results of the multi-level calibration of infiltration parameters and Manning *n* presented by

Walker (2005a). In this case, the advance, runoff and total errors were calculated by entering the infiltration parameters into IPARM as starting estimates and constraining their values to prevent optimisation. The runoff errors for the calibrations using options 1 and 2 have been calculated in a similar way by constraining the parameter values and simulating the irrigation using options 3 and 4 respectively.

Table 4-3 Infiltration parameters and volume balance errors for IPARM validation

		a	*k*	f_0	Total Error	Ad Error	Run Error
Benson	Advance	0.0000	0.00334	0.000070	1.252	1.252	[a]73.008
	Advance, V. In	0.0292	0.00531	0.000069	0.701	0.701	[a]98.188
	Advance + Runoff	0.2956	0.00159	0.000045	4.944	3.190	1.754
	Advance + Runoff, V. In	0.2234	0.00333	0.000039	4.764	1.955	2.808
	Walker Multi[b]	0.2500	0.00297	0.000040	12.045	1.948	10.097
Printz	Advance	0.0000	0.02534	0.000373	5.213	5.213	[a]618.946
	Advance, V. In	0.0000	0.01973	0.000472	3.566	3.566	[a]357.760
	Advance + Runoff	0.0927	0.01558	0.000479	8.537	7.755	0.793
	Advance + Runoff, V. In	0.0973	0.01422	0.000491	5.464	4.686	0.779
	Walker Multi[b]	0.4000	0.00429	0.000420	342.717	11.496	331.221
Downs	Advance	0.0000	0.04746	0.000320	1.044	1.044	[a]54.848
	Advance, V. In	0.0000	0.04735	0.000326	0.269	0.269	[a]67.578
	Advance + Runoff	0.2926	0.01902	0.000148	5.625	4.165	1.460
	Advance + Runoff, V. In	0.3091	0.01807	0.000136	5.112	3.522	1.590
Kooba	Advance	0.0496	0.30395	0.000000	2.603	2.603	[a]64.511
	Advance, V. In	0.2234	0.09673	0.000000	2.610	2.610	[a]35.673
	Advance + Runoff	0.0236	0.29527	0.000136	7.870	4.278	7.183
	Advance + Runoff, V. In	0.2053	0.09288	0.000100	5.889	3.622	4.534
Merungle Hill	Advance	0.0000	0.04942	0.000000	1.107	1.107	[a]90.127
	Advance, V. In	0.0020	0.01948	0.000107	0.000	0.000	[a]24.963
	Advance + Runoff	0.2359	0.01486	0.000055	10.657	7.346	3.311
	Advance + Runoff, V. In	0.0000	0.01601	0.000138	5.066	1.702	3.364
Huntawang	Advance	0.2597	0.02127	0.000169	0.900	0.900	[a]28.888
	Advance, V. In	0.3038	0.02445	0.000070	1.834	1.834	[a]21.031
	Advance + Runoff	0.3017	0.01985	0.000118	3.542	1.754	1.788
	Advance + Runoff, V. In	0.1724	0.04062	0.000159	2.939	2.205	0.735

[a] The runoff error has been calculated by constraining all parameters in IPARM and simulating with runoff included.
[b] results from Walker (2005)
V. in = variable inflow, Ad = advance data, Run = runoff data

The individual values of *a*, *k* and f_0 vary considerably between the optimisation options of each irrigation. However, in most cases the general shape of the infiltration curve is preserved between the four calibration options. Parameter *a* tended to zero for the Benson, Printz, Downs and Merungle Hill irrigations when using constant inflow and advance data. This could be considered as a limitation of the approach or for some fields (i.e. Downs) may reflect the cracking nature of the soil.

The small advance and runoff errors (Table 4-3) indicate that IPARM is predicting values close to the measured data. Generally, the use of the full inflow hydrograph (as opposed to the constant inflow assumption) reduced the advance error indicating that the volume balance was providing an improved fit to the measured advance trajectory. Considering the advance data, there appears to be a clear advantage in moving from the constant inflow calibration options 1 and 3 to the variable inflow in options 2 and 4, respectively. The reduction in runoff error between options 3 and 4 is not as evident as in half of the cases studies the error increased when moving to the variable inflow option. The general reduction in total volume balance error when using the variable inflow option demonstrates an improved overall fit to the measured data and therefore improved estimates of the three infiltration parameters.

The runoff errors calculated when using advance data alone demonstrates the failure of the resultant infiltration parameters to adequately describe the behaviour during the storage phase. In a number of cases these errors approach 100 and for Printz far exceed 100. Although the function for the runoff error is not linear, a value above 100 (from Eq. 4-45) indicates that the average error in the runoff volume prediction for each data point is above 100%. Owing to the empirical form of the infiltration function, it is more appropriate to study the performance of IPARM by observation of the infiltration curves (Figure 4-6). Relying only on advance data does not appear to introduce a systematic error into the infiltration function. Infiltration estimated from advance measurements overestimated the cumulative infiltration at the end of the irrigation time for the Benson and Downs data and underestimated for the Printz, Kooba and Merungle Hill data. However, the difference in cumulative volume is relatively insignificant at short opportunity times while the curves devised using advance data and advance plus runoff data tend to diverge as opportunity time increases. In most cases these two infiltration curves intersect in close proximity to the advance completion time. The proportional difference between the two curves will continue to increase when these curves are used to predict the infiltration volume for opportunity times greater than the measured times (Figure 4-6). This has enormous implications if the infiltration parameters are to be used in simulation or irrigation management at times greater than the advance time.

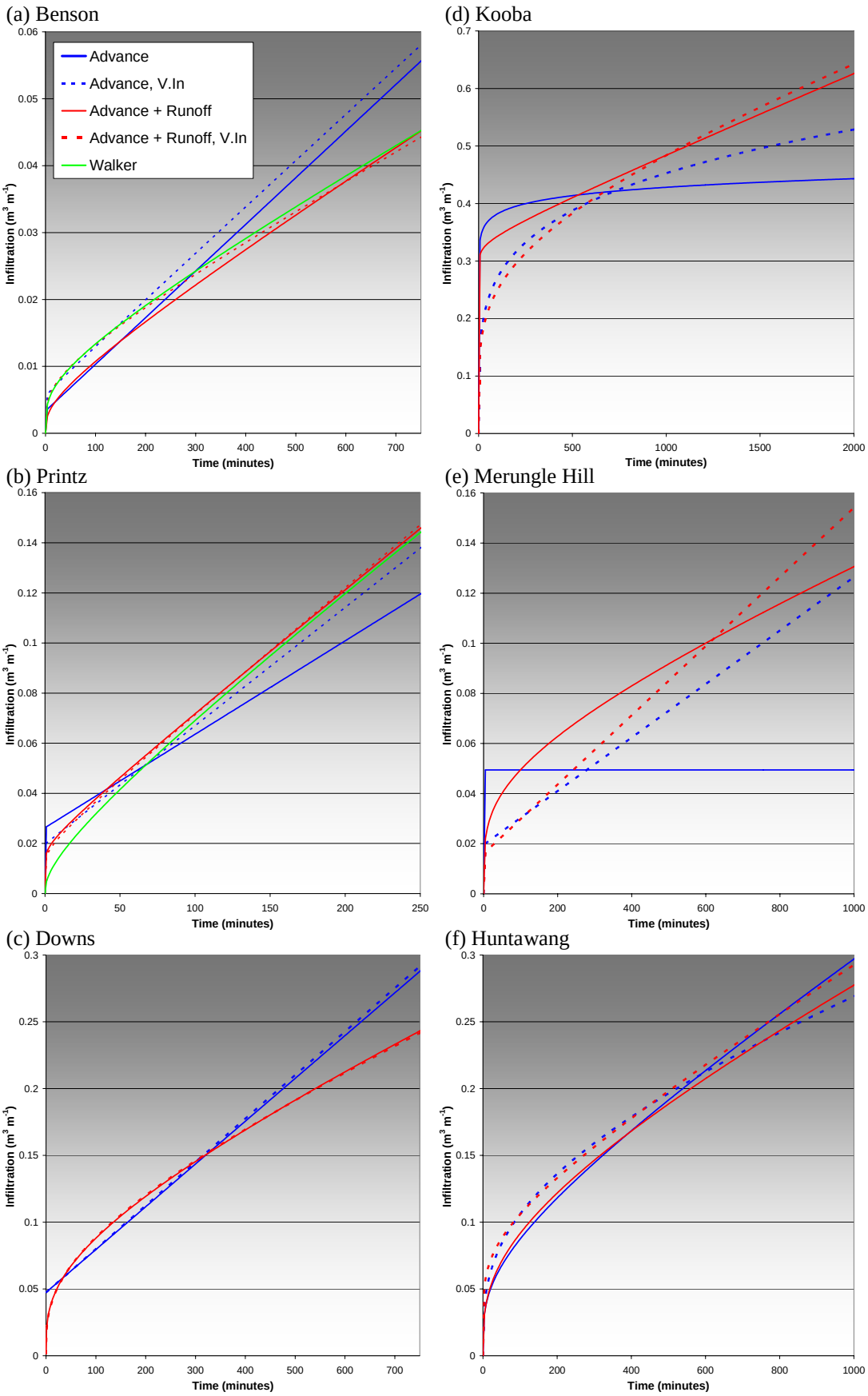

Figure 4-6 Calibrated infiltration curves for IPARM validation

The use of the variable inflow hydrograph altered the shape of the infiltration curve in all irrigations. The larger the variation in inflow rates the larger the difference between the infiltration curves. For the two irrigations where the inflow rate decreased over time (Figure 4-6.a and Figure 4-6.f), the infiltration curve derived using a constant inflow assumption underestimated the intake at early stages but tended to overestimate at longer times. The opposite behaviour can be seen in the Kooba (Figure 4-6.d) and Merungle Hill (Figure 4-6.e) irrigations where the inflow rate increased throughout the irrigation. Hence, using the average inflow rate in the calibration process introduces a systematic error into the estimated infiltration parameters, the form of which appears to depend on the shape of the inflow hydrograph. Where these infiltration parameters are used to simulate irrigation performance for a similar time, any difference in predicted efficiency and uniformity may be minor owing to the tendency of the infiltration curves to intersect close to the cut-off time. However, the process of irrigation optimisation typically involves the alteration of inflow time. Hence, the error introduced by the use of the constant inflow assumption will become more apparent.

It is also possible to estimate the final infiltration rate f_0 using the difference between inflow and outflow rates. This approach is only valid where the inflow is relatively constant and the runoff has reached final steady state conditions. The irrigations studied generally satisfy these criteria (except for Merungle Hill, and to a lesser extent for Kooba where the inflow remains unsteady). From final steady inflow and outflow discharges, the values of f_0 were found to be 0.000047 for Benson, 0.000525 for Printz, 0.000230 for Downs, 0.000172 for Kooba and 0.000212 for Huntawang. In all cases, these are higher than the values of f_0 estimated using IPARM with advance and runoff data using either a constant average inflow or the full inflow hydrograph (Table 4-3). Presumably, this indicates that the final steady intake rate was not achieved during the irrigation time or that the IPARM optimisation routine biases an underestimation of this parameter.

The accuracy of the estimated infiltration parameters can be further illustrated through a demonstration of the cumulative infiltrated volume for the whole field over time.

Figure 4-7 contains results of the four irrigations with variable inflow conditions. The "actual infiltration" volume (shown as the thin black line) is calculated by re-arrangement of equation 4-1 to make V_I the dependent variable where the inflow term has been replaced with the measured inflow hydrograph. The surface storage (V_s) term is computed by IPARM using equation 4-8 for the advance and equation 4-30 for the storage phase. The "predicted infiltration" was found by evaluating the volume balance infiltration term (equation 4-5) at each measured time using the calibrated Kostiakov parameters where the advance distances are the values predicted by IPARM. The four lines correspond to the four different combinations of input data.

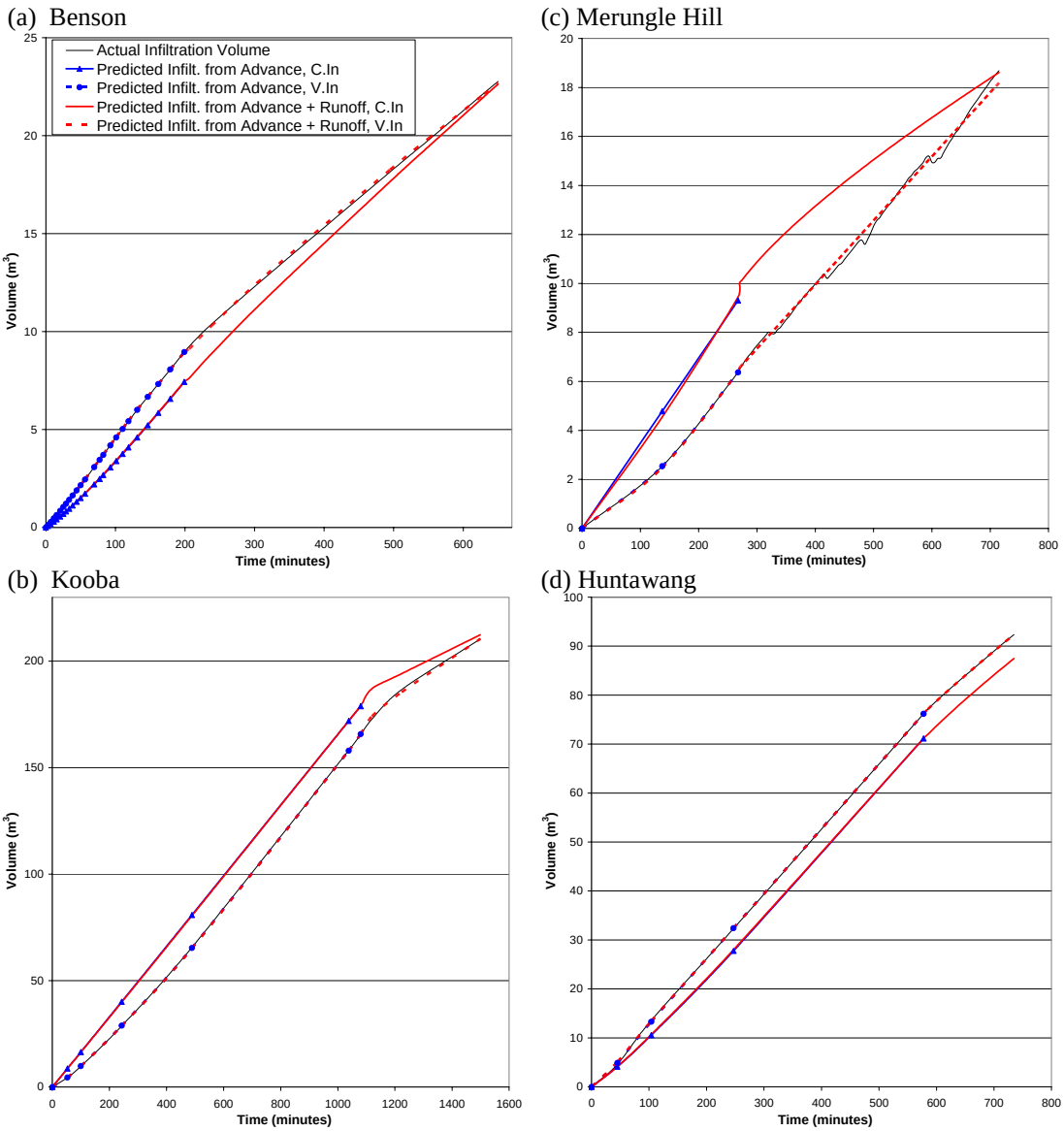

Figure 4-7 Cumulative infiltrated volumes comparing infiltration from the volume balance (actual/measured) with predicted infiltration from parameters estimated from the advance and storage phases

The stepping phenomenon, clearly visible in the "actual infiltration" line for the Merungle Hill site (Figure 4-7.c) was caused by the surface storage term reacting too quickly to the rapid variations in the inflow rate. An improved approach to estimate the surface storage may eliminate this behaviour.

In each of the irrigations presented in Figure 4-7 the actual infiltration line was best reproduced by those infiltration parameters derived using variable inflow. Where runoff data was available spanning the entire irrigation time, all lines converged at the end of the irrigation indicating that the use of the constant inflow may provide satisfactory estimates of final infiltrated volumes at the measured irrigation duration but is not appropriate for any other time, particularly mid-way through the irrigation. The predicted infiltration volume was equivalent during the advance phase regardless of whether runoff was used to estimate the infiltration parameters. This provides further evidence that the inclusion of runoff does not compromise the volume balance fit to the advance phase.

4.4.3 Validation of the Surface Storage Smoothing Approach

The surface storage smoothing (SSS) approach to calculate the surface storage offers an improved estimate for the volume balance where the inflow changes rapidly. Infiltration parameters were re-calculated using this alternative surface storage for each case study using either advance data or advance and runoff data with the variable inflow hydrograph. Comparing the results (Table 4-4) with the corresponding values from the original surface storage estimation (Table 4-3) indicates that the SSS technique has some effect on the values of a, k and f_0. The smoothing approach appeared to reduce the advance and total volume balance errors in the majority of cases where the measured inflow was varying (i.e. excluding Printz and Downs). However, the difference observed amongst the infiltration parameters failed to translate into a significant change in the infiltration curve. The greatest difference between the two methods occurred for the Kooba irrigation using advance and runoff (Figure 4-8.a). The small difference visible for the Merungle Hill (Figure 4-8.b) infiltration curves is more typical of the other case studies.

Table 4-4 Infiltration parameters from IPARM using the surface storage smoothing (SSS) approach

		a	*k*	f_0	Total Error	Ad Error	Run Error
Benson	Advance, V. In	0.0000	0.00565	0.000072	0.677	0.677	[a]99.368
	Advance + Runoff, V. In	0.2334	0.00320	0.000039	4.775	2.307	2.468
Printz	Advance, V. In	0.0000	0.01987	0.000469	3.688	3.688	[a]371.778
	Advance + Runoff, V. In	0.0972	0.01422	0.000491	5.629	4.850	0.779
Downs	Advance, V. In	0.0000	0.04724	0.000326	0.320	0.320	[a]67.961
	Advance + Runoff, V. In	0.3084	0.01812	0.000136	5.162	3.577	1.585
Kooba	Advance, V. In	0.2237	0.09664	0.000000	2.605	2.605	[a]35.218
	Advance + Runoff, V. In	0.2716	0.06640	0.000051	7.827	4.256	3.570
Merungle Hill	Advance, V. In	0.0341	0.01705	0.000109	0.000	0.000	[a]21.112
	Advance + Runoff, V. In	0.0000	0.01626	0.000140	3.408	1.314	2.094
Huntawang	Advance, V. In	0.3098	0.02346	0.000072	1.523	1.523	[a]15.549
	Advance + Runoff, V. In	0.1871	0.03804	0.000153	2.856	1.982	0.874

[a] The runoff error has been calculated by constraining all parameters in IPARM and simulating with runoff included.
V. in = variable inflow, Ad = advance data, Run = runoff data

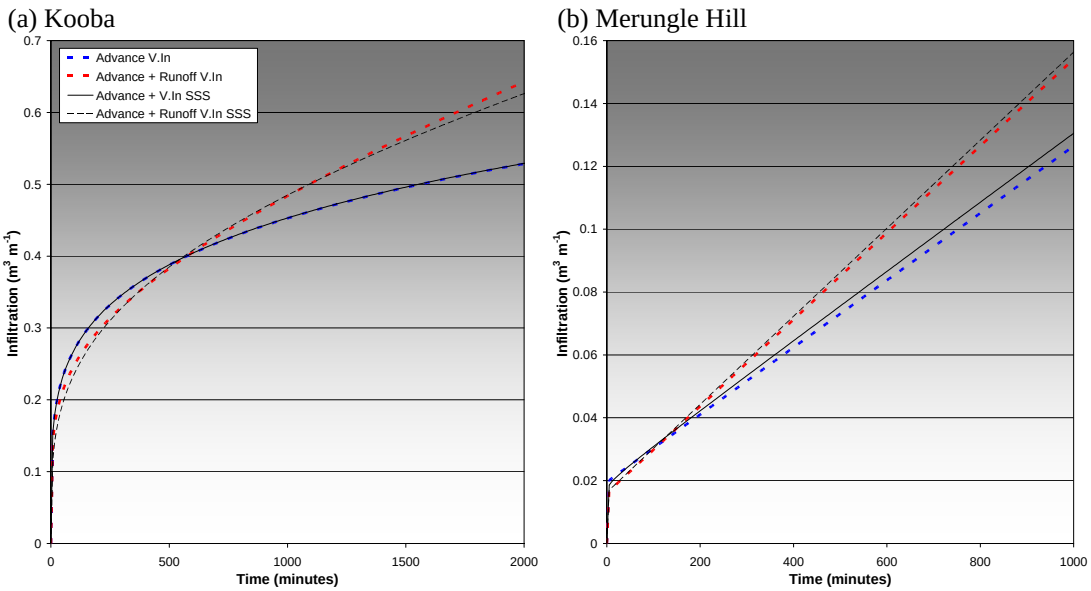

Figure 4-8 Comparing infiltration curves estimated using the variable inflow hydrograph between original surface storage and surface storage smoothing (SSS) technique

Figure 4-9 shows the volume of surface storage calculated using the constant inflow, original variable inflow and surface storage smoothing approximations. The alternative approach based on normal flow and wave celerity has been included for comparison with the adopted surface storage adjustment. The surface storage smoothing approach using wave celerity clearly failed to remove the perturbations in the actual infiltrated volume for Merungle Hill (Figure 4-7.c) since it did not have any significant effect on the estimation of the surface storage volume (Figure 4-9,

Variable Inflow SSS with Celerity). The expression for the wave celerity grossly overestimated the speed of the cross-sectional area change. However, the surface storage smoothing approach using only the equation of normal flow (i.e. *Variable Inflow SSS without Celerity*) successfully smoothed the sudden alterations in discharge.

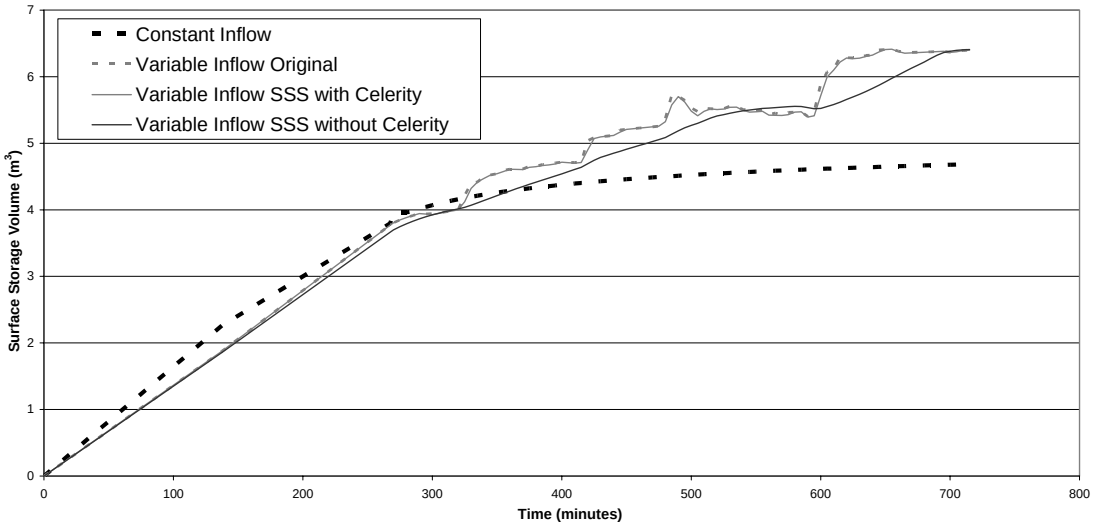

Figure 4-9 Comparing the surface storage smoothing (SSS) calculation with the standard variable and constant inflow approach (Merungle Hill data)

Although the SSS technique appeared to reduce the error in the surface term, further research is required to improve the derivation of the averaging time. SIRMOD simulations using the infiltration parameters estimated using the surface storage smoothing technique resulted in almost identical advance trajectories and runoff hydrographs. Hence, the results are not included within the SIRMOD validation that follows.

4.5 Validation of the Infiltration Parameters

To evaluate the advantages of the IPARM model each set of infiltration parameters was tested within SIRMOD III. All simulations were conducted using the full hydrodynamic model supplied with the same inflow data utilised to estimate the infiltration parameter values (i.e. parameters estimated using the full inflow hydrograph are simulated using the same hydrograph). The results titled “Advance + Runoff sim. with V.In” refer to the SIRMOD simulation using the variable inflow

while the infiltration parameters were estimated using constant inflow with advance and runoff data. The results contained in Table 4-5 refer to the complete irrigation.

Contrary to normal practice, Manning *n* was constrained to the value initially entered into IPARM to estimate the surface roughness. Commonly SIRMOD requires a final calibration, where the value of the hydraulic resistance term, is altered until the predicted advance points closely match the measured advance trajectory (Smith et al. 2005). For simplicity, time taken to reach the final advance point location is preferred rather than attempting to simultaneously match all measured points. Restraining Manning *n* to a constant value for each event separates the performance of the calibration model from any artefact of this manual adjustment within SIRMOD. Hence, the predicted advance trajectory and completion times may depart from their measured values. In fact, any disagreements between arrival times are likely caused by the simplistic and perhaps incorrect estimation of surface storage within the volume balance model.

4.5.1 Prediction of Advance Trajectory

Comparison of the different sets of infiltration parameters via the plot of simulated advance trajectories is largely subjective. Therefore, a numerical measure of fit has been included within the table of SIRMOD results (Table 4-5). In Table 4-5, the *Ad SSE per point* is the sum of squares difference between the measured and predicted advance points (from SIRMOD) divided by the number of points.

The inclusion of the runoff data did not affect the ability of SIRMOD to predict the advance trajectory (e.g. for the Benson irrigation, Figure 4-10). In many cases, it actually improved the fit to the final advance point, often at the expense of the other advance measurements. This can be clearly seen in the Printz irrigation (Figure 4-11), where the results from runoff provided an improved estimation for arrival times at 350 m but reduced accuracy for advance times between 250 and 300 m. Hence, the use of runoff data may reduce the significance of the secondary Manning *n* calibration since only minimal adjustment from the original roughness value used in IPARM appears necessary. The average difference between measured and predicted advance

times (*Ad SSE per point* Table 4-5) tends to increase when the runoff is used to estimate the infiltration curve. The simulated advance times remain similar despite clear differences in both the four sets of infiltration parameter values and the infiltration curves. The advance trajectory is relatively insensitive to the infiltration curve hence the advance measurements should not be used in isolation to estimate the values of the infiltration parameters.

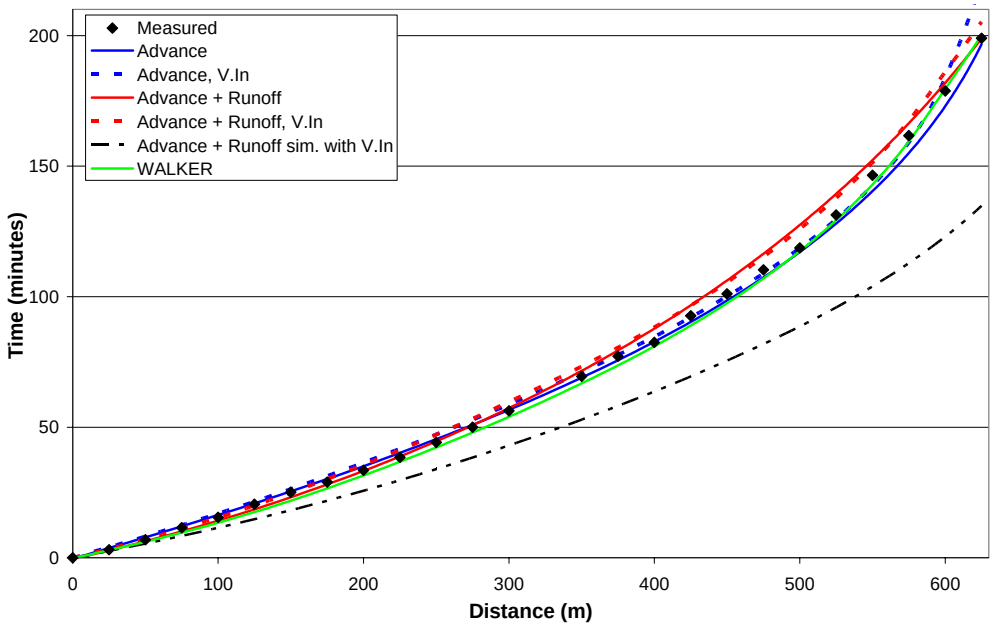

Figure 4-10 Measured and SIRMOD simulated advance (Benson data)

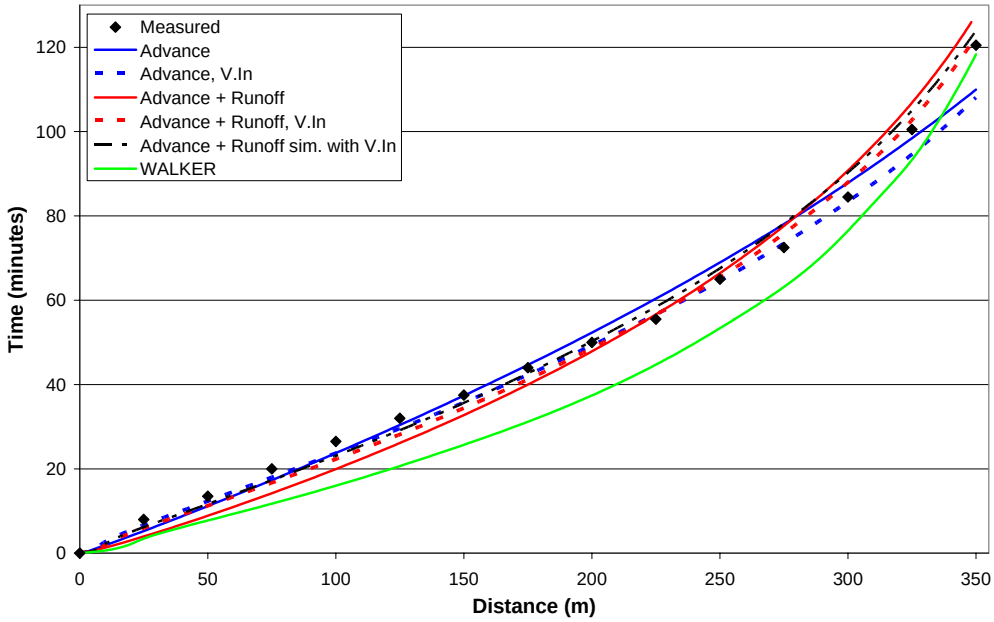

Figure 4-11 Measured and SIRMOD simulated advance (Printz data)

Generally, infiltration parameters derived using the inflow hydrograph resulted in improved predictions of the advance trajectory and reduced values of the advance SSE/point (Table 4-5) compared to those estimated using the constant inflow assumption. The only exceptions to this occurred where the simulation based on constant inflow already produced low advance errors.

Table 4-5 Summary of SIRMOD simulation results

	Infiltration Parameters	Runoff		Infiltration		Ad. SSE per point	[c] Applic. Effic. (%)	[d] Dist. Unif. (%)
		Vol. (m^3)	Error (%)	Depth (mm)	Error (%)			
Benson	Measured	7.760		26.5				
	Advance	2.025	-73.91	32.5	22.45	6.8	86.09	92.08
	Advance, V.In	0.502	-93.53	34.0	28.41	24.2	85.93	92.08
	Advance + Runoff	7.506	-3.27	26.8	0.99	13.5	77.21	92.69
	Advance + Runoff, V.In	7.764	0.06	26.5	-0.02	16.2	76.42	93.60
	Advance + Runoff sim. with V.In	6.825	-12.04	27.5	3.66	692.2	79.21	96.12
	Walker Multi[a]	7.245	-6.63	27.0	2.01	5.5	77.98	93.46
Printz	Measured	1.635		62.9				
	Advance	6.764	313.67	53.4	-15.09	15.5	73.84	85.58
	Advance, V.In	4.060	148.30	58.4	-7.14	14.6	74.36	83.60
	Advance + Runoff	2.048	25.27	62.1	-1.22	23.5	74.53	79.08
	Advance + Runoff, V.In	2.191	33.97	61.9	-1.63	7.1	74.38	80.24
	Advance + Runoff sim. with V.In	2.456	50.21	61.4	-2.42	10.2	74.12	80.23
	Walker Multi[a]	1.803	10.27	62.6	-0.49	85.4	74.42	81.15
Downs	Measured	15.130		96.1				
	Advance	5.812	-61.58	104.3	8.58	34.1	86.80	82.67
	Advance, V.In	4.520	-70.13	105.5	9.77	50.5	86.94	82.76
	Advance + Runoff	15.427	1.96	95.8	-0.27	92.4	84.97	85.60
	Advance + Runoff, V.In	15.486	2.35	95.8	-0.33	62.3	85.04	85.96
	Advance + Runoff sim. with V.In	15.304	1.15	95.9	-0.16	42.8	85.06	85.84
Kooba	Measured	52.838		248.9				
	Advance	74.063	40.17	224.1	-9.97	279.1	70.61	98.15
	Advance, V.In	63.405	20.00	236.6	-4.96	248.6	70.07	90.84
	Advance + Runoff	45.578	-13.74	257.4	3.41	985.0	70.61	87.71
	Advance + Runoff, V.In	47.577	-9.96	255.1	2.47	625.1	69.99	84.47
	Advance + Runoff sim. with V.In	51.138	-3.22	250.9	0.80	3199.1	70.24	87.49
Merungle Hill	Measured	18.431		17.0			[b]51.96	
	Advance	28.914	56.88	8.1	-52.58	247.2	24.36	100.0
	Advance, V.In	20.930	13.56	14.9	-12.53	0.2	45.58	93.53
	Advance + Runoff	17.229	-6.53	18.0	6.03	502.9	54.84	94.61
	Advance + Runoff, V.In	17.709	-3.92	17.6	3.62	12.1	53.90	92.53
	Advance + Runoff sim. with V.In	18.801	2.00	16.7	-1.85	4274.4	51.05	92.37
Huntawang	Measured	11.739		113.5				
	Advance	10.582	-9.85	114.7	1.09	611.5	77.36	79.56
	Advance, V.In	13.781	17.40	111.3	-1.93	472.7	77.91	84.31
	Advance + Runoff	13.754	17.17	111.4	-1.90	516.5	77.39	82.13
	Advance + Runoff, V.In	11.674	-0.55	113.6	0.06	487.7	77.68	81.50
	Advance + Runoff sim. with V.In	13.891	18.34	111.2	-2.03	2658.8	77.72	83.49

[a] simulated using infiltration parameters from Walker (2005)
[b] calculated from total measured runoff since no deep drainage occurred
[c] Application efficiency is calculated considering both runoff and deep drainage losses.
[d] the Distribution Uniformity is calculated separate to SIRMOD III using methods in section 6.2.3
All values for Merungle Hill assume that no deep drainage has occurred
V. in = variable inflow, Ad = simulated advance

The advance trajectory predicted by simulating the variable inflow with the infiltration parameters derived using the constant inflow assumption resulted in a poor prediction of the measured advance for Benson (Figure 4-10, *Advance + Runoff sim. with V.In*). Over the four irrigations with variable inflow conditions, the simulation of the constant inflow infiltration curve using variable inflow resulted in a five-fold increase in the advance SSE/point (Table 4-5). Hence, SIRMOD simulations are only valid when they use the same inflow type (i.e. constant or variable) used to derive the values of a, k and f_0. This behaviour is not apparent for Printz (Figure 4-11) due to the low level of inflow variance.

4.5.2 Prediction of the Runoff Hydrograph

The primary purpose of surface irrigation simulation is to evaluate the irrigation performance. Hence, the accuracy of predicted advance times is insignificant compared to that of the predicted distribution of applied depths. The infiltration curve is often extrapolated to times greater than the advance time and often to opportunity times longer than the runoff measurements. The ability of the infiltration curve to represent reality at later stages is best reflected in the predictions of the runoff hydrographs (Figure 4-12) and total volumes infiltrated (Table 4-5). In each case, infiltration parameters found using different combinations of input data resulted in outflow hydrographs that varied in shape, magnitude and time lag.

Simulations using infiltration parameters based on advance data alone were unable to reproduce the measured data. They failed to predict both the magnitude and shape of the hydrograph, particularly for Benson, Printz and Downs case studies. As expected, the inclusion of runoff in the IPARM calibration improved the prediction of runoff within SIRMOD with the fit of the simulated hydrograph being superior in every case study.

Although the simulations using runoff and constant inflow appear to match the average runoff rates, they do not recreate the shape of the measured hydrograph. This can be clearly observed in the results for the Benson irrigation (Figure 4-12.a) where the hydrograph failed to demonstrate the distinct peak observed in the measured data.

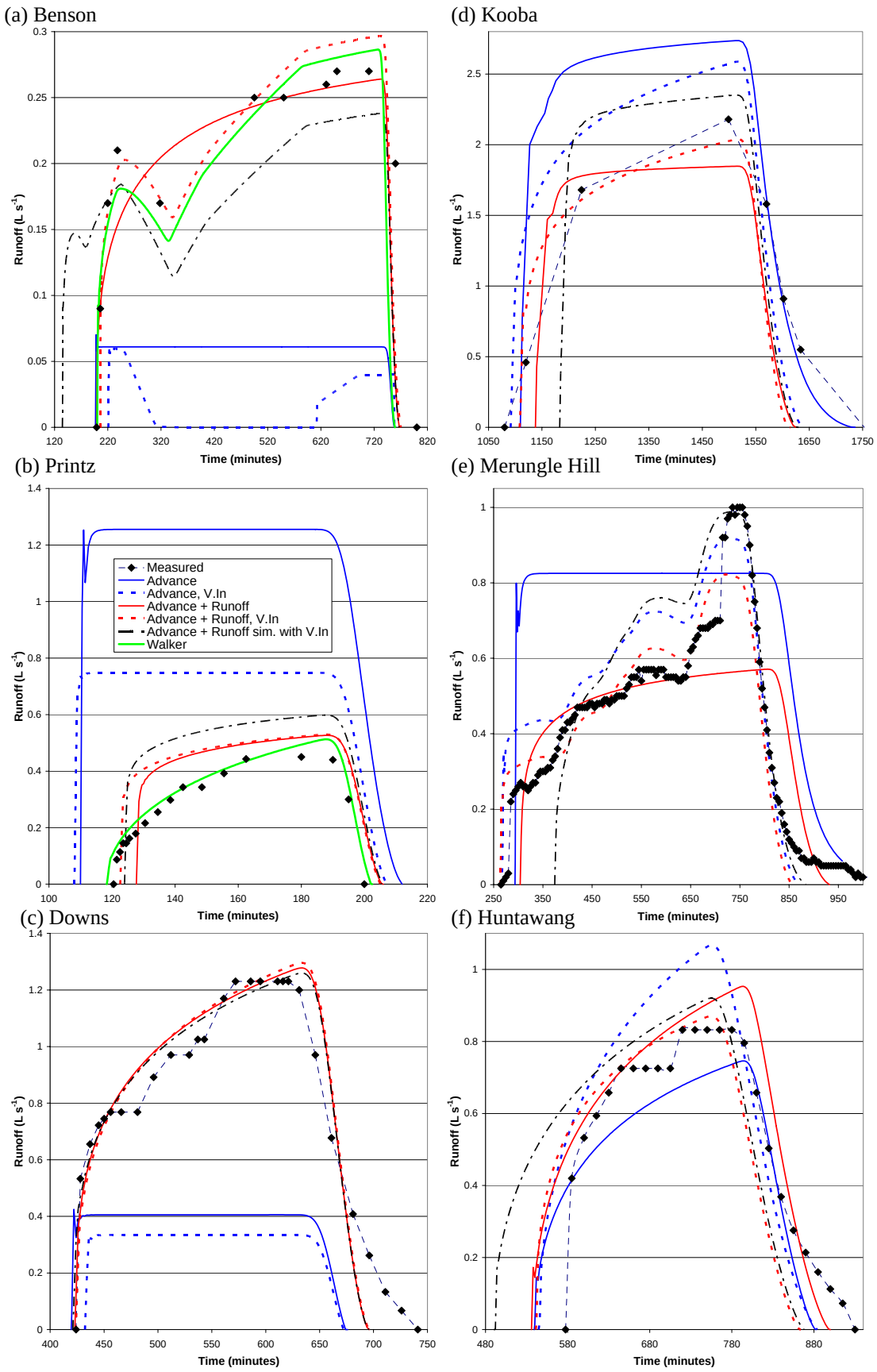

Figure 4-12 Measured and predicted runoff hydrographs using different infiltration parameters

The use of variable inflow in conjunction with runoff significantly improved the simulated results and enabled SIRMOD to accurately reproduce both the magnitude and shape of the outflow hydrograph. The results for Benson also show that use of variable inflow with advance data alters the shape of the hydrograph but does not remove the requirement to include the runoff data in the calibration.

Simulations based on advance data alone provided a poor reproduction of the runoff hydrograph and total volumes of runoff and infiltration (Table 4-5). The error introduced is not consistent between irrigations, i.e. it does not have any general convention. For Benson, the runoff volume was underestimated by almost 74% when advance data only was used to estimate the parameters. The same approach resulted in an over prediction of 313% for the Printz irrigation. The inclusion of runoff yielded improved estimates of the parameters reflected in the reduced errors (average reduction of 84%) in predicted outflow volumes. Using advance and runoff data with constant inflow, the error in the runoff estimation was reduced to -3.3% and 25.3% for Benson and Printz, respectively. However, the importance of the runoff volume varies widely between different irrigations and is a function of the relative lengths of the advance and storage phases. More crucial to irrigation performance is the average infiltrated depth (Table 4-5). Similar errors are present in the applied depths although they are proportionally smaller (compared to runoff) due to their relative magnitude. The use of advance data with the constant inflow assumption caused errors in predicted infiltrated depths ranging between -52.58% and +1.09% for the irrigations tested. Of the six data sets presented, the use of data collected during the storage phase only increased the error for one event (Huntawang). It is worth noting that in that case the decrease in accuracy was in the order of 0.81% of the infiltrated depth.

4.5.3 Prediction of Irrigation Performance and Distribution of Infiltrated Depths

In order to predict the applied depth at any point in the field, both the infiltration curve and opportunity time at that position must be known. Discrepancies in either of these will undermine the ability of simulation models to estimate the distribution of applied depths and irrigation performance. The results presented thus far confirm that

the method used to estimate the infiltration parameters influences both quantities and hence, also the predicted infiltrated depths and uniformity. This is particularly important considering that the main purpose of field evaluation is to estimate these measures.

Accurate runoff volumes may prove adequate for evaluation of the application efficiency (AE) but irrigation evaluation also considers the uniformity of applied depths. The shape of the runoff hydrograph is determined by a combination of the curvature of the infiltration curve and the variable inflow rate. Both factors also influence the distribution uniformity (DU). Therefore, it is likely that the constant inflow assumption also adds uncertainty to uniformity values. The performance parameters from SIRMOD confirm this as in some cases (for example Kooba) the DU differed between the constant and variable inflow options (Table 4-5).

For some irrigations, performance indicators of AE and DU (Table 4-5) did not differ greatly between the various calibration options. However, the difference in infiltration parameters may cause significant divergence of the performance estimates at some other combination of flow rate, time and field length. For example, under measured conditions the predicted AE and DU for Printz was found to be 73.84% and 85.58%, respectively when using advance data only or 74.53% and 79.08% when runoff data is included. However, when the inflow time was shortened to 105 minutes, the SIRMOD predicted AE and DU changed to 92.19% and 79.17%, respectively using the advance data and 99.14% and 67.38% where runoff data was included.

The differences in estimated infiltration depths are clearly visible in the extreme case of the Merungle Hill data set (Figure 4-13). Here the choice of field data used to estimate the infiltration parameters was found to cause substantial differences to the distribution of infiltrated depths, particularly when using advance data with the constant inflow assumption. The inclusion of runoff appears to account for the majority of the variance in average depth. The use of variable inflow altered the shape of the curve and hence influenced the predicted field uniformity. Where this field was evaluated by conventional means (constant inflow with advance only) the predicted

DU was an unrealistic 100% (Table 4-5). Where both the advance and runoff are used in conjunction with the variable hydrograph this value reduced to 92.5%.

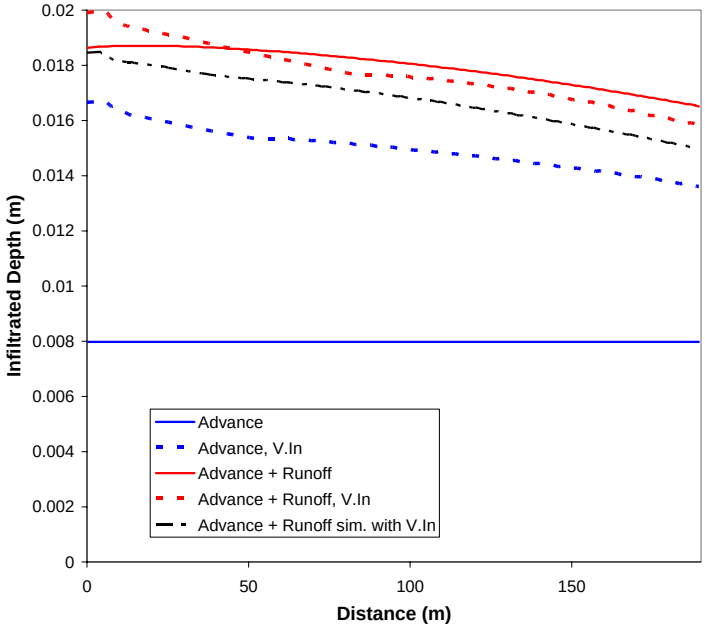

Figure 4-13 Effect of infiltration parameter estimation on the predicted water depth profile (Merungle Hill data)

4.6 Inflow as a Source of Variability in Spatial Estimates of Infiltration

It is hypothesised that part of the variance between infiltration curves estimated for furrows located in the same field is a direct result of limitations in the calibration methods. To test this hypothesis, all of the available data for the Kooba irrigation site was analysed to determine the importance of accounting for the variable inflow when assessing infiltration variability at the field scale. As mentioned previously, the irrigations were conducted within the same season over the space of three events with the inflow hydrograph recorded separately for each furrow. The inflow pattern changed significantly between each event. In irrigation 1, the inflow gradually increased to reach a value approximately double the initial rate at the cut-off time (Figure 4-14). In irrigation 2, the hydrograph demonstrates an initial increase followed by a relatively stable discharge. Irrigation 3 exhibits a typical cutback regime where the inflow declines suddenly to approximately 50% of the original discharge close to the end of the advance phase.

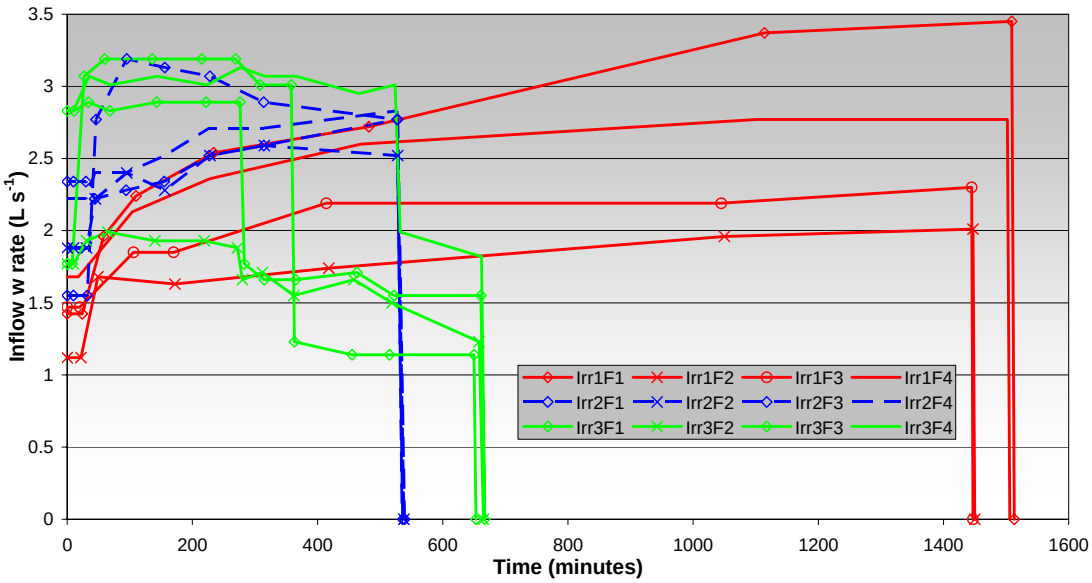

Figure 4-14 Measured inflow hydrographs for Kooba site

IPARM was used to estimate the infiltration parameters from the advance data firstly with the constant inflow equal to the average and then secondly, with the measured inflow hydrograph (Appendix C, Table C.1). The analysis was limited to the advance measurements due to the mixed quality of measured runoff hydrographs. The resultant infiltration curves are plotted for constant (Figure 4-15) and variable (Figure 4-16) inflow over a period representing the measured irrigation durations.

The use of the variable inflow was found to standardise the general shape of the infiltration curves (Figure 4-16) by reducing the apparent variation in infiltration between events. The coefficient of variation in infiltrated depths at ponding times of 100, 200, 500 and 1000 minutes was 87.3, 71.8, 51.3 and 37.8% across all furrows where parameters were calculated using constant inflow and 68.7, 58.5, 39.8 and 28.9% respectively, where the measured inflow hydrograph was used. In this case, the relative errors in infiltration caused by the constant inflow assumption were greatest during the initial stages of the irrigation and gradually declined as time increased up until the advance time. A similar but slightly smaller reduction in variance was observed when the measured inflow hydrograph was used to predict the infiltration curve from advance and runoff data (Appendix Table C.2).

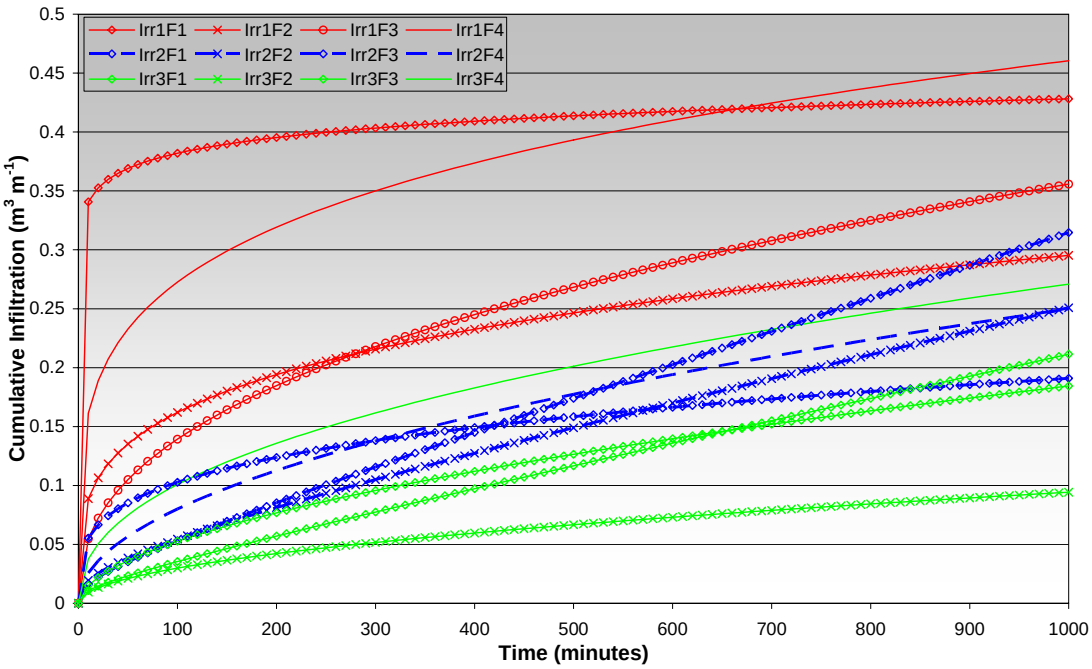

Figure 4-15 Infiltration curves for the Kooba site estimated using advance data with constant inflow

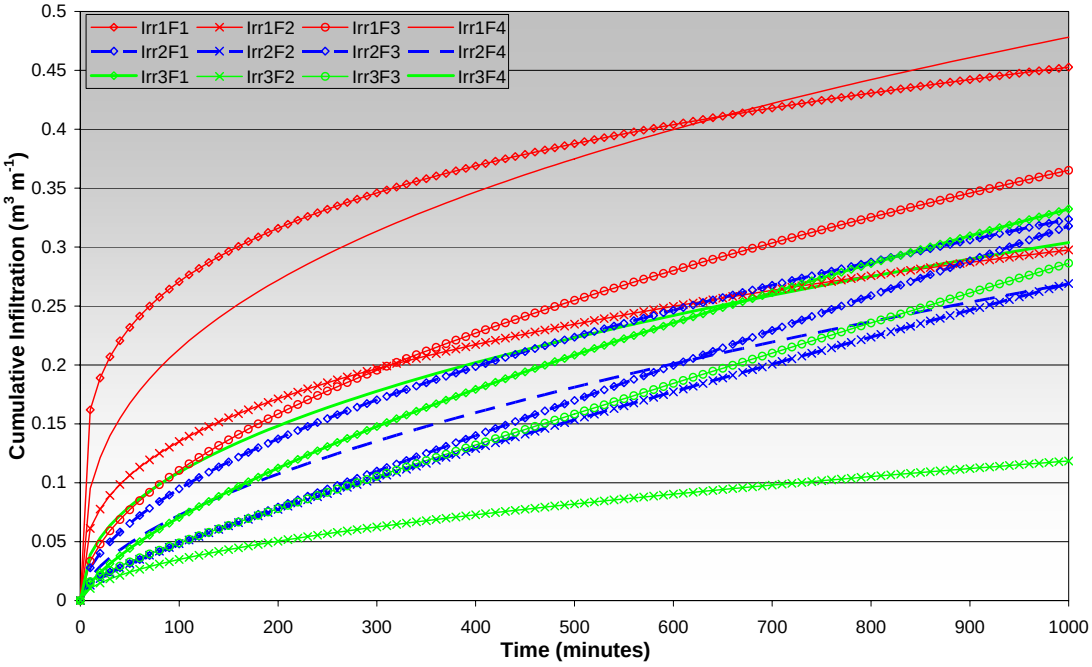

Figure 4-16 Infiltration curves for the Kooba site estimated using advance data with the measured variable inflow hydrograph

A number of the Kooba furrows experienced major inflow variations during the initial stages of the advance phase (Figure 4-14). Renault and Wallender (1996) proposed that such variations result in larger values of the Kostiakov *k* parameter and lower values of *a* when the constant inflow assumption is employed. Comparisons between

the infiltration parameters estimated using advance with constant and variable inflows (Appendix Table C.1) confirm this finding. Eight of the measured furrows exhibited inflow rates that underwent a significant increase during the initial stages of the event, In every one of these cases the constant inflow assumption produced infiltration curves where the parameter *k* was higher and *a* was lower than for the measured inflow hydrograph. In the remaining four furrows where the inflow does not change initially, *k* was lower for the constant inflow while *a* did not favour either direction. The same trends for *a* and *k* persist when considering parameters estimated from advance and runoff data (Appendix Table C.2).

4.7 Sensitivity of IPARM to Section of Input Data Points

4.7.1 Introduction

Due to the numerical nature of the model, the calibrated infiltration parameters are influenced by both the number of data points and the accuracy of their values. Although a small difference in one or more of the advance or runoff measurements may alter the values of the Kostiakov parameters, the calibration will still yield a similar infiltration curve. In the presence of sufficient advance measurements, a single error within one data point will not compromise the model since it will not substantially influence the values of the remaining data points. The advance times are considered independently within the objective function. However, for runoff, a single discrepancy within the measured runoff rates is an issue because IPARM attempts to minimise differences between measured and predicted runoff volumes instead of the instantaneous discharges. This poses a significant problem as an error early in the outflow hydrograph will shift all subsequent values by the corresponding volume.

The Merkley irrigation (Table 4-6 and Table 4-7), taken from Scaloppi et al. (1995) was chosen to study the sensitivity of the model to the selection of data points and also to the weighting between advance and runoff errors. The selected irrigation is particularly suited to this analysis due to a combination of a constant inflow rate and a small and approximately equivalent number of data points within the advance and

outflow hydrograph. In addition, any effect should be easily distinguished due to a large difference between infiltration curves derived only from advance data and advance and runoff data.

Table 4-6 Advance data for sensitivity analysis (Merkley data)

x (m)	t (min)
0	0
25	2.3
50	5.4
75	8.8
100	13.4
125	17.6
150	22.36
175	27.4
200	32
225	38.5

Table 4-7 Runoff hydrograph for sensitivity analysis (Merkley data)

t (min)	Q (L s^{-1})	calc Vol (m^3)
38.5	0.00	0.000
46.3	0.55	0.129
49.2	0.65	0.233
52.2	0.72	0.356
57.2	0.79	0.583
62.2	0.91	0.838
67.2	0.91	1.111

4.7.2 Selection of Advance Measurements

Several different combinations of advance points were chosen from the complete set of nine advance measurements to reflect possible field data collection techniques:

- all 9 advance points
- every second point (i.e. 2, 4, 6 ,8)
- typical two point method selection (i.e. 4, 9)
- first half of the field length (i.e. 1, 2, 3, 4)
- second half of the field (i.e. 5, 6, 7, 8, 9)

The infiltration parameters were estimated for each combination, firstly using advance data only and then using both the advance and runoff data. The resultant infiltration curves are shown in Figure 4-17 (infiltration parameters in Appendix Table C.3). Varying the number and selection advance points had a significant affect on the outcome where runoff was omitted from the optimisation. There was a noteworthy difference when only the first half of the field was used with the resulting parameters overestimating the cumulative infiltration at 200 minutes by greater than 200% compared to that estimated using the entire advance trajectory. By contrast, the infiltration curve resulting from advance data collected over the second half of the field differs by only 54% and compares favourably with that predicted using both runoff and advance data. Interestingly, selecting the mid-point and end-point also

provided a result that resembles the curve obtained by including the runoff data. Where runoff was included within the objective function, the curves of the five different advance selections consolidate into a single line (Figure 4-17). At 200 minutes, the five advance combinations predict cumulative infiltrated depths that differ by only 1%. Hence, including the runoff data in the estimation of the infiltration appears to overcome the problems associated with limited advance data.

4.7.3 Selection of Runoff Measurements

It is hypothesised that like the advance data, the selection of runoff measurements is crucial to the shape of the infiltration curve. The calibration of the infiltration parameters was performed using 10 different sets of outflow measurements (Appendix Table C.4). Even the addition of the first measurement of the runoff hydrograph yielded a large improvement over using advance data alone. However, the resulting infiltration curve overestimated the cumulative depths. The inclusion of each additional outflow measurement (chronologically) caused the curve to gradually approach that estimated using all nine runoff measurements (Figure 4-18). On closer inspection, the addition of each data point prolonged the time at which the two infiltration curves diverge. The omission of every second outflow measurement (i.e. points 2, 4, 6) did not undermine the performance of IPARM indicating that the reduced resolution of data points was still sufficient to describe the shape of the runoff hydrograph. The number of data points used does not appear important provided the selected measurements span the complete storage phase and describe the magnitude and shape of the outflow hydrograph. The form of equation 4-40 combined with the method by which the advance and runoff errors are calculated does not bias one side of objective function over the other with differing numbers of input measurements. Hence, the user can increase the intensity of either advance or runoff measurements without greatly influencing the outcome. The primary advantage of larger numbers of data points is to reduce the susceptibility of the model to the inevitable random measurement errors.

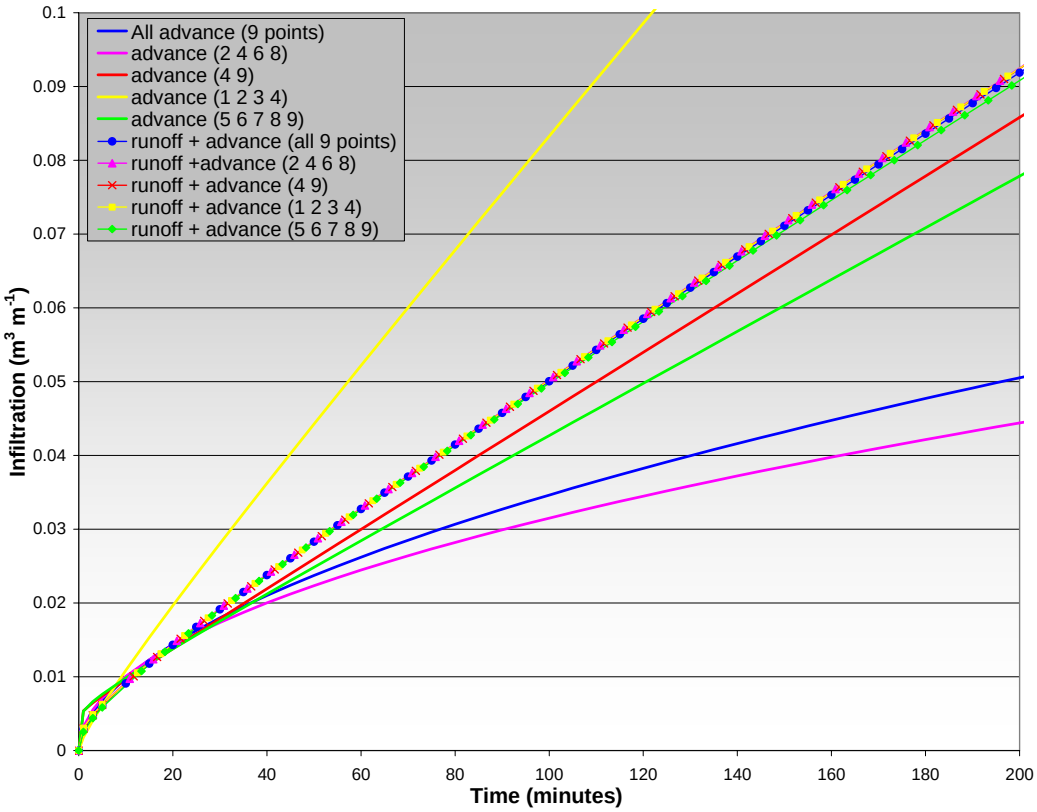

Figure 4-17 Infiltration curves estimated using different advance measurements (Merkley data)

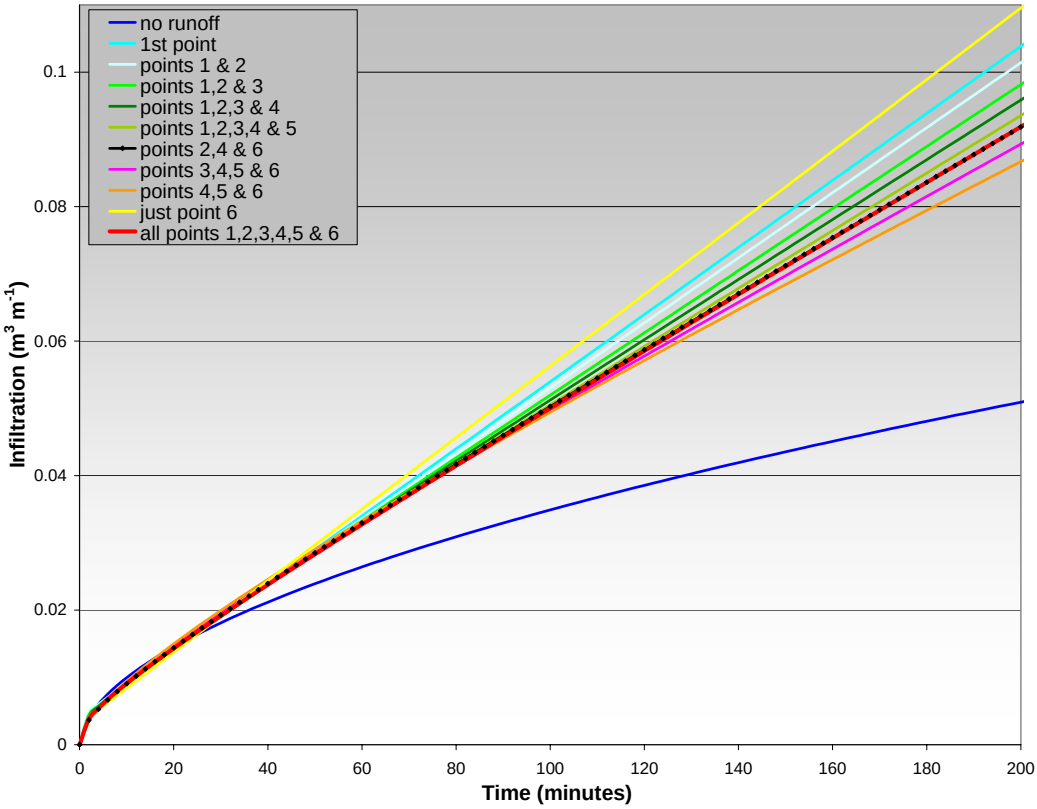

Figure 4-18 Infiltration curves estimated using different runoff measurements (Merkley data)
***all infiltration curves are estimated using the complete set of 9 advance points**

4.7.4 Weighting of Runoff Compared to Advance Data

The weighting factor allows the user to alter the relative importance between runoff and advance measurements. As stated previously, a value of 100% for *w* (Eq. 4-40) forces equal dependence on the two irrigation phases. A value of *w* = 0.0 will cause the model to completely ignore the runoff measurements. Similarly, as *w* approaches infinity the advance measurements are ignored. However, regardless of the weighting, the advance measurements retain some influence over the runoff phase due to the dependence of the subsurface shape factors (equations 4-26 and 4-27) on the power curve coefficient (*r*).

The infiltration parameters were evaluated using advance and runoff data while altering the value of *w* (Table 4-8). At low values of *w*, the high values of runoff error and low advance error indicate that IPARM concentrated primarily on the advance data. As the weighting was increased the advance error increased steadily, but the runoff error experienced a rapid decline between *w* = 0.5% and *w* = 2%. Hence, a small value of the weighting factor had a significant impact on the infiltration curve (Figure 4-19). More than half of the final change in infiltration occurred by increasing the weighting factor from zero to 1% while there was no perceivable change by increasing the value of *w* beyond 5%. As the weighting factor increased beyond unity, shown by the 10000% line (i.e. the runoff error is 100 times more important than the advance error) the infiltration curve appears to approach a second form which differs minimally from the 100% curve. The general behaviour of the infiltration curves suggest that the objective function is much more sensitive to the runoff data.

Table 4-8 Sensitivity of infiltration parameters to the runoff weighting factor (Merkley data)

	a	*k*	f_0	Total Error	Advance Error	Run Error
w = 0%	0.5449	0.00282	0.000000	1.2486	1.2486	99.7219
w = 0.5%	0.5593	0.00271	0.000000	1.7236	1.2730	90.1088
w = 1%	0.3674	0.00284	0.000290	2.0809	1.6779	40.3035
w = 2%	0.2222	0.00304	0.000420	2.1541	2.1195	1.7328
w = 5%	0.2335	0.00298	0.000417	2.1961	2.1320	1.2821
w = 10%	0.2410	0.00294	0.000415	2.2582	2.1363	1.2189
w = 50%	0.2965	0.00262	0.000399	2.7326	2.2032	1.0588
w = 100%	**0.3270**	**0.00245**	**0.000390**	**3.2553**	**2.2883**	**0.9669**
w = 200%	0.5223	0.00171	0.000303	4.0334	3.1709	0.4313
w = 1000%	0.6602	0.00146	0.000181	5.1372	3.8682	0.1269
w = 10000%	0.6776	0.00144	0.000158	15.6882	3.9526	0.1174

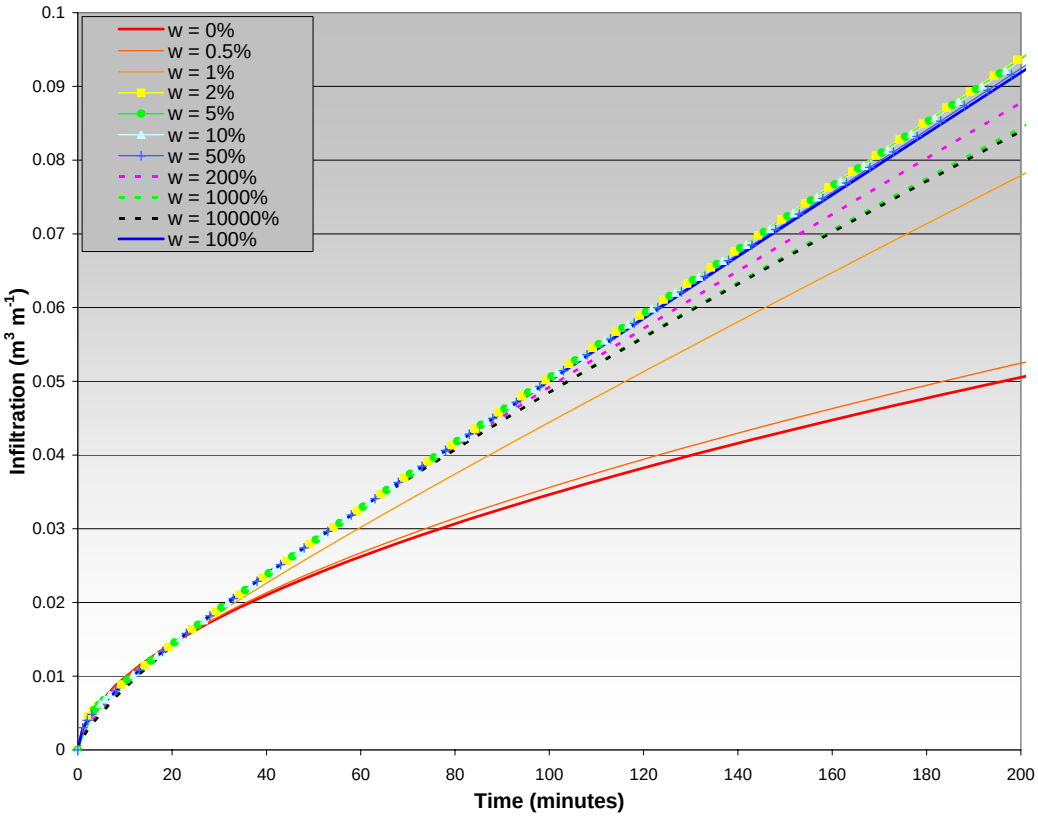

Figure 4-19 Sensitivity of IPARM to the weighting (*w*) between runoff and advance errors (Merkley data)

4.8 Discussion

4.8.1 Data Collection Recommendations

The IPARM technique has been designed to have minimal restrictions on the total number and location of field measurements. However, there are a number of recommendations regarding the collection of field data. The power advance approach requires at least three measured advance points including the start of the irrigation. However, it is recommended that at least five advance measurements are used to ensure proper calibration of the Modified Kostiakov parameters. Although in theory the advance points may be dispersed anywhere along the furrow length they should be well distributed in order to capture the true trajectory shape. Extra care should be taken where points are situated close to the supply end of the field. A unit change in measured time at this point will translate to the largest relative alteration in the advance curve. In addition, there may be some discrepancy regarding the absolute start time of inflow and the zero advance distance relative to remaining advance

points. Similarly, DeTar (1989) encountered difficulty whilst attempting to fit the first few advance points to a log transformation. They conclude that the flow-stream requires some time to reach steady state conditions and hence they neglect advance measurements from the first quarter of the field length. It is also recognised that any uncertainty in the surface storage component will have the greatest impact on the infiltration characteristic during the initial part of the advance phase.

Only runoff data collected during the storage phase can be used in the optimisation. IPARM cannot cope with runoff measurements collected after the inflow cut-off time. This form of the volume balance will not handle the sudden change in inflow rate associated with the end of the irrigation and does not include capability to simulate the recession phase. The surface storage is determined by the instantaneous inflow rate. Hence, on completion of inflow the surface storage volume is immediately shifted to the runoff resulting in a large spike in the hydrograph. The use of the surface storage smoothing estimation procedure for surface storage does not overcome this limitation but merely removes any sudden changes in the volume balance equation.

The measured inflow data should be adequate to capture the shape of the hydrograph as IPARM uses simple linear interpolation to predict the discharge for any given time. The sampling time interval for inflow should be regular in order to capture a realistic picture of the curvature between changes in discharge. Larger intervals between measurements are permitted where the variation is gradual or linear.

The measurements of furrow cross section may be located close to the supply but they must be located far enough within the field to represent typical flow conditions. Often the furrow geometry may change over the first few metres of the field due to local changes in field slope resulting from the construction of the head works. If time permits it would be advantageous to take several samples of furrow geometry along the field length to obtain a representative average cross section.

The reliance of IPARM on the volume balance model restricts its ability to function under non-standard furrow irrigation. The same equations should also apply to sloping borders but consideration should be given to the alteration of the surface storage coefficient. The surface storage approximation functions best under normal flow conditions. Hence, the model will not function correctly for fields with zero or reverse grades. Under very low grades (i.e. $S_0 < 0.0001$) it is recommended that the surface storage is calculated using a measured upstream depth or area rather than an estimated value of surface roughness. The Manning approximation will fail to provide realistic values of upstream area under such extreme shallow grades.

4.8.2 IPARM User Intervention

From experience, typical advance trajectories observed on heavy cracking clay soils tend to produce near-linear advance curves causing Kostiakov *a* to become negative. This implies an infiltration rate that increases with time which is a physical impossibility. For this reason and to ensure numerical stability, IPARM restricts this parameter to positive values. Hence, in this case the optimised value of *a* will often be zero. A linear trend exists between the values of *a* and *r*, as *r* increases *a* decreases. As *r* approaches unity (i.e. advance curve becomes linear) the parameter *a* tends to go negative, the relative error increases and the cumulative infiltration becomes less sensitive to the opportunity time (Hanson et al. 1993). In addition, the other infiltration parameters are also strongly related to advance curve exponent (*r*) (Hanson et al. 1993). Different problems occur where *r* becomes increasingly small where the advance appears to "stall" close to the end of the field. Consequently, extreme values of *r* could be used as a signal for potential problems in the final infiltration curve. The interactions between *a* and *r* change under variable inflow conditions. For example, the value of *r* may correctly become greater than unity when an increasing inflow rate causes the advance velocity to increase with distance.

One common procedure to correct for zero or negative values of *a* is to instead fix the steady intake rate (f_0) at zero, which hopefully forces part of the intake back to *a*. However, this simplistic approach causes the infiltration curve to consistently under predict the cumulative infiltration volume (Elliott and Walker 1982). A zero value for

a should not be considered as a problem, just an indicator that the linear infiltration function provides a more appropriate fit to the field conditions. However, where IPARM provides a value of $a = 0$, the user should enter a value just greater than zero (e.g. 0.00000001) into SIRMOD to prevent any divide by zero errors.

4.8.3 Parameter Starting Estimates

The default starting estimates for the infiltration parameters (shown in Table 4-2) were selected in order to achieve rapid convergence to the global minimum of model error. Like most numerical schemes the choice for starting estimates will have some influence over the final result. To illustrate the sensitivity of the calibration the Downs calibration was repeated using a total of seven different parameter starting sets. Infiltration parameters were calculated using advance and runoff data and the results are shown in Table 4-9. In this case, the use of different starting estimates had minimal influence over the final values for the infiltration parameters. These results are typical of what might be expected for any other set of field data.

Table 4-9 Infiltration parameters for Downs using different starting parameter estimates

Starting set	Starting Estimates			Infiltration Parameters			Total Error	Ad Error	Run Error
	a	*k*	f_0	*a*	*k*	f_0			
Default	0.3	0.05	0.0001	0.2927	0.01901	0.000148	5.625	4.165	1.460
1	0	0	0	0.2926	0.01902	0.000148	5.625	4.166	1.459
2	0.99	0.99	0.01	0.2906	0.01918	0.000149	5.625	4.174	1.451
3	0.99	0	0	0.2926	0.01902	0.000148	5.625	4.166	1.459
4	0	0.99	0	0.2926	0.01902	0.000148	5.625	4.166	1.459
5	0	0.99	0.01	0.2906	0.01918	0.000149	5.625	4.174	1.451
6	0.9	0	0.01	0.2906	0.01918	0.000149	5.625	4.174	1.451

4.8.4 Conclusion

An improved volume balance model is presented to correct some of the limitations of traditional infiltration from advance schemes. The procedure has been used to create a robust tool, IPARM, for simple identification of the infiltration characteristic from field measurements. Results have shown that use of the runoff hydrograph in the calibration can increase the accuracy of the infiltration curve, particularly at longer times. Where suitable outflow measurements are available the enhanced sensitivity of IPARM to runoff reduces the requirement for accurate advance measurements.

However, this also indicates the susceptibility of the model to relatively small errors in the runoff measurements. Simple modification of the volume balance equations has allowed the use of the full inflow hydrograph rather than the constant inflow assumption. Infiltration curves predicted using the full inflow hydrograph improved the fit to the measured runoff hydrograph compared to those predicted using the constant inflow assumption. It was also found that accounting for the temporal inflow variation reduced the apparent infiltration variability and standardised the shapes of the infiltration curves. The alterations to the volume balance model offer improved estimates of the infiltration curve. Hence, simulations using the resultant infiltration parameters provided improved estimates of the irrigation performance indicators.

CHAPTER 5

Field Variability of Infiltration

5.1 Introduction

This chapter provides an introduction to previous studies of infiltration variability (section 5.2) and describes some of the techniques that can be used to statistically characterise that variability (section 5.3). Section 5.4 presents the experimental data to be used in analysis of field variability. In section 5.5, IPARM is used to estimate the infiltration parameters from this data, which are used throughout the following chapters. The resultant infiltration curves are used to investigate the nature of field variability (section 5.6) and the potential to reduce data requirements whilst retaining sufficient description of that variability (section 5.7). However, the high data requirements of IPARM and similar techniques (e.g. INFILT, McClymont and Smith 1996) do not facilitate the rapid identification of infiltration curves for a large number of furrows. Hence, section 5.8 attempts to describe the infiltration variability using statistical distribution theory which is used in section 5.9 to develop a predictive procedure to estimate infiltration from reduced field measurements.

Three individual data sets have been chosen to illustrate the importance of infiltration variability at the field level. Each field will be discussed separately due to differences in soil types, field lengths, inflow rates and irrigation times. The field measurements were not collected specifically for this thesis, therefore the extent of investigation is determined by the available data. This data is also used in the following chapters to develop the whole field simulation model (chapter 6) and optimisation procedures (chapter 7).

5.2 Previous Attempts to Assess Infiltration Variability

Furrow irrigation evaluation usually entails the measurement of a number of furrows within the same field during the same irrigation. To simplify measurement, these furrows are usually located adjacent to each other. Hence, the measured furrows represent a small section of the field and therefore only describe a proportion of the possible variance within the field. In addition, the measurements are often too closely spaced to ensure spatial independence. Bautista and Wallender (1985) determined that field measurements should be spaced at least 8 m, 24 m and 32 m apart for blocked furrow, blocked continuously flowing furrow and blocked surge techniques, respectively to avoid spatial correlation when attempting to describe spatial variability. Furthermore, the strength and range of the spatial correlation increases with sample length (Wallender 1987). Oyonarte and Mateos (2002) did not find any evidence of spatial correlation at distances greater than 23 m. Other studies have suggested that soil intake rates do not show any significant spatial correlation within relatively homogeneous fields (Ben-Hur et al. 1987; Jaynes and Hunsaker 1989).

The statistical distribution of intake rates observed is dependent on the measurement procedure. In fact, for any soil characteristic, the estimated mean, variance and distribution is largely dependent on the technique and scale of measurement (van Es 2002). Ben-Hur et al. (1987) observed minimal negative skew amongst infiltration measurements made with ring infiltrometers whilst the skew of the distribution of sprinkler infiltrometer measurements was large and positive. They also found that the formation of a surface seal had caused the shape of the distribution to become more positively skewed.

Several attempts have been made to describe the variation in soil properties using distribution functions. Warrick and Nielsen (cited in Ben-Hur et al. 1987) found that the variability of hydraulic properties was large with a CV (coefficient of variance) of 100% or more. They also concluded that the clay percentage and bulk density follow normal distributions while the hydraulic conductivity tended to follow a log-normal distribution. Jaynes and Hunsaker (1989) found that the moisture content and

infiltrated depth could be described by both normal and log-normal distributions however the log-normal distribution offered a better fit to the infiltrated depths. Ersahin (2003) performed 50 infiltration measurements with a ring infiltrometer and used the Shapiro-Wilks and Kurtosis tests to prove that the variability could be described by a normal distribution. Sharma et al. (1983) found that both saturated hydraulic conductivity and sorptivity (of the Philip equation) provided a good fit to the normal distribution for measurements recorded on a fine grid (1 m spacing) but at greater spacing (i.e. 10x10 m and 100x150 m grid) they are more adequately described using a log-normal distribution. Others have simply assumed the measured data follows a given distribution to enable statistical analysis (e.g. Vieira et al. (1981) assumed a normal distribution).

Inverse estimation techniques for the infiltration parameters are suitable for use in commercial conditions. However, they are generally too measurement intensive to be used in the identification of infiltration rates at the field scale. The method introduced by Khatri and Smith (2006) was developed to make real-time infiltration estimates from reduced advance measurements. The infiltration characteristic from a single furrow is scaled using single advance measurements from other furrows in the same field (for full explanation see section 5.9.3). Such techniques would also facilitate the large scale measurement of infiltration necessary within heterogeneous fields.

5.3 Describing Infiltration Variability with Statistical Techniques

5.3.1 Review of Statistical Distribution Models

Prior to the selection of an appropriate distribution function to describe infiltration variability, it is necessary to provide a brief background for some of the available statistical models. Continuous distribution functions are used to describe the variation of a quantity that can take on any value within a specified range. Some examples include continuous uniform, normal, Gamma, Beta, Student's t and log-normal distribution (Bethea and Rhinehart 1991).

5.3.1.1 Continuous Uniform Distribution

The uniform distribution, also known as the rectangular distribution due to the shape of its frequency curve, describes the case where all possible values of the parameter have equal probability. It is most commonly used to check the adequacy of random number generators. This type of distribution is of little use in modelling engineering variables (Bury 1999) and is therefore not considered further.

5.3.1.2 Normal Distribution

The normal distribution, also known as the Gaussian distribution, has a bell shaped frequency curve that is symmetrical about the mean. The normal distribution is the most common of the continuous distribution functions and it has many convenient properties that make it the choice to represent many natural processes. It relies on the assumption that any variance in the quantity of interest is the compounded result of many independent small sources (Bethea and Rhinehart 1991). The standard normal distribution is constructed by shifting and scaling the values so that they have a mean of 0 and standard deviation of 1. It allows all the characteristics of a normal distribution to be represented in a single parameter, the standard normal variate, *ZVal*:

$$ZVal = \frac{X - \mu}{\sigma} \quad \text{..... Eq 5-1}$$

where μ is the population mean of a continuous variable X and σ is the standard deviation. When considering a sample of the population these variables are replaced with the sample mean ($\overline{X}$) and sample standard deviation σ_s:

$$\overline{X} = \frac{\sum_{i=1}^{N} X_i}{N} \quad \text{..... Eq 5-2}$$

$$\sigma_s = \sqrt{\frac{\sum_{i=1}^{N} \left(X_i - \overline{X}\right)^2}{N-1}} \quad \text{..... Eq 5-3}$$

where N is the number of X values. The CV is calculated by dividing the standard deviation by the mean.

$$CV = \frac{\sigma_S}{\overline{X}} \quad \text{..... Eq 5-4}$$

The normal distribution occurs frequently in measurement processes, can be used to study error propagation and facilitates a wide variety of numerical analysis (Allmaras and Kempthorne 2002). Hence, variables of alternative statistical distributions are often transformed into the normal form to simplify analysis. The normal distribution provides a good approximation for the central region frequencies. However, it should be used with caution where the distribution is skewed as in these cases it fails to predict the probabilities at the tails. Experience has shown that most engineering variables are constrained to positive values and their distributions are highly positively skewed (Bury 1999).

5.3.1.3 Gamma Distribution

The Gamma distribution function is adaptable to many facets of measurement due to its highly flexible shape and positive sample space. It can be used to model measurements that vary due to a small number of random underlying variables whereas the normal function is more appropriate under larger numbers of explanatory variables (Bury 1999). This distribution itself is not commonly used to model physical systems. However, the specialised case of the Chi-Squared function, given the notation χ^2, is used extensively in hypothesis testing (Montgomery and Runger 1999). If a random number of samples are selected from a normal distribution then the sampling distribution will follow a Chi-squared distribution.

Another variant of the Gamma distribution, the exponential distribution function, is commonly used to describe the elapsed time between events that occur randomly in space or time. The exponential distribution is typically used to model inter-arrival times and time to failure where the likelihood of each event follows a random distribution (Bury 1999). It cannot be applied to most measurement variables since it fails to predict the shape of the frequency distribution. None of the Gamma functions have been considered as viable options to predict the distribution function of infiltration.

5.3.1.4 Beta Distribution

The beta distribution is used to describe a random process whose values are restricted to a specified range. The function features high shape flexibility due to the two shape parameters (Bury 1999), and for this reason it has been used to model many processes such as tolerance limits, quality control and reliability (Soong 2004). The frequency distribution may be J shaped, inverted J shaped, U shaped or unimodal. The beta distribution is not likely to be of use for describing the variability of infiltration rates since it requires clearly defined upper and lower limits.

5.3.1.5 Student's t Distribution

The Student's t distribution resembles the normal probability function as the values are positioned symmetrically about the mean in a bell shape. However, more of the area under the frequency curve occurs in the tails of the distribution (Bethea and Rhinehart 1991). The t distribution is typically used to model a random sample from a normal distribution with unknown mean and variance (Montgomery and Runger 1999).

5.3.1.6 Log-Normal Distribution

If the logarithm of a variable follows a normal distribution then that variable is itself log-normally distributed. The log-normal frequency distribution function is positively skewed with values bunched at the low end of the scale with a long right tail. It only considers positive values, and hence is popular amongst the engineering disciplines as it provides a better fit to many physical processes (Bury 1999). Whereas the normal distribution function is the summation of many independent random factors, the log-normal could be considered as being the multiplicative resultant of a large number of independent factors (Allmaras and Kempthorne 2002; Soong 2004). The log-normal distribution is similar to the normal distribution and therefore shares many of the same properties. A series of values having a log-normal distribution can be transformed simply into the normal by taking the natural logarithm of all values. This transformation enables the use of all the statistical techniques available for the normal distribution.

5.3.2 Sampling Distribution, a Tool to Determine Required Number of Measurements

A description of infiltration variability is crucial to the management of surface irrigation. However, collection of field data is a time consuming and expensive process. Minimising the sample data requirement is a major priority whilst the sample should be large enough in order to provide an acceptable estimate of the mean and variance of the population. Statistical tests can be performed to determine the impact of the sample size on the estimated mean and variance (termed the sampling distribution).

If a random sample of N is taken from a population of X with an approximate normal distribution then the mean calculated from that sample ($\overline{X}$), itself follows a normal distribution with mean μ and variance σ^2/N (Bethea and Rhinehart 1991). The confidence interval for the mean at a specified significance level α, is given by:

$$P\left(\overline{X} - ZVal_{\alpha/2}\frac{\sigma}{\sqrt{N}} < \mu < \overline{X} + ZVal_{1-\alpha/2}\frac{\sigma}{\sqrt{N}}\right) = 1-\alpha \quad \text{..... Eq 5-5}$$

This equation is invalid where the population variance σ^2 is unknown. The confidence limit based on *ZVal* is only appropriate for large samples, i.e. greater than 30 (Miller and Freund 1985; Montgomery and Runger 1999) or 300 (Bethea and Rhinehart 1991) samples. For smaller sample sizes, where it is reasonable to assume that the population distribution is normal (Devore and Peck 1997), equation 5-5 is altered by replacing the normal statistic (*ZVal*) with t_{Stat}, from the t-distribution and population statistic (σ^2) by the sample variance σ_s^2.

$$P\left(\overline{X} - t_{Stat\,\alpha/2}\frac{\sigma_s}{\sqrt{N}} < \mu < \overline{X} + t_{Stat\,1-\alpha/2}\frac{\sigma_s}{\sqrt{N}}\right) = 1-\alpha \quad \text{..... Eq 5-6}$$

The same approach cannot be used to describe the behaviour of the sample variance since it cannot take on negative values. Instead, if the sampling distribution of the variance σ_s^2 calculated from a random sample size, N, is taken from a population having a normal distribution variance σ^2, then the statistic

$$\chi^2 = \frac{(N-1)\sigma_s^{\,2}}{\sigma^2} \quad \text{..... Eq 5-7}$$

follows a chi-squared distribution (χ^2) with N-1 degrees of freedom (Miller and Freund 1985). These relationships can be re-arranged to form confidence intervals for the mean and standard deviation of a sub-set of the population with known statistics. Hence, the confidence interval for the sample mean becomes:

$$\mu - ZVal_{1-\alpha/2}\frac{\sigma}{\sqrt{N}} < \overline{X} < \mu + ZVal_{\alpha/2}\frac{\sigma}{\sqrt{N}} \quad \text{..... Eq 5-8}$$

and for the sample standard deviation:

$$\sqrt{\frac{\chi^2_{N-1,1-\frac{\alpha}{2}}}{N-1}} < \frac{\sigma_S}{\sigma} < \sqrt{\frac{\chi^2_{N-1,\frac{\alpha}{2}}}{N-1}} \quad \text{..... Eq 5-9}$$

5.4 Multiple Furrow Field Data

5.4.1 Collection of Field Data using Irrimate™ Equipment

In the three data sets described below, all advance, inflow and runoff measurements were collected using the tools and techniques included within the Irrimate™ surface irrigation evaluation system, developed by the National Centre for Engineering in Agriculture (NCEA) in Toowoomba (Dalton et al. 2001). The Irrimate™ hardware for in-field measurement of surface irrigation is typically comprised of:

A) Siphon Flow-meter (Figure 5-1) – Measures and records the flow-rate within an irrigation siphon using a type of paddle wheel flow meter.

B) Advance Sensors (Figure 5-2) – Typically in a set of 6, each with 8 sensors and hence is capable of monitoring 6 advance distances in 8 adjacent furrows. Time is recorded when the water reaches each sensor (pair of exposed wires).

C) Flume Flow-meter (Figure 5-3) – Flume positioned at the downstream end of the field to measure flow within a single furrow. It measures the flow rate by inducing critical flow over a section of raised and contracted channel.

The current version of Irrimate™ flow meters measure flow rate in L s^{-1} and log at 5 minute intervals. Each advance sensor measures a single wetted time value with a resolution of 1 minute. Following collection of field data, the infiltration characteristic is estimated using the INFILT or IPARM inverse procedures. Performance evaluation and irrigation optimisation is performed using the SIRMOD II simulation model.

Figure 5-1 Irrimate™ siphon flow meter

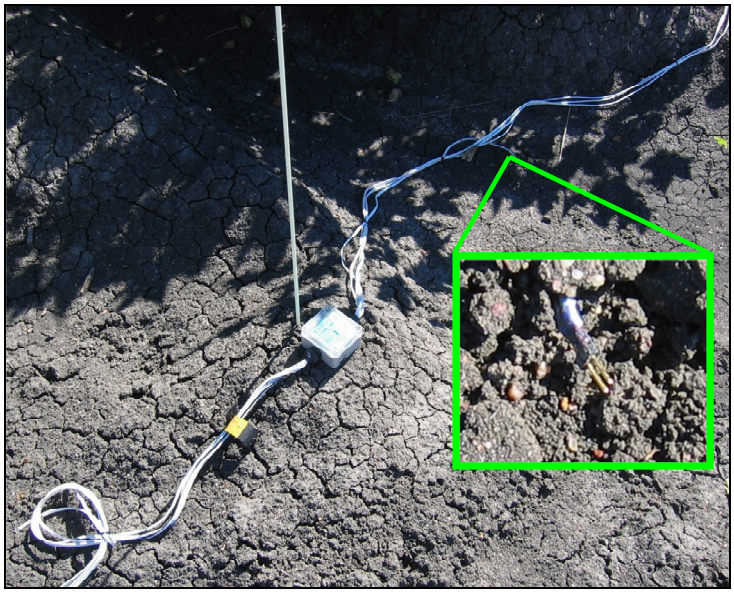

Figure 5-2 Irrimate™ advance sensor

Figure 5-3 Irrimate™ flume flow meter

Across Australia there are currently 15 consultant agents providing the Irrimate™ service (Raine et al. 2005). The service includes the measurement tools, irrigation modelling and technical expertise required to generate management and design recommendations for farmers.

5.4.2 Downs

The Downs (Dalton et al. 2001) data was collected from a cotton field at Macalister, on the Jimbour plain in southern Queensland. The field was 565 metres long and consisted of a cracking clay soil. All measurements were collected during a single season across five irrigation events with four furrows measured in each event (20 in total). In the case of the Downs data set, the inflow rates and time to cut-off do not change significantly between irrigation events. Hence, it was assumed that the combined data set could represent the field wide variation expected in a single irrigation event. Data collected for each furrow included:

- Five advance points evenly spaced down the furrow length (Appendix Table D.1).
- Inflow rate (logged every 5 minutes).
- Runoff from the end of the field (L s^{-1} at irregular intervals) (Appendix Table D.2).

No measurements were taken of the furrow cross-section. Therefore, the furrow dimensions were assumed as from previous studies as 0.6, 0.4, 0.2 and 0.1 m for the top, middle, bottom width and maximum height respectively. None of the inflow hydrographs show significant temporal variance in inflow rates (refer to the example Figure 4-5.c) and the inflow was assumed to be constant. The variation in inflow rates between furrows and irrigations was minimal (Table 5-1). The average inflow rate was 3.21 L s^{-1} with a standard deviation of 0.318 L s^{-1}. The inflow for irrigation 5, furrow 3 was unique since at 2.14 L s^{-1} it was much lower than the other measurements. This may have been an artefact of siphon meter issues. Nonetheless, in the absence of further details this data was included in the analysis. Runoff data was collected for the entire irrigation set with separate measurements for every furrow covering the total runoff duration. In most cases, the short inflow time prevented the onset of steady outflow rates. Therefore, it was not possible to estimate f_0 directly from the difference between Q_0 and Q_r as attempting to do so would result in an overestimation of the steady term.

5.4.3 Chisholm

The Chisholm data (provided by the NCEA) was collected during the 1999-2000 season on the western Darling Downs. Measurements were taken from four furrows across five irrigations with the exception of irrigations 2 and 3 where only two and three furrows were observed respectively (Appendix Table D.5). For the purpose of this analysis it was assumed that the measured furrows represent a single irrigation. In contrast to Downs, the inflow rate varied between 0.83 and 7.92 L s^{-1}. Variations of this magnitude may introduce uncertainty into the infiltration function calibration through the wetted perimeter effect. Generally, the inflow was measured for only one out of the four furrows in each event, masking the true variance in discharge. The inflow hydrographs were not recorded and a constant inflow rate over time was assumed in all cases. No observations of furrow water depths were recorded and the surface storage volumes in IPARM were estimated using a Manning *n* value of 0.04. No runoff data was collected for any of the Chisholm irrigations.

5.4.4 Turner

The Turner data (provided by the NCEA) was collected from a cotton field (Field 17) at Callondoon near Goondiwindi in southern Queensland during the 1999-2000 season. At 1120 m, the furrows are considerably longer than for the Downs or Chisholm fields. The field measurements span a total of eight irrigations with complete data for 27 furrows (Appendix Table D.6) Although the inflow measurements did not experience the same level of variance (3.97 L s^{-1} to 7.12 L s^{-1}) as for Chisholm, each irrigation event still possessed a unique discharge. No temporal inflow pattern was available, therefore, constant inflow was assumed. Similar to Chisholm, only one or two inflow measurements were collected for each event and discharges for the other furrows were assumed equal to that of furrows within the same event. This approach was considered appropriate since the measured furrows were adjacent and were subjected to the same pressure head and time of cut-off.

5.4.5 Additional Field Data for Seasonal Trends

Additional field data was obtained to describe the seasonal infiltration trends in section 5.6.2. These additional data sets were not used elsewhere in the analysis due to the reduced numbers of measured furrows for each field. The Kooba field data consisted of the 12 measured furrows (Appendix
Table A.8) described previously in section 4.6. The infiltration curves for Kooba used in this case were those estimated using the advance data and full inflow hydrograph (Appendix Table C.1). The three Coulton data sets titled Field A (Appendix Table D.7), Field B (Appendix Table D.8) and Field C (Appendix Table D.9) were collected by the NCEA from three separate fields at the same location in northern NSW. The Turner field 18 data (Appendix Table D.10) was collected from a second field at the Turner site. The infiltration parameters for the Turner field 18 and the Coulton field (Appendix D) were estimated using advance data and the constant average inflow.

5.4.6 Estimating Surface Storage using Manning's *n*

The volume balance technique of estimating the infiltration uses a simplistic approach to estimate the surface storage in the furrow. In this technique, the upstream area of flow (equation 4-20) must be estimated from the field conditions. The upstream area values provided in the field data were generally either absent or questionable. Often the upstream area does not change as expected. In one case a single value is provided when the measured inflow rate increased in magnitude by almost 10 times. This leads to an error in the estimation of the infiltration curves. It was important to remove this uncertainty from the infiltration curves, as a change in the surface storage which is proportional to the cross-sectional area of flow, will result in an equal and opposite change in the cumulative infiltrated volume. For all field data, the cross-sectional area of flow for the volume balance was estimated from an assumed value of Manning's *n* using equation 4-20. A value of $n = 0.04$ (see section 4.4.1) was selected as the default value for surface roughness. This same roughness value was also used in all the subsequent SIRMOD and IrriProb simulations that used these infiltration parameters.

5.5 Estimation of the Infiltration Curves

The three parameters of the Modified Kostiakov equation (a, k and f_0) were estimated via IPARM using all available advance and or runoff data.

5.5.1 Downs

The infiltration parameters for Downs were estimated using IPARM and the combination of the advance and runoff data. The runoff data contained no known problems hence equal weighting was given to the advance and runoff error (setting $w = 1$ in Eq 4-40). The total, advance and runoff volume balance errors (Table 5-1) do not indicate any problems within the data. Both the runoff and more significantly, the advance errors tended to be higher for the first irrigation. This is not a result of temporal variations in the inflow rate and may therefore point to increased variation in infiltration properties along the field length during the first irrigation. The reduced advance errors for the remaining events suggest that this variation in soil properties, possibly due to differences in the initial soil moisture content or surface soil structure, has been reduced either during or following the first irrigation.

Table 5-1 Infiltration parameters for Downs (whole field)

Furrow	Average Inflow (L s^{-1})	Time (min)	Infiltration Parameters			Ad SSE	Run SSE	Total SSE
			a	k	f_0			
Irr1F1	3.22	878.5	0.5543	0.00688	0.000000	13.740	7.626	21.366
Irr1F2	3.01	878.5	0.5357	0.00703	0.000000	16.487	12.723	29.210
Irr1F3	3.05	878.5	0.5191	0.00758	0.000000	22.890	14.386	37.275
Irr1F4	3.15	878.5	0.4488	0.01307	0.000000	15.333	4.140	19.473
Irr2F1	3.47	602.5	0.4856	0.01084	0.000000	7.287	6.420	13.707
Irr2F2	3.68	602.5	0.2228	0.04017	0.000139	6.252	1.405	7.656
Irr2F3	3.42	602.5	0.2921	0.01906	0.000148	4.168	1.458	5.625
Irr2F4	3.59	602.5	0.4131	0.01738	0.000035	9.881	3.289	13.170
Irr3F1	3.34	985.0	0.3984	0.02522	0.000000	5.795	7.314	13.109
Irr3F2	2.90	977.5	0.3927	0.02278	0.000000	4.716	11.215	15.931
Irr3F3	3.28	982.5	0.3999	0.02459	0.000000	5.319	12.178	17.497
Irr3F4	3.34	985.0	0.4781	0.01483	0.000000	4.179	4.678	8.857
Irr4F1	3.28	667.5	0.0196	0.09250	0.000254	2.311	0.527	2.839
Irr4F2	3.06	667.5	0.0648	0.06930	0.000220	4.620	0.375	4.995
Irr4F3	3.33	667.5	0.3601	0.02209	0.000057	5.259	2.280	7.539
Irr4F4	3.29	667.5	0.0667	0.07232	0.000249	2.783	2.807	5.590
Irr5F1	3.04	557.5	0.0351	0.05397	0.000217	6.020	1.883	7.903
Irr5F2	3.29	557.5	0.1373	0.03511	0.000217	6.576	1.297	7.873
Irr5F3	2.14	557.5	0.1609	0.02270	0.000093	7.334	0.916	8.250
Irr5F4	3.24	557.5	0.1414	0.03228	0.000228	8.936	0.516	9.452

The steady infiltration rate (f_0) remained low for all furrows, ranging between 0 and 0.000254 m^3 min^{-1} m^{-1}, indicative of the cracking clay soil. The shapes of the infiltration curves were consistent across the irrigations (Figure 5-4). The curves

appear to be clustered in groups according to the irrigation event. This indicates that the variance between furrows in the same irrigation was less than that between events during the season.

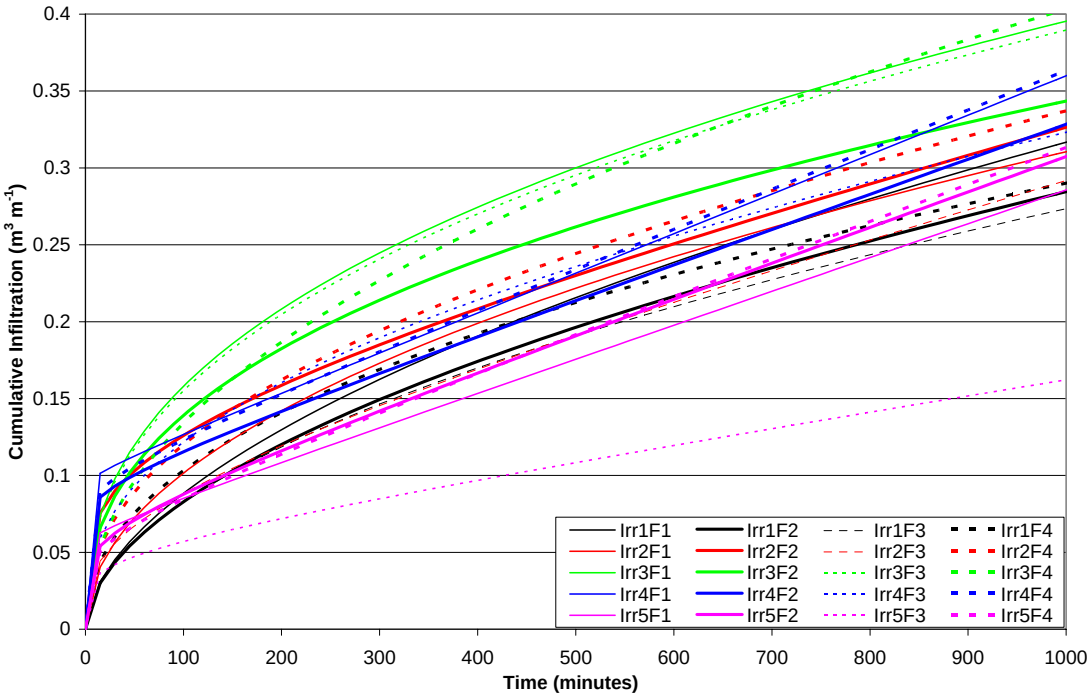

Figure 5-4 Infiltration curves estimated from advance and runoff with constant inflow (Downs field)

5.5.2 Chisholm

Infiltration parameters for the Chisholm site were calculated from advance data using a constant inflow (Table 5-2). Two furrows (irrigation 4, furrows 3 and 4) were irrigated using a 1 m wetted furrow spacing therefore the infiltration curves were adjusted to conform to the conventional 2 m spacing by doubling the value of k (f_0 is equal to zero). The measured inflow discharge for these furrows was used to estimate the infiltration parameters but was doubled for the subsequent analysis. The plotted infiltration curves (Figure 5-5) show much greater variance than for Downs. This may be a result of the short advance times and/or large variation in inflow rates. The furrow inflow durations range between 223 and 1161 minutes (Table 5-2). However, the average final advance time used to estimate the infiltration parameters is much shorter at 230 minutes with a range of 109 to 427 minutes. Hence, the advance measurements do not cover sufficient time to characterise f_0. This may cause

significant errors in predicting infiltrated depths where the infiltration curves are projected to the total irrigation time.

5.5.3 Turner

For Turner, infiltration parameters were estimated by IPARM using advance data with constant inflow (Table 5-3). The consistently low advance SSE given by IPARM does not necessarily indicate that the field measurements are of greater quality than that of Downs. In most cases they are a direct reflection of the lower numbers of measured data points. Where IPARM is optimising three infiltration parameters based on two advance points, the advance error would be greatly reduced due to the reduced degrees of freedom.

Table 5-2 Infiltration parameters (Chisholm field)

Furrow	Inflow (L s^{-1})	Time (min)	Infiltration Parameters			Ad SSE
			a	*k*	f_0	
Irr1F1	0.83	1161	0.3514	0.00867	0.000000	4.839
Irr1F2	0.83	1161	0.3789	0.00806	0.000000	0.282
Irr1F3	0.83	1161	0.4143	0.00735	0.000000	6.420
Irr1F4	0.83	1161	0.3515	0.01207	0.000000	1.698
Irr2F1	5	559	0.4132	0.03550	0.000165	0.000
Irr2F2	5	559	0.0000	0.14871	0.001174	3.440
Irr3F1	2.6	807	0.3519	0.02520	0.000000	3.937
Irr3F2	2.6	807	0.2127	0.05102	0.000000	2.193
Irr3F3	2.6	807	0.2493	0.02728	0.000236	0.000
Irr4F1	3.74	300	0.2892	0.04599	0.000300	0.000
Irr4F2	7.92	223	0.2621	0.04668	0.000567	0.000
Irr4F3	**3.78**	230	0.0804	**0.08864**	0.000000	1.617
Irr4F4	**7.6**	231	0.3561	**0.04523**	0.000000	2.408
Irr5F1	4.5	973	0.3470	0.04220	0.000000	2.747
Irr5F2	4.5	973	0.1881	0.07896	0.000000	0.999
Irr5F3	4.5	973	0.2259	0.06230	0.000000	0.411
Irr5F4	4.5	973	0.2427	0.05609	0.000000	0.891

The *k* values and inflows in bold have been doubled to enable valid comparison with the other furrows at the 2 m furrow spacing. The measured inflow rate was used to estimate the parameters within IPARM.

Table 5-3 Infiltration parameters (Turner field)

Furrow	Inflow (L s^{-1})	Time (min)	Infiltration Parameters			Ad SSE
			a	*k*	f_0	
Irr1F1	5.06	688	0.0523	0.11822	0.000004	0.000
Irr1F2	5.06	531	0.0487	0.12662	0.000004	0.000
Irr2F1	5.63	635	0.1025	0.09269	0.000000	1.515
Irr2F2	5.63	615	0.1054	0.06421	0.000119	0.000
Irr2F3	5.91	457	0.1849	0.06127	0.000000	0.700
Irr2F4	5.91	654	0.2526	0.04182	0.000000	0.699
Irr3F1	5.84	476	0.0940	0.10266	0.000002	0.000
Irr3F2	5.84	673	0.1743	0.06725	0.000000	0.385
Irr3F3	5.84	667	0.1451	0.08099	0.000000	3.286
Irr3F4	5.84	662	0.1600	0.07395	0.000000	3.703
Irr3F5	5.84	670	0.0503	0.13618	0.000000	0.000
Irr4F1	5.36	483	0.0898	0.06609	0.000019	0.000
Irr4F2	5.36	316	0.0000	0.06811	0.000148	1.062
Irr4F3	5.36	446	0.1170	0.04400	0.000078	0.672
Irr4F4	5.36	448	0.2661	0.02430	0.000000	0.527
Irr5F1	6.13	383	0.0779	0.04168	0.000155	0.041
Irr5F2	6.13	199	0.0000	0.02557	0.000274	1.276
Irr5F3	6.13	329	0.6563	0.00246	0.000000	2.509
Irr5F4	6.13	306	0.5409	0.00402	0.000027	0.000
Irr6F1	3.97	616	0.0000	0.09516	0.000043	0.457
Irr6F2	3.97	612	0.0456	0.07156	0.000049	0.000
Irr7F1	6.87	440	0.0000	0.10240	0.000115	0.798
Irr7F2	6.89	439	0.0000	0.10670	0.000096	1.795
Irr7F3	5.77	455	0.0000	0.09158	0.000083	1.928
Irr7F4	7.12	312	0.0000	0.11531	0.000055	2.475
Irr8F1	6.46	498	0.1281	0.06540	0.000039	0.000
Irr8F2	6.46	481	0.0586	0.08944	0.000051	0.000

Calibration of infiltration for the Turner field resulted in zero values for the Kostiakov *a* parameter for seven furrows (Table 5-3), caused by the linear nature of the advance trajectory. Wherever this occurs, the infiltration function is biased towards the *k* and f_0 parameters, in some cases causing the steady infiltration rate to reach excessive values. This is shown clearly in the line representing irrigation 5, furrow 2 (Figure

5-6). A similar problem can be observed in irrigation 2 furrow 2 of the Chisholm field (Figure 5-5) which caused the infiltration curve to rise above the other furrows at long opportunity times. In this analysis, no attempt was made to constrain f_0 in order to force the infiltration back to the transient term.

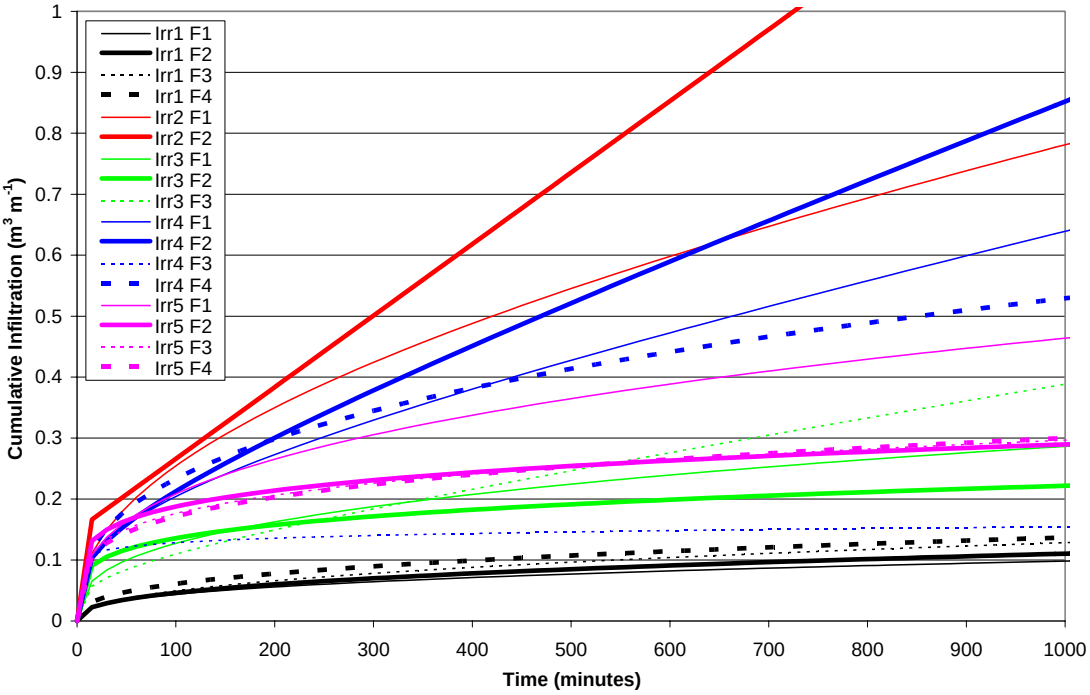

Figure 5-5 Infiltration curves estimated from advance with constant inflow (Chisholm field)

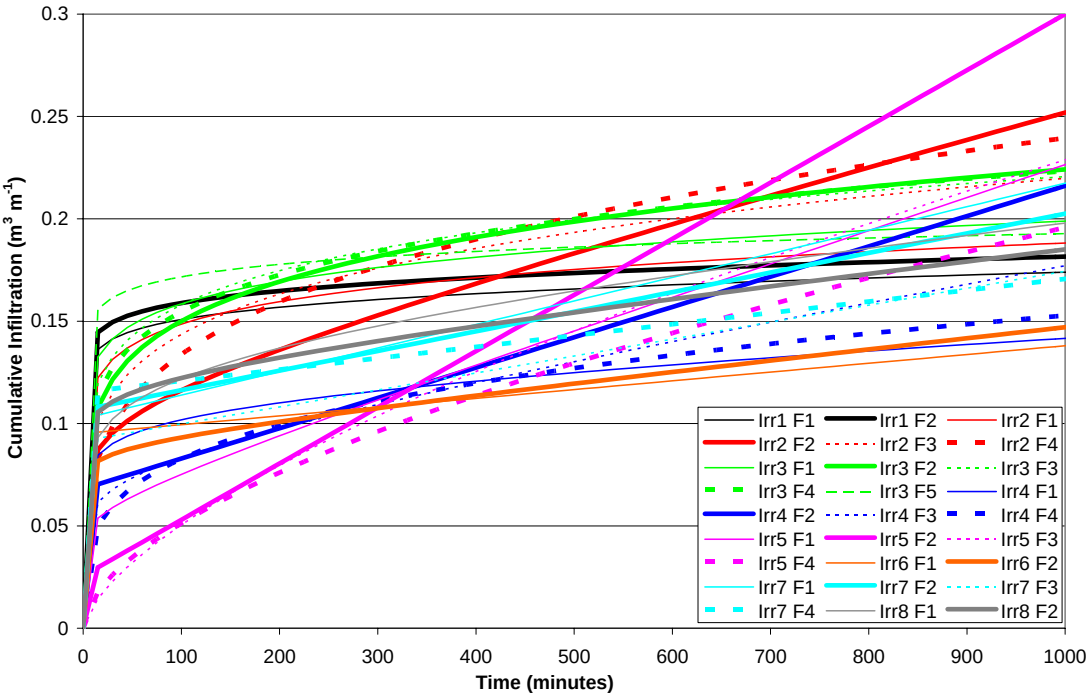

Figure 5-6 Infiltration curves estimated from advance with constant inflow (Turner field)

5.6 Variability of Infiltration

Although soil conditions might vary considerably along the length of a furrow, this study focused on the variation between adjacent furrows and across irrigation events within the same field. It is difficult to infer a series of infiltration rates along the furrow length from sparse advance measurements since the intake at a single point will have an impact on the opportunity times at all points downstream of that location. Treating a furrow as the basic soil unit is a gross simplification of the actual field behaviour as it assumes that the soil does not show any spatial trends. In reality, many soil properties do exhibit spatial correlation due to a combination of factors outlined in section 2.3. The analysis in this dissertation also assumes that the water applied to a given furrow does not re-distribute laterally. Hence, this analysis assumes that (1) the surface and subsurface flow of water in one furrow is independent of its neighbouring furrows and (2) infiltration rates are constant over the field length.

5.6.1 Variability between Infiltration Curves

On observation of the infiltration curves for Downs (Figure 5-4), Chisholm (Figure 5-5) and Turner (Figure 5-6), it is clear that each field experiences a different level of variation. The same curves also indicate that this variability is not fixed as the curves tend to converge or diverge with changing opportunity time. To observe the time-dependent nature of the variability, the CV of infiltrated depths was calculated across the measured furrows for each field over opportunity times between 0 and 1000 minutes (Figure 5-7). The CV was calculated by dividing the standard deviation of cumulative depths at a given time by the mean depth corresponding to that opportunity time.

Both the Downs and Turner infiltration curves show significant variation at early times with the CV declining to below 20% after 500 minutes (Figure 5-7). This suggests that for these soils there is a large variation influencing the initial infiltration rates (i.e. pre-irrigation moisture content, cracking) but over time the cumulative intake of all furrows becomes similar. Chisholm behaves very differently, the minimum CV of 46% occurs at < 100 minutes and the CV continues to increase with

time. At 1000 minutes, the CV of the Chisholm infiltration curves is 80%, over 4 times the variation observed in the other fields. The large discrepancy in steady intake rates results in an enormous variation in infiltrated depth at long ponding times. One reason for the increasing variance for Chisholm at long opportunity times may be the extrapolation of the infiltration curves beyond the relatively short duration of advance data. However, this does not explain the relatively large variability observed at this site for short opportunity times.

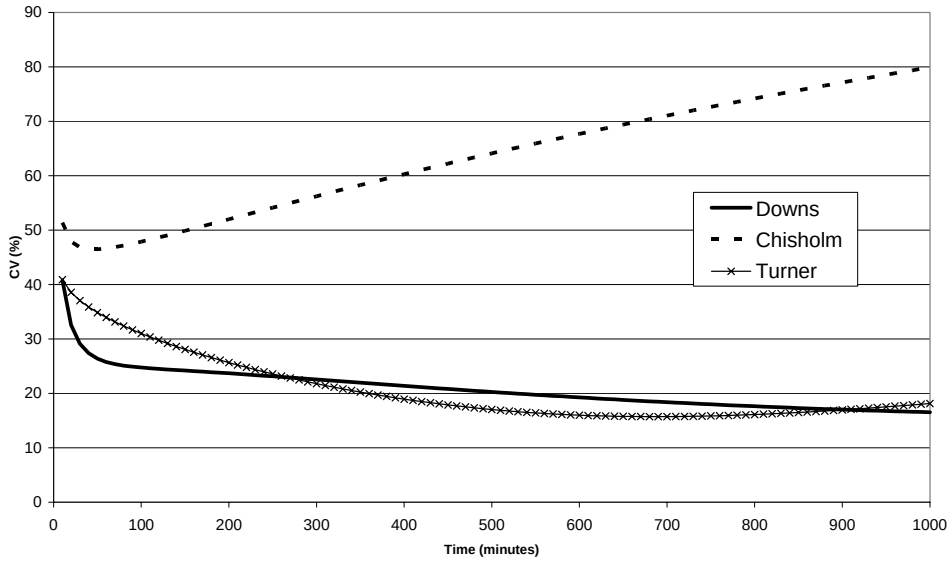

Figure 5-7 CV of infiltration with opportunity time (Downs, Chisholm and Turner fields)

5.6.2 Seasonal (Between Irrigation Events) Infiltration Variability

The nature of the irrigation measurements facilitated the observation of seasonal trends in the infiltration parameters and curves. To evaluate the seasonal trends attempts were made to correlate each quantity with the irrigation number. Linear correlation tests were conducted using SPSS v12.0 (SPSS Inc., Chicago IL).

5.6.2.1 Seasonal Trends in the Infiltration Parameters

For the Downs field, all three infiltration parameters were found to be significantly correlated with the irrigation number at the 0.01 level with Pearson correlations (R) of -0.807, 0.587 and 0.69 for a, k and f_0 (Table 5-4). An initial test for the Chisholm data did not identify any significant correlation with the irrigation number. However, the

infiltration curve corresponding to irrigation 2, furrow 2 appeared to be an outlier and possibly masked any correlation. Hence, analysis for Chisholm was repeated, this time removing the offending furrow (Table 5-4). In this case, *a* was negatively correlated at the 0.05 level (R = -0.603), *k* was positively correlated at the 0.01 level (R = 0.828) but f_0 was not correlated (R = 0.123). None of the infiltration parameters from Turner were significantly correlated with the irrigation number but the parameter f_0 demonstrated the same increasing trend (R = 0.364) as for Downs and Chisholm. The low significance in the correlations of the infiltration parameters observed for Turner is probably a result of the zero values for *a*.

The same analysis was repeated for Coulton A, B and C, Kooba and Turner Field 18 (Table 5-4). However, the validity of any conclusions made based on these fields is questionable due to the limited number of measured furrows. In these fields the trends in infiltration parameters are reduced, or in the case of Kooba, reversed.

Table 5-4 Seasonal correlation between infiltration parameters and infiltrated depths

Field	No.	*a*		*k*		f_0	
		sig	*R*	sig	*R*	sig	*R*
Downs	20	**0.000**	**-0.807**	**0.006**	**0.587**	**0.001**	**0.690**
Chisholm[1]	17[1]	**0.013**	**-0.603**	**0.000**	**0.828**	0.651	0.123
Turner	27	0.481	-0.142	0.797	-0.052	0.062	0.364
Kooba	12	0.298	0.328	**0.044**	**-0.589**	0.469	0.231
Coulton A	9	0.102	-0.580	0.283	-0.402	0.637	0.183
Coulton B	7	0.957	0.025	0.060	0.734	0.200	-0.551
Coulton C	11	0.676	-0.143	0.632	-0.163	0.916	0.036
Turner F18	13	0.575	-0.172	0.794	-0.080	0.410	0.250

- The results in the shaded rows are based on fewer furrows hence it is difficult to make conclusions
- Numbers in bold font represent correlations that are significant (sig.) at the 0.05 level
[1] Analysis for Chisholm was carried out with the outlier (Irr2Fur2) removed, and hence uses 16 furrows

Considering all fields, there did not appear to be any consistent significant trends in the infiltration parameters. However, the R values demonstrated weak correlations between *a* and f_0 and the irrigation number. The Modified Kostiakov *a* term tended to decline, indicating that the infiltration curve had reached steady conditions earlier in the opportunity time. For the majority of fields the steady infiltration term f_0 exhibits a weak increasing trend with time. The apparent general increase in steady intake conflicts with the expected decline associated with the accumulated compaction throughout the season. In all cases, except for Downs, the infiltration parameters were

estimated using advance data only. In the Downs case, the runoff data does not extend the infiltration curve to opportunity times much longer than the advance phase. Hence, it is likely that the IPARM calibration process was unable to correctly identify the value of f_0. The increasing trend for f_0, combined with the negative trend for a, possibly indicates that the infiltration curve is changing form by becoming increasingly linear rather than insinuating an increase in the saturated hydraulic conductivity.

It may appear obvious to describe the variability using the infiltration parameters, as they are simple numerical constants. However, this approach is not justified since the parameters are empirical and therefore have no physical meaning. Attempts in the literature to observe the parameters individually have not been successful, as the parameters are interdependent (e.g. a and k (Hopmans 1989)). Even where strong relationships exist between infiltrated depths there does not appear to be any correlation between the raw values of the parameters (Jaynes and Hunsaker 1989). Hence, studies of the infiltration variability should instead consider the infiltration rates or cumulative depths.

5.6.2.2 Seasonal Trends in the Cumulative Infiltration

The infiltration curves are not suited to statistical analysis. It is easier to describe the infiltration characteristic at a number of defined opportunity times rather than attempting to analyse the full infiltration curve. In this analysis, the linear correlation tests were conducted using the infiltrated depths at opportunity times of 200, 500 and 1000 minutes.

For the Downs field no significant seasonal trends in the cumulative infiltrated depths were found (R values of -0.183, -0.219 and -0.057) for the three opportunity times (Table 5-5). However, for the Chisholm field the cumulative infiltrated depth at 200 minutes was significantly correlated at the 0.05 level (R = 0.619) while the depths at 500 and 1000 minutes were not correlated with Pearson correlations of 0.478 and 0.374, respectively. For Turner, the cumulative infiltrated depths demonstrated a significant seasonal relationship at 200 (R = -0.525) and 500 minutes (R = -0.554),

which was opposite to that of Chisholm. Amongst the additional fields (Kooba, Coulton A, B and C and Turner F18), the correlation of infiltrated depths with time is generally stronger and negative.

Table 5-5 Seasonal correlation of infiltrated depths with irrigation number

Field	No.	200 minutes		500 minutes		1000 minutes	
		sig	*R*	sig	*R*	sig	*R*
Downs	20	0.441	-0.183	0.354	-0.219	0.811	-0.057
Chisholm[1]	17[1]	**0.011**	**0.619**	0.061	0.478	0.154	0.374
Turner	27	**0.001**	**-0.525**	**0.003**	**-0.554**	0.350	-0.187
Kooba	12	**0.011**	**-0.701**	**0.011**	**-0.704**	**0.024**	**-0.642**
Coulton A	9	**0.010**	**-0.796**	**0.006**	**-0.830**	**0.029**	**-0.718**
Coulton B	7	0.730	-0.161	0.289	-0.469	0.233	-0.518
Coulton C	11	**0.005**	**-0.775**	**0.036**	**-0.634**	0.064	-0.576
Turner F18	13	0.466	-0.222	0.719	-0.111	0.850	0.058

- The results in the shaded rows are based on fewer furrows hence it is difficult to make conclusions
- Numbers in bold font represent correlations that are significant (sig.) at the 0.05 level
[1] Analysis for Chisholm was carried out with the outlier (Irr2Fur2) removed, and hence uses 16 furrows

In the majority of fields considered, the cumulative infiltration curve experienced a significant decrease over the season. However, for Chisholm the infiltrated depth tends to increase with increasing irrigation number. A number of seasonal relationships could be identified amongst the fields considered but the lack of consistency between the different fields indicates that the seasonal variance is governed by a series of complex processes. It is difficult to generalise the relationship of infiltration with time, each field may have a unique history sequence of cultural practices (i.e. cultivation and compaction) and moisture status (due to rainfall and irrigation scheduling).

5.6.3 Significance of Temporal and Spatial Variability

The analysis of variance test (ANOVA) can be used to determine if the variability in a sample can be explained by a factor or is caused by random variation. In this way the ANOVA test can be used to assess the significance of the temporal and spatial variability in infiltration rates. Unfortunately, the data sets do not allow analysis of the spatial component as there is no guarantee that the same furrows were tested in each irrigation event. The data does however permit statistical inference on the temporal component, i.e. the irrigation number. The ANOVA test was performed on each of the three fields using the cumulative infiltrated depths at 200, 500 and 1000 minutes.

Furrows were grouped according to the irrigation number and the results are presented in Table 5-6. The F statistic is the ratio of the between group variability to the within group variability while the significance value is the probability that the result occurred by chance. The results in Table 5-6 clearly show that the temporal or between irrigation variability is significant.

Table 5-6 Significance of temporal variability using ANOVA

Field	No.	200 minutes		500 minutes		1000 minutes		F_{crit}
		F	*sig*	F	*sig*	F	*sig*	
Downs	20	20.7	0.000	14.6	0.000	5.9	0.005	3.1
Chisholm[1]	17[1]	20.1	0.000	12.5	0.000	8.8	0.001	3.3
Turner	27	68.4	0.000	25.3	0.000	3.9	0.009	2.5

- F is the F-ratio and sig is the significance.

[1] Analysis for Chisholm was carried out with the outlier (Irr2Fur2) removed, and hence uses 16 furrows

5.6.4 Seasonal Compared to Spatial Variability

The selected data sets contain measurements that represent both multiple furrows from a single irrigation event and multiple irrigations throughout the same season. It therefore should be possible to evaluate the relative importance of spatial (closely spaced) variation and seasonal variation. The CV was calculated from the infiltrated depths at 200, 500 and 1000 minutes for the furrows within each irrigation event. The seasonal CV (Table 5-7) represents the variance between the average infiltrated depth for each irrigation at the given opportunity time. The total CV was calculated from the entire number of available furrows.

Table 5-7 Comparison between spatial and seasonal variability (coefficient of variation)

	Downs			Chisholm			Turner		
Irrigation	200 (min)	500 (min)	1000 (min)	200 (min)	500 (min)	1000 (min)	200 (min)	500 (min)	1000 (min)
1	8.07	5.95	6.29	14.71	14.51	14.74	3.50	3.24	3.04
2	13.46	10.08	6.23	6.47	21.02	36.40	8.07	6.01	12.36
3	6.54	6.01	7.03	4.26	12.54	28.12	2.09	3.85	7.04
4	5.08	4.45	6.07	31.14	42.76	53.71	5.94	5.87	19.19
5	20.16	23.72	26.56	13.14	19.70	25.00	9.56	9.34	18.57
6	-	-	-	-	-	-	1.95	1.73	4.47
7	-	-	-	-	-	-	7.31	8.16	11.77
8	-	-	-	-	-	-	2.42	4.65	4.76
Average Spatial	10.66	10.04	10.44	13.94	22.11	31.59	5.11	5.36	10.15
Total[1]	23.70	20.27	16.55	52.00	64.10	79.91	25.66	17.04	18.15
Seasonal[2]	23.76	19.71	14.10	52.82	63.88	76.27	23.48	15.82	14.87

[1] The total CV is calculated from the total set of measured furrows for each field.

[2] The seasonal CV is calculated from the average infiltrated depth of each irrigation event.

No temporal trends could be found in the results (Table 5-7) indicating that the spatial variability did not experience a consistent change over time. For Downs, the fifth and final irrigation had the greatest variation. However, for Chisholm this occurred in the second last (4th) irrigation while in the Turner field no particular irrigation demonstrated a clear increase in variation. In most cases the variability between irrigation events (i.e. seasonal) was higher than the variability within any particular irrigation event. For example, the average spatial variability in cumulative infiltration for the three fields was found to be 10.0, 22.1 and 5.4% at an opportunity time of 500 minutes compared to the seasonal variability at 19.7, 63.9 and 15.8% (Table 5-7). Hence, it appears that the temporal variability in infiltration is greater than the spatial component. This is further supported by the fact that the value for the seasonal CV is close to or in some cases exceeds the total CV. The relative importance of the temporal and spatial components of variability, given by the ratio between the two appears to follow a trend with the opportunity time The CV within an event tended to increase for larger opportunity times but the CV between events typically decreased with opportunity time. This indicates that the temporal (seasonal) variability in infiltration rates is greatest at short opportunity times whilst the spatial variation in soil properties has the greatest influence over the steady intake rates. Since the temporal variability is most important during the early stage of infiltration, a major part of this variability may be explained by the moisture dependent crack fill volume.

It must be remembered that the sampled furrows were located adjacent to each other. Hence, this analysis can only take into account the spatial variability that occurs within the space of less than 10 metres. It is expected that the spatial variability at the whole field scale will be much greater in most instances and therefore may exceed the seasonal variability.

5.7 Minimum Number of Infiltration Curves Required to Estimate Whole Field Variability

5.7.1 Method

The sampling distribution (5.3.2) was constructed by calculating the infiltrated depth for each furrow at a selected opportunity time (i.e. 25%, 50%, 75%, 100% and 150% of the average final advance time). A random sample was taken and the sample mean and standard deviation were calculated. This procedure was repeated 100 times storing the values of mean and standard deviation each time. Sampling distributions under different sample sizes were created by repeating this process with sample sizes ranging from one up to the total number of measurements. The sampling distributions were plotted against increasing sample size (e.g. Figure 5-8) by representing the average of each sample with a separate dot. This procedure was repeated to create sampling distributions for the mean and standard deviation of the infiltrated depth at opportunity times equal to 25%, 50%, 75%, 100%, and 150% of the average final advance time (AT). This was replicated for each of the three fields of interest.

The data sets used in this analysis contain between 17 and 27 measured furrows. This is lower than the sample number of 30 (Devore and Peck 1997) typically specified for application of the Central Limit Theorem. Hence, the confidence intervals for the mean should be calculated using the t statistic (i.e. Eq. 5-6). However, the form of this expression is not suited for application to the simulated sampling process. The sample standard deviation and hence also the confidence intervals will change significantly between each individual sample. Instead it was assumed that the sampling distribution is approximately normal, hence equation 5-5 provides an approximate confidence interval for the mean (Devore and Peck 1997). As this expression requires the population standard deviation it will be assumed that the population mean and variance for each field is equal to that of the complete sample of furrows (i.e. $\mu = \overline{X}$ and $\sigma = \sigma_s$). The resultant confidence intervals should be used with care due to the uncertainty of the sample standard deviation. Application of equation 5-9 indicates that the sample standard deviation should be within ± 31.5%, ± 34.3% and ± 27.0% of the population standard deviation for Downs, Chisholm and Turner, respectively with

95% confidence. The upper and lower theoretical confidence lines based on equation 5-8 were plotted on the same axes using the *ZVal* (Eq. 5-1) to provide the probability statistic for the desired confidence intervals.

5.7.2 Sampling Distributions

The example provided in Figure 5-8 was constructed from the cumulative infiltration (*Z*) for Downs at an opportunity time of 615.1 minutes, where each dot represents the average calculated from a random sample of the population.

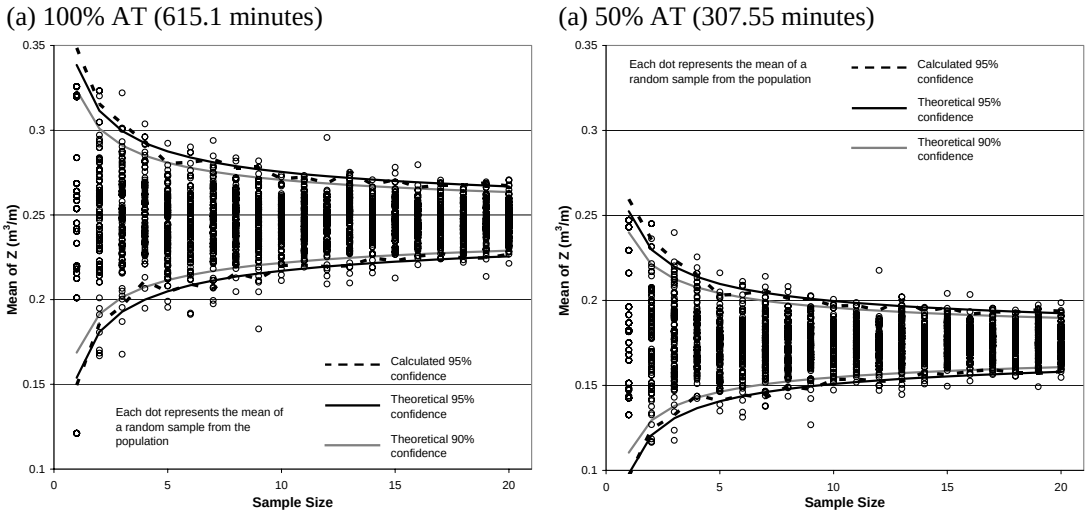

Figure 5-8 Sampling distribution of mean of Z with increasing sample size (Downs field)

The "Theoretical confidence" lines were calculated by applying equation 5-8 using the *ZVal* for the 90% and 95% confidence intervals, respectively. The points plotted at a sample size of one represent the individual infiltrated depth in each furrow, selecting two or three furrows generally improves the approximation of the mean but does not alter the spread of values. As the number of samples increases, the possible range of the estimated mean decreases. After ten samples, the use of any additional points does not significantly improve the estimate. The same trends are visible in the theoretical lines of the confidence intervals. Because the spread of the infiltration curves changes with time (Figure 5-4), the sampling distributions are shown for two different opportunity times (i.e. for Downs at 615.1 (Figure 5-8.a) and 307.55 minutes (Figure 5-8.b)). The confidence intervals for the mean satisfactorily approximate the variance of the curves over the range of sample sizes considered. A further check is provided

by the "Calculated 95% confidence", which is based on the mean and standard deviation of sampled values at each sample size (i.e. dots on Figure 5-8).

The sampling distributions for the standard deviation (Figure 5-9.a) was constructed using a similar process as for the mean. The range of estimated standard deviations decreases as the number of sampled furrows is increased. When the opportunity time is reduced (Figure 5-9.b) the magnitude of the standard deviations are decreased but the trend remains the same. Again, the confidence intervals (calculated by equation 5-9) appear to be able to characterise the sampling distribution for the standard deviation. It is worth noting that the precise location of each point within either of the sampling distributions (Figure 5-8 and Figure 5-9) is not important as the position of the individual depth measures will change on a repeat of the sampling procedure.

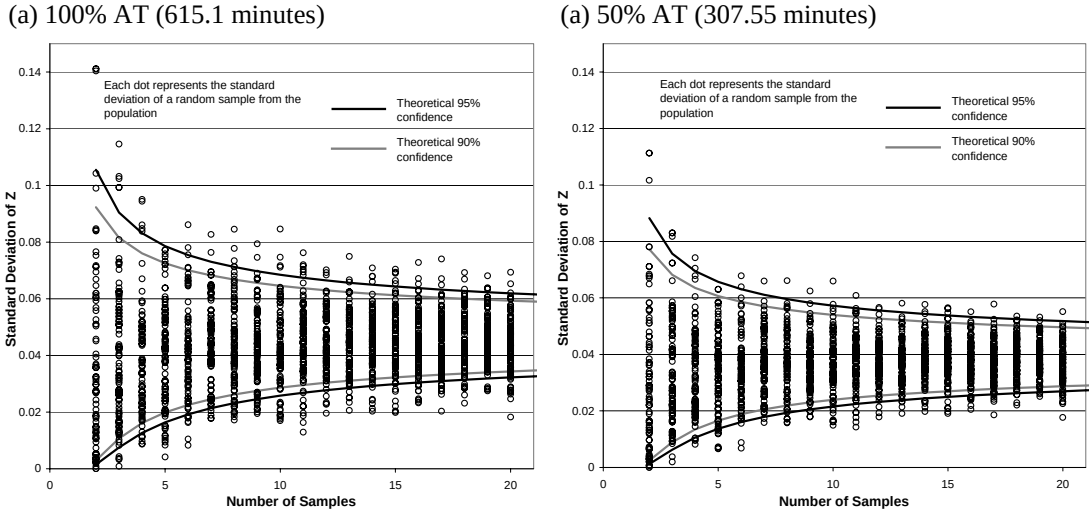

Figure 5-9 Sampling distribution of standard deviation of Z with increasing sample size (Downs field)

This process was replicated for opportunity times ranging from 25-150% of the average advance time for both the Chisholm and Turner fields. The results convey the same findings as above and have not been included here (some selected sampling distributions are presented in Appendix E). In all cases, the theoretical significance lines provide a satisfactory prediction for the calculated confidence intervals and describe the spread of the sampled points. For further validation, the procedure was repeated for the infiltrated depths at 615.1 minutes for Downs, this time using 900 replicates (Figure 5-10) of the sampling procedure instead of the 100 replicates used

previously. The increase in replicate number has improved the fit of the calculated confidence intervals to the theoretical lines. This further validates the use of the central limit theorem and equation 5-8 to predict the confidence intervals for the sample mean.

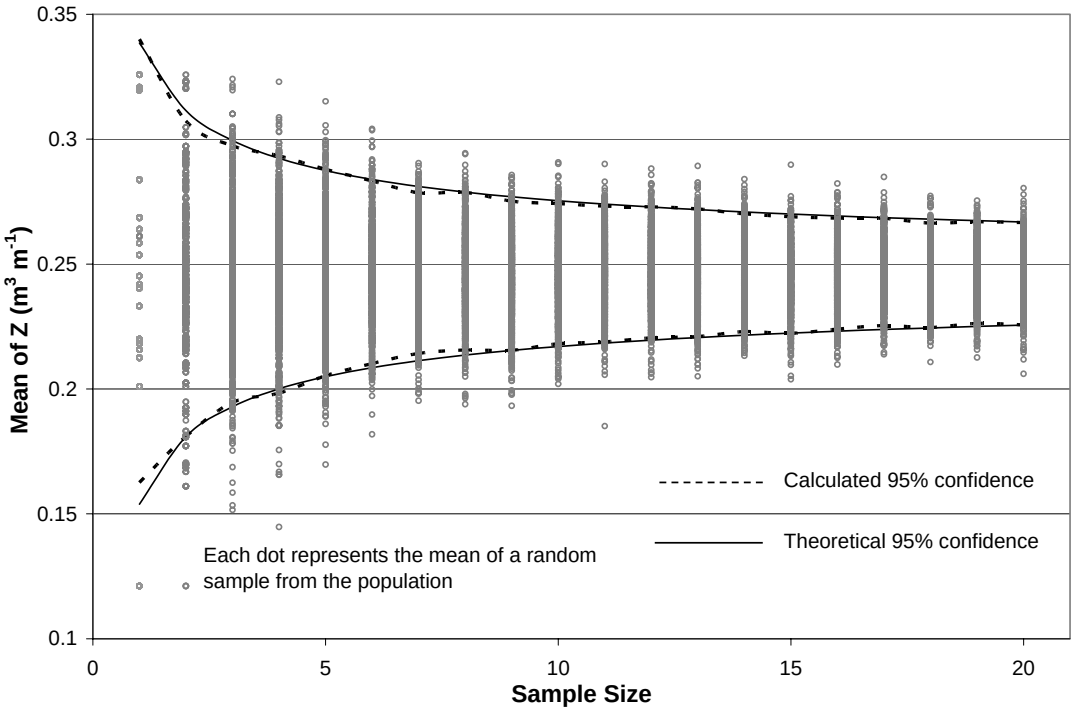

Figure 5-10 Sampling distribution of mean of Z using 900 random samples for each sample size (Downs field)

5.7.3 Number of Field Samples Required to Reach a Given Accuracy

The theoretical confidence expressions appear to describe the spread of the sampling distributions. Where the theoretical lines provide a good fit to the sampling distributions the sampling distributions should follow a normal distribution (Sakai et al. 1992). Where this is the case, the expression for the confidence interval (Eq. 5-8) can be rearranged to predict the number of samples required to determine the mean to an accuracy of $\overline{X} - \mu$ with a given confidence α:

$$N = \left(\frac{\sigma Z Val_{1-\alpha/2}}{\overline{X} - \mu} \right)^2 \quad \text{..... Eq 5-10}$$

Replacing the denominator with the relative error of the infiltration function, E_μ, this becomes (Sakai et al. 1992):

$$N = \left(\frac{\sigma ZVal_{1-\alpha/2}}{E_\mu \mu} \right)^2 \quad \text{..... Eq 5-11}$$

where the error term is given by.

$$E_\mu = \frac{\overline{X} - \mu}{\mu} \quad \text{..... Eq 5-12}$$

In a similar manner, where the plot of the sampling distribution for the standard deviation is adequately described by the curves constructed according to the confidence intervals, equation 5-9 can be used to estimate the number of samples necessary to evaluate the variance to a given level of accuracy. The term E_σ is proposed to represent the proportional error in the estimated standard deviation:

$$E_\sigma = \frac{\sigma_S}{\sigma} \quad \text{..... Eq 5-13}$$

and hence, equation 5-9 becomes:

$$\sqrt{\frac{\chi^2_{N-1,1-\frac{\alpha}{2}}}{N-1}} < E_\sigma < \sqrt{\frac{\chi^2_{N-1,\frac{\alpha}{2}}}{N-1}} \quad \text{..... Eq 5-14}$$

Sampling distributions for the mean and standard deviation were performed for the Downs, Chisholm and Turner data sets (i.e. the same procedure used to derive Figures 5-8 and 5-9) for values of opportunity time of 25%, 50%, 75%, 100%, and 150% of the average final advance time (AT) for Figure 5-11 was generated by applying equation 5-11 to the resultant sampling distributions. Similarly Figure 5-12 was created by applying equation 5-14 to the sampling distributions.

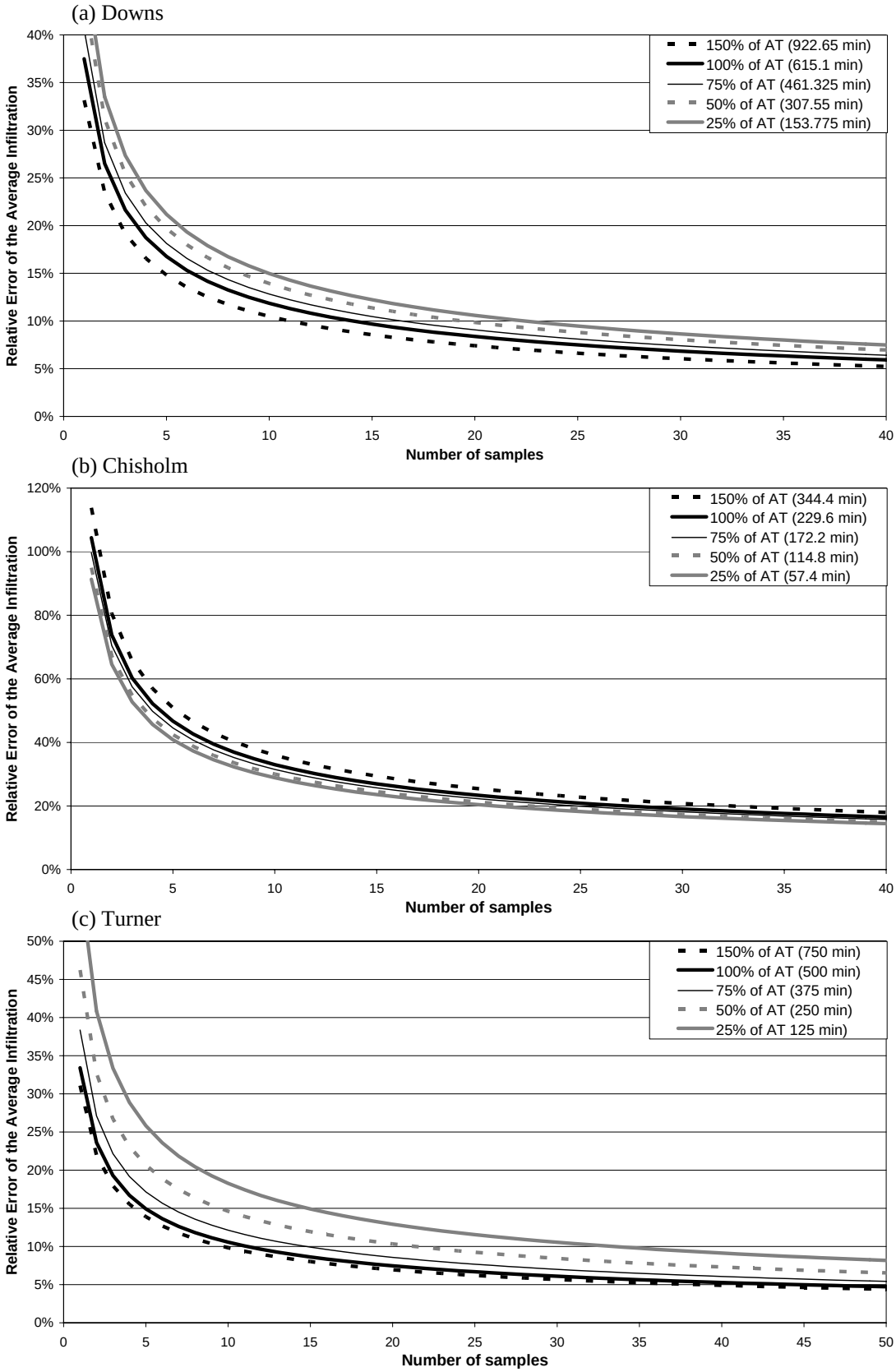

Figure 5-11 Maximum relative error in the estimated population mean (E_μ) according to sample size

- These lines are based on Eq. 5-11 with 95% confidence, AT = average final advance time

Increasing the sample size will increase the accuracy of the population statistics but the marginal improvement per additional sample declines exponentially. For Downs, increasing the sample size from three to four furrows decreases the error in the estimated mean by 2.6% (Figure 5-11.a) whilst increasing the sample from five to six furrows only decreases the error by 1.0%. The error (E_μ) on the vertical axis is a dimensionless value and hence should behave independently of the magnitude of infiltration. Despite this, the five lines corresponding to different opportunity times do exhibit some variance in the predicted error for a given sample size. In the Downs and Turner data, the mean has a greater relative error at shorter opportunity times whilst Chisholm instead demonstrates increased errors with time (Figure 5-11.b). Chisholm also features the highest error in estimation of the mean; this is caused by the high variability in soil intake between the measured furrows.

The form of the deviation error (E_σ) in equation 5-14 means that the relationship with sample size is consistent across all fields and opportunity times (Figure 5-12). With a sample of 10 furrows the estimate of the standard deviation could be in error by a factor of approx. 50% ($0.55 < E_\sigma < 1.45$. However, under the typical four furrow field evaluation technique of Irrimate™ the results indicate that the predicted variance may range anywhere between 0.268 and 1.765 as a ratio of the true value.

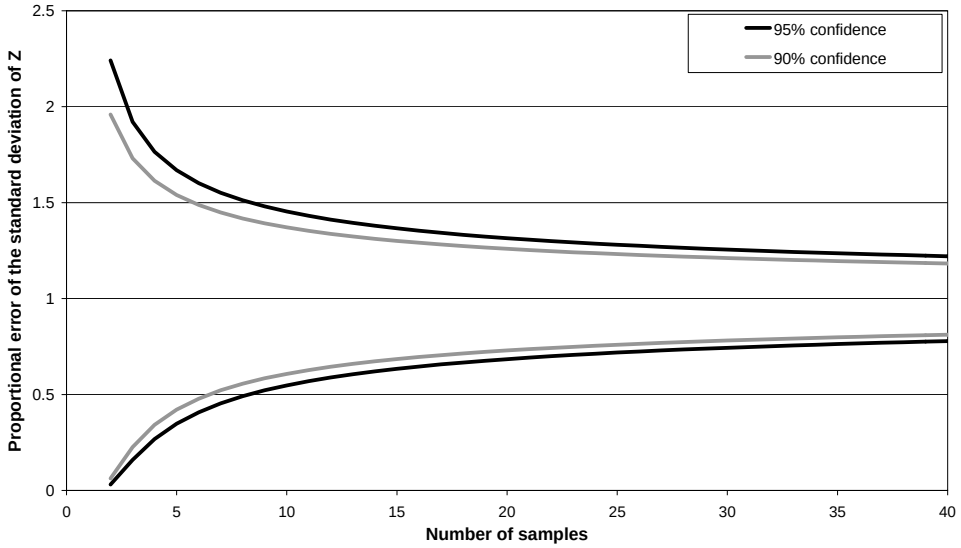

Figure 5-12 Maximum relative error in the estimated standard deviation (E_σ) according to sample size
- These lines are based on Eq. 5-14

It would be advantageous to pick a sample size that can reach the desired accuracy over a wide range of opportunity time. For Downs, to estimate the average infiltration to an accuracy of ± 10% at 923 minutes 11 furrows should be measured (Figure 5-11.a), but to obtain the same accuracy at 154 minutes the field trial must be expanded to include at least 24 furrows. Similar conclusions can be drawn from the Turner results (Figure 5-11.c). Figure 5-11.b indicates that it is impossible to achieve the same level of accuracy for Chisholm; over 30 furrows must be sampled just to decrease the error to ± 20%.

Unfortunately irrigation measurement is not free. The extra costs incurred through increasing the sample size should be weighed up against the potential benefits. This study does not include any consideration of crop yields hence it is worthless to factor in the measured costs since the likely influence on the profit is not known. The analysis of three data sets has shown that the furrow sample size required in order to produce reliable estimates of the mean infiltration is determined by the level of the infiltration variability. In highly variable conditions the field evaluation must include measurement of increasing numbers of furrows to maintain the same level of accuracy. Generally, a sample size of five furrows reduces the error of the predicted mean by over 50% compared to the use of a single furrow. Increasing the sample to 10 furrows only reduces this error approximately by a further 12% while 20 samples will further reduce this by 10% compared to the original error (Figure 5-11). From the results presented it appears that a sample size of 10 furrows is sufficient to capture the majority of the variance in infiltration while there is little benefit in increasing the sample size much past 20 measured furrows. It is important to note that these recommendations are based on furrows having constant infiltration. It is anticipated that a similar sampling distribution exists for talking multiple infiltration measurements within a single furrow. Hence, determination of the average infiltration rate along the furrow length should require a similar number of samples.

5.8 Describing Infiltration Variability using Statistical Distribution Functions

5.8.1 Statistical Test Methodology

The normal and log-normal distributions were selected as candidates to describe the variability of infiltration. The log-normal distribution is the most appropriate option but is a more complex relationship than the normal distribution. The distribution models are traditionally applied to the analysis of single random values. In this analysis, the variability in infiltration will be assessed by observing the cumulative infiltration at several periods of opportunity time. Accuracy problems may arise wherever the infiltration curve is extrapolated to times greater than the measured data from which they are estimated (chapter 4). Hence, the opportunity times were calculated as a proportion of the average final advance time (AT) for each field. The four opportunity times selected were 150%, 100%, 75% and 50% of the AT. The data analysis and statistical tests were carried out primarily using SPSS v12.0.

The first stage in the test for normality is to sort the observations by magnitude and divide the values into a number of equal intervals. The frequency histogram is constructed by plotting the number of observations that fall into each interval. The data provides a good fit to the proposed distribution where the measured frequencies approximate the theoretical frequency distribution. To test for the log-normal distribution, the data is transformed by taking the natural logarithm of the original values. Commonly, the test for normality is conducted graphically using the normal probability and detrended normal probability plots. The former is constructed by plotting the expected value of each point against the measured value (Norusis 1993). The resulting plot should approximate a straight line with any points that depart significantly from this line considered as possible outliers. The detrended normal plot is the plot of the residuals between the observed and expected values. Any trends observed in the plot of the residuals indicate a possible failure of the proposed distribution.

Further validation of the normal distribution can be conducted numerically by inspection of various statistics. The normal distribution is characterised by a symmetrical spread about the mean. Therefore, the median value should be approximately equal to the mean and the skew should be close to zero. If the absolute value of the skewness divided by its standard error is greater than 2, then the asymmetry observed in the sample did not occur by chance (Myers and Well 2003). The kurtosis value is an indication of the relationship between the sizes of the peak and tails of a distribution and its value reflects the departure from the normal curve (Myers and Well 2003). A high kurtosis value indicates a sharper peak while a low value infers a more rounded, flattened shape with thin tails (tending towards a uniform distribution). The kurtosis of a normal distribution is zero.

The Chi-squared goodness of fit test is preferred for hypothesis testing of a probability function but the small sample sizes involved in this analysis do not facilitate its use. The Lilliefors test based on a modification of the Kolmogorov-Smirnov test, is most commonly used but the Shapiro-Wilks significance test is more powerful for sample sizes smaller than 50 (Myers and Well 2003). The test hypothesis proposed is: *"the measured values can be approximated by a normal distribution"*. Where the value for α is less than 0.05 one can neglect the null hypothesis with a 95% significance level and conclude that the data does not follow a normal distribution. A higher value does not prove the fit to the proposed distribution but indicates that the distribution is a possible solution.

5.8.2 Downs

The average time of the final advance point (AT) (i.e. start of runoff) was found to be 615.1 minutes. The frequency histograms for the cumulative infiltration and logarithm of the cumulative infiltration at this opportunity time (Figure 5-13.a & b) identify a single outlier that appears to be an issue for both distributions. The log-normal probability plot (Figure 5-14.a) indicates that this point alone compromises the fit of the distribution function. This furrow (Irr.5 Fur.3) was identified earlier (section 0) as having possible issues with the measured inflow rate. Hence, the analysis for both normal and log-normal distributions was repeated omitting this furrow. Removing the

outlier caused the log-transformed values to more closely fit the normal distribution (Figure 5-13.d) and transformed the probability plot into a straight line (Figure 5-14.b).

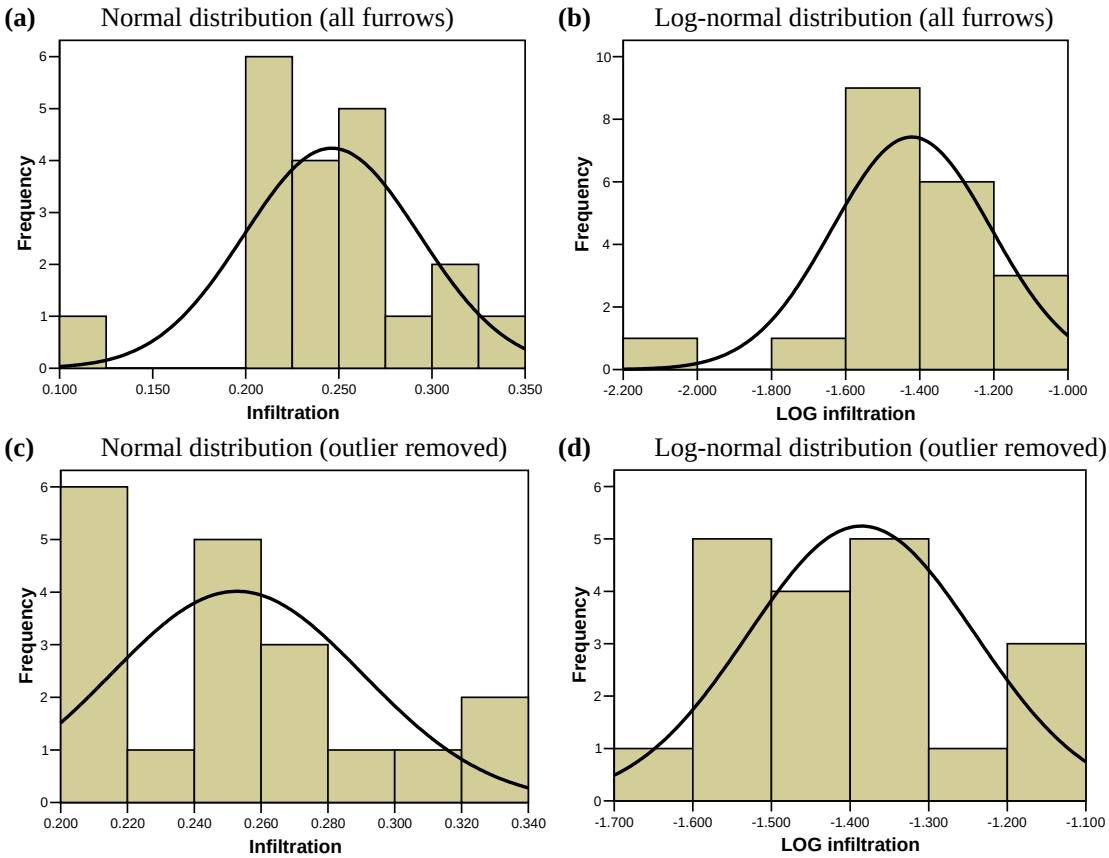

Figure 5-13 Frequency histograms of cumulative infiltration at 615.1 minutes opportunity time (Downs field)

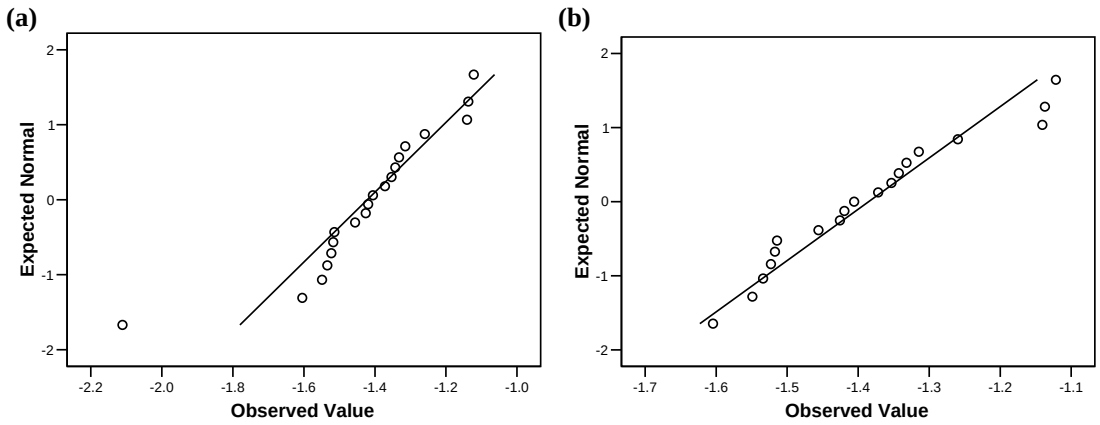

Figure 5-14 Log-normal probability plot of cumulative infiltration at 615.1 minutes with (a) all furrows and (b) outlier removed (Downs field)

Similar conclusions can be made from the numerical indicators of the distribution (Table 5-8). Considering all data (Table 5-8.a) the normal distribution is a possible candidate while the log-normal distribution fails the hypothesis test for most opportunity times. Where the outlier is removed, the Shapiro-Wilks significance test yielded 0.077 and 0.221 at 100% of the AT for the normal and log-normal data, respectively (Table 5-8.b). Hence, both distributions are possible fits to the data. However, the raw infiltration values have a larger skew than the logarithm of the infiltration values (e.g. 0.76 compared to 0.52) indicating that the log-normal distribution is more suitable. Both distributions provide acceptable levels of kurtosis where the outlier is omitted.

Table 5-8 Statistical summary of infiltration curves and test for normality considering both (a) all data and (b) outlier removed (Downs field)

(a)

	All Curves							
	Infiltration				**LOG Infiltration**			
% of AT[a]	**150%**	**100%**	**75%**	**50%**	**150%**	**100%**	**75%**	**50%**
Opp. time (min.)	922.7	615.1	461.3	307.6	922.7	615.1	461.3	307.6
Mean	0.306	0.246	0.213	0.175	-1.200	-1.422	-1.570	-1.768
Median	0.307	0.244	0.210	0.173	-1.182	-1.413	-1.562	-1.755
Min	0.154	0.121	0.104	0.086	-1.870	-2.111	-2.264	-2.457
Max	0.388	0.326	0.290	0.247	-0.947	-1.122	-1.236	-1.398
Skew	-0.95	-0.44	-0.20	0.01	-2.02	-1.54	-1.23	-0.92
Skew/SE	1.9	0.9	0.4	0.0	4.0	3.0	2.4	1.8
Kurtosis	3.02	1.68	0.99	0.39	6.91	4.94	3.65	2.32
Shapro-Wilk								
Stat	0.910	0.931	0.947	0.967	0.812	0.859	0.892	0.931
Sig	0.063	0.163	0.329	0.682	0.001	0.007	0.029	0.160
	OK	OK	OK	OK	Fail	Fail	Fail	OK

(b)

	Outlier Removed							
	Infiltration				**LOG Infiltration**			
% of AT[a]	**150%**	**100%**	**75%**	**50%**	**150%**	**100%**	**75%**	**50%**
Opp. time (min.)	922.7	615.1	461.3	307.6	922.7	615.1	461.3	307.6
Mean	0.314	0.253	0.218	0.180	-1.165	-1.385	-1.534	-1.732
Median	0.311	0.245	0.213	0.175	-1.169	-1.406	-1.545	-1.742
Min	0.262	0.201	0.167	0.133	-1.338	-1.605	-1.790	-2.020
Max	0.388	0.326	0.290	0.247	-0.947	-1.122	-1.236	-1.398
Skew	0.66	0.76	0.73	0.67	0.47	0.52	0.45	0.36
Skew/SE	1.3	1.4	1.4	1.3	0.9	1.0	0.9	0.7
Kurtosis	0.66	-0.27	-0.31	-0.41	-0.66	-0.55	-0.60	-0.72
Shapro-Wilk								
Stat	0.929	0.911	0.916	0.930	0.946	0.936	0.940	0.954
Sig	0.164	0.077	0.094	0.176	0.341	0.221	0.266	0.466
	OK	OK	OK	OK	OK	OK	OK	OK

[a] ***% of AT*** **refers to a percentage of the average final advance time**

5.8.3 Chisholm

The same statistical procedures were carried out for Chisholm. Histograms were constructed for opportunity times of 100% of the AT (230 minutes) and 800 minutes (Figure 5-15). The 230 minute data clearly demonstrates a positive skew whilst the log-transformed data is approximately equally distributed around the mean. This skew becomes stronger as time increases. At 800 minutes, the normal distribution struggles to fit the distribution of the infiltrated volumes (Figure 5-15.c).

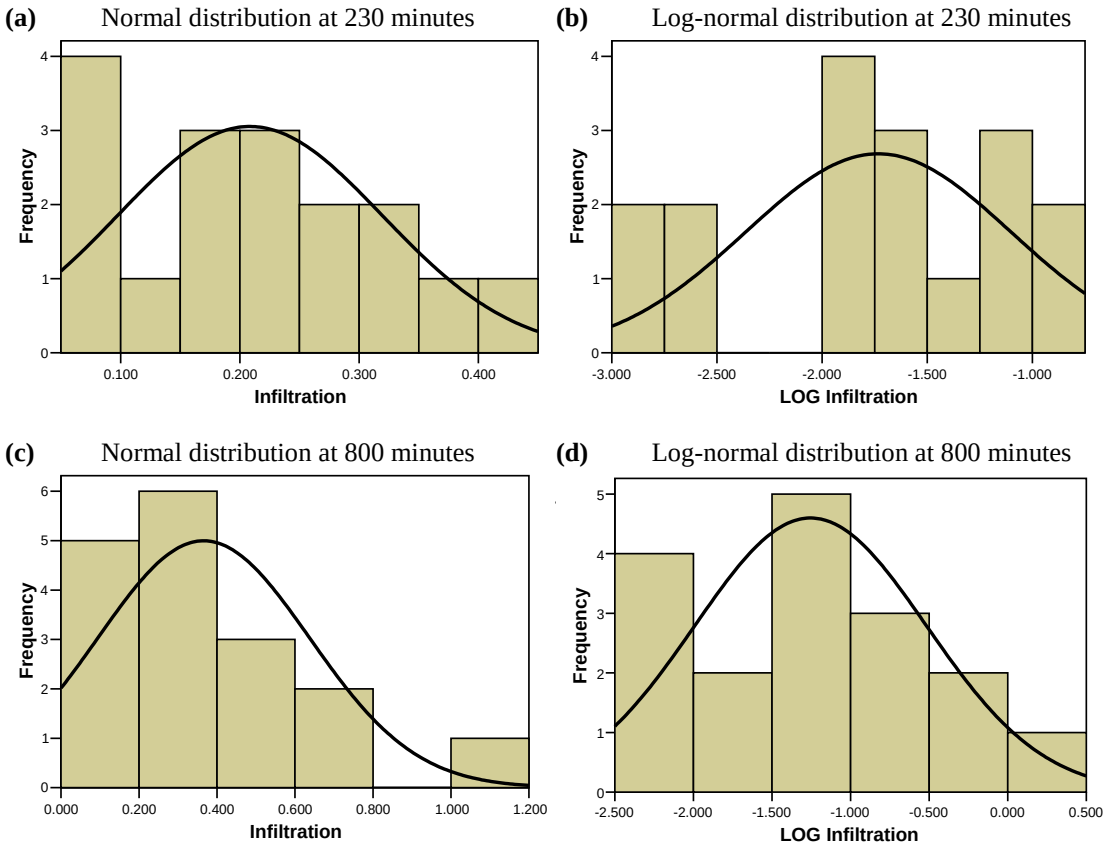

Figure 5-15 Frequency histograms of cumulative infiltration at 230 and 800 minutes opportunity time (Chisholm field)

At times greater than the AT (i.e. 150% and 800 minutes), the skew of the infiltration was large and positive while the log-transformed values showed minimal skew (Table 5-9). For a normal distribution, the mean and median should be equal. In general, the mean and median were closer to each other for the log-transformed values compared to the untransformed data. The moderate values for kurtosis, although still within tolerable limits, indicate that the distribution was less peaked than expected.

Generally, the logarithm of the infiltration function resulted in kurtosis values closer to zero. The infiltration volumes satisfy the significance test for times equal to or less than 1½ times the AT but fail at 800 minutes. In contrast, the significance test indicated that the log-normal cannot predict the distribution at 50% of the AT but provides a better fit at longer opportunity times.

Table 5-9 Statistical summary of infiltration curves and test for normality (Chisholm field)

	Infiltration					LOG Infiltration				
% of AT	**348%**	**150%**	**100%**	**75%**	**50%**	**348%**	**150%**	**100%**	**75%**	**50%**
Opp. time (min.)	800	344	230	172	115	800	344	230	172	115
Mean	0.366	0.246	0.208	0.187	0.161	-1.254	-1.583	-1.733	-1.835	-1.974
Median	0.282	0.232	0.210	0.196	0.177	-1.266	-1.463	-1.561	-1.631	-1.729
Min	0.091	0.068	0.059	0.053	0.046	-2.399	-2.695	-2.837	-2.939	-3.081
Max	1.088	0.553	0.418	0.351	0.283	0.084	-0.592	-0.872	-1.047	-1.261
Skew	1.35	0.61	0.29	0.09	-0.14	0.05	-0.38	-0.57	-0.68	-0.82
Skew/SE	2.5	1.1	0.5	0.2	0.3	0.1	0.7	1.0	-0.7	1.5
Kurtosis	1.73	-0.37	-0.86	-1.04	-1.14	-0.89	-0.90	-0.84	-0.78	-0.69
Shapro-Wilk										
Stat	0.868	0.940	0.951	0.948	0.939	0.964	0.942	0.918	0.898	0.870
Sig	0.020	0.314	0.466	0.429	0.307	0.712	0.342	0.139	0.062	0.022
	Fail	OK	OK	OK	OK	OK	OK	OK	OK	Fail

5.8.4 Turner

Turner is the most appropriate field for this analysis due to the larger number of observations. The frequency histograms (Figure 5-16) do not favour one model over the other and at both 500 and 1000 minutes both the normal and log-normal distributions are poor but possible fits to the data. The statistical summary (Table 5-10) indicates that the mean and median were approximately equal for both cases at all times considered. Neither model considered departs significantly from the expected symmetry, as the relative skewness did not reach values above 2. The log-transformed infiltration generally offered an improved fit to the shape of the curve particularly at longer times indicated by the lower kurtosis values. The significance test indicates that neither distribution should be used to describe the distribution of infiltrated depths at times less than the AT (i.e. 375 and 250 minutes).

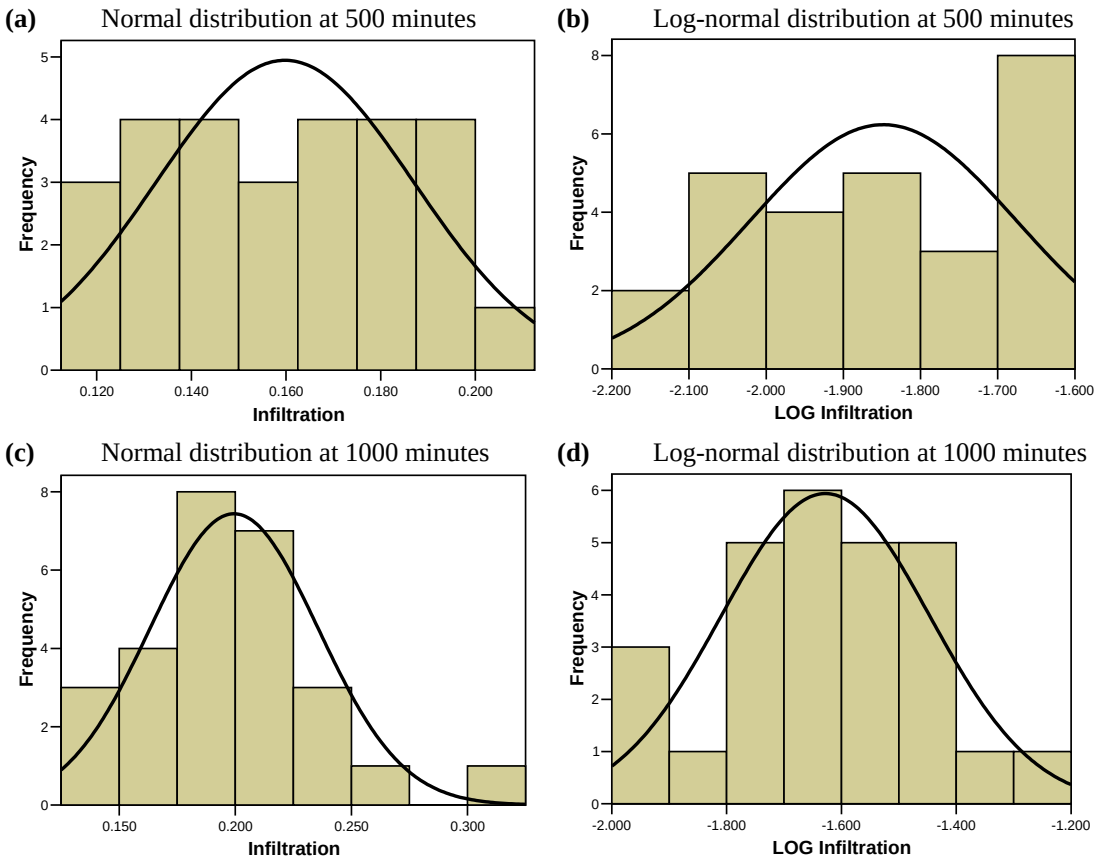

Figure 5-16 Frequency histograms of cumulative infiltration at 500 and 1000 minutes opportunity time (Turner field)

Table 5-10 Statistical summary of infiltration curves and test for normality (Turner field)

	Infiltration					LOG Infiltration				
% of AT		150%	100%	75%	50%		150%	100%	75%	50%
Opp. time (min.)	1000	750	500	375	250	1000	750	500	375	250
Mean	0.199	0.180	0.160	0.148	0.135	-1.628	-1.725	-1.848	-1.927	-2.027
Median	0.198	0.182	0.160	0.146	0.131	-1.620	-1.702	-1.833	-1.927	-2.031
Min	0.138	0.127	0.117	0.109	0.086	-1.980	-2.061	-2.149	-2.213	-2.448
Max	0.300	0.231	0.201	0.191	0.180	-1.204	-1.464	-1.605	-1.654	-1.713
Skew	0.50	-0.15	0.07	0.19	0.07	-0.08	-0.45	-0.13	0.05	-0.13
Skew/SE	1.1	0.3	0.2	0.4	0.2	0.2	1.0	0.3	0.1	0.3
Kurtosis	0.98	-0.70	-1.27	-1.56	-1.56	0.14	-0.50	-1.22	-1.59	-1.47
Shapro-Wilk										
Stat	0.964	0.968	0.939	0.894	0.901	0.974	0.956	0.942	0.900	0.908
Sig	0.443	0.558	0.118	0.010	0.014	0.704	0.293	0.138	0.013	0.020
	OK	OK	OK	Fail	Fail	OK	OK	OK	Fail	Fail

5.8.5 Discussion

Three different fields were used to determine if the variability in the infiltration curves at the field scale can be described by either the normal or log-normal distribution functions. Both statistical models passed the significance test at times

equal to the last measured advance point but fail under some circumstances. Since the infiltration curves were based on data collected during the advance (all data) and storage phases (Downs only) it is anticipated that these curves are only applicable over opportunity times close to and less than the measured field data. At longer times, these curves are simply extrapolated and often do not reflect the real infiltration behaviour. However, the initial shape of the infiltration curve is vulnerable to initial variations in the inflow rate (all infiltration parameters in this section are based on the constant inflow assumption). Therefore, studies of the infiltration rates should focus on the later stages of the opportunity time. There is a tendency for the log-normal function to provide a better fit compared to the normal at longer times, where the variability is greatest, whilst at 50% of the AT the inverse is true. This supports the findings of Sharma et al. (1983) who concluded that the distribution of infiltration is influenced by the magnitude of variability, which in their case was determined by measurement spacing. Jaynes and Clemmens (1986) propose that use of the normal distribution is justified if the CV is less than 50%, which is clearly not the case for the Chisholm infiltration curves (Figure 5-7). In general, the log-normal distribution function provides a slightly better fit to the variation and is therefore the preferred choice for the predictive procedure proposed in section 5.9.

5.9 Estimating Infiltration using Probability

It is hypothesised that the statistical distribution of infiltration between furrows can be estimated from other simple field measurements. It should be possible to define the mean and variance of the population but also estimate the intake of individual furrows using the chosen measurement. IPARM has shown that the parameters of the infiltration function can be estimated from advance measurements. However, the high data requirements restrict the use of these techniques to capture the full extent of the field variability. It would be a great advantage to be able to estimate the infiltration curve from a single advance measurement at the tail end of the furrow. In addition to the reduced data requirements, the positioning of the measurement at the end of the field facilitates easy access for observation, setup and recovery of measurement apparatus.

5.9.1 Development of an Infiltration Prediction Procedure

It is proposed that a strong relationship exists between the Modified Kostiakov infiltration function (Eq. 2-6) Z and the infiltration estimated by a rearrangement of the volume balance. The traditional volume balance equation for advance can be re-arranged to form an expression for the infiltration volume:

$$V_I = \frac{Q_0 t - \sigma_y A_0 x}{x} \quad \text{..... Eq 5-15}$$

where Z can be expressed as:

$$Z = k\tau^a + f_0\tau \quad \text{..... Eq 5-16}$$

A direct relationship between V_I and Z will eliminate the subsurface storage factors (σ_{z1} and σ_{z2}) from the volume balance (Eq. 4-9). Hence, the approach will also remove the requirement to calculate the power curve exponent (r) of the advance trajectory.

The volume of infiltration calculated from equation 5-15 at a single advance point yields a single value whereas the expression for infiltration is a function of opportunity time. Hence, it would be beneficial to describe the variability of infiltration as a difference between infiltration curves rather than merely a difference in cumulative volume at a single time. Therefore, the proposed procedure will need to consider the infiltration curve Z over a range of opportunity times. Previous work (chapter 4) has indicated that the early part of the infiltration curve is subject to uncertainty due to initial inflow rate variation. Hence, it may be sensible to reduce the importance of that part of the infiltration curve. Also, the typical concave shape of the advance curve means that the distribution of the opportunity times over the furrow length is skewed towards higher values. From the validation of IPARM (chapter 4), it is clear that the estimated infiltration curves are only applicable over times less than or equal to the field measurements on which they are based. Hence, the range of opportunity times used to describe the infiltration curve will be restricted to values less than the final advance time.

An initial evaluation of the proposed model involved testing with a number of different ranges of opportunity times (i.e. 0 to 100% and 50 to 150% of the AT). From this analysis it was found that the logarithm of the section of the infiltration curve

between 50% and 100% of the AT had the highest correlation with the logarithm of the volume balance calculated at the final advance point. This section of the infiltration curve resulted in the best correlation between the *ZVal* and CV of the logarithm of infiltration (logarithm of Eq. 5-16) with the logarithm of the volume balance (logarithm of Eq. 5-15).

The approach selected to predict infiltration involves calculating the average *ZVal* of the natural logarithm of cumulative infiltration volumes for opportunity times (τ) over the time interval from 50% to 100% of the AT:

$$ZVal_{Infiltration} = \frac{\sum_{i=0}^{N} \frac{\ln(Z(\tau)) - \overline{\ln(Z(\tau))}}{\sigma_{S\ln(z(\tau))}}}{N} \quad \text{..... Eq 5-17}$$

where

$$\tau = \frac{AT}{2} + i\left(\frac{\frac{AT}{2}}{N-1}\right) \quad \text{..... Eq 5-18}$$

where $Z(\tau)$ is the Modified Kostiakov infiltration at opportunity time τ for the furrow of interest and $\overline{\ln(Z(\tau))}$ is the average of the natural logarithm of infiltration calculated across all furrows at time τ. In a similar fashion, *ZVal* for V_I of the volume balance equation is calculated from the measured inflow and a single advance point:

$$ZVal_{VB} = \frac{\ln(V_I) - \overline{\ln(V_I)}}{\sigma_{S\ln(V_I)}} \quad \text{..... Eq 5-19}$$

From the direct relationship between equations 5-15 and 5-16 it follows that $ZVal_{VB}$ should be positively correlated with $ZVal_{Infiltration}$ with a scaling factor, ω_{ZVal}:

$$ZVal_{Infiltration} = \omega_{ZVal} ZVal_{VB} \quad \text{..... Eq 5-20}$$

Substitution into equation 5-1 results in an expression to estimate the infiltration from the single advance point. The only remaining unknown is σ, the standard deviation of the infiltration function. The standard deviation is non-dimensionalised by dividing by the mean to enable comparison between the different units:

$$CV_{Infiltration} = \frac{\sum_{i=0}^{N}\left(\sigma_{S\ln(z(\tau))} \Big/ \overline{\ln(Z(\tau))}\right)}{N} \quad \text{..... Eq 5-21}$$

where $CV_{Infiltration}$ is calculated over the same time interval as for $ZVal_{Infiltration}$. In a similar manner to before, the CV calculated from the logarithm of the infiltration curve (CV_{VB}) should be related to the CV of the logarithm of the volume balance multiplied by the scaling coefficient ω_{CV}:

$$CV_{Infiltration} = \omega_{CV} CV_{VB} \quad \text{..... Eq 5-22}$$

where:

$$CV_{VB} = \frac{\sigma_{S\ln(V_I)}}{\overline{\ln(V_I)}} \quad \text{..... Eq 5-23}$$

Re-arrangement of equation 5-17 and substitution of the standard deviation term with

$$\sigma_{S\ln(Z(\tau))} = CV_{Infiltration}.\overline{\ln(Z(\tau))} \quad \text{..... Eq 5-24}$$

leads to an expression to predict the average infiltrated depth at a given opportunity time from one or more known infiltration curves (N_K):

$$\overline{\ln(Z(\tau))} = \frac{\sum_{j=0}^{N_K}\left(\frac{\ln(Z(\tau)_j)}{CV_{Infiltration} ZVal_{Infiltration} + 1}\right)}{N_K} \quad \text{..... Eq 5-25}$$

The infiltration parameters of any infiltration curve are found by minimising the sum of squares between the predicted *ZVal* and $ZVal_{Infiltration}$

$$Objective = \frac{\sum_{i=0}^{N}\left[\left(\frac{\left(\ln(Zp(\tau)) - \overline{\ln(Z(\tau))}\right)}{CV_{Infiltration}.\overline{\ln(Z(\tau))}} - ZVal_{Infiltration}\right)^2\right]}{N} \quad \text{..... Eq 5-26}$$

where τ is given by equation 5-18 and *Zp* is the infiltration depth calculated from the predicted infiltration parameters of the Modified Kostiakov equation. This expression is evaluated and averaged over opportunity times from 50%-100% of the AT to form a single time-averaged value. Finally, the infiltration parameters (i.e. *a*, *k*, and f_0) are solved via a regression technique similar to that used by IPARM. Similarly, the parameters corresponding to the average infiltration curve can be found by setting $ZVal_{Infiltration}$ to zero and solving for the infiltration parameters.

The proposed procedure to predict the infiltration parameters from a single advance point is described as follows:

1. Obtain measurements from a number of furrows (inflow rate, slope, furrow geometry and single advance point) and detailed measurements of advance and or advance and runoff for one or more furrows.
2. Calculate the infiltration parameters for those furrows with detailed measurement using IPARM or INFILT (these are the "known" furrows).
3. Calculate the volume of infiltration using the volume balance for each furrow at the single advance point (using Eq. 5-15).
4. Calculate the CV_{VB} of the population (Eq. 5-23) and $ZVal_{VB}$ (Eq. 5-19) for each furrow from the logarithm of the values in step 3.
5. Estimate $CV_{Infiltration}$ from CV_{VB} calculated in step 4 (Eq. 5-22) and $ZVal_{Infiltration}$ from $ZVal_{VB}$ for each furrow (Eq. 5-20).
6. Use $CV_{Infiltration}$ and the $ZVal_{Infiltration}$ of the selected furrow(s) in step 5 to estimate the average infiltration curve, using equation 5-25.
7. Use $CV_{Infiltration}$, $ZVal_{VB}$ for the first furrow with the single advance point and the average infiltration curve ($\overline{\ln(Z(\tau))}$) in step 6 to predict the infiltration parameters for that furrow using equation 5-26.
8. Repeat step 7 for each of the furrows with a single advance point.

This procedure was coded in C++ and developed into an executable file using Borland C++ Builder 6. The software is divided into three tabbed sections. The first screen uses the expression for the $ZVal_{Infiltration}$ (Eq. 5-17) to determine the probabilities for a given set of infiltration curves. The second screen prompts the user for the field data and calculates the probabilities for each furrow and total variance according to the single advance points (Eq. 5-19 and Eq. 5-23, respectively). The third screen prompts the user to choose one or more "base" furrows with known infiltration and then predicts the infiltration parameters for all remaining furrows using the eight step process described above.

This predictive procedure assumes that the distribution of the infiltration curves is correlated to that of the infiltration terms derived using the volume balance approach.

Hence, the probability calculated from the logarithm of the volume balance infiltrations should be correlated with the time averaged logarithm of the infiltration curve. The field measurements from Downs, Chisholm and Turner were used to evaluate this relationship. The *ZVal* values for the infiltration curves (Eq. 5-17) and volume balance approach (Eq. 5-19) were calculated for each furrow within the three fields (Figure 5-17).

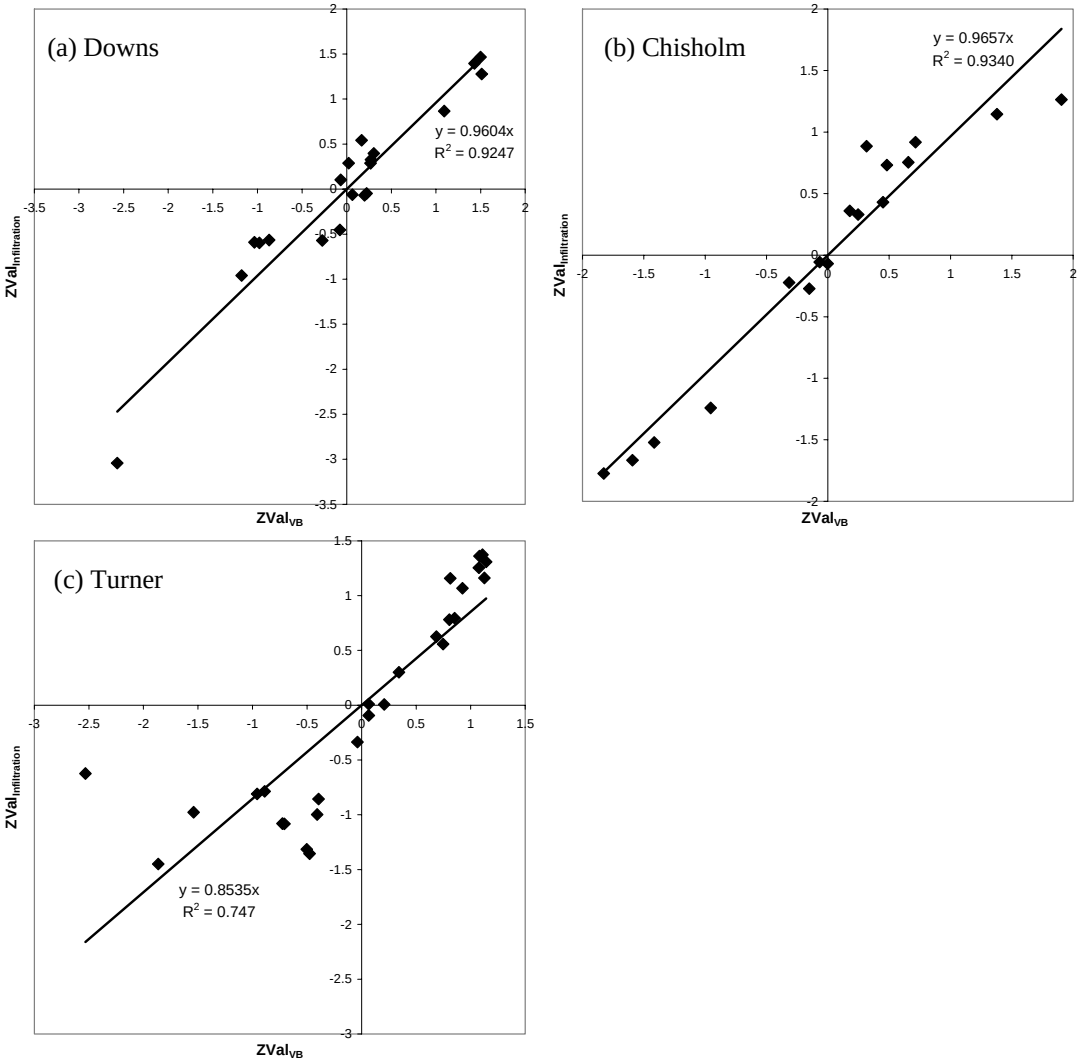

Figure 5-17 Scatter plot between the *ZVal* of the infiltration curve and *ZVal* of the volume balance infiltration term

In the analysis for Downs, the *ZVal* values were positively correlated (t_{Stat} = 15.28, α < 0.001) with a slope of 0.960 and R^2 of 0.925 (Figure 5-17.a). For Chisholm (Figure 5-17.b), they were correlated (t_{Stat} = 15.05, α < 0.001) with a slope of 0.966 and R^2 of 0.934. However, for the Turner data (Figure 5-17.c), they were correlated

(t_{Stat} = 8.76, α < 0.001) with a lower slope (0.854) and R^2 of 0.747. In this case, it appears that the departure from the power relationship was caused by a single outlying point at $ZVal_{Infiltration}$ = -2.5. When the *ZVal* values were re-calculated removing this outlying furrow the correlation improved (slope = 0.923, R^2 = 0.867). The slope of the linear correlation does not depart significantly from unity for any of the fields considered. Hence the scaling factor for the *ZVal* will be assigned a value of ω_{ZVal} = 1.0.

The proposed method of predicting infiltration requires a strong relationship between the magnitude of the variance of the infiltration curves and the variance in infiltration calculated by the volume balance. If all other sources of variability are eliminated, the relative variance and hence, the CV of these two quantities should be equal. A series of correlations were performed using the data from the Downs, Chisholm and Turner sites as well as data from four additional fields (i.e. Coulton A, B and C and Turner Field 18). The CV values were found to be positively correlated with a slope of 0.95 and R^2 of 0.756 for the three primary fields and 0.662 where additional fields were included (Figure 5-18).

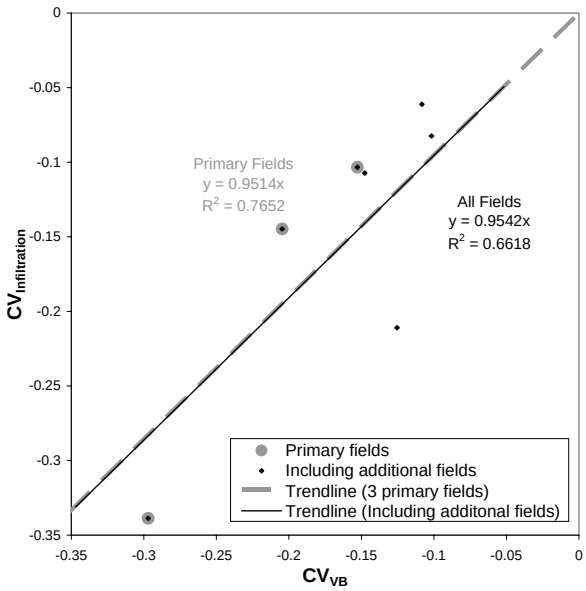

Figure 5-18 Correlation of CV between logarithm infiltration and logarithm of volume balance

An R^2 less than unity indicates that some of the variance in the volume balance is caused by factors other than infiltration (such as uncertainty in inflow rates or surface

roughness). The scaling coefficient ω_{CV} for the CV relationship in equation 5-22 is equal to the slope of this line. The limited number of points in Figure 5-18 makes it difficult to obtain a reliable estimate of this statistic. It was found that the removal of one or two fields significantly altered the trend line position. In the subsequent validation of this method (section 5.9.2) the coefficient will be given the value ω_{CV} = 1.0. However, further testing may be required to validate this assumption or determine a more reliable value for this coefficient.

5.9.2 Validation of the Infiltration Prediction Procedure

The Downs, Chisholm and Turner fields were used to validate the predictive technique. Several tests were performed using different selections and numbers of "known" infiltration curves to predict the infiltration curves for the remaining furrows. Each case study used the final advance point in every furrow combined with the IPARM calibrated infiltration curve(s) from:

- Case Study A: Downs using Irr1Fur1
- Case Study B: Downs using all furrows from the second irrigation (Irr2F1-4)
- Case Study C: Chisholm using Irr3Fur1
- Case Study D: Chisholm using Irr1Fur1 and Irr2Fur1
- Case Study E: Turner using the two furrows of irrigation 1 (Irr1Fur1 and Irr1Fur2)
- Case Study F: Turner using the single furrow, Irr2Fur1

In some instances, the time value for the last advance distance was not measured. Hence, the final measured advance point distance varied between the furrows of each field. The estimated infiltration parameters for each of the six case studies can be found in Appendix F.

Comparison between the "actual" infiltration curves (from IPARM) and predicted infiltration curves for case study A (Figure 5-19) demonstrates the ability of the procedure to estimate the sets of infiltration parameters using only a single known furrow. In this case, the predictive procedure has overestimated the spread of the infiltration curves but has provided a good reproduction of the relative position of

each curve. In most cases, the relative positions of the infiltration curves are preserved in relation to the known furrow (irrigation 1 furrow 1, given by the shaded circles).

(a) Actual infiltration curves from IPARM

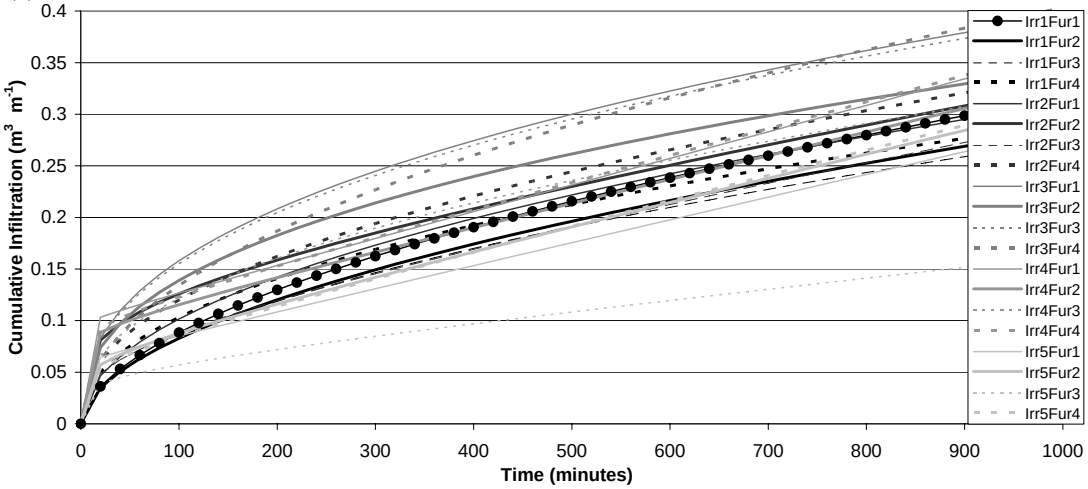

(b) Predicted using final advance points and infiltration parameters from Irr1Fur1 (case study A)

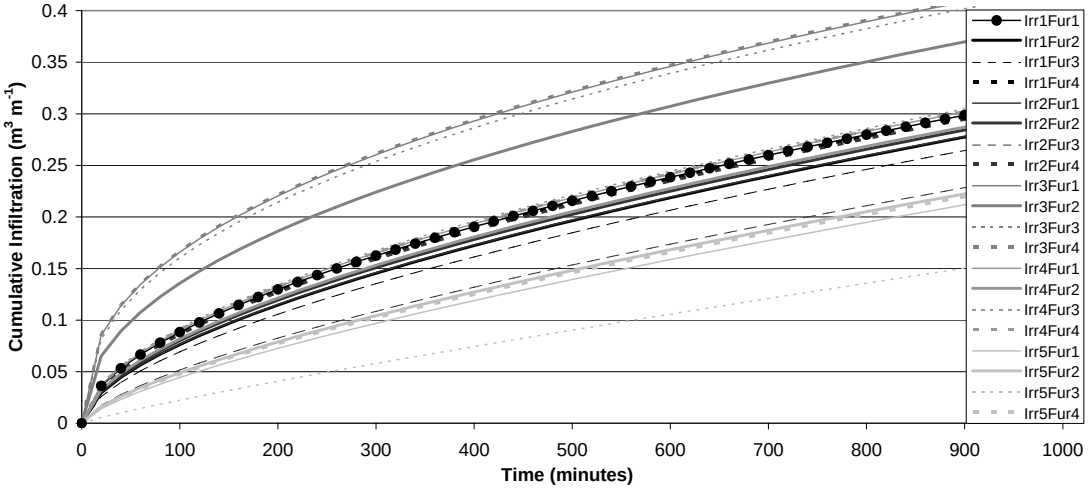

Figure 5-19 Comparing predicted and IPARM estimated infiltration curves (Downs field, using Irr1Fur1)

The accuracy of the proposed technique is best evaluated by the ability of the trend line fitted to the predicted and actual infiltrated depths at a given opportunity time to approximate a 1:1 line with $R^2 = 1$. This regression was performed at four values of opportunity time or each case study, at approximately one third of, two thirds of and the average final advance time with an additional later time point (Figure 5-20). In this analysis all infiltration curves are generated from the predicted infiltration parameters, even for the "known" furrows. This will remove any bias introduced by the known points as they will always lie on the 1:1 correlation line.

(a) Downs using Irr1Fur1

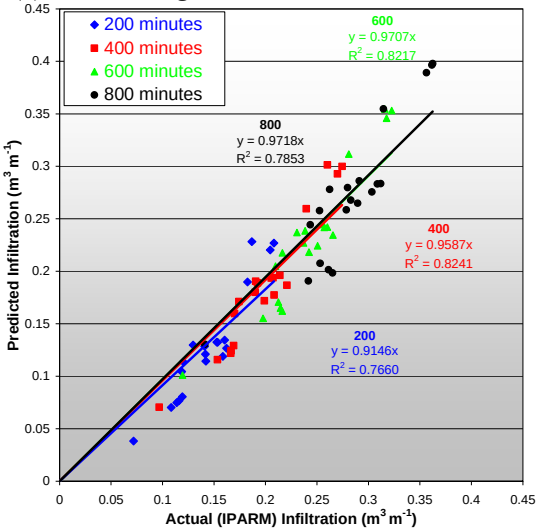

(b) Downs using Irr2, Fur1, Fur2, Fur3, Fur 4

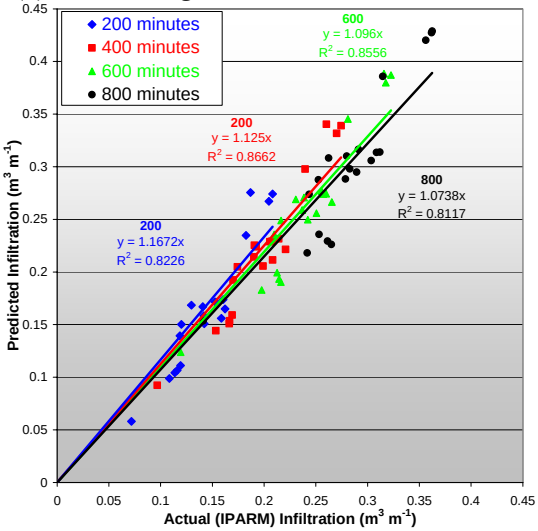

(c) Chisholm using Irr3Fur1

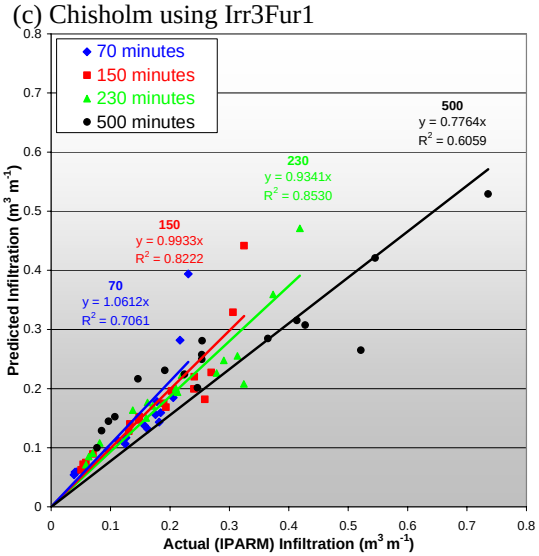

(d) Chisholm using Irr1Fur1, Irr2Fur1

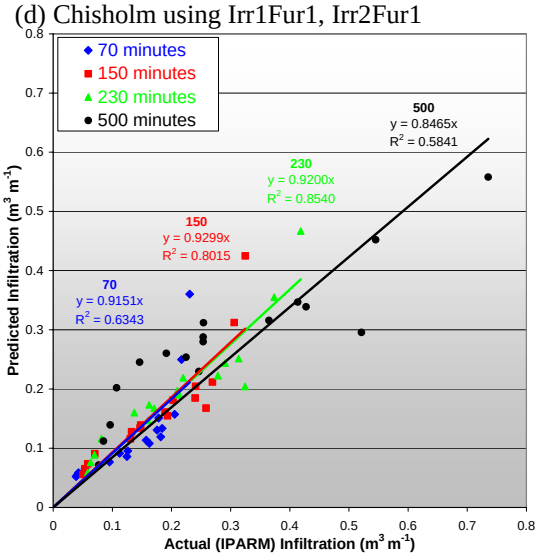

(e) Turner with Irr1Fur1, Irr1Fur2

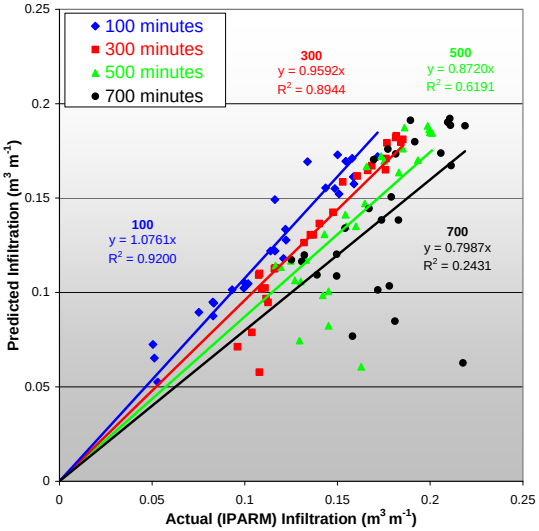

(f) Turner with Irr7Fur1,Irr7Fur2, Irr7Fur3, Irr7F4

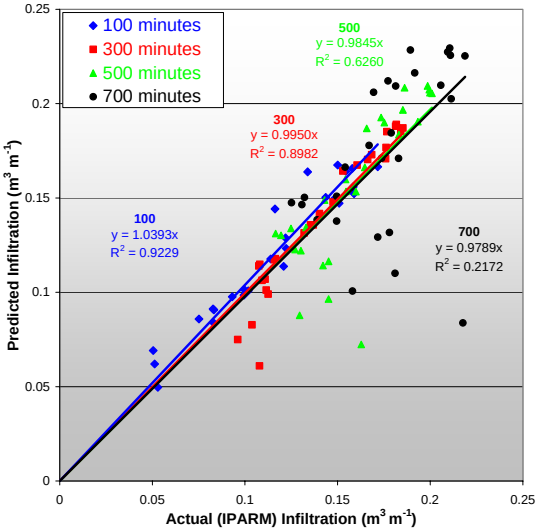

Figure 5-20 Comparison between infiltration depths from the predictive procedure and those estimated using IPARM (actual)

For case study A, the infiltration parameters are estimated using a single furrow from the first irrigation. The points of the scatter plot approximate a straight line (Figure 5-20.a) and the slope and R^2 value of the regression between predicted and actual infiltrated depths is close to unity. The slight improvement in R^2 for case B indicates that the prediction can be improved by using an increased number of "known" furrows (i.e. all four furrows of the second irrigation). In case C, the infiltration curves are predicted using a furrow with an infiltration curve that falls close to the average. For case D, the infiltration parameters are predicted using two furrows that represent the maximum (Irr2 Fur1) and minimum (Irr1 Fur1) for the field. There is little difference in the fit between the predicted and actual values indicating that the furrow selection is not crucial to the outcome. For Turner, the curves estimated using all four furrows of the seventh irrigation (Figure 5-20.f, case study F) provide a slight improvement in correlation compared to those based on the 2 furrows from the first irrigation (case study E). Generally, the predicted infiltrations provide reliable estimates for the majority of furrows for times less than the final advance point. Thereafter, the correlation decreases (declining R^2) and the slope of the trend lines tend to depart from unity. Further validation of the estimated infiltration curves is provided by comparison of the infiltrated depths at given opportunity times (Table 5-11).

Table 5-11 Comparison between actual (IPARM estimated) and predicted infiltration curves

	Opportunity Time (min)	Mean Z ($m^3\ m^{-1}$)	CV (%)	Mean Z ($m^3\ m^{-1}$)	CV (%)	Mean Z ($m^3\ m^{-1}$)	CV (%)
Downs		Actual (IPARM)		Case A		Case B	
	200	0.1446	23.7	0.1281	41.0	0.1651	35.9
	400	0.1984	21.4	0.1863	33.5	0.2199	30.2
	600	0.2430	19.3	0.2325	29.1	0.2635	26.6
	800	0.2831	17.6	0.2724	25.9	0.3018	23.9
Chisholm		Actual (IPARM)		Case C		Case D	
	70	0.1369	46.9	0.1432	60.3	0.1237	63.0
	150	0.1774	49.9	0.1768	54.0	0.1650	55.6
	230	0.2086	53.3	0.2001	50.1	0.1964	51.1
	500	0.2908	64.1	0.2535	41.7	0.2765	42.4
Turner		Actual (IPARM)		Case E		Case F	
	100	0.1153	31.0	0.1251	29.0	0.1207	29.4
	300	0.1408	21.8	0.1336	28.1	0.1387	27.7
	500	0.1598	17.0	0.1381	27.7	0.1563	26.1
	700	0.1765	15.7	0.1414	27.4	0.1737	24.9

results are based on the infiltration parameters in Appendix F

The results in Table 5-11 demonstrate that the predicted infiltration curves provide good estimates of the average infiltration over a range of opportunity times. However, the approach does have some difficulty in reproducing the observed variance between furrows, indicated by poor estimates of the CV between furrows. The difference between predicted and actual CV changes between case studies and fields but tends to be higher for the predicted infiltration curves of Downs and Turner than for Chisholm. The difference between the two values of CV possibly signals the need to revise the value of the ω_{CV} parameter in equation 5-22 to relate infiltration variability to the variation in the final advance point.

5.9.3 The Predictive Procedure Compared to Scaling

The technique developed here predicts the parameters of the infiltration function from limited field data using the correlation between the distributions of the infiltration curves and that of the volume balance evaluated at a single advance point. The scaling method proposed by Khatri and Smith (2006) functions in a similar way, requiring only the inflow rate, furrow geometry and a single advance point for each furrow. In the Khatri and Smith (2006) method, the traditional inverse technique is applied to a single furrow using INFILT to determine the model infiltration curve (MIC). A scaling factor (F_S) is determined for each furrow by application of the volume balance equation:

$$F_S = \frac{Q_0 t - \sigma_y A_0 x}{\sigma_{Z1} k t^a x + \frac{f_0 t x}{1+r}} \quad \text{..... Eq 5-27}$$

and the scaled cumulative infiltration (Z_S) is calculated from the MIC using:

$$Z_S = F_S\left(k\tau^a + f_0\tau\right) \quad \text{..... Eq 5-28}$$

The coefficient F_S, determined individually for each furrow, is used to scale the model infiltration curve. The parameters k and f_0 are altered accordingly. Unlike the technique described in section 5.9.1, the parameter a cannot change between furrows and the characteristic curve shape is maintained. This may be an advantage for clay dominant soil types where the majority of variation is caused by a moisture dependent change in the crack volume. The main disadvantage of the MIC approach is the reliance on a single known infiltration curve. However, this limitation can be

overcome by careful observation of the estimated MIC or by some form of averaging process to determine a more appropriate MIC.

Unlike the MIC approach, the predictive technique is not restricted to using a single advance point within each furrow. It should be possible to adapt this procedure to predict the infiltration parameters for a set of furrows using some other indicator or surrogate measure of the variability. For example, it may be possible to relate the infiltration variance to the variance in soil moisture deficit. Alternatively, this procedure could be modified to estimate the potential range of infiltration curves under a different level of variability.

5.10 Conclusions

The IPARM infiltration estimation method developed in chapter 4 enables the identification of soil intake rates from easily obtainable field irrigation measurements. Applying these techniques to field data collected in typical irrigated fields has shown that the infiltration rates vary within a single field both spatially (i.e. between furrows in the same irrigation) and temporally (i.e. over the duration of the cropping season). From the limited data available, it was not possible to distinguish the causes of the variability although some basic trends can be inferred from the changes in the magnitude and shape of the infiltration curves.

The analysis in this chapter was based on previously collected field measurements. The data was limited to small numbers of furrows and did not include any information regarding the soil or crop conditions or the general field management. Further studies to investigate the variability of infiltration should include collection of advance measurements encompassing a larger area of the field in addition to suitable descriptors of the spatial distribution of soil conditions and initial moisture contents. Future field trials should also include measurements of the spatial variability in crop growth and performance (yield).

The sampling distribution analysis provided insight into the number of furrows that should be measured in order to predict the average infiltration curve and estimate the

field variance. Even with access to complete irrigation data for 20 or more furrows the uncertainty of the average infiltration curve could not be reduced to much less than ±5%. However, in practice the minimum number of furrows needed to reach a specified level of accuracy is field specific as it was found to be a function of the infiltration variability. Hence, it is inappropriate to specify a single value for the number of furrows required to characterise the population in heterogeneous conditions. Every furrow that is added to the evaluation results in an improvement in accuracy for the estimated average infiltration and variance. However, the marginal benefit diminishes with increasing sample number. For the sites evaluated, the measurement of approximately 10 furrows should provide an adequate estimation of the population statistics. The benefits associated with higher sampling numbers is unlikely to justify the additional equipment and labour costs due to the diminishing unit increase in accuracy at higher sample numbers.

The variance of soil intake rates between furrows located within the same field was adequately described by both the normal and log-normal distributions. However, the log-normal probability function provided a better fit to the field data. The infiltration variability was expressed in the form of a log-normal probability function and a technique was developed to estimate the distribution parameters and infiltration curve parameters from reduced quantities of field data. This technique provided estimates for the infiltration curves from single advance points and also offers the possibility of estimating the infiltration parameters using other measures of field variability. However, further testing with additional data sets is required to validate the approach and revise the values of the ω_{ZVal} and ω_{CV} coefficients.

The uncertainty in soil intake parameters is a large problem for irrigation evaluation since many aspects of field performance are highly sensitive to infiltration. The large variability, and difficultly in assessing that variability leads to the conclusion that the simulation of furrow irrigation must consider multiple furrows rather than attempting to predict the field performance using a single representative furrow. Chapter 6 follows to develop this multiple furrow simulation procedure.

CHAPTER 6

Whole Field Simulation Model

6.1 Introduction

Simple hydraulic models based on the volume balance (e.g. IPARM), can be useful in the calibration of infiltration parameters but generally provide substandard predictions of the irrigation performance. The volume balance model can predict the total infiltration volume, advance trajectory and runoff providing that all the necessary assumptions are satisfied but cannot adequately describe the distribution of applied depths. Hence, more complex models are employed to calculate irrigation performance values such as the distribution uniformity and requirement efficiency. Some notable examples of these models were discussed in section 3.5.

The field data introduced in chapter 5 clearly demonstrates that soil infiltration rates vary considerably between furrows within the same field. Past research has indicated that this variation between furrows is a significant concern for the performance of surface irrigation. However, none of the models considered can accommodate the simulation of more than one furrow simultaneously. There is no simple procedure to estimate the performance of furrow irrigation at the whole field scale in heterogeneous conditions. Often a single representative furrow is selected and used to estimate the field performance, thereby ignoring inter-furrow variability. The typical procedure to account for variability is to simulate each furrow individually and then combine the performance parameter values of the furrows in some simple average. However, the average of each performance term may not correspond well to the true field performance, particularly considering the uniformity terms. The purpose of this chapter is to describe the software package, IrriProb which is designed to simulate the whole field water application under variable conditions. IrriProb also includes an optimisation capability to identify the combinations of inflow rate and cut-off time to improve irrigation performance.

The application of water to the field is a three dimensional process comprised of (1) water flow in the primary furrow direction, (2) infiltration in the vertical dimension and (3) lateral water movement between adjacent furrows. The IrriProb simulation model as developed in this chapter relies on two major underlying assumptions:

1. That the surface and subsurface water flow within each furrow is independent of all surrounding furrows, and
2. That the variation in infiltration along the length of a furrow can be ignored and represented with a single infiltration characteristic.

Hence, it is possible to simplify the hydraulic model by dividing the spatial application into a series of individual longitudinal transects. The common hydrodynamic modelling approach is applied to each furrow to predict the distribution of water depths. Each furrow is simulated with an infiltration curve representative of the soil properties in that furrow and the predicted longitudinal profiles of applied depths are combined to form a two dimensional grid of applied depths. The irrigation performance is calculated based on this spatial distribution of infiltrated depths.

6.2 Components of the Simulation Model

6.2.1 Introduction to IrriProb

The IrriProb software package (Figure 6-1) was developed as a tool to evaluate and manage the whole field performance of furrow irrigation. The functionality of this software is best understood by dividing the package into four components (i.e. surface irrigation simulation engine, whole field performance evaluation, batch simulation and optimisation tool). The remaining parts of section 6.2 describe the first two of these components, the simulation engine and field performance evaluation.

IrriProb was developed in object orientated C++ with charting capabilities provided by TeeChart (Steema Software SL, Girona, Spain). Several minor alterations were made to the original FIDO simulation code throughout the developmental process to ensure smooth uninterrupted operation even in the instance of numerical convergence failure. For compatibility with existing techniques, IrriProb utilises the standard format of input data used in SIRMOD and IPARM. Inputs include field length, slope, furrow dimensions and spacing. Soil infiltration rates are described using the

Modified Kostiakov equation (Eq. 2-6) where the empirical factors of a, k and f_0 can differ between furrows. The values of inflow rate (L s^{-1}), cut off time (minutes) and soil moisture deficit (m) can also vary between separate furrows within the same field.

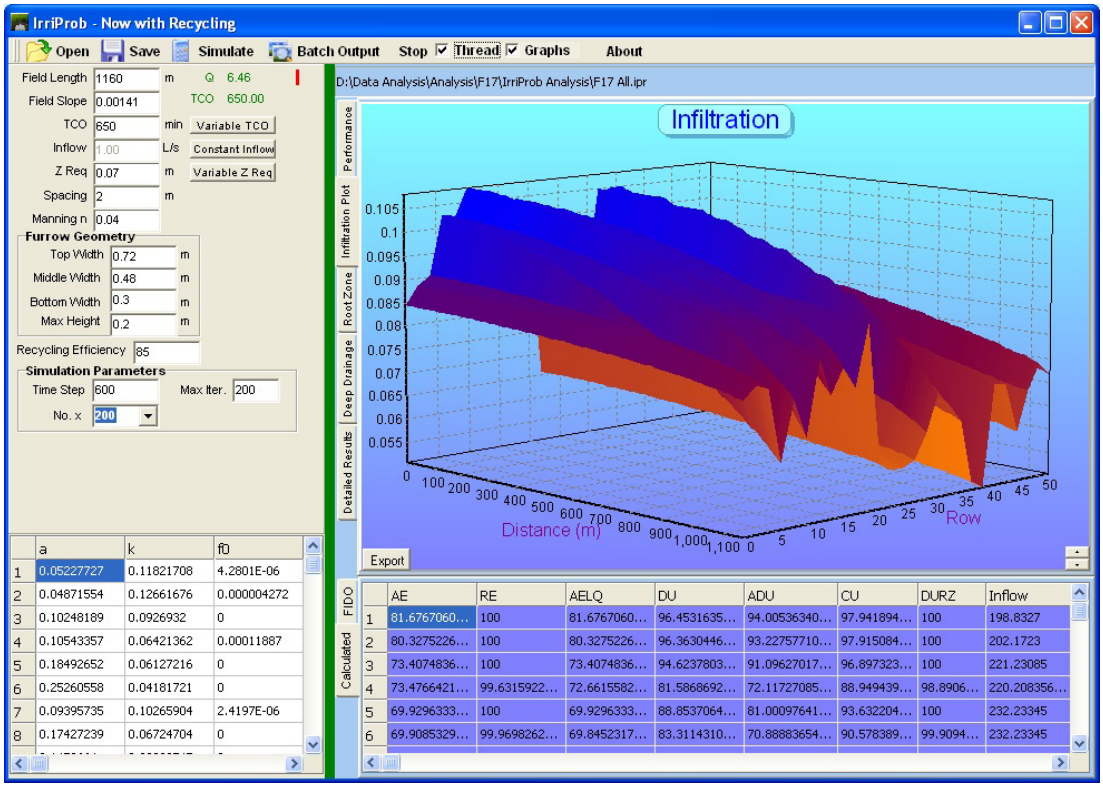

Figure 6-1 IrriProb screen shot: Simulation of Turner field

6.2.2 FIDO Simulation Engine

The single most important component of IrriProb is the furrow simulation model. The simulation engine from FIDO (McClymont et al. 1999) was selected as it performs favourably against other alternatives, has been found to remain stable for a wide range of field conditions (McClymont 2007) and provides outputs suitable for secondary processing. The simulation engine of FIDO, like SIRMOD is based on a fixed time step for the full hydrodynamic equations and is solved via the Priessman double sweep technique (described in (Walker 2005b)). This approach starts from a known upstream condition and proceeds in the forward direction, calculating the coefficients for each cell and finally the distance of the advancing water front. Starting from this estimated advance distance, the changes in flow area and discharge at each numerical node are calculated in the reverse direction. This process is repeated using the revised estimates of flow area and discharge at each cell boundary. Convergence of the

numerical solution for each time step is realised when the differences in calculated flow area (m^2) and discharge ($m^3 s^{-1}$) at every node between two consecutive iterations is less than $1x10^{-5}$.

The FIDO simulation engine, and therefore IrriProb requires the following inputs:

- parameters of the Modified Kostiakov equation (a, k, and f_0),
- description of inflow (inflow rate and cut-off time),
- field characteristics (field length, slope and surface roughness), and
- furrow dimensions (top width, middle width, bottom width and max. depth).

The model does not include any adjustment to the infiltration function for changing water depth. Hence, the infiltration parameters must have already been adjusted for changes in the wetted perimeter if desired.

Following successful execution, the simulation engine creates an output object that contains the infiltrated depth profile (infiltrated volume per unit length against furrow distance), runoff hydrograph and water advance and recession trajectories. FIDO performs well during all phases of the irrigation and copes with those situations where recession commences before the advance reaches the end of the field. Hence, the model is suitable for an optimisation procedure because stability is ensured even with unrealistic combinations of input parameters (McClymont 2007). The simulation engine has the provision to accommodate a variable inflow hydrograph. However, for simplicity variable inflow has not been incorporated in the original FIDO interface nor the model developed herein.

The FIDO model assumes that the inflow rate is zero at the start time and increases to the constant inflow value during the first numerical time step. For this research, the code was modified to commence normal inflow at time zero. This alteration is expected to have some impact on the performance indicators, particularly considering that the time step commonly ranges between 5 and 10 minutes. It was found that attempts to reduce the initial time step below 10 minutes compromised the stability of the simulation. Hence, the default time step was fixed at 10 minutes throughout this research.

6.2.3 Calculation of Performance Parameters

Although FIDO contains procedures to calculate the standard performance indicators, these procedures were re-written in IrriProb to ensure compatibility with the aggregation of multiple furrows. The original simulation is based on a semi-constant time step therefore the resultant infiltrated depth profiles are expressed in respect to intervals of advance time. Hence, in order to properly calculate the low-quarter based distribution uniformity and facilitate the combination of separate furrows these results require some simple post-processing. The field length is divided into a pre-determined number of distance intervals, Δx and the infiltrated depth at each node is calculated by linear interpolation. This results in two vectors for each furrow, one being the displacement values and the other the corresponding infiltrated depth at each location. IrriProb allows the user to choose the number of intervals depending on output requirements and memory. Either 100 or 200 intervals (per furrow) are preferred and the latter is used throughout this dissertation. Increasing the number of intervals further (i.e. to 500) may result in memory problems within the charting components with no significant increase in accuracy.

The next step is to extract meaningful information from the raw infiltrated volume profiles. The row spacing, W_s (m) is used to calculate the equivalent applied depth from Z (m^3 m^{-1}), the infiltrated volume per unit length. The required depth (D_{req}) is used to designate the total depth into the depths of root-zone storage (D_{RZ}) and deep percolation (D_{DD}):

$$D = \frac{Z}{W_s} \quad \text{..... Eq 6-1}$$

$$\begin{aligned} if\,(D < D_{req}) &\Rightarrow D_{RZ} = D \\ if\,(D > D_{req}) &\Rightarrow D_{RZ} = D_{req} \end{aligned} \quad \text{..... Eq 6-2}$$

$$\begin{aligned} if\,(D < D_{req}) &\Rightarrow D_{DD} = 0 \\ if\,(D > D_{req}) &\Rightarrow D_{DD} = D - D_{req} \end{aligned} \quad \text{..... Eq 6-3}$$

where D (m) is the volume of infiltration per unit area of soil, commonly expressed as an equivalent depth and D_{req} (m) is the required or desired depth of application. For surface irrigation, D_{req} is typically equal to the soil moisture deficit. In the current version of IrriProb, the required depth is assumed constant over the furrow length but

can be assigned individual magnitudes for different furrows. The value of *D* for each interval is calculated by averaging the values of the two adjacent nodes. In this fashion the volume of infiltration ($Vol_{Infiltration}$), rootzone storage (Vol_{RZ}) and deep drainage (Vol_{DD}) are calculated using the trapezium rule:

$$Vol_{Infiltration} = \sum_{i=1}^{N-1}\left(\left(\frac{D_{i+1}+D_i}{2}\right)\times\Delta x\times W_s\right) \quad \text{..... Eq 6-4}$$

The volumes of total inflow (Vol_{Inflow}) and runoff (Vol_{Runoff}) are calculated by finding the average value of inflow (Q_0) and runoff (Q_r) rates, respectively for each time step (t_i - t_{i-1}) multiplied by the time interval and then summing all values.

$$Vol_{Inflow} = \sum_{i=1}^{N}\left(\left(\frac{Q_{0_i}+Q_{0\,i-1}}{2}\right)(t_i - t_{i-1})\right) \quad \text{..... Eq 6-5}$$

$$Vol_{Runoff} = \sum_{i=1}^{N}\left(\left(\frac{Q_{r_i}+Q_{r\,i-1}}{2}\right)(t_i - t_{i-1})\right) \quad \text{..... Eq 6-6}$$

The application efficiency (AE) is the most common term used to assess surface irrigation. It represents the percentage of total applied water that is beneficially used by the crop or stored in the root zone (Walker and Skogerboe 1987).

$$AE = 100\% \times \frac{Vol_{RZ}}{Vol_{Inflow}} \quad \text{..... Eq 6-7}$$

This term becomes less relevant where runoff is recovered through a tail-water return system. Instead, the AE is adjusted to account for the seepage and evaporation that occurs during the recycling process to create a new expression, application efficiency with recycling (AER).

$$AER = 100\% \times \frac{Vol_{RZ} + E_R \times Vol_{Runoff}}{Vol_{Inflow}} \quad \text{..... Eq 6-8}$$

E_R represents the efficiency of the tail-water recovery process. The AER may give false indications of irrigation performance as it does not account for the costs incurred in lifting the excess water back to the storage. The value of E_R typically includes the channel losses that occur between when water leaves the end of the field and is returned to the supply reservoir or the next field in the farm system. This term may also be adjusted to account for the proportion of the recycled water that is lost during

the storage time before that water can be used (may be significant in those systems where water is not normally stored on the property). In reality, it is unlikely that the recycling losses are strictly proportional to the volume of runoff. For example, the transport seepage loss is influenced by the duration of the recycling process and the dead storage in the channel that cannot be pumped.

In most cases, particularly in non-water limited conditions, it is more important that the irrigation refills a significant portion of the profile over the field area. The requirement efficiency (RE), otherwise known as storage efficiency or effective water (Bali and Wallender 1987), serves as a check of the irrigation adequacy:

$$RE = 100\% \times \frac{Vol_{RZ}}{Vol_{req}} \quad \text{..... Eq 6-9}$$

where Vol_{req} is the volume of infiltration required to satisfy the field deficit. Low values indicate that large portions of the field do not receive adequate water application. In most cases, the farmer will endeavour to supply adequate moisture to the entire field (RE ≈ 100%) often at the expense of other performance indicators. The RE does not give any indication of the proportion of the field that receives the full application. It is possible to have high values of RE (i.e. >90%) whilst having parts of the field with zero application. For this type of information, the efficiency value must be complemented by some indication of application uniformity.

Calculations of uniformity require the re-arrangement of the two dimensional grid of infiltrated depths in ascending order. This may not be crucial for a single open ended furrow, where these values will almost certainly be already ordered in declining order of magnitude. However, sorting is necessary for multiple furrows where the minimum applied depths may occur in any given furrow(s). The distribution uniformity (DU) is probably the most common uniformity term employed for surface irrigation and is expressed as the ratio of the average depth in the quarter of the field with the lowest infiltrated depths ($\overline{D_{LQ}}$) to the average infiltrated depth ($\overline{D}$) over the entire field area (Kruse 1978).

$$DU = 100\% \times \frac{\overline{D_{LQ}}}{\overline{D}} \quad \text{..... Eq 6-10}$$

The absolute distribution uniformity (ADU) instead considers the ratio of the absolute minimum depth of infiltration (D_{min}) to the field average.

$$ADU = 100\% \times \frac{D_{\min}}{\overline{D}} \quad \text{..... Eq 6-11}$$

The DU is usually preferred since if any part of the field receives a zero application, the ADU cannot describe any further decrease in uniformity.

Christiansen's Coefficient of Uniformity (CU) is another popular uniformity measure, usually applied to sprinkler systems but equally applicable in the context of surface irrigation.

$$CU = 100\% \times \left(1 - \frac{\sum_{i=0}^{N_D} \left| D_i - \overline{D} \right|}{N_D \times \overline{D}} \right) \quad \text{..... Eq 6-12}$$

These are the traditional measures of uniformity. However, for surface irrigation where a significant part of the field can be over-irrigated, a more appropriate calculation may be the distribution uniformity of the root zone (DURZ). This expression has similar meaning to the DU and is most probably linked to the value of the requirement efficiency:

$$DURZ = 100\% \times \frac{\overline{D_{RZ_{LQ}}}}{\overline{D_{RZ}}} \quad \text{..... Eq 6-13}$$

where $\overline{D_{RZ_{LQ}}}$ is equivalent to $\overline{D_{LQ}}$ but applied to the depths in the root zone.

The application efficiency of the low quarter (AELQ) refers to the average depth of water stored in the root zone in the quarter of the field with the lowest application divided by the average depth of infiltration. In some situations it may serve as a more useful alternative to the AE since it includes the effects of uniformity of application and fulfilment of the irrigation requirement (Kruse 1978).

$$AELQ = 100\% \times \frac{\overline{D_{RZ_{LQ}}}}{\overline{D}} \quad \text{..... Eq 6-14}$$

Additional performance indicators provided by IrriProb include values such as the average infiltrated depth, root zone depth and deep percolation depth, total volumes of inflow, runoff and infiltration and percentages by inflow of storage, deep percolation and runoff. Other expressions have been used to describe the performance of surface irrigation (e.g. the potential application efficiency of the low quarter, PELQ (Santos 1996)) but it is believed that the set described here will suffice for most requirements.

6.2.4 Calculation and Visualisation of the Whole Field Performance

The performance parameters above have been used to describe the single furrow application within various simulation models such as SIRMOD, SRFR and FIDO. IrriProb applies the same expressions to describe the performance of a collection of furrows. In the single furrow case, the field is divided into a number of intervals with an infiltration depth for each. For the whole field case, each furrow is divided into an equal number of intervals and the infiltration is calculated based on a two dimensional grid. IrriProb provides graphical representations of the infiltrated depths, root-zone storage and deep percolation over the furrow group. Although not used in the optimisation process these graphics may be useful to visually demonstrate the irrigation variability. An example is provided in Figure 6-2 which was generated by simulating all 20 furrows of the Downs field (chapter 5) using the measured flow rate and time for each furrow and the individual infiltration curves.

The vectors of total infiltration, root-zone storage and deep percolation are joined to form one complete set of values. In this form, the standard suit of performance parameters is evaluated via identical methods as for the single furrow. The total volumes of infiltration are found by summing these vectors while the inflow and runoff volumes come from a simple addition of the individual furrows. The results from the entire field performance will be different from the simple averages of the individual furrows. Basic averages of these measures may lead to satisfactory approximations of the RE and AE but will fail to yield accurate values for the uniformity indicators.

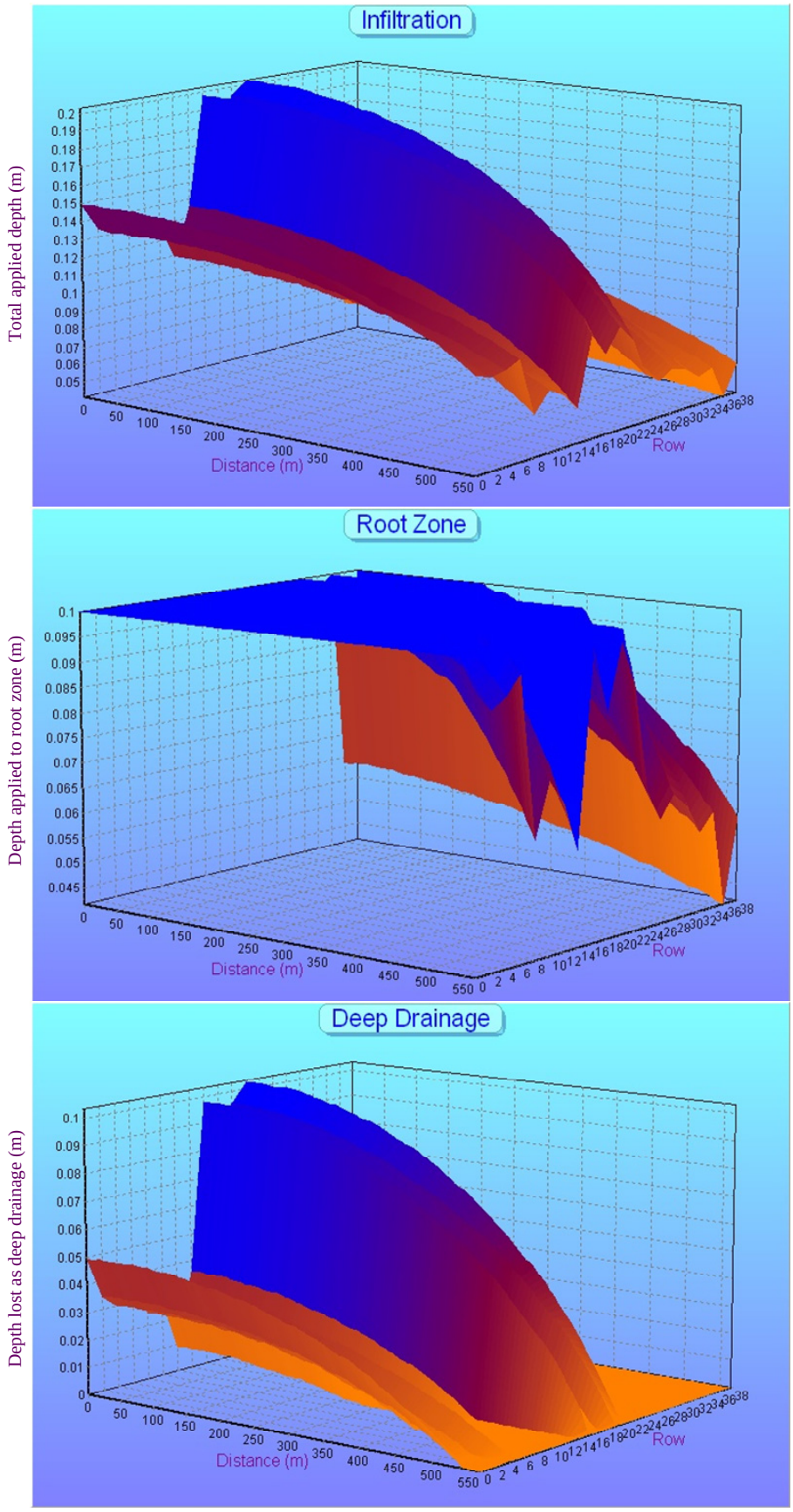

Figure 6-2 Three dimensional IrriProb plots of (a) infiltration, (b) root zone and (c) deep drainage (Downs trial site under measured conditions)

6.3 Surface Irrigation Optimisation Framework

6.3.1 Development of the Optimisation Tool

Although simulation tools can adequately assess irrigation performance, system optimisation remains a repetitive trial and error procedure. The approach outlined in this section is applicable for any number of the continuous management variables. However, the analysis presented here using IrriProb only considers inflow characteristics since most other factors cannot be altered after the initial field construction.

Once the IrriProb hydraulic model has been used to evaluate the irrigation performance under the existing management, the next step is to simulate the field irrigation using a range of inflow rates and times, termed the "batch simulation". When the batch simulation option is selected, the user is prompted to enter the ranges of values for the management variables. IrriProb simulates all combinations of inflow rates (Q) and times to cut off (TCO) within the user defined range for the given furrow or group of furrows and stores the results for later use. For example, if the user supplies the conditions shown in Figure 6-3, IrriProb will create a 31x31 grid containing the specified inflow rates and cut-off times and simulate the furrow(s) for each. The simulation will start with Q = 1 L s^{-1} at TCO = 200 minutes, then Q = 1.33 L s^{-1}, 1.66 L s^{-1}, 1.99 L s^{-1} ….. 11 L s^{-1}. The TCO is then increased to 233.3 minutes and the cycle repeats

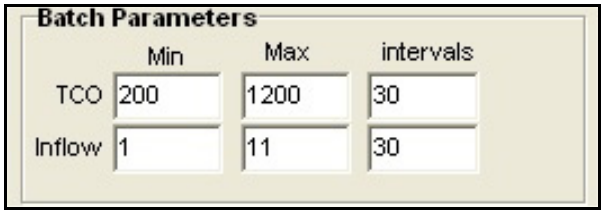

Figure 6-3 Batch simulation parameter input box

Once the batch simulation process is completed, IrriProb will contain the performance indicators, average infiltrated depths and water volumes for every combination of the specified inflow conditions. Each performance parameter is plotted over those ranges of Q and TCO to create a three dimensional surface plot (e.g. Figures 6-4 and 6-5). This data can be viewed in spreadsheet format or saved to a comma delimited text file

(*.csv) for later use. The charts shown in Figures 6-4 and 6-5 were created by simulating all 20 furrows of the Downs field (chapter 5) using the batch limits defined in Figure 6-3 except the number of intervals for the TCO and inflow was increased from 30 to 100.

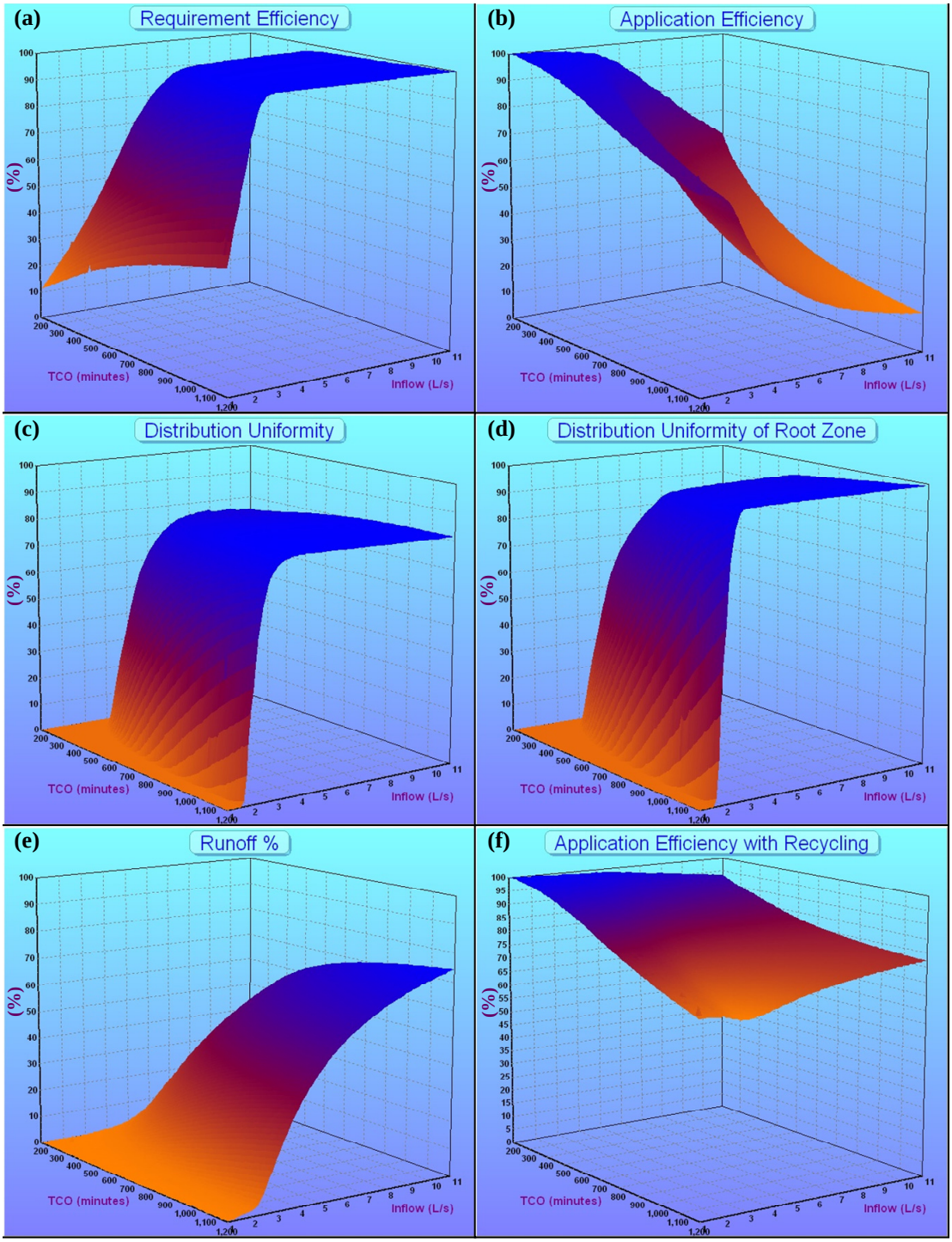

Figure 6-4 Screenshot from IrriProb: Performance indicators for Downs field (Q = 1 to 11 L s^{-1} and TCO = 200 to 1200 minutes)

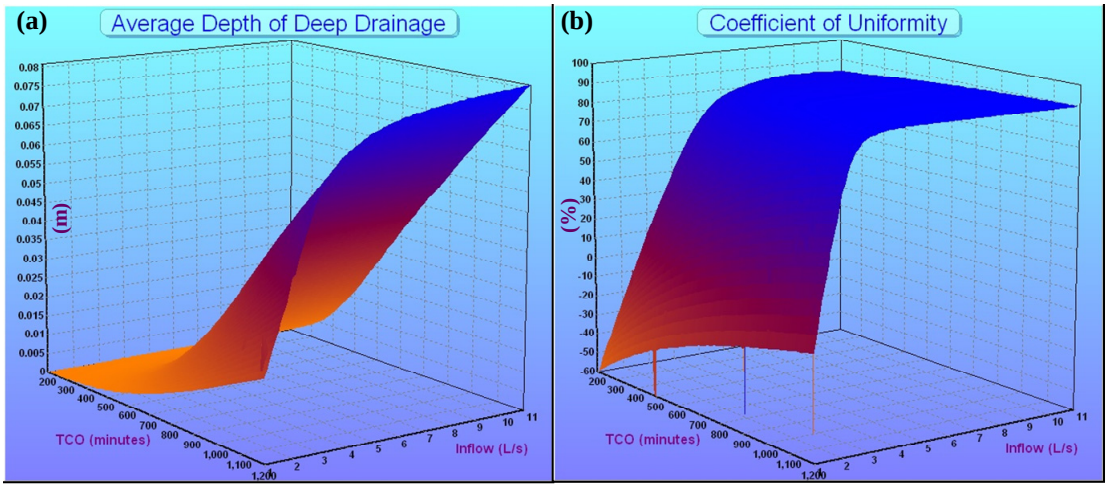

Figure 6-5 Screenshot from IrriProb continued: Performance indicators for Downs field (Q = 1 to 11 L s^{-1} and TCO = 200 to 1200 minutes)

These plots (Figures 6-4 and 6-5) may be useful for the analysis of one performance parameter in isolation. However, presented in this form, the data does not easily lend itself to optimisation as it difficult to interpret or visualise the interactions between two or more of these expressions. Instead, the "optimise grid" tool was developed to collate and simplify the three dimensional behaviour of the performance indicators. The optimise grid (Figure 6-6) is constructed by taking a horizontal slices through the results presented in Figures 6-4 and 6-5 for specified values of each performance parameter.

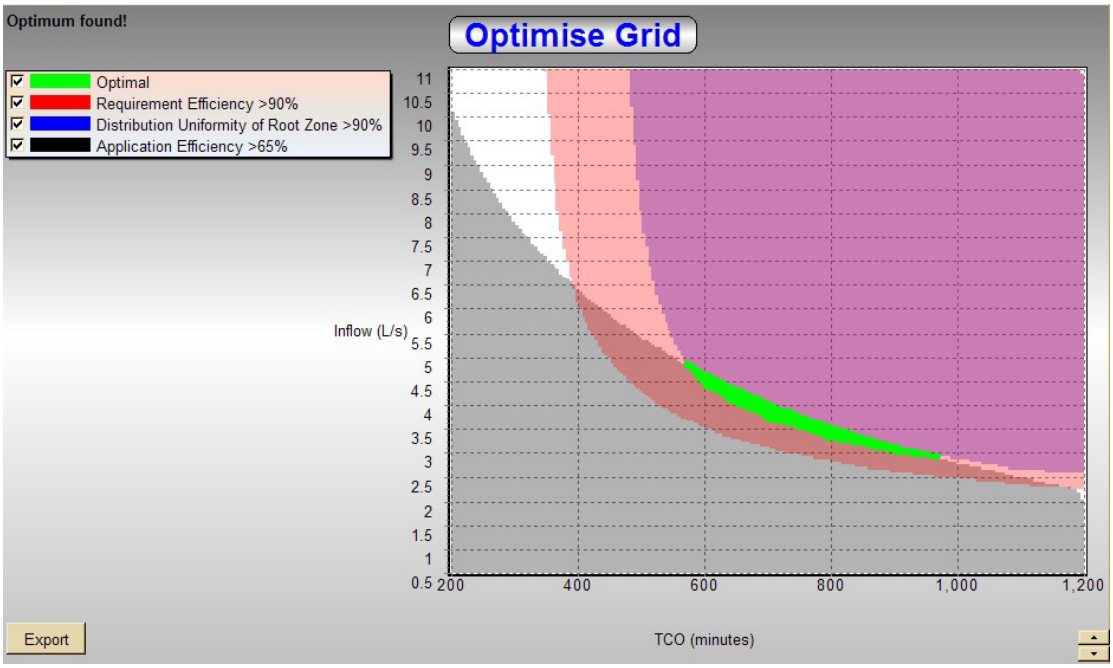

Figure 6-6 IrriProb screen shot: Using the optimising tool to determine inflows that achieve RE>90%, DURZ>90% and AE>65% (Downs field)

The value of the optimisation tool is derived from the ability to superimpose several different performance criteria to quickly identify the optimal irrigation strategy. The vertical axis of the optimise grid plot (Figure 6-6) is the inflow rate and the time to cut off is given on the horizontal axis. The objective function for optimisation is a Boolean expression containing any number of conditions. Hence, the resulting expression is entirely user customisable and therefore flexible to any situation that may be encountered. Each condition includes a performance parameter, a value for that parameter and either an inequality, or equality with corresponding tolerance level (i.e. greater than, less than or approximately equal to). Each selected performance parameter is plotted on the same set of axes with a different colour (currently up to eight conditions can be selected). The points or regions that satisfy all criteria are shaded in bright green to signify the "optimal" inflow characteristics. Clicking on an parameter within the chart legend will hide the corresponding series and cause the chart to "zoom in" to the remaining regions. The example in Figure 6-6 shows where the user has identified the combinations of Q and TCO that will accomplish both a RE and DURZ of over 90% and AE of above 65%. The area shaded green (optimal) represents those combinations of inflow rates and times that satisfy all three criteria.

The optimisation tool has been found to perform best using a 200x200 grid of inflow rates and times. However, simulation at this increased resolution of Q and TCO would require excessive numbers of field simulations. For example, computation at the 200x200 level for the Downs field (20 furrows) would involve 40,000 replicates of the field simulation (total of 800,000 individual simulations). Instead, IrriProb facilitates calculation of the performance parameters at some coarse resolution (e.g. 30x30) and the extra points are estimated using bi-linear interpolation.

6.3.2 Validation of the IrriProb Simulation Model

The completed simulation model, IrriProb was evaluated prior to any field analysis. McClymont (2007) found that the FIDO simulation engine performed favourably against alternative models. However, a further validation was conducted using a number of data sets chosen to illustrate potential differences between FIDO and other simulation models (Appendix G). The simulation results compared favourably with

the results of the SIRMOD III (Walker 2003) and SRFR (Clemmens and Strelkoff 1999) models. Operation of IrriProb in single furrow simulation mode resulted in predictions of the advance trajectories (Figure G.1) runoff hydrographs (Figure G.2) and infiltrated depth profiles (Figure G.3) that were almost identical to the other models. Comparison of the performance terms (Table G.1) with the other models uncovered minor differences indicating the existence of potential numerical issues. These differences were explained by further investigation of the models. For example, the larger numerical time step used by IrriProb can introduce a small systematic error into the estimated volumes. However, this does not translate to significant differences in the performance terms.

6.4 Simple Furrow Averages Cannot Represent the Field Performance

Conventional logic may suggest that the field performance can be estimated by averaging the terms of the individual furrows. However, as the majority of quantities behave in a non-linear fashion this approach is likely to be inadequate. The IrriProb whole field simulation model enables the rapid and automated evaluation of multiple furrows but it also ensures accurate calculation of the performance indicators. A small trial was undertaken using IrriProb to demonstrate that the performance indicators should not be simply averaged across the individual furrows. To illustrate the importance of the whole field simulation model, all furrows from the Downs field (chapter 5) were simulated using the measured inflow rates and times. The "Average of individual furrows" (Table 6-1) was calculated by a simple arithmetic average of the single furrow efficiency terms. The "Total whole field" values were calculated using IrriProb and the two dimensional grid of applied depths.

The "Calculated using average infiltration" data was obtained by simulating the average infiltration curve for Downs with the average values for inflow rate and time to cut-off. The average infiltration curve was found through application of equation 5-26 with $ZVal_{Infiltration} = 0$ and $CV_{Infiltration} = CV_{VB}$ (Eq. 5-23) to obtain a value for $\overline{\ln(Z(\tau))}$. The average infiltration curve is estimated by solving for the unknown

infiltration parameters over range of opportunity times, τ between 50% and 100% of the average final advance time. The resulting infiltration parameters were found to be a = 0.3271, k = 0.02061 and f_0 = 0.000119.

Table 6-1 Differences in the performance indicators between simple furrow averages and the true field performance (Downs field)

	Average of Individual Furrows	Standard Deviation of Individual Furrows	Maximum Furrow	Minimum Furrow	Calculated using Average Infiltration[1]	Total Whole Field (IrriProb)
AE (%)	76.14	11.39	91.16	56.66	76.72	73.81
AER (%)[2]	82.82	12.36	98.35	59.21	83.32	80.25
RE (%)	93.91	10.66	99.99	52.77	98.07	93.91
AELQ (%)	68.45	5.50	74.01	56.38	72.18	59.84
DU (%)	78.50	4.62	86.18	72.29	79.01	64.75
ADU (%)	65.07	8.20	78.99	53.22	66.47	35.46
CU (%)	87.62	2.64	92.18	83.83	87.93	77.27
DURZ (%)	90.93	7.66	99.97	79.41	94.08	81.07

[1] calculated using average infiltration curve and average values of inflow rate and inflow time
[2] recycling efficiency of E_R = 85%

The AE for the individual furrows varied between 56.7% and 91.2% with an average of 76.1% (Table 6-1). The total AE of the field was 73.8%, which was lower than the simple average value. The RE of the whole field was identical to the average of the individual furrows but this will only be the case in situations where the deficit is spatially constant. The values for the field and furrow RE will be significantly different where the water deficit varies between furrows. The field based DU of applied depths was 64.8% while the average of individual furrows was much higher at 78.5%. Similarly, the ADU of the field was much lower than the value indicated by the averages of the single furrow simulations. Using simple averages of the performance indicators resulted in overestimates for all parameters except the RE where they were equal. Simulation using the average infiltration curve and inflow also provided poor predictions of the performance parameters. The resultant performance estimates were found to be further removed from the total whole field performance than the simple averaged performance parameters.

The values for the field wide uniformity terms (DU and CU) were lower than that of the furrow with the poorest individual uniformity. This indicates that even within a relatively homogeneous field the variability between adjacent furrows is more

important than the variation in applied depths along the furrow length resulting from differences in opportunity time alone (i.e. ignoring the variation in soil properties along the field length). Measures of uniformity calculated from the averages of individual furrows will be unable to adequately represent the field wide variability resulting from variations in inflow regimes or infiltration curves between furrows. Descriptions of the uniformity of applied depths based on a single furrow only reflect the variation directly caused by the disparity in opportunity time.

It should be noted that the total whole field performance is based on spatial averages of the infiltration characteristic along the furrow length. IrriProb is restricted to a single infiltration characteristic for each furrow resulting in an overestimation of the DU. The true uniformity of applied depths would be expected to be significantly lower than that estimated by merely considering the inter-furrow variation in soil characteristics (i.e. lower than the "Total whole field" DU in Table 6-1). If the analysis considered this extra source of variation it is predicted that the combined effects of variations in opportunity time and infiltration rate may exceed the inter-furrow variation.

6.5 Irrigation Performance in Heterogeneous Conditions under Measured Field Management

The modelling approach developed in this chapter has been found to provide an improved description of the irrigation performance under variable conditions. The procedures included within IrriProb facilitate the optimisation of field management. However, the first stage in any field optimisation is to benchmark the irrigation performance under the existing field conditions and inflow management. The performance for the Downs, Chisholm and Turner fields (Table 6-2) was determined by simulation using the calibrated infiltration parameters in Tables 5-1, 5-2 and 5-3, respectively combined with the individual inflow time and discharge for each furrow. A summary of the field performance is given in Table 6-2 with complete results provided in Appendix H. The performance parameters were found to vary both between irrigations in the same field and between furrows in the same irrigation (Appendix Tables H.1, H.2 and H.4). In these simulations, the performance

parameters were based on a constant deficit for each field. However, the field data for the Chisholm field also included individual event assessments of the deficit. Hence, the Chisholm field was also simulated for a second time using the measured (variable) soil moisture deficit (Appendix Table H.3) which had different values for each irrigation event. In this case the use of the variable deficit only resulted in minor differences in the efficiencies and deep drainage depths.

The Downs field experienced a high AE and an acceptable level of RE with poor uniformity (Table 6-2). For the majority of furrows, the inflow was stopped within 1 to 4 hours after the completion of the advance phase. This resulted in reduced runoff and deep drainage losses and hence, higher application efficiency. Unfortunately, the decreased inflow duration also resulted in low values for uniformity (DU = 64.8%) due to insufficient opportunity times at the tail end of the field.

Table 6-2 Field irrigation performance under the measured irrigation management

	AE (%)	AER[a] (%)	RE (%)	DU (%)	ADU (%)	CU (%)	DURZ (%)	Inflow[b] (m^3)	Run. (%)	Deep Drain. (%)	D (mm)	D_{RZ} (mm)	D_{DD} (mm)
Downs	73.81	80.25	93.91	64.75	35.46	77.27	81.07	143.77	7.58	18.60	117.6	93.9	23.7
Chisholm	21.37	62.37	98.82	42.60	24.74	61.19	96.41	138.73	48.24	30.16	143.0	59.3	83.7
Chisholm variable Defict	20.71	61.71	96.34	42.60	24.74	61.19	86.90	138.73	48.24	30.82	142.96	57.46	85.50
Turner	68.62	84.96	94.62	73.89	44.98	80.41	86.85	223.92	19.22	12.04	77.9	66.2	11.6

[a] Application efficiency with recycling is based on a tail water recycling efficiency of E_R = 85%
[b] Field inflow is expressed as a average volume per furrow

In contrast, the Chisholm field had higher RE due to the longer inflow times and as a result the AE decreased to 21% as almost half of the water applied ended up as runoff and close to a third was lost as deep percolation. The average deep drainage depth (D_{DD} = 83.7 mm) exceeded the soil moisture deficit (60 mm). The Chisholm field was found to have lower uniformity (DU = 42.6%) than the Downs field, caused by the increased magnitude and variance of the steady infiltration rates (Figure 5-5). However, the uniformity of water added to the root zone was much higher (DURZ = 96.4%) because the deficit was satisfied over the majority of the field area. The high predicted value for the deep drainage may indicate that the estimated soil moisture deficit is incorrect. One might expect that the RE should be higher and D_{DD} lower

when simulating using the measured (variable) moisture deficits rather than seasonal average. However, there was minimal change in these performance terms (Table 6-2), even considering individual furrows (Appendix Table H.3) This raises questions over the accuracy of the measured moisture deficits for the Chisholm field. However, for the purpose of this analysis, the values were assumed to be correct.

The Turner field was found to have higher uniformity than the other fields (DU = 73.9%). The AE was lower (68.6%) than for the Downs field but since a substantial proportion of the applied water ends up as runoff this value increases to 85% when tail water recycling is considered (Table 6-2). The deep drainage depth was much lower for the Turner field compared to the Downs and Chisholm fields. However, the irrigation was still able to satisfy the majority of the moisture deficit (RE = 94.6%). Such behaviour is explained by the cracking nature of the infiltration curves (Figure 5-6) for this field.

All three fields have high RE indicating that the irrigation successfully satisfied the requirement. However, the low values for AE imply that it is possible to modify the irrigation management in order to reduce the total volume of water applied. The consistently low uniformity values suggest that the irrigation performance may be improved through adoption of increased inflow discharges. Hence, it should be possible to considerably improve the performance of all three fields through adjustment of inflow rates and cut-off times

6.6 Conclusion

A model has been developed to extend the simulation of surface irrigation from a single furrow event to the field application. The resulting model facilitates the estimation of irrigation performance of furrow irrigation at the field scale while considering infiltration variability. The two dimensional based values of the performance terms enable calculation of the true uniformity of surface irrigation at the whole field scale. The two dimensional nature of the performance parameters also facilitates valid field scale comparisons of furrow irrigation with the performance of other irrigation systems (e.g. centre pivot sprinkler and subsurface drip). The software

interface, IrriProb, also features a novel approach to optimise the irrigation performance according to customisable criteria. The objective function is based on a Boolean expression combining any number of performance parameters.

The development of this tool has proven the inability of simple furrow averages to adequately describe the field scale performance. The averaged furrow performance estimates do not capture the true irrigation performance at the field level and significantly over predict the uniformity of applied depths. IrriProb, the whole field simulation model, provides improved estimates of the irrigation performance over single furrow or simple furrow averages but still remains unable to capture the full impact of longitudinal, within furrow variation in soil infiltration characteristics.

Single furrow simulations are inadequate to predict the field scale irrigation performance. In a similar manner it is postulated that optimisation of irrigation management at the field scale is also compromised by ignoring the spatial variance in infiltration rates between furrows. Chapter 7 follows to demonstrate the importance of accounting for this variability during the optimisation of furrow irrigation and attempts to optimise the irrigation performance under spatially variable conditions.

CHAPTER 7
Optimising Irrigation Performance Considering Infiltration Variability

7.1 Introduction

The evaluation of soil infiltration rates (chapter 4) combined with the appropriate simulation model (chapter 6) may facilitate the identification of the current irrigation performance. However, the ultimate value of these techniques is to define benchmarks and propose changes to field management to improve the system performance. In Australia, the majority of irrigation farms are water limited. Hence, the cultivated land area and total potential yields are directly linked to the water use efficiency. Increases in the application efficiency will make more water available to support an additional area of crop. In water limited conditions, it is possible to express incremental improvements in application efficiency as a dollar benefit to the farmer. This is not the case in all farming regions. For example, small farmers in the Fergana Valley in central Asia consider land as being a limited resource and therefore find it hard to justify water savings (Horst et al. 2007). Although reductions in water extractions may benefit the natural environment, it may not be possible for the individual farmer to recoup the costs of infrastructure investment and altered management practices. Hence, where improvements to an irrigation system result in "public good", it may be more appropriate to encourage society to provide financial incentives to farmers.

This chapter provides some background to the process of irrigation optimisation and introduces the Boolean objective function as used by IrriProb. Prior to application of the proposed optimisation technique it is important to understand the behaviour and interactions of the irrigation performance components and how this may differ

between the single furrow and furrow group. This chapter demonstrates the use of IrriProb (developed in chapter 6), by optimising the performance of three selected fields. It focuses particularly on the ramifications of optimising management at a field scale using limited infiltration information. Several alternate optimisation strategies are tested including individual furrow optimisation, optimisation based on the average infiltration curve, whole field optimisation and recipe management.

7.2 The Furrow Irrigation Optimisation Process

7.2.1 Factors to Consider in Addition to the Standard Performance Terms

7.2.1.1 Maximum Inflow Rate

Optimisation of furrow irrigation using computer simulation commonly indicates that an increase in the inflow rate will result in improvements to uniformity and reductions in deep percolation at the upstream end. The resultant increase in the advance velocity may reduce the detrimental effects of the infiltration variability along the furrow. With increased advance velocities, the opportunity time at any point in the field becomes less sensitive to upstream variations in the infiltration rate. The maximum allowable inflow rates are dependent on many factors (Fernandez-Gomez et al. 2004) and must be determined for each case as the water velocity may vary considerably over the furrow length. However, the majority of simulation models neglect the soil erosion and subsequent change in furrow cross section that typically occurs at elevated flow velocities. Smith et al. (2005) propose a maximum inflow rate of 6 L s^{-1} for the Australian cotton industry, which in most cases corresponds to an increase above the current practice.

7.2.1.2 Deep Drainage and Leaching Requirement

The factors chosen as the basis for irrigation performance optimisation are determined by the type of application system. For pressurised systems with a high capacity for volumetric control, the uniformity becomes the dominant consideration. However, for furrow irrigation the application efficiency is considered as the index most indicative of performance due to the high potential for water losses through deep percolation and runoff. Many soil and crop combinations require a certain volume of the applied water

(either by natural rainfall or artificial irrigation) to be drained from the bottom of the profile to prevent salt accumulation. This additional infiltration requirement, termed the leaching fraction is determined by the salinity of the applied water, the salinity of the soil solution and the crop salt tolerance. Optimising solely on the basis of application efficiency will lead to a general reduction in deep percolation volumes which may decline below the leaching requirement. Where leaching is important it will impose an upper limit on the application efficiency. One alternative is to include the leaching fraction in the numerator of Eq 6-7 as a beneficial use (not used in this thesis). Leaching is not a common concern for the cotton growing areas of Australia since the cotton plant has a relatively high salt tolerance, the irrigation water has low salinity and sufficient natural drainage commonly occurs during summer storms (Smith et al. 2005). However, other surface irrigated crops such as maize (1.7 dS m^{-1}) and sugarcane (1.7 dS m^{-1}) experience yield losses at lower levels of salinity (Ayers and Westcot 1994) compared to cotton (7.7 dS m^{-1}).

7.2.1.3 Irrigation Management Constraints

The irrigation management practices may impose a number of constraints on the optimisation process. These factors do not readily become part of the objective function and may be overlooked in the process of optimisation. One major example is the issues associated with increasing inflow discharges. Generally, increased inflow rates will result in increases in uniformity and volumetric efficiency but may exceed the discharge capacity of the supply system. To implement the increased inflow without upgraded supply infrastructure (e.g. pipe sizes, pumps, channel dimensions or supply channel head) the farmer will be forced to reduce the set size hence, increasing labour requirements. The reduced run times associated with higher flow rates may be beneficial to irrigation performance however, it is often more preferable to remain using the longer inflow times for labour management. For example, a 12 hour shift (e.g. 6am and 6pm) may be chosen because most operations can occur in daylight, the majority of the day free for other activities and the farmer can catch a full night sleep.

Changes to field layout (e.g. slope and furrow length) may include a direct capital cost associated with the required earthworks. However, the alterations may have other

subtle impacts that can be overlooked. For example, shortening of field lengths may reduce the cropping area due to increased space required for headland and channel structures as well as add to machinery costs due to the extra time spent turning at either end of the field.

7.2.2 Existing Techniques to Optimise Irrigation Management

The uniformity of applied depths and the application efficiency (AE) are strongly influenced by the advance velocity and field length. Trials have indicated that high application efficiencies are possible over a wide range of furrow lengths providing the correct inflow (i.e. low inflows for short furrows) is used (Eldeiry et al. 2005). The same trials also indicated that for longer furrow lengths, the irrigation performance is less sensitive to variations in inflow rates, furrow shape, field slope and surface roughness. Simulations using the Furdev (FURrow Design, operation and EValuation) model indicated that the optimal field length was longer for a heavy clay soil (Jurriëns and Lenselink 2001). Jurriëns and Lenselink (2001) concluded that for a light, medium and heavy soil the maximum AE can be achieved by increasing the flow rate by 0.5 L s^{-1}, 0.3 L s^{-1} and 0.2 L s^{-1}, respectively for every additional 100 m in field length. Increases in furrow inflow are commonly associated with increased performance as water reaches the end of the field more rapidly. However, for a light textured (high infiltration alluvial) soil, decreasing the inflow rate was found to increase the AE due to a decrease in the wetted furrow cross section reducing the infiltration rates (Raine and Bakker 1996). Wallender and Rayej (1987) develop a volume balance based economic model to optimise profitability considering intra-furrow variability. They discovered that the optimal flow rate was higher and cut-off time was shorter for heterogeneous compared to homogeneous infiltration conditions.

Design charts (design curves) offer potential to reduce the computer simulation requirement associated with irrigation optimisation. The curves are created by simulating a given field and varying the key management parameters. The resulting charts facilitate the rapid identification of improved irrigation strategies without the need for further computer simulation. Examples include the design charts for

infiltration volume, runoff, AE and distribution uniformity (DU) for various inflow rates and times by Hornbuckle (1999) and the "Management-design charts" developed by Santos (1996) plotting contours of CU (Christiansen's coefficient of uniformity) and low quarter depth over unit inflow rate and cut-off time. In practice, the applicability of design charts is limited due to the requirement to develop individual charts for each combination of soil characteristics and field design.

7.2.3 Optimising Irrigation Performance at the Field Scale

A number of techniques have been proposed to derive the optimal irrigation strategy at the field scale. For example, as an alternative to considering all furrows during the optimisation process, Izadi et al. (1991) considered only the furrows with the highest and lowest infiltration. They found that if the inflow rate is sufficient to ensure rapid completion of the advance phase, the furrow with the lowest intake defines the maximum time to cut-off (TCO). In the situation where the advance accounts for a large proportion of the irrigation time, the furrow with the highest intake defines the maximum TCO.

Optimising more than one management parameter simultaneously requires extensive computational power. Realising this, Ito et al. (1999) devised a "Box Search" algorithm that determines the optimal TCO for a given inflow rate (Q), followed by an equivalent search for the optimal Q for that sub-optimal TCO. The process is repeated to arrive at the absolute optimal combination of the two. This technique was included within an optimisation scheme that considers spatially variable infiltration and maximises the return for water by calculating the expected yield under a seasonal irrigation application.

Many optimisation procedures require extensive field measurement and considerable technical capacity on the part of the farmer in order to adjust management to changes in infiltration. Hence, others have suggested the use of simple "recipe" strategies to improve irrigation performance (Smith et al. 2005). The recipe strategy describes the procedure where the inflow is cut-off at some multiple of the advance completion time (e.g. 90% or 100% of the advance time). Smith et al. (2005) found that

substantial improvements can be made to the AE and deep drainage via this type of recipe management. The recipe strategy can effectively adjust the inflow time to account for the variations in infiltration rates. However, additional gains are possible with specialist optimisation using simulation models.

7.3 The Optimisation Objective Function

The irrigation performance is not simply described by any single numerical expression. It is a complex combination of in excess of seven separate parameters, the values of which are partly dependent on each other. Hence, the "objective function" is created to compound the different aspects of irrigation performance. The objective function has no general rules. The performance parameters which are included and their relative weights will depend on the water supply, soil condition, crop physiology, environmental conditions and management constraints. Hence, it is conceivable that the objective function derived for a given field will not be appropriate for other fields without some form of adjustment. To account for the multi-dimensional interaction of the performance indicators our irrigation guidelines and recommendations also need to be multi-dimensional (Raine et al. 1997).

7.3.1 Arithmetic Objective Function

One option is to create an objective function in the form of a mathematical expression (e.g. FIDO, McClymont 2007). In this case, several performance terms are combined using weightings to arrive at a single numerical value. The weightings are chosen based on the relative importance of each parameter. This approach is often preferred since the numerical nature of the objective function enables its use within an automated optimisation procedure. The computer continues to alter the management variables until the objective function cannot be improved any further. In some cases, the complexity of the solution surface will prevent identification of the global optimum as the optimisation converges to local maxima points.

The major difficulty for arithmetic objective functions is the formulation of the relative parameter weightings. There are no standard values for these weights as they

will vary depending on the particular objectives for that irrigation. For example, all twenty furrows of the Downs field were simulated over realistic ranges for Q (0.5 to 11 L s^{-1}) and TCO (200 to 1200 minutes). The total field performance parameters were calculated on a 105x101 grid made up of Q and TCO values (inflow at 0.1 L s^{-1} and time at 10 minute increments).

An objective function (*OBJ*) was proposed:

$$OBJ = \frac{25}{100}(RE) + \frac{25}{100}(AE) + \frac{25}{100}(DU) + \frac{25}{100}(1 - DD\%) \quad \textbf{..... Eq 7-1}$$

where the requirement efficiency (RE), AE, DU and deep drainage percentage (DD%) have equal weighting. In this case, the objective function appears to identify a single optimised point (e.g. at Q = 4.9 L s^{-1} and TCO = 470 minutes) within the range of management variables considered (Figure 7-1). However, the form of this surface and the position of the optimal management point will change considerably when either the weightings or selected performance terms are altered.

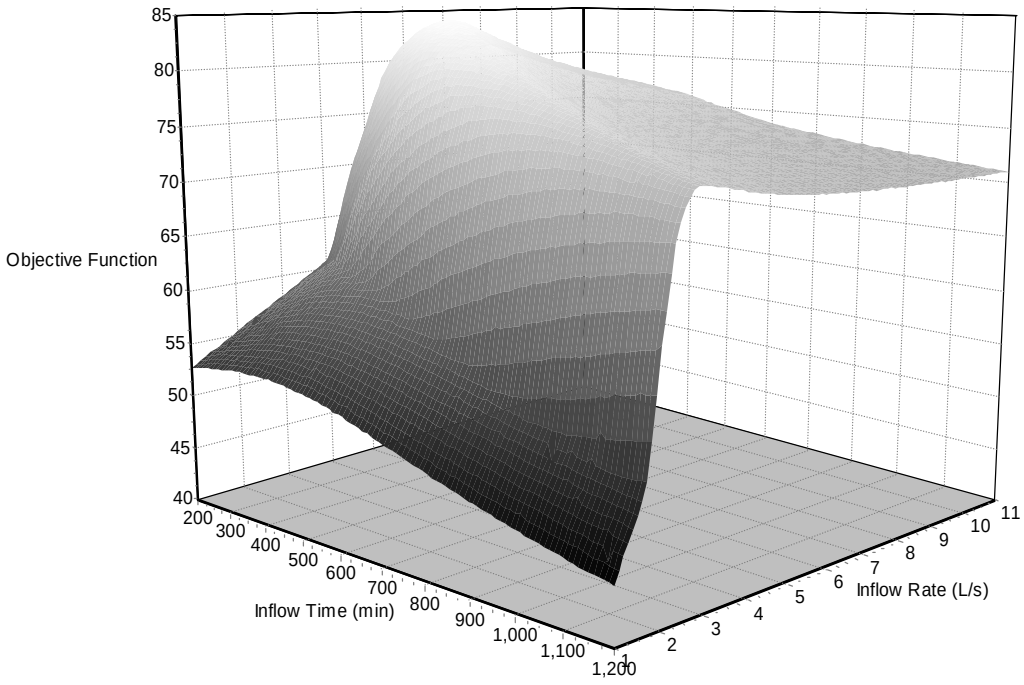

Figure 7-1 Optimising using an Arithmetic objective function: ¼(RE) ¼AE) + ¼DU + ¼(1-DD%) (Downs field)

In this example it might be possible that the optimised inflow rate and time only results in high values for three of the performance terms at the expense of the fourth

parameter. However, there is no way to know for sure since the numerical value given by the objective function (e.g. Eq. 7-1) does not provide any information regarding the values of the individual performance parameters. Hence, optimisation procedures employing such objective functions should contain an additional checking mechanism to guarantee satisfactory irrigation performance (i.e. minimum limits or restrictions for each performance term).

7.3.2 Boolean Objective Function

The optimisation procedure employed by IrriProb differs from the arithmetic objective function in that it identifies the range of management variables that fulfil a "Boolean objective function". The Boolean expression defines the "optimised" irrigation as one that simultaneously satisfies a series of defined performance criteria. The user selects any number of performance terms and provides conditions or limits (i.e. greater than, less than or equal to) for each. This objective function is implemented in graphical form as the "optimise grid", explained in section 6.3.1. The domains of management variables that satisfy given criteria are shaded in separate colours whilst the optimised (overlapped) region is easily distinguishable (e.g. Figure 6-6). In some cases the objective function of IrriProb may fail to distinctly identify the optimal region and require redefinition of the performance criteria. Hence, this style of objective function is less suited to autonomous operation than the arithmetic based objective functions described previously.

The major advantage of this approach is derived via the use of performance limits. The optimisation will not become biased towards certain parameters, even if their values increase far above the specified minimum conditions. Hence, none of the parameters included within the objective function loose significance when the values of the other performance terms increase. In addition, the user will be immediately aware when any part of the supplied objective function is not satisfied. In these cases, the criteria can be sequentially revised until a "optimal" combination of Q and TCO is found.

7.3.3 Optimisation Methodology

The optimisation tool within IrriProb is flexible as it can be adapted for use within almost any furrow irrigation system. Hence, a full validation of the procedure considering all possible scenarios would is beyond the scope of this discussion. The analysis presented in this chapter was carried out according to a standard methodology. The first stage in the optimisation process is to simulate the field or furrow of interest for combinations of Q and TCO within specified limits according to the batch simulation process (6.3.1). In each case, simulations were conducted using all possible combinations of inflow rates between 0.1 and 28 L s^{-1} and cut off times between 20 and 5000 minutes. However, the middle of this region (i.e. Q = 1 to 11 L s^{-1} and TCO = 200 to 1200 minutes for Downs) was simulated at higher resolution (smaller Q and TCO intervals) and serves as the primary focus region for the remainder of this chapter. The bounds of the simulated region were modified according to the average measured inflow rates and times for each field.

As the Boolean objective function can take on endless possible combinations of the various performance terms, the region identified as “optimal” may be quite large in some cases. For this analysis the unique optimal field management combination was found by selecting two performance parameters with appropriate minimum requirements. This restricted the optimisation to a limited combination of Q and TCO values within the total area of consideration. A third parameter was selected and its performance limit was gradually increased until the overlapping region of the three criteria converged to a single point or small range of optimal points. Where this procedure did not converge to a single clear solution for the Q and TCO the optimal point was chosen by manual observation of the optimise grid (e.g. Figure 6-6).

For purposes of illustration, this study considered two different optimisations, described by the following formulations of the objective function:

Opt 1. Maintain the requirement efficiency and distribution uniformity of the root zone (DURZ) above 90% whilst the optimal point is found by maximising the application efficiency (i.e. RE > 90%, DURZ > 90% and maximise AE).

Opt 2. Maintain the requirement efficiency above 95% while achieving an application efficiency of greater than 70% and the optimal point is found by minimising the deep drainage (i.e. RE > 95%, AE > 70% and minimise D_{DD}).

It should be noted that the performance criteria that make up these objective functions are arbitrary and that these options merely represent two possible scenarios for optimisation. The analysis in this chapter is entirely theoretical and was in no way restricted by the practical limitations on inflow rates or cut-off times as discussed previously in section 7.2.1. It is assumed that the findings based on the use of these optimisation criteria (Opt 1 and Opt 2) are applicable across a wide range of possible formulations of the objective function.

7.4 Behaviour of the Irrigation Performance Objective Function

7.4.1 Interactions between Inflow and Performance

The results used to generate Figure 7-1 for the Downs data were also used to study the relationship of the inflow time (TCO) (Figure 7-2) and inflow rate (Q) (Figure 7-3) with the values of AE and RE. Each point on these figures represents the combined "field" performance of the 20 furrows for a particular value of Q and TCO. In both cases, the four subfigures contain the same information where each is simply rotated 90 degrees clockwise from the previous sub-figure. The points that do not conform to the general curvature should be ignored as they simply indicate that the simulation encountered an error within one of the furrows for that combination of Q and TCO.

Observation of the relationship between TCO and performance (Figure 7-2) clearly demonstrates a trade-off between application efficiency and requirement efficiency

that occurs at any value of inflow time. The points align roughly in a set of near vertical lines, where each line symbolises a different value of inflow rate. Given a constant inflow time, increasing the RE will cause a decline in the AE. At low inflow times (i.e. TCO = 200 minutes) it is possible to achieve higher values of the AE (i.e. above 80%) but such management is associated with unacceptably low values for the RE. At higher values of TCO, it becomes easier to improve the RE.

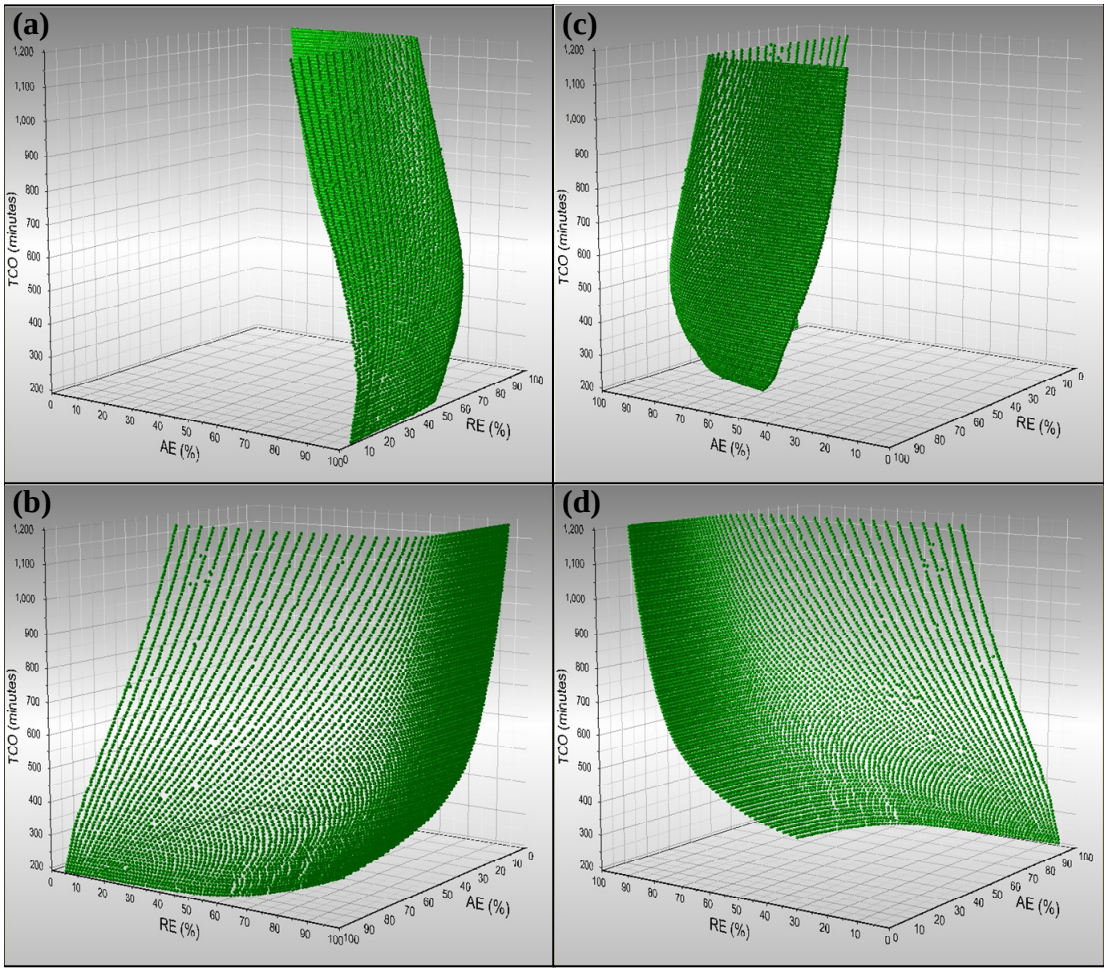

Figure 7-2 Cut-off time plotted against application efficiency and requirement efficiency (Downs field)

At low inflow rates (Figure 7-3) the AE tends to be higher at the expense of the RE (e.g. RE < 25% for Q = 0.5 L s^{-1}), thus indicating that a significant portion of the field would receive zero application. The RE increases rapidly with increasing flow rate up to a certain inflow (determined by the TCO), thereafter further increases will not improve the RE. The approximate position of this region represents the range of inflow rates that achieve maximum benefit for the irrigation adequacy whilst

minimising deep percolation and runoff losses. Generally, increases in the inflow rate were found to cause decreased values for the AE. This incremental decrease in AE appears to become more significant at higher inflows (i.e. greater than 4 L s^{-1}).

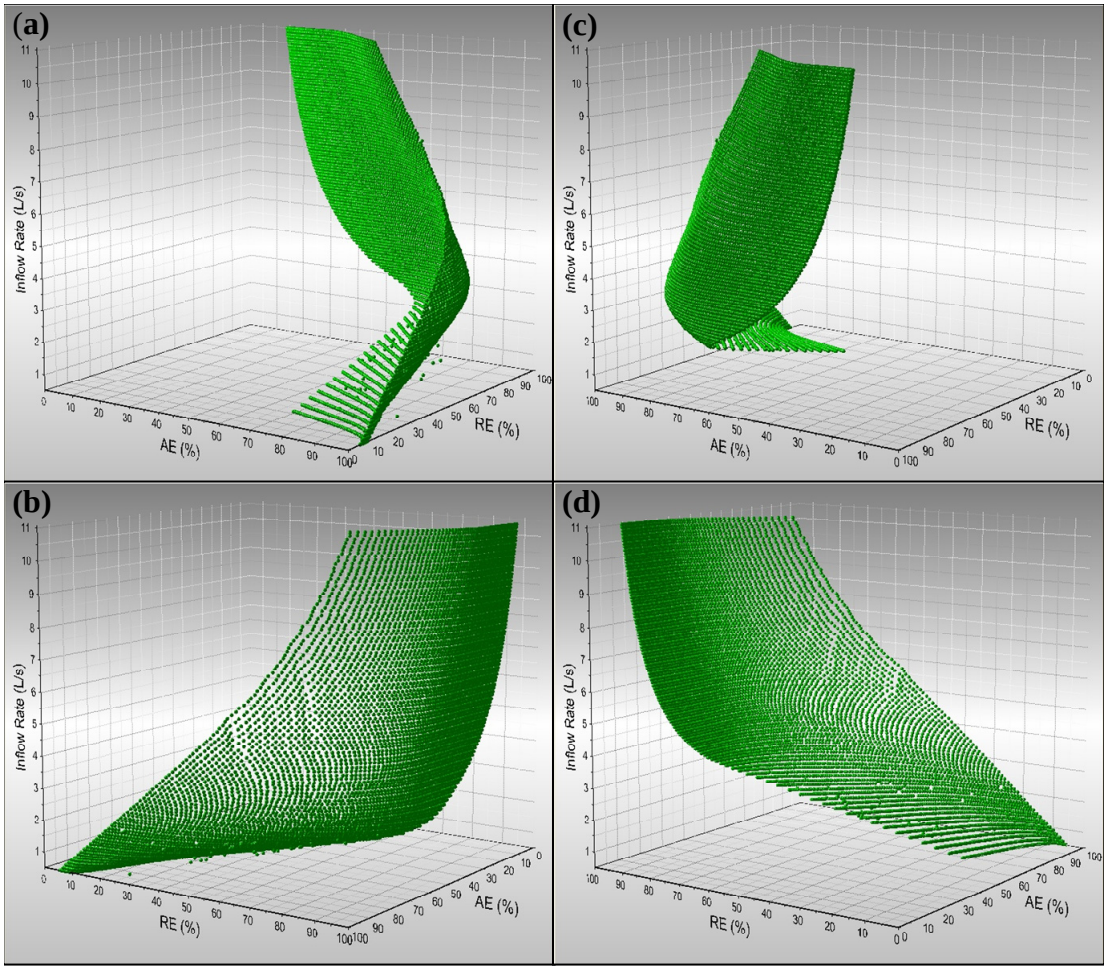

Figure 7-3 Inflow rate plotted against application efficiency and requirement efficiency (Downs field)

This analysis is limited to the application efficiency and requirement efficiency. However, several observations can be made from the plotted surfaces of the individual performance terms against inflow rates and times presented in chapter 6 (Figure 6-4 and Figure 6-5). The AE appears to follow an inverse relationship with the RE. At low inflow rates and times the AE reaches 100% whilst the RE is at minimum. Increasing Q and/or TCO will cause the AE to decline and RE to increase. The application efficiency with recycling (AER) (Figure 6-4.f) follows similar trends to the AE except that its values are generally much closer to 100%. Low inflow rates result in poor values of RE, DU, CU and DURZ as the water advance never reaches

the end of the field. Short inflow times may reduce the losses due to deep percolation and runoff but will also cause low values of RE and uniformity. The DURZ surface (Figure 6-4.d) appears to be a hybrid of the RE and DU terms. The DURZ and RE are similar except that low values of the RE correspond to zero values for the DURZ. As anticipated the surfaces of DU (Figure 6-4.c) and CU (Figure 6-5.b) are essentially identical. Hence, there is little value in considering both terms within a single objective function. The average depth of deep drainage (D_{DD}) (Figure 6-5.a) appears to be more sensitive to the inflow time than to the inflow rate. The opposite is true of the runoff percentage (Figure 6-4.e) as it appears to be more sensitive to changes in the inflow rate.

From the results presented in chapter 6 (Figure 6-4 and Figure 6-5) it is concluded that similar relationships must exist amongst all performance terms as those identified in Figure 7-2 and Figure 7-3 for the AE and RE. Hence, it is evident that no performance parameter should be considered in isolation. For example, a strategy that alone strives for maximum application efficiencies will result in unacceptable levels of uniformity and irrigation adequacy.

7.4.2 The Trade-off between the Performance Terms in the Objective Function

The interactions observed amongst the parameters in the previous section indicate that there is a trade-off between many of the different irrigation performance terms. Improving the value of one parameter may adversely influence the potential level of the other parameters. The same simulation results for the Downs field (used in 7.4.1) were used to demonstrate the relationships between the three parameters of the proposed objective functions. The two performance terms with limiting criteria are plotted on the horizontal axes while the third optimised term is located on the vertical axis.

For optimisation 1 (Opt 1) the RE follows a general positive relationship (Figures 7-4.a and 7-5) with the DURZ that appears to be strongest for DURZ values between 5 and 75%. Considering a fixed value of DURZ, the maximum AE tends to occur at

the lowest value of RE. It is possible to achieve high levels of application efficiency (i.e. AE > 70%) over the majority of RE and DURZ values. However, the AE experiences a rapid decline as the RE and DURZ criteria increase above 95% and 90%, respectively. Hence, the shape of the surface at this point (Figures 7-4.a and 7-5) appears to define the maximum optimised values for the RE and DURZ. For this objective function (Opt 1) the optimal management will occur somewhere close to this sudden turning point (maximum curvature).

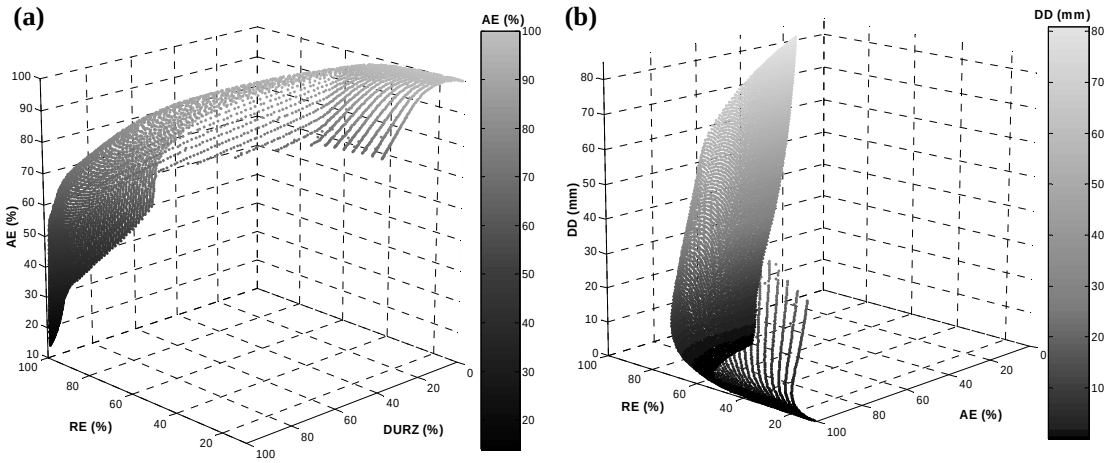

Figure 7-4 Behaviour of the objective function of a) Opt 1 and b) Opt 2 (Downs field)
Figure 7-4.a contains the same results as Figure 7-5 and,
Figure 7-4.b contains the same results as Figure 7-6

Considering the second objective function (Opt 2), the average depth of deep percolation (D_{DD}) is plotted over axes of RE and AE (Figures 7-4.b and 7-6). In this case the plotted surface appears to be more complex in nature within the region of interest. In one section of the figure there exists two widely different values of D_{DD} for a given combination of RE and AE (Figure 7-6). This behaviour would have been expected to occur over a wider range of AE and RE if the field had been simulated using an increased domain for the inflow rates and times. Observation of the same surface from an alternate angle (Figure 7-4.b) provides further insight into the behaviour of the objective function. The multiple solutions for D_{DD} suggests that the process of optimisation should not be performed considering only one of the performance terms at a time. The user should be aware of the general relationship with the other performance terms in case some adjustment of the other optimisation criteria is required.

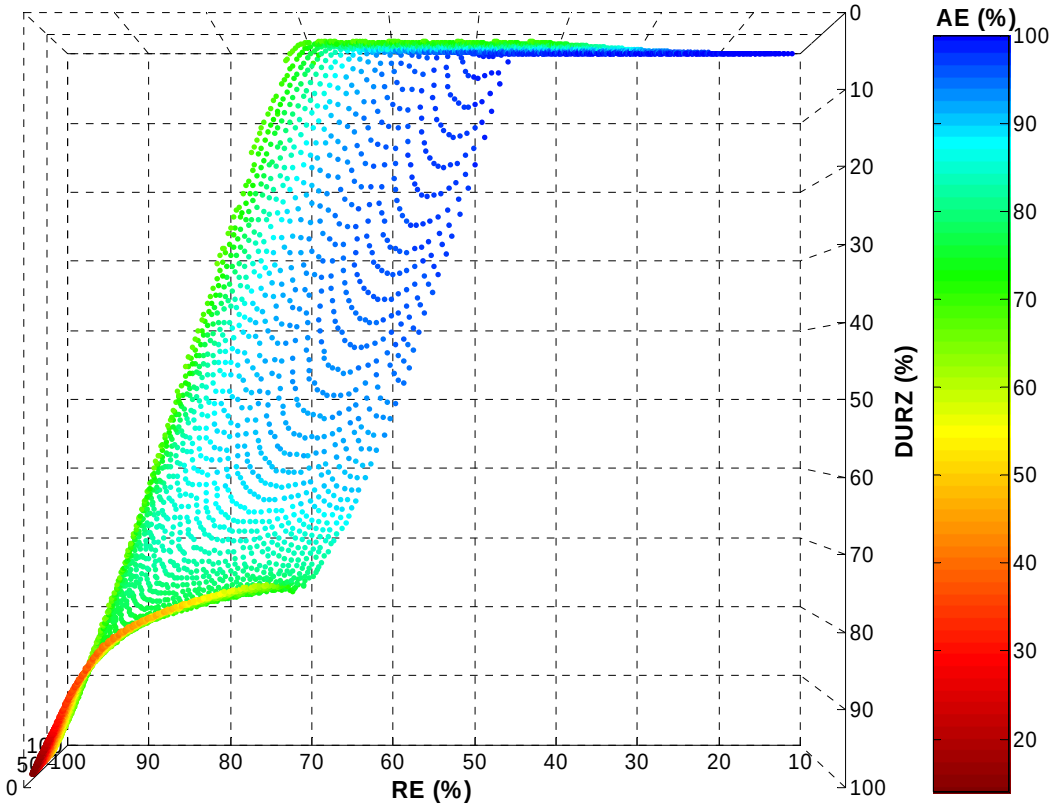

Figure 7-5 Behaviour of AE in relation to RE and DURZ (Downs field)

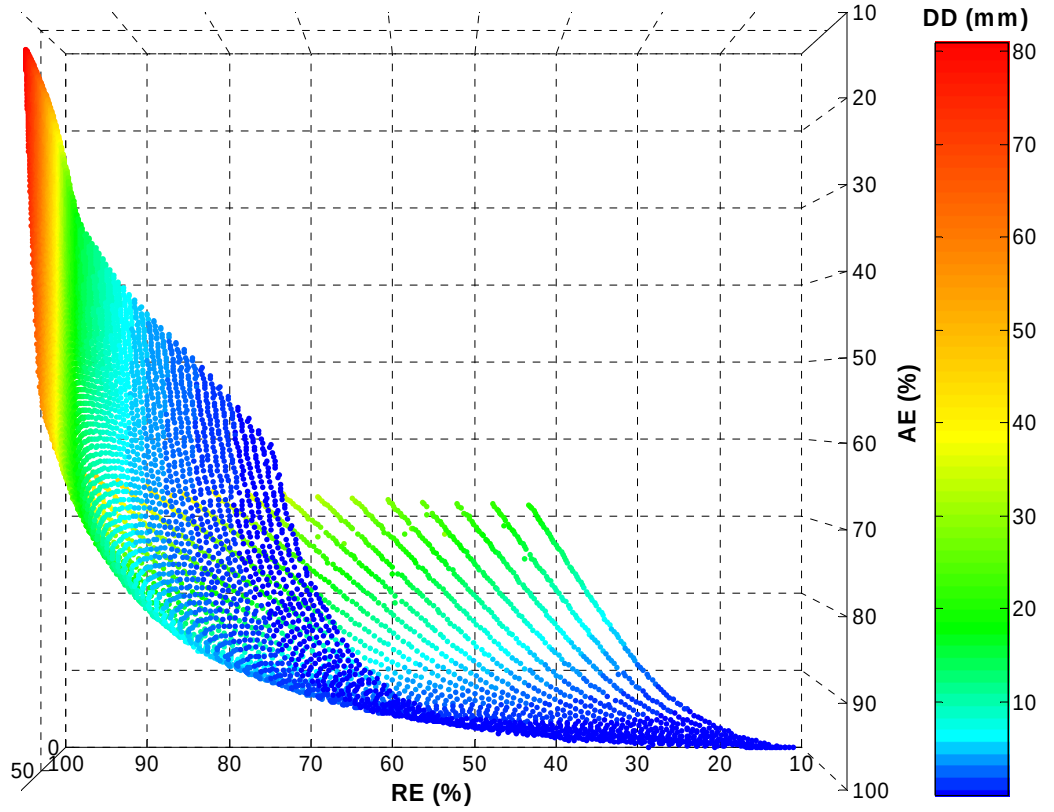

Figure 7-6 Behaviour of D_{DD} in relation to RE and AE (Downs field)

Considering the large variation between the surfaces of these two optimisations it is concluded that alternative formulations for the objective function will behave differently and perhaps with greater complexity than observed for Opt 1 and Opt 2. Optimisation of irrigation management employing a variant of the arithmetic objective function may still identify an appropriate optimal point but will mask the true nature of the individual performance terms. The findings from this investigation provide support for the use of the IrriProb optimisation tool, not just to identify the optimal irrigation strategy but also to observe the behaviour of the performance terms in the vicinity of the optimal point.

7.4.3 Movement of the Optimised Point in the Inflow Rate/Inflow Time Domain

The two objective functions chosen to demonstrate the optimisation of irrigation management contain two minimum performance constraints or criteria. The optimal inflow rate and TCO were identified by optimising the value of a third parameter. Relationships were observed between the components of the objective function in Figures 7-4, 7-5 and 7-6. However, these charts do not illustrate the impact of changing values of the performance terms on the optimised values of inflow rate and time. An analysis was conducted to determine the sensitivity of this optimal point to the values of the performance criteria. The 20 furrows of the Downs field were optimised using the objective functions described earlier (Opt 1 and Opt 2). The value for one criteria was altered and the optimisation repeated to identify a new optimised combination of Q and TCO. The resulting movement of the optimal inflow management is plotted in Figure 7-7 for Opt 1 and Figure 7-8 for Opt 2. Three additional lines are included to represent the inflow rates and times that correspond to each constant component of the original objective function.

For optimisation 1 (Figure 7-7), altering the RE requirement does not have any effect on the optimised inflow management (at DURZ = 90%) until it exceeds 96%. Thereafter the position of the optimal point is highly sensitive to the RE and further increases cause the inflow rate to decline and TCO to increase. The DURZ has a similar effect over the optimised inflow. The influence of the DURZ occurs over a

wider range of parameter values compared to the RE and the values of optimised Q and TCO become increasingly sensitive as the value of DURZ criterion increases. The movement of the optimised inflow point is explained by visualising the movement of the three lines corresponding to RE = 90%, DURZ = 90% and AE = 70%. Increasing the value of the RE and DURZ will cause these lines to shift in an approximately parallel fashion from left to right and in the opposite direction for the AE.

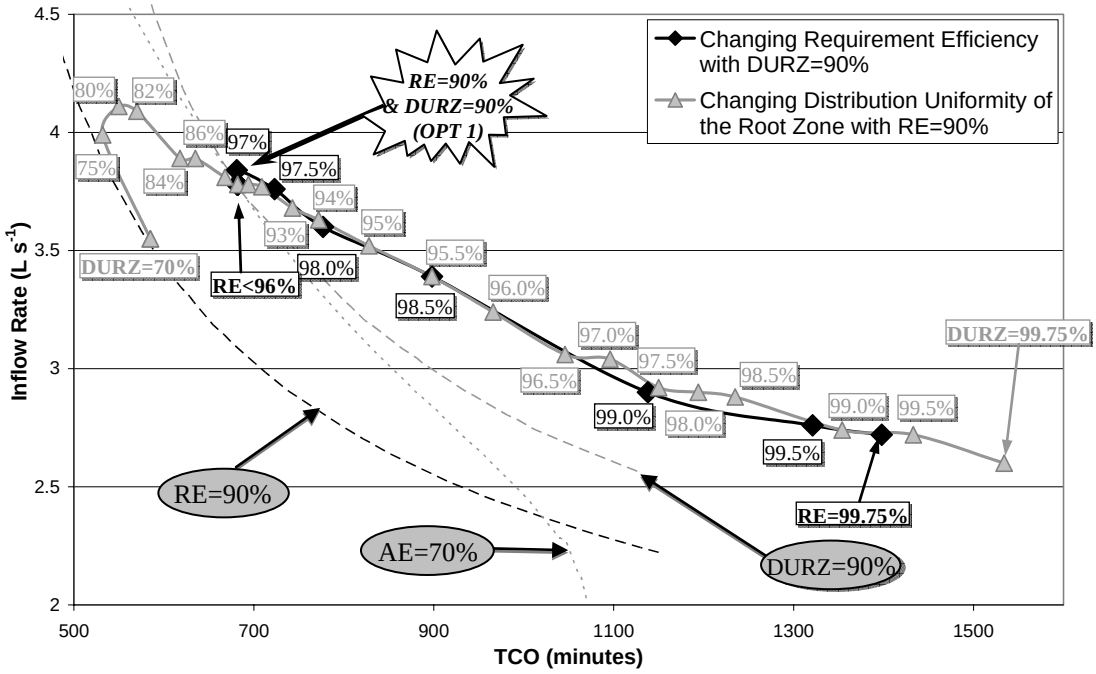

Figure 7-7 Movement of the optimal inflow point to maximise application efficiency while varying the RE and DURZ criteria (Downs field)

For optimisation 2, the direct influence of each performance parameter criteria on the position of the optimal point is more evident (Figure 7-8). The application and requirement efficiencies are opposing in nature. Hence, the regions that satisfy the stipulated requirements for these parameters intersect over a narrow band of Q and TCO. Altering the value of RE causes the optimal point to move along the line corresponding to AE = 70%. To achieve higher values of requirement efficiency at the same level of AE, the farmer must extend the TCO to increase the average opportunity time but simultaneously reduce the inflow discharge to prevent an increase in runoff losses. Similarly, the optimal point (minimal D_{DD}) follows the line of RE = 95% when AE is altered. The application efficiency reaches an upper limit of 73.65% (at RE = 95%) indicating that the regions of inflow in the rate/time domain

for RE and AE no longer intersect for further increases in performance. In a similar way Figure 7-8 also illustrates the maximum value of RE under the fixed requirement for AE. Although the values of Q and TCO may differ the movement of these two optimisation objective functions should behave in similar manner for any field considered.

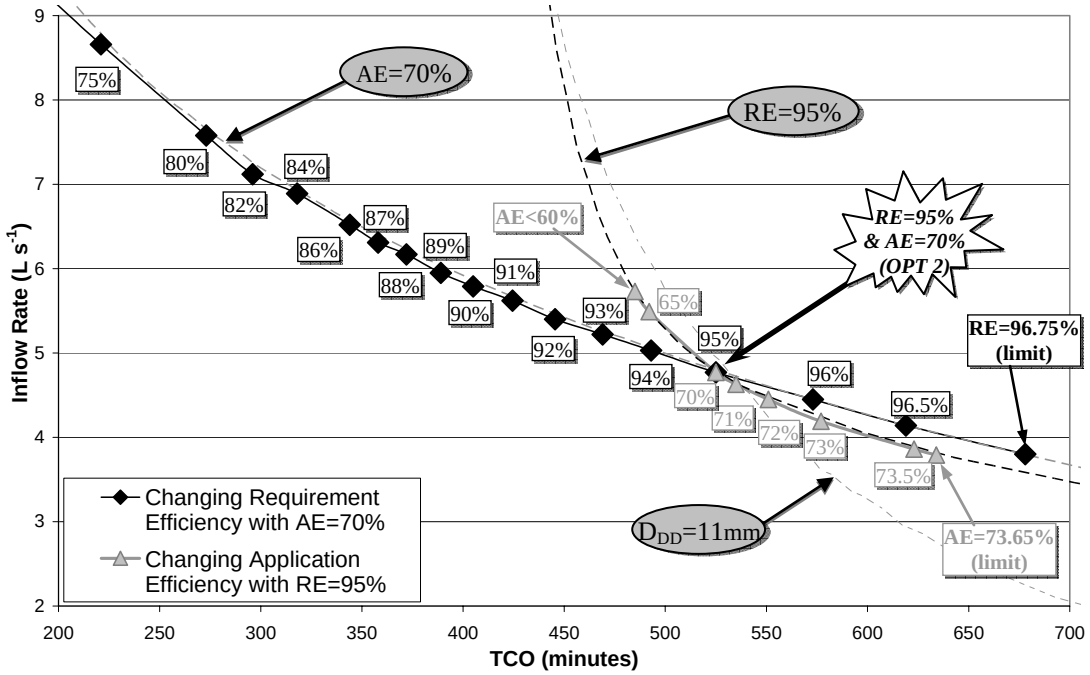

Figure 7-8 Movement of the optimal inflow point to minimise deep drainage while varying the RE and AE criteria (Downs field)

The results indicate that the point of optimal inflow rate and TCO is sensitive to the values of the performance criteria. The level of sensitivity is determined by the type of interaction between the selected performance terms. Under some objective functions individual performance terms may become redundant once they reach certain thresholds and have no effect on the optimal point (e.g. Opt 1, reducing the RE below 96%). In other cases, altering the values of the performance criteria may prevent the identification optimisation (e.g. attempting to increase the AE above 73.65% for Opt 2).

7.5 Can the Optimal Field Management be identified from a Single Furrow?

7.5.1 Introduction

For furrow irrigation, the optimal field management is traditionally determined based on the evaluation and optimisation of one furrow or possibly a small number of furrows. This practice is fundamentally flawed due to the large variance in soil intake rates (chapter 5) and other field characteristics. The optimal irrigation management identified from the measurements of one furrow may not necessarily correlate with that of other furrows or with the field as a whole. The Downs, Chisholm and Turner (field 17) fields (chapter 5) were chosen to evaluate the potential to identify the whole field irrigation management using measurements from a single furrow.

Batch simulations (chapter 6) were performed over an appropriate range of inflow rates and times for each individual furrow and group of furrows as a whole and the results were stored for subsequent analysis and optimisation. The field was optimised using IrriProb following the criteria of Opt 1 and Opt 2 by considering each furrow independently. This resulted in a unique optimal inflow rate and time for each furrow. The whole field was simulated using each optimal inflow recommendation to assess the true improvements to irrigation performance.

7.5.2 Furrow Based Performance Terms Compared to Field Values

Before attempting to optimise the whole field management based on the results of any single furrow it would be beneficial to compare the behaviour of the performance terms of those furrows with that of the combined furrow group. The results in Figure 7-9 illustrate the values of Q and TCO that correspond to the performance criteria that make up the objective functions, Opt 1 (a, b and c) and Opt 2 (c, d and e).

The field based values for the RE follow a similar shape to that of the individual furrows at both the 90% (Figure 7-9.a) and 95% (Figure 7-9.d) levels. The line generated from the field simulation is located approximately centrally amongst the

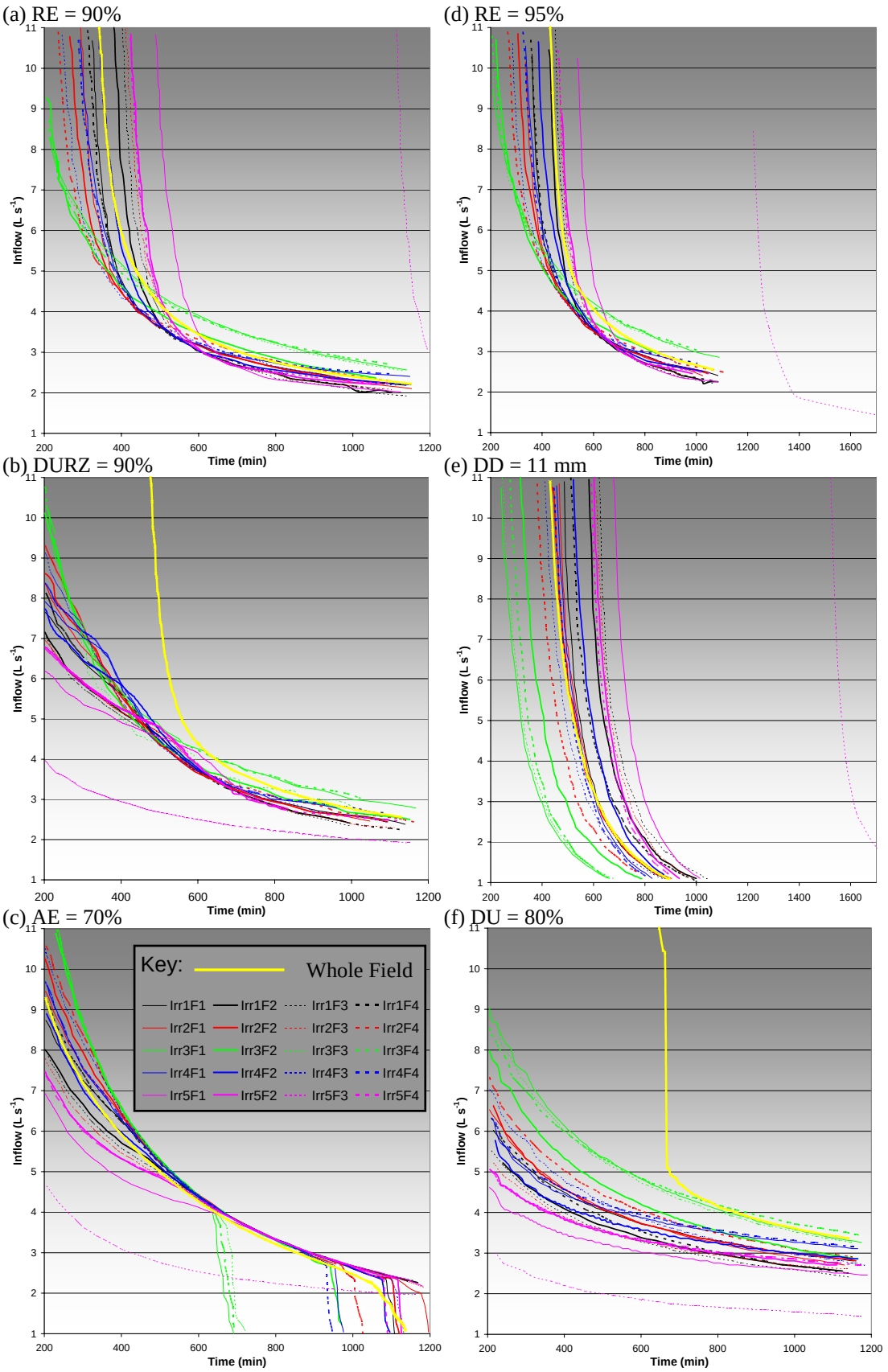

Figure 7-9 Comparing the inflow rates and times that meet each performance criteria for Opt 1 (a – c) and Opt 2 (c - d) and DU = 80% between the individual furrows and the whole field

furrow based results. The lines of constant AE and deep drainage demonstrate similar trends as the field based inflow rates and times appear to correspond with the average of the individual furrows. In contrast the DURZ does not conform to the same relationships (Figure 7-9.b). The individual furrow simulations suggest that the 90% requirement for the DURZ can be satisfied using high inflow rates for shorter times (e.g. 6 L s^{-1} for 400 minutes). However, simulation of the 20 furrows as a group indicates that this level of root zone uniformity requires the farmer to extend the TCO. The field management required to achieve the 90% value of DURZ appears to be similar for the single furrow compared to the field for lower inflow rates and longer times but the lines diverge as the inflow rates increase. The DU does not feature in either of the selected objective functions but has been included (Figure 7-9.f) since it often forms the basis for the optimisation of irrigation management. The Q and TCO values required to reach the DU requirement behave similarly to that of the root zone uniformity. However, in this case the field based values are further removed from those indicated by the furrow simulations.

It is believed that the general shapes observed in Figure 7-9 will persist for any surface irrigated field. However, the relative spread of the curves and the dissimilarity compared to the field performance should increase under higher levels of infiltration variability. The optimisation technique behaves similarly for the whole field as for the majority of the individual furrows since the lines of constant performance follow the same general shape. Hence, it is valid to employ the procedures developed here to identify the optimal management practices for both the individual furrow and the field as a whole. The strong correlation between furrow and field based values of the RE, AE and D_{DD} suggests that it should be possible to adjust the furrow based optimal management to optimise the performance of the group. However, both the DU and DURZ prevent any direct association. The inflow rate and/or time must be increased significantly to achieve the same level of uniformity as for the single furrow.

7.5.3 Example: Optimising the Downs Field using Opt 1

Each furrow of the Downs field was optimised according to Opt 1, i.e. to maintain both the RE and DURZ above 90% while maximising the application efficiency. The

results of the "Furrow selected for optimisation" (Table 7-1) indicate that in every case it is possible to manage the single furrows in order to satisfy the performance criteria. In this case, the optimised inflow rates for individual furrows ranged between 1.43 to 8.84 L s^{-1} while the TCO values ranged from 238 to 1673 minutes. For the majority of furrows, the AE was improved beyond that of the measured irrigation (original performance for each furrow located in Appendix Table H.1). In a number of instances a slight decrease in the AE was required to increase the levels of RE and DURZ to 90%.

Table 7-1 Optimisation 1: RE>90%, DURZ>90% and AE is maximised (Downs field)

			Furrow selected for optimisation			Whole field under furrow optimum			Error in predicted field performance		
	TCO (min)	**Inflow (L s^{-1})**	**RE (%)**	**DURZ (%)**	**AE (%)**	**RE (%)**	**DURZ (%)**	**AE (%)**	**RE (%)**	**DURZ (%)**	**AE (%)**
Actual Calculated from Individual Furrows						**93.9**	**81.1**	**73.8**			
Irr1 F1	554	4.04	97.0	90.9	80.6	92.8	80.1	76.9	4.2	10.7	3.7
Irr1 F2	667	3.39	97.2	91.5	79.6	93.3	79.0	76.5	4.0	12.5	3.0
Irr1 F3	748	3.04	97.4	92.1	79.3	92.8	76.9	75.9	4.6	15.1	3.4
Irr1 F4	642	3.46	97.0	90.7	81.2	92.8	77.9	77.5	4.2	12.8	3.7
Irr2 F1	554	4.04	97.4	91.9	79.9	92.8	80.1	76.9	4.6	11.8	3.0
Irr2 F2	557	4.02	97.1	91.3	80.8	92.7	79.9	77.0	4.4	11.4	3.8
Irr2 F3	738	3.09	97.4	92.0	78.9	93.0	77.7	75.8	4.4	14.3	3.1
Irr2 F4	444	4.94	96.9	90.6	81.5	90.1	80.3	75.9	6.8	10.3	5.6
Irr3 F1	238	8.84	95.5	87.4	88.0	77.7	77.0	66.7	17.9	10.4	21.4
Irr3 F2	363	5.95	97.2	91.6	82.4	86.6	79.9	73.5	10.6	11.7	8.9
Irr3 F3	243	8.74	97.3	91.7	82.4	78.1	77.1	66.6	19.2	14.6	15.9
Irr3 F4	301	7.23	97.3	91.7	80.9	82.9	78.5	69.4	14.4	13.2	11.5
Irr4 F1	594	3.84	97.1	91.2	78.9	93.7	81.2	76.0	3.5	10.0	2.9
Irr4 F2	672	3.41	97.1	91.2	79.0	93.7	80.2	75.9	3.4	11.0	3.1
Irr4 F3	481	4.57	96.9	90.6	81.9	91.4	80.5	76.6	5.4	10.1	5.3
Irr4 F4	579	3.91	97.2	91.4	79.0	93.4	80.7	76.2	3.8	10.7	2.7
Irr5 F1	836	2.73	97.3	91.8	79.5	91.6	72.8	74.6	5.7	19.1	4.9
Irr5 F2	735	3.09	97.2	91.5	79.6	92.9	77.3	76.1	4.4	14.2	3.5
Irr5 F3	1673	1.43	97.8	93.5	76.6	71.6	0.0	56.0	26.2	93.5	20.7
Irr5 F4	718	3.16	97.5	92.2	79.3	93.0	77.8	76.1	4.4	14.4	3.3
Combined[1]	**-**	**-**	**-**	**-**	**-**	**97.1**	**91.3**	**80.4**	-	-	-
average	616.9	4.35	97.1	91.3	80.5			**average**	**7.8**	**16.6**	**6.7**

[1] Represents the maximum performance where each furrow was optimised individually.

The values under "Whole field under furrow optimum" (Table 7-1) describe the performance of the whole field under the same optimal inflow management identified for the single furrow. When the whole field was simulated using the optimum Q and TCO for each furrow, the RE, DURZ and AE were found to be lower than that predicted by simulation of the respective furrow in every case. On average, the single furrow optimisation overestimated the RE by 7.8%, the DURZ by 16.6% and the AE by 6.7% (Table 7-1). In some cases, the use of the single furrow optimum practice to

manage the whole field could create significant problems. For example, consider if the field evaluation only included measurements from furrow 3 of irrigation 3. In this case, it would be considered valid to optimise the irrigation management based on the infiltration curve estimated from the measurements in that furrow alone. The subsequent optimisation procedure would suggest that the farmer should increase the inflow rate to 8.74 L s^{-1} and cease the flow after 243 minutes to achieve 97% RE, 92% DURZ and an AE of 82%. The farmer would be led to believe that the recommended management practices would almost fully replenish the root zone. However, in reality, the irrigation would only satisfy 78% of the requirement with a root zone uniformity and application efficiency of 77% and 67%, respectively. In general, the optimisations based on the measurements from individual furrows do not offer any advantage over the current performance (first row of Table 7-1). On average they tend to result in a reduction of the field-wide AE, RE and DURZ from the measured irrigation conditions.

"Combined" (Table 7-1) refers to the situation where each furrow was individually optimised and was simulated with that individual inflow time and application rate. This represents the maximum possible AE (80.4%) while adhering to the RE and DURZ requirements of 90%. If it was possible to implement these variable inflow rates and times in this case, the total water use could be reduced by 0.064 ML ha^{-1} per irrigation or 0.321 M ha^{-1} over the season (5 irrigations). In the case of 85% tail-water recovery these figures improve further to result in savings of 0.094 ML ha^{-1} and 0.47 ML ha^{-1}, respectively.

7.5.4 Summary of Results

The Downs field was also optimised using Opt 2 (RE > 95%, AE > 70% and minimise D_{DD}) resulting in similar trends (Appendix Table I.1) to that of Opt 1. On average the individual furrow optimum overestimated the RE by 8.29% (Table 7-2) compared to the field performance. However, optimising using the furrows of irrigation 3 caused the RE to be overestimated by between 18.9 to 27.7%. In most cases the furrow based optimum underestimated the D_{DD}. In one case (Irrigation 5 furrow 3), the optimisation resulted in an average deep drainage across the field of

52.2 mm when only 1.3 mm was predicted by the simulation of that individual furrow. Optimisation using the single furrow was generally found to result in a reduction in the deep drainage at the expense of lower efficiency values.

Table 7-2 Average difference (overestimation) between the single furrow and the field performance simulated with the individual furrow optimum management

	Opt 1.			Opt 2.		
Field	Error in RE (%)	Error in DURZ (%)	Error in AE (%)	Error in RE (%)	Error in AE (%)	Error in D_{DD} (mm)
Downs	7.81	16.59	6.68	8.29	6.00	-7.6
Chisholm	26.04	65.54	17.94	19.76	9.52	-7.4
Turner	11.10	26.56	10.09	7.16	6.22	-19.8

In fields with greater variability in infiltration the differences between individual furrow and whole field performances should also increase. To test this hypothesis optimisation procedure was repeated for the Chisholm (Appendix Tables I.2 and I.3) and Turner (Appendix Tables I.5 and I.6) fields. The infiltration curves of the Chisholm field (Figure 5-5) and Turner field (Figure 5-6) possessed greater variance than those of the Downs field. In both cases the problems associated with the use of the single furrow for optimisation were magnified. The individual furrow optimisations were found to overestimate the field performance by a greater extent (Table 7-2) than for the Downs field. These additional fields are not discussed further here as the key findings are similar to that of the Downs field. One notable exception was for the Chisholm field, Opt 2 where it was necessary to reduce the 70% criteria for the application efficiency to 60% to enable optimisation (Appendix Table I.3).

The optimisation process was repeated for the Chisholm field using the variable soil moisture deficit measurements and Opt 2 (Appendix Table I.4). As discussed previously (section 6.5), there are some concerns regarding the accuracy of these measured moisture deficits. However, it was clear that the variation in initial moisture content influenced both the optimised inflow conditions and the differences between the individual furrow and whole field performance values. In general, the issues associated with the use of the single furrow tended to be more significant in conditions of variable moisture deficit.

7.5.5 Optimising Using the Average Infiltration Curve

The results of the previous sections indicate that it is inappropriate to evaluate and optimise the field performance relying on the measurements of a single furrow. The infiltration curve estimated from the measurements within a single random furrow may not provide an adequate representation of the soil properties over the entire field area. The selected furrow may lie anywhere within the spread of infiltration curves experienced within a typical irrigated field, which can be considerable (section 5.5). Many of the issues associated with optimising field performance with limited field data may be corrected by improving the quality of the soil infiltration information. Hence, the identification of an average infiltration curve for the field should improve the accuracy of whole field evaluation and performance of the optimal irrigation strategy compared to the use of infiltration information from a single random furrow.

To evaluate the potential of the average infiltration curve to identify the whole field optimisation, the process previously described (section 7.3.3) to optimise individual furrows was repeated using the parameters of the average infiltration curve. The average infiltration parameters (Table 7-3) were estimated by application of equation 5-26 with $ZVal_{Infiltration}$ = 0 and $CV_{Infiltration}$ = CV_{VB} (Eq. 5-23) to obtain a value for $\overline{\ln(Z(\tau))}$ representative of the average infiltration curve over all furrows within each field. The infiltration parameters were estimated using a similar procedure to that of the predictive technique in section 5.9. Hence, the resulting values of a, k and f_0 represent the best fit to the average of the log-transformed infiltration curves for opportunity times (τ) between 50% and 100% of the average final advance time.

Table 7-3 Average infiltration parameters for Downs, Chisholm and Turner

Field	Infiltration Parameters		
	a	***k***	***f_0***
Downs	0.3271	0.02061	0.000119
Chisholm	0.2940	0.03161	0.000092
Turner F17	0.0721	0.07534	0.000080

The results (Table 7-4) suggest that optimisation of field management based on simulation of the average infiltration curve suffers from many of the same problems

as the use of the single random furrow. The performance level indicated by the optimisation using the average infiltration curve overestimated the field performance (of the terms in the objective function) at the resultant optimal inflow rate and time to cut-off (Table 7-4). In a number of cases (e.g. the AE for Chisholm and Turner and the D_{DD} for Chisholm) the optimisation based on the average infiltration curve is associated with larger errors than compared to the average error found when using the single random furrow approach.

Table 7-4 Optimising inflow rates and TCO using the average infiltration curve

				Optimised performance as predicted by simulation of average infiltration curve				Whole field performance under implementation of the this optimal inflow				Error in predicted field performance			
Field	**Opt**	**TCO (min)**	**Inflow ($L\ s^{-1}$)**	**RE (%)**	**DURZ (%)**	**AE (%)**	**D_{DD} (mm)**	**RE (%)**	**DURZ (%)**	**AE (%)**	**D_{DD} (mm)**	**RE (%)**	**DURZ (%)**	**AE (%)**	**D_{DD} (mm)**
Downs	**1**	597	3.76	97.21	91.45	79.63		93.16	79.70	76.86		4.1	11.7	2.8	
	2	409	6.1	95.06		70.36	0.41	91.08		66.91	5.76	4.0		3.5	-5.4
Chisholm	**1**	47	9.61	95.24	90.78	90.23		70.90	25.45	67.00		24.3	65.3	23.2	
	2	54	10.07	94.61		86.76	0.30	79.38		61.88	13.47	15.2		24.9	-13.2
Turner (field 17)	**1**	277	9.06	91.84	91.26	96.29		81.15	62.41	84.70		10.7	28.9	11.6	
	2	289	11.77	94.85		76.93	0.00	90.51		70.28	5.75	4.3		6.7	-5.7

The results presented here indicate that the use of the average infiltration curve to optimise field management may provide improved performance compared to the use of the single furrow. However, the small benefit observed probably does not warrant the extra measurement and analysis required to estimate the average infiltration parameters for the field.

7.6 Improving the Performance of Furrow Irrigation using Recipe Management Strategies

Recipe irrigation strategies are often preferred since if they are properly prescribed improvements in irrigation performance may be obtained without the need for detailed advance measurements and computer modelling. The performance of several

different recipe management strategies were compared with the whole field optimisation techniques. The recipe strategies selected for the analysis included:

1) Measured Q and TCO equal to final advance,
2) Measured Q and TCO equal to 110% completion of advance,
3) Measured Q and TCO equal to completion time + 60 minutes,
4) Measured Q and TCO equal to completion time + 120 minutes,
5) Q = 6 L s^{-1} and TCO equal to completion of advance,
6) Q = 6 L s^{-1} and TCO equal to 110% of completion time,
7) Q = 6 L s^{-1} and TCO equal to completion time + 60 minutes, and
8) Q = 6 L s^{-1} and TCO equal to completion time + 120 minutes.

where "measured" Q refers to the inflow rate measured in each separate furrow (given in Tables 5-1, 5-2 and 5-3).

The inflow rate of 6 L s^{-1} was selected as it represents the maximum flow discharge used by the cotton industry without risk of erosion (Smith et al. 2005). In each case, the individual completion time for each furrow was determined by simulating that furrow with the treatment flow rate (i.e. the completion times are not those from the advance data). All furrows within each field were simulated using the specified recipe to determine the TCO and a summary of the field performance values are presented in Table 7-5 (full results are presented in Appendix Table I.7).

For the majority of furrows, implementation of the recipe management shortened the TCO compared to that measured in the field (Table 7-5). Hence, the recipe strategy was found to result in moderate increases in the application efficiency through decreased runoff and deep percolation at the expense of the RE and DURZ. The Chisholm field experienced the largest benefit from the recipe management technique as the D_{DD} was reduced from 85.5 mm to between 32.8 and 69.5 mm for the various strategies. As a result the AE increased by up to 35% over the measured conditions while the RE and uniformity declined. Generally, the recipe management did not fully satisfy the moisture deficit and resulted in a decrease in the DURZ. However, the recipe strategies achieved application efficiency values that were better than the AE achieved by optimisation using a single flow rate and time for the Chisholm field (e.g.

for Opt 2 AE = 21% (Appendix Table I.3)). The benefits of the recipe management technique were less obvious for the Downs and Turner fields. For these fields, the recipe strategies did not offer any significant advantage over the measured irrigation practice (Table 6-2).

Table 7-5 Irrigation performance with various different recipe management strategies for the (a) Downs, (b) Chisholm and (c)Turner fields

(a)

	Downs								
Recipe	**Meas.**	**1**	**2**	**3**	**4**	**5**	**6**	**7**	**8**
RE (%)	93.91	86.68	90.62	91.05	93.66	70.66	75.31	79.42	85.15
AE (%)	73.81	82.98	77.27	77.78	73.64	89.11	82.88	78.21	70.57
DU (%)	64.75	57.61	60.37	61.44	63.92	62.87	63.62	66.44	68.49
DURZ (%)	81.07	68.19	74.33	75.20	80.57	65.35	67.00	70.37	74.16
D_{DD} (mm)	23.7	15.9	20.9	20.4	24.4	2.8	4.0	4.7	7.0

(b)

	Chisholm								
Recipe	**Meas.**	**1**	**2**	**3**	**4**	**5**	**6**	**7**	**8**
RE (%)	98.82	89.95	91.27	91.80	92.85	83.80	84.47	87.92	89.50
AE (%)	21.37	52.06	46.08	40.89	34.65	56.50	48.64	37.46	29.31
DU (%)	42.60	35.78	35.95	35.42	34.66	27.85	26.24	31.28	31.83
DURZ (%)	96.41	66.65	71.30	73.20	76.91	46.02	46.49	58.80	64.80
D_{DD} (mm)	85.50	46.6	54.1	59.7	69.5	32.8	39.1	47.0	57.3

(c)

	Turner								
Recipe	**Meas.**	**1**	**2**	**3**	**4**	**5**	**6**	**7**	**8**
RE (%)	94.62	91.90	94.14	94.77	96.53	91.49	93.73	94.35	96.10
AE (%)	68.62	76.73	69.97	70.10	65.22	76.23	69.40	69.35	64.34
DU (%)	73.89	70.80	72.95	73.93	75.62	70.35	72.08	73.07	74.66
DURZ (%)	86.85	81.83	85.63	86.67	90.04	81.35	84.69	85.77	89.04
D_{DD} (mm)	11.6	10.0	11.5	11.4	12.9	10.0	11.5	11.5	13.0

The use of these recipe strategies facilitates rapid identification of appropriate cut off times from field observations, effectively bypassing the need to estimate soil intake rates and model the irrigation using computer simulations. However, the ability to implement individual variations in TCO at the single furrow scale is often not practical. It is more likely that the farmer will manage the field in a series of furrow groups or sets. Hence, the TCO for the furrow set is usually determined by the completion time for the slowest advancing furrow within that set. Recipe techniques still require field evaluations to assess the current performance and to identify the most appropriate recipe strategy. It should also be noted that the recipe strategies proposed here may be sub-optimal. Higher levels of irrigation performance may be possible under different inflow rates and/or TCO recipes.

7.7 Optimising Irrigation Management in Heterogeneous Conditions using the Whole Field Approach

To demonstrate the power of the whole field simulation approach the Downs, Chisholm and Turner (field 17) fields were optimised according to the two objective functions, Opt 1 and Opt 2 (section 7.3.3). The process used was identical to that used to optimise the single furrows (section 7.5.3) but in this case was based on the simulation of all 20, 17 or 27 furrows of the three fields, respectively, as a single unit. The results (Table 7-6) indicate that it was possible to manage the irrigations of the Downs and Turner fields to satisfy the performance criteria (Opt 1 and Opt 2) using a single combination of inflow rate and time.

Table 7-6 Optimising irrigation inflow rates and TCO considering the whole field

Field	Treatment	TCO (min)	Q (L/s)	RE (%)	DURZ (%)	AE (%)	D_{DD} (mm)
Downs	Performance under measured conditions	--	--	93.91	81.07	73.81	23.7
	Opt 1.	687	3.80	97.17	91.26	69.04	--
	Opt 2.	529	4.75	95.24	--	70.02	10.9
Chisholm	Performance under measured conditions	--	--	98.82	96.41	21.37	83.7
	Opt 1.	788	4.02	96.81	90.12	15.06	--
	Opt 2.	665	3.36	95.06	--	21.01	89.4
Turner (F17)	Performance under measured conditions	--	--	94.62	86.85	68.62	11.6
	Opt 1.	620	5.73	97.39	92.09	73.03	--
	Opt 2.	449	7.81	95.31	--	72.22	7.9

For the Downs field, the inflow management identified by Opt 1 resulted in a slight improvement in the AE, a 3% increase in the RE and an improvement in the DURZ from 81.1% to 91.3%. However, implementation of this recommendation would increase the total application volume by 0.135 ML ha^{-1} (0.023 ML ha^{-1} with 85% recycling) per irrigation due to increased runoff. Similarly, optimising the Downs field according to Opt 2 was found to reduce the average depth of deep drainage from 24 mm to 11 mm. Optimisation of the Downs field using a single value of Q and TCO provided modest improvements in the irrigation performance but also required small

increases in the gross water use. The consequence of increasing inflow diminishes in significance where tailwater recycling is practiced.

For the Chisholm field, Opt 1 satisfied the 90% requirements for RE and DURZ but the long opportunity times required to reach these values restricted the AE to a maximum value of 15.1%. Optimisation of this field according to Opt 2 provided similar results. Hence, the Chisholm field data demonstrates that in situations of substantial infiltration variability it is difficult and even inappropriate to improve irrigation performance using a single combination of inflow rate and time. Instead, it may be more appropriate to split the recommendation into two or more management zones. In this case, the greatest proportion of the infiltration variability is attributed to temporal changes rather than spatial variation. The nature of the infiltration curves and individual furrow optima suggest that the first irrigation requires low inflow rates and long opportunity times while the remaining furrows benefit from increased discharges and reduced inflow times. It is worth noting that the large level of infiltration variability measured for the Chisholm field surpasses the magnitude of variation typically expected within a single irrigation event.

Simulation of a single furrow using the optimal management practices identified for that furrow (Table 7-1 and Appendix Table I.1 to I.6) often predicted levels of irrigation performance that were significantly higher than the performance obtained when optimising the whole field under a single combination of Q and TCO (Table 7-6). For example, optimisation of the Turner field using Opt 2 in 17 out of 27 furrows indicated that the average deep drainage could be reduced to less than 1 mm (Table I.6). However, the minimum predicted achievable deep drainage using a single inflow rate and TCO for the whole field was 7.9 mm.

In this study no restrictions were imposed on the range of possible values of inflow rate or TCO. As a result, many of the optimisations based on single furrow data suggested inflow rates that transcended practical limits. In some cases, the optimal inflow rates were found to exceed 20 L s^{-1} (e.g. Chisholm irrigation 3 furrow 2). Discharges of this magnitude would be difficult to achieve under siphon application.

More importantly such flow rates would result in destruction of the upstream end of the field, severe erosion of the furrow profile and furrow overtopping or breakthrough into unwatered furrows. Using single infiltration functions, simulation models may suggest that high performance can be achieved at high inflow rates. However, without appropriate constraints such information may lead to impractical and inappropriate recommendations that discourage farmers from using field evaluation and optimisation procedures in the future. In all cases the optimisation process using the multiple furrow simulation resulted in realistic and practical recommendations for the inflow rate whilst fulfilling the desired performance criteria in the majority of cases.

7.8 Relationships between Individual Furrow Optima and the Whole Field Optimum

The optimal combination of inflow rate (Q) and time to cut off (TCO) obtained using the whole field data was generally found to be located centrally within the range of the individual furrow optima However, the values did not correlate particularly well with the average inflow rate or average time. The optimised inflow rates and times from the Downs field under Opt 1 (Table 7-1) were plotted to better observe the nature of this variation (Figure 7-10).

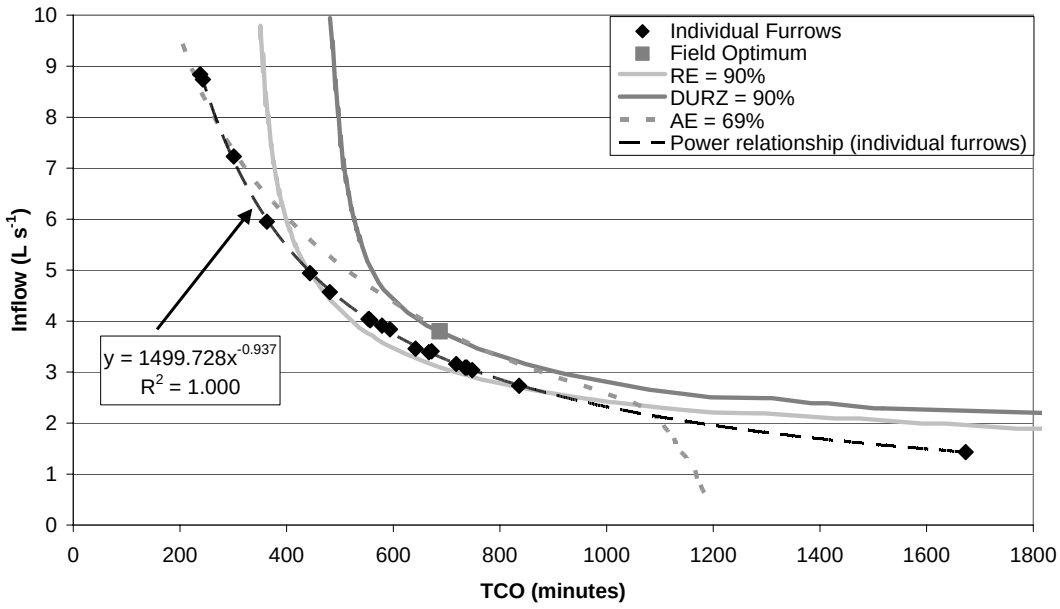

Figure 7-10 Relationship between the optimised Q and TCO amongst individual furrows and the field optimum for the Downs field using Opt 1

There appeared to be some form of relationship between the individual furrow optima for Downs Opt 1 (Figure 7-10). Fitting various trend lines to the results determined that the distribution of points was best described by a power curve (R^2 = 0.9997). The point corresponding to the whole field optimum is situated close to, but does not lie on, the fitted regression curve. The three curves corresponding to the three components of the objective function for the whole field simulation were also plotted. The curves corresponding to DURZ = 90% and AE = 69% (for the whole field) intersect at the field optimum point. It appears that the power curve is related to a combination of the these three curves for AE, RE and DURZ. The results for the Downs field using Opt 2 were found to behave in a similar manner (not presented).

The same procedure was employed to study the distribution of optimised inflow rates and times for the Chisholm field (Figure 7-11) for Opt 1 (Table I.2) and Opt 2 (Table I.3). The individual furrow optimum points were found to follow similar power relationships as for the Downs field. The field based optimal combination of Q and TCO was located close to the middle of the individual furrow optima but this time positioned further from the fitted regression line. Similarly to the Downs field, these points were found to be offset on the positive side of the regression line in respect to both axes (i.e. higher than expected Q and TCO).

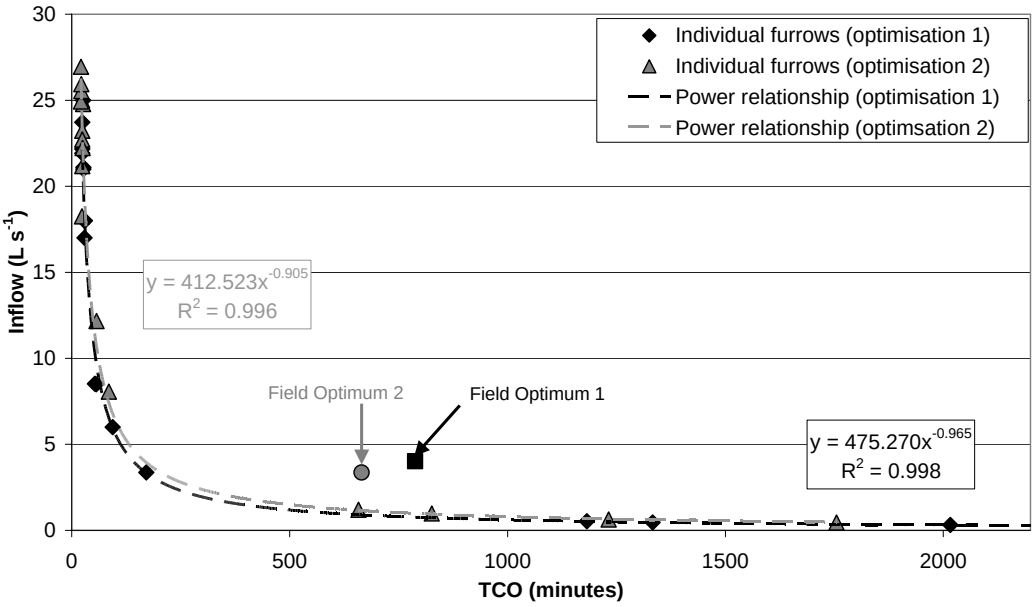

Figure 7-11 Relationship between the optimised Q and TCO amongst individual furrows and the field optimum for the Chisholm field using Opt 1 and Opt 2

From the trends identified in Figures 7-10 and 7-11, it is proposed that a relationship exists between the global (i.e. whole field or season) optimum inflow rate and cut off time and the individual optimised inflow rates and times. The power curve relationships in Figures 7-10 and 7-11 were simplified to linear form by taking the natural logarithms of both optimised inflow rates and times (Figure 7-12). The resulting values were found to follow a strong negative linear trend across the six optimisation case studies, inferred by R^2 values of 0.99 or greater. The relative position of these regression lines varied between the three fields and two optimisation objectives. However, the gradient of the trend lines remained relatively constant throughout (between -0.858 and -0.963).

The optimal points corresponding to the average infiltration curves were found to lie on the regression line of the individual furrow optima (Figure 7-12). In addition, these points appeared to be positioned close to the middle of the individual furrow optima. However, optimised Q and TCO based on the average infiltration curve did not coincide with the whole field optimal point for any of the fields (very close in the case of Downs Opt 1). Across all the fields and optimisation objective functions tested the field optimum is positioned at lower inflow rate and higher inflow time compared to the optimum derived from the average infiltration curve. The results indicate that it is not appropriate to use a simple averaged infiltration curve to derive the optimal irrigation strategy.

For Downs and Turner, the field optimum points lie close to the fitted trend line (Figure 7-12 a, b, e and f) but for the Chisholm data are offset from this line by some distance. This may be partly due to the relaxation of the 70% AE criteria for the identification of the field optimum. The departure of the global optimum point from the regression line may also be caused by the behaviour of the uniformity term as the distance tended to be greater for Opt 1. The results in section 7.5.2 (Figures 7-9.b and 7-9.f) indicated that the whole field optimum required a greater TCO than any individual furrow and greater Q than the majority of the furrows to reach the same level of DU or DURZ.

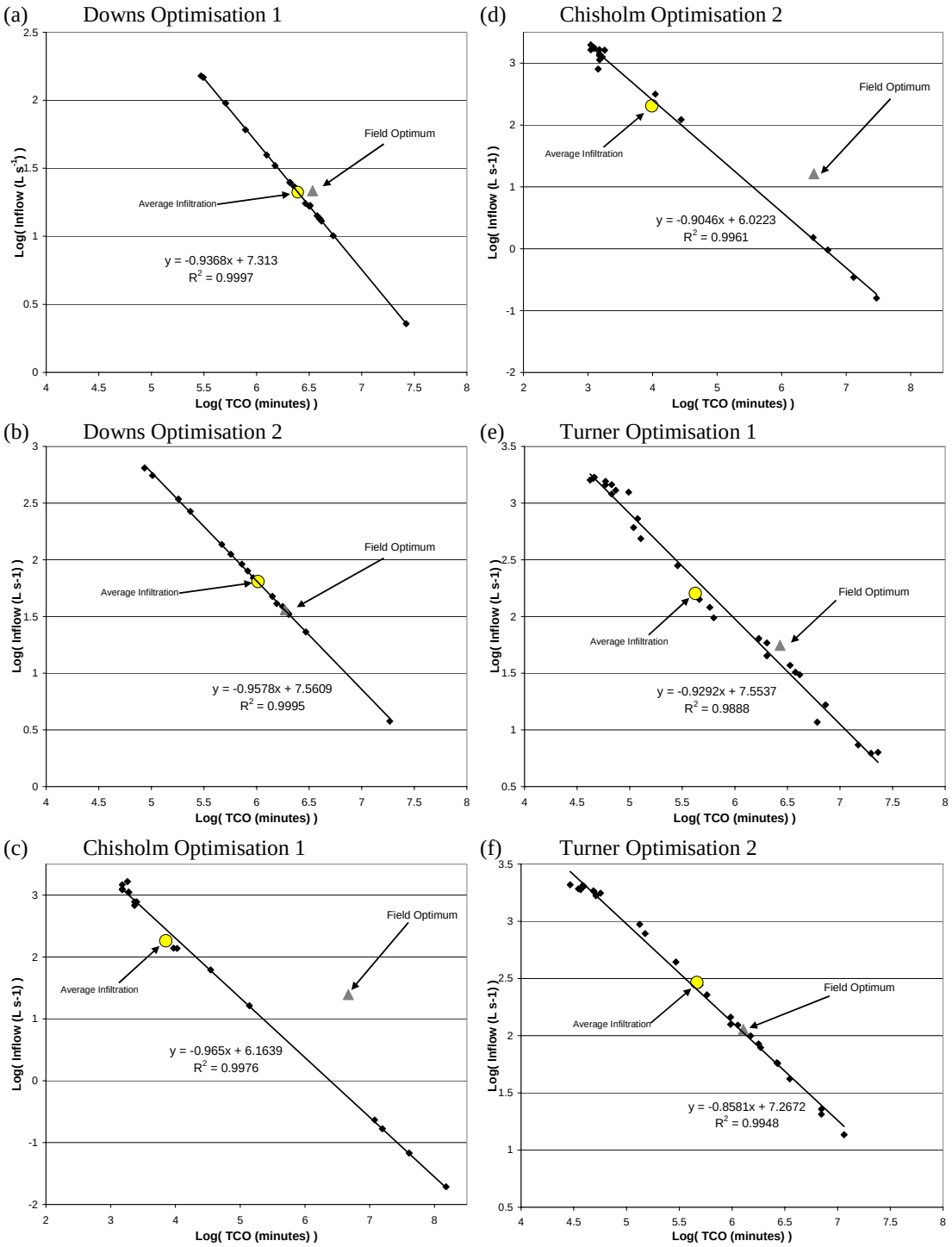

Figure 7-12 Log-Log relationships between optimised Q and TCO for each single furrow and whole field optimisation

Attempts to relate the whole field optimum to various numerical combinations of the individual furrows failed to find any correlations. Further analysis was conducted using the average, median and middle (i.e. (maximum + minimum)/2) of the values and log transformed values of the individual furrow optima. It was found that the

optimal field TCO was best correlated with the average TCO while the optimal field Q was best correlated with the middle of the log-transformed individual optimal Q values. Despite the absence of any simple relationship, the strong linear behaviour common to all single furrow optimisations and consistent dispersion of the individual points suggests that the single furrow and field optima can be predicted using reduced numbers of field measurements. Perhaps these relationships can be identified through the collection and analysis of additional field data.

7.9 Conclusion

Simulation of the Downs field over a range of inflow rates (Q) and cut off times (TCO) has identified associations between the various parameters that make up the irrigation performance. Several clear relationships could be identified, such as the universal trade-off between high application efficiencies and requirement efficiencies. Analysis of a wide range of performance terms has shown that no parameter is independent of the other terms. The results indicate that the performance terms are inter-related at a range of different levels. Hence, it is clear that no aspect of irrigation performance should be considered in isolation. The irrigation performance terms behave similarly between the individual furrow and the whole field. However, it was found that the uniformity terms are generally lower at the whole field scale compared to single furrows. On the basis of these findings it was concluded that the same approach to optimise furrow performance can be directly applied to optimisation of field management.

This chapter demonstrates the potential of IrriProb (developed in chapter 6) to evaluate and optimise surface irrigation at both the furrow and field levels. The Boolean objective function was chosen over alternative optimisation techniques due to its power to optimise field management using a wide range of performance parameters while not ignoring the significance of any of the individual performance components.

Optimisation of three irrigated fields using the IrriProb approach has shown that the use of the single furrow to evaluate field performance (chapter 6) and optimise

irrigation management across the whole field and over the season is unacceptable. The irrigation management can be easily tailored to optimise the performance of one furrow but the optimal value of Q and TCO is unlikely to result in favourable performance over the entire field. The optimal Q and TCO identified using a single furrow approach are based on overestimations of the irrigation performance as the true whole field application efficiency, requirement efficiency and uniformity are consistently lower than predicted at the single furrow scale. Furthermore, the single furrow optimisation often indicates a level of irrigation performance that is significantly higher than the maximum potential performance when managing the field with a single combination of inflow rate and time.

The consequences of using a single furrow to optimise irrigation management are far greater under conditions of increased variability in soil characteristics. For fields with moderate to low variability in infiltration rates it was found to be adequate to optimise the irrigation performance using a single value of Q and TCO. However, it is not possible to achieve the same high levels of irrigation performance using a single combination of Q and TCO to irrigate a field that contains high levels of spatial variability. Similarly, specifying a single set of inflow management parameters is not appropriate where there is significant temporal variation in infiltration rates between irrigation events or between seasons.

Many of these problems may be attributed to the inability of the estimated infiltration parameters to provide a representative measure of the soil infiltration across the field. However, it was found that the optimisations arising from the average infiltration parameters also failed to predict the optimal field inflow rates and times. Furthermore, the optimisation based on the average infiltration curve overestimated the field performance by a similar magnitude as for many of the individual furrows.

Although not considered in this analysis the unavoidable intra-furrow variation in infiltration rates is expected to pose similar limitations on the ability to derive singular optima inflow rates and cut off times. Random within furrow variability would result in greater variation of applied depths and hence lower values of uniformity and

application efficiency and higher values of deep percolation. A further consequence would be the increased inflow times required to reach the same level of requirement efficiency. The increased inflow time would result in increased runoff and deep drainage losses and hence lower application efficiency.

Often the Q and TCO values identified by the optimisation of single furrows lead to inappropriate values for the inflow rate. In some instances, the optimal inflow identified would have resulted in massive soil losses and difficulties with supply infrastructure. However, the optimised Q and TCO based on the whole field set of measurements tended to remain well within commonly acceptable limits.

Recipe irrigation strategies offer the potential to estimate optimal inflow times with reduced requirements for infield measurement and modelling. However, the recipe management strategies evaluated here were generally out-performed by the optimised irrigation management practices identified by IrriProb. With sufficient modelling, it may be possible to identify a recipe strategy that increases the irrigation performance to a level comparable with the numerical optimisation. However, it is important to note that any such recipe strategy would be unique to that field. Hence, application to other fields would require a separate modelling evaluation to refine the recipe characteristics

A strong relationship exists between the individual optimised Q and TCO for different furrows in the same field. In addition, it appears that the point corresponding to the whole field optimal combination of Q and TCO may be related to the midpoint of the line formed by single furrow optimisations. This suggests that it may be possible to develop a predictive capability whereby the whole field management could be determined using limited numbers of field measurements. Hence, it may be possible to estimate the optimal whole field inflow discharge and time to cut-off providing that the infiltration variability is known.

CHAPTER 8

Practical Demonstration: The Lagoona Field Trial

8.1 Introduction

Close to the completion of this work, a field trial was conducted in an attempt to quantify the whole field irrigation performance. The resulting experimental data (Lagoona) provides an opportunity to demonstrate application of the techniques developed throughout the preceding chapters. Detailed advance and runoff measurements from a small number of furrows enabled the use of the IPARM model (chapter 4) to estimate the infiltration curves. The procedure introduced in section 5.9 was used to predict the infiltration parameters based on completion times for a large number of additional furrows. The resulting soil data was used to demonstrate the use of the whole field simulation and optimisation tool developed in chapter 6.

8.2 Field Data

The Lagoona data was collected from a furrow irrigated cotton field, south of Theodore in the Dawson River valley in central Queensland (Figure 8-1). Unlike the field data presented in chapter 5, all measurements were collected during a single event, the second irrigation (first after planting) of the season. The measured furrows were located within a single siphon set hence inflow rates should be relatively spatially uniform. Field inflow was measured using a STARFLOW Doppler meter mounted within the inlet pipe, upstream of the supply head ditch, logging velocity and area of flow at 5 minute intervals. The resulting hydrograph did not exhibit any significant temporal changes therefore the inflow was assumed to be constant over time. This was further confirmed by an Irrimate™ siphon flow meter installed in one of the furrows. Advance and flume data were also recorded using Irrimate™ equipment. A number of siphon head measurements were also collected and the

discharge was estimated using the procedure explained by Bos (1979). The resulting flow rates were found to be in close agreement with the STARFLOW measurements.

Figure 8-1 Advance meter at 0 m (head-ditch) in Lagoona trial

Figure 8-2 depicts the layout of the trial field showing the relative positions of advance sensors and runoff flumes. Normal advance data was collected at four or five positions along the length of the furrow length for eight wetted furrows and limited measurements were collected for an additional 76 wetted furrows (Appendix Table J.1). The furrows with detailed advance measurements were situated close to, but not adjacent to the edge of the field (on both sides of the field). The time taken to reach the final advance distance of 761 m was measured for all 84 wetted furrows. In addition, the time taken to reach the midpoint (460 m) was measured for 20 furrows located approximately in the middle of the field (Figure 8-2). Flumes were positioned in wetted furrows numbers 5, 39 and 67 to measure runoff. Runoff discharges were recorded in 5 minute intervals for these furrows (Appendix Table J.2). Due to difficulties with furrow breakthrough, the flow of one of the adjacent "unwetted" furrows was directed across into the wetted furrow upstream of the flume.

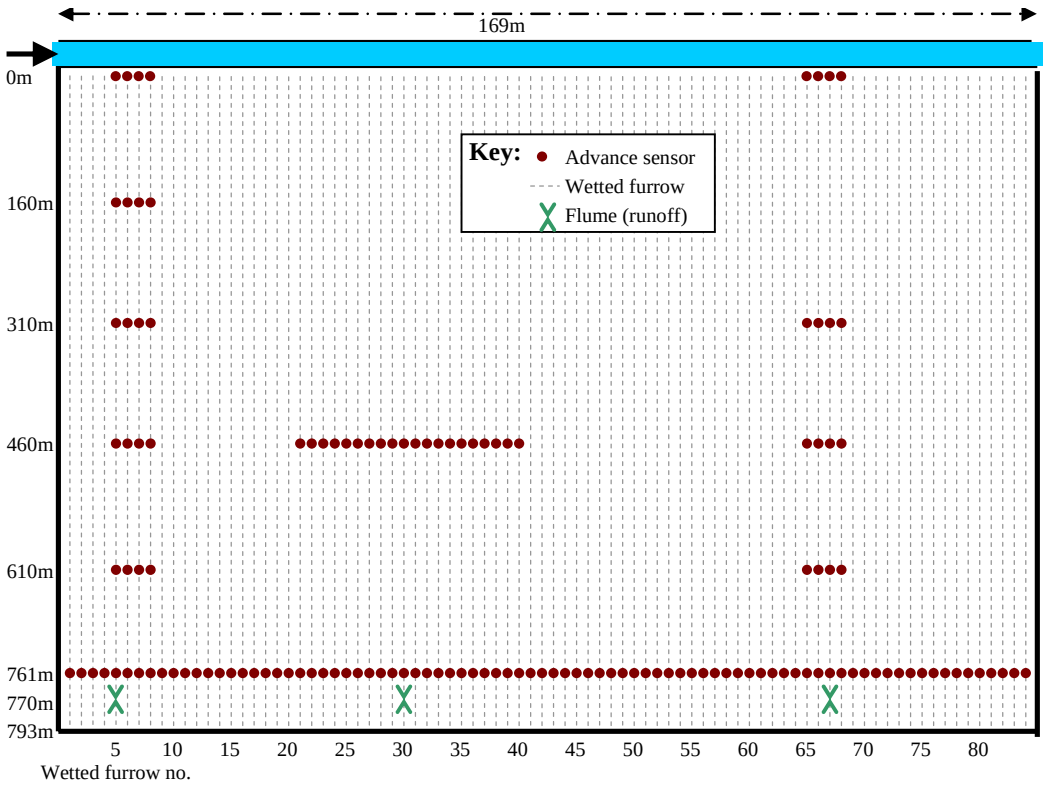

Figure 8-2 Lagoona field trial layout

Initial observation of the advance completion times (Figure 8-3) indicates that the furrows with detailed measurement experienced advance rates that were representative of the remainder of the field. The variation of advance times does not appear entirely random. The wetted furrows numbered 15 to 50 tend to have slower advance rates than the other furrows. This effect may be caused by decreased inflow rates as the result of changing siphon head. The large-scale spatial change in infiltration may be also caused by subtle differences in soil composition as the field has undergone some major levelling operations in the recent past. Part of the variation between adjacent furrows is due to the compaction during machinery operations. Field observations indicated that every second furrow was compacted starting with furrow 1 (i.e. furrows 1, 3, 5… are compacted). The wheeled furrows have decreased advance times at a significance level of 0.013 assuming independent sampling. Considering the difference between adjacent furrows (paired t test), the compacted furrows have decreased advance times at a 0.000 level of significance. Furthermore, the decrease in advance time between adjacent furrows due to compaction was found to be 36.5 and 47.3 minutes ($\alpha = 0.05$) moving forwards (furrow 1 vs. 2, 3 vs. 4,...) and backwards (furrow 2 vs. 3, 4 vs. 5,…) across the furrows, respectively.

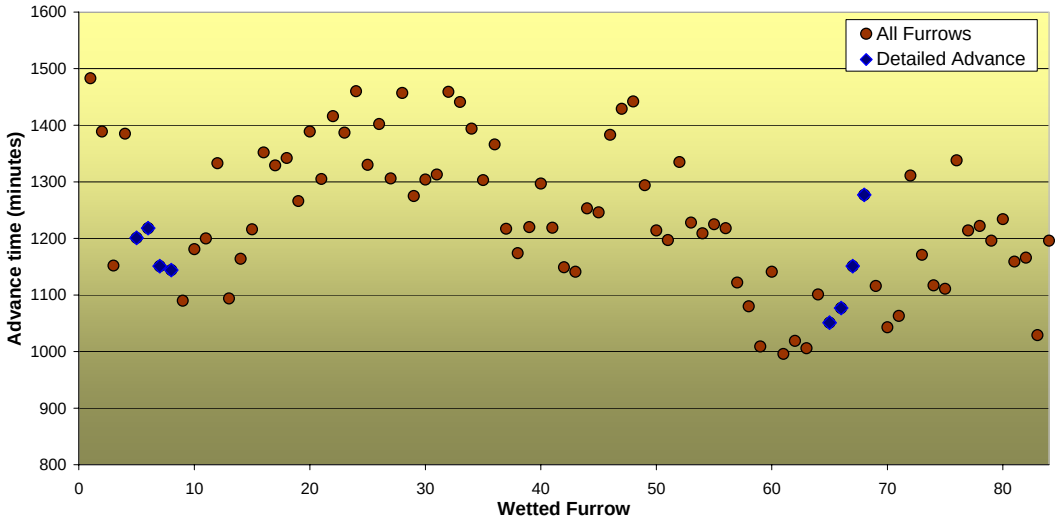

Figure 8-3 Time taken to reach final advance point (761 m) for the Lagoona field

8.3 Calibration of the Infiltration Curve

8.3.1 Estimation of Infiltration Curves using IPARM

Infiltration parameters (Appendix Table J.3) were estimated using IPARM from the advance data and constant inflow rate for all furrows with two or more measured advance points. For furrows 5, 30 and 67 the infiltration parameters were estimated using the advance and runoff data collected during the storage phase (i.e. times less than 1410 minutes). The resulting infiltration curves are shown in Figure 8-4. The surface storage was estimated using the average wetted furrow dimensions and the upstream flow depth of 50 mm. This resulted in a Manning's roughness value of $n = 0.0377$.

The infiltration curves produced from two advance points (furrows 21 to 40) have widely varying shapes (Figure 8-4). However, those estimated using increased numbers of data points have both reduced variability and relatively uniform shape. The use of runoff data to estimate the infiltration parameters appears to standardise the curves further. This demonstrates the apparent variability that can arise through inadequate field data. The infiltration curves from two advance points had increased variability at both short and long opportunity times (Figure 8-4). However, they tend to have reduced variance and match the curves estimated from the detailed

measurements at opportunity times between 800 and 1200 minutes. These two time values correspond approximately with the measured advance times at the middle and final advance points, respectively. Hence, the infiltration curves estimated from the two advance points should not be used to predict infiltrated depths at opportunity times widely departed from the measured advance times.

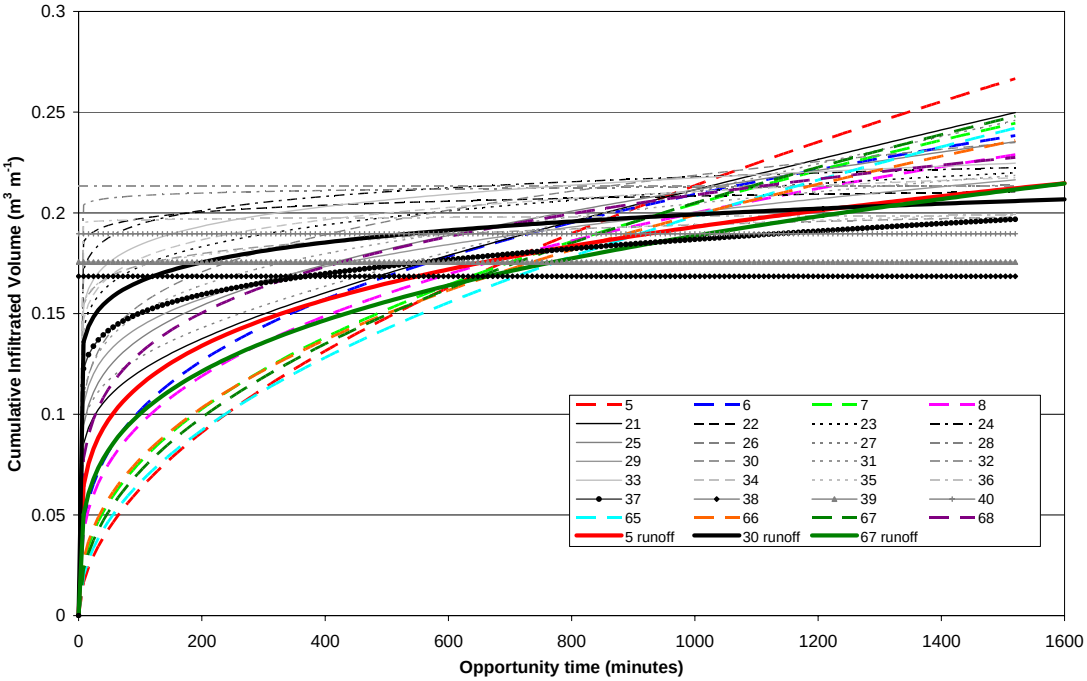

Figure 8-4 Infiltration curves for Lagoona estimated using IPARM

8.3.2 Minimum Distance for Field Measurement

The advance times are not randomly distributed but appear to follow a mild spatial trend. The correlogram (section 2.7.2.1) is a tool for predicting the minimum spacing of field measurements in order to achieve spatial independence. The correlogram is constructed by plotting the autocorrelation coefficient (*ACF*) as defined in Eq. 2-14 over an increasing number of lags *h* (Bautista and Wallender 1985).

The autocorrelation coefficient was computed for the final advance distances of the Lagoona Field and plotted over 20 lags (40 metres) (Figure 8-5). Two measurements are said to be spatially dependent over distances (lags) less than the critical value where the standard error of the *ACF* crosses the origin. The standard error of the

autocorrelation can be approximated by $1/\sqrt{N}$ where *N* is the number of lagged pairs used to calculate the *ACF* (Box and Pierce 1970). The resulting correlogram (Figure 8-5) shows that the final advance times are spatially correlated to a lag distance of approximately 9-11 wetted furrows or 18-22 m. This compares favourably with the value of 24 m given by Bautista and Wallender (1985) even though in that case they measured a series of short furrow sections along the length of a single furrow. These findings indicate that in order to gain the most benefit from each measured furrow the monitored furrows should be spaced greater than 20 m apart. However, Wallender (1987) demonstrated that autocorrelation increases with the scale of measurement. Hence this critical distance should decrease from 20 m when measuring shorter lengths of furrow on the same soil. The findings should be similar when considering the infiltration curves themselves since they are strongly influenced by this final advance point. In this case the apparent spatial trend is expected to reduce the value of field measurements collected at spacings less than 20 m.

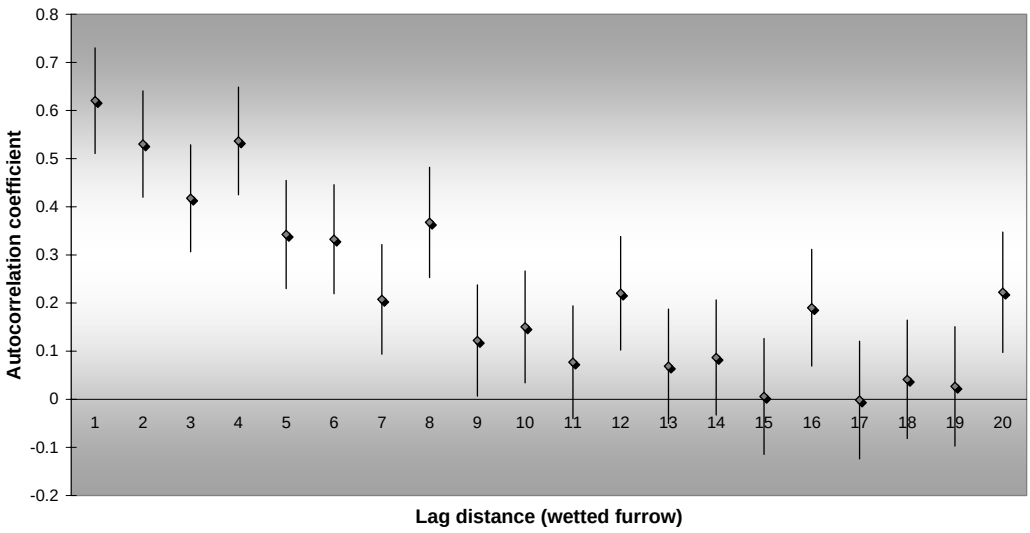

Figure 8-5 Correlogram of final advance times (761 m) for Lagoona

8.3.3 Predicting Infiltration Parameters using the Final Advance Time

The plot of final advance times (Figure 8-3) shows that the nine furrows with sufficient data for operation of IPARM do not cover the full range of variance seen in the field. Simulation and optimisation based on these furrows alone will not be able to predict the range of applied depths and runoff volumes that would occur in the field. Hence, it is necessary to identify the soil infiltration rates for additional furrows. The procedure described in section 5.9 was used to predict the infiltration parameters for all furrows. The process requires one advance measurement for each furrow, in this instance, the time for the water to traverse a distance of 761 m. The infiltration curves estimated using advance and runoff data (furrows 5, 30 and 67) were used as the known infiltration curves since they should be the most accurate. These selected furrows are reasonably spread throughout the variance in final advance times with probabilities calculated from $ZVal_{VB}$ (Eq. 5-19) of 40.9%, 72.1% and 25.7%.

The infiltration parameters were predicted for all furrows with less than three advance measurements, excluding furrow 30 (i.e. furrows 1 - 4, 9 - 29, 31 - 64 and 69 - 84). It is presumed that the remaining furrows contain sufficient advance measurements for the IPARM inverse technique. The resulting predicted and IPARM estimated infiltration parameters are given in Appendix Table J.4 and are plotted in Figure 8-6. The predicted infiltration curves take on a similar shape to that of the three base furrows (furrows 5, 30 and 67). The CV between the resulting curves declines slightly with increasing opportunity time, the CV in cumulative infiltration is 11.6%, 10.0% and 9.6% at 400, 800 and 1200 minutes respectively. This is significantly lower than the variability observed within the Downs, Chisholm and Turner fields in chapter 5 (Figure 5-7). The infiltration rates vary (CV) by 19.7%, 25.5% and 29.3% at 400, 800 and 1200 minutes, respectively.

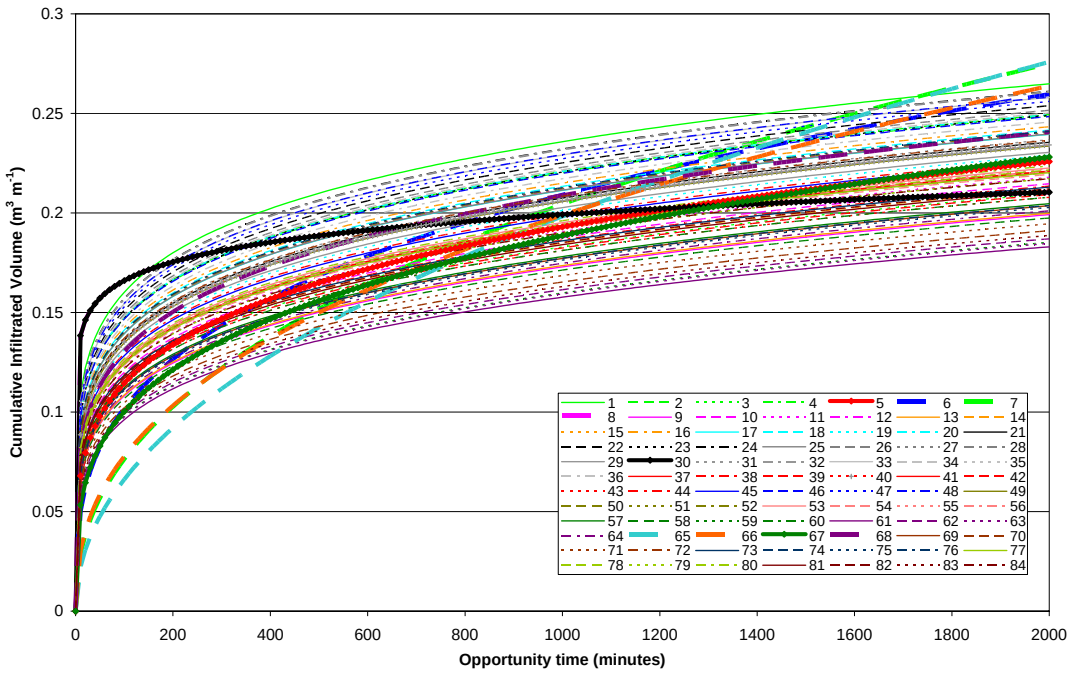

Figure 8-6 Predicted infiltration curves for Lagoona
(IPARM calibrated furrows are 5-8, 30 and 65-68; predicted infiltration in remainder)

8.4 Optimising Performance

The Lagoona irrigation was optimised using IrriProb according to similar objective functions as those used in chapter 7. The field was optimised according to two main criteria. The first optimisation objective (Opt 1) was to achieve both a requirement efficiency (RE) and distribution uniformity of the root zone (DURZ) of 90% while maximising the application efficiency (AE). The second objective (Opt 2) is to maintain a RE of at least 95% and AE of 70% while minimising the average depth of deep percolation (D_{DD}). For this field it should be possible to attain a higher level of irrigation adequacy compared to the case studies of chapter 7 as the infiltration curves exhibit lower variance (Figure 8-6). Hence, the two objective functions were repeated using a RE > 99% criteria (i.e. Opt 1.b and Opt 2.b).

8.4.1 Current Performance

A simulation was carried out by IrriProb using the infiltration parameters identified by IPARM for nine furrows and predicted infiltration parameters for the remaining furrows (Appendix Table J.4). The value of Manning *n* used in the simulations was

maintained at the same value used to estimate the infiltration parameters (0.03769). The resulting field simulation reproduced the final advance point (761 m) over the 84 furrows with a root mean square error (RMSE) of 35.2 and average deviation of +4.63 minutes. Hence, further attempts to calibrate a field wide value for *n* was not deemed necessary. Simulation deviation error changes to -11.76 minutes whilst *n* = 0.04 results in an RMSE of 35.9 and average deviation of +9.47. It was found that small changes to Manning *n* improved the fit to the final advance point but compromised the ability to predict other advance points (for those furrows with additional advance measurements).

The whole field simulation indicated that the Lagoona field had high irrigation adequacy with a RE of 98.87% whilst also having relatively high AE (78.21%) and application efficiency with recycling (AER = 85.74%) values. The irrigation also had high uniformity, with a low quarter distribution uniformity (DU) equal to 83.57% and DURZ = 96.57%. The average runoff per furrow was 14.752 m^3, and the average depths applied to the root zone and deep drainage were 82.06 mm and 13.80 mm, respectively. As the performance of the Lagoona field is considerably high (Table 8-1) only minimal performance gains can be expected through optimisation of irrigation management. The variance present in the infiltration curves brought about a corresponding variance in many of the performance indicators (Appendix Table J.5). The AE and RE only vary by 1.30% and 1.31% (CV), respectively but other terms experienced greater levels of variability between furrows (e.g. CV = 6.7% for DU and CV = 6.2% for AER). The majority of the variability manifests itself within the predicted runoff (CV = 72.1%) and deep drainage (CV = 50.3%) volumes.

It was noted that the simulations provided poor predictions of measured runoff volumes (i.e. 19.62 m^3, 15.34 m^3 and 21.51 m^3 compared to measured values of 50.66 m^3, 41.28 m^3 and 22.02 m^3, respectively). However, the runoff accounts for less than 9% of the total inflow volume. In addition, the measured outflow hydrographs far exceed the time of cut-off (Appendix Table J.2) suggesting that the flumes may have been submerged during the later stages of the irrigation due to restricted drainage within the tail drain.

8.4.2 Optimising the Time to Cut-off

Firstly, the optimisation process considered the potential to improve irrigation performance by altering the time to cut-off (TCO) alone. The inflow rate (Q) was constrained to the measured discharge of 1.95 L s^{-1} and all other field characteristics are as measured. The field was simulated for TCO values ranging from 200 to 2000 minutes and the optimisation tool within IrriProb was used to determine the optimal TCO. Opt 1.a shows that a minimal increase in the AE is possible by reducing the TCO to 1303 minutes with a slight penalty in the RE and DURZ (Table 8-1). In this case the reduced uniformity indicates that the water would not have reached the end of the field within a small number of furrows. Objective Opt 1.b suggests that the TCO should be increased slightly to 1420 minutes to ensure adequate water application over a greater proportion of the field.

Optimisation according to Opt 2 demonstrated that it is possible to reduce the average deep drainage (D_{DD}) by 2.9 mm and increase the AE to 85% by decreasing the TCO to 1247 minutes. However, to maintain the same RE as measured in the field the inflow time must be restored to the higher value of 1420 minutes (Opt 2.b). This time is almost identical to the measured TCO (1410 minutes). Hence, there is minimal potential for improvement of the irrigation performance over measured conditions by altering only the time to cut-off.

Table 8-1 Optimising Lagoona by time to cut-off

	Objective	TCO (min)	AE (%)	AER (%)	RE (%)	DU (%)	ADU (%)	CU (%)	DURZ (%)	Inflow (m^3)	Run. (m^3)	D (mm)	DRZ (mm)	D_{DD} (mm)
	Current Manage.	1410	78.21	85.74	98.87	83.57	0.00	89.65	96.57	166.4	14.75	95.9	82.1	13.8
Opt 1.a	RE>90, DURZ>90 Max AE	1303	82.80	87.37	96.80	78.59	0.00	87.48	90.08	153.9	8.28	92.2	80.3	11.8
Opt 1.b	RE>99, DURZ>90 Max AE	1420	77.78	85.57	99.00	83.89	0.00	89.79	96.98	167.6	15.36	96.2	82.2	14.0
Opt 2.a	RE>95, AE>70 Min D_{DD}	1247	85.03	88.54	95.00	74.13	0.00	85.57	84.26	147.1	6.09	89.6	78.8	10.8
Opt 2.b	RE>99, AE>70 Min D_{DD}	1420	77.78	85.57	99.00	83.89	0.00	89.79	96.98	167.6	15.36	96.2	82.2	14.0

The "Inflow" and Runoff ("Run.") are expressed in terms of average volumes per furrow.

8.4.3 Optimising Inflow

Assuming that it is possible to alter siphon sizes and/or head ditch conditions, further increases may be possible through altered inflow discharges. This time the field was simulated using inflow rates between 1 and 7 L s^{-1} and inflow times between 400 and 1600 minutes. The first optimisation, Opt 1.a provided an increase in the AE and demonstrated that the D_{DD} could be reduced by 50% through increased inflow rates (Table 8-2). Attempting to increase the irrigation adequacy (Opt 1.b) causes the AE to drop as the runoff volume increases from measured conditions. However, the behaviour of the AER indicates that this decline in efficiency can be overcome if the tail-water is recovered.

In all the optimisations of the Lagoona field thus far, the absolute distribution uniformity (ADU) has been equal to zero. An ADU = 0% indicates some part of the field, no matter how small has received zero application. Optimising the field based on objective 2 (both Opt 2.a and Opt 2.b) improved the ADU to values greater than 75%. Hence, no part of the field has received less than 75% of the average applied depth. This example illustrates the problems involved with using the RE as the solitary indicator of irrigation adequacy as the RE of Opt 2.a was less than the measured irrigation. It is possible to improve the uniformity and AER by increasing the inflow discharge. However, the ability to increase inflow rates is limited where the farmer is attempting to achieve perfect RE with minimal water wastage.

Table 8-2 Optimising Lagoona by time inflow rate and time to cut-off

	Objective	Q (L s^{-1})	TCO (min)	AE (%)	AER (%)	RE (%)	DU (%)	ADU (%)	CU (%)	DURZ (%)	Inflow (m^3)	Run. (m^3)	D (mm)	D_{RZ} (mm)	D_{DD} (mm)
	Current Manage.	1.953	1410	78.21	85.74	98.87	83.57	0.00	89.65	96.57	166.4	14.75	95.9	82.1	13.8
Opt 1.a	RE>90, DURZ>90 Max AE	3.170	790	83.67	91.90	96.71	84.24	0.00	89.95	91.01	152.2	14.74	86.7	80.3	6.5
Opt 1.b	RE>99, DURZ>90 Max AE	2.150	1311	76.65	86.21	99.30	85.27	0.00	90.43	97.88	170.5	19.20	95.6	82.4	13.2
Opt 2.a	RE>95, AE>70 Min D_{DD}	5.820	480	73.11	93.16	95.15	86.41	75.79	91.05	90.12	171.3	40.41	82.4	79.0	3.4
Opt 2.b	RE>99, AE>70 Min D_{DD}	3.280	933	70.36	88.31	99.04	87.03	75.33	91.60	97.09	185.3	39.13	92.1	82.2	9.9

The "Inflow" and Runoff ("Run.") are expressed in terms of average volumes per furrow.

The results suggest two possible scenarios to improve irrigation performance. Firstly, the inflow discharge can be increased slightly to 3.17 L s^{-1} for 790 minutes to reduce the deep percolation loss. The second scenario, where the farmer can re-capture the tail water, the inflow rate can be further increased to shorten the advance phase. This will ensure adequate application at the downstream end of the field and improve the overall uniformity of applied depths. The increase in inflow volume associated with Opt 2.a and Opt 2.b can is misleading. After subtracting the water recovered from the runoff (recycling efficiency of 85%), the net depth of water applied to field was found to be 86.4 mm and 95.9 mm for Opt 2.a and Opt 2.b, respectively compared to the measured irrigation at 97.0 mm.

8.5 Sensitivity of Optimisation Process to Uncertainties in Field Measurements

Both throughout this chapter and the body of the dissertation it has been assumed that field data was collected following the best possible procedures. All field measurements, regardless of the apparatus used are subject to some element of uncertainty. These errors or uncertainties will influence all stages of the measurement analysis and optimisation process, however the sensitivity analysis required to describe the influence of measurement errors is beyond the scope of this research.

One example which is particularly relevant to this case study is the inflow rate. In the Lagoona analysis it was assumed that all furrows received the same inflow rate. Apart from the systematic variation that may result from trends in head channel height or field cross-slope, the siphon tubes will impose some level of random variability in discharge rates between furrows. In addition, the estimated total discharge provided by the STARFLOW meter may include a margin of error. An error in the inflow rate will influence all stages of the analysis process. A unit change in inflow will have a similar and almost proportional effect on the soil infiltration characteristic. For the simulation model, the altered infiltration rates combined with the direct impact of changes in inflow on introduces uncertainty into the predicted performance and optimised values of inflow rate and cut off time.

Some of the optimised inflow rates and times presented in Tables 8.1 and 8.2 represent changes from the measured values by less than 10%. These changes may be less than the uncertainty in the optimised management resulting from errors in field measurements. The accuracy of field measurements and limited capacity to implement optimised inflow rates and times restricts the maximum achievable performance to some level below the theoretical optimum.

8.6 Conclusions

The Lagoona field trial has provided valuable information describing the spatial variation in infiltration that occurs within a single irrigation event. Autoregressive analysis has shown that the advance times and therefore infiltration rates are partly spatially dependent. Statistical analysis of the variability in final advance times indicated that furrows subject to machinery traffic had advance times that were increased by approximately 42 minutes (3.4% faster) than uncompacted furrows. The effect of soil compaction only explained a small part of the total infiltration variance observed. Statistical analysis of the spatial variability indicated that maximum benefit is obtained from the measured data where the sampled furrows are located at least 20 m apart. However, such sampling is not implemented in current measurement procedures and not practical with the existing suite of measurement tools.

The Lagoona field trial demonstrated the ability of the IPARM procedure to estimate accurate infiltration curves from field measurements. By combining this information with simple single advance point measurements it was possible to predict the infiltration curves across the entire field. Irrigation simulation indicated that the field was managed under a near optimum combination of inflow rate and time. Hence, there was minimum potential for improving irrigation performance by changing only inflow rates and times. Optimisation using IrriProb has suggested that the uniformity can be improved via the adoption of increased inflow rates. This chapter has demonstrated the successful operation of the procedures for field measurement, infiltration estimation, performance evaluation and management optimisation developed within this research.

CHAPTER 9

Conclusions and Recommendations

9.1 Conclusions from this Research

Infiltration variability is a significant concern during the measurement and management of surface irrigation. The infiltration characteristic of the soil governs both the depth applied at any given point and the distribution of water throughout the field. This study has addressed the issue of infiltration variability through work in three main areas:

1) Improving the techniques to estimate infiltration parameters thereby reducing the apparent variability arising from the constant inflow assumption and the restriction to data collected during the advance phase.
2) Evaluating the statistical nature of field scale infiltration variability and using this statistical information to predict the field scale infiltration variability from a surrogate measure.
3) Development of a simulation model to evaluate performance and optimise irrigation management at the field scale in heterogeneous conditions.

9.1.1 Estimation of Infiltration Parameters from Field Measurements

Previous studies (chapter 2) have identified significant spatial and temporal variability in infiltration rates. However, a proportion of this apparent variation has been caused by inadequacies within field measurement and modelling techniques. In chapter 4, a procedure was developed to extend the inverse solution for the parameters of the Modified Kostiakov infiltration function to accommodate runoff measurements and variable inflow rates. The resulting model forms the foundation of IPARM, a robust tool to estimate the soil infiltration characteristic from field measurements. Apart

from the numerical model, IPARM also includes an intuitive user interface to facilitate data capture and interpretation of the volume balance model fit to the advance and runoff measurements.

Calibration of the infiltration function from advance data only provides infiltration parameters that adequately describe the soil behaviour over opportunity times less than the length of the advance phase. However, the same curve must be extrapolated beyond the known values to predict infiltration at greater times. IPARM optimises the infiltration parameter values by minimising the difference between measured and predicted runoff volumes. The estimation of infiltration parameters from runoff data in conjunction with the advance measurements was found (section 4.4.2) to extend the infiltration curve to greater opportunity times with greater accuracy. However, estimation from runoff did not significantly alter the form of the infiltration curve for opportunity times less than the length of the advance phase.

Simple modifications to the volume balance model enabled the use of the full inflow hydrograph rather than relying on the constant inflow assumption. Tests (section 4.4.2) using IPARM indicated that the assumption of constant inflow introduced a systematic error into the infiltration curve whenever the measured inflow changes with time. The magnitude and sign of this error was determined by the shape of the inflow hydrograph. The analysis was extended to estimate the infiltration parameters from several furrows within a single field with varying inflow patterns. It was found (section 4.6) that accounting for the temporal inflow variation during the irrigation event reduced the variability in predicted infiltrated depths at any given opportunity time and also tended to standardise the shape of the infiltration curves. Hence, a significant proportion of the apparent infiltration variability measured in the field is caused by the constant inflow assumption associated with the inverse solution for the infiltration parameters.

Trials (section 4.4.2) suggested that the simplified approach adopted by IPARM overestimated the change in surface storage that occurs due to rapid changes in the inflow discharge. The surface storage smoothing (SSS) technique was developed in an

attempt to dampen the step change in the surface storage. Evaluation of the SSS procedure (section 4.4.3) demonstrated small improvements to the accuracy of the volume balance model but the resultant effect on the estimated infiltration parameters was minimal.

SIRMOD simulations using the estimated infiltration parameters indicated that IPARM produces reliable estimates of the infiltration curve (section 4.5). Generally, all sets of infiltration parameters provided accurate predictions of the advance trajectory. However, SIRMOD simulations using parameters estimated from runoff data resulted in greatly improved estimates of the total runoff and infiltration volumes. Use of the full inflow hydrograph was found (section 4.5.2) to improve the fit of SIRMOD to the measured runoff rates. Sensitivity analysis (section 4.7) confirmed that the IPARM procedure was not influenced by the number of measured data points as long as those points chosen are sufficient in number to capture the shape of the advance trajectory or runoff hydrograph. The predicted infiltration curves were found (section 4.7.4) to be relatively insensitive to the value of the weighting coefficient between advance and runoff errors. Hence, the model was found to be far more sensitive to the runoff measurements than compared to the advance data.

9.1.2 Statistical Nature of Infiltration Variability

The severity and behaviour of infiltration variability at the field scale was investigated using data collected from three representative cotton fields in the Darling Downs region (chapter 5). Infiltration curves estimated by IPARM indicated that soil infiltration rates vary significantly at both the spatial (between furrows) and temporal (during the season) scales. Statistical analysis of the sampling distribution showed (section 5.7) that the number of curves required to characterise the population is determined by the expected variance of infiltration rates. The accuracy in the predicted field mean and variance increases with additional measured furrows. However, the incremental gain in accuracy diminishes with increasing sampling size. Measurement of approximately ten furrows was found to provide the greatest value in terms of reducing the error of estimated means and standard deviations.

Both the normal and log-normal distribution functions were found to be possible descriptors of the infiltration variability between furrows. However, the log-normal model appeared to provide the better fit to the frequency distribution (section 5.8). Hence, the variance between infiltration curves was described by applying the normal distribution to a logarithmic transform of the infiltration curves. As the infiltration depth is a function of time, the variance terms were adapted to describe the variability over a range of opportunity times rather than a single value. A strong correlation was identified between the parameters of this distribution and the log-transformed infiltration term from the volume balance. Hence, a procedure was devised (section 5.9) to predict the Modified Kostiakov infiltration parameters from a single measured advance point from each furrow and any number of known infiltration curves from the same field. The resulting predictive technique offers potential to increase field infiltration information without substantially increased field measurement requirements.

9.1.3 Whole Field Simulation and Optimisation Model

The IrriProb simulation model (chapter 6) was developed to extend the simulation of furrow irrigation to the field scale. This model predicts the water application to individual furrows but then calculates the irrigation performance based on a group of any number of these furrows. It was found (section 6.4) that furrow based estimates of irrigation performance do not necessarily equate to field based values. The same is true for simple averaging of the performance parameters across individual furrows. Generally, the averaging process grossly overestimates the uniformity terms since under full irrigation the variation in applied depths is usually greater between furrows than longitudinally down a single furrow. IrriProb provides improved estimates of the whole field application while simultaneously capturing the full impact of the distribution of opportunity times within furrows and infiltration variability between furrows. IrriProb calculates two-dimensional based estimates of the irrigation performance. Hence, it facilitates valid comparison of surface irrigation with the spatially based performance estimates of pressurised systems (e.g. sprinkler and subsurface drip).

IrriProb also features a tool to optimise the management of surface irrigation by maximising the irrigation performance of a single furrow or group of furrows (chapter 7). The optimisation tool simulates the field application over predetermined ranges of inflow rates and times and enables the user to provide appropriate optimisation criteria. Rather than a strict numerical function, the objective function for optimisation takes the form of a Boolean expression combining any number of performance criteria. The tool is graphically based to demonstrate the interactions between the various performance terms and to simplify modification (if required) of the optimisation criteria. Alternative optimisation procedures such as the weighted combination of various performance terms may be able to identify the optimal performance. However, such schemes do not provide any information regarding the values of the individual performance components. The adopted optimisation approach facilitates identification of the optimal field management while the criteria themselves provide a check for the values of each performance indicator.

Although IrriProb is capable of modelling the inter-furrow variation of infiltration it does not currently have the capacity for multiple infiltration characteristics along the length of a single furrow. Therefore it is highly likely the whole field model is still overestimating the distribution uniformity. In the same way the optimisation routines do not consider the full impact of infiltration variation on the optimal values of inflow rate and time to cut-off.

Simulation of the field application under ranges of inflow rates and inflow times uncovered significant interactions between the common performance terms (section 7.4). There appears to be a consistent trade-off between the application efficiency (AE) and requirement efficiency (RE) as maximising one parameter will ultimately lead to lower values in the other parameter. Extending this analysis indicated the existence of similar trends amongst the other performance parameters. It is clear that no performance term acts independently of the others, hence none should be considered in isolation during the process of optimisation.

The performance terms, and hence the optimisation processes, behave similarly whether considering a single furrow or a large group of furrows. Hence, it is valid to scale up the process of furrow optimisation to maximise the field performance. The results (section 7.7) have shown that it is possible to optimise and manage the irrigation of a group of furrows using single combinations of inflow rate and time to cut off (TCO). However, under increased levels of infiltration variability it is instead more appropriate to split the recommendations into two or more branches with separate management regimes. Optimisations based on the measurements from a single furrow failed to identify the optimal management strategy resulting in sub-optimal combinations of inflow rate and TCO (section 7.5). When the inflow rate and time recommended from any single furrow is applied to the whole field the AE, RE and uniformity (DU & DURZ) are consistently lower than that indicated by the single furrow simulation. Often the single furrow optimisation suggested a level of irrigation performance that is unachievable under any single combination of inflow rate and TCO. In the majority of cases, optimising based on the single furrow resulted in a decrease in performance compared to the measured irrigation conditions. Under increased levels of infiltration variability the consequences are far greater. In addition, many of the inflow rates suggested by the single furrow optimisations tended to be outside the normal practical range of inflow rates whereas the combination of inflow rate and TCO arising from the whole field optimisation remained within practical limits (section 7.7). Similar problems were encountered when attempting to use the average infiltration parameters.

A strong power relationship was identified (section 7.8) between the optimised inflow rates and TCO values for individual furrows for any particular field under a constant optimisation objective function. Furthermore, the field based optimal point tended to lie towards the middle of these points but consistently offset from the midpoint of the regression line at some higher value of inflow rate and TCO.

Data collected from the Lagoona field site (chapter 8) served as a demonstration of the techniques developed within this thesis. IPARM was used to accurately estimate the infiltration parameters for a small number of furrows. The predictive technique

was successfully employed to estimate the infiltration curves for 84 furrows within the same field during a single irrigation. Observation of trends within the final advance points indicated that the variation was not entirely random. One such trend was explained by the compacted furrows, found to be approximately 42 minutes faster than the uncompacted furrows. Autoregressive analysis of the advance data indicated that the sample furrows should be a minimum of 20 m apart to gain the maximum benefit from the measured data. Optimisation of the Lagoona field did not offer substantial improvements to the irrigation performance since the existing management is already close to optimal. However, the optimisation suggested that some further performance gains would be possible with increased inflow discharges.

9.2 Key Research Outcomes

The most significant findings of this research can be summarised as:

- Modification of the inverse volume balance approach to accommodate runoff data and the full inflow hydrograph has reduced the uncertainty in estimated infiltration characteristics and extended the "known" infiltration curve to greater opportunity times.
- In heterogeneous conditions, optimising irrigation management on the basis of simulation of any single furrow or the field average infiltration leads to sub-optimal management recommendations and overestimations of potential irrigation performance.
- The IrriProb simulation model makes it possible to evaluate existing irrigation performance and optimise whole field irrigation management while accounting for the effects of spatial and temporal variability.

9.3 Recommendations for Further Research

The issue of infiltration variability as it concerns furrow irrigation is far wider than the scope of work contained in this dissertation. Several areas were identified for investigation as part of this study whilst a range of other areas require further research.

9.3.1 Inverse Techniques to Estimate Infiltration

The volume balance model used in IPARM, like earlier approaches (e.g. Two Point method), remains dependent on the power curve advance assumption. The subsurface shape terms for infiltration (i.e. σ_{Z1}, Eq. 4-26 and σ_{Z2}, Eq. 4-27) are functions of the power curve exponent r during both the advance and storage phases. Hence, infiltration parameters cannot be estimated on the basis of runoff data alone as the solution for r requires a minimum of two measured advance points. Temporal changes in the inflow rate may cause the advance trajectory to depart significantly from the power curve shape. IPARM can cope with either increasing or decreasing advance velocity providing that the curvature of the advance trajectory is constant. However, a sudden change in discharge may significantly alter the form of the advance curve midway down the field. Further research is required to investigate options to remove the r term from the volume balance equations through an alternative formulation of the subsurface storage terms.

Regardless of the inflow regime, the surface storage is assumed to follow a constant shape where the volume of water within the furrow is defined as a multiple of the upstream flow area. The surface storage smoothing approach (section 4.3.4.2) provided some improvement to model accuracy under conditions with rapid changes in inflow rate. The surface storage component is also limited exclusively to constant positively sloping (i.e. in the flow direction) furrows. However, it may be possible to adapt the volume balance model to zero-slope or reverse grade fields through measurement of furrow water depths and modification of the surface storage equation. Alternatively it may be more appropriate to adopt one of the more complex models such as the kinematic wave, which can readily accommodate calculation of the subsurface and surface storage profiles by division of the furrow length into a number of discrete cells.

IPARM estimates infiltration rates from field measurements collected during the advance and storage phases (i.e. during the inflow time). This approach is sufficient for the majority of furrow systems since the duration of inflow almost entirely covers the full range of opportunity times. However, in some instances such as for surged

furrow and some border irrigation systems, the inflow is shut off well before the water reaches the end of the field. Hence, the entire runoff hydrograph and a significant portion of the advance may occur during the depletion and recession phases. One potential development to IPARM is to extend the inverse technique to accommodate these later stages of irrigation. This procedure would enable the estimation of infiltration parameters for these alternative surface irrigation systems where inflow is cut off before the end of the advance phase and possibly further improve the accuracy of the inverse technique for traditional furrow irrigation.

It is also likely that further improvements to the inverse procedure will only be possible through the adoption of one of the more complex hydraulic models. The improvements to the personal computer over recent years have dramatically reduced the run-time of these models. Hence, it may be more appropriate to adapt one of the zero inertia or full hydrodynamic models to perform the optimisation of infiltration parameters rather than attempting to further improve the volume balance model.

9.3.2 Field Experimentation

This research has focussed on the hydraulic performance of surface irrigation and in doing so has largely ignored the crop response. The work has assumed that the plant will receive maximum benefit from the irrigation when the deficit is fully satisfied. The nature of field measurements did not permit correlation between the irrigation application and crop growth or yield. Future research in this subject area should consider measures of crop variability. Not simply measurements of crop yield but also plant vigour, root profiles and possibly spatially based estimates of the evapotranspiration.

The field measurements used within this research are also devoid of any information describing the soil properties. It is likely that a significant component of the infiltration variability can be explained by soil properties such as measurements of the bulk density, texture and soil solute composition. One important parameter, particularly for the cracking clay soils is the pre-irrigation moisture content. On many soils it should be possible to scale the infiltration characteristic based on

measurements of the soil moisture deficit. Electromagnetic surveys (section 2.7.1) can be used to quickly assess the spatial variability of soil properties over a large area. It might be possible to combine such measurements with the current simulation and optimisation techniques to account for infiltration variability at both smaller scales (i.e. within furrow) and larger scales (across the field) than is currently possible under standard Irrimate™ measurements (section 5.4.1).

9.3.3 Statistical Description of Infiltration Variability

The statistical analysis covered in chapter 5 of this dissertation suffers from two major deficiencies. Firstly the description of variability is restricted to the inter-furrow variability using spatial averages of infiltration characteristics across the length of the furrow. With the appropriate field studies future research could apply similar methodologies to analyse the distribution of infiltration characteristics over the furrow length. The second area for future studies is the investigation of alternative statistical probability models. This dissertation has focussed on the normal and lognormal distributions with some inconclusive results. Future research could be directed to alternative statistical distributions such as the Box-Cox distribution which offer greater flexibility and share some of the convenient properties of both models.

9.3.4 Simulation Models for Heterogeneous Conditions

The simulation model (IrriProb) developed in chapter 6 provides an opportunity to study the impact of the variations in infiltration, inflow rates, inflow times and moisture deficit between furrows on the irrigation efficiency and uniformity. However, it does not provide any provision for the variance in infiltration and soil moisture deficit that commonly occurs along the length of a single furrow. This inter-furrow variability was not considered as the limited field measurements available did not provide sufficient information to identify multiple sets of infiltration parameters from within the single furrow.

The lack of sampling techniques and excessive measurement requirements impedes the estimation of infiltration rates at the sub-furrow length scale. However, modelling of the within furrow infiltration variation may be of value in research applications. It

may be valid to assume that the fit of the between furrow infiltration variability to the log-normal distribution function (section 5.8) also extends to the intra-furrow infiltration variability. Hence, Monte Carlo simulation techniques could be used to estimate the infiltration parameters at the sub-furrow scale. Alternatively it may be more appropriate to link the longitudinal variance in infiltration rates with the uniformity of the previous irrigation event. To utilise this information it would be necessary to modify the simulation approach to account for this variability. The same basic optimisation procedure used to optimise irrigation management within IrriProb (chapter 7) should apply equally to this smaller scale variability but would require validation in the field.

LIST OF REFERENCES

1. Abbasi, F., Adamsen, F. J., Hunsaker, D. J., Feyen, J., Shouse, P., and van Genuchten, M. T. (2003a). "Effects of flow depth on water flow and solute transport in furrow irrigation: Field data analysis." *Journal of Irrigation and Drainage Engineering*, 129(4), 237-246.

2. Abbasi, F., Shooshtari, M. M., and Feyen, J. (2003b). "Evaluation of various surface irrigation numerical simulation models." *Journal of Irrigation and Drainage Engineering*, 129(3), 208-213.

3. ABS. (2006a). "Water account, Australia, 2004-05." Australian Bureau of Statistics.

4. ABS. (2006b). "Water use on Australian farms, 2004-05." Australian Bureau of Statistics.

5. Ahuja, L. R., and Williams, R. D. (1991). "Scaling water characteristic and hydraulic conductivity based on Gregson-Hector-McGowan approach." *Soil Science Society of America Journal*, 55(2), 308-319.

6. Alazba, A. A. (1999). "Simulating furrow irrigation with different inflow patterns." *Journal of Irrigation and Drainage Engineering*, 125(1), 12-18.

7. Allen, R. R., and Musick, J. T. (1992). "Furrow traffic and ripping for control of irrigation intake." *Applied Engineering in Agriculture*, 8(2), 243-248.

8. Allen, R. R., and Musick, J. T. (1997). "Furrow irrigation infiltration with multiple traffic and increased axle mass." *Applied Engineering in Agriculture*, 13(1), 49-53.

9. Allmaras, R. R., and Kempthorne, O. (2002). "Errors, variability, and precision." Methods of soil analysis. Part 4, Physical methods, G. C. Topp and J. H. Dane, eds., Soil Science Society of America, Madison.

10. Amali, S., Rolston, D. E., Fulton, A. E., Hanson, B. R., Phene, C. J., and Oster, J. D. (1997). "Soil water variability under subsurface drip and furrow irrigation." *Irrigation Science*, 17(4), 151-155.

11. Antonio, J., and Alvarez, R. (2003). "Estimation of advance and infiltration equations in furrow irrigation for untested discharges." *Agricultural Water Management*, 60(3), 227-239.

12. ASAE. (2003). "Evaluation of Irrigated Furrows." ASAE EP419.1 FEB03, American Society of Agricultural Engineers.

13. Austin, N. R., and Prendergast, J. B. (1997). "Use of kinematic wave theory to model irrigation on cracking soil." *Irrigation Science*, 18(1), 1-10.

14. Ayers, R. S., and Westcot, D. W. (1994). "Water quality for agriculture." FAO Irrigation and Drainage Paper 29, Food and Agriculture Organization of the United Nations, Rome.

15. Baker, S. W. (1979). "Pore size distribution - A factor to be considered in infiltration studies?" *Journal of Hydrology*, 41(3-4), 279-290.

16. Bakker, D. M., Plunkett, G., and Sherrard, J. (2006). "Application efficiencies and furrow infiltration functions of irrigations in sugar cane in the Ord River Irrigation Area of North Western Australia and the scope for improvement." *Agricultural Water Management*, 83(1-2), 162-172.

17. Bali, K., and Wallender, W. W. (1987). "Water application under varying soil and intake opportunity time." *Transactions of the ASAE*, 30(2), 442-448.

18. Bautista, E., and Wallender, W. W. (1985). "Spatial variability of infiltration in furrows." *Transactions of the ASAE*, 28(6), 1846-1851.

19. Bautista, E., and Wallender, W. W. (1993a). "Identification of furrow intake parameters from advance times and rates." *Journal of Irrigation and Drainage Engineering*, 119(2), 295-311.

20. Bautista, E., and Wallender, W. W. (1993b). "Optimal management strategies for cutback furrow irrigation." *Journal of Irrigation and Drainage Engineering*, 119(6), 1099-1114.

21. Bautista, E., and Wallender, W. W. (1993c). "Reliability of optimized furrow-infiltration parameters." *Journal of Irrigation and Drainage Engineering*, 119(5), 784-800.

22. Ben-Hur, M., Shainberg, I., and Morin, J. (1987). "Variability of infiltration in a field with surface-sealed Soil." *Soil Science Society of America Journal*, 51(5), 1299-1302.

23. Bethea, R. M., and Rhinehart, R. R. (1991). *Applied engineering statistics*, M. Dekker, New York.

24. Bjorneberg, D. L., Sojka, R. E., and Aase, J. K. (2002). "Pre-wetting effect on furrow irrigation erosion: A field study." *Transactions of the American Society of Agricultural Engineers*, 45(3), 717-722.

25. Bos, M. G. (1979). *Discharge measurement structures*, Third Edition, International Institute for Land Reclamation and Improvement, Wageningen, The Netherlands.

26. Box, G. E. P., and Pierce, D. A. (1970). "Distribution of residual autocorrelations in autoregressive-integrated moving average time series models." *Journal of the American Statistical Association - Theory and Methods*, Vol. 65(No. 332), 1509-1526.

27. Brady, N. C., and Weil, R. R. (2002). *The nature and properties of soils*, 13th, Prentice Hall, Upper Saddle River, N.J.

28. Bresler, E., Dagan, G., Wagenet, R. J., and Laufer, A. (1984). "Statistical analysis of salinity and texture effects on spatial variability of soil hydraulic conductivity." *Soil Science Society of America Journal*, 48(1), 16-25.

29. Brown, M. J., Kemper, W. D., Trout, T. J., and Humpherys, A. S. (1988). "Sediment, erosion and water-intake in furrows." *Irrigation Science*, 9(1), 45-55.

30. Brye, K. R., Slaton, N. A., and Norman, R. J. (2006). "Soil physical and biological properties as affected by land leveling in a clayey aquert." *Soil Science Society of America Journal*, 70(2), 631-642.

31. Brye, K. R., Slaton, N. A., Savin, M. C., Norman, R. J., and Miller, D. M. (2003). "Short-term effects of land leveling on soil physical properties and microbial biomass." *Soil Sci Soc Am J*, 67(5), 1405-1417.

32. Burt, C. (1995). *The surface irrigation manual: A comprehensive guide to design and operation of surface irrigation systems*, Waterman Industries, Exeter.

33. Bury, K. V. (1999). *Statistical distributions in engineering*, Cambridge University Press, New York.

34. Cahoon, J. E. (1995). "Defining furrow cross section." *Journal of Irrigation and Drainage Engineering*, 121(1), 114-119.

35. Camacho, E., Perez-Lucena, C., Roldan-Canas, J., and Alcaide, M. (1997). "IPE: Model for management and control of furrow irrigation in real time." *Journal of Irrigation and Drainage Engineering*, 123(4), 264-268.

36. Cantor, L. M. (1970). *A world geography of irrigation*, Praeger Publishers Inc., New York.

37. Cavero, J., Playan, E., Zapata, N., and Faci, J. M. (2001). "Simulation of maize grain yield variability within a surface-irrigated field." *Agronomy Journal*, 93(4), 773-782.

38. Chan, K. Y., and Hodgson, A. S. (1981). "Moisture regimes of a cracking clay soil under furrow irrigation." *The Properties and Utilization of Cracking Clay Soils*, University of New England, Armidale, New South Wales, Australia.

39. Chiang, S. C., Radcliffe, D. E., and Miller, W. P. (1993). "Hydraulic properties of surface seals in Georgia soils." *Soil Science Society of America Journal*, 57(6), 1418-1426.

40. Childs, J. L., Wallender, W. W., and Hopmans, J. W. (1993). "Spatial and seasonal variation of furrow infiltration." *Journal of Irrigation and Drainage Engineering*, 119(1), 74-90.

41. Chow, V. T. (1959). *Open-channel hydraulics*, McGraw-Hill, New York.

42. Clemmens, A. J. (1983). "Infiltration equations for border irrigation models." *Advances in Infiltration, Proceedings of the National Conference.*, Chicago, IL, USA.

43. Clemmens, A. J. (1988). "Method for analyzing field scale surface irrigation Uniformity." *Journal of Irrigation and Drainage Engineering*, 114(1), 74-88.

44. Clemmens, A. J. (1991). "Direct solution to surface irrigation advance inverse problem." *Journal of Irrigation and Drainage Engineering*, 117(4), 578-593.

45. Clemmens, A. J. (2003). "Field Verification of a Two-Dimensional Surface Irrigation Model." *Journal of Irrigation and Drainage Engineering*, 129(6), 402-411.

46. Clemmens, A. J., and Strelkoff, T. (1999). "SRFR." U.S. Water Conservation Laboratory, Agricultural Research Service, Phoenix, A Surface Irrigation Simulation Model.

47. Dalton, P., Raine, S. R., and Bradfoot, K. (2001). "Best management practices for maximising whole farm irrigation efficiency in the Australian cotton industry." USQ, Toowoomba.

48. DeTar, W. R. (1989). "Infiltration function from furrow stream advance." *Journal of Irrigation and Drainage Engineering*, 115(4), 722-733.

49. Devore, J. L., and Peck, R. (1997). *Statistics : the exploration and analysis of data*, 3rd, Duxbury Press, Belmont.

50. Dowling, A. J., Thorburn, P. J., Ross, P. J., and Elliot, P. J. (1991). "Estimation of infiltration and deep drainage in a furrow-irrigated sodic duplex soil." *Australian Journal of Soil Research*, 29, 363-375.

51. Duke, H. R. (1992). "Water temperature fluctuations and effect on irrigation infiltration." *Transactions of the ASAE*, 35(1), 193-199.

52. Eldeiry, A. A., Garcia, L. A., El-Zaher, A. S. A., and Kiwan, M. E.-S. (2005). "Furrow irrigation system design for clay soils in arid regions." *Applied Engineering in Agriculture*, 21(3), 411-420.

53. El-Dine, T. G., and Hosny, M. M. (2000). "Field evaluation of surge and continuous flows in furrow irrigation systems." *Water Resources Management*, 14(2), 77-87.

54. Elliott, R. L., and Walker, W. R. (1982). "Field evaluation of furrow infiltration and advance functions." *Transactions of the ASAE*, 25(2), 396-400.

55. Elliott, R. L., Walker, W. R., and Skogerboe, G. V. (1983). "Infiltration parameters from furrow irrigation advance data." *Transactions of the ASAE*, 26(6), 1726-1731.

56. Emdad, M. R., Raine, S. R., Smith, R. J., and Fardad, H. (2004). "Effect of water quality on soil structure and infiltration under furrow irrigation." *Irrigation Science*, 23(2), 55-60.

57. Enciso-Medina, J., Martin, D., and Eisenhauer, D. (1998). "Infiltration model for furrow irrigation." *Journal of Irrigation and Drainage Engineering*, 124(2), 73-80.

58. Ersahin, S. (2003). "Comparing ordinary kriging and cokriging to estimate infiltration rate." *Soil Science Society of America Journal*, 67(6), 1848-1855.

59. Esfandiari, M., and Maheshwari, B. L. (1997). "Field values of the shape factor for estimating surface storage in furrows on a clay soil." *Irrigation Science*, 17(4), 157-161.

60. Fattah, H. A., and Upadhyaya, S. K. (1996). "Effect of soil crust and soil compaction of infiltration in a Yolo loam soil." *Transactions of the ASAE*, 39(1), 79-84.

61. Featherstone, R. E., and Nalluri, C. (1995). *Civil engineering hydraulics : Essential theory with worked examples*, 3rd, Blackwell Science, Oxford ; Cambridge.

62. Fekersillassie, D., and Eisenhauer, D. E. (2000). "Feedback-controlled surge irrigation: I. Model development." *Transactions of the American Society of Agricultural Engineers*, 43(6), 1621-1630.

63. Fernandez-Gomez, R., Mateos, L., and Giraldez, J. V. (2004). "Furrow irrigation erosion and management." *Irrigation Science*, 23(3), 123-131.

64. Fonteh, M., and Podmore, T. (1994a). "Furrow irrigation with physically based spatially varying infiltration." *Journal of Agricultural Engineering Research*, 57(4), 229-236.

65. Fonteh, M. F., and Podmore, T. (1994b). "Application of geostatistics to characterize spatial variability of infiltration in furrow irrigation." *Agricultural Water Management*, 25(2), 153-165.

66. Fornstrom, K. J., Michel, J. A. J., Borrelli, J., and Jackson, G. D. (1985). "Furrow firming for control of irrigation advance rates." *Transactions of the ASAE*, 28(2), 529-531.

67. Foroud, N., George, E. S., and Entz, T. (1996). "Determination of infiltration rate from border irrigation advance and recession trajectories." *Agricultural Water Management*, 30(2), 133-142.

68. Furman, A., Warrick, A. W., Zerihun, D., and Sanchez, C. A. (2006). "Modified Kostiakov infiltration function: Accounting for initial and boundary conditions." *Journal of Irrigation and Drainage Engineering*, 132(6), 587-596.

69. Gharbi, A., Daghari, H., and Cherif, K. (1993). "Effect of flow fluctuations on free draining, sloping furrow and border irrigation systems." *Agricultural Water Management*, 24(4), 299-319.

70. Gish, T. J., and Starr, J. L. (1983). "Temporal variability of infiltration under field conditions." *Advances in Infiltration, Proceedings of the National Conference.*, Chicago, IL, USA, 122-131 BN - 0-916150-58-5.

71. Glanville, S., and Smith, G. (1988). "Aggregate breakdown in clay soils under simulated rain and effects on infiltration." *Australian Journal of Soil Research*, 26(1), 110-126.

72. Guardo, M., Oad, R., and Podmore, T. H. (2000). "Comparison of zero-inertia and volume balance advance-infiltration models." *Journal of Hydraulic Engineering*, 126(6), 457-465.

73. Gupta, R. K., Rudra, R. P., Dickinson, W. T., and Elrick, D. E. (1994). "Modeling spatial patterns of three infiltration parameters." *Canadian Agricultural Engineering*, 36(1), 9-13.

74. Haining, R. P. (2003). *Spatial data analysis: Theory and practice*, Cambridge University Press, New York.

75. Hallows, P. J., and Thompson, D. G. (1995). *The history of irrigation in Australia*, ANCID First Mildura Irrigation Trust, Mildura.

76. Hanson, B. R., and Kaita, K. (1997). "Response of electromagnetic conductivity meter to soil salinity and soil-water content." *Journal of Irrigation and Drainage Engineering*, 123(2), 141-143.

77. Hanson, B. R., Prichard, T. L., and Schulbach, H. (1993). "Estimating furrow infiltration." *Agricultural Water Management*, 24(4), 281-298.

78. Hedley, C. B., Yule, I. J., Eastwood, C. R., Shepherd, T. G., and Arnold, G. (2004). "Rapid identification of soil textural and management zones using electromagnetic induction sensing of soils." *Australian Journal of Soil Research*, 42(4), 389-400.

79. Hidore, J. J., and Oliver, J. E. (1993). *Climatology: An atmospheric science*, Maxwell Macmillan International, New York, Toronto.

80. Hodges, M. E., Stone, J. F., Garton, J. E., and Weeks, D. L. (1989). "Variance of water advance in wide-spaced furrow irrigation." *Agricultural Water Management*, 16(1-2), 5-13.

81. Holzapfel, E., A., Marino, M. A., Valenzuela, A., and Diaz, F. (1988). "Comparison of infiltration measuring methods for surface irrigation." *Journal of Irrigation and Drainage Engineering*, 114(1), 130-142.

82. Holzapfel, E. A., Jara, J., Zuniga, C., Marino, M. A., Paredes, J., and Billib, M. (2004). "Infiltration parameters for furrow irrigation." *Agricultural Water Management*, 68(1), 19-32.

83. Hopmans, J. W. (1989). "Stochastic description of field-measured infiltration data." *Transactions of the ASAE*, 32(6), 1987-1993.

84. Hornbuckle, J. W. (1999). "Modelling furrow irrigation on heavy clays, high water tables and tiled drained soils using SIRMOD in the Murrumbidgee irrigation area.," Undergraduate Thesis, University of New England, Armidale, NSW, Australia.

85. Horst, M. G., Shamutalov, S. S., Goncalves, J. M., and Pereira, L. S. (2007). "Assessing impacts of surge-flow irrigation on water saving and productivity of cotton." *Agricultural Water Management*, 87(2), 115-127.

86. Horst, M. G., Shamutalov, S. S., Pereira, L. S., and Goncalves, J. M. (2005). "Field assessment of the water saving potential with furrow irrigation in Fergana, Aral Sea basin." *Agricultural Water Management*, 77(1), 210-231.

87. House, M. L., Powers, W. L., Eisenhauer, D. E., Marx, D. B., and Fekersillassie, D. (2001). "Spatial analysis of machine-wheel traffic effects on soil physical properties." *Soil Science Society of America Journal*, 65(5), 1376-1384.

88. Hunsaker, D. J., Clemmens, A. J., and Fangmeier, D. D. (1999). "Cultural and irrigation management effects on infiltration, soil roughness, and advance in furrowed level basins." *Transactions of the ASAE*, 42(6), 1753-1764.

89. Ito, H., Wallender, W. W., and Raghuwanshi, N. S. (1999). "Economics of furrow irrigation under partial infiltration information." *Journal of Irrigation and Drainage Engineering*, 125(3), 105-111.

90. Ito, H., Wallender, W. W., and Raghuwanshi, N. S. (2005). "Optimal sample size for furrow irrigation design." *Biosystems Engineering*, 91(2), 229-237.

91. Iwata, S., Tabuchi, T., and Warkentin, B. P. (1995). *Soil-water interactions: Mechanisms and applications*, 2nd ed, rev. and expand, M. Dekker, New York.

92. Izadi, B., Studer, D., and McCAnn, I. (1991). "Maximizing set-wide furrow irrigation application efficiency under full irrigation strategy." *Transactions of the ASAE*, 34(5), 2006-2014.

93. Izadi, B., and Wallender, W. W. (1985). "Furrow hydraulic characteristics and infiltration." *Transactions of the ASAE*, 28(6), 1901-1908.

94. Jaynes, D. B., and Clemmens, A. J. (1986). "Accounting for spatially variable infiltration in border irrigation models." *Water Resources Research*, 22(8), 1257-1262.

95. Jaynes, D. B., and Hunsaker, D. J. (1989). "Spatial and temporal variability of water content and infiltration on a flood irrigated field." *Transactions of the ASAE*, 32(4), 1229-1238.

96. Jurriëns, M., and Lenselink, K. J. (2001). "Straightforward furrow irrigation can be 70% efficient." *Irrigation and Drainage*, 50(3), 195-204.

97. Kang, S. Z., Shi, P., Pan, Y. H., Liang, Z. S., Hu, X. T., and Zhang, J. (2000). "Soil water distribution, uniformity and water-use efficiency under alternate furrow irrigation in arid areas." *Irrigation Science*, 19(4), 181-190.

98. Katopodes, N. D., Tang, J.-H., and Clemmens, A. J. (1990). "Estimation of surface irrigation parameters." *Journal of Irrigation and Drainage Engineering*, 116(5), 676-696.

99. Kemper, W. D., Trout, T. J., Humpherys, A. S., and Bullock, M. S. (1988). "Mechanisms by which surge irrigation reduces furrow infiltration rates in a silty loam soil." *Transactions of the ASAE*, 31(3), 821-829.

100. Kemper, W. D., Trout, T. J., and Kincaid, D. C. (1987). "Cablegation: Automated supply for surface irrigation." Advances in Irrigation, D. Hillel, ed., Academic Press Inc., London, 1-66.

101. Khanna, M., and Malano, H. M. (2006). "Modelling of basin irrigation systems: A review." *Agricultural Water Management*, 83(1-2), 87-99.

102. Khatri, K., and Smith, R. (2006). "Real-time prediction of soil infiltration characteristics for the management of furrow irrigation." *Irrigation Science*, 1-11.

103. Khatri, K. L., and Smith, R. J. (2005). "Evaluation of methods for determining infiltration parameters from irrigation advance data." *Irrigation and Drainage*, 54(4), 467-482.

104. Kruse, E. G. (1978). "Describing irrigation efficiency and uniformity." *Journal of Irrigation and Drainage Engineering*, 104(1), 35-41.

105. Lal, R., and Pandya, A. C. (1970). "Furrow irrigation with decreasing inflow rate." *Journal of the Irrigation and Drainage Division*, 96(4), 451-460.

106. Lal, R., and Shukla, M. K. (2004). *Principles of soil physics*, Marcel Dekker ;Taylor & Francis, New York & London.

107. Lentz, R. D., and Bjorneberg, D. L. (2001). "Influence of irrigation water properties on furrow infiltration: Temperature effects."

108. Lentz, R. D., and Bjorneberg, D. L. (2003). "Polyacrylamide and straw residue effects on irrigation furrow erosion and infiltration." *Journal of Soil and Water Conservation*, 58(5), 312-318.

109. Lentz, R. D., Sojka, R. E., and Mackey, B. E. (2002). "Fate and efficacy of polyacrylamide applied in furrow irrigation: Full-advance and continuous treatments." *Journal of Environmental Quality*, 31(2), 661-670.

110. Levien, S. L. A., and de Souza, F. (1987). "Algebraic computation of flow in furrow irrigation." *Journal of Irrigation and Drainage Engineering*, 113(3), 367-377.

111. Li, Y., Tullberg, J. N., and Freebairn, D. M. (2001). "Traffic and residue cover effects on infiltration." *Australian Journal of Soil Research*, 39(2), 239-247.

112. Maheshwari, B. L., and Kelly, D. (1997). "Evaluation of time-rated infiltration families for noncracking soils." *Journal of Irrigation and Drainage Engineering*, 123(4), 238-245.

113. Mailhol, J.-C. (2003). "Validation of a predictive form of Horton infiltration for simulating furrow irrigation." *Journal of Irrigation and Drainage Engineering*, 129(6), 412-421.

114. Mailhol, J.-C., and Gonzalez, J.-M. (1993). "Furrow irrigation model for real-time applications on cracking soils." *Journal of Irrigation and Drainage Engineering*, 119(5), 768-783.

115. Mailhol, J. C., Priol, M., and Benali, M. (1999). "A furrow irrigation model to improve irrigation practices in the Gharb valley of Morocco." *Agricultural Water Management*, 42(1), 65-80.

116. Mailhol, J. C., Ruelle, P., and Popova, Z. (2005). "Simulation of furrow irrigation practices (SOFIP): A field-scale modelling of water management and crop yield for furrow irrigation." *Irrigation Science*, 1-12.

117. Mateos, L., and Oyonarte, N. A. (2005). "A spreadsheet model to evaluate sloping furrow irrigation accounting for infiltration variability." *Agricultural Water Management*, 76(1), 62-75.

118. McClymont, D. J. (2007). "Development of a Decision Support System for Furrow and Border Irrigation," University of Southern Queensland, Toowoomba.

119. McClymont, D. J., and Smith, R. J. (1996). "Infiltration parameters from optimization on furrow irrigation advance data." *Irrigation Science*, 17(1), 15-22.

120. McClymont, D. J., Smith, R. J., and Raine, S. R. (1999). "An integrated numerical model for the design and management of furrow irrigation." *2nd International Conference on Multiple Objective Decision Support Systems for Land, Water and Environmental Management*, Brisbane, Australia.

121. McKenzie, N. J., and Cresswell, H. P. (2002). "Selecting a method for hydraulic conductivity." Soil Physical Measurement and Interpretation for Land Evaluation, N. J. McKenzie, K. J. Coughlan, and H. P. Cresswell, eds., CSIRO Publishing, Collingwood.

122. Mehuys, G. R., Stolzy, L. H., Letey, J., and Weeks, L. V. (1975). "Effect of stones on the hydraulic conductivity of relatively dry desert soils." *Proceedings of the Soil Science Society of America*, 39(1), 37-42.

123. Miller, I., and Freund, J. E. (1985). *Probability and statistics for engineers*, 3rd, Prentice Hall, Englewood Cliffs.

124. Mitchell, A. R., and van Genuchten, M. T. (1993). "Flood irrigation of a cracked soil." *Soil Science Society of America journal*, 57(2), 490-497.

125. Montgomery, D. C., and Runger, G. C. (1999). *Applied statistics and probability for engineers*, 2nd, John Wiley Sons, New York.

126. Myers, J. L., and Well, A. (2003). *Research design and statistical analysis*, 2nd, Lawrence Erlbaum Associates, Mahwah.

127. Naney, J. W., Ahuja, L. R., and Barnes, B. B. (1983). "Variability and interrelation of soil-water and some related soil properties in a small watershed." *Advances in Infiltration, Proceedings of the National Conference.*, Chicago, IL, USA, 92-100.

128. Northcote, K. H. (1979). *A factual key for the recognition of Australian soils*, 4th, Rellim Technical Publications, Adelaide.

129. Norum, D. I., and Gray, D. M. (1970). "Infiltration equations from rate of advance data." *Journal of Irrigation and Drainage Engineering*, 96(2), 111-119.

130. Norusis, M. J. (1993). *SPSS for Windows: Base system user's guide, release 6.0*, SPSS Inc., Chicago.

131. Oliveira, M. R. G., Serralheiro, R. P., Reis, M. P. Z., and Santos, F. L. (1998). "Maize root system response to furrow irrigation in a Mediterranean brown soil: root growth related to water distribution." *Journal of Agricultural Engineering Research*, 71(1), 13-17.

132. O'neill, C. J., Humphreys, E., and Katupiyiya, A. (2006). "Comparison of sprinkler, subsurface drip and flood irrigation for maize in the Coleambally irrigation area, NSW." *Irrigation Association of Australia National Conference*, Brisbane, Qld, Australia, 97-98.

133. Or, D., and Silva, H. R. (1996). "Prediction of surface irrigation advance using soil intake properties." *Irrigation Science*, 16(4), 159-167.

134. Oster, J. D., and Schroer, F. W. (1979). "Infiltration as influenced by irrigation water-quality." *Soil Science Society of America Journal*, 43(3), 444-447.

135. Oyonarte, N. A., and Mateos, L. (2002). "Accounting for soil variability in the evaluation of furrow irrigation." *Transactions of the American Society of Agricultural Engineers*, 45(6), 85-94.

136. Oyonarte, N. A., Mateos, L., and Palomo, M. J. (2002). "Infiltration variability in furrow irrigation." *Journal of Irrigation and Drainage Engineering*, 128(1), 26-33.

137. Popova, Z., and Kuncheva, R. (1996). "Modeling in water losses evaluation for nonhomogeneous furrow set." *Journal of Irrigation and Drainage Engineering*, 122(1), 1-6.

138. Postel, S. (1999). *Pillar of sand: Can the irrigation miracle last?*, Norton, New York ; London.

139. Purkey, D. R., and Wallender, W. W. (1989). "Surge flow infiltration variability." *Transactions of the ASAE*, 32(3), 894-900.

140. Raghuwanshi, N. S., and Wallender, W. W. (1996). "Modeling seasonal furrow irrigation." *Journal of Irrigation and Drainage Engineering*, 122(4), 235-242.

141. Raghuwanshi, N. S., and Wallender, W. W. (1997). "Economic optimization of furrow irrigation." *Journal of Irrigation and Drainage Engineering*, 123(5), 377-385.

142. Ragusa, S. R., Zoysa, D. S., and Rengasamy, P. (1994). "The effect of microorganisms, salinity and turbidity on hydraulic conductivity of irrigation channel soil." *Irrigation Science*, 15(4), 159-166.

143. Raine, S. R., and Bakker, D. M. (1996). "Increased furrow irrigation efficiency through better design and management of cane fields." *Australian Society of Sugar Can Technologists*, Mackay, 114 - 124.

144. Raine, S. R., McClymont, D. J., and Smith, R. J. (1997). "The development of guidelines for surface irrigation in areas with variable infiltration." *Australian Society of Sugar Cane Technologists*, Cairns; Australia, 293-301.

145. Raine, S. R., McClymont, D. J., and Smith, R. J. (1998). "The effect of variable infiltration on design and management guidelines for surface irrigation." ASSCI National Soils Conference.

146. Raine, S. R., Purcell, J., and Schmidt, E. (2005). "Improving whole farm and infield irrigation efficiencies using Irrimate tools." *Irrigation 2005: Restoring the Balance*, Townsville, Australia.

147. Rasoulzadeh, A., and Sepaskhah, A. R. (2003). "Scaled infiltration equations for furrow irrigation." *Biosystems Engineering*, 86(3), 375-383.

148. Rayej, M., and Wallender, W. W. (1988). "Time solution of Kinematic-wave model with stochastic infiltration." *Journal of Irrigation and Drainage Engineering*, 114(4), 605-621.

149. Reddell, D. L., and Latimer, E. A. (1987). "Field evaluation of an advance rate feedback irrigation system." *Irrigation Systems for the 21st Century, Proceedings of a Conference. Papers Presented at the 1987 Irrigation and Drainage Division Specialty Conference.*, Portland, OR, USA, 317-324 BN - 0-87262-609-1.

150. Renault, D., and Wallender, W. W. (1994). "Furrow advance-rate solution for stochastic infiltration properties." *Journal of Irrigation and Drainage Engineering*, 120(3), 617-633.

151. Renault, D., and Wallender, W. W. (1996). "Initial-inflow-variation impacts on furrow irrigation evaluation." *Journal of Irrigation and Drainage Engineering*, 122(1), 7-14.

152. Renault, D., and Wallender, W. W. (1997). "Surface storage in furrow irrigation evaluation." *Journal of Irrigation and Drainage Engineering*, 123(6), 415-422.

153. Reynolds, W. D., Elrick, D. E., Youngs, E. G., Amoozegar, A., Booltink, H. W. G., and Bouma, J. (2002). "Section 3.4 Saturated and Field-Saturated Water Flow Meters." Methods of soil analysis. Part 4, Physical methods, G. C. Topp and J. H. Dane, eds., Soil Science Society of America, Madison, 797 - 878.

154. Robertson, D., Wood, M., and Wang, Q. J. (2004). "Estimating hydraulic parameters for a surface irrigation model from field conditions." *Australian Journal of Experimental Agriculture*, 44(2), 173-179.

155. Sakai, K., Upadhyaya, S. K., and Sime, M. (1992). "Variability of a double ring infiltration test." *Transactions of the ASAE*, 35(4), 1221-1226.

156. Santos, F. L. (1996). "Evaluation and adoption of irrigation technologies. I. Management-design curves for furrow and level basin systems." *Agricultural Systems*, 52(2-3), 317-329.

157. Santos, F. L., and Serralheiro, R. P. (2000). "Improving infiltration of irrigated Mediterranean soils with polyacrylamide." *Journal of Agricultural Engineering Research*, 76(1), 83-90.

158. Scaloppi, E. J., Merkley, G. P., and Willardson, L. S. (1995). "Intake parameters from advance and wetting phases of surface irrigation." *Journal of Irrigation and Drainage Engineering*, 121(1), 57-70.

159. Schmitz, G. H., and Seus, G. J. (1992). "Mathematical zero-inertia modeling of surface irrigation. Advance in furrows." *Journal of Irrigation and Drainage Engineering*, 118(1), 1-18.

160. Schwankl, L. J., Raghuwanshi, N. S., and Wallender, W. W. (2000). "Furrow irrigation performance under spatially varying conditions." *Journal of Irrigation and Drainage Engineering*, 126(6), 355-361.

161. Schwankl, L. J., and Wallender, W. W. (1988). "Zero inertia furrow modeling with variable infiltration and hydraulic characteristics." *Transactions of the ASAE*, 31(5), 1470-1475.

162. Segeren, A. G., and Trout, T. J. (1991). "Hydraulic resistance of soil surface seals in irrigated furrows." *Soil Science Society of America Journal*, 55(3), 640-646.

163. Sepaskhah, A. R., and Afshar-Chamanabad, H. (2002). "SW--Soil and water: Determination of infiltration rate for every-other furrow irrigation." *Biosystems Engineering*, 82(4), 479-484.

164. Sepaskhah, A. R., and Ghahraman, B. (2004). "The effects of irrigation efficiency and uniformity coefficient on relative yield and profit for deficit irrigation." *Biosystems Engineering*, 87(4), 495-507.

165. Shafique, M. S., and Skogerboe, G. V. (1983). "Impact of seasonal infiltration function variation on furrow irrigation performance." *Advances in Infiltration, Proceedings of the National Conference.*, Chicago, IL, USA, 292-301.

166. Sharma, M. L., Barron, R. J. W., and De Boer, E. S. (1983). "Spatial structure and variability of infiltration parameters." *Advances in Infiltration, Proceedings of the National Conference.*, Chicago, IL, USA, 113-121 BN - 0-916150-58-5.

167. Shepard, J. S., Wallender, W. W., and Hopmans, J. W. (1993). "One-point method for estimating furrow infiltration." *Transactions of the ASAE*, 36(2), 395-404.

168. Simpson, J. A., and Weiner, E. S. C. (1989). *The Oxford English dictionary*, 2nd, Clarendon Press, Oxford University Press, Oxford, New York.

169. Singer, M. J., and Munns, D. N. (1999). *Soils: An introduction*, 4th, Prentice Hall, Upper Saddle River.

170. Smith, R. J. (1990). "The distribution of water from rigid and layflat gated pipe." Proceedings of Australian Society of Sugar Cane Technologists.

171. Smith, R. J., Raine, S. R., and Minkevich, J. (2005). "Irrigation application efficiency and deep drainage potential under surface irrigated cotton." *Agricultural Water Management*, 71(2), 117-130.

172. Smith, R. J., Walton, R. S., and Loxton, T. (1992). "Infiltration and surge irrigation on two clay soils in Queensland." *8th Conference on Engineering in Agriculture - Quality Soils, Quality Food, Quality Environment, Oct 4-7 1992*, Albury, Australia, 127-131.

173. Soong, T. T. (2004). *Fundamentals of probability and statistics for engineers*, Wiley, Hoboken.

174. Sousa, P. L. d., Silva, L. L., and Serralheiro, R. P. (1999). "Comparative analysis of main on-farm irrigation systems in Portugal." *Agricultural Water Management*, 40(2-3), 341-351.

175. "SPSS V12.0". (2005), SPSS Inc., Chicago, IL

176. Strelkoff, T., and Souza, F. (1984). "Modeling effect of depth on furrow infiltration." *Journal of Irrigation and Drainage Engineering*, 110(4), 375-387.

177. Sturm, T. W. (2001). *Open channel hydraulics*, McGraw-Hill, Boston.

178. Sudduth, K. A., Drummond, S. T., and Kitchen, N. R. (2001). "Accuracy issues in electromagnetic induction sensing of soil electrical conductivity for precision agriculture." *Computers and Electronics in Agriculture*, 31(3), 239-264.

179. Tarboton, K. C., and Wallender, W. W. (1989). "Field-wide furrow infiltration variability." *Transactions of the ASAE*, 32(3), 913-918.

180. "TeeChart Pro v7". (2006), Steema Software SL, Girona, Spain

181. Trout, T. J. (1990). "Furrow inflow and infiltration variability impacts on irrigation management." *Transactions of the ASAE*, 33(4), 1171-1178.

182. Trout, T. J. (1992a). "Flow velocity and wetted perimeter effects on furrow infiltration." *Transactions of the ASAE*, 35(3), 855-863.

183. Trout, T. J. (1992b). "Furrow flow velocity effect on hydraulic roughness." *Journal of Irrigation and Drainage Engineering*, 118(6), 981-987.

184. Trout, T. J. (1996). "Furrow irrigation erosion and sedimentation: On-field distribution." *Transactions of the ASAE*, 39(5), 1717-1723.

185. Trout, T. J., and Kemper, W. D. (1983). "Factors which affect furrow intake rates." *Advances in Infiltration, Proceedings of the National Conference.*, Chicago, IL, USA, 302-312 BN - 0-916150-58-5.

186. Trout, T. J., and Mackey, B. E. (1988a). "Furrow inflow and infiltration variability." *Transactions of the ASAE*, 31(2), 531-537.

187. Trout, T. J., and Mackey, B. E. (1988b). "Inflow-outflow infiltration measurement accuracy." *Journal of Irrigation and Drainage Engineering*, 114(2), 256-265.

188. Turnell, D. J., Deep, G. S., and Freire, R. C. S. (1997). "A low-cost water detection method for furrow irrigation control." *Instrumentation and Measurement, IEEE Transactions on*, 46(4), 986-990.

189. Turral, H. N., Malano, H. M., and McMahon, T. A. (1992). "Evaluation of surge flow in border irrigation." *8th Conference on Engineering in Agriculture - Quality Soils, Quality Food, Quality Environment, Oct 4-7 1992*, Albury, Aust, 137-141.

190. Upton, G. J. G., and Cook, I. (2002). *A dictionary of statistics*, Oxford University Press, New York.

191. Valiantzas, J. D. (1997). "Volume balance irrigation advance equation: Variation of surface shape factor." *Journal of Irrigation and Drainage Engineering*, 123(4), 307-312.

192. Valiantzas, J. D. (2000). "Surface water storage independent equation for predicting furrow irrigation advance." *Irrigation Science*, 19(3), 115-123.

193. Valiantzas, J. D., Aggelides, S., and Sassalou, A. (2001). "Furrow infiltration estimation from time to a single advance point." *Agricultural Water Management*, 52(1), 17-32.

194. van Es, H. M. (2002). "Soil variability." Methods of soil analysis. Part 4, Physical methods, G. C. Topp and J. H. Dane, eds., Soil Science Society of America, Madison.

195. van Es, H. M., Cassel, D. K., and Daniels, R. B. (1991). "Infiltration variability and correlations with surface soil properties for an eroded Hapludult." *Soil Science Society of America Journal*, 55(2), 486-492.

196. van Es, H. M., Ogden, C. B., Hill, R. L., Schindelbeck, R. R., and Tsegaye, T. (1999). "Integrated assessment of space, time, and management-related variability of soil hydraulic properties." *Soil Science Society of America Journal*, 63(6), 1599-1608.

197. Vazquez-Fernandez, E. (2006). "Comparison between continuous-flow and increased-discharge irrigations in blocked-end furrows using a mathematical model." *Applied Engineering in Agriculture*, 22(3), 375-380.

198. Vazquez-Fernandez, E., Lopez-Tellez, P., and Chagoya-Amador, B. (2005). "Comparison of water distribution uniformities between increased-discharge and continuous-flow irrigations in blocked-end furrows." *Journal of Irrigation and Drainage Engineering*, 131(4), 379-382.

199. Vervoort, R. W., Cattle, S. R., and Minasny, B. (2003). "The hydrology of Vertosols used for cotton production: I. Hydraulic, structural and fundamental soil properties." *Australian Journal of Soil Research*, 41(7), 1255-1272.

200. Vieira, S. R., Nielsen, D. R., and Biggar, J. W. (1981). "Spatial variability of field-measured infiltration rate." 45(6), 1040-1048.

201. Viviani, G., and Iovino, M. (2004). "Wastewater reuse effects on soil hydraulic conductivity." *Journal of Irrigation and Drainage Engineering*, 130(6), 476-484.

202. Walker, W. R. (2003). "Surface irrigation simulation, evaluation and design." User Guide and Technical Documentation, Utah State University, Logan, Utah, 145.

203. Walker, W. R. (2005a). "Multilevel calibration of furrow infiltration and roughness." *Journal of Irrigation and Drainage Engineering*, 131(2), 129-136.

204. Walker, W. R. (2005b). "SIRMOD III - Online help." Utah State University, Logan, Utah.

205. Walker, W. R., Prestwich, C., and Spofford, T. (2006). "Development of the revised USDA-NRCS intake families for surface irrigation." *Agricultural Water Management*, 85(1-2), 157-164.

206. Walker, W. R., and Skogerboe, G. V. (1987). *Surface irrigation: Theory and practice*, Prentice-Hall, Englewood Cliffs.

207. Walker, W. R., and Willardson, L. S. (1983). "Infiltration measurements for simulating furrow irrigation." *Advances in Infiltration, Proceedings of the National Conference.*, Chicago, IL, USA, 241-248.

208. Wallender, W. W. (1986). "Furrow model with spatially varying infiltration." *Transactions of the ASAE*, 29(4), 1012-1016.

209. Wallender, W. W. (1987). "Sample Volume Statistical Relations for Water Content, Infiltration and Yield." *Transactions of the American Society of Agricultural Engineers*, 30(4), 1043 - 1050.

210. Wallender, W. W., Ardila, S., and Rayej, M. (1990). "Irrigation optimization with variable water quality and nonuniform soil." *Transactions of the ASAE*, 33(5), 1605-1611.

211. Wallender, W. W., and Rayej, M. (1987). "Economic optimization of furrow irrigation with uniform and nonuniform soil." *Transactions of the ASAE*, 30(5), 1425-1429.

212. Warrick, A. W., Zerihun, D., Sanchez, C. A., and Furman, A. (2005). "Infiltration under variable ponding depths of water." *Journal of Irrigation and Drainage Engineering*, 131(4), 358-363.

213. Wichelns, D., and Oster, J. D. (1990). "Potential economic returns to improved irrigation infiltration uniformity." *Agricultural Water Management*, 18(3), 253-266.

214. Yinong, L., Shaohui, Z., Di, X., and Meijian, B. (2006). "An optimised inverse model used to estimate soil infiltration parameters and the Manning's roughness coefficient under surface irrigation condition." *CIGR World Congress - Agricultural Engineering for a Better World*, Bonn, Germany, 43-44.

215. Young, A. R. M., and Young, R. W. (2002). *Soils in the Australian landscape*, Oxford University Press, Melbourne.

APPENDIX A

Field Data for IPARM

Validation

Table A.1 Field data for Benson

Irrigation Name: **Benson**
Source: Walker 2005
Location: Benson Farm near Greeley, Colorado, US
Details corn planted on clay loam, 7/07/1997

Field length: 625 m
Slope: 0.004174
Furrow Spacing 1.542 m

Average Inflow 0.78198 L s^{-1}

Furrow Dimensions

Top Width 0.311 m
Middle Width 0.263 m
Bottom Width 0.083 m
Max Height 0.036 m

Advance Data

x (m)	t (min)
0	0
25	3.1
50	6.9
75	11.5
100	15.5
125	20.5
150	25.1
175	29
200	33.5
225	38.5
250	44.2
275	50
300	56.3
350	69.5
375	77.2
400	82.5
425	92.7
450	101.1
475	110.3
500	118.7
525	131.3
550	146.5
575	161.7
600	178.8
625	199

Inflow Data

t (min)	Q (L s^{-1})	calc Vol (m^3)
0	1.11	0.000
6	1.11	0.400
20	1.04	1.303
56	1.02	3.527
135	0.80	7.841
145	0.80	8.321
202	0.79	11.040
296	0.68	15.185
360	0.71	17.854
550	0.76	26.233
705	0.76	33.301
705.1	0.00	33.303

Runoff Data

t (min)	Q (L s^{-1})	calc Vol (m^3)
199	0.00	0.000
206	0.09	0.019
220	0.17	0.128
238	0.21	0.333
318	0.17	1.245
495	0.25	3.476
550	0.25	4.301
630	0.26	5.525
650	0.27	5.843
710	*0.27*	*6.815*
760	*0.20*	*7.520*
800	*0.00*	*7.760*

Cells in italic grey have been guessed to estimate the total runoff volume

Table A.2 Field data for Printz

Irrigation Name: **Printz**
Source: Walker 2005
Location: Printz Farm near Ft. Morgan, Colorado, US
Details corn planted on loamy sand, 26/08/1979

Field length: 350 m
Slope: 0.002483
Furrow Spacing 1.544 m

Average Inflow 3.4316 L s^{-1}

Furrow Dimensions

Top Width 0.360 m
Middle Width 0.270 m
Bottom Width 0.160 m
Max Height 0.060 m

Advance Data

x (m)	t (min)
0	0.0
25	8.0
50	13.5
75	20.0
100	26.5
125	32.0
150	37.5
175	44.0
200	50.0
225	55.5
250	65.0
275	72.5
300	84.5
325	100.5
350	120.5

Inflow Data

t (min)	Q (L s^{-1})	calc Vol (m^3)
0	*1.165*	0.000
2	1.165	0.140
3	1.917	0.232
4.5	2.466	0.429
5.5	2.727	0.585
7.5	3.101	0.935
9.5	3.101	1.307
12.5	3.299	1.883
14.5	3.299	2.279
17.5	3.504	2.891
20.5	3.504	3.522
23.5	3.504	4.153
29.5	3.504	5.414
35.5	3.504	6.676
41.5	3.610	7.956
44.5	3.610	8.606
46.5	3.610	9.039
48.5	3.504	9.466
52.5	3.504	10.307
56.5	3.504	11.148
61.5	3.504	12.199
66.5	3.610	13.266
71.5	3.504	14.333
80.5	3.504	16.225
95.5	3.504	19.379
103.5	3.504	21.061
112.5	3.504	22.953
135.5	3.504	27.789
152.5	3.504	31.363
172.5	3.504	35.567
173	0.000	35.620

Runoff Data

t (min)	Q (L s^{-1})	calc Vol (m^3)
120.5	0.000	0.000
121.5	0.087	0.003
122.5	0.114	0.009
123.5	0.145	0.016
124.5	0.145	0.025
125.5	0.162	0.034
127.5	0.179	0.055
130.5	0.216	0.090
134.5	0.255	0.147
138.5	0.298	0.213
142.5	0.343	0.290
148.5	0.343	0.414
155.5	0.392	0.568
162.5	0.443	0.743
180	*0.450*	*1.016*
190	*0.440*	*1.283*
195	*0.300*	*1.394*
200	*0.000*	*1.439*

Cells in italic grey have been guessed to estimate the total runoff volume

Table A.3 Field data for Downs (Irrigation 2 Furrow 3)

Irrigation Name: **Downs**
Source: NCEA
Location: Macalister near Dalby, Qld, Australia
Details Cotton planted on cracking clay soil
Furrow: Irrigation 2 Furrow 3

Field length: 565 m
Slope: 0.001
Furrow Spacing 2 m

Average Inflow 3.4224 L s^{-1}

Furrow Dimensions

Top Width 0.600 m
Middle Width 0.400 m
Bottom Width 0.200 m
Max Height 0.100 m

Advance Data

x (m)	t (min)
0	0.0
110	45.0
220	97.0
330	162.0
440	257.0
550	397.0

Inflow Data

t (min)	Q (L s^{-1})	calc Vol (m^3)
0	2.400	0.000
5	2.400	0.720
10	3.500	1.605
15	3.400	2.640
20	3.200	3.630
25	3.300	4.605
30	3.600	5.640
100	3.600	20.760
105	3.500	21.825
160	3.500	33.375
165	3.400	34.410
170	3.400	35.430
175	3.500	36.465
180	3.400	37.500
185	3.500	38.535
190	3.400	39.570
600	3.400	123.210
602.5	3.400	123.720

Redundant cells have been removed from the data where the inflow remains constant for 3 or more adjacent cells

Runoff Data

t (min)	Q (L s^{-1})	calc Vol (m^3)
424	0.000	0.000
428	0.533	0.064
437	0.655	0.385
445	0.722	0.715
450	0.745	0.935
456	0.768	1.208
466	0.768	1.669
481	0.768	2.360
496	0.892	3.107
512	0.970	4.001
529	0.970	4.991
537	1.025	5.470
543	1.025	5.839
561	1.170	7.024
572	1.230	7.816
586	1.230	8.850
595	1.230	9.514
611	1.230	10.695
616	1.230	11.064
621	1.230	11.433
631	1.200	12.162
646	0.970	13.139
661	0.677	13.880
681	0.408	14.531
696	0.262	14.833
711	0.133	15.010
726	0.067	15.100
741	0.000	15.130

Table A.4 Field data for Kooba

Irrigation Name:	**Kooba**
Source:	Hornbuckle 1999
Location:	Kooba Station, Wunnamurra near Jerilderie, NSW, Australia
Details	corn planted on self mulching clay, 1989-1999
Furrow:	Irrigation 1 Furrow 1

Field length:	443 m
Slope:	0.0005
Furrow Spacing	1.93 m
Average Inflow	2.9265 L s^{-1}

Furrow Dimensions

Top Width	0.500 m
Middle Width	0.300 m
Bottom Width	0.100 m
Max Height	0.200 m

Inflow Data

t (min)	Q (L s^{-1})	calc Vol (m^3)
0	1.424	0.000
24	1.424	2.051
58	1.960	5.502
110	2.240	12.054
234	2.540	29.836
482	2.720	68.970
1114	3.370	184.437
1509	3.450	265.254
1513	0.000	265.668

Runoff Data

t (min)	Q (L s^{-1})	calc Vol (m^3)
1080	0.000	0.000
1120	0.460	0.552
1224	1.680	7.229
1499	2.180	39.074
1570	1.580	47.083
1602	0.910	49.473
1634	0.550	50.875
1753	0.000	52.838

Advance Data

x (m)	t (min)
0	0.0
25	53.0
50	100.0
113	243.0
194	489.0
414	1038.0
443	1080.0

Table A.5 Field data for Merungle Hill

Irrigation Name: **Merungle Hill**
Source: Hornbuckle 1999
Location: Merungle Hill near Leeton, NSW, Australia
Details Citrus planted on Merungle loam (red-brown earth), 1992
Furrow: Chemical treatment, furrow 2

Field length: 189.3 m
Slope: 0.0025
Furrow Spacing 6.2 m

Average Inflow 0.8251 L s^{-1}

Furrow Dimensions

Top Width 1.300 m
Middle Width 0.800 m
Bottom Width 0.100 m
Max Height 0.200 m

Advance Data

x (m)	t (min)
0	0.0
94.67	137.5
189.3	267.5

Inflow Data

t (min)	Q (L s^{-1})	calc Vol (m^3)
0	0.000	0.000
5	0.030	0.005
10	0.090	0.023
15	0.120	0.054
20	0.140	0.093
25	0.140	0.135
30	0.150	0.179
35	0.390	0.260
40	0.480	0.390
45	0.490	0.536
50	0.500	0.684
55	0.510	0.836
60	0.590	1.001
65	0.690	1.193
70	0.720	1.404
75	0.730	1.622
100	0.730	2.717
105	0.720	2.934
110	0.730	3.152
115	0.720	3.369
120	0.730	3.587
150	0.730	4.901
155	0.720	5.118
160	0.730	5.336
165	0.720	5.553
170	0.720	5.769
175	0.730	5.987
180	0.720	6.204
185	0.720	6.420
190	0.730	6.638
195	0.730	6.857
200	0.750	7.079
210	0.750	7.529
215	0.760	7.755
240	0.760	8.895
245	0.780	9.126
250	0.780	9.360
255	0.760	9.591
260	0.780	9.822
290	0.780	11.226
295	0.760	11.457
320	0.760	12.597
325	0.820	12.834
330	0.870	13.088
335	0.870	13.349
340	0.890	13.613
350	0.890	14.147
355	0.900	14.415
360	0.900	14.685
365	0.890	14.954
370	0.890	15.221
375	0.900	15.489
380	0.890	15.758
385	0.900	16.026
390	0.890	16.295
395	0.900	16.563
400	0.900	16.833
405	0.890	17.102
415	0.890	17.636
420	0.980	17.916
425	0.990	18.212
440	0.990	19.103
445	1.010	19.403
475	1.010	21.221
480	1.040	21.528
485	1.140	21.855
490	1.120	22.194
495	1.090	22.526
500	1.040	22.845
505	1.040	23.157
510	1.070	23.474
515	1.060	23.793
525	1.060	24.429
530	1.070	24.749
535	1.060	25.068
540	1.040	25.383
555	1.040	26.319
560	1.010	26.627
565	1.030	26.933
570	1.010	27.239
575	1.030	27.545
585	1.030	28.163
590	0.990	28.466
595	1.030	28.769
600	1.140	29.094
605	1.190	29.444
610	1.200	29.802
615	1.250	30.170
620	1.240	30.543
630	1.240	31.287
635	1.250	31.661
640	1.250	32.036
645	1.270	32.414
655	1.270	33.176
660	1.250	33.554
695	1.250	36.179
700	1.240	36.552
705	1.250	36.926
715	1.250	37.676
720	0.990	38.012
725	0.260	38.199
730	0.080	38.250
735	0.070	38.273
740	0.060	38.292
745	0.040	38.307
750	0.040	38.319
755	0.050	38.333
760	0.030	38.345
765	0.040	38.355
770	0.020	38.364
775	0.000	38.367

Redundant cells have been removed from the data where the inflow remains constant for 3 or more adjacent cells

Runoff Data

t (min)	Q (L s^{-1})	calc Vol (m^3)
267.5	0.000	0.000
270	0.010	0.001
275	0.020	0.005
280	0.030	0.013
285	0.220	0.050
290	0.240	0.119
295	0.250	0.193
300	0.260	0.269
305	0.270	0.349
310	0.260	0.428
315	0.260	0.506
320	0.250	0.583
325	0.260	0.659
330	0.270	0.739
335	0.270	0.820
340	0.290	0.904
345	0.300	0.992
350	0.300	1.082
355	0.300	1.172
360	0.310	1.264
365	0.310	1.357
370	0.330	1.453
375	0.340	1.553
380	0.360	1.658
385	0.390	1.771
390	0.410	1.891

t (min)	Q (L s^{-1})	calc Vol (m^3)	t (min)	Q (L s^{-1})	calc Vol (m^3)	t (min)	Q (L s^{-1})	calc Vol (m^3)
395	0.410	2.014	710	0.700	12.352	1025	0.020	18.328
400	0.430	2.140	715	0.920	12.595	1030	0.020	18.334
405	0.430	2.269	720	0.920	12.871	1035	0.018	18.339
410	0.440	2.399	725	0.970	13.154	1040	0.018	18.345
415	0.450	2.533	730	0.980	13.447	1045	0.018	18.350
420	0.470	2.671	735	1.000	13.744	1050	0.018	18.356
425	0.470	2.812	740	0.980	14.041	1055	0.018	18.361
430	0.470	2.953	745	1.000	14.338	1060	0.018	18.366
435	0.470	3.094	750	1.000	14.638	1065	0.018	18.372
440	0.470	3.235	755	1.000	14.938	1070	0.018	18.377
445	0.480	3.377	760	0.980	15.235	1075	0.018	18.383
450	0.480	3.521	765	0.950	15.524	1080	0.015	18.388
455	0.470	3.664	770	0.900	15.802	1085	0.015	18.392
460	0.480	3.806	775	0.820	16.060	1090	0.010	18.396
465	0.480	3.950	780	0.750	16.295	1095	0.010	18.399
470	0.480	4.094	785	0.680	16.510	1100	0.010	18.402
475	0.490	4.240	790	0.590	16.700	1105	0.008	18.405
480	0.490	4.387	795	0.520	16.867	1110	0.008	18.407
485	0.480	4.532	800	0.470	17.015	1115	0.006	18.409
490	0.490	4.678	805	0.410	17.147	1120	0.006	18.411
495	0.490	4.825	810	0.350	17.261	1125	0.006	18.413
500	0.500	4.973	815	0.310	17.360	1130	0.004	18.414
505	0.500	5.123	820	0.270	17.447	1135	0.006	18.416
510	0.500	5.273	825	0.230	17.522	1140	0.006	18.417
515	0.500	5.423	830	0.220	17.590	1145	0.004	18.419
520	0.520	5.576	835	0.190	17.651	1150	0.004	18.420
525	0.530	5.734	840	0.160	17.704	1155	0.004	18.421
530	0.550	5.896	845	0.140	17.749	1160	0.003	18.422
535	0.550	6.061	850	0.120	17.788	1165	0.003	18.423
540	0.550	6.226	855	0.110	17.822	1170	0.003	18.424
545	0.570	6.394	860	0.100	17.854	1175	0.001	18.425
550	0.540	6.560	865	0.090	17.882	1180	0.001	18.425
555	0.570	6.727	870	0.090	17.909	1185	0.006	18.426
560	0.570	6.898	875	0.070	17.933	1190	0.006	18.428
565	0.570	7.069	880	0.070	17.954	1195	0.006	18.430
570	0.570	7.240	885	0.060	17.974	1200	0.000	18.431
575	0.570	7.411	890	0.060	17.992			
580	0.555	7.580	895	0.060	18.010			
585	0.570	7.748	900	0.070	18.029			
590	0.570	7.919	905	0.060	18.049			
595	0.570	8.090	910	0.060	18.067			
600	0.550	8.258	915	0.050	18.083			
605	0.550	8.423	920	0.050	18.098			
610	0.550	8.588	925	0.050	18.113			
615	0.550	8.753	930	0.050	18.128			
620	0.550	8.918	935	0.050	18.143			
625	0.540	9.082	940	0.050	18.158			
630	0.540	9.244	945	0.050	18.173			
635	0.550	9.407	950	0.050	18.188			
640	0.550	9.572	955	0.050	18.203			
645	0.580	9.742	960	0.050	18.218			
650	0.620	9.922	965	0.050	18.233			
655	0.630	10.109	970	0.040	18.247			
660	0.650	10.301	975	0.040	18.259			
665	0.660	10.498	980	0.030	18.269			
670	0.680	10.699	985	0.020	18.277			
675	0.680	10.903	990	0.030	18.284			
680	0.680	11.107	995	0.020	18.292			
685	0.680	11.311	1000	0.020	18.298			
690	0.690	11.516	1005	0.020	18.304			
695	0.690	11.723	1010	0.020	18.310			
700	0.700	11.932	1015	0.020	18.316			
705	0.700	12.142	1020	0.020	18.322			

Table A.6 Field data for Huntawang

Irrigation Name: **Huntawang**
Source: Hornbuckle personal communication
Location: Huntawang near Hillston, NSW, Australia
Details Cotton
Furrow: Cotton treatment, furrow 3

Field length: 500 m
Slope: 0.0001
Furrow Spacing 2 m

Average Inflow 2.5162 L s^{-1}

Furrow Dimensions

Top Width 0.700 m
Middle Width 0.500 m
Bottom Width 0.260 m
Max Height 0.250 m

Advance Data

x (m)	t (min)
0	0.0
81	45.0
146	104.0
279	247.0
467	577.5

Inflow Data

t (min)	Q (L s^{-1})	calc Vol (m^3)
0	2.614	0.000
15	2.614	2.352
30	3.303	5.015
45	3.303	7.987
60	3.230	10.927
75	3.158	13.801
90	3.088	16.612
105	2.880	19.297
120	2.812	21.858
135	2.745	24.359
150	2.679	26.800
165	2.679	29.211
180	2.614	31.592
195	2.614	33.945
210	2.614	36.297
225	2.549	38.620
240	2.549	40.914
255	2.549	43.209
270	2.614	45.532
285	2.549	47.855
300	2.549	50.149
315	2.614	52.472
330	2.549	54.796
345	2.549	57.090
360	2.549	59.384
375	2.549	61.678
390	2.549	63.972
405	2.614	66.296
420	2.485	68.590
435	2.485	70.827
450	2.485	73.064
465	2.485	75.301
480	2.485	77.538
495	2.485	79.774
510	2.485	82.011
525	2.485	84.248
540	2.485	86.485
555	2.485	88.722
570	2.485	90.959
585	2.485	93.196
600	2.485	95.432
615	2.485	97.669
630	2.485	99.906
645	2.485	102.143
660	2.485	104.380
675	2.485	106.617
690	2.485	108.854
705	2.485	111.090
720	2.485	113.327
735	2.485	115.564
750	0.691	116.993
765	0.503	117.531
780	0.000	117.757

Runoff Data

t (min)	Q (L s^{-1})	calc Vol (m^3)
577.5	0.000	0.000
585	0.420	0.095
600	0.532	0.523
615	0.593	1.030
630	0.658	1.593
645	0.725	2.215
660	0.725	2.867
675	0.725	3.520
690	0.725	4.172
705	0.725	4.825
720	0.832	5.526
735	0.832	6.274
750	0.832	7.023
765	0.832	7.772
780	0.832	8.521
795	0.796	9.254
810	0.658	9.907
825	0.503	10.430
840	0.369	10.822
855	0.275	11.112
870	0.214	11.332
885	0.160	11.500
900	0.113	11.623
915	0.073	11.706
930	0.000	11.739

Table A.7 Field data for Merkley

Irrigation Name: **Merkley**
Source: Merkley 1983 cited in Scaloppi et al. 1995
Location:
Details

Field length: 225 m
Slope: 0.00289
Furrow Spacing 0.8 m

Average Inflow 2.67 L s^{-1}

Furrow Dimensions

Top Width 0.433 m
Middle Width 0.272 m
Bottom Width 0.130 m
Max Height 0.080 m

Advance Data

x (m)	t (min)
0	0
25	2.3
50	5.4
75	8.8
100	13.4
125	17.6
150	22.36
175	27.4
200	32
225	38.5

Runoff Data

t (min)	Q (L s^{-1})	calc Vol (m^3)
38.5	0.00	0.000
46.3	0.55	0.129
49.2	0.65	0.233
52.2	0.72	0.356
57.2	0.79	0.583
62.2	0.91	0.838
67.2	0.91	1.111
70.0	*0.91*	*1.264*
80.0	*0.90*	*1.807*
90.0	*0.20*	*2.137*
100.0	*0.00*	*2.197*

Cells in italic grey have been guessed to estimate the total runoff volume

Table A.8 All advance data for Kooba

Irrigation 1 Furrow 1

See Table A-4

Irrigation 1 Furrow 2

x (m)	t (min)
0	0
25	13
50	38
75	69
100	131
131	240
215	490
430	1030
443	1054

Irrigation 1 Furrow 3

x (m)	t (min)
0	0
25	10
50	27
75	55
100	86
170	240
253	490
443	1027

Irrigation 1 Furrow 4

x (m)	t (min)
0	0
25	24
75	96
115	234
204	481
400	1090
443	1210

Irrigation 2 Furrow 1

x (m)	t (min)
0	0
25	6
50	25
75	31
100	62
150	93
200	154

Irrigation 2 Furrow 2

x (m)	t (min)
0	0
25	5
50	14
75	21
100	31
150	54
200	81
300	146
350	188
400	237
443	288

Irrigation 2 Furrow 3

x (m)	t (min)
0	0
25	7
50	13
75	18
100	27
150	49
200	72
350	182
400	241
443	296

Irrigation 2 Furrow 4

x (m)	t (min)
0	0
25	6
50	13
75	23
100	38
150	64
250	158
300	228
443	390

Irrigation 3 Furrow 1

x (m)	t (min)
0	0
25	5
50	12
75	21
100	31
150	54
200	79
250	115
300	156
350	209
400	249
443	298

Irrigation 3 Furrow 2

x (m)	t (min)
0	0
25	4
50	12
75	18
100	27
150	47
200	69
250	91.2
300	118.2
350	148
400	178
443	211

Irrigation 3 Furrow 3

x (m)	t (min)
0	0
25	5
75	16
100	25
150	42
200	60
250	83
300	104
350	133
400	169
443	203

Irrigation 3 Furrow 4

x (m)	t (min)
0	0
25	4
50	14
75	26
100	46
163	99
200	139
300	259
350	324
443	442

Table A.9 All inflow data for Kooba

Irrigation 1 Furrow 1

See Table A-4

Irrigation 1 Furrow 2

t (min)	Q (L s^{-1})
0	1.12
22	1.12
49	1.68
172	1.63
418	1.74
1050	1.96
1447	2.01
1450	0

Irrigation 1 Furrow 3

t (min)	Q (L s^{-1})
0	1.47
20	1.47
106	1.85
170	1.85
414	2.19
1045	2.19
1445	2.30
1447	0

Irrigation 1 Furrow 4

t (min)	Q (L s^{-1})
0	1.68
18	1.68
104	2.13
228	2.36
469	2.60
1101	2.77
1502	2.77
1506	0

Irrigation 2 Furrow 1

t (min)	Q (L s^{-1})
0	1.55
10	1.55
32	1.55
46	2.77
95	3.19
156	3.13
228	3.07
314	2.89
528	2.77
539	0

Irrigation 2 Furrow 2

t (min)	Q (L s^{-1})
0	1.88
10	1.88
31	1.88
45	2.22
95	2.4
156	2.28
228	2.52
315	2.59
528	2.52
538	0

Irrigation 2 Furrow 3

t (min)	Q (L s^{-1})
0	2.34
10	2.34
30	2.34
44	2.22
94	2.28
155	2.34
227	2.52
314	2.59
527	2.77
536	0

Irrigation 2 Furrow 4

t (min)	Q (L s^{-1})
0	2.22
10	2.22
30	2.22
44	2.40
94	2.40
156	2.52
227	2.71
314	2.71
527	2.83
535	0

Irrigation 3 Furrow 1

t (min)	Q (L s^{-1})
0	1.77
8	1.77
27	3.07
60	3.19
136	3.19
215	3.19
269	3.19
308	3.01
358	3.01
363	1.23
455	1.14
515	1.14
650	1.14
653	0

Irrigation 3 Furrow 2

t (min)	Q (L s^{-1})
0	1.77
10	1.77
31	1.93
65	1.99
140	1.93
219	1.93
272	1.88
280	1.66
312	1.71
362	1.55
458	1.66
519	1.50
658	1.23
665	0

Irrigation 3 Furrow 3

t (min)	Q (L s^{-1})
0	2.83
11	2.83
34	2.89
68	2.83
143	2.89
222	2.89
276	2.89
283	1.77
315	1.66
365	1.66
463	1.71
522	1.55
661	1.55
667	0

Irrigation 3 Furrow 4

t (min)	Q (L s^{-1})
0	2.83
10	2.83
35	3.07
69	3.01
144	3.07
223	3.01
277	3.13
316	3.07
366	3.07
466	2.95
524	3.01
532	1.99
662	1.82
667	0

Table A.10 All runoff data for Kooba

Irrigation 1 Furrow 1

See Table A-4

Irrigation 1 Furrow 2

t (min)	Q_r (L s^{-1})
1054	0
1062	0.11
1090	0.43
1118	0.76
1140	1.63
1248	2.19
1523	1.23
1594	0.58
1626	0.23
1744	0

Irrigation 1 Furrow 3

t (min)	Q_r (L s^{-1})
1027	0
1044	0.21
1052	0.21
1087	0.46
1117	0.62
1220	1.12
1439	1.68
1506	0.91
1538	0.49
1570	0.21
1687	0

Irrigation 1 Furrow 4

t (min)	Q_r (L s^{-1})
1210	0
1218	0.55
1484	1.58
1564	0.92
1596	0.49
1627	0.30
1744	0

Irrigation 2 Furrow 1

t (min)	Q_r (L s^{-1})
0	0
400	0
522	1.77
566	1.93
744	0

Irrigation 2 Furrow 2

t (min)	Q_r (L s^{-1})
288	0
293	0.20
304	0.38
322	0.66
520	2.2
563	2.59
743	0

Irrigation 2 Furrow 3

t (min)	Q_r (L s^{-1})
296	0
301	0.16
321	0.41
517	2.05
559	2.05
741	0

Irrigation 2 Furrow 4

t (min)	Q_r (L s^{-1})
390	0
514	1.05
556	1.14
740	0

Irrigation 3 Furrow 1

t (min)	Q_r (L s^{-1})
298	0
303	0.24
335	0.92
337	0.81
357	0.81
450	0.81
511	0.74
649	0.78
816	0

Irrigation 3 Furrow 2

t (min)	Q_r (L s^{-1})
211	0
223	0.41
243	0.49
305	0.78
337	0.96
357	0.92
453	1.05
513	1.05
651	1.05
817	0

Irrigation 3 Furrow 3

t (min)	Q_r (L s^{-1})
203	0
208	0.31
227	0.49
244	0.59
248	0.92
358	1.09
454	1.09
516	1.14
654	1.07
819	0

Irrigation 3 Furrow 4

t (min)	Q_r (L s^{-1})
442	0
446	0.28
473	0.59
507	0.88
645	0.78
809	0

APPENDIX B

C++ code for

KostiakovCalibrationObject

"KostiakovCalibrationObject" represents the part of IPARM that performs the majority of the parameter optimisation process. Prior to the calibration process, IPARM loads all necessary data from the interface into the KostiakovCalibrationObject. The software code is comprised of a header (*.h*) file containing the declarations and a *.cpp* file containing the functions. The code refers to "_MainForm" which represents the main unit of IPARM. The code is written in C++ for Borland Builder 6.

KostiakovCalibrationObject.h

```
//---------------------------------------------------------------------------
#ifndef KostiakovCalibrationObjectH
#define KostiakovCalibrationObjectH
#include <algorithm>
#include <numeric>
#include <Classes.hpp>
#pragma package(smart_init)
#include <iostream>
#include <vector>
using namespace std;
class TKostiakovCalibrationObject;

class TWaitThread;

class TKostiakovCalibrationObject:public TObject
{
   public:
   __fastcall TKostiakovCalibrationObject(void);
   bool __fastcall ExecuteCalibration(void);
   double TopWidth,MiddleWidth,BottomWidth,MaxHeight;
   double Inflow,Qpm,Slope,FieldLength,RunoffPos;
   double n,sy,Beta,MidDepth,MidDist;
   long double c,m;
   long double a,k,f0,C;
   double Inia,Inik,Inif0,IniC;
   long double a_Upper,k_Upper,f0_Upper,C_Upper;
   long double a_Lower,k_Lower,f0_Lower,C_Lower;
   double Sastep,Skstep,Sf0step,SCstep;
   bool aOP,kOP,f0OP,COP;
   int OptimisationType;
   int SurfaceStorageType;
   int InflowVariationType;
   bool AlternativeSurfaceStorage;
   double num_P;
   vector<double> VolInflow_P,UpStreamA0_P,VCalc_P;
   double RunoffWeight,StartOfRunoff;
   double UpStreamDepth,UpStreamArea;
   long double __fastcall WettedPerim(long double y, long double Bw);
   double __fastcall WettedPerimSimple(double y);
   double __fastcall nFromA0(double Qinsec, double Bw, double S0, double Ym, double A0);
   long double __fastcall Normaldepth(double Qinsec, double Bw, double S0, double n, double Ym);
   vector<double> MeasuredAdvanceX,MeasuredAdvanceT;
   vector<double> RawInflowTime,RawInflowRate;
   vector<double> MeasuredRunoffT,MeasuredRunoffR,MeasuredRunoffV;
   vector<long double> sz1,sz2;
   vector<double> CalculatedRunoffV;
   long double PowerError,p,r;
   long double SSSERun,SSSEad;
   vector<double> ProcessedInflowT,ProcessedInflowV;
   long double SSSECurrent;
   vector<double> __fastcall CalcX(vector<double> MeasT,long double t_a, long double t_k, long double t_f0,
long double t_C, vector<double> VolInflow, vector<double> UpStreamA0);
   vector<double> __fastcall CalcXAdvanced(vector<double> MeasT,long double t_a, long double t_k,
long double t_f0, long double t_C, vector<double> VolInflow, vector<double> UpStreamA0);
   vector<double> __fastcall CalcXImagine(vector<double> MeasT,long double t_a, long double t_k,
long double t_f0, long double t_C, vector<double> VolInflow, vector<double> UpStreamA0);
   vector<double> __fastcall Calcrun(vector<double> VolInflowRunoff, long double t_a, long double t_k,
long double t_f0, long double t_C, vector<double> UpStreamA0Runoff);
```

```
    vector<double> __fastcall CalcrunAdvanced(vector<double> VolInflowRunoff, long double t_a, long double t_k,
long double t_f0, long double t_C, vector<double> UpStreamA0Runoff);
    long double __fastcall Objective_Advance(vector<double> VolInflow, long double t_a, long double t_k,
long double t_f0, long double t_C, vector<double> UpStreamA0);
    void __fastcall UpdateDisplayRunoff(long double SSSE1, double num, vector<double> VolInflow,
vector<double> UpStreamA0, vector<double> VCalc);
    void __fastcall UpdateDisplayAdvance(long double SSSE1, double num, vector<double> VolInflow,
vector<double> UpStreamA0);
    __property bool StopOptimising = { read = GetStopOptimising, write = SetStopOptimising };
    bool finished;
    __property double MaxTime = { read = GetMaxTime };
    vector<double> VSMeasAd,VSMeasRun;
    vector<double> VSCalcAd,VSCalcRun;
    vector<double> VIMeasAd,VIMeasRun;
    vector<double> VICalcAd,VICalcRun;
    bool AdvancedResultsReady;
    __property bool IsUsingRunoff = { read = GetIsUsingRunoff };
private:
    void ThreadedCalibration(void* Data);
    long double __fastcall CalPower(vector<double> MeasX, vector<double> MeasT, long double & t_pm,
long double & t_rm);
    long double __fastcall DiffPower(vector<double> MeasX, vector<double> MeasT, long double t_p,
long double t_r);
    void __fastcall CalculateSurfaceStorageFactor(void);
    vector<double> __fastcall RunoffVolume(vector<double> MRT, vector <double> MRR, double ST);
    bool V_StopOptimising;
    void __fastcall GetVariableInflow_Advance(vector<double> MT, vector<double> &VolInflowm,
vector<double> &UpStreamA0m);
    void __fastcall GetVariableInflow_Runoff(vector<double> MRT, vector<double> &VolInflowRunoffm,
vector<double> &UpStreamA0Runoffm);
    void __fastcall Initial_Search(vector<double> VolInflow, vector<double> VolInflowRunoff,long double
&t_am,long double &t_km,long double &t_f0m,long double &t_Cm, vector<double> UpStreamA0,
vector<double> UpStreamA0Runoff, int sc);
    void __fastcall new_a(long double t_a,int sc);
    long double __fastcall SubShape(double La,long double t_a, int sc);
    long double __fastcall Objective_Run(vector<double> VolInflow, vector<double> VolInflowRunoff,
long double t_a, long double t_k, long double t_f0, long double t_C, vector<double> UpStreamA0,
vector<double> UpStreamA0Runoff, int sc);
    long double __fastcall SStorage(double t_A0, double Xi,double CurrentT);
    void __fastcall SetStopOptimising(bool value);
    bool __fastcall GetStopOptimising();
    long double __fastcall IterA(vector<double> VolInflow, vector<double> VolInflowRunoff, long double & t_am,
long double t_k, long double t_f0, long double t_C, vector<double> UpStreamA0, vector<double>
UpStreamA0Runoff,long double astep, long double & Ja1m, int sc);
    long double __fastcall IterA_Advance(vector<double> VolInflow,long double & t_am, long double t_k,
long double t_f0, long double t_C, vector<double> UpStreamA0,long double astep, long double & Ja1m);
    long double __fastcall IterK(vector<double> VolInflow, vector<double> VolInflowRunoff, long double t_a,
long double & t_km, long double t_f0, long double t_C, vector<double> UpStreamA0, vector<double>
UpStreamA0Runoff, long double kstep, long double & Jk1m,int sc);
    long double __fastcall IterK_Advance(vector<double> VolInflow, long double t_a, long double & t_km,
long double t_f0, long double t_C, vector<double> UpStreamA0, long double kstep, long double & Jk1m);
    long double __fastcall IterF(vector<double> VolInflow, vector<double> VolInflowRunoff, long double t_a,
long double t_k, long double & t_f0m, long double t_C, vector<double> UpStreamA0, vector<double>
UpStreamA0Runoff, long double fstep, long double & Jf1m,int sc);
    long double __fastcall IterF_Advance(vector<double> VolInflow, long double t_a, long double t_k,
long double & t_f0m, long double t_C, vector<double> UpStreamA0, long double fstep, long double & Jf1m);
    long double __fastcall IterC(vector<double> VolInflow, vector<double> VolInflowRunoff, long double t_a,
ong double t_k, long double t_f0, long double & t_Cm, vector<double> UpStreamA0, vector<double>
UpStreamA0Runoff, long double Cstep, long double & JC1m,int sc);
    long double __fastcall IterC_Advance(vector<double> VolInflow, long double t_a, long double t_k,
long double t_f0, long double & t_Cm, vector<double> UpStreamA0, long double Cstep, long double & JC1m);
    double __fastcall GetMaxTime();
    double __fastcall GetVariableSSadvance(double currentT,int advancepoint,double tempdist,
double CurrentUSarea);
    double __fastcall GetVariableSSrunoff(double currentT,int advancepoint,double CurrentUSarea);
    vector<double> RawUpstreamArea;
    vector<double> RawUpstreamAreaChange;
    vector<double> InstQadvance;
    vector<double> InstQrunoff;
    vector<double> OldCalcX,OldCalcXImagine;
    bool __fastcall GetIsUsingRunoff();
};
#endif
```

KostiakovCalibrationObject.cpp

```
#pragma hdrstop
#include "KostiakovCalibrationObject.h"
#include "math.h"
#include "SynchedThreads.h"
#include "math.h"
#include "IPARM.h"
#pragma package(smart_init)
#include <vcl.h>
#pragma hdrstop
#include <stdio.h>
#include <stdlib.h>
#include <conio>
#include <iostream>
#include <math>
#include <dos.h>
#pragma argsused
using namespace std;
#include <algorithm>
#include <clx.h>
#include <string>
////////////////////////////////////////////////////////////////////////////////////////////////////////////////////////////////////////////////////////
__fastcall TKostiakovCalibrationObject::TKostiakovCalibrationObject(void)
{
   c=0.0;
   m=0.0;
   V_StopOptimising=false;
   a_Upper=0.9999999999999999;        //these values may have to modified for use in border irrigation
   k_Upper=0.9999999999999999;
   f0_Upper=0.9999999999999999;
   C_Upper=0.9999999999999999;
   a_Lower=0.0;
   k_Lower=0.0;
   f0_Lower=0.0;
   C_Lower=0.0;
   AlternativeSurfaceStorage=false;
   AdvancedResultsReady=false;
}
////////////////////////////////////////////////////////////////////////////////////////////////////////////////////////////////////////////////////////
bool __fastcall TKostiakovCalibrationObject::ExecuteCalibration(void)
{                                                  //the main driver for the calibration, started in a thread
   AdvancedResultsReady=false;                     //to free up the user interface
   if ((InflowVariationType==1)&&(OptimisationType>1))
      AlternativeSurfaceStorage=true;
   else
      AlternativeSurfaceStorage=false;
   TWaitThread* CalibrationThread;
   CalibrationThread=NULL;
   MsgWaitForThread(CalibrationThread, ThreadedCalibration);
   if (CalibrationThread!=NULL)  CalibrationThread->AbortThread();
   delete CalibrationThread;
   return true;
}
////////////////////////////////////////////////////////////////////////////////////////////////////////////////////////////////////////////////////////
void __fastcall TKostiakovCalibrationObject::SetStopOptimising(bool value)
{
   V_StopOptimising = value;
}
////////////////////////////////////////////////////////////////////////////////////////////////////////////////////////////////////////////////////////
bool __fastcall TKostiakovCalibrationObject::GetStopOptimising()
{
   return V_StopOptimising;
}
////////////////////////////////////////////////////////////////////////////////////////////////////////////////////////////////////////////////////////
void TKostiakovCalibrationObject::ThreadedCalibration(void* Data)
{                                  //this is the main calibration function
   finished=false;
   int Actual_Numad=MeasuredAdvanceX.size();
   int Actual_Numrun=MeasuredRunoffT.size();     //determine the number of input data points
   int Actual_Numinflow=RawInflowTime.size();
   OldCalcX.resize(MeasuredAdvanceX.size(),0);
   OldCalcXImagine.resize(MeasuredRunoffT.size(),0);
```

```
    for (int kk=0;kk<MeasuredAdvanceX.size();kk++)
       OldCalcX[kk]=MeasuredAdvanceX[kk];
    for (int kk=0;kk<MeasuredRunoffT.size();kk++)
       OldCalcXImagine[kk]=RunoffPos+10.0;
    long double SSSE,SSSE1,SSSE2, astep,kstep,fstep,rstep,Cstep,Ja,Ja1,Jk,Jk1,Jf,Jf1,JC,JC1,Jr,Jr1;
    PowerError=CalPower(MeasuredAdvanceX, MeasuredAdvanceT, p, r);          //fit the power curve
    CalculateSurfaceStorageFactor();                    // calculate the surface storage
    int startnum=1, num=startnum, repeat=25, sc=20;
    int sw=0,sw1=0;
    if ((OptimisationType==1)||(OptimisationType==3))          //optimise based on the advance and runoff data
    {
       MeasuredRunoffV.resize(Actual_Numrun);
       sz1.resize(Actual_Numrun);
       sz2.resize(Actual_Numrun);
       CalculatedRunoffV.resize(Actual_Numrun);
       long double sum,sum2;
       MeasuredRunoffV=RunoffVolume(MeasuredRunoffT, MeasuredRunoffR, StartOfRunoff);
       vector<double> VolInflow, UpStreamA0, VolInflowRunoff, UpStreamA0Runoff;
       GetVariableInflow_Advance(MeasuredAdvanceT,VolInflow,UpStreamA0);
       GetVariableInflow_Runoff(MeasuredRunoffT,VolInflowRunoff,UpStreamA0Runoff);
       _MainForm->UpdateProcessedInflow();          //outputs estimated inflow volumes to the GUI
       Initial_Search(VolInflow,VolInflowRunoff,a,k,f0,C,UpStreamA0,UpStreamA0Runoff,sc);
       int lc=0;
       while (num<=repeat)
       {
          astep= Sastep*pow(0.5,(num-1));              //reduces the steps sizes by half for every new iteration
          kstep= Skstep*pow(0.5,(num-1));
          fstep= Sf0step*pow(0.5,(num-1));
          Cstep=SCstep*pow(0.5,(num-1));
          new_a(a,sc);
          SSSE1=Objective_Run(VolInflow,VolInflowRunoff,a,k,f0,C,UpStreamA0,UpStreamA0Runoff,sc);
          _MainForm->SSSEOut=SSSE1;
          sw=0;
          Ja=0;
          Jk=0;
          Jf=0;
          JC=0;
          while (sw<1)
          {
             Ja1=0;
             Jk1=0;                  //reset the J storage parameters for new step sizes
             Jf1=0;
             JC1=0;
             _MainForm->SGo();               //just lets the user know that  the calibration is still working
             lc++;
             if (aOP)                  //tests to see if the user wants to optimise a
             {
                SSSE=IterA(VolInflow,VolInflowRunoff,a,k,f0,C,UpStreamA0,UpStreamA0Runoff,astep,Ja1,sc);
                new_a(a,sc);          //a has changed so recalculate storage factors
             }
             else
                SSSE=Objective_Run(VolInflow,VolInflowRunoff,a,k,f0,C,UpStreamA0,UpStreamA0Runoff,sc);
             if (StopOptimising)  sw=1;
             if (kOP)
                SSSE=IterK(VolInflow,VolInflowRunoff,a,k,f0,C,UpStreamA0,UpStreamA0Runoff,kstep,Jk1,sc);
             else
                SSSE=Objective_Run(VolInflow,VolInflowRunoff,a,k,f0,C,UpStreamA0,UpStreamA0Runoff,sc);
             if (StopOptimising)  sw=1;
             if (f0OP)
                SSSE=IterF(VolInflow,VolInflowRunoff,a,k,f0,C,UpStreamA0,UpStreamA0Runoff,fstep,Jf1,sc);
             else
                SSSE=Objective_Run(VolInflow,VolInflowRunoff,a,k,f0,C,UpStreamA0,UpStreamA0Runoff,sc);
             if (StopOptimising)  sw=1;
             if (COP)
                SSSE=IterC(VolInflow,VolInflowRunoff,a,k,f0,C,UpStreamA0,UpStreamA0Runoff,Cstep,JC1,sc);
             else
                SSSE=Objective_Run(VolInflow,VolInflowRunoff,a,k,f0,C,UpStreamA0,UpStreamA0Runoff,sc);
             SSSE=IterR(L,VolInflow,VolInflowRunoff,MeasX,MeasT,MeasRT,MeasRV,a,k,f0,UpStreamA0,
UpStreamA0Runoff,r,sy,sz,sz2,weight,rstep,Jr1,sc,runoffstart);
             Ja+=Ja1;
             Jk+=Jk1;                  //adds the new values of J to the old values
             Jf+=Jf1;
             JC+=JC1;
             sw1=0;
             while (sw1==0)            //////////---GROUP ITERATIONS
```

```
            {
               if (StopOptimising)  sw1=1;
               if (StopOptimising)  sw=1;
               if (aOP)
               {
                  a=a+(astep*Ja)*0.01;
                  if (a<a_Lower)  a=a_Lower;
                  if (a>a_Upper)  a=a_Upper;
                  new_a(a,sc);
               }
               if (kOP)
               {
                  k=k+(kstep*Jk)*0.01;
                  if (k>k_Upper)  k=k_Upper;
                  if (k<k_Lower)  k=k_Lower;
               }
               if (f0OP)
               {
                  f0=f0+(fstep*Jf)*0.01;
                  if (f0<f0_Lower)  f0=f0_Lower;
                  if (f0>f0_Upper)  f0=f0_Upper;
               }
               if (COP)
               {
                  C=C+(Cstep*JC)*0.01;
                  if (C<C_Lower)  C=C_Lower;
                  if (C>C_Upper)  C=C_Upper;
               }
               SSSE2=Objective_Run(VolInflow,VolInflowRunoff,a,k,f0,C,UpStreamA0,UpStreamA0Runoff,sc);
               if (SSSE2>=SSSE)
               {
                  if (num==repeat)  finished=true;
                  sw1=1;
                  if (aOP)  a=a-(astep*Ja)*0.005;
                  if (kOP)  k=k-(kstep*Jk)*0.005;          //moves the parameters back one half step
                  if (f0OP)  f0=f0-(fstep*Jf)*0.005;
                  if (COP)   C=C-(Cstep*JC)*0.005;
                  SSSE2=Objective_Run(VolInflow,VolInflowRunoff,a,k,f0,C,UpStreamA0,UpStreamA0Runoff,sc);
               }
               SSSE=SSSE2;
            }
            if (SSSE>=SSSE1)  sw=sw+1;
            SSSE1=SSSE;
         }
         double percentdone,numd=num,repeatd=repeat;
         percentdone=(numd/repeatd)*100;
         CalculatedRunoffV=Calcrun(VolInflowRunoff,a,k,f0,C,UpStreamA0Runoff);
         sum=0;
         sum2=0;
         for (int I=0;I<Actual_Numrun;I++)
         {
            sum=sum+pow((MeasuredRunoffV[I]-CalculatedRunoffV[I]),2);
            sum2=sum2+powI(MeasuredRunoffV[I],2);
         }
         SSSERun=100*(powI((sum/sum2),0.5));
         _MainForm->SSSErunOut=SSSERun;
         UpdateDisplayRunoff(SSSE1,percentdone,VolInflow,UpStreamA0,CalculatedRunoffV);
         if (StopOptimising)
           num=100;
         num=num+1;
      }
      vector<double> Xcalctemp, Vcalctemp;          //adanced results for the main interface
      Xcalctemp= CalcXAdvanced(MeasuredAdvanceT,a,k,f0,C,VolInflow,UpStreamA0);
      Vcalctemp=CalcrunAdvanced(VolInflowRunoff,a,k,f0,C,UpStreamA0Runoff);
      AdvancedResultsReady=true;
   }
   else
   {                          //using advance data only
      vector<double> VolInflow, UpStreamA0;
      GetVariableInflow_Advance(MeasuredAdvanceT,VolInflow,UpStreamA0);
      _MainForm->UpdateProcessedInflow();
      while (num<=repeat)
      {
         astep= Sastep*pow(0.5,(num-1));
         kstep= Skstep*pow(0.5,(num-1));         //reduces the steps sizes by half for every new iteration
```

```
fstep= Sf0step*pow(0.5,(num-1));
Cstep=SCstep*pow(0.5,(num-1));
SSSE1= Objective_Advance(VolInflow,a,k,f0,C,UpStreamA0);
_MainForm->SSSEOut=SSSE1;
sw=0;
Ja=0;          //reset the J storage parameters for new step sizes
Jk=0;
Jf=0;
JC=0;
while (sw<1)
{
   _MainForm->SGo();    //just lets the user know that  the calibration is still working
   Ja1=0;
   Jk1=0;
   Jf1=0;
   JC1=0;
   if (aOP)
      SSSE=IterA_Advance(VolInflow,a,k,f0,C,UpStreamA0,astep,Ja1);
   else
      SSSE= Objective_Advance(VolInflow,a,k,f0,C,UpStreamA0);
   if (StopOptimising)  sw=1;
   if (kOP)
      SSSE=IterK_Advance(VolInflow,a,k,f0,C,UpStreamA0,kstep,Jk1);
   else
      SSSE= Objective_Advance(VolInflow,a,k,f0,C,UpStreamA0);
   if (StopOptimising)  sw=1;
   if (f0OP)
      SSSE=IterF_Advance(VolInflow,a,k,f0,C,UpStreamA0,fstep,Jf1);
   else
      SSSE= Objective_Advance(VolInflow,a,k,f0,C,UpStreamA0);
   if (StopOptimising)  sw=1;
   if (COP)
      SSSE=IterC_Advance(VolInflow,a,k,f0,C,UpStreamA0,Cstep,JC1);
   else
      SSSE= Objective_Advance(VolInflow,a,k,f0,C,UpStreamA0);
   if (StopOptimising)  sw=1;
   Ja=Ja+Ja1;
   Jk=Jk+Jk1;
   Jf=Jf+Jf1;
   JC=JC+JC1;
   sw1=0;
   while (sw1==0)              //////////---GROUP ITERATIONS
   {
      if (StopOptimising)  sw1=1;
      if (StopOptimising)  sw=1;
      if (aOP)
      {
         a=a+(astep*Ja)*0.01;
         if (a<a_Lower)  a=a_Lower;
         if (a>a_Upper)  a=a_Upper;
      }
      if (kOP)
      {
         k=k+(kstep*Jk)*0.01;
         if (k<k_Lower)  k=k_Lower;
         if (k>k_Upper)  k=k_Upper;
      }
      if (f0OP)
      {
         f0=f0+(fstep*Jf)*0.01;
         if (f0<f0_Lower)  f0=f0_Lower;
         if (f0>f0_Upper)  f0=f0_Upper;
      }
      if (COP)
      {
         C=C+(Cstep*JC)*0.01;
         if (C<C_Lower)  C=C_Lower;
         if (C>C_Upper)  C=C_Upper;
      }
      SSSE2=Objective_Advance(VolInflow,a,k,f0,C,UpStreamA0);
      if (SSSE2>=SSSE)
      {
         sw1=1;
         if (aOP)  a=a-(astep*Ja)*0.005;
         if (kOP)  k=k-(kstep*Jk)*0.005;
```

```
                if (f0OP)  f0=f0-(fstep*Jf)*0.005;
                if (COP)  C=C-(Cstep*JC)*0.005;
                SSSE2=Objective_Advance(VolInflow,a,k,f0,C,UpStreamA0);
              }
              SSSE=SSSE2;
            }
            if (SSSE>=SSSE1)  sw=sw+1;
            SSSE1=SSSE;
          }
          double percentdone,numd=num,repeatd=repeat;
          percentdone=(numd/repeatd)*100;
          UpdateDisplayAdvance(SSSE1,percentdone,VolInflow,UpStreamA0);
          if (StopOptimising)  num=100;
          num=num+1;
        }
        vector<double> Xcalctemp;
        Xcalctemp= CalcXAdvanced(MeasuredAdvanceT,a,k,f0,C,VolInflow,UpStreamA0);
        AdvancedResultsReady=true;
    }
}
//////////////////////////////////////////////////////////////////////////////////////////////////////////////////////////////////////////////////////
long double __fastcall TKostiakovCalibrationObject::CalPower(vector<double> MeasX, vector<double> MeasT,
long double & t_p, long double & t_r)
{                                          //fits the power curve to the advance data and calcaultes p and r
    int t1,sw1,t2,sw;
    long double diff,diff1,newdiff,diff2;
    double pstep=0.1, rstep=0.1,jpstep=1, jrstep=1;
    int lastpoint=MeasX.size()-1;
    float jr,jp;
    for (t1=0;t1<lastpoint;t1++)
    {
        if (MeasT[t1]<=0)
            MeasT[t1]=0.001;
    }
    t_p=MeasX[0]/( powl((MeasT[0]),(log(MeasX[0]/MeasX[lastpoint]))/log(MeasT[0]/MeasT[lastpoint])));
    t_r=(log(MeasX[0]/MeasX[lastpoint]))/(log(MeasT[0]/MeasT[lastpoint]));
    diff= DiffPower(MeasX,MeasT,t_p,t_r);
    for (t1=1;t1<=10;t1++)                          //repeats the process 10 times with reducing step sizes
    {
        jr=0;
        jp=0;
        sw1=0;
        while (sw1==0)
        {
            diff1= DiffPower(MeasX,MeasT,t_p,t_r);
            for (t2=1;t2<=2;t2++)
            {
                sw=0;
                diff= DiffPower(MeasX,MeasT,t_p,t_r);
                while (sw==0)
                {
                    t_p=t_p+pstep;
                    jp=jp+jpstep;
                    if (t_p<=0)            // prevents p from becoming negative
                    {
                        t_p=0.00000001;
                        sw=1;
                    }
                    newdiff = DiffPower(MeasX,MeasT,t_p,t_r);
                    if (newdiff>=diff)
                    {
                        sw=1;
                        t_p=t_p-pstep;
                        jp=jp-jpstep;
                    }
                    diff=newdiff;
                }
                pstep=(-1)*pstep;
                jpstep=jpstep*(-1);
            }
            for (t2=1;t2<=2;t2++)
            {
                diff= DiffPower(MeasX,MeasT,t_p,t_r);
                sw=0;
                while (sw==0)
```

```
            {
               t_r=t_r+rstep;
               jr=jr+jrstep;
               if (t_r<=0)          // prevents r from becoming negative
               {
                  t_r=0.00000001;
                  sw=1;
               }
               newdiff = DiffPower(MeasX,MeasT,t_p,t_r);
               if (newdiff>=diff)
               {
                  sw=1;
                  t_r=t_r-rstep;
                  jr=jr-jrstep;
               }
               diff=newdiff;
            }
            rstep=(-1)*rstep;
            jrstep=jrstep*(-1);
         }
         diff= DiffPower(MeasX,MeasT,t_p,t_r);
         sw=0;
         while (sw==0)
         {
            t_r=t_r+jr*rstep*0.1;
            t_p=t_p+jp*pstep*0.1;
            newdiff = DiffPower(MeasX,MeasT,t_p,t_r);
            if (newdiff>=diff)
            {
               sw=1;
               t_r=t_r-jr*rstep*0.1;
               t_p=t_p-jp*pstep*0.1;
            }
            diff=newdiff;
         }
         diff2= DiffPower(MeasX,MeasT,t_p,t_r);
         if (diff2>=diff1)  sw1=1;
      }
      pstep=pstep*0.1;
      rstep=rstep*0.1;
      PowerError=diff2;
      _MainForm->DisplayPowerResults();
   }
   return diff2;
}
//////////////////////////////////////////////////////////////////////////////////////////////////////////////////////////////////////////////
long double __fastcall TKostiakovCalibrationObject::DiffPower(vector<double> MeasX, vector<double> MeasT,
long double t_p, long double t_r)
{                                   //the objective function to fit the power curve
   int Xsize=MeasX.size();
   long double Xsize1=MeasX.size();
   long double X1,Xdiffsum=0;
   for (int num1=0;num1<Xsize;num1++)
   {
      X1=t_p*powl(MeasT[num1],t_r);
      Xdiffsum=Xdiffsum+ powl((MeasX[num1]-X1),2);          //sum of square errors between measured advance
   }                                                        // and power curve
   return (Xdiffsum)/Xsize1;
}
//////////////////////////////////////////////////////////////////////////////////////////////////////////////////////////////////////////////
void __fastcall TKostiakovCalibrationObject::CalculateSurfaceStorageFactor(void)
{                           //calculates the surface storage factor sy via the user choice
   int problemin=0, num_area_points=500;
   double xs,Yis,area;
   if (SurfaceStorageType==2)              //calculates sy from two depth measurements
   {
      if (MidDepth==0)
      {
         sy=0.77;
         problemin=1;
      }
      else
      {
         if (MidDist==0)
         {
```

```
            sy=0.77;
            problemin=1;
         }
         else
         {
            if (MidDepth<0)
            {
               sy=0.77;
               problemin=1;
            }
            else
            {
               if (MidDist<0)
               {
                  sy=0.77;
                  problemin=1;
               }
               else
               {
                  if (MidDepth<(UpStreamDepth-0.0001))
                  {
                     Beta=(log(MidDepth/UpStreamDepth))/(log(1-MidDist/FieldLength));
                     double VSs=0;
                     for (int xpoint=0;xpoint<=500;xpoint++)
                     {
                        xs=xpoint*(FieldLength/num_area_points);
                        Yis=UpStreamDepth*pow((1-xs/FieldLength),Beta);
                        area = BottomWidth*Yis+(c*powl(Yis,(m+1)))/(m+1);
                        VSs=VSs+area*(FieldLength/num_area_points);
                     }
                     sy=VSs/(FieldLength*UpStreamArea);
                  }
                  else
                  {
                     Yis=(UpStreamDepth+MidDepth)*0.5;
                     area = BottomWidth*Yis+(c*powl(Yis,(m+1)))/(m+1);
                     double VSs=MidDist*area;
                     for (int xpoint=0;xpoint<=500;xpoint++)
                     {
                        xs=xpoint*((FieldLength-MidDist)/num_area_points);
                        Yis=MidDepth*pow((1-xs/(FieldLength-MidDist)),Beta);
                        area = BottomWidth*Yis+(c*powl(Yis,(m+1)))/(m+1);
                        VSs=VSs+area*((FieldLength-MidDist)/num_area_points);
                     }
                     sy=VSs/(FieldLength*UpStreamArea);
                  }
               }
            }
         }
      }
   }
   else
   {
      if (SurfaceStorageType==1)
      {                    ///calculate surface storage coefficient from beta
         double VSs=0;
         for (int xpoint=0;xpoint<=500;xpoint++)
         {
            xs=xpoint*(FieldLength/num_area_points);
            Yis=UpStreamDepth*pow((1-xs/FieldLength),Beta);
            area = BottomWidth*Yis+(c*powl(Yis,(m+1)))/(m+1);
            VSs=VSs+area*(FieldLength/num_area_points);
         }
         sy=VSs/(FieldLength*UpStreamArea);
      }
      else
         sy=sy;
   }
   if (problemin==1)
   {
      Application->MessageBox("There is a problem with midpoint depth/distance.  A value for the shape factor of
0.77 has been assumed","Input Error", MB_OK | MB_ICONEXCLAMATION);
   }
   _MainForm->DisplaySurfaceStorage();
}
```

```
////////////////////////////////////////////////////////////////////////////////////////////////////////////////////////////////////////////////////
vector<double> __fastcall TKostiakovCalibrationObject::RunoffVolume(vector<double> MRT, vector <double>
MRR, double ST)
{                                   //estimates runoff volumes from measured rates and times
   int s=MRT.size();
   vector<double> MRV(s);
   MRV[0]=((MRR[0])/2)*(MRT[0]-ST)*60.0;
   for (int num=1;num<s;num++)
      MRV[num]=MRV[num-1]+ (((MRR[num]+MRR[num-1]))*0.5)*(60.0*MRT[num]-60.0*MRT[num-1]);
   return MRV;
}
////////////////////////////////////////////////////////////////////////////////////////////////////////////////////////////////////////////////////
void __fastcall TKostiakovCalibrationObject::GetVariableInflow_Advance(vector<double> MT, vector<double>
&VolInflow, vector<double> &UpStreamA0)
{                                   //calculates the upstream area from measured inflow and supplied advance times
   int PrevRowCount=0,  vsize=MT.size();
   double oldrate=1.2;
   ProcessedInflowT.resize(vsize+1);
   ProcessedInflowV.resize(vsize+1);
   VolInflow.resize(vsize);
   UpStreamA0.resize(vsize);
   InstQadvance.resize(vsize);
   ProcessedInflowT[0]=0.0;
   ProcessedInflowV[0]=0.0;
   int NumIR=RawInflowTime.size();
   RawUpstreamArea.resize(NumIR,0);
   if (NumIR>0)
      RawUpstreamAreaChange.resize((NumIR-1),0);
   else
      RawUpstreamAreaChange.resize(0,0);
   long double VarY;
   if (OptimisationType>1)       //variable inflow
   {
      double tempUSarea;
      if (AlternativeSurfaceStorage)         //the SSS (surface storage smoothing) technique
      {
         for (int kk=0;kk<NumIR;kk++)
         {
            if (oldrate!=RawInflowRate[kk])
            {
               VarY = Normaldepth(RawInflowRate[kk],BottomWidth,Slope,n,MaxHeight);
               tempUSarea=BottomWidth*VarY+(c*powl(VarY,(m+1)))/(m+1);
               oldrate=RawInflowRate[kk];
            }
            RawUpstreamArea[kk]=tempUSarea;
            if (kk>0)
               RawUpstreamAreaChange[kk-1]=(RawUpstreamArea[kk]-RawUpstreamArea[kk-
1])/(RawInflowTime[kk]-RawInflowTime[kk-1]);
         }
      }
      double Vol,Vol2,CurrentQ,a,b;
      for (int J=0;J<vsize;J++)
      {
         Vol=0;
         Vol2=0;
         for (int K=0;K<(NumIR-1);K++)
         {
            if (RawInflowTime[K+1]>=MT[J])
            {
               b = (RawInflowRate[K+1]-RawInflowRate[K])/(RawInflowTime[K+1]-RawInflowTime[K]);
               Vol2=(( (2*RawInflowRate[K]+b*(MT[J]-RawInflowTime[K]))*0.5)*60.0)*(MT[J]-RawInflowTime[K]);
               CurrentQ=(RawInflowRate[K]+b*(MT[J]-RawInflowTime[K]));
               K=NumIR;
            }
            else
               Vol=Vol+(((RawInflowRate[K]+RawInflowRate[K+1])*0.5)*60.0)*(RawInflowTime[K+1]-
RawInflowTime[K]);
         }
         VolInflow[J]=Vol+Vol2;
         VarY = Normaldepth(CurrentQ,BottomWidth,Slope,n,MaxHeight);
         UpStreamA0[J]= BottomWidth*VarY+(c*powl(VarY,(m+1)))/(m+1);
         ProcessedInflowV[1+J+PrevRowCount]=VolInflow[J];
         ProcessedInflowT[1+J+PrevRowCount]=MT[J];
         InstQadvance[J]=CurrentQ;
      }
```

```
    }
    else     //constant inflow
    {
       for (int J=0;J<vsize;J++)
       {
          UpStreamA0[J]= UpStreamArea;
          VolInflow[J]=Inflow*MT[J]*60.0;
          ProcessedInflowV[1+J+PrevRowCount]=VolInflow[J];
          ProcessedInflowT[1+J+PrevRowCount]=MT[J];
          InstQadvance[J]=Inflow;
       }
    }
    return;
}
////////////////////////////////////////////////////////////////////////////////////////////////////////////////////////////////////////////////////////////
void __fastcall TKostiakovCalibrationObject::GetVariableInflow_Runoff(vector<double> MRT, vector<double> &
VolInflowRunoff, vector<double> &UpStreamA0Runoff)
{                                //calculates the upstream area from measured inflow and supplied runoff times
    int vsize=MRT.size();
    VolInflowRunoff.resize(vsize);
    UpStreamA0Runoff.resize(vsize);
    InstQrunoff.resize(vsize);
    int PrevRowCount=ProcessedInflowT.size();
    ProcessedInflowT.resize(vsize+PrevRowCount);
    ProcessedInflowV.resize(vsize+PrevRowCount);
    if (OptimisationType>1)                    //variable inflow
    {
       int NumIR=RawInflowTime.size();
       double Vol,Vol2,a,b,OldQCurrentQ=0;
       for (int J=0;J<vsize;J++)
       {
          OldQ=CurrentQ;
          Vol=0;
          Vol2=0;
          for (int K=0;K<(NumIR-1);K++)
          {
             if (RawInflowTime[K+1]>=MRT[J])
             {
                b = (RawInflowRate[K+1]-RawInflowRate[K])/(RawInflowTime[K+1]-RawInflowTime[K]);
                Vol2=(( (2*RawInflowRate[K]+b*(MRT[J]-RawInflowTime[K]))*0.5)*60.0)*(MRT[J]-RawInflowTime[K]);
                CurrentQ=(RawInflowRate[K]+b*(MRT[J]-RawInflowTime[K]));
                K=NumIR;
             }
             else
                Vol=Vol+(((RawInflowRate[K]+RawInflowRate[K+1])*0.5)*60.0)*(RawInflowTime[K+1]-
RawInflowTime[K]);
          }
          VolInflowRunoff[J]=Vol+Vol2;
          ProcessedInflowV[PrevRowCount+J]=VolInflowRunoff[J];
          ProcessedInflowT[PrevRowCount+J]=MRT[J];
          if(CurrentQ<OldQ)
             CurrentQ=(CurrentQ+OldQ)*0.5;
          long double VarY = Normaldepth(CurrentQ,BottomWidth,Slope,n,MaxHeight);
          UpStreamA0Runoff[J]= BottomWidth*VarY+(c*powl(VarY,(m+1)))/(m+1);
          InstQrunoff[J]=CurrentQ;
       }
    }
    else                    //constant inflow
    {
       for (int J=0;J<vsize;J++)
       {
          UpStreamA0Runoff[J]= UpStreamArea;
          VolInflowRunoff[J]=Inflow*MRT[J]*60.0;
          ProcessedInflowV[PrevRowCount+J]=VolInflowRunoff[J];
          ProcessedInflowT[PrevRowCount+J]=MRT[J];
          InstQrunoff[J]=Inflow;
       }
    }
}
////////////////////////////////////////////////////////////////////////////////////////////////////////////////////////////////////////////////////////////
double __fastcall TKostiakovCalibrationObject::nFromA0(double Qinsec, double Bw, double S0, double Ym,
double A0)
{                                    //estimates Mannings roughness from a measured cross sectional area of flow
    long double diff1,diff2,Perim,y=Ym/2;
    double G,Area, ystep=-0.01;
```

```
    int num2;
    Area=Bw*y+(c*powl(y,(m+1)))/(m+1);
    diff1=powl((Area-A0),2);
    for (num2=1; num2<=10; num2++)
    {
       int sw=0;
       while (sw==0)
       {
          y=y+ystep;
          if (y<=0)
          {
             y=0.00000001;
             sw=1;
          }
          Area=Bw*y+(c*powl(y,(m+1)))/(m+1);
          diff2=powl((Area-A0),2);
          if (diff2>=diff1)  sw=1;
          diff1=diff2;
       }
       ystep=ystep/(-10);
    }
    Perim=WettedPerim(y,Bw);
    double n=(1/Qinsec)*((powl(A0,(5*0.333333333333)))/(powl(Perim,(2*0.333333333333))))*(powl(S0,0.5));
    return n;
}
//////////////////////////////////////////////////////////////////////////////////////////////////////////////////////////////////////////////////////////////
long double __fastcall TKostiakovCalibrationObject::Normaldepth(double Qinsec, double Bw, double S0, double
n, double Ym)
{                                          //estimates the normal depth from discharge
    long double diff1,diff2,Perim,y=Ym;
    double G,Area, ystep=-0.01;
    int num1,num2;
    G=(Qinsec*n)/(pow(S0,0.5));
    Area=Bw*y+(c*powl(y,(m+1)))/(m+1);
    Perim=WettedPerim(y,Bw);
    diff1=powl(G-(pow(Area,(5*0.33333333333333333)))/(powl(Perim,(2*0.3333333333333333333))),2);
    for (num2=1; num2<=10; num2++)
    {                                  //loops testing values for the normal depth
       int sw=0;
       while (sw==0)
       {
          y=y+ystep;
          if (y<=0)
          {
             y=0.00000001;
             sw=1;
          }
          Area=Bw*y+(c*powl(y,(m+1)))/(m+1);
          Perim=WettedPerim(y,Bw);
          diff2=powl(G-(powl(Area,(5*0.33333333333333333)))/(powl(Perim,(2*0.3333333333333333333))),2);
          if (diff2>=diff1)  sw=1;
          diff1=diff2;
       }
       ystep=ystep/(-10);          //reduces the step size for the normal depth
    }
    return y;
}
//////////////////////////////////////////////////////////////////////////////////////////////////////////////////////////////////////////////////////////////
long double __fastcall TKostiakovCalibrationObject::WettedPerim(long double y, long double Bw)
{                                                  //calculates the wetted perimeter for a given depth of water
    long double perim, yc,w=0;
    double h=500;
    long double s=y/h;
    int ycount;
    for (ycount=(1);ycount<=500;ycount++)
    {
       yc=ycount*s;
       w=w + powl(((powl(((c*0.5)*(powl(yc,m)-powl(yc-s,m))),2))+(powl(s,2))),0.5);
    }
    perim = w*2+Bw;
    return perim;
}
//////////////////////////////////////////////////////////////////////////////////////////////////////////////////////////////////////////////////////////////
void __fastcall TKostiakovCalibrationObject::Initial_Search(vector<double> VolInflow, vector<double>
VolInflowRunoff,long double &t_a,long double &t_k,long double &t_f0,long double &t_C, vector<double>
```

```
UpStreamA0, vector<double> UpStreamA0Runoff, int sc)
{           //performs an initial search for the infiltration parameters for the advance and runoff data
   long double SSSEmin,SSSE1, a_search,k_search,f_search,C_search;
   long double a_inistep=0.0005, k_inistep=0.0002, f_inistep=0.00001,C_inistep=0.0002;
   int valcount,Actual_Numrun=MeasuredRunoffT.size();
   sz1.resize(Actual_Numrun);
   sz2.resize(Actual_Numrun);
   SSSEmin=10000000000;      //investigate a
   new_a(t_a,sc);
   if (aOP)
   {
      for (valcount=0;valcount<=1000;valcount++)
      {
         a_search=a_inistep*valcount;
         new_a(a_search,sc);
         SSSE1=Objective_Run(VolInflow,VolInflowRunoff,a_search,t_k,t_f0,t_C,UpStreamA0,
UpStreamA0Runoff,sc);
         if (SSSE1<SSSEmin)
         {
            SSSEmin=SSSE1;
            t_a=a_search;
         }
      }
   }                 //investigates k
   SSSEmin=10000000000;
   if (kOP)
   {
      for (valcount=0;valcount<=1000;valcount++)
      {
         k_search=k_inistep*valcount;
         SSSE1=Objective_Run(VolInflow,VolInflowRunoff,t_a,k_search,t_f0,t_C,UpStreamA0,
UpStreamA0Runoff,sc);
         if (SSSE1<SSSEmin)
         {
            SSSEmin=SSSE1;
            t_k=k_search;
         }
      }
   }                //investigates f0
   SSSEmin=10000000000;
   if (f0OP)
   {
      for (valcount=0;valcount<=1000;valcount++)
      {
         f_search=f_inistep*valcount;
         SSSE1=Objective_Run(VolInflow,VolInflowRunoff,t_a,t_k,f_search,t_C,UpStreamA0,
UpStreamA0Runoff,sc);
         if (SSSE1<SSSEmin)
         {
            SSSEmin=SSSE1;
            t_f0=f_search;
         }
      }
   }
   if (COP)             //investigates C
   {
      for (valcount=0;valcount<=1000;valcount++)
      {
         C_search=C_inistep*valcount;
         SSSE1=Objective_Run(VolInflow,VolInflowRunoff,t_a,t_k,t_f0,C_search,UpStreamA0,
UpStreamA0Runoff,sc);
         if (SSSE1<SSSEmin)
         {
            SSSEmin=SSSE1;
            t_C=C_search;
         }
      }
   }
}
////////////////////////////////////////////////////////////////////////////////////////////////////////////////////////////////////////////////////////////
void __fastcall TKostiakovCalibrationObject::new_a(long double t_a,int sc)
{           //calculates new values for the surface storage parameters, saves having to evaluate this every time
      int loopc,numRT=MeasuredRunoffT.size();
      double La;
      for (loopc=0;loopc<numRT;loopc++)
```

```
        {
            La = StartOfRunoff/MeasuredRunoffT[loopc];
            sz1[loopc]=SubShape(La,t_a,sc);
            sz2[loopc]=(1-(r*La)/(r+1));
        }
}
////////////////////////////////////////////////////////////////////////////////////////////////////////////////////////////////////////////////////
long double __fastcall TKostiakovCalibrationObject::SubShape(double La,long double t_a, int sc)
{                       calculates the new value of subshape factor 1 based on the time and a
   long double sz=1;
   int signSz=-1;
   long double num=t_a*r*La;
   long double dem=r+1;
   sz=sz+signSz*num/dem;
   signSz=(-1)*signSz;
   for (int pr=2;pr<=sc;pr++)
   {
      num=num*(t_a-(pr-1))*La;
      dem=dem*pr*(r+pr)/(r+pr-1);
      sz=sz+signSz*num/dem;
      signSz=(-1)*signSz;
   }
   return sz;
}
////////////////////////////////////////////////////////////////////////////////////////////////////////////////////////////////////////////////////
long double __fastcall TKostiakovCalibrationObject::Objective_Run(vector<double> VolInflow, vector<double>
VolInflowRunoff, long double t_a, long double t_k, long double t_f0, long double t_C, vector<double>
UpStreamA0, vector<double> UpStreamA0Runoff, int sc)
{                       //objective function for the advance and runoff data
   int sa=MeasuredAdvanceX.size(),sr=MeasuredRunoffT.size();
   vector<double> Xcalc,Vcalc;
   Xcalc= CalcX(MeasuredAdvanceT,t_a,t_k,t_f0,t_C,VolInflow,UpStreamA0);
   long double SSSEX,SSSER,SSSE, sum=0, sum2=0;
   for (int num=0;num<sa;num++)
   {                            //loops for each data point
      sum=sum+pow((MeasuredAdvanceX[num]-Xcalc[num]),2);
      sum2=sum2+powl(MeasuredAdvanceX[num],2);
   }
   SSSEX=sum/sum2;          //advance data error
   Vcalc=Calcrun(VolInflowRunoff,t_a,t_k,t_f0,t_C,UpStreamA0Runoff);
   sum=0;
   sum2=0;
   for (int num=0;num<sr;num++)
   {                            //loops for each data point
      sum=sum+pow((MeasuredRunoffV[num]-Vcalc[num]),2);
      sum2=sum2+powl(MeasuredRunoffV[num],2);
   }
   SSSER=sum/sum2;                      //runoff data error
   SSSE=100*(powl(SSSEX,0.5)+RunoffWeight*powl(SSSER,0.5));     //combine using weighting
   return SSSE;
}
////////////////////////////////////////////////////////////////////////////////////////////////////////////////////////////////////////////////////
long double __fastcall TKostiakovCalibrationObject::Objective_Advance(vector<double> VolInflow, long double
t_a, long double t_k, long double t_f0, long double t_C, vector<double> UpStreamA0)
{                            //objective function for the advance data
   vector<double> Xcalc;
   Xcalc= CalcX(MeasuredAdvanceT,t_a,t_k,t_f0,t_C,VolInflow,UpStreamA0);
   int sa=MeasuredAdvanceT.size();
   long double SSSEX,SSSER,SSSE,sum=0, sum2=0;
   for (int num=0;num<sa;num++)
   {                            //loops for each data point
      sum=sum+pow((MeasuredAdvanceX[num]-Xcalc[num]),2);
      sum2=sum2+powl(MeasuredAdvanceX[num],2);
   }
   SSSEX=sum/sum2;
   SSSE=100*(powl(SSSEX,0.5));
   return SSSE;
}
////////////////////////////////////////////////////////////////////////////////////////////////////////////////////////////////////////////////////
vector<double> __fastcall TKostiakovCalibrationObject::CalcX(vector<double> MeasT,long double t_a, long
double t_k, long double t_f0, long double t_C, vector<double> VolInflow, vector<double> UpStreamA0)
{                       //calculate the advance distance from measured time
   if (t_a<=0)   t_a=0.0000000001;    //stops errors from powl
   long double szaold = (t_a + r * (1 - t_a) + 1) / ((1 + t_a) * (1 + r));  //not used
   long double sza=SubShape(1,t_a,20);
```

```
    int s=MeasT.size();
    vector<double> Xcalc(s);
    double tempSS;
    for (int num=0;num<s;num++)
    {
       if (AlternativeSurfaceStorage)     //SSS technique
          tempSS=GetVariableSSadvance(MeasT[num],num,OldCalcX[num],UpStreamA0[num]);
       else
          tempSS=UpStreamA0[num];
       Xcalc[num]=VolInflow[num]/(sy*tempSS+sza*t_k*powl(MeasT[num],t_a)+(t_f0*MeasT[num]/(1+r))+t_C);
       OldCalcX[num]=Xcalc[num];
    }
    return Xcalc;
}
////////////////////////////////////////////////////////////////////////////////////////////////////////////////////////////////////////////////////////
vector<double> __fastcall TKostiakovCalibrationObject::CalcXImagine(vector<double> MeasT,long double t_a,
long double t_k, long double t_f0, long double t_C, vector<double> VolInflow, vector<double> UpStreamA0)
{             //calculates the advance distance past the end of the field
    if (t_a<=0)  t_a=0.0000000001;    //stops errors from powl
    long double szaold = (t_a + r * (1 - t_a) + 1) / ((1 + t_a) * (1 + r));     //not used
    long double sza=SubShape(1,t_a,20);
    int s=MeasT.size();
    vector<double> Xcalc(s);
    double tempSS;
    for (int num=0;num<s;num++)
    {
       if (AlternativeSurfaceStorage)          //SSS technique
          tempSS=GetVariableSSadvance(MeasT[num],num,OldCalcXImagine[num],UpStreamA0[num]);
       else
          tempSS=UpStreamA0[num];
       Xcalc[num]=VolInflow[num]/(sy*tempSS+sza*t_k*powl(MeasT[num],t_a)+(t_f0*MeasT[num]/(1+r))+t_C);
       OldCalcXImagine[num]=Xcalc[num];
    }
    return Xcalc;
}
////////////////////////////////////////////////////////////////////////////////////////////////////////////////////////////////////////////////////////
vector<double> __fastcall TKostiakovCalibrationObject::Calcrun(vector<double> VolInflowRunoff, long double
t_a, long double t_k, long double t_f0, long double t_C, vector<double> UpStreamA0Runoff)
{                          //calculate the runoff volume from measured time
    if (t_a<=0)   t_a=0.0000000001;    //stops errors from powl
    int s=MeasuredRunoffT.size();
    long double VS;
    double Vrun,tempAveArea,tempAveUSArea,tempShapeFactor, Vold=-1000;
    vector<double> Ximagine(s),Vcalc(s);
    Ximagine= CalcXImagine(MeasuredRunoffT,t_a,t_k,t_f0,t_C,VolInflowRunoff,UpStreamA0Runoff);
    for (int num=0;num<s;num++)
    {          //loops for each data point
       VS=SStorage(UpStreamA0Runoff[num],Ximagine[num],MeasuredRunoffT[num]);
       tempAveArea=VS/RunoffPos;
       tempShapeFactor=tempAveArea/UpStreamA0Runoff[num];
       if (AlternativeSurfaceStorage)          //SSS technique
       {
          tempAveUSArea=GetVariableSSrunoff(MeasuredRunoffT[num],num,tempAveArea);
          VS=tempAveUSArea*RunoffPos*tempShapeFactor;
       }
       Vrun=VolInflowRunoff[num] - (RunoffPos*sz1[num]*t_k*powl(MeasuredRunoffT[num],t_a) +
RunoffPos*sz2[num]*t_f0*MeasuredRunoffT[num] + VS+RunoffPos*t_C);
       Vcalc[num]=Vrun;
       if (Vcalc[num]<Vold)
          Vcalc[num]=Vold;
       Vold=Vcalc[num];
    }
    return Vcalc;
}
////////////////////////////////////////////////////////////////////////////////////////////////////////////////////////////////////////////////////////
long double __fastcall TKostiakovCalibrationObject::SStorage(double t_A0, double Xi,double CurrentT)
{                          //calculates the surface storage by assuming that the advance proceeds past the end
    long double VS;                  //of the field
    double sy_storage;
    Xi=((Xi-RunoffPos)+ powl((pow((Xi-RunoffPos),2)),0.5) )/2+RunoffPos;
    sy_storage=sy*(Xi/RunoffPos)*(1-pow((1-RunoffPos/Xi),(1./sy)) );
    VS=sy_storage*t_A0*RunoffPos;
    return VS;
}
////////////////////////////////////////////////////////////////////////////////////////////////////////////////////////////////////////////////////////
```

```
long double __fastcall TKostiakovCalibrationObject::IterA(vector<double> VolInflow, vector<double>
VolInflowRunoff, long double & t_a, long double t_k, long double t_f0, long double t_C, vector<double>
UpStreamA0, vector<double> UpStreamA0Runoff,long double astep, long double & Ja1, int sc)
{           //iterate a for advance and runoff data
   Ja1=0;
   long double SSSE1,SSSE2;
   int sw,Jastep=1;
   if (astep<0)  Jastep=-1;
   for (int num=1;num<=2;num++)
   {
      SSSE1=Objective_Run(VolInflow,VolInflowRunoff,t_a,t_k,t_f0,t_C,UpStreamA0,UpStreamA0Runoff,sc);
      sw=0;
      while (sw==0)
      {
         t_a=t_a+astep;
         Ja1=Ja1+Jastep;
         if (t_a<0)
         {
            t_a=0;
            sw=1;
         }
         if (t_a>0.99)
         {
            t_a=0.99;
            sw=1;
         }
         new_a(t_a,sc);
         SSSE2=Objective_Run(VolInflow,VolInflowRunoff,t_a,t_k,t_f0,t_C,UpStreamA0,UpStreamA0Runoff,sc);
         if (SSSE2>=SSSE1)
         {
            sw=1;
            t_a=t_a-astep/2;                    //go back one half step
            Ja1=Ja1-Jastep/2;
         }
         SSSE1=SSSE2;
      }
      astep=(-1)*astep;
      Jastep=Jastep*(-1);
   }
   return SSSE2;
}
////////////////////////////////////////////////////////////////////////////////////////////////////////////////////////////////////////////////////////////
long double __fastcall TKostiakovCalibrationObject::IterA_Advance(vector<double> VolInflow,long double & t_a,
long double t_k, long double t_f0, long double t_C, vector<double> UpStreamA0,long double astep, long double &
Ja1)
{           //iterate a for advance data
   Ja1=0;
   long double SSSE1,SSSE2;
   int sw,Jastep=1;
   if (astep<0)  Jastep=-1;
   for (int num=1;num<=2;num++)
   {
      SSSE1= Objective_Advance(VolInflow,t_a,t_k,t_f0,t_C,UpStreamA0);
      sw=0;
      while (sw==0)
      {
         t_a=t_a+astep;
         Ja1=Ja1+Jastep;
         if (t_a<0)
         {
            t_a=0;
            sw=1;
         }
         if (t_a>0.99)
         {
            t_a=0.99;
            sw=1;
         }
         SSSE2=Objective_Advance(VolInflow,t_a,t_k,t_f0,t_C,UpStreamA0);
         if (SSSE2>=SSSE1)
         {
            sw=1;
            t_a=t_a-astep/2;
            Ja1=Ja1-Jastep/2;
         }
```

```
            SSSE1=SSSE2;
        }
        astep=(-1)*astep;
        Jastep=Jastep*(-1);
    }
    return SSSE2;
}
////////////////////////////////////////////////////////////////////////////////////////////////////////////////////////////////////////////////////////////
long double __fastcall TKostiakovCalibrationObject::IterK(vector<double> VolInflow, vector<double>
VolInflowRunoff, long double t_a, long double & t_k, long double t_f0, long double t_C, vector<double>
UpStreamA0, vector<double> UpStreamA0Runoff, long double kstep, long double & Jk1,int sc)
{           //iterate k for advance and runoff data
    Jk1=0;
    long double SSSE1,SSSE2;
    int int sw,Jkstep=1;
    if (kstep<0)  Jkstep=-1;
    for (int num=1;num<=2;num++)
    {
        SSSE1=Objective_Run(VolInflow,VolInflowRunoff,t_a,t_k,t_f0,t_C,UpStreamA0,UpStreamA0Runoff,sc);
        sw=0;
        while (sw==0)
        {
            t_k=t_k+kstep;
            Jk1=Jk1+Jkstep;
            if (t_k<0)
            {
                t_k=0;
                sw=1;
            }
            if (t_k>0.99)
            {
                t_k=0.99;
                sw=1;
            }
            SSSE2=Objective_Run(VolInflow,VolInflowRunoff,t_a,t_k,t_f0,t_C,UpStreamA0,UpStreamA0Runoff,sc);
            if (SSSE2>=SSSE1)
            {
                sw=1;
                t_k=t_k-kstep/2;
                Jk1=Jk1-Jkstep/2;
            }
            SSSE1=SSSE2;
        }
        kstep=(-1)*kstep;
        Jkstep=Jkstep*(-1);
    }
    return SSSE2;
}
////////////////////////////////////////////////////////////////////////////////////////////////////////////////////////////////////////////////////////////
long double __fastcall TKostiakovCalibrationObject::IterK_Advance(vector<double> VolInflow, long double t_a,
long double & t_k, long double t_f0, long double t_C, vector<double> UpStreamA0, long double kstep, long
double & Jk1)
{           //iterate k for advance data
    Jk1=0;
    long double SSSE1,SSSE2;
    int sw,Jkstep=1;
    if (kstep<0)  Jkstep=-1;
    for (int num=1;num<=2;num++)
    {
        SSSE1= Objective_Advance(VolInflow,t_a,t_k,t_f0,t_C,UpStreamA0);
        sw=0;
        while (sw==0)
        {
            t_k=t_k+kstep;
            Jk1=Jk1+Jkstep;
            if (t_k<0)
            {
                t_k=0;
                sw=1;
            }
            if (t_k>0.99)
            {
                t_k=0.99;
                sw=1;
            }
```

```
        SSSE2=Objective_Advance(VolInflow,t_a,t_k,t_f0,t_C,UpStreamA0);
        if (SSSE2>=SSSE1)
        {
          sw=1;
          t_k=t_k-kstep/2;
          Jk1=Jk1-Jkstep/2;
        }
        SSSE1=SSSE2;
      }
      kstep=(-1)*kstep;
      Jkstep=Jkstep*(-1);
    }
    return SSSE2;
}
////////////////////////////////////////////////////////////////////////////////////////////////////////////////////////////////////////////////////////////
long double __fastcall TKostiakovCalibrationObject::IterF(vector<double> VolInflow, vector<double>
VolInflowRunoff, long double t_a, long double t_k, long double & t_f0, long double t_C, vector<double>
UpStreamA0, vector<double> UpStreamA0Runoff, long double fstep, long double & Jf1,int sc)
{           //iterate f0 for advance and runoff data
    Jf1=0;
    long double SSSE1,SSSE2;
    int sw,Jfstep=1;
    if (fstep<0)  Jfstep=-1;
    for (int num=1;num<=2;num++)
    {
      SSSE1=Objective_Run(VolInflow,VolInflowRunoff,t_a,t_k,t_f0,t_C,UpStreamA0,UpStreamA0Runoff,sc);
      sw=0;
      while (sw==0)
      {
        t_f0=t_f0+fstep;
        Jf1=Jf1+Jfstep;
        if (t_f0<0)
        {
          t_f0=0;
          sw=1;
        }
        if (t_f0>0.99)
        {
          t_f0=0.99;
          sw=1;
        }
        SSSE2=Objective_Run(VolInflow,VolInflowRunoff,t_a,t_k,t_f0,t_C,UpStreamA0,UpStreamA0Runoff,sc);
        if (SSSE2>=SSSE1)
        {
          sw=1;
          t_f0=t_f0-fstep/2;
          Jf1=Jf1-Jfstep/2;
        }
        SSSE1=SSSE2;
      }
      fstep=(-1)*fstep;
      Jfstep=Jfstep*(-1);
    }
    return SSSE2;
}
////////////////////////////////////////////////////////////////////////////////////////////////////////////////////////////////////////////////////////////
long double __fastcall TKostiakovCalibrationObject::IterF_Advance(vector<double> VolInflow, long double t_a,
long double t_k, long double & t_f0, long double t_C, vector<double> UpStreamA0, long double fstep, long double
& Jf1)
{           //iterate f0 for advance data
    Jf1=0;
    long double SSSE1,SSSE2;
    int sw,Jfstep=1;
    if (fstep<0)  Jfstep=-1;
    for (int num=1;num<=2;num++)
    {
      SSSE1= Objective_Advance(VolInflow,t_a,t_k,t_f0,t_C,UpStreamA0);
      sw=0;
      while (sw==0)
      {
        t_f0=t_f0+fstep;
        Jf1=Jf1+Jfstep;
        if (t_f0<0)
        {
          t_f0=0;
```

```
            sw=1;
         }
         if (t_f0>0.99)
         {
            t_f0=0.99;
            sw=1;
         }
         SSSE2=Objective_Advance(VolInflow,t_a,t_k,t_f0,t_C,UpStreamA0);
         if (SSSE2>=SSSE1)
         {
            sw=1;
            t_f0=t_f0-fstep/2;
            Jf1=Jf1-Jfstep/2;
         }
         SSSE1=SSSE2;
      }
      fstep=(-1)*fstep;
      Jfstep=Jfstep*(-1);
   }
   return SSSE2;
}
////////////////////////////////////////////////////////////////////////////////////////////////////////////////////////////////////////////////////////////
long double __fastcall TKostiakovCalibrationObject::IterC(vector<double> VolInflow, vector<double>
VolInflowRunoff, long double t_a, long double t_k, long double t_f0, long double & t_C, vector<double>
UpStreamA0, vector<double> UpStreamA0Runoff, long double Cstep, long double & JC1,int sc)
{            //iterate C for advance and runoff data
   JC1=0;
   long double SSSE1,SSSE2;
   int sw,JCstep=1;
   if (Cstep<0)  JCstep=-1;
   for (int num=1;num<=2;num++)
   {
      SSSE1=Objective_Run(VolInflow,VolInflowRunoff,t_a,t_k,t_f0,t_C,UpStreamA0,UpStreamA0Runoff,sc);
      sw=0;
      while (sw==0)
      {
         t_C=t_C+Cstep;
         JC1=JC1+JCstep;
         if (t_C<0)
         {
            t_C=0;
            sw=1;
         }
         if (t_C>0.99)
         {
            t_C=0.99;
            sw=1;
         }
         SSSE2=Objective_Run(VolInflow,VolInflowRunoff,t_a,t_k,t_f0,t_C,UpStreamA0,UpStreamA0Runoff,sc);
         if (SSSE2>=SSSE1)
         {
            sw=1;
            t_C=t_C-Cstep/2;
            JC1=JC1-JCstep/2;
         }
         SSSE1=SSSE2;
      }
      Cstep=(-1)*Cstep;
      JCstep=JCstep*(-1);
   }
   return SSSE2;
}
////////////////////////////////////////////////////////////////////////////////////////////////////////////////////////////////////////////////////////////
long double __fastcall TKostiakovCalibrationObject::IterC_Advance(vector<double> VolInflow, long double t_a,
long double t_k, long double t_f0, long double & t_C, vector<double> UpStreamA0, long double Cstep, long
double & JC1)
{            //iterate C for advance data
   JC1=0;
   long double SSSE1,SSSE2;
   int sw,JCstep=1;
   if (Cstep<0)  JCstep=-1;
   for (int num=1;num<=2;num++)
   {
      SSSE1= Objective_Advance(VolInflow,t_a,t_k,t_f0,t_C,UpStreamA0);
      sw=0;
```

```
        while (sw==0)
        {
           t_C=t_C+Cstep;
           JC1=JC1+JCstep;
           if (t_C<0)
           {
              t_C=0;
              sw=1;
           }
           if (t_C>0.99)
           {
              t_C=0.99;
              sw=1;
           }
           SSSE2=Objective_Advance(VolInflow,t_a,t_k,t_f0,t_C,UpStreamA0);
           if (SSSE2>=SSSE1)
           {
              sw=1;
              t_C=t_C-Cstep/2;
              JC1=JC1-JCstep/2;
           }
           SSSE1=SSSE2;
        }
        Cstep=(-1)*Cstep;
        JCstep=JCstep*(-1);
     }
     return SSSE2;
}
////////////////////////////////////////////////////////////////////////////////////////////////////////////////////////////////////////////////////////
void __fastcall TKostiakovCalibrationObject::UpdateDisplayRunoff(long double SSSE1, double num,
vector<double> VolInflow, vector<double> UpStreamA0, vector<double> VCalc)
{               //send some of the results to screen
     SSSECurrent=SSSE1;
     num_P=num;
     VolInflow_P=VolInflow;
     UpStreamA0_P=UpStreamA0;
     VCalc_P=VCalc;
     _MainForm->DisplayRunoffResults();
}
////////////////////////////////////////////////////////////////////////////////////////////////////////////////////////////////////////////////////////
void __fastcall TKostiakovCalibrationObject::UpdateDisplayAdvance(long double SSSE1, double num,
vector<double> VolInflow, vector<double> UpStreamA0)
{               //send some of the results to screen
     SSSECurrent=SSSE1;
     num_P=num;
     VolInflow_P=VolInflow;
     UpStreamA0_P=UpStreamA0;
     _MainForm->DisplayAdvanceResults();
}
////////////////////////////////////////////////////////////////////////////////////////////////////////////////////////////////////////////////////////
double __fastcall TKostiakovCalibrationObject::GetMaxTime()
{               //determine the maximum time of any of the supplied data
     double MaxTime_Temp=0;
     int asize=MeasuredAdvanceT.size(),rsize=MeasuredRunoffT.size(),isize=RawInflowTime.size();
     if (MeasuredAdvanceT[asize-1]>MaxTime_Temp)
        MaxTime_Temp=MeasuredAdvanceT[asize-1];
     if (rsize>0)
     {
        if (MeasuredRunoffT[rsize-1]>MaxTime_Temp)
           MaxTime_Temp=MeasuredRunoffT[rsize-1];
     }
     if (isize>0)
     {
        if (RawInflowTime[asize-1]>MaxTime_Temp)
           MaxTime_Temp=RawInflowTime[asize-1];
     }
     return MaxTime_Temp;
}
////////////////////////////////////////////////////////////////////////////////////////////////////////////////////////////////////////////////////////
double __fastcall TKostiakovCalibrationObject::GetVariableSSadvance(double currentT,int advancepoint,double
tempdist,double CurrentUSarea)
{                       //calculate the surface storage during the advance phase using the SSS technique
     double CurrentAverageArea=CurrentUSarea*sy;
     double initime, Vol,Vol2,a,b,tempy=0.001;
     for (int kk=0;kk<16;kk++)
```

```
        tempy=CurrentAverageArea/(BottomWidth+(c*powl(tempy,m))/(m+1));
    double tempw=WettedPerimSimple(tempy);
    double averagey=CurrentAverageArea/(BottomWidth+c*powl(tempy,m));
    double tempv=(1.0/n)*(pow(Slope,0.5))*pow(CurrentAverageArea/tempw,(2.0/3.0));
              //+pow((9.81*averagey),0.5); //extra for celerity has been removed
    double tempt=tempdist/tempv;    //seconds
    tempt=tempt/60.0;
    initime=currentT-tempt;
    int K, StartIndex,EndIndex,PrevRowCount=0,NumIR=RawInflowTime.size();
    bool logerror=false,foundit=false;
    Vol=0;
    if (initime<=0.0)
    {
       initime=0.0;
       K=0;
       StartIndex=0;
    }
    else
    {
       K=0;
       foundit=false;
       while (!foundit)
       {
          if (RawInflowTime[K+1]>=initime)
          {
             StartIndex=K;
             foundit=true;
          }
          else
          {
             K++;
             if (K>(NumIR-2))
             {
                foundit=true;
                logerror=true;
             }
          }
       }
    }
    K=StartIndex;
    if (logerror)
          return CurrentAverageArea;
    else
    {
       if (RawInflowTime[K+1]>=currentT)
       {            //the current time is in the same interval
          b = RawUpstreamAreaChange[K];
         Vol= (currentT-initime)*(RawUpstreamAreaArea[K]+b*(initime-RawInflowTime[K])+RawUpstreamAreaArea[K]
+b*(currentT-RawInflowTime[K]))/2.0;
       }
       else
       {
          b = RawUpstreamAreaChange[K];
          Vol+=((RawUpstreamAreaArea[K]+b*(initime-RawInflowTime[K])+RawUpstreamAreaArea[K+1])*0.5)
*(RawInflowTime[K+1] -initime);
          K++;
          foundit=false;
          while (!foundit)
          {
             if (RawInflowTime[K+1]>=currentT)
             {
                b = RawUpstreamAreaChange[K];
                Vol+= (currentT-RawInflowTime[K])*((RawUpstreamAreaArea[K]+b*(currentT-RawInflowTime[K])
+RawUpstreamAreaArea[K])/2.0);
                EndIndex=K;
                foundit=true;
             }
             else
             {
                Vol+=((RawUpstreamAreaArea[K]+RawUpstreamAreaArea[K+1])*0.5)*(RawInflowTime[K+1]-
RawInflowTime[K]);
                K++;
                if (K>(NumIR-2))
                   foundit=true;
             }
```

```
            }
        }
    }
    double aarea=Vol/(currentT-initime);
    return aarea;
}
////////////////////////////////////////////////////////////////////////////////////////////////////////////////////////////////////////////////////////////
double __fastcall TKostiakovCalibrationObject::WettedPerimSimple(double y)
{               // a rapid version of the wetted permeter calculation
    double perim, yc, t1=0,t2=0, w=0,h=50;
    double s=y/h;
    for (int ycount=(1);ycount<=h;ycount++)
    {
        t1=t2;
        t2=powl(yc,m);
        yc=ycount*s;
        w=w + pow(((c*0.5)*(t2-t1))*((c*0.5)*(t2-t1))+(s*s),0.5);
    }
    perim = w*2+BottomWidth;
    return perim;
}
////////////////////////////////////////////////////////////////////////////////////////////////////////////////////////////////////////////////////////////
double __fastcall TKostiakovCalibrationObject::GetVariableSSrunoff(double currentT,int advancepoint,double
CurrentUSarea)
{                           //calculate the surface storage during the runoff phase using the SSS technique
    double CurrentAverageArea=CurrentUSarea;
    double initime,Vol,Vol2,a,b,tempy=0.001;
    for (int kk=0;kk<16;kk++)
        tempy=CurrentAverageArea/(BottomWidth+(c*powl(tempy,m))/(m+1));
    double tempw=WettedPerimSimple(tempy);
    double averagey=CurrentAverageArea/(BottomWidth+c*powl(tempy,m));
    double wavev=pow((9.81*averagey),0.5);
    double tempv=(1.0/n)*(pow(Slope,0.5))*pow(CurrentAverageArea/tempw,(2.0/3.0));
    tempv=tempv;//+wavev; //removed the wave celerity
    double tempt=RunoffPos/tempv;    //seconds
    tempt=tempt/60.0;
    initime=currentT-tempt;
    int K, StartIndex,EndIndex, PrevRowCount=0, NumIR=RawInflowTime.size();
    bool logerror=false, foundit=false;
    Vol=0;
    if (initime<=0.0)        //find the start
    {
        initime=0.0;
        K=0;
        StartIndex=0;
    }
    else
    {
        K=0;
        foundit=false;
        while (!foundit)
        {
            if (K>(NumIR-2))
            {
                foundit=true;
                logerror=true;
            }
            else
            {
                if (RawInflowTime[K+1]>=initime)
                {
                    StartIndex=K;
                    foundit=true;
                }
                K++;
            }
        }
    }
    K=StartIndex;
    if (logerror)
        return CurrentAverageArea;
    else
    {
        if (K>(NumIR-2))
        {
```

```
            foundit=true;
            logerror=true;
         }
         else
         {
            if (RawInflowTime[K+1]>=currentT)
            {              //the current time is in the same interval
               b = RawUpstreamAreaChange[K];
               Vol= (currentT-initime)*(RawUpstreamArea[K]+b*(initime-RawInflowTime[K])+RawUpstreamArea[K]
+b*(currentT-RawInflowTime[K]))/2.0;
            }
            else
            {
               b = RawUpstreamAreaChange[K];
               Vol+=((RawUpstreamArea[K]+b*(initime-RawInflowTime[K])+RawUpstreamArea[K+1])
*0.5)*(RawInflowTime[K+1]-initime);
               K++;
               foundit=false;
               while (!foundit)
               {
                  if (K>(NumIR-2))
                     foundit=true;
                  else
                  {
                     if (RawInflowTime[K+1]>=currentT)
                     {
                        b = RawUpstreamAreaChange[K];
                        Vol+= (currentT-RawInflowTime[K])*((RawUpstreamArea[K]+b*(currentT-RawInflowTime[K])
+RawUpstreamArea[K])/2.0);
                        EndIndex=K;
                        foundit=true;
                     }
                     else
                        Vol+=((RawUpstreamArea[K]+RawUpstreamArea[K+1])*0.5)*(RawInflowTime[K+1]
-RawInflowTime[K]);
                     K++;
                  }
               }
            }
         }
      }
      double aarea=CurrentUSarea;
      if (!logerror)
         aarea=Vol/(currentT-initime);
      return aarea;
}
////////////////////////////////////////////////////////////////////////////////////////////////////////////////////////////////////////////////////////////////////////
vector<double> __fastcall TKostiakovCalibrationObject::CalcXAdvanced(vector<double> MeasT,long double t_a,
long double t_k, long double t_f0, long double t_C, vector<double> VolInflow, vector<double> UpStreamA0)
{              //calculates the advance distances and extra results for the user
      if (t_a<=0)  t_a=0.0000000001;    //stops errors from powl
      long double szaold = (t_a + r * (1 - t_a) + 1) / ((1 + t_a) * (1 + r));  //not used
      long double sza=SubShape(1,t_a,20);
      int s=MeasT.size();
      vector<double> Xcalc(s);
      VSMeasAd.resize(s);
      VSCalcAd.resize(s);
      VIMeasAd.resize(s);
      VICalcAd.resize(s);
      double tempSS,tempMeasSS;
      for (int num=0;num<s;num++)
      {
         if (AlternativeSurfaceStorage)         //SSS technique
         {
            tempSS=GetVariableSSadvance(MeasT[num],num,OldCalcX[num],UpStreamA0[num]);
            tempMeasSS=GetVariableSSadvance(MeasT[num],num, MeasuredAdvanceX[num],UpStreamA0[num]);
         }
         else
         {
            tempSS=UpStreamA0[num];
            tempMeasSS=UpStreamA0[num];
         }
        Xcalc[num]=VolInflow[num]/(sy*tempSS+sza*t_k*powl(MeasT[num],t_a)+(t_f0*MeasT[num]/(1+r))+t_C);
        OldCalcX[num]=Xcalc[num];
        VSMeasAd[num]=sy*tempMeasSS*MeasuredAdvanceX[num];
```

```
      VSCalcAd[num]=sy*tempSS*Xcalc[num];
      VIMeasAd[num]=VolInflow[num]-sy*tempMeasSS*MeasuredAdvanceX[num];
      VICalcAd[num]=(sza*t_k*powl(MeasT[num],t_a)+(t_f0*MeasT[num]/(1+r))+t_C)*Xcalc[num];
   }
   return Xcalc;
}
////////////////////////////////////////////////////////////////////////////////////////////////////////////////////////////////////////////////////
vector<double> __fastcall TKostiakovCalibrationObject::CalcrunAdvanced(vector<double> VolInflowRunoff, long
double t_a, long double t_k, long double t_f0, long double t_C, vector<double> UpStreamA0Runoff)
{            //calculates the runoff volumes and extra results for the user
   if (t_a<=0)  t_a=0.0000000001;    //stops errors from powl
   int s=MeasuredRunoffT.size();
   long double VS;
   double Vrun,tempAveArea,tempAveUSArea,tempShapeFactor,Vold=-1000;
   vector<double> Ximagine(s), Vcalc(s);
   VSMeasRun.resize(s);
   VSCalcRun.resize(s);
   VIMeasRun.resize(s);
   VICalcRun.resize(s);
   Ximagine= CalcXImagine(MeasuredRunoffT,t_a,t_k,t_f0,t_C,VolInflowRunoff,UpStreamA0Runoff);
   for (int num=0;num<s;num++)
   {
      VS=SStorage(UpStreamA0Runoff[num],Ximagine[num],MeasuredRunoffT[num]);
      tempAveArea=VS/RunoffPos;
      tempShapeFactor=tempAveArea/UpStreamA0Runoff[num];
      if (AlternativeSurfaceStorage)
      {
         tempAveUSArea=GetVariableSSrunoff(MeasuredRunoffT[num],num,tempAveArea);
         VS=tempAveUSArea*RunoffPos*tempShapeFactor;
      }
      VSMeasRun[num]=VS;
      VSCalcRun[num]=VS;
      VICalcRun[num]=RunoffPos*sz1[num]*t_k*powl(MeasuredRunoffT[num],t_a)+RunoffPos
*sz2[num]*t_f0*MeasuredRunoffT[num] + RunoffPos*t_C;
      VIMeasRun[num]=VolInflowRunoff[num]-VS-MeasuredRunoffV[num];
      Vrun=VolInflowRunoff[num] - (RunoffPos*sz1[num]*t_k*powl(MeasuredRunoffT[num],t_a) + RunoffPos
*sz2[num]*t_f0*MeasuredRunoffT[num] + VS+RunoffPos*t_C);
      Vcalc[num]=Vrun;
      if (Vcalc[num]<Vold)
         Vcalc[num]=Vold;
      Vold=Vcalc[num];
   }
   return Vcalc;
}
////////////////////////////////////////////////////////////////////////////////////////////////////////////////////////////////////////////////////
bool __fastcall TKostiakovCalibrationObject::GetIsUsingRunoff()
{
   bool tempIsRunoff=false;
   switch (OptimisationType)
   {
      case 0:
         tempIsRunoff=false;
         break;
      case 1:
         tempIsRunoff=true;
         break;
      case 2:
         tempIsRunoff=false;
         break;
      case 3:
         tempIsRunoff=true;
         break;
      default:
         tempIsRunoff=false;
         break;
   }
   return tempIsRunoff;
}
```

APPENDIX C

Extra Results for IPARM

Validation

Table C.1 Infiltration parameters for Kooba from advance with constant and variable inflow

Constant Inflow	*a*	*k*	f_0	Error (IPARM)	Infiltration ($m^3 m^{-1}$)			
					100 min	200 min	500 min	1000 min
Irr 1 Fur 1	0.0496	0.30395	0.000000	2.60	0.3820	0.3953	0.4137	0.4282
Irr 1 Fur 2	0.2607	0.04875	0.000000	6.38	0.1620	0.1941	0.2464	0.2952
Irr 1 Fur 3	0.4073	0.02134	0.000000	5.09	0.1393	0.1847	0.2683	0.3558
Irr 1 Fur 4	0.2278	0.09549	0.000000	3.10	0.2726	0.3192	0.3932	0.4605
Irr 2 Fur 1	0.2692	0.02973	0.000000	4.76	0.1027	0.1238	0.1584	0.1909
Irr 2 Fur 2	0.3251	0.00834	0.000172	0.70	0.0545	0.0811	0.1489	0.2508
Irr 2 Fur 3	0.2846	0.00724	0.000263	1.32	0.0531	0.0853	0.1739	0.3147
Irr 2 Fur 4	0.4950	0.00818	0.000000	3.39	0.0800	0.1127	0.1774	0.2499
Irr 3 Fur 1	0.5444	0.00429	0.000000	1.28	0.0526	0.0768	0.1265	0.1844
Irr 3 Fur 2	0.4998	0.00298	0.000000	0.99	0.0298	0.0422	0.0666	0.0942
Irr 3 Fur 3	0.2926	0.00460	0.000177	1.13	0.0354	0.0570	0.1167	0.2114
Irr 3 Fur 4	0.4294	0.01396	0.000000	3.23	0.1008	0.1357	0.2012	0.2709
Coefficient of Variation					**87.2817**	**71.8247**	**51.3075**	**37.8372**
Full Inflow Hydrograph	*a*	*k*	f_0	Error (IPARM)	Infiltration ($m^3 m^{-1}$)			
					100 min	200 min	500 min	1000 min
Irr 1 Fur 1	0.2234	0.09673	0.000000	2.61	0.2706	0.3160	0.3878	0.4527
Irr 1 Fur 2	0.3435	0.02775	0.000000	6.69	0.1349	0.1712	0.2345	0.2976
Irr 1 Fur 3	0.5193	0.01011	0.000000	5.40	0.1105	0.1583	0.2548	0.3652
Irr 1 Fur 4	0.3506	0.04244	0.000000	3.27	0.2133	0.2720	0.3750	0.4781
Irr 2 Fur 1	0.5336	0.00812	0.000000	5.68	0.0947	0.1371	0.2236	0.3237
Irr 2 Fur 2	0.4184	0.00422	0.000193	0.92	0.0483	0.0773	0.1533	0.2690
Irr 2 Fur 3	0.1685	0.00876	0.000290	1.41	0.0480	0.0793	0.1698	0.3178
Irr 2 Fur 4	0.5702	0.00524	0.000000	2.76	0.0723	0.1074	0.1810	0.2688
Irr 3 Fur 1	0.6735	0.00317	0.000000	2.69	0.0705	0.1124	0.2084	0.3323
Irr 3 Fur 2	0.5315	0.00301	0.000000	1.03	0.0348	0.0504	0.0819	0.1184
Irr 3 Fur 3	0.2601	0.00750	0.000241	1.21	0.0489	0.0780	0.1583	0.2863
Irr 3 Fur 4	0.4458	0.01397	0.000000	3.36	0.1088	0.1482	0.2230	0.3038
Coefficient of Variation					**68.7868**	**56.4653**	**39.7989**	**28.8557**

Table C.2 Infiltration parameters for Kooba from advance and runoff data with constant and variable inflow

Constant Inflow	*a*	*k*	f_0	Error (IPARM)	Infiltration ($m^3 m^{-1}$)			
					100 min	200 min	500 min	1000 min
Irr 1 Fur 1	0.0236	0.29527	0.000136	7.87	0.3429	0.3619	0.4101	0.4839
Irr 1 Fur 2	0.1292	0.11059	0.000000	18.62	0.2005	0.2193	0.2469	0.2700
Irr 1 Fur 3	0.3291	0.03471	0.000000	11.83	0.1580	0.1984	0.2683	0.3370
Irr 1 Fur 4	0.2467	0.08464	0.000000	4.01	0.2636	0.3127	0.3920	0.4651
Irr 2 Fur 1	0.2036	0.03407	0.000139	5.25	0.1009	0.1279	0.1901	0.2778
Irr 2 Fur 2	0.4021	0.00958	0.000000	8.30	0.0610	0.0806	0.1165	0.1540
Irr 2 Fur 3	0.4553	0.00766	0.000000	8.34	0.0623	0.0855	0.1297	0.1778
Irr 2 Fur 4	0.4912	0.00833	0.000000	3.40	0.0800	0.1124	0.1763	0.2479
Irr 3 Fur 1	0.5012	0.00490	0.000028	4.54	0.0521	0.0753	0.1244	0.1842
Irr 3 Fur 2	0.4883	0.00300	0.000015	1.71	0.0299	0.0428	0.0699	0.1025
Irr 3 Fur 3	0.5065	0.00300	0.000050	3.31	0.0360	0.0540	0.0951	0.1497
Irr 3 Fur 4	0.2367	0.02599	0.000184	6.34	0.0957	0.1278	0.2050	0.3171
Coefficient of Variation					**79.8979**	**68.5543**	**54.6463**	**46.0443**
Full Inflow Hydrograph	*a*	*k*	f_0	Error (IPARM)	Infiltration ($m^3 m^{-1}$)			
					100 min	200 min	500 min	1000 min
Irr 1 Fur 1	0.2053	0.09288	0.000100	5.89	0.2491	0.2957	0.3828	0.4838
Irr 1 Fur 2	0.1774	0.07863	0.000000	19.44	0.1780	0.2013	0.2368	0.2678
Irr 1 Fur 3	0.3745	0.02523	0.000000	14.52	0.1415	0.1834	0.2585	0.3351
Irr 1 Fur 4	0.2775	0.05969	0.000064	3.90	0.2206	0.2725	0.3669	0.4699
Irr 2 Fur 1	0.4410	0.01244	0.000000	6.45	0.0948	0.1287	0.1927	0.2616
Irr 2 Fur 2	0.4751	0.00619	0.000000	9.40	0.0552	0.0767	0.1186	0.1649
Irr 2 Fur 3	0.5250	0.00499	0.000000	6.78	0.0560	0.0806	0.1304	0.1877
Irr 2 Fur 4	0.5651	0.00536	0.000000	2.77	0.0724	0.1071	0.1797	0.2658
Irr 3 Fur 1	0.3379	0.01828	0.000000	20.93	0.0866	0.1095	0.1492	0.1886
Irr 3 Fur 2	0.4960	0.00356	0.000000	5.14	0.0349	0.0492	0.0776	0.1094
Irr 3 Fur 3	0.4760	0.00567	0.000000	9.05	0.0508	0.0706	0.1092	0.1519
Irr 3 Fur 4	0.3909	0.01859	0.000000	7.82	0.1125	0.1475	0.2111	0.2768
Coefficient of Variation					**62.3880**	**55.5892**	**48.3224**	**44.8534**

Table C.3 Infiltration parameters for Merkley estimated by selecting different advance measurements

Input data selection	*a*	*k*	f_0	Power Curve Error	Total Error	Advance Error	Run Error
All advance (9 points)	0.544925	0.0028164	0	2.086	1.249	1.249	-
advance (2 4 6 8)	0.495231	0.0032205	0	0.361	1.174	1.174	-
advance (4 9)	0.054970	0.0049864	0.0003957	0.000	0.000	0.000	-
advance (1 2 3 4)	0.568661	0.0010931	0.0006828	1.442	0.871	0.871	-
advance (5 6 7 8 9)	0.106659	0.0049854	0.0003454	2.310	0.699	0.699	-
runoff + advance (all 9 points)	0.326952	0.0024476	0.0003902	2.086	3.255	2.288	0.967
runoff +advance (2 4 6 8)	0.288773	0.0027222	0.0003998	0.361	3.426	2.392	1.034
runoff + advance (4 9)	0.302232	0.0025807	0.0003981	0.000	3.454	2.429	1.025
runoff + advance (1 2 3 4)	0.290879	0.0026638	0.0004001	1.442	4.773	3.695	1.079
runoff + advance (5 6 7 8 9)	0.383343	0.002156	0.0003719	2.310	3.033	2.202	0.832

Table C.4 Infiltration parameters for Merkley estimated by selecting different runoff measurements

Runoff Points	*a*	*k*	f_0	Total Error	Advance Error	Run Error
no runoff	0.544925	0.0028384	0	1.249	1.249	
1st point	0.02759	0.0036886	0.0004978	2.419	2.419	0.000
points 1 & 2	0.052236	0.0038009	0.0004819	2.276	2.276	0.000
points 1,2 & 3	0.154475	0.0031935	0.0004546	2.770	2.218	0.552
points 1,2,3 & 4	0.217655	0.0028954	0.0004334	2.874	2.213	0.661
points 1,2,3,4 & 5	0.281327	0.0026234	0.0004094	3.168	2.245	0.924
points 2,4 & 6	0.366633	0.0022599	0.0003804	2.789	2.420	0.370
points 3,4,5 & 6	0.415141	0.0022264	0.0003461	2.807	2.437	0.370
points 4,5 & 6	0.503477	0.002055	0.0002854	2.873	2.864	0.009
just point 6	0.003188	0.0030613	0.0005321	3.310	3.310	0.000
all points 1,2,3,4,5 & 6	0.326952	0.0024476	0.0003902	3.255	2.288	0.967

For explanations of the Total, Advance and Runoff Errors see chapter 4.

APPENDIX D

Field Data for Infiltration Variability and Whole Field Simulation

The data sets contained within this appendix are described in chapter 5 and used within chapters 6 and 7.

Table D.1 Field data for Downs (whole field)

Field Name: **Downs**
Source: NCEA
Location: Macalister near Dalby, Qld, Australia
Details Cotton planted on cracking clay soil
Number of Furrows: 20
Field length: 565 m
Slope: 0.001
Furrow Spacing 2 m
Deficit 100 mm

Furrow Dimensions

Top Width 0.600 m
Middle Width 0.400 m
Bottom Width 0.200 m
Max Height 0.100 m

Advance Data

Irrigation 1

Furrow	1	2	3	4
distance (m)	time (min)	time (min)	time (min)	time (min)
0	0	0	0	0
110	35	31	33	37
220	69	63	62	76
330	133	123	109	149
440	301	282	192	428
550	595	581	498	637

Irrigation 2

Furrow	1	2	3	4
distance (m)	time (min)	time (min)	time (min)	time (min)
0	0	0	0	0
110	84	45	89	52
220	137	97	167	212
330	215	162	238	334
440	337	257	358	596
550	493	397	527	820

Irrigation 3

Furrow	1	2	3	4
distance (m)	time (min)	time (min)	time (min)	time (min)
0	0	0	0	0
110	52	44	40	49
220	212	228	233	174
330	334	421	419	322
440	596	624	626	537
550	820	858	866	923

Irrigation 4

Furrow	1	2	3	4
distance (m)	time (min)	time (min)	time (min)	time (min)
0	0	0	0	0
110	83	71	72	75
220	155	147	159	163
330	269	245	246	256
440	425	389	387	397
550	590	574	573	575

Irrigation 5

Furrow	1	2	3	4
distance (m)	time (min)	time (min)	time (min)	time (min)
0	0	0	0	0
110	133	119	103	125
220	201	210	197	218
330	269	271	260	283
440	324	320	302	321
550	419	411	370	413

Inflow rates and times are located in section 5.5

Table D.2 Runoff data for Downs (whole field) Irr1 Fur1 – Irr2 Fur3

Irrigation 1 Furrow 1

t (min)	Q_r (L s^{-1})	Vol (m^3)
628	0	0.000
630	0.1159	0.007
650	0.3604	0.293
658	0.3919	0.473
673	0.4773	0.864
695	0.6554	1.612
725	0.6772	2.811
755	0.841	4.178
783	1.1997	5.892
810	1.3247	7.937
821	1.4231	8.843
850	1.6684	11.533
900	1.6684	16.538
905	1.6684	17.039
913	1.6684	17.839
918	1.6684	18.340
927	1.596	19.221
937	1.4909	20.147
947	1.2613	20.973
962	0.9174	21.953
972	0.7449	22.452
982	0.6554	22.872
992	0.5331	23.229
1010	0.3604	23.711
1040	0.1241	24.147
1055	0.093	24.245
1070	0	24.287

Irrigation 1 Furrow 2

t (min)	Q_r (L s^{-1})	Vol (m^3)
607	0	0.000
609	0.0504	0.003
611	0.0793	0.011
613	0.1003	0.022
615	0.1079	0.034
620	0.1604	0.074
625	0.1805	0.125
637	0.2747	0.289
639	0.3018	0.324
650	0.376	0.548
669	0.4594	1.024
690	0.5525	1.661
695	0.841	1.870
725	1.0252	3.550
755	1.2613	5.608
782	1.4231	7.782
811	1.5255	10.348
821	1.6684	11.306
850	1.6684	14.209
900	1.6684	19.214
905	1.6684	19.714
913	1.6684	20.515
918	1.6684	21.016
927	1.4909	21.869
937	1.3247	22.713
947	1.1398	23.453
962	1.0252	24.427
972	0.8164	24.979
982	0.6554	25.421
992	0.5723	25.789
1010	0.3604	26.293
1040	0.2248	26.819
1055	0.1604	26.993
1100	0	27.209

Irrigation 1 Furrow 3

t (min)	Q_r (L s^{-1})	Vol (m^3)
565	0	0.000
569	0.1604	0.019
572	0.202	0.052
573	0.202	0.064
574	0.202	0.076
579	0.2248	0.140
585	0.2881	0.232
590	0.3018	0.321
595	0.3159	0.414
615	0.3604	0.819
625	0.5331	1.087
636	0.5525	1.446
650	0.6994	1.971
668	0.8164	2.790
690	0.8661	3.900
697	1.0532	4.303
725	1.3247	6.301
762	1.5605	9.504
781	1.8963	11.474
812	2.0989	15.189
821	2.2261	16.357
850	2.1833	20.193
900	2.0575	26.554
905	1.9359	27.153
913	1.8185	28.054
918	1.7802	28.594
927	1.4909	29.478
937	1.3899	30.342
962	1.1105	32.217
972	0.9976	32.849
982	0.6554	33.345
992	0.5331	33.702
1010	0.3018	34.153
1040	0.1327	34.544
1055	0.0611	34.631
1085	0	34.686

Irrigation 1 Furrow 4

t (min)	Q_r (L/s)	Vol (m^3)
635	0	0.000
666	0.4082	0.380
696	0.8164	1.482
725	1.1695	3.210
780	1.4231	7.487
813	1.667	10.547
821	1.668	11.347
850	1.6684	14.250
900	1.6684	19.255
905	1.6684	19.755
913	1.4909	20.513
918	1.4568	20.956
927	1.3247	21.707
937	1.1695	22.455
947	0.8915	23.073
962	0.6554	23.769
972	0.5331	24.126
982	0.3919	24.403
992	0.376	24.634
1010	0.202	24.946
1040	0.0365	25.161
1055	0.0365	25.193
1085	0	25.226

Irrigation 2 Furrow 1

t (min)	Q_r (L s^{-1})	Vol (m^3)
535	0	0.000
543	0.1159	0.028
551	0.3604	0.142
556	0.3919	0.255
561	0.4773	0.385
570	0.6554	0.691
575	0.6772	0.891
586	0.841	1.392
595	1.1997	1.943
611	1.3247	3.155
616	1.4231	3.567
621	1.6684	4.031
631	1.6684	5.032
646	1.6684	6.533
661	1.6684	8.035
681	1.6684	10.037
696	1.596	11.506
711	1.4909	12.895
726	1.2613	14.133
741	0	14.701

Irrigation 2 Furrow 2

t (min)	Q_r (L s^{-1})	Vol (m^3)
522	0	0.000
524	0.3604	0.022
526	0.5525	0.076
529	0.5525	0.176
536	0.841	0.468
543	0.9437	0.843
561	1.1105	1.953
571	1.1105	2.619
586	1.1695	3.645
595	1.1695	4.276
611	1.1695	5.399
616	1.1695	5.750
621	1.1695	6.101
631	1.1695	6.803
646	0.841	7.707
661	0.6554	8.381
681	0.442	9.039
696	0.3018	9.374
711	0.1703	9.586
726	0.073	9.696
741	0	9.729

Irrigation 2 Furrow 3

see Appendix A

Table D.3 Runoff data for Downs (whole field) Irr2 Fur4– Irr4 Fur4

Irrigation 2 Furrow 4

t (min)	Q_r (L s^{-1})	Vol (m^3)
558	0	0.000
561	0.1241	0.011
572	0.2132	0.122
575	0.2368	0.163
581	0.4955	0.295
586	0.4955	0.443
595	0.4955	0.711
611	0.4955	1.187
616	0.4955	1.335
621	0.4955	1.484
631	0.4773	1.776
646	0.3604	2.153
661	0.2881	2.445
681	0.1159	2.687
696	0.0793	2.775
711	0.0409	2.829
726	0.0135	2.853
741	0	2.860

Irrigation 3 Furrow 2

t (min)	Q_r (L s^{-1})	Vol (m^3)
917	0	0.000
920	0.0611	0.005
925	0.1703	0.040
930	0.376	0.122
935	0.4955	0.253
940	0.6554	0.425
945	0.8661	0.654
950	0.8915	0.917
955	0.8915	1.185
960	0.8915	1.452
980	0.8915	2.522
995	0.8915	3.325
1010	0.8915	4.127
1025	0.8915	4.929
1040	0.5925	5.597
1055	0.2881	5.993
1070	0.0669	6.153
1085	0	6.183

Irrigation 3 Furrow 4

t (min)	Q_r (L s^{-1})	Vol (m^3)
919	0	0.000
925	0.0015	0.000
930	0.1604	0.025
935	0.5925	0.137
940	0.5925	0.315
945	0.613	0.496
950	0.634	0.683
955	0.6554	0.877
960	0.6554	1.073
980	0.6554	1.860
995	0.6554	2.449
1010	0.6554	3.039
1025	0.6554	3.629
1040	0.4249	4.115
1055	0.2132	4.402
1070	0.0611	4.526
1085	0	4.553

Irrigation 4 Furrow 3

t (min)	Q_r (L s^{-1})	Vol (m^3)
625	0	0.000
630	0.2881	0.043
635	0.4594	0.155
645	0.5141	0.447
655	0.7449	0.825
665	0.7449	1.272
675	0.7449	1.719
685	0.7449	2.166
700	0.613	2.777
715	0.4594	3.260
725	0.3159	3.492
735	0.1911	3.644
745	0.1241	3.739
755	0.073	3.798
765	0.0325	3.830
775	0.0058	3.841
785	0	3.843

Irrigation 3 Furrow 1

t (min)	Q_r (L s^{-1})	Vol (m^3)
915	0	0.000
917	0.0325	0.002
920	0.1604	0.019
925	0.2881	0.087
930	0.4773	0.201
935	0.8661	0.403
940	0.8915	0.667
945	0.9437	0.942
950	0.9437	1.225
955	0.9437	1.508
960	0.9437	1.791
980	0.9437	2.924
995	0.9437	3.773
1010	0.9437	4.622
1025	0.613	5.323
1040	0.4082	5.783
1055	0.2248	6.067
1070	0.0669	6.199
1085	0	6.229

Irrigation 3 Furrow 3

t (min)	Q_r (L s^{-1})	Vol (m^3)
910	0	0.000
915	0.0188	0.003
920	0.0504	0.013
925	0.2747	0.062
930	0.5331	0.183
935	0.8661	0.393
940	0.8661	0.653
945	0.9174	0.920
950	0.9976	1.208
955	0.9976	1.507
960	0.9976	1.806
980	0.9976	3.003
995	0.9976	3.901
1010	0.9976	4.799
1025	0.9976	5.697
1040	0.634	6.431
1055	0.3159	6.859
1070	0.1703	7.077
1085	0.0365	7.171
1100	0	7.187

Irrigation 4 Furrow 1

t (min)	Q_r (L s^{-1})	Vol (m^3)
625	0	0.000
630	0.5723	0.086
635	0.6994	0.277
645	0.6994	0.696
655	0.6994	1.116
670	0.6994	1.745
685	0.6994	2.375
700	0.6994	3.004
715	0.6994	3.633
725	0.5331	4.003
735	0.4082	4.286
745	0.2491	4.483
755	0.1241	4.595
765	0.0556	4.649
775	0.0251	4.673
785	0	4.680

Irrigation 4 Furrow 4

t (min)	Q_r (L s^{-1})	Vol (m^3)
625	0	0.000
630	0.0504	0.008
635	0.5925	0.104
645	0.5925	0.459
655	0.5925	0.815
665	0.5925	1.170
675	0.5925	1.526
685	0.5925	1.881
700	0.4773	2.363
715	0.4594	2.784
725	0.442	3.055
735	0.3159	3.282
745	0.2132	3.441
755	0.1327	3.545
765	0.0793	3.608
775	0.0251	3.640
785	0	3.647

Irrigation 4 Furrow 2

t (min)	Q_r (L s^{-1})	Vol (m^3)
625	0	0.000
630	0.613	0.092
635	0.613	0.276
645	0.613	0.644
655	0.6994	1.037
670	0.6994	1.667
685	0.6994	2.296
700	0.6772	2.916
715	0.6772	3.525
725	0.6772	3.931
735	0.3919	4.252
745	0.2248	4.437
755	0.1416	4.547
765	0.0409	4.602
775	0.0135	4.618
785	0	4.622

Table D.4 Runoff data for Downs (whole field) Irr5 Fur1 – Irr5 Fur4

Irrigation 5 Furrow 1

t (min)	Q_r (L s^{-1})	Vol (m^3)
429	0	0.000
431	0.0325	0.002
433	0.2368	0.018
436	0.4955	0.084
441	0.5525	0.241
446	0.634	0.419
471	0.841	1.525
481	0.841	2.030
501	0.841	3.039
511	0.841	3.544
521	0.8164	4.041
531	0.8164	4.531
541	0.7921	5.013
551	0.7921	5.489
561	0.7921	5.964
571	0.7921	6.439
581	0.7683	6.907
596	0.7449	7.588
611	0.6994	8.238
626	0.4773	8.768
641	0.2747	9.106
656	0.1805	9.311
671	0.086	9.431
686	0.0218	9.480
701	0	9.489

Irrigation 5 Furrow 2

t (min)	Q_r (L s^{-1})	Vol (m^3)
425	0	0.000
426	0.0188	0.001
429	0.2491	0.025
431	0.376	0.062
436	0.376	0.175
441	0.5141	0.308
446	0.6554	0.484
471	0.6994	1.500
481	0.7219	1.926
491	0.7449	2.366
501	0.7683	2.820
511	0.7921	3.289
521	0.7921	3.764
531	0.8164	4.246
541	0.8661	4.751
551	0.8661	5.271
561	0.8661	5.790
571	0.8661	6.310
581	0.8164	6.815
596	0.7921	7.539
611	0.7683	8.241
626	0.5925	8.853
641	0.3304	9.268
656	0.1703	9.494
671	0.086	9.609
686	0.0409	9.666
701	0	9.685

Irrigation 5 Furrow 3

t (min)	Q_r (L s^{-1})	Vol (m^3)
389	0	0.000
390	0.0455	0.001
391	0.2491	0.010
393	0.3604	0.047
395	0.4249	0.094
397	0.4773	0.148
399	0.4955	0.206
401	0.5141	0.267
409	0.613	0.537
416	0.634	0.799
426	0.6772	1.193
431	0.7219	1.403
436	0.7449	1.623
441	0.7921	1.853
446	0.7921	2.091
471	0.8661	3.334
481	0.8661	3.854
491	0.8661	4.374
501	0.8661	4.893
511	0.8661	5.413
521	0.8661	5.933
531	0.8915	6.460
541	0.9437	7.011
551	0.9437	7.577
561	0.9437	8.143
571	0.9437	8.709
581	0.8915	9.260
596	0.8661	10.051
611	0.7683	10.786
626	0.4955	11.355
641	0.3159	11.720
656	0.2248	11.963
671	0.1003	12.110
686	0.0287	12.168
701	0	12.181

Irrigation 5 Furrow 4

t (min)	Q_r (L s^{-1})	Vol (m^3)
424	0	0.000
425	0.0287	0.001
428	0.1911	0.021
431	0.3452	0.069
436	0.376	0.177
441	0.4249	0.297
446	0.4594	0.430
471	0.5525	1.189
481	0.5723	1.526
491	0.613	1.882
501	0.6554	2.262
511	0.6554	2.656
521	0.6554	3.049
531	0.6772	3.449
541	0.7219	3.868
551	0.7219	4.302
561	0.7219	4.735
571	0.7219	5.168
581	0.7219	5.601
596	0.6772	6.231
611	0.6772	6.840
626	0.442	7.344
641	0.3018	7.678
656	0.2491	7.926
671	0.1508	8.106
686	0.0218	8.184
701	0	8.194

Table D.5 Field data for Chisholm

Field Name: **Chisholm**
Source: NCEA
Location: Western Darling Downs, Qld, Australia
Details Cotton planted on cracking clay (Kildonan) soil 1999-2000
Number of Furrows: 17
Field length: 250 m
Slope: 0.0008
Furrow Spacing *2 m
Average Deficit 60 mm

Furrow Dimensions

Top Width 0.800 m
Middle Width 0.400 m
Bottom Width 0.150 m
Max Height 0.180 m

Advance Data

Irrigation 1

Furrow	1	2	3	4
Original[1]	F8	F10	F12	F14
distance (m)	time (min)	time (min)	time (min)	time (min)
0	0	0	0	0
60	30	41	28	53
120	116		134	163
180	192	202	243	287
240	273	307	336	427

Irrigation 2

Furrow	1	2
Original[1]	F8	F10
distance (m)	time (min)	time (min)
0	0	0
60	30	46
120		109
180	170	179
240	277	367

Irrigation 3

Furrow	1	2	3
Original[1]	F8	F10	F14
distance (m)	time (min)	time (min)	time (min)
0	0	0	0
60	27	42	30
120	98	111	
180	165	169	135
240	238	246	210

Irrigation 4

Furrow	1	2	3	4
Original[1]	8a	8b	8c	8d
distance (m)	time (min)	time (min)	time (min)	time (min)
0	0	0	0	0
60	38	17	35	19
120	101		81	56
180	186	72	122	89
240		109	164	136

Irrigation 5

Furrow	1	2	3	4
Original[1]	F8	F10	F12	F14
distance (m)	time (min)	time (min)	time (min)	time (min)
0	0	0	0	0
60	29	35	32	30
120	87	85	76	72
180	144	134	124	122
240		189		171

Soil water deficit

Furrow	Defict (m)
Irr1F1	0.07
Irr1F2	0.07
Irr1F3	0.07
Irr1F4	0.07
Irr2F1	0.057
Irr2F2	0.057
Irr3F1	0.06
Irr3F2	0.06
Irr3F3	0.06
Irr4F1	0.06
Irr4F2	0.06
Irr4F3	0.06
Irr4F4	0.06
Irr5F1	0.05
Irr5F2	0.05
Irr5F3	0.05
Irr5F4	0.05

Note: that unless otherwise specified the deficit will be assumed to be equal to the average (0.06).

* The furrow spacing for Irr4 F3 and Irr4 F4 was 1 m

Inflow rates and times are located in section 5.5

[1] **Original refers to the original furrow name in the NCEA database**

Table D.6 Field data for Turner

Field Name: **Turner Field 17**
Source: NCEA
Location: Near Goondiwindi, Qld, Australia
Details Cotton planted on cracking clay (Callondoon) soil 1999-2000
Number of Furrows: 27
Field length: 1120 m
Slope: 0.00141
Furrow Spacing 2 m
Deficit 70 mm

Inflow rates and times are located in section 5.5

Furrow Dimensions

Top Width 0.720 m
Middle Width 0.480 m
Bottom Width 0.300 m
Max Height 0.200 m

Advance Data

Irrigation 1

Furrow	1	2
Original[1]	F4	F8
distance (m)	time (min)	time (min)
0	0	0
280		168
560		
840	508	531
1120	688	

Irrigation 2

Furrow	1	2	3	4
Original[1]	F2	F4	F6	F8
distance (m)	time (min)	time (min)	time (min)	time (min)
0	0	0	0	0
280	131	110	123	0
560	307		287	269
840	470	417	457	461
1120	635	615		654

Irrigation 3

Furrow	1	2	3	4	5
Original[1]	F2	F4	F6	F8	F10
distance (m)	time (min)	time (min)	time (min)	time (min)	time (min)
0	0	0	0	0	0
280	144		132	131	
560		297	307	298	
840	476	484	520	520	496
1120		673	667	662	670

Irrigation 4

Furrow	1	2	3	4
Original[1]	F2	F4	F6	F8
distance (m)	time (min)	time (min)	time (min)	time (min)
0	0	0	0	0
280		92	87	78
560	216	190	188	190
840	351	316	314	310
1120	483		446	448

Irrigation 5

Furrow	1	2	3	4
Original[1]	F2	F4	F6	F8
distance (m)	time (min)	time (min)	time (min)	time (min)
0	0	0	0	0
280	69	50		
560	155	109	96	104
840	258	199	211	192
1120	383		329	306

Irrigation 6

Furrow	1	2
Original[1]	F2	F4
distance (m)	time (min)	time (min)
0	0	0
280	144	131
560	289	278
840		
1120	616	612

Irrigation 7

Furrow	1	2	3	4
Original[1]	F2	F4	F6	F8
distance (m)	time (min)	time (min)	time (min)	time (min)
0	0	0	0	0
280	99	106	110	106
560	197	197	203	196
840	315	314	325	312
1120	440	439	455	

Irrigation 8

Furrow	1	2
Original[1]	F4	F6
distance (m)	time (min)	time (min)
0	0	0
280		
560	222	
840		348
1120	498	481

[1] **Original refers to the original furrow name in the NCEA database**

Table D.7 Field data and infiltration parameters for Coulton A

Field Name: **Coulton Field A**
Source: NCEA
Location: Near Boggabilla, NSW, Australia
Details Cotton planted on cracking clay (Morella) soil 1999-2000
Number of Furrows: 9
Field length: 600 m
Slope: 0.001
Furrow Spacing 1 m for Irrigations 1 and 2, 2 m for Irrigations 4, 5, 6 and 7

Furrow Dimensions

Top Width 0.640 m
Middle Width 0.400 m
Bottom Width 0.200 m
Max Height 0.120 m

Advance Data

Irrigation 1

Furrow	1	2
Original[1]	F5	F6
distance (m)	time (min)	time (min)
0	0	0
150	86	
300		267
450	409	381
600	542	519

Irrigation 4

Furrow	1
Original[1]	F8
distance (m)	time (min)
0	0
150	69
300	151
450	257
600	

Irrigation 6

Furrow	1
Original[1]	F9
distance (m)	time (min)
0	0
150	89
300	202
450	311
600	396

Irrigation 2

Furrow	1	2	3
Original[1]	F10	F14	F16
distance (m)	time (min)	time (min)	time (min)
0	0	0	0
150	86		81
300	229	193	204
450	351	308	364
600		405	549

Irrigation 5

Furrow	1
Original[1]	F8
distance (m)	time (min)
0	0
150	78
300	165
450	244
600	336

Irrigation 7

Furrow	1
Original[1]	F10
distance (m)	time (min)
0	0
150	
300	159
450	234
600	332

Infiltration Parameters

Furrow	Inflow (L s^{-1})	Time (min)	Infiltration			Ad SSE
			a	*k*	f_0	
Irr1F1	2.42	799	0.2587	0.02760	0.000000	3.617
Irr1F2	4.85	799	0.0000	0.22074	0.000000	1.565
Irr2F1	2.25	959	0.2238	0.02873	0.000000	3.135
Irr2F2	2.65	959	0.0619	0.06483	0.000000	1.433
Irr2F3	2.65	959	0.2984	0.02125	0.000039	0.255
Irr4F1	5.14	450	0.0000	**0.04803**	**0.000171**	0.371
Irr5F1	2.79	484	0.0076	**0.03275**	**0.000016**	1.011
Irr6F1	2.65	404	0.0274	**0.03820**	**0.000000**	2.844
Irr7F1	2.26		0.0000	**0.02440**	**0.000025**	1.574

The *k* values and f_0 values in bold have been halved to conform with the 1 m furrow spacing (following identification in IPARM)

[1] Original refers to the original furrow name in the NCEA database

Table D.8 Field data and infiltration parameters for Coulton B

Field Name: **Coulton Field B**
Source: NCEA
Location: Near Boggabilla, NSW, Australia
Details Cotton planted on cracking clay (Morella) soil 1999-2000
Number of Furrows: 7
Field length: 350 m
Slope: 0.001
Furrow Spacing 2 m

Furrow Dimensions

Top Width 0.640 m
Middle Width 0.400 m
Bottom Width 0.200 m
Max Height 0.120 m

Advance Data

Irrigation 3

Furrow	1	2	2	3
Original[1]	F1	F3	F5	F7
distance (m)	time (min)	time (min)	time (min)	time (min)
0	0	0	0	0
80	28	25		33
160	51	49	55	63
240	101	106	85	132
320	188	226	127	195

Irrigation 4

Furrow	1	2	3
Original[1]	F1	F3	F5
distance (m)	time (min)	time (min)	time (min)
0	0	0	0
80	28	25	33
160	55	53	68
240		92	
320	138	133	150

Infiltration Parameters

Furrow	Inflow (L s^{-1})	Time (min)	Infiltration			Ad SSE
			a	*k*	f_0	
Irr3F1	4.54	494	0.0000	0.02841	0.000784	4.004
Irr3F2	4.54	494	0.0000	0.02062	0.000887	3.392
Irr3F3	4.54	494	0.0000	0.05062	0.000400	1.355
Irr3F4	4.54	494	0.1002	0.04741	0.000560	4.069
Irr4F1	5.51	366	0.0000	0.06654	0.000559	1.875
Irr4F2	5.51	366	0.0815	0.05025	0.000464	1.185
Irr4F3	5.51	366	0.0000	0.09625	0.000322	0.263

[1] **Original refers to the original furrow name in the NCEA database**

Table D.9 Field data for and infiltration parameters for Coulton C

Field Name: **Coulton Field C**
Source: NCEA
Location: Near Boggabilla, NSW, Australia
Details Cotton planted on cracking clay (Morella) soil 1999-2000
Number of Furrows: 11
Field length: 450 m
Slope: 0.001
Furrow Spacing 2 m

Furrow Dimensions

Top Width 0.640 m
Middle Width 0.400 m
Bottom Width 0.200 m
Max Height 0.120 m

Advance Data

Irrigation 3

Furrow	1	2	2	3
Original[1]	F8	F10	F12	F14
distance (m)	time (min)	time (min)	time (min)	time (min)
0	0	0	0	0
110	17	21		15
220	59	62	78	57
330	113	123	140	115
440	187	195	171	154

Irrigation 7

Furrow	1	2	3
Original[1]	F8	F10	F14
distance (m)	time (min)	time (min)	time (min)
0	0	0	0
110	24	23	19
220			
330	132	129	112
440	169	171	149

Irrigation 4

Furrow	1	2	2	3
Original[1]	F8	F10	F12	F14
distance (m)	time (min)	time (min)	time (min)	time (min)
0	0	0	0	0
110	34	18	32	18
220	50	59	81	59
330	83	107	134	100
440	122	146	161	151

Infiltration Parameters

Furrow	Inflow (L s^{-1})	Time (min)	Infiltration			Ad SSE
			a	*k*	f_0	
Irr3F1	6.15	578	0.6610	0.00511	0.000000	2.793
Irr3F2	6.15	578	0.5996	0.00718	0.000000	1.483
Irr3F3	6.15	578	0.1302	0.06437	0.000000	5.226
Irr3F4	6.15	578	0.5301	0.00923	0.000000	6.255
Irr4F1	5.60	577	0.0000	0.04358	0.000231	6.212
Irr4F2	5.60	577	0.4357	0.01220	0.000000	4.458
Irr4F3	5.60	577	0.1118	0.05936	0.000000	5.878
Irr4F4	5.60	577	0.5106	0.00868	0.000000	2.330
Irr7F1	4.43	472	0.4091	0.01250	0.000000	5.358
Irr7F2	4.43	472	0.4066	0.01263	0.000000	4.814
Irr7F3	4.43	472	0.4646	0.00848	0.000000	5.168

[1] **Original refers to the original furrow name in the NCEA database**

Table D.10 Field data and infiltration parameters for Turner Field 18

Field Name: **Turner Field 18**
Source: NCEA
Location: Near Goondiwindi, Qld, Australia
Details Cotton planted on cracking clay (Callondoon) soil 1999-2000
Number of Furrows: 13
Field length: 725 m
Slope: 0.00151
Furrow Spacing 2 m

Furrow Dimensions

Top Width 0.720 m
Middle Width 0.480 m
Bottom Width 0.300 m
Max Height 0.200 m

Advance Data

Irrigation 1

Furrow	1
Original[1]	F8
distance (m)	time (min)
0	0
175	111
350	261
525	397
700	

Irrigation 4

Furrow	1	2	3
Original[1]	F2	F4	F8
distance (m)	time (min)	time (min)	time (min)
0	0	0	0
175	78	75	59
350	215	205	215
525	344	347	373
700	520	529	593

Irrigation 6

Furrow	1	2	3
Original[1]	F2	F4	F6
distance (m)	time (min)	time (min)	time (min)
0	0	0	0
175			
350			175
525	338	346	
700	464	553	598

Irrigation 3

Furrow	1
Original[1]	F4
distance (m)	time (min)
0	0
175	176
350	336
525	575
700	

Irrigation 5

Furrow	1	2	2	3
Original[1]	F2	F4	F6	F8
distance (m)	time (min)	time (min)	time (min)	time (min)
0	0	0	0	0
175	56	46	60	57
350	143	125	166	136
525	245	218	272	233
700	350	360	438	367

Irrigation 8

Furrow	1
Original[1]	F2
distance (m)	time (min)
0	0
175	
350	272
525	
700	583

Infiltration Parameters

Furrow	Inflow (L s^{-1})	Time (min)	Infiltration			Ad SSE
			a	*k*	f_0	
Irr1F1	3.64	873	0.1314	0.07434	0.000000	1.856
Irr3F1	3.18	703	0.0000	0.14730	0.000136	2.859
Irr4F1	3.50	600	0.2947	0.02647	0.000000	1.793
Irr4F2	3.50	600	0.3350	0.02125	0.000000	0.957
Irr4F3	3.50	600	0.4279	0.01333	0.000000	2.696
Irr5F1	3.28	425	0.3005	0.01706	0.000000	0.955
Irr5F2	3.28	425	0.2755	0.01260	0.000132	1.151
Irr5F3	3.28	425	0.2608	0.01950	0.000092	1.944
Irr5F4	3.28	425	0.0931	0.02941	0.000171	0.423
Irr6F1	4.00	546	0.0699	0.09071	0.000026	0.000
Irr6F2	4.00	546	0.1040	0.05335	0.000209	0.000
Irr6F3	4.00	546	0.0773	0.04632	0.000290	0.000
Irr8F1	3.32	773	0.1023	0.08352	0.000001	0.000

[1] **Original refers to the original furrow name in the NCEA database**

APPENDIX E

Results from Sample Size

Analysis

The figures in this section follow from the results presented in section 5.7. The sampling distributions were constructed from random sampling (with replacement) of the cumulative infiltration volumes at the specified opportunity times with 50 random samples for each sample size.

(a) 100% average advance time (229.6 minutes) (a) 50% average advance time (114.8 minutes)

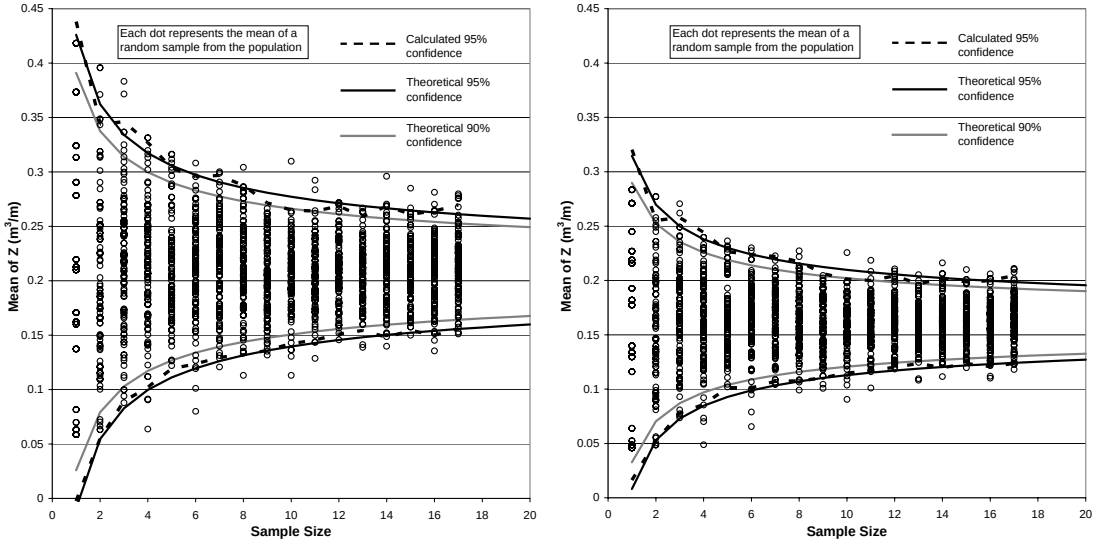

Figure E.1 Chisholm: Sampling distributions of the mean

(a) 100% average advance time (500 minutes) (a) 50% average advance time (250 minutes)

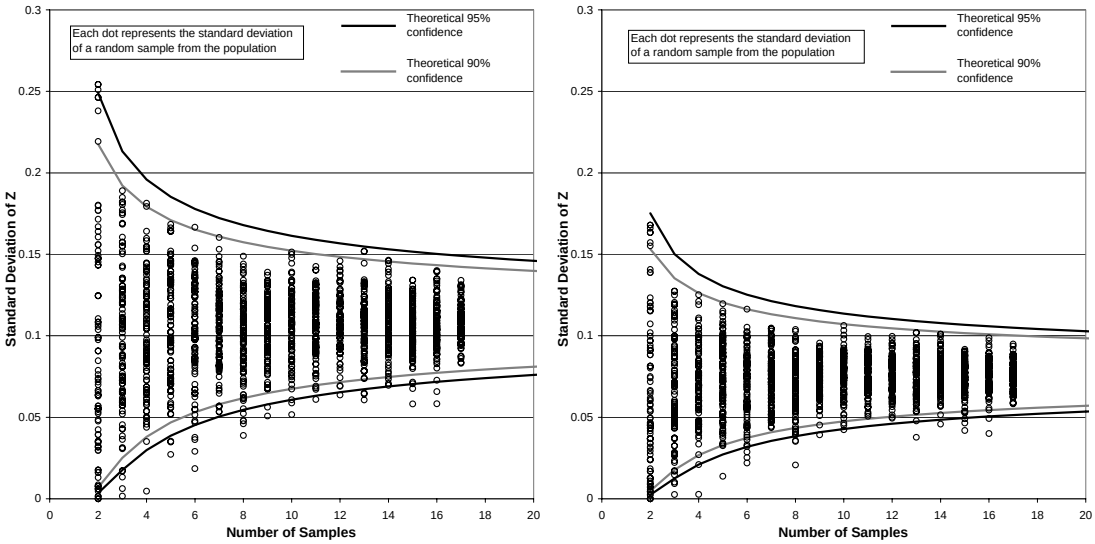

Figure E.2 Chisholm: Sampling distributions of the standard deviation

(a) 100% average advance time (500 minutes) (a) 50% average advance time (250 minutes)

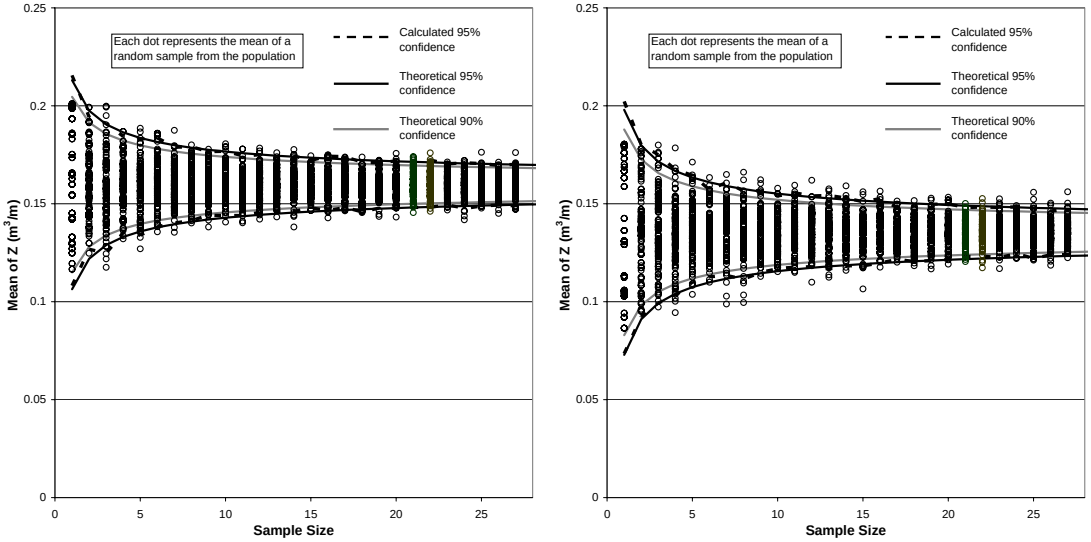

Figure E.3 Turner: Sampling distributions of the mean

(a) 100% average advance time (500 minutes) (a) 50% average advance time (250 minutes)

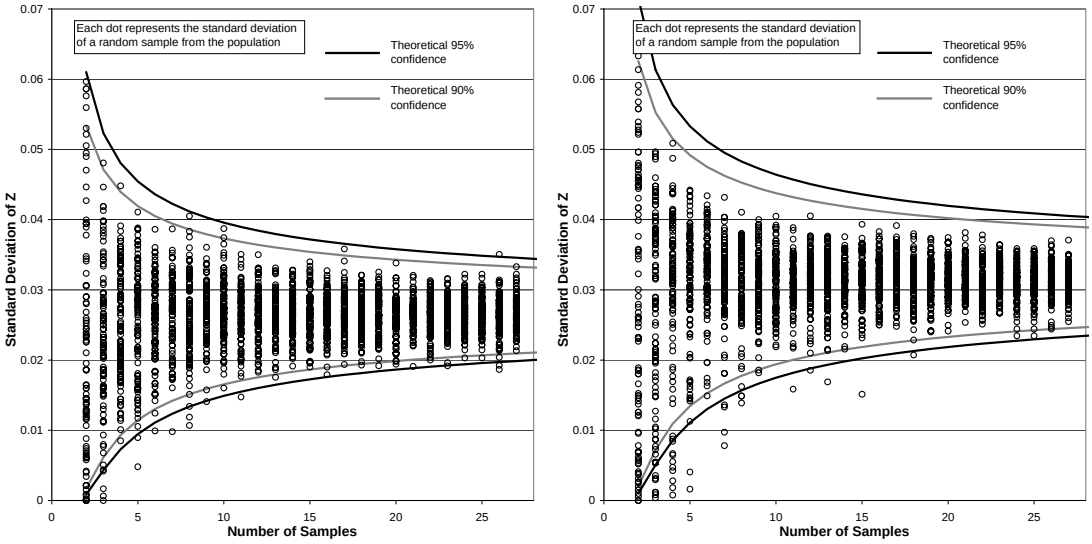

Figure E.4 Turner: Sampling distributions of the standard deviation

APPENDIX F

Results from Infiltration

Prediction

This section contains the infiltration parameters estimated using IPARM from the data introduced in chapter 5. These infiltration parameters are used as the basis of the analysis conducted within chapters 5, 6 and 7.

Table F.1 Estimated infiltration parameters for Downs

	Estimated using Irr1Fur1			Estimated using Irr2 (Fur1,Fur2,Fur3,Fur4)		
	a	***k***	f_0	***a***	***k***	f_0
Irr1 F1	0.5543	0.00688	0.0000000	0.3402	0.02478	0.0000849
Irr1 F2	0.5880	0.00508	0.0000000	0.3552	0.02015	0.0000887
Irr1 F3	0.6101	0.00417	0.0000000	0.3642	0.01764	0.0000912
Irr1 F4	0.5568	0.00673	0.0000000	0.3414	0.02439	0.0000851
Irr2 F1	0.5869	0.00514	0.0000000	0.3546	0.02030	0.0000886
Irr2 F2	0.5769	0.00562	0.0000000	0.3503	0.02157	0.0000874
Irr2 F3	0.6772	0.00228	0.0000000	0.3876	0.01191	0.0000987
Irr2 F4	0.5605	0.00650	0.0000000	0.3431	0.02384	0.0000856
Irr3 F1	0.4105	0.02504	0.0000000	0.2660	0.06166	0.0000675
Irr3 F2	0.4563	0.01660	0.0000000	0.2909	0.04596	0.0000734
Irr3 F3	0.4181	0.02338	0.0000000	0.2699	0.05880	0.0000688
Irr3 F4	0.4090	0.02538	0.0000000	0.2647	0.06240	0.0000677
Irr4 F1	0.5493	0.00720	0.0000000	0.3379	0.02556	0.0000843
Irr4 F2	0.5723	0.00585	0.0000000	0.3483	0.02218	0.0000869
Irr4 F3	0.5451	0.00747	0.0000000	0.3360	0.02623	0.0000838
Irr4 F4	0.5488	0.00723	0.0000000	0.3377	0.02563	0.0000842
Irr5 F1	0.7119	0.00167	0.0000001	0.3966	0.00981	0.0001025
Irr5 F2	0.6895	0.00204	0.0000000	0.3910	0.01111	0.0001001
Irr5 F3	0.8684	0.00041	0.0000007	0.3935	0.00464	0.0001173
Irr5 F4	0.6957	0.00193	0.0000001	0.3927	0.01072	0.0001007

Infiltration parameters were predicted according to the technique developed in section 5.9

Table F.2 Estimated infiltration parameters for Chisholm

	Estimated using Irr3Fur1			Estimated using Irr1Fur1 and Irr2Fur1		
	a	***k***	f_0	***a***	***k***	f_0
Irr1 F1	0.0000	0.04660	0.0001250	0.0000	0.04635	0.0000970
Irr1 F2	0.0000	0.04460	0.0001975	0.0000	0.04370	0.0001735
Irr1 F3	0.0000	0.04630	0.0002085	0.0000	0.04425	0.0002105
Irr1 F4	0.4385	0.01019	0.0000000	0.0000	0.04290	0.0003350
Irr2 F1	0.2111	0.10991	0.0000001	0.2832	0.07145	0.0000504
Irr2 F2	0.1599	0.18783	0.0000000	0.2159	0.13511	0.0000419
Irr3 F1	0.3519	0.02520	0.0000000	0.4591	0.01260	0.0000722
Irr3 F2	0.3456	0.02692	0.0000000	0.4516	0.01362	0.0000712
Irr3 F3	0.3762	0.01955	0.0000000	0.4871	0.00937	0.0000766
Irr4 F1	0.2815	0.05264	0.0000000	0.3733	0.02993	0.0000611
Irr4 F2	0.3146	0.03721	0.0000000	0.4144	0.01990	0.0000661
Irr4 F3	0.3601	0.02313	0.0000000	0.4686	0.01140	0.0000737
Irr4 F4	0.2758	0.05585	0.0000000	0.3662	0.03209	0.0000602
Irr5 F1	0.2986	0.04403	0.0000000	0.3946	0.02425	0.0000636
Irr5 F2	0.3016	0.04264	0.0000000	0.3984	0.02336	0.0000641
Irr5 F3	0.3280	0.03235	0.0000000	0.4306	0.01689	0.0000683
Irr5 F4	0.3213	0.03470	0.0000000	0.4225	0.01834	0.0000672

Table F.3 Estimated infiltration parameters for Turner

	Estimated using Irr1Fur1 and Irr1Fur2			Estimated using Irr7 (Fur1,Fur2,Fur3,Fur4)		
	a	***k***	f_0	***a***	***k***	f_0
Irr1 F1	0.0523	0.11822	0.0000043	0.0499	0.09896	0.0001645
Irr1 F2	0.0487	0.12662	0.0000043	0.0516	0.10187	0.0001651
Irr2 F1	0.1025	0.09269	0.0000000	0.0508	0.10049	0.0001648
Irr2 F2	0.1054	0.06421	0.0001189	0.0488	0.09728	0.0001641
Irr2 F3	0.1849	0.06127	0.0000000	0.0509	0.10069	0.0001649
Irr2 F4	0.2526	0.04182	0.0000000	0.0547	0.10844	0.0001662
Irr3 F1	0.0940	0.10266	0.0000024	0.0526	0.10389	0.0001655
Irr3 F2	0.1743	0.06725	0.0000000	0.0556	0.11054	0.0001665
Irr3 F3	0.1451	0.08099	0.0000000	0.0552	0.10949	0.0001664
Irr3 F4	0.1600	0.07395	0.0000000	0.0548	0.10862	0.0001663
Irr3 F5	0.0503	0.13618	0.0000001	0.0554	0.11002	0.0001664
Irr4 F1	0.0898	0.06609	0.0000187	0.0212	0.07514	0.0001545
Irr4 F2	0.0000	0.06811	0.0001480	0.0000	0.06811	0.0001480
Irr4 F3	0.1170	0.04400	0.0000783	0.0096	0.07077	0.0001508
Irr4 F4	0.2661	0.02430	0.0000000	0.0103	0.07100	0.0001511
Irr5 F1	0.0779	0.04168	0.0001550	0.0028	0.06881	0.0001488
Irr5 F2	0.0000	0.02557	0.0002744	0.0000	0.03749	0.0001165
Irr5 F3	0.6563	0.00246	0.0000000	0.0000	0.05475	0.0001360
Irr5 F4	0.5409	0.00402	0.0000270	0.0000	0.04848	0.0001294
Irr6 F1	0.0000	0.09516	0.0000428	0.0190	0.07416	0.0001537
Irr6 F2	0.0456	0.07156	0.0000490	0.0181	0.07382	0.0001535
Irr7 F1	0.0000	0.10240	0.0001150	0.0351	0.08315	0.0001592
Irr7 F2	0.0000	0.10670	0.0000958	0.0351	0.08317	0.0001592
Irr7 F3	0.0000	0.09158	0.0000828	0.0216	0.07532	0.0001546
Irr7 F4	0.0000	0.11531	0.0000553	0.0323	0.08119	0.0001582
Irr8 F1	0.1281	0.06540	0.0000395	0.0419	0.08895	0.0001616
Irr8 F2	0.0586	0.08944	0.0000509	0.0388	0.08604	0.0001605

APPENDIX G

Validation of the FIDO

Simulation Engine Used by

IrriProb

Introduction

It is important to validate the completed simulation model of IrriProb prior to any field analysis. McClymont (2007) found that the FIDO simulation engine performed favourably against alternative models. The analysis presented here aims to provide further justification for the use of the FIDO simulation model. Data sets have been chosen to illustrate potential differences between FIDO and other surface irrigation models. SIRMOD (Walker 2003) has been used extensively in the past to verify the performance of other simulation models (Abbasi et al. 2003b), therefore it was selected as the basis for validation. The results of the SRFR (Clemmens and Strelkoff 1999) irrigation model were used as a secondary comparison. However, SRFR utilises the zero inertia approximation rather than the hydrodynamic approach of IrriProb and SIRMOD and may have slightly altered results.

Prediction of the Advance Trajectory and Runoff Hydrograph

The furrow from the Downs field, irrigation two furrow three was simulated using IrriProb, SIRMOD III and SRFR with field characteristics contained in The data sets contained within this appendix are described in chapter 5 and used within chapters 6 and 7.

Table D.1 and infiltration parameters presented in Table 5-1. The resultant advance trajectories are plotted against the measured data in Figure G.1, and similarly for the runoff hydrograph in Figure G.2. The advance trajectories are almost identical between SIRMOD and IrriProb, with an R^2 of 0.99999 and a SSE per point of 0.55. The advance predicted by SRFR diverged slightly from the other models at greater distances. However, this was expected since SRFR uses the simpler, zero inertia model.

All three models provided accurate predictions of the runoff hydrograph from the end of the field when compared to the measured data (Figure G.2). However, SRFR suffers from instability during the initial time steps of the storage phase. The hydrograph from IrriProb also exhibits the same type of instability during the initial

minutes of runoff. The jagged shape at the commencement of runoff is more pronounced for some other data sets (not presented here). This effect is most likely a result of differences in step size; SIRMOD was using a 2 minute time step whilst IrriProb used the initial 10 minute time step. The use of the larger time step tends to cause the simulation to overestimate the runoff rate for the first time step of the storage phase. This reduces the volume available for runoff at the subsequent time step and hence the discharge is underestimated.

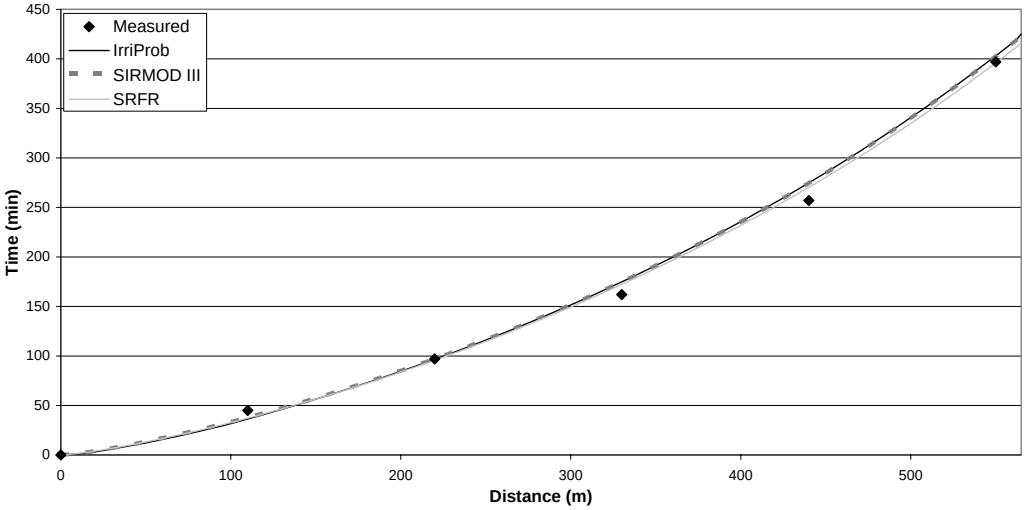

Figure G.1 Simulated advance trajectories (Downs, Irr2 Fur3)

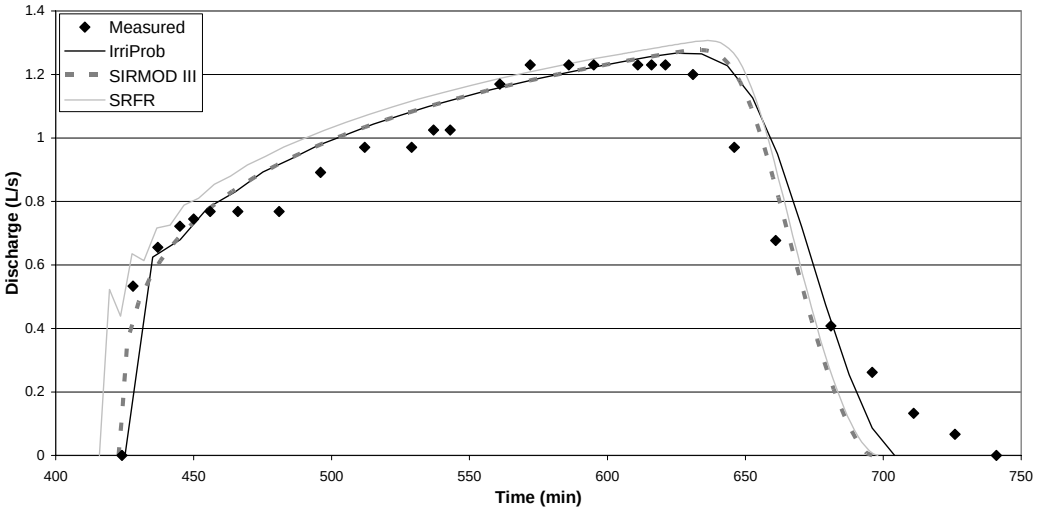

Figure G.2 Simulated runoff hydrographs (Downs, Irr2 Fur3)

Similar conclusions can be made from the distribution of applied depths (Figure G.3). Although no measured data was available, any difference in the predicted infiltrated

depths between the three models is trivial. All results confirm the accuracy of the FIDO simulation.

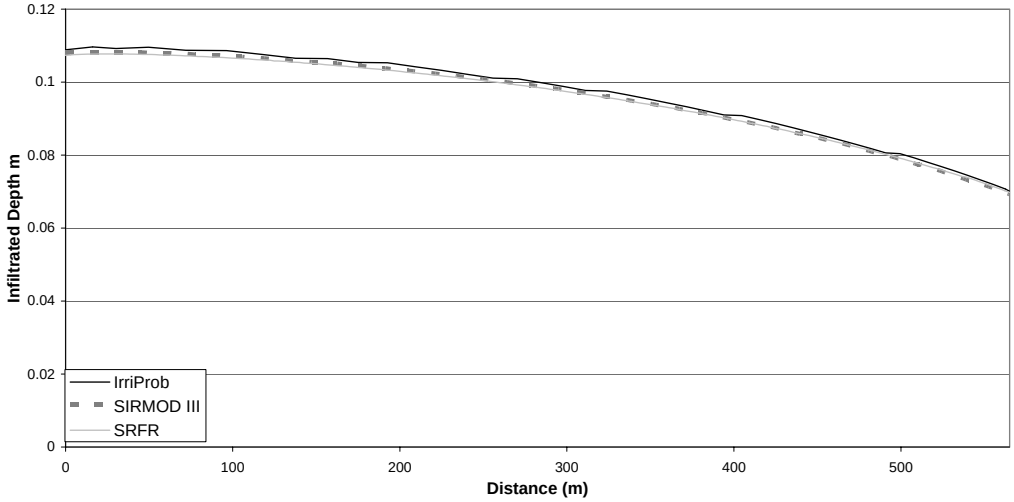

Figure G.3 Simulated infiltration profiles (Downs, Irr2 Fur3)

Ability to Predict the Performance Parameters

Regardless of the fit to the measured advance trajectory and runoff hydrograph the primary function of IrriProb is the prediction and management of irrigation performance. Hence, more emphasis will be given towards the ability to provide reliable values for the performance indicators and total volumes of runoff and infiltration. Four furrows were chosen from the Downs data set for comparison; irrigation 1 furrow 3, irrigation 2 furrow 2, irrigation 3 furrow 4 and irrigation 5 furrow 3. For valid comparison, all simulations were conducted using the constant average inflow rate with all input parameters equal (including Manning *n*) between the different models. The comparisons between the different software packages are presented in Appendix Table G.1. Although the numerical method is consistent between the two versions of SIRMOD (II and III) they were considered separately due to the differences in estimated performance parameters. The final row titled VB (volume balance) error represents the numerical accuracy of the model and was calculated using a simple difference between the volumes of predicted inflow, infiltration and runoff. A volume balance error of less than 5% is acceptable; a value of approximately 1% is typical (Walker 2005b). The volume balance error was low in all simulations therefore the models performed satisfactory for the furrows tested.

Table G.1 Comparison of SIRMOD and IrriProb Performance Terms

(a) Downs Irrigation 1 Furrow 3

	SIRMOD III	SIRMOD II	SRFR	IrriProb	Difference between IrriProb and		Measured
					SIRMOD III (%)	SIRMOD II (%)	
Advance Time (min)	522.60	522.20	521.00	524.32	0.33	0.41	565.00
AE (%)	69.89	70.34	70.07	69.28	-0.87	-1.50	
RE (%)	99.28	99.59		99.68	0.41	0.09	
DU (%)	90.17	86.08	85.96	86.18	-4.42	0.12	
ADU (%)		77.28	77.05	77.67		0.51	
Runoff (%)	16.97		16.78	16.98	0.08		21.60
Deep Drainage (%)	13.14		***13.14***	13.63	3.75		
Inflow (1000 L)	160.50	160.00	***160.63***	162.58	1.30	1.61	160.62
Runoff (1000 L)	26.90	26.70	***26.95***	27.61	2.65	3.42	34.69
Infiltration (1000 L)	133.30	133.50	***133.62***	134.81	1.13	0.98	125.93
VB error (%)	0.22	-0.15		0.10			

(b) Downs Irrigation 2 Furrow 2

	SIRMOD III	SIRMOD II	SRFR	IrriProb	Difference between IrriProb and		Measured
					SIRMOD III (%)	SIRMOD II (%)	
Advance Time (min)	532.80	533.40	532.33	535.09	0.43	0.32	522.00
AE (%)	82.05	82.19	82.20	81.50	-0.67	-0.84	
RE (%)	96.38	96.64		97.02	0.66	0.39	
DU (%)	83.55	79.65	79.56	80.04	-4.20	0.49	
ADU (%)		67.71	67.27	68.36		0.97	
Runoff (%)	7.53		7.29	7.43	-1.29		7.32
Deep Drainage (%)	10.43		***10.50***	10.96	5.06		
Inflow (1000 L)	132.70	132.90	***132.83***	134.51	1.36	1.21	132.86
Runoff (1000 L)	9.70	9.70	***9.68***	10.00	3.07	3.07	9.73
Infiltration (1000 L)	122.80	123.10	***123.17***	124.37	1.27	1.03	123.13
VB error (%)	0.22	0.00		0.11			

(c) Downs Irrigation 3 Furrow 4

	SIRMOD III	SIRMOD II	SRFR	IrriProb	Difference between IrriProb and		Measured
					SIRMOD III (%)	SIRMOD II (%)	
Advance Time (min)	896.70	895.60	895.33	897.54	0.09	0.22	919.00
AE (%)	56.93	57.06	57.03	56.66	-0.47	-0.70	
RE (%)	99.45	99.79		99.84	0.39	0.05	
DU (%)	79.11	72.41	72.00	72.65	-8.17	0.33	
ADU (%)		51.63	50.58	52.67		2.02	
Runoff (%)	3.10		2.96	2.99	-3.43		2.30
Deep Drainage (%)	39.97		***40.00***	40.33	0.90		
Inflow (1000 L)	197.40	197.60	***197.64***	199.11	0.86	0.76	197.61
Runoff (1000 L)	5.80	5.90	***5.85***	5.96	2.77	1.03	4.55
Infiltration (1000 L)	191.30	192.20	***191.76***	193.12	0.95	0.48	193.06
VB error (%)	0.18	-0.22		0.01			

(d) Downs Irrigation 5 Furrow 3

	SIRMOD III	SIRMOD II	SRFR	IrriProb	Difference between IrriProb and		Measured
					SIRMOD III (%)	SIRMOD II (%)	
Advance Time (min)	401.50	402.20	401.17	403.50	0.50	0.32	389.00
AE (%)	82.09	82.50	82.33	81.88	-0.26	-0.75	
RE (%)	51.75	51.92		52.77	1.97	1.64	
DU (%)	88.02	85.66	85.57	85.87	-2.44	0.25	
ADU (%)		78.48	78.16	78.99		0.65	
Runoff (%)	17.91		17.64	18.05	0.78		17.05
Deep Drainage (%)	0.00		***0.00***	0.00	0.0		
Inflow (1000 L)	71.20	71.10	***71.42***	72.83	2.29	2.43	71.43
Runoff (1000 L)	12.60	12.50	***12.60***	13.15	4.33	5.16	12.18
Infiltration (1000 L)	58.50	58.70	***58.82***	59.63	1.93	1.59	59.25
VB error (%)	0.21	-0.08		0.07			

The values in bold have been calculated outside SRFR using the simulation output file from the predicted average depths of runoff, deep percolation, infiltration and total application

The four selected furrows provided further confirmation that the three simulation models provide similar accuracy. Much of the difference in the results was a direct consequence of the handling of the time step and is clearly visible as differences in the total inflow volume. IrriProb consistently overestimated the inflow volume since it continues the inflow for one time interval past the specified cut-off time. This resulted in slightly higher values for the runoff and infiltration volumes and hence caused the model to overestimate the deep drainage and RE.

The DU was similar between IrriProb and SIRMOD II, with less than 0.5% difference over the irrigations studied. However, there was a significant difference between the DU predicted by IrriProb and SIRMOD III, ranging between -2.44% and -8.17%, indicating the use of a different formula. Manual evaluation of the low quarter DU from predicted depth profiles using equation 6-10 matched the values predicted by SIRMOD II and IrriProb. SIRMOD III consistently exaggerated the DU and the difference increased where the advance did not reach the end of the field. The remaining performance indicators behaved similarly between the three models. The results from SRFR also matched the performance estimates of SIRMOD and IrriProb, which is significant since SRFR uses the kinematic wave approximation.

APPENDIX H

IrriProb: Irrigation

Performance Under Measured

Conditions

Table H.1 Downs: irrigation performance under measured conditions

	AE (%)	AER[a] (%)	RE (%)	AELQ (%)	DU (%)	ADU (%)	CU (%)	DURZ (%)	Inflow (m^3)	Runoff (%)	Deep Drainage (%)	D (mm)	D_{RZ} (mm)	D_{DD} (mm)
Irr1F1	66.16	75.47	99.88	65.91	82.06	70.44	89.95	99.63	170.6	11.0	22.8	134.3	99.9	34.4
Irr1F2	70.38	81.91	99.59	69.50	84.12	74.30	91.03	98.75	159.9	13.6	16.0	122.2	99.6	22.6
Irr1F3	69.28	83.72	99.68	68.62	86.18	77.67	92.18	99.05	162.6	17.0	13.6	119.3	99.7	19.6
Irr1F4	67.06	80.18	99.92	66.91	85.33	76.62	91.57	99.77	168.4	15.4	17.4	125.8	99.9	25.9
Irr2F1	83.98	88.36	95.52	72.40	76.45	60.54	86.74	86.21	128.5	5.2	10.7	107.7	95.5	12.2
Irr2F2	81.50	87.82	97.01	74.01	80.04	68.66	88.25	90.80	134.5	7.4	11.0	110.1	97.0	13.0
Irr2F3	84.57	95.23	93.75	72.40	82.88	72.98	90.08	85.61	125.3	12.5	2.8	96.8	93.7	3.1
Irr2F4	81.90	83.78	95.89	71.38	72.99	53.73	84.75	87.16	132.3	2.2	15.9	114.5	95.9	18.6
Irr3F1	56.83	60.96	99.99	56.81	75.98	58.86	86.38	99.97	198.8	4.9	39.2	169.0	100.0	69.1
Irr3F2	65.33	68.45	99.60	64.55	75.97	59.24	86.38	98.80	172.3	3.7	30.9	146.8	99.6	47.2
Irr3F3	57.69	60.93	99.99	57.67	75.94	59.67	86.34	99.97	195.9	3.8	38.5	166.7	100.0	66.7
Irr3F4	56.66	59.21	99.84	56.38	72.64	53.22	84.63	99.51	199.1	3.0	40.3	170.9	99.8	71.1
Irr4F1	80.90	84.01	96.18	71.27	74.07	59.88	84.65	88.09	134.3	3.7	15.3	114.4	96.2	18.2
Irr4F2	86.04	89.25	94.11	71.57	74.47	59.73	84.90	83.19	123.6	3.8	10.1	105.1	94.1	11.0
Irr4F3	80.64	83.50	96.63	72.20	74.93	58.13	85.78	89.54	135.4	3.4	15.9	115.7	96.6	19.0
Irr4F4	81.41	83.52	95.68	70.39	72.29	56.28	83.83	86.47	132.8	2.5	16.0	114.4	95.7	18.8
Irr5F1	89.75	98.35	82.99	71.83	80.04	69.90	88.09	80.04	104.5	10.1	0.0	83.0	83.0	0.0
Irr5F2	89.72	97.28	89.65	72.44	79.62	67.53	88.04	80.74	112.9	8.9	1.3	90.9	89.7	1.3
Irr5F3	81.88	97.22	52.77	70.31	85.87	78.99	91.57	85.87	72.8	18.1	0.0	52.8	52.8	0.0
Irr5F4	91.16	97.28	89.46	72.39	78.10	65.00	87.34	79.41	110.9	7.2	1.5	91.0	89.5	1.5
Field	**73.81**	**80.25**	**93.91**	**59.84**	**64.75**	**35.46**	**77.27**	**81.07**	**143.8**	**7.6**	**18.6**	**117.6**	**93.9**	**23.7**

Field inflow is expressed as a volume per furrow

[a] Application efficiency with recycling is based on a tail water recycling efficiency of 85%

Table H.2 Chisholm: irrigation performance under measured conditions using a constant deficit equal to 0.06 m

	AE (%)	AER[a] (%)	RE (%)	AELQ (%)	DU (%)	ADU (%)	CU (%)	DURZ (%)	Inflow (m^3)	Runoff (%)	Deep Drainage (%)	D (mm)	D_{RZ} (mm)	D_{DD} (mm)
Irr1F1	43.73	91.48	85.04	42.37	96.89	95.27	98.12	96.89	58.3	56.2	0.0	51.0	51.0	0.0
Irr1F2	49.10	92.29	95.42	47.18	96.10	94.23	97.66	96.10	58.3	50.8	0.0	57.3	57.3	0.0
Irr1F3	51.47	88.00	100.00	51.47	94.67	92.01	96.83	100.00	58.3	43.0	5.5	66.4	60.0	6.4
Irr1F4	51.42	85.76	100.00	51.42	94.15	91.31	96.50	100.00	58.3	40.4	8.1	69.4	60.0	9.4
Irr2F1	17.48	35.22	100.00	17.48	87.68	80.79	92.79	100.00	171.6	20.9	61.5	271.0	60.0	211.0
Irr2F2	17.72	17.80	100.00	17.72	69.91	33.37	83.44	100.00	169.3	0.1	81.3	335.4	60.0	275.4
Irr3F1	23.68	64.95	100.00	23.68	95.69	93.45	97.41	100.00	126.7	48.6	27.6	130.0	60.0	70.0
Irr3F2	23.62	73.47	100.00	23.62	97.67	96.67	98.54	100.00	127.0	58.6	17.6	104.7	60.0	44.7
Irr3F3	23.46	54.41	100.00	23.46	93.10	89.35	95.83	100.00	127.9	36.4	40.0	162.4	60.0	102.4
Irr4F1	43.60	43.60	99.44	42.87	65.07	26.22	80.25	98.32	68.4	0.0	55.0	134.9	59.7	75.2
Irr4F2	27.48	51.11	100.00	27.48	90.25	84.78	93.82	100.00	109.2	27.8	44.4	157.0	60.0	97.0
Irr4F3	54.22	86.01	100.00	54.22	98.32	97.42	99.01	100.00	55.3	37.4	7.9	68.8	60.0	8.8
Irr4F4	27.23	51.91	100.00	27.23	92.40	88.19	95.35	100.00	110.2	29.0	43.3	155.4	60.0	95.4
Irr5F1	11.34	59.81	100.00	11.34	96.94	95.35	98.13	100.00	264.5	57.0	31.5	226.7	60.0	166.7
Irr5F2	11.29	73.18	100.00	11.29	98.83	98.24	99.28	100.00	265.7	72.8	15.8	143.9	60.0	83.9
Irr5F3	11.31	72.62	100.00	11.31	98.71	98.09	99.20	100.00	265.2	72.1	16.5	147.3	60.0	87.3
Irr5F4	11.36	72.34	100.00	11.36	98.59	97.89	99.13	100.00	264.1	71.7	16.8	148.8	60.0	88.8
Field	**21.37**	**62.37**	**98.82**	**20.60**	**42.60**	**24.74**	**61.19**	**96.41**	**138.7**	**48.2**	**30.2**	**143.0**	**59.3**	**83.7**

Table H.3 Chisholm: irrigation performance under measured conditions using measured (variable) soil water deficits

	AE (%)	AER[a] (%)	RE (%)	AELQ (%)	DU (%)	ADU (%)	CU (%)	DURZ (%)	Inflow (m^3)	Runoff (%)	Deep Drainage (%)	D (mm)	D_{RZ} (mm)	D_{DD} (mm)
Irr1F1	43.73	91.48	72.89	42.37	96.89	95.27	98.12	96.89	58.3	56.2	0.0	51.0	51.0	0.0
Irr1F2	49.10	92.29	81.79	47.18	96.10	94.23	97.66	96.10	58.3	50.8	0.0	57.3	57.3	0.0
Irr1F3	56.94	93.47	94.82	53.90	94.67	92.01	96.83	94.67	58.3	43.0	0.0	66.4	66.4	0.0
Irr1F4	58.73	93.06	97.89	56.04	94.15	91.31	96.50	95.42	58.3	40.4	0.8	69.4	68.5	0.9
Irr2F1	16.61	34.35	100.00	16.61	87.68	80.79	92.79	100.00	171.6	20.9	62.4	271.0	57.0	214.0
Irr2F2	16.83	16.92	100.00	16.83	69.91	33.37	83.44	100.00	169.3	0.1	82.2	335.4	57.0	278.4
Irr3F1	23.68	64.95	100.00	23.68	95.69	93.45	97.41	100.00	126.7	48.6	27.6	130.0	60.0	70.0
Irr3F2	23.62	73.47	100.00	23.62	97.67	96.67	98.54	100.00	127.0	58.6	17.6	104.7	60.0	44.7
Irr3F3	23.46	54.41	100.00	23.46	93.10	89.35	95.83	100.00	127.9	36.4	40.0	162.4	60.0	102.4
Irr4F1	43.60	43.60	99.44	42.87	65.07	26.22	80.25	98.32	68.4	0.0	55.0	134.9	59.7	75.2
Irr4F2	27.48	51.11	100.00	27.48	90.25	84.78	93.82	100.00	109.2	27.8	44.4	157.0	60.0	97.0
Irr4F3	54.22	86.01	100.00	54.22	98.32	97.42	99.01	100.00	55.3	37.4	7.9	68.8	60.0	8.8
Irr4F4	27.23	51.91	100.00	27.23	92.40	88.19	95.35	100.00	110.2	29.0	43.3	155.4	60.0	95.4
Irr5F1	9.45	57.92	100.00	9.45	96.94	95.35	98.13	100.00	264.5	57.0	33.4	226.7	50.0	176.7
Irr5F2	9.41	71.30	100.00	9.41	98.83	98.24	99.28	100.00	265.7	72.8	17.7	143.9	50.0	93.9
Irr5F3	9.43	70.74	100.00	9.43	98.71	98.09	99.20	100.00	265.2	72.1	18.3	147.3	50.0	97.3
Irr5F4	9.47	70.45	100.00	9.47	98.59	97.89	99.13	100.00	264.1	71.7	18.7	148.8	50.0	98.8
Field	**20.71**	**61.71**	**96.34**	**18.00**	**42.60**	**24.74**	**61.19**	**86.90**	**138.7**	**48.2**	**30.8**	**143.0**	**57.5**	**85.5**

Table H.4 Turner: irrigation performance under measured conditions

	AE (%)	AER[a] (%)	RE (%)	AELQ (%)	DU (%)	ADU (%)	CU (%)	DURZ (%)	Inflow (m^3)	Runoff (%)	Deep Drainage (%)	D (mm)	D_{RZ} (mm)	D_{DD} (mm)
Irr1F1	59.34	83.14	100.00	59.34	97.93	96.88	98.74	100.00	273.7	28.0	12.5	84.8	70.0	14.8
Irr1F2	59.26	80.47	100.00	59.26	97.89	96.85	98.72	100.00	274.1	25.0	15.7	88.5	70.0	18.5
Irr2F1	64.19	80.19	100.00	64.19	95.93	93.62	97.61	100.00	253.0	18.8	17.0	88.5	70.0	18.5
Irr2F2	64.21	74.36	100.00	64.21	83.74	75.93	90.18	100.00	252.9	11.9	23.8	95.9	70.0	25.9
Irr2F3	60.93	73.26	100.00	60.93	91.72	87.01	95.16	100.00	266.6	14.5	24.4	98.1	70.0	28.1
Irr2F4	60.96	70.19	100.00	60.96	87.73	80.49	92.89	100.00	266.4	10.9	28.1	102.2	70.0	32.2
Irr3F1	54.42	76.40	100.00	54.42	96.69	94.98	98.02	100.00	298.4	25.9	19.6	95.2	70.0	25.2
Irr3F2	55.03	71.01	100.00	55.03	93.03	89.12	95.89	100.00	295.1	18.8	26.1	103.1	70.0	33.1
Irr3F3	54.95	71.23	100.00	54.95	94.17	90.98	96.56	100.00	295.6	19.2	25.8	102.8	70.0	32.8
Irr3F4	54.45	70.86	100.00	54.45	93.64	90.11	96.24	100.00	298.3	19.3	26.1	103.6	70.0	33.6
Irr3F5	55.03	76.87	100.00	55.03	98.42	97.55	99.05	100.00	295.1	25.7	19.1	94.3	70.0	24.3
Irr4F1	68.90	95.20	90.68	66.12	95.96	94.01	97.53	95.96	213.7	30.9	0.0	63.5	63.5	0.0
Irr4F2	74.73	90.87	97.41	69.13	85.43	78.70	91.08	92.51	211.7	19.0	6.2	73.8	68.2	5.6
Irr4F3	72.88	94.89	95.55	66.69	90.15	85.40	94.00	91.51	212.9	25.9	1.1	67.9	66.9	1.0
Irr4F4	71.54	95.61	93.93	66.85	93.44	90.09	96.15	93.44	213.2	28.3	0.0	65.8	65.8	0.0
Irr5F1	91.59	98.61	79.84	74.90	81.78	71.88	89.10	81.78	141.6	8.3	0.0	55.9	55.9	0.0
Irr5F2	95.36	99.24	83.96	73.02	76.57	59.58	86.73	76.57	143.0	4.6	0.0	58.8	58.8	0.0
Irr5F3	93.15	98.85	82.36	74.08	79.53	62.95	88.95	79.53	143.6	6.7	0.0	57.7	57.7	0.0
Irr5F4	86.25	97.78	76.20	73.50	85.21	74.84	91.87	85.21	143.5	13.6	0.0	53.3	53.3	0.0
Irr6F1	72.52	95.78	87.67	67.91	93.65	91.19	95.95	93.65	196.3	27.4	0.0	61.4	61.4	0.0
Irr6F2	75.12	96.26	91.35	68.84	91.63	88.10	94.78	91.63	197.5	24.9	0.0	63.9	63.9	0.0
Irr7F1	81.61	93.91	97.73	76.75	89.71	85.57	93.55	94.04	194.5	14.5	3.9	71.7	68.4	3.3
Irr7F2	83.93	95.58	97.20	78.74	91.40	87.84	94.61	93.82	188.1	13.7	2.2	69.8	68.0	1.8
Irr7F3	88.19	98.07	85.52	80.27	91.02	87.18	94.36	91.02	157.5	11.6	0.0	59.9	59.9	0.0
Irr7F4	85.46	97.62	95.52	81.63	95.52	93.54	97.17	95.52	181.5	14.3	0.0	66.9	66.9	0.0
Irr8F1	73.69	87.33	99.99	73.67	91.58	87.36	94.94	99.98	220.4	16.0	10.2	79.7	70.0	9.7
Irr8F2	74.43	91.38	99.82	74.04	93.46	90.35	95.96	99.47	217.8	19.9	5.5	75.0	69.9	5.1
Field	**68.62**	**84.96**	**94.62**	**59.60**	**73.89**	**44.98**	**80.41**	**86.85**	**223.9**	**19.2**	**12.0**	**77.9**	**66.2**	**11.6**

APPENDIX I

Analysis of the Optimisation

Objective Function

This results in this appendix have been generated using the methodology discussed in section 7.5. The key findings of these tables have been summarised within section 7.5.4.

Table I.1 Downs Opt 2: RE>95%, AE>70% and D_{DD} is minimised

			Furrow selected for optimisation			Whole field under furrow optimum			Error in predicted field performance		
	TCO (min)	**Inflow ($L\ s^{-1}$)**	**RE (%)**	**AE (%)**	**D_{DD} (mm)**	**RE (%)**	**AE (%)**	**D_{DD} (mm)**	**RE (%)**	**AE (%)**	**D_{DD} (mm)**
Actual Calculated from Individual Inflows						**93.9**	**81.1**	**23.7**			
Irr1 F1	398	6.25	95.0	70.5	0.0	90.5	66.7	5.3	4.5	3.7	-5.3
Irr1 F2	489	5.02	95.8	71.4	0.3	93.8	70.7	8.6	2.0	0.7	-8.3
Irr1 F3	517	4.89	95.8	69.7	0.2	94.9	69.6	10.2	0.9	0.0	-10.0
Irr1 F4	401	6.23	94.7	70.2	0.0	90.6	66.7	5.4	4.1	3.5	-5.4
Irr2 F1	371	6.7	94.9	70.8	0.0	89.0	65.7	4.3	5.9	5.0	-4.3
Irr2 F2	351	7.11	95.8	69.6	0.7	87.9	64.4	3.8	7.8	5.2	-3.1
Irr2 F3	532	4.74	95.0	70.2	0.5	95.2	70.1	11.0	-0.2	0.2	-10.5
Irr2 F4	290	8.46	95.2	71.4	0.1	83.4	61.9	2.3	11.8	9.5	-2.2
Irr3 F1	139	16.59	95.7	72.6	0.0	68.5	52.1	0.0	27.1	20.5	0.0
Irr3 F2	215	11.32	95.9	70.3	0.1	77.0	56.9	0.9	18.9	13.5	-0.7
Irr3 F3	150	15.54	96.6	71.3	0.4	69.9	53.0	0.0	26.7	18.3	0.4
Irr3 F4	192	12.62	95.5	70.7	0.0	74.7	55.3	0.4	20.8	15.4	-0.4
Irr4 F1	401	6.18	95.4	70.3	1.9	90.6	67.1	5.3	4.8	3.2	-3.5
Irr4 F2	469	5.35	95.7	69.8	2.0	93.6	68.6	8.2	2.2	1.2	-6.3
Irr4 F3	316	7.76	95.7	70.8	0.4	85.3	63.4	2.9	10.3	7.4	-2.5
Irr4 F4	391	6.3	95.5	70.9	1.9	90.0	67.2	4.9	5.6	3.7	-3.0
Irr5 F1	645	3.91	95.3	70.4	1.8	96.4	70.9	17.4	-1.1	-0.5	-15.6
Irr5 F2	549	4.57	95.7	70.0	1.5	95.5	70.5	11.9	0.1	-0.5	-10.4
Irr5 F3	1432	1.78	95.9	70.2	1.3	82.4	60.3	52.2	13.5	9.9	-50.9
Irr5 F4	544	4.62	95.5	70.5	1.3	95.5	70.4	11.6	0.0	0.1	-10.2
TOTAL[1]	**529**	**4.75**	**95.2**	**70.0**	**10.9**	**95.2**	**70.0**	**10.9**	-	-	-
COMBINED[2]	**-**	**-**	**-**	**-**	**-**	**95.5**	**70.6**	**0.7**	-	-	-
average	439.6	7.30	95.5	70.6	0.7			**average**	**8.3**	**6.0**	**-7.6**
Average Infiltration	409	6.10	95.1	70.4	0.4	91.1	66.9	5.8	4.0	3.5	-5.4

[1] Where all furrows within the field were optimised as a group using the same inflow rate and TCO.
[2] Represents the maximum performance where each furrow was optimised individually

Table I.2 Chisholm Opt 1: RE>90%, DURZ>90% and AE is maximised

			Furrow selected for optimisation			Whole field under furrow optimum			Error in predicted field performance		
	TCO (min)	**Inflow (L s^{-1})**	**RE (%)**	**DURZ (%)**	**AE (%)**	**RE (%)**	**DURZ (%)**	**AE (%)**	**RE (%)**	**DURZ (%)**	**AE (%)**
Actual Calculated from Individual Inflows						**98.8**	**96.4**	**21.4**			
Irr1 F1	3564	0.18	94.7	84.7	84.8	48.3	0.0	37.4	46.3	84.7	47.4
Irr1 F2	2016	0.31	97.8	93.2	77.9	53.4	0.0	42.3	44.4	93.2	35.6
Irr1 F3	1333	0.46	97.4	92.2	79.0	56.0	0.0	45.3	41.4	92.2	33.8
Irr1 F4	1182	0.53	98.2	94.6	77.6	57.6	0.0	45.5	40.6	94.6	32.1
Irr2 F1	26.5	21.00	99.7	99.1	68.0	81.1	42.1	63.2	18.6	57.0	4.8
Irr2 F2	26	25.00	99.8	99.5	57.2	82.9	48.6	53.3	16.9	50.9	3.9
Irr3 F1	94	6.00	96.1	89.4	87.4	75.2	31.0	60.1	20.8	58.4	27.3
Irr3 F2	56	8.49	99.6	98.7	90.3	71.7	27.0	65.3	27.8	71.7	25.0
Irr3 F3	171	3.36	97.5	92.2	80.1	71.4	20.5	57.8	26.1	71.7	22.3
Irr4 F1	24	22.17	100.0	100.0	65.5	82.1	46.1	57.8	17.9	53.9	7.7
Irr4 F2	29	18.00	98.3	94.9	78.2	77.8	36.1	69.5	20.6	58.8	8.8
Irr4 F3	53	8.52	100.0	100.0	90.4	71.5	26.2	66.6	28.5	73.8	23.8
Irr4 F4	26.5	21.10	99.6	98.9	67.6	81.1	42.2	63.7	18.5	56.8	3.9
Irr5 F1	30	18.00	94.7	83.0	75.3	77.8	36.1	69.5	16.9	46.9	5.8
Irr5 F2	24	23.73	100.0	100.0	60.3	82.6	63.3	55.5	17.4	36.7	4.8
Irr5 F3	24	21.92	100.0	100.0	65.3	81.2	43.9	57.9	18.8	56.1	7.4
Irr5 F4	29	17.00	96.8	90.2	81.6	75.8	33.4	70.9	21.1	56.8	10.7
TOTAL[1]	**788**	**4.02**	**96.8**	**90.1**	**15.1**	**96.8**	**90.1**	**15.1**	-	-	-
COMBINED[2]	**-**	**-**	**-**	**-**	**-**	**98.2**	**94.7**	**74.2**	-	-	-
average	512.2	12.69	98.2	94.7	75.7			**average**	**26.0**	**65.5**	**17.9**
Average Infiltration	47	9.61	95.2	90.8	90.2	70.9	25.5	67.0	24.3	65.3	23.2

Table I.3 Chisholm Opt 2: RE>95%, AE>60% and D_{DD} is minimised

			Furrow selected for optimisation			Whole field under furrow optimum			Error in predicted field performance		
	TCO (min)	**Inflow (L s^{-1})**	**RE (%)**	**AE (%)**	**D_{DD} (mm)**	**RE (%)**	**AE (%)**	**D_{DD} (mm)**	**RE (%)**	**AE (%)**	**D_{DD} (mm)**
Actual Calculated from Individual Inflows						**98.8**	**21.4**	**83.7**			
Irr1 F1	1755	0.45	95.5	60.0	0.0	61.7	38.7	51.8	33.8	21.3	-51.8
Irr1 F2	1232	0.63	95.6	61.0	0.1	64.7	41.2	46.9	30.9	19.8	-46.8
Irr1 F3	826	0.98	96.4	58.6	0.1	70.1	42.8	44.3	26.3	15.8	-44.2
Irr1 F4	658	1.20	95.5	60.0	0.0	71.2	44.5	40.7	24.4	15.5	-40.7
Irr2 F1	23.93	25.00	100.0	59.9	32.3	82.9	53.3	13.7	17.1	6.5	18.6
Irr2 F2	26	24.78	99.2	57.3	42.0	82.9	53.6	13.7	16.3	3.7	28.3
Irr3 F1	57	12.17	99.8	57.5	2.9	84.9	53.2	16.8	14.9	4.2	-13.9
Irr3 F2	24	21.17	99.7	71.3	2.3	81.1	63.6	12.8	18.6	7.7	-10.5
Irr3 F3	85	8.06	95.3	62.7	0.1	83.6	54.5	19.0	11.6	8.2	-19.0
Irr4 F1	21	24.93	100.0	61.7	19.6	82.9	53.4	13.7	17.1	8.3	5.9
Irr4 F2	22	25.54	100.0	62.7	20.2	83.2	51.5	13.9	16.8	11.2	6.3
Irr4 F3	23.5	18.25	100.0	78.5	3.1	78.3	69.0	10.7	21.7	9.5	-7.5
Irr4 F4	21	26.95	100.0	56.5	32.3	83.2	50.0	14.0	16.8	6.5	18.3
Irr5 F1	22	25.94	100.0	59.8	23.6	83.4	51.4	13.9	16.6	8.4	9.7
Irr5 F2	24	23.23	100.0	61.6	25.4	82.5	56.4	13.3	17.5	5.3	12.1
Irr5 F3	24	22.72	100.0	63.0	19.4	82.4	56.6	13.2	17.6	6.4	6.1
Irr5 F4	25	22.22	100.0	60.5	16.8	82.1	57.0	13.0	17.9	3.5	3.8
TOTAL[1]	**665**	**3.36**	**95.1**	**21.0**	**89.4**	**95.1**	**21.0**	**89.4**	-	-	-
COMBINED[2]	**-**	**-**	**-**	**-**	**-**	**98.6**	**61.6**	**14.1**	-	-	-
average	286.4	16.72	98.6	61.9	14.1			**average**	**19.8**	**9.5**	**-7.4**
Average Infiltration	54	10.07	94.6	86.8	0.3	79.4	61.9	13.5	15.2	24.9	-13.2

Table I.4 Chisholm Opt 3: RE>95%, AE>60% and D_{DD} is minimised with variable irrigation requirement

			Furrow selected for optimisation			Whole field under furrow optimum			Error in predicted field performance		
	TCO (min)	**Inflow ($L\ s^{-1}$)**	**RE (%)**	**AE (%)**	**D_{DD} (mm)**	**RE (%)**	**AE (%)**	**D_{DD} (mm)**	**RE (%)**	**AE (%)**	**D_{DD} (mm)**
Actual Calculated from Individual Inflows						**96.4**	**20.7**	**85.5**			
Irr1 F1	2750	0.34	95.6	59.4	0.0	63.8	33.7	66.0	31.8	25.6	-66.0
Irr1 F2	1855	0.49	95.4	60.8	0.0	66.2	35.9	60.2	29.1	24.9	-60.1
Irr1 F3	1202	0.75	95.4	61.3	0.0	69.2	37.7	55.0	26.2	23.5	-55.0
Irr1 F4	1051	0.84	95.4	62.3	0.1	69.4	38.6	52.6	26.1	23.8	-52.5
Irr2 F1	23.88	25.00	100.0	56.9	35.3	78.9	50.4	16.4	21.1	6.4	18.9
Irr2 F2	33	22.62	100.0	46.8	50.9	81.1	45.4	17.2	18.9	1.3	33.7
Irr3 F1	57	12.17	99.8	57.5	2.9	80.9	50.4	19.5	18.9	7.0	-16.5
Irr3 F2	24	21.17	99.7	71.3	2.3	77.1	60.1	15.5	22.6	11.2	-13.2
Irr3 F3	85	8.06	95.3	62.7	0.1	79.7	51.7	21.6	15.5	11.0	-21.6
Irr4 F1	21	24.93	100.0	61.7	19.6	78.9	50.5	16.4	21.1	11.2	3.2
Irr4 F2	22	25.54	100.0	62.7	20.2	79.2	48.7	16.6	20.8	14.0	3.6
Irr4 F3	23.5	18.25	100.0	78.5	3.1	74.5	65.3	13.2	25.5	13.2	-10.1
Irr4 F4	21	26.95	100.0	56.5	32.3	79.1	47.3	16.7	20.9	9.2	15.6
Irr5 F1	24	22.52	100.0	53.4	31.6	78.2	53.8	15.5	21.8	-0.4	16.1
Irr5 F2	26	19.91	98.2	58.8	32.3	77.2	62.1	15.1	21.0	-3.3	17.2
Irr5 F3	24	22.52	100.0	53.0	28.0	78.2	53.8	15.5	21.8	-0.8	12.5
Irr5 F4	24	22.17	100.0	62.6	22.4	78.1	54.7	15.4	21.9	8.0	7.0
TOTAL[1]	**869**	**4.87**	**95.1**	**11.0**	**128.5**	**95.1**	**11.0**	**128.5**	-	-	-
COMBINED[2]	**-**	**-**	**-**	**-**	**-**	**98.3**	**59.8**	**16.5**	-	-	-
average	427.4	16.13	98.5	60.4	16.5			**average**	**22.6**	**10.9**	**-9.8**

Table I.5 Turner Opt 1: RE>90%,DURZ>90% and AE is maximised

			Furrow selected for optimisation			Whole field under furrow optimum			Error in predicted field performance		
	TCO (min)	**Inflow (L s^{-1})**	**RE (%)**	**DURZ (%)**	**AE (%)**	**RE (%)**	**DURZ (%)**	**AE (%)**	**RE (%)**	**DURZ (%)**	**AE (%)**
Actual Calculated from Individual Inflows						**94.6**	**86.9**	**68.6**			
Irr1 F1	160	17.50	96.0	87.6	90.1	82.5	69.2	76.9	13.5	18.4	13.2
Irr1 F2	130	22.50	96.1	87.7	85.6	82.6	69.5	73.5	13.5	18.2	12.1
Irr2 F1	125	21.75	98.8	96.5	91.2	81.9	68.0	75.2	16.9	28.5	16.0
Irr2 F2	165	14.68	91.2	91.3	96.1	78.2	58.3	82.4	13.0	33.1	13.6
Irr2 F3	105	25.00	98.8	96.3	93.1	80.4	64.4	76.0	18.4	31.9	17.1
Irr2 F4	102	24.63	97.9	94.0	93.7	79.6	62.5	76.7	18.3	31.4	17.0
Irr3 F1	125	23.63	99.8	99.3	84.7	83.3	70.7	71.0	16.4	28.6	13.7
Irr3 F2	106	25.25	96.8	90.2	90.3	80.5	64.6	75.3	16.4	25.6	15.0
Irr3 F3	118	24.33	100.0	100.0	83.7	82.5	69.4	72.9	17.5	30.6	10.8
Irr3 F4	118	23.60	95.8	87.0	87.3	81.6	67.4	74.6	14.3	19.6	12.7
Irr3 F5	147	22.12	99.8	99.4	78.8	84.7	73.2	67.3	15.1	26.2	11.5
Irr4 F1	883	2.91	91.0	90.1	94.6	78.5	25.6	81.5	12.5	64.5	13.0
Irr4 F2	748	4.42	97.2	91.6	78.5	94.7	83.3	76.6	2.6	8.2	1.9
Irr4 F3	956	3.39	97.1	91.3	80.5	91.9	73.6	75.9	5.2	17.6	4.6
Irr4 F4	1303	2.38	97.4	92.1	84.5	84.9	47.0	73.5	12.5	45.1	11.1
Irr5 F1	682	4.80	97.0	90.8	79.5	95.0	84.6	77.4	2.0	6.2	2.1
Irr5 F2	507	6.08	97.0	90.8	84.1	92.5	80.4	79.7	4.5	10.5	4.4
Irr5 F3	547	5.85	97.6	92.7	80.4	94.2	84.0	78.3	3.4	8.7	2.1
Irr5 F4	718	4.52	97.4	91.8	80.0	94.1	81.6	77.5	3.3	10.2	2.5
Irr6 F1	1574	2.23	97.6	93.6	74.8	88.6	61.3	68.2	9.1	32.3	6.6
Irr6 F2	1473	2.21	97.3	92.2	80.4	84.9	46.5	70.1	12.5	45.7	10.3
Irr7 F1	288	8.59	91.3	91.5	97.6	80.2	59.0	85.7	11.1	32.4	11.9
Irr7 F2	318	8.01	92.8	92.5	96.5	82.1	62.4	85.4	10.7	30.1	11.2
Irr7 F3	547	5.22	90.0	90.2	84.4	89.2	69.8	83.1	0.8	20.4	1.3
Irr7 F4	330	7.30	90.4	89.5	100.0	79.4	53.4	87.6	11.0	36.1	12.4
Irr8 F1	154	16.19	93.6	94.6	94.9	80.0	63.1	81.2	13.7	31.6	13.7
Irr8 F2	234	11.57	95.2	95.8	91.0	83.6	70.3	80.2	11.6	25.6	10.7
TOTAL[1]	**620**	**5.73**	**97.4**	**92.1**	**73.0**	**97.4**	**92.1**	**73.0**	-	**-**	**-**
COMBINED[2]	**-**	**-**	**-**	**-**	**-**	**96.0**	**89.6**	**86.6**	-	**-**	-
average	469.0	12.62	96.0	92.6	87.3			**average**	**11.1**	**26.6**	**10.1**
Average Infiltration	277	9.06	91.8	91.3	96.3	81.2	62.4	84.7	10.7	28.9	11.6

Table I.6 Turner Opt 2: RE>95%, AE>70% and D_{DD} is minimised

			Furrow selected for optimisation			Whole field under furrow optimum			Error in predicted field performance		
	TCO (min)	**Inflow (L s^{-1})**	**RE (%)**	**AE (%)**	**D_{DD} (mm)**	**RE (%)**	**AE (%)**	**D_{DD} (mm)**	**RE (%)**	**AE (%)**	**D_{DD} (mm)**
Actual Calculated from Individual Inflows						**94.6**	**68.6**	**11.6**			
Irr1 F1	99	27.3	96.0	90.7	6.5	80.6	75.4	9.2	15.4	15.4	-2.8
Irr1 F2	111	25.14	99.8	86.0	11.0	82.8	71.6	10.7	17.0	14.4	0.3
Irr2 F1	98	27.25	96.9	91.8	5.8	80.7	75.4	9.5	16.3	16.4	-3.7
Irr2 F2	177	18.05	95.4	77.4	0.0	86.1	69.7	13.8	9.3	7.7	-13.8
Irr2 F3	94	26.69	98.3	95.0	3.9	79.1	76.9	8.6	19.2	18.1	-4.7
Irr2 F4	87	27.65	96.0	99.0	0.3	76.9	79.5	7.7	19.1	19.5	-7.4
Irr3 F1	109	26.04	95.0	85.9	10.6	81.6	73.7	9.9	13.5	12.2	0.7
Irr3 F2	96	26.49	93.6	91.1	6.3	78.5	77.1	8.4	15.1	14.0	-2.1
Irr3 F3	108.5	26.24	100.0	81.9	12.4	81.7	72.8	10.3	18.3	9.1	2.1
Irr3 F4	98	27.5	100.0	86.4	9.9	80.4	74.7	9.5	19.6	11.7	0.4
Irr3 F5	116	25.69	94.1	79.4	16.5	83.0	69.9	11.0	11.1	9.4	5.5
Irr4 F1	941	3.72	95.4	72.8	0.0	95.6	72.9	55.1	-0.2	-0.1	-55.1
Irr4 F2	519	6.88	95.3	70.7	1.2	96.6	72.0	29.0	-1.2	-1.3	-27.8
Irr4 F3	622	5.8	95.3	70.2	0.6	97.6	72.0	36.2	-2.3	-1.8	-35.7
Irr4 F4	697	5.07	95.1	72.3	0.0	97.3	73.4	40.4	-2.2	-1.1	-40.4
Irr5 F1	481	7.38	95.4	70.9	1.0	96.0	71.4	27.1	-0.6	-0.5	-26.1
Irr5 F2	398	8.69	95.6	72.6	0.6	94.0	72.2	22.1	1.5	0.4	-21.5
Irr5 F3	426	8.11	95.3	73.0	0.0	94.7	72.8	23.3	0.6	0.2	-23.3
Irr5 F4	529	6.66	94.9	72.0	0.0	96.6	72.8	29.6	-1.7	-0.8	-29.6
Irr6 F1	1167	3.11	95.1	70.5	0.5	94.9	70.1	69.1	0.3	0.4	-68.6
Irr6 F2	941	3.89	95.3	69.6	0.5	97.1	70.9	57.4	-1.7	-1.2	-56.9
Irr7 F1	298	11.52	94.5	75.8	0.0	90.8	70.0	18.5	3.7	5.8	-18.5
Irr7 F2	318	10.56	95.3	76.0	0.0	91.3	71.9	18.8	4.0	4.1	-18.8
Irr7 F3	617	5.83	95.3	70.4	0.4	97.5	72.3	35.7	-2.2	-1.9	-35.2
Irr7 F4	398	8.16	95.6	78.6	0.0	92.9	75.7	21.0	2.7	2.9	-21.0
Irr8 F1	168	19.56	96.6	76.4	0.0	85.7	67.8	13.6	10.9	8.6	-13.6
Irr8 F2	237	14.08	96.7	75.9	0.0	88.6	69.4	16.2	8.0	6.5	-16.2
TOTAL[1]	**449**	**7.81**	**95.3**	**72.2**	**7.9**	**95.3**	**72.2**	**7.9**	-	**-**	**-**
COMBINED[2]	**-**	**-**	**-**	**-**	**-**	**96.0**	**78.2**	**3.3**	-	**-**	-
average	458.8	11.75	95.7	75.3	2.5			**average**	**7.2**	**6.2**	**-19.8**
Average Infiltration	289	11.77	94.9	76.9	0.0	90.5	70.3	5.7	4.3	6.7	-5.8

Table I.7 Recipe field performance

	Recipe	AE (%)	AER[a] (%)	RE (%)	AELQ (%)	DU (%)	ADU (%)	CU (%)	DURZ (%)	Inflow (m^3)	Runoff (%)	Deep Drainage (%)	D (mm)	D_{RZ} (mm)	D_{DD} (mm)
Downs	1	82.98	84.63	86.68	56.58	57.61	28.80	71.38	68.19	118.0	1.9	15.2	102.6	86.7	15.9
	2	77.27	81.34	90.62	57.43	60.37	30.40	73.32	74.33	132.5	4.8	17.9	111.6	90.6	20.9
	3	77.78	82.05	91.05	58.49	61.44	31.07	74.16	75.20	132.3	5.0	17.4	111.4	91.1	20.4
	4	73.64	79.66	93.66	59.33	63.92	33.16	75.98	80.57	143.7	7.1	19.2	118.1	93.7	24.4
	5	89.11	95.28	70.66	58.23	62.87	39.88	73.09	65.35	89.6	7.3	3.5	73.4	70.7	2.8
	6	82.88	93.50	75.31	55.53	63.62	39.70	74.01	67.00	102.7	12.5	4.4	79.3	75.3	4.0
	7	78.21	92.62	79.42	55.04	66.44	41.53	76.36	70.37	114.7	16.9	4.6	84.1	79.4	4.7
	8	70.57	90.44	85.15	52.34	68.49	42.24	78.20	74.16	136.3	23.4	5.8	92.2	85.1	7.0
Chisholm	1	52.06	54.46	89.95	34.70	35.78	18.07	52.77	66.65	51.8	2.8	44.9	100.5	54.0	46.6
	2	46.08	52.89	91.27	32.86	35.95	20.55	52.38	71.30	59.4	8.0	45.5	108.8	54.8	54.1
	3	40.89	53.12	91.80	29.93	35.42	21.79	52.48	73.20	67.4	14.4	44.3	114.8	55.1	59.7
	4	34.65	53.17	92.85	26.65	34.66	22.86	50.52	76.91	80.4	21.8	43.2	125.2	55.7	69.5
	5	56.50	61.98	83.80	26.00	27.85	20.95	52.17	46.02	44.5	6.4	36.8	83.1	50.3	32.8
	6	48.64	59.99	84.47	22.61	26.24	19.38	51.04	46.49	52.1	13.4	37.5	89.8	50.7	39.1
	7	37.46	61.83	87.92	22.03	31.28	25.02	53.55	58.80	70.4	28.7	33.4	99.8	52.8	47.0
	8	29.31	62.48	89.50	18.99	31.83	25.39	52.85	64.80	91.6	39.0	31.3	111.0	53.7	57.3
Turner	1	76.73	86.29	91.90	62.79	70.80	39.59	78.81	81.83	194.5	11.2	11.9	74.3	64.3	10.0
	2	69.97	85.05	94.14	59.92	72.95	45.27	80.18	85.63	218.5	17.7	12.2	77.4	65.9	11.5
	3	70.10	85.14	94.77	60.75	73.93	49.97	81.09	86.67	219.6	17.7	12.1	77.8	66.3	11.4
	4	65.22	84.11	96.53	58.73	75.62	56.74	82.75	90.04	240.3	22.2	12.4	80.5	67.6	12.9
	5	76.23	86.31	91.49	62.01	70.35	37.99	78.52	81.35	194.9	11.9	11.9	74.1	64.0	10.0
	6	69.40	84.98	93.73	58.77	72.08	45.01	79.91	84.69	219.3	18.3	12.1	77.1	65.6	11.5
	7	69.35	85.04	94.35	59.48	73.07	50.07	80.76	85.77	220.9	18.5	12.1	77.5	66.0	11.5
	8	64.34	84.02	96.10	57.29	74.66	56.92	82.39	89.04	242.5	23.1	12.4	80.2	67.3	13.0

Recipe	Inflow	time
1	measured	advance completion
2	measured	advance completion x 110%
3	measured	advance completion + 60 minutes
4	measured	advance completion + 120 minutes
5	6 L s^{-1}	advance completion
6	6 L s^{-1}	advance completion x 110%
7	6 L s^{-1}	advance completion + 60 minutes
8	6 L s^{-1}	advance completion + 120 minutes

For explanation of these results see section 7.6

APPENDIX J

Lagoona Field Trial

Table J.1 Advance data for Lagoona Trial

Field Name:	**Lagoona**		
Location:	Theodore, Dawson River, Qld, Australia		
Details	Cotton planted on clay soil, second irrigation		
Number of Furrows:	84		
Field length:	793 m	Average inflow rate	1.952775 L s^{-1}
Slope:	0.00156	Average TCO	1410 min
Furrow Spacing	2 m		
Deficit	83 mm		

Furrow Dimensions

Top Width	0.578 m	Upstream Flow Depth	0.05 m
Middle Width	0.423 m		
Bottom Width	0.263 m		
Max Height	0.128 m		

Advance Data

Wetted Furrow	0m	160m	310m	460m	610m	761m
1	0					1483
2	0					1389
3	0					1152
4	0					1385
5	0	53	201	619	879	1201
6	0	103	365	669	951	1218
7	0	71	268	589	851	1151
8	0	89	339	635	880	1144
9	0					1090
10	0					1181
11	0					1200
12	0					1333
13	0					1094
14	0					1164
15	0					1216
16	0					1352
17	0					1329
18	0					1342
19	0					1266
20	0					1389
21	0			658		1305
22	0			846		1416
23	0			801		1387
24	0			861		1460
25	0			714		1330
26	0			777		1402
27	0			674		1306
28	0			877		1457
29	0			709		1275
30	0			770		1304
31	0			736		1313
32	0			897		1459
33	0			839		1441
34	0			811		1394
35	0			768		1303
36	0			824		1366
37	0			699		1217
38	0			714		1174
39	0			742		1220
40	0			819		1297
41	0					1219
42	0					1149

Wetted Furrow	0m	160m	310m	460m	610m	761m
43	0					1141
44	0					1253
45	0					1246
46	0					1383
47	0					1429
48	0					1442
49	0					1294
50	0					1214
51	0					1197
52	0					1335
53	0					1228
54	0					1209
55	0					1225
56	0					1218
57	0					1122
58	0					1080
59	0					1009
60	0					1141
61	0					996
62	0					1019
63	0					1006
64	0					1101
65	0		184	566	815	1051
66	0		223	609	850	1077
67	0		218	578	854	1151
68	2		410	713	1028	1277
69	0					1116
70	0					1043
71	0					1063
72	0					1311
73	0					1171
74	0					1117
75	0					1111
76	0					1338
77	0					1214
78	0					1222
79	0					1196
80	0					1234
81	0					1159
82	0					1166
83	0					1029
84	0					1196

Table J.2 Runoff data for Lagoona Trial

Furr 5		Furr 30		Furr 67	
t min	Q_r L s^{-1}	t min	Q_r L s^{-1}	t min	Q_r L s^{-1}
1251	0.0	1320	0.0	1175	0.0
1256	0.2	1325	0.4	1180	0.1
1261	0.3	1330	0.6	1185	0.2
1266	0.4	1335	0.8	1190	0.3
1271	0.5	1340	0.9	1195	0.3
1276	0.7	1345	1.0	1200	0.4
1281	0.8	1350	1.0	1205	0.5
1286	0.8	1355	1.3	1210	0.5
1291	0.9	1360	1.5	1215	0.6
1296	0.9	1365	1.6	1220	0.7
1301	1.0	1370	1.7	1225	0.7
1306	1.0	1375	1.9	1230	0.8
1311	1.1	1380	2.1	1235	0.8
1316	1.1	1385	1.8	1240	0.8
1321	1.2	1390	1.7	1245	0.8
1326	1.2	1395	1.7	1250	0.9
1331	1.2	1400	1.6	1255	0.9
1336	1.2	1405	1.6	1260	0.9
1341	1.3	1410	1.6	1265	1.0
1346	1.3	1415	1.6	1270	1.0
1351	1.3	1420	1.7	1275	1.1
1356	1.4	1425	1.7	1280	1.1
1361	1.4	1430	1.6	1285	1.1
1366	1.4	1435	1.6	1290	1.1
1371	1.4	1440	1.7	1295	1.2
1376	1.4	1445	1.7	1300	1.1
1381	1.4	1450	1.6	1305	1.1
1386	1.4	1455	1.7	1310	1.1
1391	1.5	1460	1.7	1315	1.2
1396	1.5	1465	1.6	1320	1.2
1401	1.5	1470	1.6	1325	1.2
1406	1.6	1475	1.6	1330	1.2
1411	1.6	1480	1.7	1335	1.2
1416	1.6	1485	1.6	1340	1.2
1421	1.6	1490	1.6	1345	1.2
1426	1.6	1495	1.7	1350	1.2
1431	1.6	1500	1.7	1355	1.3
1436	1.6	1505	1.7	1360	1.3
1441	1.6	1510	1.7	1365	1.2
1446	1.6	1515	1.7	1370	1.2
1451	1.6	1520	1.7	1375	1.2
1456	1.6	1525	1.7	1380	1.3
1461	1.6	1530	1.7	1385	1.3
1466	1.6	1535	1.7	1390	1.2
1471	1.6	1540	1.8	1395	1.3
1476	1.6	1545	1.7	1400	1.2
1481	1.6	1550	1.8	1405	1.3
1486	1.6	1555	1.8	1410	1.2
1491	1.6	1560	1.8	1415	1.2
1496	1.6	1565	1.7	1420	1.2
1501	1.7	1570	1.8	1425	1.1
1506	1.7	1575	1.8	1430	1.1
1511	1.7	1580	1.7	1435	1.1
1516	1.7	1585	1.8	1440	1.1
1521	1.7	1590	1.8	1445	1.1
1526	1.7	1595	1.7	1450	1.1
1531	1.7	1600	1.7	1455	1.0
1536	1.7	1605	1.7	1460	0.9
1541	1.7	1610	1.6	1465	0.9
1546	1.7	1615	1.6	1470	0.9
1551	1.7	1620	1.5	1475	0.8
1556	1.7	1625	1.4	1480	0.8
1561	1.7	1630	1.4	1485	0.7
1566	1.7	1635	1.4	1490	0.7
1571	1.7	1640	1.3	1495	0.7
1576	1.7	1645	1.3	1500	0.6
1581	1.7	1650	1.2	1505	0.6
1586	1.7	1655	1.2	1510	0.6
1591	1.7	1660	1.1	1515	0.6
1596	1.7	1665	1.1	1520	0.5
1601	1.7	1670	1.0	1525	0.5
1606	1.7	1675	1.0	1530	0.5
1611	1.7	1680	1.0	1535	0.4
1616	1.7	1685	1.0	1540	0.4
1621	1.7	1690	0.9	1545	0.4
1626	1.7	1695	0.9	1550	0.3
1631	1.7	1700	0.8	1555	0.4
1636	1.7	1705	0.8	1560	0.3
1641	1.7	1710	0.8	1565	0.3
1646	1.7	1715	0.7	1570	0.3
1651	1.7	1720	0.8	1575	0.3
1656	1.7	1725	0.7	1580	0.3
1661	1.7	1730	0.7	1585	0.2
1666	1.7	1735	0.6	1590	0.3
1671	1.7	1740	0.6	1595	0.2
1676	1.6	1745	0.6	1600	0.2
1681	1.5	1750	0.6	1605	0.2
1686	1.5	1755	0.6	1610	0.2
1691	1.5	1760	0.6	1615	0.1
1696	1.4	1765	0.6	1620	0.2
1701	1.4	1770	0.5	1625	0.2
1706	1.3	1775	0.5	1630	0.1
1711	1.3	1780	0.5	1635	0.1
1716	1.2	1785	0.5	1640	0.1
1721	1.2	1790	0.5	1645	0.1
1726	1.2	1795	0.4	1650	0.2
1731	1.1	1800	0.5	1655	0.2
1736	1.1	1805	0.4	1660	0.2
1741	1.0	1810	0.3	1665	0.1
1746	1.0	1815	0.4	1670	0.1
1751	1.0	1820	0.4	1675	0.1
1756	1.0	1825	0.3	1680	0.1
1761	0.9	1830	0.4	1685	0.1
1766	0.9	1835	0.4	1690	0.1
1771	0.8	1840	0.4	1695	0.0
1776	0.8	1845	0.4	1700	0.0
1781	0.8	1850	0.3	1705	0.1
1786	0.8	1855	0.4	1710	0.1
1791	0.7	1860	0.4	1715	0.1
1796	0.7	1865	0.4	1720	0.1
1801	0.7	1870	0.3	1725	0.0
1806	0.7	1875	0.3	1730	0.1
1811	0.6	1880	0.3	1735	0.0
1816	0.6	1885	0.2	1740	0.1
1821	0.6	1890	0.2	1745	0.0
1826	0.6	1895	0.3		
1831	0.6	1900	0.3		
1836	0.6	1905	0.3		
1841	0.6	1910	0.2		
1846	0.6	1915	0.2		
1851	0.5	1920	0.3		
1856	0.5	1925	0.3		
1861	0.5	1930	0.2		
1866	0.5	1935	0.3		
1871	0.5	1940	0.2		
1876	0.5	1945	0.1		
1881	0.5	1950	0.2		
1886	0.4	1955	0.2		
1891	0.4	1960	0.2		
1896	0.4	1965	0.1		
1901	0.4	1970	0.2		
1906	0.4	1975	0.1		
1911	0.4	1980	0.1		
1916	0.4	1985	0.2		
1921	0.4	1990	0.2		
1926	0.4	1995	0.2		
1931	0.4	2000	0.1		
1936	0.4	2005	0.1		
1941	0.4	2010	0.1		
1946	0.4	2015	0.1		
1951	0.4	2020	0.1		
1956	0.4	2025	0.1		
1961	0.4	2030	0.1		
1966	0.4	2035	0.1		
1971	0.4	2040	0.1		
1976	0.3	2045	0.1		
1981	0.3	2050	0.1		
1986	0.3	2055	0.1		
1991	0.3	2060	0.0		
1996	0.3				
2001	0.3				

The runoff start time for furrow 30 and 67 was estimated using the final advance time and advance trajectory speed (from the power curve advance) and the final advance point.
The shaded values signify the storage phase, and were used by IPARM to estimate infiltration.

Table J.3 Infiltration parameters for Lagoona from IPARM

Wetted Furrow	*a*	*k*	f_0	Ad. Error	Run. Error
5	0.5299	0.00549	0.0000000	6.90	
6	0.3121	0.02421	0.0000000	4.23	
7	0.4280	0.01063	0.0000000	4.44	
8	0.3228	0.02150	0.0000000	4.77	
21	0.1225	0.06575	0.0000582	0.00	
22	0.0238	0.17667	0.0000001	0.00	
23	0.0755	0.12216	0.0000049	0.00	
24	0.0491	0.15506	0.0000002	0.00	
25	0.1425	0.07014	0.0000238	0.00	
26	0.1391	0.08097	0.0000069	0.00	
27	0.1015	0.07699	0.0000552	0.00	
28	0.0087	0.20037	0.0000000	0.00	
29	0.1215	0.08139	0.0000119	0.00	
30	0.0474	0.13988	0.0000000	0.00	
31	0.1221	0.08518	0.0000067	0.00	
32	0.0000	0.21310	0.0000000	0.75	
33	0.0686	0.13416	0.0000019	0.00	
34	0.0743	0.12590	0.0000003	0.00	
35	0.0428	0.14229	0.0000031	0.00	
36	0.0025	0.19418	0.0000007	0.00	
37	0.0786	0.10407	0.0000077	0.00	
38	0.0000	0.16848	0.0000000	0.27	
39	0.0000	0.17557	0.0000000	0.27	
40	0.0000	0.18958	0.0000000	1.95	
65	0.4766	0.00737	0.0000000	7.04	
66	0.4075	0.01191	0.0000000	6.66	
67	0.4558	0.00879	0.0000000	4.85	
68	0.2044	0.05090	0.0000000	2.31	
5 runoff	0.2268	0.04029	0.0000000	14.84	6.01
30 runoff	0.0790	0.11538	0.0000000	0.72	8.13
67 runoff	0.2742	0.02837	0.0000000	8.48	4.91

Shaded furrows are based on two advance points only
The final three rows are estimated using advance and runoff data with weighting of 100%

Table J.4 Infiltration parameters predicted using final advance point

Wetted Furrow	*a*	*k*	f_0
1	0.1691	0.07262	1.208E-09
2	0.1763	0.06492	1.265E-09
3	0.1971	0.04701	8.030E-09
4	0.1766	0.06460	9.955E-10
5**	**0.2268**	**0.04029**	**0**
6	0.3121	0.02421	0
7	0.4280	0.01063	0
8	0.0790	0.11538	0
9	0.2033	0.04270	6.567E-09
10	0.1943	0.04909	8.319E-09
11	0.1925	0.05046	4.347E-09
12	0.1808	0.06050	5.831E-09
13	0.2028	0.04299	2.500E-08
14	0.1960	0.04786	4.351E-12
15	0.1911	0.05163	8.851E-10
16	0.1793	0.06198	5.476E-09
17	0.1811	0.06021	2.989E-08
18	0.1801	0.06120	3.336E-09
19	0.1866	0.05535	2.384E-13
20	0.1763	0.06492	1.265E-09
21	0.1832	0.05832	3.967E-09
22	0.1742	0.06709	1.192E-13
23	0.1765	0.06476	1.718E-09
24	0.1707	0.07073	2.001E-08
25	0.1810	0.06029	2.623E-08
26	0.1753	0.06597	5.442E-09
27	0.1831	0.05840	3.528E-09
28	0.1710	0.07046	1.435E-09
29	0.1858	0.05604	8.152E-09
30**	**0.0790**	**0.11538**	**0**
31	0.1825	0.05894	4.152E-09
32	0.1709	0.07062	2.354E-12
33	0.1722	0.06914	3.587E-09
34	0.1759	0.06532	1.186E-11
35	0.1834	0.05817	4.936E-09
36	0.1782	0.06309	1.980E-09
37	0.1910	0.05170	1.498E-09
38	0.1950	0.04858	7.635E-10
39	0.1907	0.05192	6.760E-10
40	0.1839	0.05771	3.240E-09
41	0.1908	0.05185	2.270E-09
42	0.1974	0.04680	1.036E-08

Wetted Furrow	*a*	*k*	f_0
43	0.1981	0.04625	1.670E-08
44	0.1877	0.05437	1.884E-09
45	0.1884	0.05385	4.974E-10
46	0.1768	0.06444	2.688E-10
47	0.1732	0.06815	1.040E-10
48	0.1722	0.06922	9.322E-10
49	0.1841	0.05748	6.783E-09
50	0.1912	0.05149	1.242E-08
51	0.1928	0.05024	2.286E-09
52	0.1807	0.06065	3.661E-09
53	0.1900	0.05251	1.261E-10
54	0.1917	0.05112	4.268E-09
55	0.1903	0.05229	2.384E-13
56	0.1908	0.05181	3.558E-08
57	0.2001	0.04490	1.037E-11
58	0.2041	0.04206	5.351E-08
59	0.2119	0.03732	3.252E-08
60	0.1981	0.04625	1.670E-08
61	0.2135	0.03646	6.427E-09
62	0.2109	0.03794	2.013E-10
63	0.2124	0.03710	1.492E-09
64	0.2022	0.04345	4.514E-09
65	0.4766	0.00737	0
66	0.4075	0.01191	0
67**	**0.2742**	**0.02837**	**0**
68	0.2044	0.05090	0
69	0.2006	0.04450	2.109E-08
70	0.2083	0.03953	4.775E-09
71	0.2062	0.04086	4.768E-13
72	0.1827	0.05878	1.788E-09
73	0.1953	0.04836	1.770E-09
74	0.2006	0.04455	6.802E-10
75	0.2012	0.04413	5.960E-14
76	0.1804	0.06088	5.067E-09
77	0.1912	0.05149	1.242E-08
78	0.1905	0.05207	3.514E-09
79	0.1929	0.05017	5.524E-09
80	0.1894	0.05295	7.651E-10
81	0.1964	0.04750	6.062E-10
82	0.1958	0.04800	2.008E-09
83	0.2098	0.03860	2.675E-09
84	0.1929	0.05017	5.524E-09

**** The furrows used to predict the unshaded furrows.**
All shaded furrows are those estimated using IPARM

Table J.5 Irrigation performance of the Lagoona field under measured conditions

Wetted Furrow	AE (%)	AER (%)	RE (%)	DU (%)	DURZ (%)	Runoff (m^3)	D (mm)	D_{DD} (mm)
1	74.44	76.22	93.74	65.65	79.97	3.5	104.6	26.8
2	78.57	79.60	99.44	83.31	98.31	2.0	104.6	22.0
3	78.70	90.29	99.33	89.90	97.99	22.7	90.4	8.0
4	78.60	80.38	99.48	83.59	98.44	3.5	104.4	21.8
5*	**78.47**	**86.86**	**99.41**	**87.11**	**98.21**	**16.5**	**94.7**	**12.2**
6	77.86	81.11	98.45	78.90	95.26	6.4	100.9	19.2
7	76.90	80.09	97.36	74.35	91.86	6.2	101.1	20.3
8	78.90	84.75	100.00	94.37	100.00	11.5	97.9	14.9
9	78.05	93.04	98.65	90.97	95.93	29.3	86.3	4.5
10	78.63	88.83	99.54	89.42	98.60	20.0	92.4	9.8
11	78.56	87.87	99.63	89.09	98.88	18.3	93.7	11.0
12	79.20	82.21	99.64	85.42	98.91	5.9	101.4	18.7
13	77.94	92.82	98.74	90.95	96.19	29.2	86.7	4.7
14	78.59	89.66	99.44	89.73	98.31	21.7	91.3	8.7
15	78.59	87.08	99.66	88.71	98.97	16.7	94.7	11.9
16	79.07	80.72	99.57	84.64	98.72	3.2	102.4	19.8
17	79.29	81.91	99.63	85.48	98.88	5.1	101.1	18.4
18	79.10	82.48	99.62	85.13	98.85	6.6	101.9	19.2
19	78.94	84.76	99.70	87.40	99.09	11.4	97.6	14.8
20	78.57	79.60	99.44	83.31	98.31	2.0	104.6	22.0
21	78.98	82.89	99.71	86.41	99.12	7.6	99.9	17.2
22	78.04	80.96	98.28	79.56	94.76	5.7	104.9	23.4
23	78.90	80.49	99.36	83.06	98.06	3.1	104.2	21.7
24	75.75	75.79	95.40	70.66	85.53	0.1	104.8	25.6
25	79.28	81.87	99.63	85.47	98.89	5.1	101.1	18.4
26	78.40	78.42	99.23	82.50	97.66	0.0	105.2	22.8
27	78.95	82.85	99.71	86.40	99.13	7.6	100.0	17.2
28	75.94	75.99	95.64	71.38	86.32	0.1	104.9	25.5
29	78.90	84.31	99.74	87.35	99.23	10.6	98.2	15.4
30*	**78.90**	**84.75**	**100.00**	**94.37**	**100.00**	**11.5**	**97.9**	**14.9**
31	78.98	82.51	99.70	86.19	99.11	6.9	100.4	17.6
32	75.59	75.94	95.67	71.50	86.42	0.7	105.2	25.8
33	76.67	76.67	96.55	74.19	89.28	0.0	104.8	24.6
34	78.54	79.92	99.40	83.09	98.18	2.7	104.8	22.3
35	78.71	82.89	99.73	86.58	99.20	8.2	99.9	17.2
36	79.02	80.65	99.52	84.09	98.54	3.2	103.2	20.6
37	78.91	87.15	99.63	88.59	98.89	16.1	94.6	11.9
38	78.55	89.16	99.50	89.57	98.51	20.8	92.0	9.4
39	78.77	86.94	99.65	88.58	98.96	16.0	94.8	12.1
40	78.98	83.27	99.71	86.62	99.12	8.4	99.4	16.7
41	78.81	87.00	99.65	88.58	98.93	16.0	94.8	12.1
42	78.46	90.36	99.34	90.00	98.00	23.3	90.3	7.9
43	78.41	90.73	99.27	90.14	97.80	24.2	89.8	7.4
44	78.79	85.33	99.73	87.90	99.18	12.8	96.9	14.1
45	78.74	85.66	99.72	88.07	99.16	13.6	96.5	13.7
46	78.93	80.53	99.40	83.28	98.19	3.1	104.0	21.5
47	77.07	79.61	97.54	77.46	92.44	5.0	105.2	24.3
48	76.66	76.71	96.54	74.16	89.26	0.1	104.8	24.7
49	78.76	83.33	99.73	86.79	99.19	9.0	99.4	16.6
50	78.67	87.21	99.64	88.73	98.93	16.7	94.5	11.8
51	78.68	88.06	99.60	89.11	98.81	18.4	93.4	10.7
52	79.15	82.90	99.63	85.38	98.90	7.3	101.5	18.8
53	78.79	86.55	99.67	88.41	99.02	15.2	95.3	12.6
54	78.89	87.53	99.60	88.75	98.81	16.9	94.1	11.4
55	78.93	86.76	99.65	88.43	98.96	15.3	95.1	12.4
56	78.88	87.11	99.64	88.58	98.91	16.1	94.7	12.0
57	78.40	91.65	99.08	90.46	97.21	25.9	88.5	6.2
58	78.00	93.48	98.46	91.11	95.48	30.3	85.6	3.9
59	76.29	95.77	96.34	92.17	93.08	38.1	80.8	0.8
60	78.41	90.73	99.27	90.14	97.80	24.2	89.8	7.4
61	75.65	95.95	95.75	92.37	92.86	39.8	79.9	0.4
62	76.52	95.49	96.79	92.05	93.37	37.2	81.5	1.2
63	75.97	95.75	96.27	92.25	93.09	38.8	80.6	0.7
64	78.06	92.53	98.84	90.83	96.47	28.4	87.1	5.1
65	76.83	80.57	97.37	74.71	91.90	7.3	100.5	19.7
66	77.41	82.12	97.87	77.50	93.46	9.2	99.0	17.8
67*	**78.10**	**87.50**	**98.99**	**85.92**	**96.95**	**18.5**	**93.5**	**11.4**
68	78.48	82.28	99.53	84.86	98.59	7.5	100.5	17.9
69	78.26	91.89	99.02	90.58	97.04	26.7	88.1	5.9
70	77.18	94.79	97.61	91.70	94.12	34.5	83.2	2.1
71	77.43	94.04	98.16	91.42	94.92	32.6	84.6	3.1
72	78.71	82.52	99.73	86.37	99.19	7.5	100.4	17.6
73	78.67	89.34	99.48	89.59	98.42	20.9	91.7	9.1
74	78.23	91.83	99.04	90.57	97.10	26.7	88.2	6.0
75	78.09	92.07	98.99	90.70	96.92	27.5	87.8	5.7
76	79.10	81.40	99.62	85.17	98.85	4.5	101.7	19.0
77	78.67	87.21	99.64	88.73	98.93	16.7	94.5	11.8
78	78.69	86.82	99.67	88.57	99.00	15.9	95.0	12.3
79	78.72	88.12	99.60	89.12	98.79	18.4	93.3	10.7
80	78.92	86.33	99.68	88.25	99.03	14.5	95.7	12.9
81	78.44	89.86	99.42	89.85	98.25	22.4	91.0	8.5
82	78.52	89.54	99.46	89.72	98.38	21.6	91.4	8.9
83	76.74	95.20	97.18	91.92	93.69	36.2	82.2	1.6
84	78.72	88.12	99.60	89.12	98.79	18.4	93.3	10.7

**** The furrows used to predict the unshaded furrows.**
All shaded furrows are those estimated using IPARM